สำนักงานกองทุนสนับสนุนการวิจัย
The Thailand Research Fund

รายงานการวิจัยฉบับสมบูรณ์

โครงการวิจัยทุนส่งเสริมกลุ่มวิจัย (เมธีวิจัยอาวุโส สกว.)

ชื่อโครงการ

การกระตุ้นด้วยฮอร์โมนเพื่อเพิ่มประสิทธิภาพกระบวนการสืบพันธุ์ของหอยเป๋าฮื้อและกุ้งก้ามกราม

Endocrine manipulation of the reproduction in the tropical abalone, *Haliotis asinina*, and the giant freshwater prawn, *Macrobrachium rosenbergii*

โดย

ศ. ดร. ประเสริฐ โศภน และคณะ

สัญญาเลขที่ RTA4780014

รายงานการวิจัยฉบับสมบูรณ์

โครงการวิจัยทุนส่งเสริมกลุ่มวิจัย (เมธีวิจัยอาวุโส สกว.)

(31 สิงหาคม 2547- 28 กุมภาพันธ์ 2551)

ชื่อโครงการ

การกระตุ้นด้วยฮอร์โมนเพื่อเพิ่มประสิทธิภาพกระบวนการสืบพันธุ์ของหอยเป๋าฮื้อและกุ้งก้ามกราม

Endocrine manipulation of the reproduction in the tropical abalone, *Haliotis asinin*a, and the giant freshwater prawn, *Macrobrachium rosenbergii*

คณะผู้วิจัย

ชื่อ	ตำแหน่ง	สังกัด
นายประเสริฐ โศภน	ศ. ดร.	คณะวิทยาศาสตร์ ม. มหิดล
นายชัยทิพย์ วนิชานนท์	รศ. ดร.	คณะวิทยาศาสตร์ ม. มหิดล
นางประพีร์ เศรษฐรักษ์	รศ. ดร.	คณะวิทยาศาสตร์ ม. มหิดล
นางจิตติพันธุ์ ชวเดช	รศ. ดร.	คณะวิทยาศาสตร์ ม. มหิดล
น.ส. พรจันทร์ สายทองดี	รศ. ดร.	คณะวิทยาศาสตร์ ม. มหิดล
นายวัฒนา วีรชาติยานุกูล	รศ. ดร.	คณะวิทยาศาสตร์ ม. มหิดล
นายวิชัย ลิ้นทอง	นักวิทยาศาสตร์	คณะวิทยาศาสตร์ ม. มหิดล
นายธเนศ พุ่มทอง	นักวิชาการประมง	ศูนย์วิจัยและพัฒนาประมงชายฝั่ง คลองวาฬ ประจวบคีรีขันต์

สนับสนุนโดยสำนักงานกองทุนสนับสนุนการวิจัย

(ความเห็นในรายงานนี้เป็นของผู้วิจัย สกว. ไม่จำเป็นต้องเห็นด้วยเสมอไป)

สารบัญ

หน้า

บทคัดย่อ (Abstract)……...5

บทสรุปสำหรบผู้บริหาร(Executive summary)……. 9

เนื้อหางานวิจัย.....11

โครงการวิจัย: การกระตุ้นด้วยฮอร์โมนเพื่อเพิ่มประสิทธิภาพกระบวนการสืบพันธุ์ของหอยเป๋าฮื้อ.....11
และกุ้งก้ามกราม (Endocrine manipulation of the reproduction in the tropical abalone, *Haliotis asinine*,
and the giant freshwater prawn, *Macrobrachium rosenbergii*)

โครงการที่ 1 หอยเป๋าฮื้อ.....11

หัวข้อที่ 1 บทนำ……11

หัวข้อที่ 2 วงจรชีวิตและระบบสืบพันธุ์ของหอยเป๋าฮื้อ.....12

หัวข้อที่ 3 ระบบประสาทและฮอร์โมนที่ควบคุมการสืบพันธุ์และการเจริญเติบโต.....13

หัวข้อที่ 4 การศึกษาฮอร์โมนกระตุ้นการตกไข่ (egg-laying hormone-ELH) และยีนที่ควบคุม..... 16

หัวข้อที่ 5 ฮอร์โมนที่ควบคุมการเจริญเติบโตและการพัฒนาของตัวอ่อน..... 17

หัวข้อที่ 6 การลงเกาะ (settlement) และเมตามอร์โฟซิส (metamorphosis) ในหอยเป๋าฮื้อ..... 19

หัวข้อที่ 7 การศึกษาบทบาทของฮอร์โมน aELH และ GnRH ที่มีผลต่อการเจริญเติบโต และพัฒนาการ.....21
ของเซลล์สืบพันธุ์ในหอยเป๋าฮื้อตัวอ่อน

หัวข้อที่ 8 การกระตุ้นการพัฒนาของต่อมสืบพันธุ์ในหอยเป๋าฮื้อตัวเต็มวัยด้วยฮอร์โมน aELH และ GnRH…… 32

หัวข้อที่ 9 การทดสอบการกระตุ้นการปล่อยเซลล์สืบพันธุ์ในหอยเป๋าฮื้อตัวเต็มวัยด้วยสาร aELH และ GnRH…….. 36

โครงการที่ 2 กุ้งก้ามกราม.....40

หัวข้อที่ 1 บทนำ.....40

หัวข้อที่ 2 การศึกษาโครงสร้างของต่อมอัณฑะและการพัฒนาของเซลล์อสุจิในกุ้งก้ามกรามเปรียบเทียบกับกุ้งกุลาดำ.....40

หัวข้อที่ 3 การศึกษาโครงสร้างของไข่และการพัฒนาของเซลล์ไข่ในกุ้งก้ามกรามเปรียบเทียบกับกุ้งกุลาดำและ.....51
กระบวนการปฏิสนธิระหว่างไข่กับอสุจิ

หัวข้อที่ 4 การวิเคราะห์การกระจายและวัดระดับของสารสื่อประสาทเซโรโทนิน (5-HT) โดปามีน (DA)……..52
ออกโตปามีน (OA) ในระบบประสาทและรังไข่กุ้งโดยวิธี immunocytochemistry (ICC) และ high performance
liquid chromatography (HPLC)

หัวข้อที่ 5. การศึกษาผลกระตุ้นการพัฒนาของรังไข่กุ้งด้วยสารสื่อประสาท 5-HT และ DA…… 54

หัวข้อที่ 6 การวิเคราะห์การกระจายของฮอร์โมน gonadotropin-releasing hormone (GnRH) และ..... 55
egg-laying hormone (ELH)โดยวิธี immunocytochemistry (ICC)

หัวข้อที่ 7 การวิเคราะห์คุณลักษณะของฮอร์โมน GnRH และ ELH ของกุ้งโดยวิธี high performance……60
liquid chromatography (HPLC)

หัวข้อที่ 8 ทดสอบการกระตุ้นพัฒนาการของรังไข่กุ้งด้วยฮอร์โมน GnRH, ELH และ methyl farnesoate (MF)……..61

หัวข้อที่ 9 การศึกษาโครงสร้างและเซลล์ในต่อมเพศผู้(Androgenic gland) ของกุ้งก้ามกราม.....62

หัวข้อที่ 10 การศึกษาคุณลักษณะของ Androgenic gland hormone (AGH) และ Insulin –like peptide hormone (ILP)….. 66

หน้า

หัวข้อที่ 11 การกระตุ้นการเปลี่ยนเพศกุ้งก้ามกรามด้วย 17 α methyltestosterone (17 αMT)..... 70
และ สารสกัดรวมจาก androgenic gland
ผลลัพธ์ที่ได้จากโครงการ.....72
ผลงานที่ตีพิมพ์ในวารสารวิชาการนานาชาติ.....72
การเสนอผลงานในที่ประชุมระดับนานาชาติ……75
บทความวิชาการภาษาไทยสำหรับบุคคลทั่วไป.....77
รหัสพันธุกรรมของฮอร์โมนกุ้งในฐานข้อมูล.....77
นักวิจัยในโครงการที่ได้รับทุนอื่นในระหว่างรับทุนส่งเสริมกลุ่มวิจัย.....78
การผลิตบุคลากรและนักวิจัย.....78
ผลิตภัณฑ์ที่ได้ซึ่งมีโอกาสนำไปประยุกต์ใช้ในเชิงพาณิชย์หรือเชิงสาธารณะ…….. 80
ภาคผนวก
ผลงานตีพิมพ์ในวารสารวิชาการนานาชาติ
ผลงานที่นำเสนอในที่ประชุมระดับนานาชาติ

บทคัดย่อ (Abstract)

ประเทศไทยได้มีการพัฒนาระบบเพาะเลี้ยงหอยเป๋าฮื้อและกุ้งก้ามกรามที่ก้าวหน้าไปมากแต่การผลิตตัวอ่อนที่สามารถอยู่รอดและพัฒนาไปเป็นตัวเต็มวัยยังมีอัตราเพิ่มขึ้นไม่มากนัก อีกทั้งการเลี้ยงพ่อ-แม่พันธุ์ในสภาพที่ไม่เหมือนธรรมชาติทำให้พ่อ-แม่พันธุ์ลดประสิทธิภาพการสืบพันธุ์ลงเนื่องจากเกิดความเครียด จึงมีความจำเป็นที่จะต้องใช้สารฮอร์โมนช่วยกระตุ้น แต่จะกระทำเช่นนั้นได้ต้องมีองค์ความรู้พื้นฐานและความเข้าใจเกี่ยวกับการควบคุมกระบวนการพัฒนาและการทำงานของระบบสืบพันธุ์ซึ่งควบคุมโดยฮอร์โมนจากระบบประสาท ฮอร์โมนที่ควบคุมการทำงานของระบบสืบพันธุ์เหล่านี้อาจถูกควบคุมอีกต่อหนึ่งโดยสารสื่อประสาท (neurotransmitters-NE) เช่น serotonin (5-HT) และ dopamine (DA) และ/หรือสารปรับสัญญาณประสาท (neuromodulator-NM) เช่น FMRF APGW amides และ GnRH สาร NE และ NM อาจเป็นสารสื่อกลาง (chemical mediators) ตัวแรกที่รับรู้การเปลี่ยนแปลงของสภาพแวดล้อมภายนอก โดยเฉพาะอุณหภูมิ ความยาวของกลางวันต่อกลางคืน (photo period) ปริมาณอาหาร ฯลฯ ทั้งนี้เพื่อจะได้ควบคุมการหลั่งฮอร์โมนเพศและฮอร์โมนเร่งการเจริญเติบโตที่กระตุ้นให้หอยหรือกุ้งปรับตัวเข้าสู่ช่วงการเจริญพันธุ์ (reproductive growth) หรือช่วงการเจริญเติบโตของร่างกาย (somatic growth) ที่เหมาะสมกับสภาพแวดล้อม

หอยเป๋าฮื้อ

คณะผู้วิจัยได้ศึกษาลักษณะโครงสร้างของระบบประสาทและระบบสืบพันธุ์ของหอยเป๋าฮื้อและการกระจายของสารสื่อประสาท เซอโรโตนิน (5-HT) และสารปรับสัญญาณประสาท gonadotropin-releasing hormone (GnRH) ซึ่งเป็นสารที่ผลิตโดยเซลล์ประสาทรับสัมผัสที่รับรู้การเปลี่ยนแปลงภายนอกที่มีอิทธิพลต่อการพัฒนาของระบบสืบพันธุ์ พบว่า 5-HT และ GnRH ส่วนใหญ่มีอยู่ในเซลล์ประสาทของปมประสาท cerebral และ pleuropedal โดยเซลล์เหล่านี้ไม่มีการรวมกลุ่มชัดเจน นอกจากนี้ยังได้ศึกษาความสัมพันธ์ระหว่างสาร 5-HT, GnRH และฮอร์โมน์ที่ควบคุมการสืบพันธุ์ในหอยเป๋าฮื้อโดยเฉพาะฮอร์โมนประสาทที่คุมการหลั่งเซลล์สืบพันธุ์ (abalone egg-laying hormone-aELH) ในหอยเป๋าฮื้อพันธุ์พื้นเมือง *(Haliotis asinina)* โดยได้ทำการสังเคราะห์ aELH ด้วยวิธีพันธุวิศวกรรมแล้วนำไปฉีดกระตุ้นหอยพ่อ-แม่พันธุ์ พบว่าสารสื่อประสาทเซโรโทนิน (serotonin-5HT), GnRH และ aELH สามารถกระตุ้นการพัฒนาของรังไข่กับเซลล์ไข่และการตกไข่ได้ ซึ่งช่วยเพิ่มประสิทธิภาพของแม่พันธุ์ที่เลี้ยงแบบกักขังได้ และถ้าหากนำไปฉีดในหอยวัยอ่อนอายุก่อน 4 เดือนทำให้ได้หอยเพศเมียมากขึ้น นอกจากนั้นยังพบว่าสารปรับสัญญาณ APGW สามารถกระตุ้นการปล่อยเซลล์อสุจิจากพ่อพันธุ์ได้ทั้งหมด ทำให้สะดวกต่อการกำหนดระยะเวลาปล่อยเซลล์สืบพันธุ์เพศผู้และเพศเมียจากพ่อ-แม่พันธุ์ที่พร้อมกัน ทำให้สะดวกต่อการเก็บเซลล์สืบพันธุ์เพื่อนำไปปฏิสนธิโดยวิธี *in vitro* fertilization โดยใช้อัตราส่วนไข่ต่ออสุจิที่ได้ผลมากที่สุดคือ 1:100

การศึกษากลไกการลงเกาะ(settlement) ของตัวอ่อนของหอยเป๋าฮื้อพบว่า γ aminobutyric acid (GABA) 5γ aminovaleric acid (5AVA) ที่ความเข้มข้น 1 μM และ monosodium glutamate (MSG) ที่ความเข้มข้น 5 mM สามารถกระตุ้นการลงเกาะได้มากกว่า 50% เมื่อเปรียบเทียบกับกลุ่มควบคุมทำให้อัตราการลงเกาะและการอยู่รอดของตัวอ่อนหอยเป๋าฮื้อเพิ่มขึ้นมาก โดยกลุ่มควบคุมที่มีการลงเกาะเพียง 10-15% องค์ความรู้ที่ได้จากงานวิจัยพื้นฐานดังกล่าวแล้วสามารถนำไปประยุกต์ใช้เพิ่มประสิทธิภาพการเพาะเลี้ยงหอยเป๋าฮื้อโดยเกษตกรรายย่อยและการเพาะเลี้ยงระดับเชิงพาณิชย์ได้

กุ้งก้ามกราม

การหลั่งฮอร์โมนที่ควบคุมวงจรการสืบพันธุ์กับการพัฒนาของต่อมสืบพันธุ์ และเซลล์สืบพันธุ์ของกุ้งก้ามกรามมีการส่งสัญญาณเป็นทอดๆ ผ่านเซลล์ประสาทลำดับแรกที่อยู่ใน optic lobe ซึ่งสร้างสารสื่อประสาท (neurotransmitters) ในกลุ่ม indolamine ได้แก่ เซโรโทนิน (serotonin or 5-hydroxytryptamine-5-HT) และสารสื่อประสาทในกลุ่ม catecholamines (dopamine-DA และ octopamine-OA) โดย 5-HT และ DA ทำหน้าที่ตรงกันข้าม การฉีด 5-HT ในกุ้งก้ามกรามที่ระดับ2.5x10^{-}

^{5}-2.5 x 10^{-7} mol/ตัว และ DA antagonist (spiperone-SP) ที่ระดับ 5.4 x 10^{-7} mol/ตัว ทำให้รังไข่พัฒนาเร็วขึ้นกว่าปกติ และมีการปล่อยไข่ออกมาในปริมาณและคุณภาพใกล้เคียงกับปกติ และยังทำให้ระยะการพัฒนาของเอมบริโอลดลงด้วย แต่การฉีด DA ในปริมาณใกล้เคียงกัน มีผลตรงกันข้าม พบว่า 5-HT และ DA มีการกระจายอยู่ในเกือบทุกส่วนของสมอง แต่จะมีความเข้มข้นสูงในปมประสาท thoracic และต่อมสืบพันธุ์ ระดับ 5-HT มีเพิ่มขึ้นเรื่อยๆ จากระยะที่ 1 ของวงจรรังไข่จนมีระดับสูงสุดในระยะที่ 4 ส่วน DA มีระดับความเข้มข้นที่สวนทางกัน

การออกฤทธิ์ของ 5-HT อาจถูกขยายสัญญาณด้วยสารปรับสัญญาณประสาท (neuromodulator) ซึ่งมักเป็นสารเปปไทด์ขนาดเล็กหรือ เอไมด์ โดยเฉพาะ gonadotropin-releasing hormone (GnRH) และ Enkephalin (Enk) ซึ่งพบว่าการฉีด GnRH ที่ระดับ 50-500 ng/gm น้ำหนักตัว หรือ GnRH agonist ที่ระดับ 1000 ng/gm น้ำหนักตัว สามารถกระตุ้นให้วงจรของการพัฒนารังไข่และการตกไข่เร็วขึ้นกว่าปกติ อีกทั้งมีปริมาณและคุณภาพของไข่ใกล้เคียงกับกลุ่มควบคุม พบว่า GnRH มีกระจายอยู่ในสมอง ปมประสาท thoracic และต่อมสืบพันธุ์

ฮอร์โมนที่เป็นสารออกฤทธิ์ระดับสุดท้ายคือ gonadotropins ซึ่งแบ่งเป็นสองกลุ่มคือ กลุ่มที่กระตุ้นการพัฒนาของต่อมเพศได้แก่ gonad-stimulating hormone (GSH) ซึ่งกระตุ้นการพัฒนาของรังไข่และเซลล์ไข่, vitellogenin stimulating ovarian hormone (VSOH) ซึ่งกระตุ้นการสร้างสารไข่ในเซลล์ไข่ ส่วนในเพศผู้มี androgenic gland hormone (AGH) ซึ่งกระตุ้นการพัฒนาของต่อมอัณฑะ ส่วนฮอร์โมนที่ห้ามการพัฒนาของต่อมสืบพันธุ์ ได้แก่ gonad-inhibiting hormone (GIH) ซึ่งทำหน้าที่ตรงกันข้ามกับฮอร์โมนกลุ่มแรก นอกจากฮอร์โมนดังกล่าวเรายังพบว่าในกุ้งมีฮอร์โมนคล้ายๆกับ abalone egg-laying hormone (aELH) กระจายอยู่ในปมประสาท thoracic และรังไข่ การฉีดฮอร์โมน ELH ที่ระดับ 5-500 ng/gm น้ำหนักตัว ทำให้วงจรของการพัฒนารังไข่และการตกไข่ของกุ้งสั้นลงโดยมีการปล่อยไข่ในปริมาณและคุณภาพที่ปกติ เนื่องจากพบว่า ELH เป็นฮอร์โมนที่มีการอนุรักษ์สูงในกุ้งก้ามกราม กุ้งกุลาดำ และสัตว์พวก crustaceans ชนิดอื่นๆ เราจึงเชื่อว่า ELH เป็น gonadotropin ที่สำคัญมากตัวหนึ่งที่มีบทบาทในการพัฒนาของต่อมสืบพันธุ์และเซลล์สืบพันธุ์ ทั้งนี้เป็นไปได้ว่า ELH อาจเป็นหรือทำหน้าที่คล้าย GSH ซึ่งเป็นฮอร์โมนที่มีผู้เสนอว่ามีการออกฤทธิ์กระตุ้นการพัฒนาของรังไข่ในกุ้ง แต่ยังไม่เคยมีผู้ใดสามารถสกัดฮอร์โมนดังกล่าวออกมาได้

การเลี้ยงในสภาพกักขังทำให้กุ้งเกิดความเครียดเป็นเหตุให้การพัฒนาของต่อมสืบพันธุ์และการสืบพันธุ์ของพ่อ-แม่พันธุ์กุ้งลดลงจนกระทั่งอาจจะไม่มีเพศสัมพันธ์เลย ทั้งนี้เป็นไปได้ว่าความเครียดมีผลกระทบต่อความสมดุลของฮอร์โมน gonadotropins โดยตรง การฉีด 5-HT และ/หรือ GnRH หรือแม้กระทั่งการให้ ELH โดยตรง สามารถกระตุ้นให้ประสิทธิภาพการสืบพันธุ์ของพ่อ-แม่พันธุ์เพิ่มขึ้นได้ นอกจากนั้นการฉีดสารห้าม DA เช่น SP ช่วยเป็นปัจจัยเสริมที่ผลักดันให้มีการสร้างและหลั่ง gonadotropin ที่มีฤทธิ์กระตุ้นการพัฒนาต่อมสืบพันธุ์ และพฤติกรรมสืบพันธุ์เพิ่มขึ้นได้ ในทำนองเดียวกับการกระตุ้นตัวอ่อนทั้งสองเพศด้วยฮอร์โมนกำหนดเพศผู้ที่อยู่ในกลุ่ม insulin-like growth factor (IGF) และ/หรือ AGH และ/หรือ testosterone อาจทำให้เกิดการเปลี่ยนเพศของลูกกุ้งที่เป็นเพศผู้มากขึ้นได้ ซึ่งจะทำให้การเลี้ยงแต่เพศผู้อย่างเดียว (male sex monoculture)เป็นไปได้ และให้ผลตอบแทนแก่เกษตกรเพิ่มสูงขึ้น

The tropical abalone, *Haliotis asinina*, and the giant freshwater prawn, *Macrobrachium rosenbergii*, gear their reproductive and growth activities to fit the changing of environmental conditions. The most powerful environmental stimuli are light, photoperiod, lunar cycle, temperature, and availability of food. These cues are perceived by many specialized sense organs concentrating in the eyes and appendages around the head region. Specialized receptor cells and associated neurons in these structures and various neural ganglia are the principal structures that perceive and act in the signaling pathway to mediate the physiological and behavioral changes of these animals in response to the changes of environmental conditions.

Abalone

The anatomical organization and detailed histology of the abalone nervous and reproductive systems together with the distribution of the controlling neurotransmitters (NE), 5-HT, and neuromodulators (NM), GnRH, have been studied. These NE and NM have been localized principally in the cerebral and pleuropedal ganglia. Furthermore, the neurohormone, especially the abalone egg-laying hormone (aELH) have also been detected in these ganglia and the gonads. Recombinant aELH has been synthesized. The administrations of serotonin (5-HT), GnRH, or aELH could shorten the ovarian cycle and the maturation of oocytes in female broodstocks. 5-HT and aELH could also stimulate spawning in female. On the other hand, APGW could stimulate spermiation in mature males. These treatments could stimulate the simultaneous spawning and spermiation which allow expedient collection of the gametes for the *in vitro* fertilization. Administration of 5-HT, aELH and GnRH in juvenile abalone with age less than 4 months could also stimulate the ovarian and testicular maturation at the earlier age. Furthermore, 5-HT and aELH tend to increase the number of females more than males. In addition to the endocrine manipulation of the reproductive processes, we have also studied the factors that could increase the settlement and metamorphosis of the abalone larvae. It was demonstrated that GABA, 5AVA at 1 μM and MSG at 5 mM could enhance settlement rate of the veliger larvae by 50% when compared to the control which was at 10-15%. This endocrine manipulation could also increase the rate of metamorphosis and survival of the abalone spats. This technique could be used for small as well as large scale aquaculture.

Prawn

Major neurotransmitters that could stimulate the reproduction and growth of the giant freshwater prawn are indolamine (serotonin or 5-hydroxytryptamine-5HT), and catecholamines (dopamine-DA, octopamine-OA). Indolamine and catecholamine are usually antagonistic in their actions; for example, 5-HT was found to stimulate hyperglycemic hormone (CHH) and gonadotrophic hormone (GSH) which stimulate the ovarian maturation, while DA and OA

inhibit the releases and consequently the actions of these hormones. The actions of neurotransmitters may be mediated and modified by groups of neuromodulators, which are usually composed of short peptides or amides, the most prominent of which are enkephalin and GnRH. Gonadotrophic hormones themselves are classified into stimulatory group (GSH/VSH, VSOH, AGH) and inhibitory group (GIH) which inhibit the syntheses and releases of the formers. In addition to these two groups of hormone, we have detected the presence the prawn egg-laying hormone (ELH) which is similar to abalone ELH, in thoracic ganglia and ovary of prawn. The administration of this hormone (aELH) at the dosages of 5 ng/gm BW to 500 ng/gm BW could significantly shortening the ovarian cycle and spawning period. When characterized by HPLC, the prawn ELH is very similar to abalone ELH. Other vertebrate-type hormones is present including insulin-like growth factor (IGF). This hormone was detected in the androgenic gland of the giant freshwater prawn, which is highly similar to that of the closely related species, *Cherax destructor*. This hormone could be male-sex determining factors acting in addition to or in place of AGH, as up to date AGH could not yet be isolated in the freshwater prawn. In addition, the evidence for the presence of vertebrate-type sex steroids (testosterone, estradiol), and their stimulating effects on the prawn gonads has been demonstrated by our group.

When reared in captivity, the fecundity of the broodstocks always decline which is due to the imbalance of gonadotrophins, perhaps caused by unnatural environment and stress. The restoration of stimulatory gonadotrophins by direct supplementation of ELH, and/or by stimulation with 5-HT, and/or neuromediators like GnRH, could improved the gonadal maturation and greater production of gametes. Furthermore, this processes could be enhanced by the inhibition of the inhibitory hormones with DA inhibitor. Likewise, we demonstrated that the male-sex determination of freshwater prawn could be controlled by the antagonistic hormones, ie, IGF and GIH. If such endocrine manipulative strategies are possible, then they could be applied for economic benefit in aquaculture, such as in avoiding eyestalk-ablation in prawn (especially *P. monodon* and *P. vannamei*) which is routinely employed to stimulate the ovarian maturation and spawning, as well as in the sex conversion to obtain and culture only male prawn.

บทสรุปสำหรับผู้บริหาร(Executive Summary)

ประเทศไทยมีชายฝั่งทะเลที่ยาวเกือบตลอดทั้งอ่าวไทยและทางด้านทะเลอันดามันรวมกัน 2,760กิโลเมตร อีกทั้งยังมีแหล่งน้ำจืดธรรมชาติและที่เกิดขึ้นจากการสร้างเขื่อนเกิดขึ้นอีกมากมาย การประมงจากทะเลและจากแหล่งน้ำจืดจึงมีความสำคัญทั้งในระดับเกษตรกรรมแบบพอเพียงและเกษตรกรรมเชิงพาณิชย์เพื่อการบริโภคภายในประเทศ และเพื่อการส่งออก ตัวอย่างที่เป็นต้นแบบของเกษตรกรรมทั้งสองระดับที่มีความสัมพันธ์กันคือการเลี้ยงกุ้งโดยเฉพาะกุ้งกุลาดำ (*Penaeus monodon*) และกุ้งขาว (*Penaeus vannamei*) ซึ่งสามารถใช้บริโภคภายในประเทศและทำรายได้ให้ประเทศไทยจากการส่งออกไม่ต่ำกว่าปีละ 70,000 ล้านบาท ตั้งแต่ปี 2543 เป็นต้นมา นอกจากกุ้งกุลาดำและกุ้งขาวแล้ว กุ้งก้ามกรามก็เป็นสินค้าซึ่งเป็นที่ต้องการของตลาดทั้งภายในและภายนอกประเทศซึ่งเป็นผู้บริโภคที่มีกำลังซื้อสูง หอยเป๋าฮื้อก็เป็นสัตว์น้ำอีกตัวหนึ่งที่น่าจะมีศักยภาพในการส่งออกและทำรายได้ให้แก่เกษตรกรสูง เนื่องจากเป็นที่นิยมของผู้บริโภคตั้งแต่สมัยโบราณมาแล้ว โดยเฉพาะในประเทศจีน ญี่ปุ่น เกาหลี ไต้หวัน นอกจากนั้นแล้วค่านิยมในการบริโภคหอยเป๋าฮื้อก็สูงขึ้นอย่างรวดเร็วในประเทศยุโรปตะวันตก และอเมริกาเหนือเนื่องจากมีประชากรเชื้อสายเอเชียมากขึ้น ตลอดจนมีการแลกเปลี่ยนและคลุกเคล้าวัฒนธรรมการบริโภคอาหารระหว่างตะวันตกและตะวันออกเพิ่มขึ้นเรื่อย ๆ

ประเทศไทยได้มีการพัฒนาระบบเพาะเลี้ยงหอยเป๋าฮื้อและกุ้งก้ามกรามที่ก้าวหน้าไปมากแต่การผลิตตัวอ่อนที่สามารถอยู่รอดและพัฒนาไปเป็นตัวเต็มวัยยังมีอัตราเพิ่มขึ้นไม่มากนัก อีกทั้งการเลี้ยงพ่อ-แม่พันธุ์ในสภาพที่ไม่เหมือนธรรมชาติทำให้พ่อ-แม่พันธุ์ลดประสิทธิภาพการสืบพันธุ์ลงเนื่องจากความเครียด จึงมีความจำเป็นที่จะต้องใช้สารฮอร์โมนช่วยกระตุ้น แต่จะกระทำเช่นนั้นได้ต้องมีองค์ความรู้พื้นฐานและความเข้าใจเกี่ยวกับการควบคุมกระบวนการพัฒนาและการทำงานของระบบสืบพันธุ์ซึ่งควบคุมโดยระบบประสาทและฮอร์โมนจากระบบประสาท ฮอร์โมนที่ควบคุมการทำงานของระบบสืบพันธุ์เหล่านี้อาจถูกควบคุมอีกต่อหนึ่งโดยสารสื่อประสาท (neurotransmitters-NE) เช่น serotonin และ dopamine และ/หรือสารปรับสัญญาณประสาท (neuromodulator-NM) เช่น FMRF APGW amides และ GnRH สาร NE และ NM อาจเป็นสารสื่อกลาง (chemical mediators) ตัวแรกที่รับรู้การเปลี่ยนแปลงของสภาพแวดล้อมภายนอก โดยเฉพาะอุณหภูมิ ความยาวของกลางวันต่อกลางคืน (photo period) ปริมาณอาหาร ฯลฯ ทั้งนี้เพื่อจะได้ควบคุมการหลั่งฮอร์โมนเพศและฮอร์โมนเร่งการเจริญเติบโตที่กระตุ้นให้สัตว์ทั้งสองชนิดปรับตัวเข้าสู่ช่วงการเจริญพันธุ์ (reproductive growth) หรือช่วงการเจริญเติบโตของร่างกาย (somatic growth) ให้เหมาะสมกับสภาวะแวดล้อม

หอยเป๋าฮื้อ

คณะผู้วิจัยได้ศึกษาลักษณะโครงสร้างของระบบประสาทและระบบสืบพันธุ์ของหอยเป๋าฮื้อและการกระจายของสารสื่อประสาท เซอโรโตนิน (5-HT) และสารปรับสัญญาณประสาท gonadotropin-releasing hormone (GnRH) ซึ่งเป็นสารที่ผลิตโดยเซลล์ประสาทรับสัมผัสที่รับรู้การเปลี่ยนแปลงภายนอกที่มีอิทธิพลต่อการพัฒนาของระบบสืบพันธุ์ พบว่า 5-HT และ GnRH ส่วนใหญ่มีอยู่ในเซลล์ประสาทของปมประสาท cerebral และ pleuropedal โดยเซลล์เหล่านี้ไม่มีการรวมกลุ่มชัดเจน นอกจากนี้ยังได้ศึกษาความสัมพันธ์ระหว่างสาร 5-HT, GnRH และฮอร์โมน์ที่ควบคุมการสืบพันธุ์ในหอยเป๋าฮื้อโดยเฉพาะฮอร์โมนประสาทที่คุมการหลั่งเซลล์สืบพันธุ์ (abalone egg-laying hormone-aELH) ในหอยเป๋าฮื้อพันธุ์พื้นเมือง *(Haliotis asinina)* โดยได้ทำการสังเคราะห์ aELH ด้วยวิธีพันธุวิศวกรรมแล้วนำไปฉีดกระตุ้นหอยพ่อ-แม่พันธุ์ พบว่าสารสื่อประสาทเซโรโทนิน (serotonin-5HT), GnRH และ aELH สามารถกระตุ้นการพัฒนาของรังไข่กับเซลล์ไข่และการตกไข่ได้ ซึ่งช่วยเพิ่มประสิทธิภาพของแม่พันธุ์ที่เลี้ยงแบบกักขังได้ และถ้าหากนำไปฉีดในหอยวัยอ่อนอายุก่อน 4 เดือนทำให้ได้หอยเพศเมียมากขึ้น นอกจากนั้นยังพบว่าสารปรับสัญญาณ APGW สามารถกระตุ้นการปล่อยเซลล์อสุจิจากพ่อพันธุ์ได้ทั้งหมด ทำให้สะดวกต่อการกำหนดระยะเวลาปล่อยเซลล์สืบพันธุ์เพศผู้และเพศเมียจากพ่อ-แม่พันธุ์ที่พร้อมกัน ทำให้สะดวกต่อการเก็บเซลล์สืบพันธุ์เพื่อนำไปปฏิสนธิโดยวิธี *in vitro* fertilization โดยใช้อัตราส่วนไข่ต่ออสุจิที่ได้ผลมากที่สุดคือ 1:100

การศึกษากลไกการลงเกาะ(settlement) ของตัวอ่อนของหอยเป๋าฮื้อพบว่า γ aminobutyric acid (GABA) 5γ aminovaleric acid (5AVA) ที่ความเข้มข้น 1 μM และ monosodium glutamate (MSG) ที่ความเข้มข้น 5 mM สามารถกระตุ้นการลงเกาะได้มากกว่า 50% เมื่อเปรียบเทียบกับกลุ่มควบคุมทำให้อัตราการลงเกาะและการอยู่รอดของตัวอ่อนหอยเป๋าฮื้อ

เพิ่มขึ้นมาก โดยกลุ่มควบคุมที่มีการลงเกาะเพียง 10-15% องค์ความรู้ที่ได้จากงานวิจัยพื้นฐานดังกล่าวแล้วสามารถนำไปประยุกต์ใช้เพิ่มประสิทธิภาพการเพาะเลี้ยงหอยเป๋าฮื้อโดยเกษตกรรายย่อยและการเพาะเลี้ยงระดับเชิงพาณิชย์ได้

กุ้งก้ามกราม

การหลั่งฮอร์โมนที่ควบคุมวงจรการสืบพันธุ์กับการพัฒนาของต่อมสืบพันธุ์ และเซลล์สืบพันธุ์ของกุ้งก้ามกรามมีการส่งสัญญาณเป็นทอดๆ ผ่านเซลล์ประสาทลำดับแรกที่อยู่ใน optic lobe ซึ่งสร้างสารสื่อประสาท (neurotransmitters) ในกลุ่ม indolamine ได้แก่ เซโรโทนิน (serotonin or 5-hydroxytryptamine-5-HT) และสารสื่อประสาทในกลุ่ม catecholamines (dopamine-DA และ octopamine-OA) โดย 5-HT และ DA ทำหน้าที่ตรงกันข้าม การฉีด 5-HT ในกุ้งก้ามกรามที่ระดับ$2.5x10^{-5}$-2.5×10^{-7} mol/ตัว และ DA antagonist (spiperone-SP) ที่ระดับ 5.4×10^{-7} mol/ตัว ทำให้รังไข่พัฒนาเร็วขึ้นกว่าปกติ และมีการปล่อยไข่ออกมาในปริมาณและคุณภาพใกล้เคียงกับปกติ และยังทำให้ระยะการพัฒนาของเอมบริโอลดลงด้วย แต่การฉีด DA ในปริมาณใกล้เคียงกัน มีผลตรงกันข้าม พบว่า 5-HT และ DA มีการกระจายอยู่ในเกือบทุกส่วนของสมอง แต่จะมีความเข้มข้นสูงในปมประสาท thoracic และต่อมสืบพันธุ์ ระดับ 5-HT มีเพิ่มขึ้นเรื่อยๆ จากระยะที่ 1 ของวงจรรังไข่จนมีระดับสูงสุดในระยะที่ 4 ส่วน DA มีระดับความเข้มข้นที่สวนทางกัน

การออกฤทธิ์ของ 5-HT อาจถูกขยายสัญญาณด้วยสารปรับสัญญาณประสาท (neuromodulator) ซึ่งมักเป็นสารเปปไทด์ขนาดเล็กหรือ เอไมด์ โดยเฉพาะ gonadotropin-releasing hormone (GnRH) และ Enkephalin (Enk) ซึ่งพบว่าการฉีด GnRH ที่ระดับ 50-500 ng/gm น้ำหนักตัว หรือ GnRH agonist ที่ระดับ 1000 ng/gm น้ำหนักตัว สามารถกระตุ้นให้วงจรของการพัฒนารังไข่และการตกไข่เร็วขึ้นกว่าปกติ อีกทั้งมีปริมาณและคุณภาพของไข่ใกล้เคียงกับกลุ่มควบคุม พบว่า GnRH มีกระจายอยู่ในสมอง ปมประสาท thoracic และต่อมสืบพันธุ์

ฮอร์โมนที่เป็นสารออกฤทธิ์ระดับสุดท้ายคือ gonadotropins ซึ่งแบ่งเป็นสองกลุ่มคือ กลุ่มที่กระตุ้นการพัฒนาของต่อมเพศได้แก่ gonad-stimulating hormone (GSH) ซึ่งกระตุ้นการพัฒนาของรังไข่และเซลล์ไข่, vitellogenin-stimulating ovarian hormone (VSOH) ซึ่งกระตุ้นการสร้างสารไข่ในเซลล์ไข่ ส่วนในเพศผู้มี androgenic gland hormone (AGH) ซึ่งกระตุ้นการพัฒนาของต่อมอัณฑะ ส่วนฮอร์โมนที่ห้ามการพัฒนาของต่อมสืบพันธุ์ ได้แก่ gonad-inhibiting hormone (GIH) ซึ่งทำหน้าที่ตรงกันข้ามกับฮอร์โมนกลุ่มแรก นอกจากฮอร์โมนดังกล่าวเรายังพบว่าในกุ้งมีฮอร์โมนคล้ายๆกับ abalone egg laying hormone (aELH) กระจายอยู่ในปมประสาท thoracic และรังไข่ การฉีดฮอร์โมน ELH ที่ระดับ 5-500 ng/gm น้ำหนักตัว ทำให้วงจรของการพัฒนารังไข่และการตกไข่ของกุ้งสั้นลงโดยมีการปล่อยไข่ในปริมาณและคุณภาพที่ปกติ เนื่องจากพบว่า ELH เป็นฮอร์โมนที่มีการอนุรักษ์สูงในกุ้งก้ามกราม กุ้งกุลาดำ และสัตว์พวก crustaceans ชนิดอื่นๆ เราจึงเชื่อว่า ELH เป็น gonadotropin ที่สำคัญมากตัวหนึ่งที่มีบทบาทในการพัฒนาของต่อมสืบพันธุ์และเซลล์สืบพันธุ์ ทั้งนี้เป็นไปได้ว่า ELH อาจเป็นหรือทำหน้าที่คล้าย GSH ซึ่งเป็นฮอร์โมนที่มีผู้เสนอว่ามีการออกฤทธิ์กระตุ้นการพัฒนาของรังไข่ในกุ้ง แต่ยังไม่เคยมีผู้ใดสามารถสกัดฮอร์โมนดังกล่าวออกมาได้

การเลี้ยงในสภาพกักขังทำให้กุ้งเกิดความเครียดเป็นเหตุให้การพัฒนาของต่อมสืบพันธุ์และการสืบพันธุ์ของพ่อ-แม่พันธุ์กุ้งลดลงจนกระทั่งอาจจะไม่มีเพศสัมพันธ์เลย ทั้งนี้เป็นไปได้ว่าความเครียดมีผลกระทบต่อความสมดุลของฮอร์โมน gonadotropins โดยตรง การฉีด 5-HT และ/หรือ GnRH หรือแม้กระทั่งการให้ ELH โดยตรง สามารถกระตุ้นให้ประสิทธิภาพการสืบพันธุ์ของพ่อ-แม่พันธุ์เพิ่มขึ้นได้ นอกจากนั้นการฉีดสารห้าม DA เช่น SP ช่วยเป็นปัจจัยเสริมที่ผลักดันให้มีการสร้างและหลั่ง gonadotropin ที่มีฤทธิ์กระตุ้นการพัฒนาต่อมสืบพันธุ์ และพฤติกรรมสืบพันธุ์เพิ่มขึ้นได้ ในทำนองเดียวกับการกระตุ้นตัวอ่อนทั้งสองเพศด้วยฮอร์โมนกำหนดเพศผู้ที่อยู่ในกลุ่ม insulin-like growth factor (IGF) และ/หรือ AGH และ/หรือ testosterone อาจทำให้เกิดการเปลี่ยนเพศของลูกกุ้งที่เป็นเพศผู้มากขึ้นได้ ซึ่งจะทำให้การเลี้ยงแต่เพศผู้อย่างเดียว (male sex monoculture)เป็นไปได้ และให้ผลตอบแทนแก่เกษตกรเพิ่มสูงขึ้น

เนื้อหางานวิจัย

โครงการวิจัย: การกระตุ้นด้วยฮอร์โมนเพื่อเพิ่มประสิทธิภาพกระบวนการสืบพันธุ์ของหอยเป๋าฮื้อและกุ้งก้ามกราม

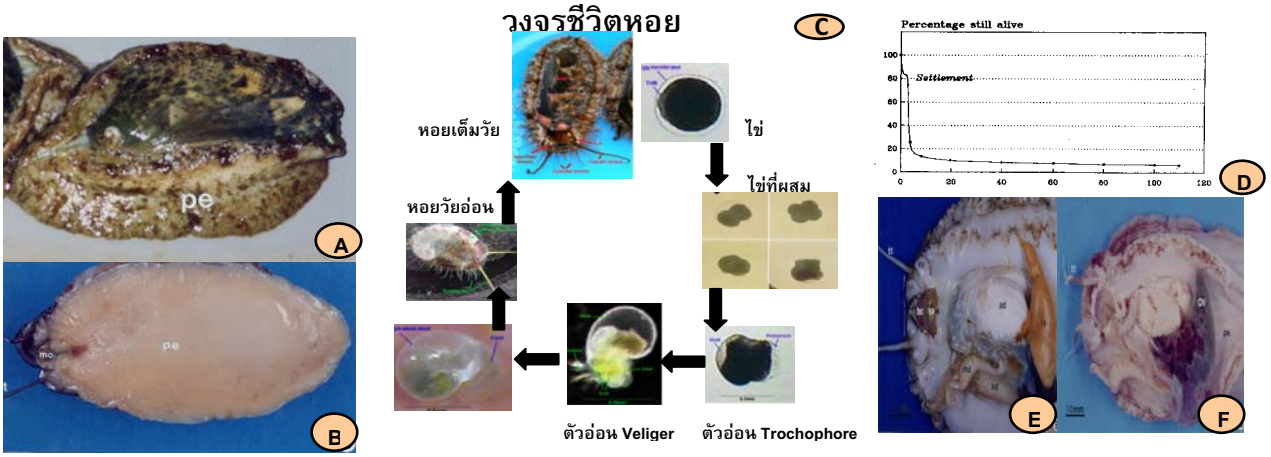
Endocrine manipulation of the reproduction in the tropical abalone, *Haliotis asinina*, and the giant freshwater prawn, *Macrobrachium rosenbergii*

โครงการที่ 1 หอยเป๋าฮื้อ

หัวข้อที่ 1. บทนำ

หอย *H. asinina* (รูปที่ 1A) มีขนาดใหญ่ที่สุดในกลุ่มของหอยเป๋าฮื้อที่พบในฝั่งทะเลของประเทศไทย โดยมีขนาดโตเต็มที่ประมาณ 5x8 ซม. มีอัตราการเจริญเติบโตสูงสุด และมีขนาดเปลือกเล็กและอัตราส่วนเนื้อต่อเปลือกสูงสุด จึงเป็นที่ยอมรับว่าน่าจะเป็นชนิดที่ควรสนับสนุนให้เกษตรกรเลี้ยงทั้งในระดับครัวเรือน ระดับกลาง และระดับใหญ่เชิงพาณิชย์ หอยเป๋าฮื้อชนิดนี้มักอาศัยอยู่ในบริเวณที่มีน้ำขึ้นน้ำลงที่ระดับ 1-7 เมตร หอยเคลื่อนตัวไปช้า ๆ บนโขดหินหรือปะการังที่ตายแล้ว และมีสาหร่ายเกาะอยู่อย่างหนาแน่นซึ่งสาหร่ายที่หอยกินเป็นอาหารหลักคือสาหร่ายผมนางสกุล Gracillaria และ Laminaria ขณะนี้ศูนย์วิจัยและพัฒนาประมงชายฝั่ง คลองวาฬ ประจวบคีรีขันธ์ สามารถทำผสมเทียมและออกแบบระบบการเพาะเลี้ยงหอยบนบกแบบปิดที่ได้ผลดี แต่อย่างไรก็ตามการเลี้ยงหอยเป๋าฮื้อโดยเกษตรกรรายย่อยยังไม่แพร่หลายนัก เนื่องจากมีปัญหาหลายอย่างโดยเฉพาะด้านเงินลงทุนและการตลาด ตลอดจนการแนะนำสินค้าให้ผู้บริโภครู้จักอย่างจริงจังและต่อเนื่อง อย่างไรก็ดีนับได้ว่าหอยเป๋าฮื้อ *H. asinina* เป็นสินค้าที่มีศักยภาพสูง

การเพาะเลี้ยงหอยในสภาพกักขัง ซึ่งไม่เหมือนสภาพธรรมชาติทำให้พ่อ-แม่พันธุ์มีความเครียดสูง การเจริญเติบโตและความสมบูรณ์เพศลดลงมาก การผลิตเซลล์สืบพันธุ์และอัตราการปฏิสนธิเพื่อให้กำเนิดตัวอ่อนก็ลดลงอย่างมากด้วย แม้แต่ในสภาพธรรมชาติอัตราการรอดของตัวอ่อนต่ำมาก โดยเฉพาะในช่วงไซโกตเปลี่ยนเป็นตัวอ่อนระยะ trochophore และตัวอ่อนระยะ veliger และในช่วงการลงเกาะ (settlement) บนพื้นที่มีสาหร่ายปกคลุม และระยะเมตามอร์โฟซิส (metamorphosis) ไปเป็นหอยวัยอ่อน (juvenile) (รูปที่ 1C) โดยทั่วไปหอยวัยอ่อนที่อยู่รอด และมีโอกาสเจริญเติบโตต่อไปมีแค่ 2-5 % (รูปที่ 1D) ถ้าหากเราสามารถหาวิธีทำให้อัตราการลงเกาะ อัตราการเมตามอร์โฟซิส และอัตราการอยู่รอดสูงขึ้นก็น่าจะช่วยลดให้ต้นทุนการผลิตต่ำลง นอกจากนั้นแล้วการกระตุ้นพ่อ-แม่พันธุ์ที่เลี้ยงในสภาพกักขังโดยการให้สารอาหารและฮอร์โมนที่ควบคุมการสืบพันธุ์ในปริมาณที่เหมาะสมก็อาจช่วยเพิ่มความสมบูรณ์เพศได้ ซึ่งจะนำไปสู่การเพิ่มปริมาณเซลล์สืบพันธุ์ที่พ่อ-แม่พันธุ์ผลิตได้ ดังนั้นงานวิจัยพื้นฐานด้านชีววิทยาการสืบพันธุ์โดยเฉพาะการสร้างองค์ความรู้และความเข้าใจเกี่ยวกับอวัยวะสืบพันธุ์ กระบวนการผลิตเซลล์สืบพันธุ์ การลงเกาะ การเมตามอร์โฟซิส รวมทั้งการควบคุมการสืบพันธุ์และการเจริญเติบโตของหอยโดยระบบประสาทและฮอร์โมน น่าจะสามารถนำมาประยุกต์ใช้เพื่อเพิ่มผลผลิตหอยเป๋าฮื้อได้



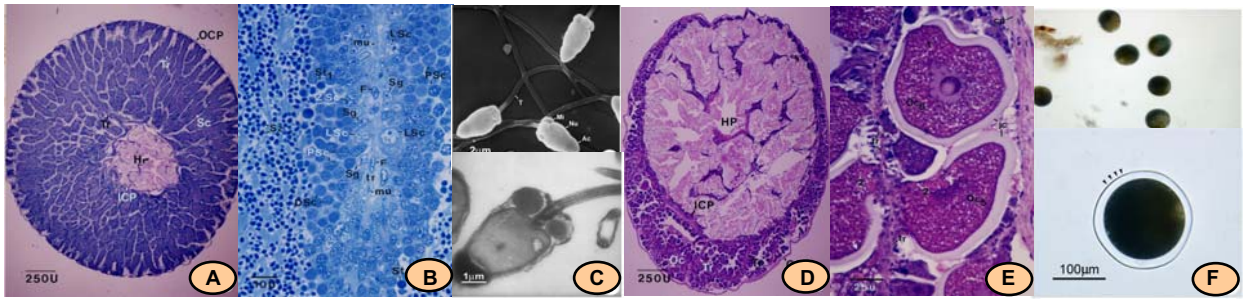
รูปที่ 1. หอยเป๋าฮื้อ H.asinina ตัวเต็มวัย ด้านบน (A) ด้านล่าง (B) (C) วงจรชีวิตของหอยเป๋าฮื้อ ซึ่งประกอบด้วยระยะไข่ที่ผสมแล้วหรือไซโกต (zycote) บลาสตูล่า (blastula) ตัวอ่อน (larvae) ระยะ trochophore และ veliger หอยวัยอ่อน (spat หรือ juvenile) ระยะตัวเต็มวัยซึ่งผลิตเซลล์สืบพันธุ์เพื่อปฏิสนธิเป็นไซโกต (D) กราฟการอยู่รอดในช่วงชีวิตต่างๆ ของหอยที่เจริญตามธรรมชาติ (ปรับจาก Fallu, 1991) (E) อัณฑะในหอยตัวผู้ (F) รังไข่ในหอยตัวเมีย

หัวข้อที่ 2. วงจรชีวิตและระบบสืบพันธุ์ของหอยเป๋าฮื้อ

องค์ความรู้เกี่ยวกับชีววิทยาการสืบพันธุ์ของหอยเป๋าฮื้อมีค่อนข้างจำกัดและโดยมากก็มักจะได้จากการศึกษาในหอยเป๋าฮื้อชนิดที่อาศัยอยู่ในเขตอบอุ่นและเขตหนาวซึ่งมีช่วงของวงจรชีวิตยาวกว่าพันธุ์ที่อยู่ในเขตร้อน คณะผู้ทำวิจัยได้ทำการศึกษาวงจรชีวิตและช่วงของการพัฒนาในระยะต่างๆ ของหอยเป๋าฮื้อ *H.asinina* (รูปที่ 1 C และ ตารางที่ 1) พบว่าจากไข่ที่ถูกผสมแล้วคือ ระยะไซโกตถึงระยะ first cleavage ใช้เวลา 15 -20 นาที ถึงระยะ blastula 75-85 นาที ถึงระยะ trochophore 90-120 นาที ถึงระยะ late veliger 28-40 ชั่วโมง และลงเกาะเมื่อ 48-72 ชั่วโมง และกลายเป็นตัวอ่อนเมื่อ 3-6 วัน ในที่สุดจะเจริญเติบโตเป็นหอยวัยเยาว์ (juvenile) ขนาด 2 มม. เมื่อประมาณ 30 วัน

ตารางที่ 1 ขั้นตอน ขนาด และระยะเวลา ของการพัฒนาของหอยเป๋าฮื้อ *H. asinina*

Stages	Diameter	Time
Unfertilized eggs	180 µm	0 sec
Sperm attach to egg	185 µm	20-30 sec
Sperm acrosome reaction	185 µm	~ 1 min
Appearance of 1st polar body	185 µm	8-9 min
Appearance of 2nd polar body	185 µm	10 min
First cleavage	220 µm	15-20 min
Second cleavage	195 µm	35-40 min
Morula	200 µm	45-55 min
Blastulation	192 µm	75-85 min
Gastrulation	192 µm	85-90 min
Trochophore larvae	210 µm	90-250 min
Early veliger	225 µm	5-24 hours
Late veliger	228 µm	28-40 hours
Early creeping larvae	230 µm	48-72 hours
Creeping larvae	300 µm	3-6 days
Juvenile	2 mm	30 days



รูปที่ 2 (A) ส่วนตัดขวางต่อมอัณฑะ (B) เซลล์สืบพันธุ์ขั้นต่างๆ ในอัณฑะ (C) เซลล์อสุจิถ่ายโดยจุลทรรศน์อิเล็กตรอน (D) ส่วนตัดขวางรังไข่ (E) เซลล์ไข่ในรังไข่ (F) ไข่ที่สุกและปล่อยออกมา

พบว่าหอยตัวผู้เริ่มมีต่อมอัณฑะชัดเจน (รูปที่ 1E, 2A) เมื่ออายุได้ 4 เดือน และตัวเมียมีรังไข่ (รูปที่ 1F, 2D)ปรากฏชัดเจนเมื่ออายุได้ 7 เดือนโดยพบว่าต่อมสืบพันธุ์ (gonad) ทั้งรังไข่และอัณฑะเป็นอวัยวะรูปกรวยห่อหุ้มตับและตับอ่อน (hepatopancreas) อยู่โดยรอบ (รูปที่ 1E, F) ต่อมสืบพันธุ์ถูกห่อหุ้มโดยถุง (capsule) ที่ประกอบด้วยเยื่อเกี่ยวพัน กล้ามเนื้อ และเส้นประสาท ภายในต่อมสืบพันธุ์ถูกแบ่งออกเป็นห้องเล็ก ๆ โดยแผ่นเยื่อเกี่ยวพัน (trabeculae) ที่ยื่นแผ่เข้าไปภายในต่อมจากถุงหุ้ม (รูปที่ 2A, D)

เซลล์สืบพันธุ์เพศผู้ (male germ cells) แบ่งออกเป็น 12 ระยะ คือ spermatogonia, primary spermatocytes (6 ระยะ) secondary spermatocyte spermatids (3 ขั้น) (รูปที่ 2B) และเซลล์อสุจิ (spermatozoa) (รูปที่ 2C) ซึ่งมีหัวลักษณะเป็นรูปโคน มีอะโครโซม (acrosome) ลักษณะคล้ายถ้วยคว่ำปิดอยู่ด้านหน้า หางยาวและมีเฉพาะ axoneme ซึ่งประกอบด้วย microtubules จำนวน 9+2 หุ้มรอบโดยเยื่อหุ้มเซลล์ ที่ด้านท้ายของส่วนหัวมีไมโตคอนเดรียลักษณะเป็นก้อนกลมอยู่ 4-5 ก้อนเรียงต่อกันเป็นวงกลม ในนิวเคลียสของเซลล์อสุจิบรรจุไยโครมาตินซึ่งมีโปรตีน nucleosomal histones (H_{2A}, H_{2B}, H_3, H_4) อยู่ครบและมีโปรตีนที่คล้าย protamines (PL proteins) อยู่ซึ่งอาจเป็นปัจจัยที่ทำให้โครมาตินในนิวเคลียสขดพันกันแน่นเช่นเดียวกับที่เกิดในสัตว์ชั้นสูง เซลล์อสุจิสามารถปฏิสนธิได้ทันทีหลังจากที่ถูกปล่อยออกมาจากหอยพ่อพันธุ์ ซึ่งแสดงว่ากระบวนการกระตุ้นอสุจิให้มีประสิทธิภาพ (sperm capacitation) เกิดขึ้นเรียบร้อยแล้วในต่อมอัณฑะและใช้เพียงน้ำทะเลเป็นตัวกระตุ้นเท่านั้น

เซลล์สืบพันธุ์เพศเมีย (female germ cells) แบ่งออกเป็น 6 ระยะ คือ oogonia (Og), และ primary oocytes ห้าขั้น (Oc_1-Oc_5) เซลล์สืบพันธุ์เพศเมียมีขนาดขยายใหญ่ขึ้นมากจาก 12 μmในระยะ Og ถึง 140 μmในระยะ Oc_5 ซึ่งมีชั้น jelly coat หนาที่ประกอบด้วยสารไกลโคโปรตีนหุ้มอยู่รอบ (รูปที่ 2E) หลังจาก Oc_5 ตกออกจากรังไข่และผสมกับเซลล์อสุจิก็จะมี first polar body เกิดขึ้นเมื่อ 8-9 นาที และ second polar body เกิดขึ้นเมื่อ 10 นาที หลังจากนั้นก็จะเกิด hatching envelope โดยการหนาตัวของชั้น vitelline envelope (รูปที่ 2F) ที่ป้องกันการเข้าผสมของอสุจิตัวอื่นๆ (polyspermy) พบว่าอัตราส่วนที่เหมาะสมสำหรับการทำผสมเทียมระหว่างไข่กับอสุจิคือ 1:100 ซึ่งเป็นสัดส่วนที่ทำให้ได้อัตราการปฏิสนธิสูงสุด และถ้าหากจะชักนำให้เกิด polyploidy ในหอยเป๋าฮื้อเพื่อให้ได้หอยตัวใหญ่ก็ควรชักนำภายใน 10 นาทีแรกหลังจากปฏิสนธิเพื่อป้องกันการเกิด polar bodies

(ดูรายละเอียดในเอกสารหมายเลข 1.2, 1.16, 1.25 และ 1.26 ในภาคผนวก)

หัวข้อที่ 3. ระบบประสาทและฮอร์โมนที่ควบคุมการสืบพันธุ์และการเจริญเติบโต

การพัฒนาของต่อมสืบพันธุ์ในหอยอยู่ภายใต้การควบคุมโดยระบบประสาทที่สร้างและหลั่งฮอร์โมนประสาท (neurohormones) มีการศึกษาเกี่ยวกับระบบประสาท สารสื่อประสาท ตลอดจนฮอร์โมนประสาทที่ควบคุมการพัฒนาของต่อมสืบพันธุ์ การแยกเพศ ตลอดจนการเติบโตในหอยเป๋าฮื้อน้อยมาก องค์ความรู้ส่วนใหญ่ได้มาจากการศึกษาในหอย gastropods ชั้นสูงกว่าหอยเป๋าฮื้อคือ หอยกลุ่ม pulmonates โดยเฉพาะในหอยทาก *Lymnea stagnalis, Helix aspersa* และ *Achatina fulica* และในหอย gastropod กลุ่ม opisthobranchs เช่น *Aplysia spp*. โครงสร้างและการทำงานของระบบประสาทและฮอร์โมนประสาทในหอยเป๋าฮื้อน่าจะมีส่วนคล้ายคลึงกับในหอย gastropod สองประเภทที่กล่าวแล้วและน่าจะมีส่วนที่แตกต่างเป็นลักษณะเฉพาะด้วย ดังนั้นการวิจัยเพื่อสร้างองค์ความรู้เกี่ยวกับระบบประสาทของหอยว่ามีลักษณะเป็นอย่างไรมีฮอร์โมนประสาท(neurohormones) อะไรบ้างที่ควบคุมกระบวนการสร้างเซลล์สืบพันธุ์ (gametogenesis) การปล่อยเซลล์สืบพันธุ์ (spawning) การลงเกาะ (settlement) และเมตามอร์โฟซิส (metamorphosis) การจำแนกเพศ (sexual differentration) และการเจริญเติบโต (growth) จะช่วยทำให้เราเข้าใจกลไกการควบคุมกระบวนการสืบพันธุ์และการเจริญเติบโตของหอย แล้วสามารถนำความรู้เหล่านี้มาช่วยปรับปรุงแก้ไขจุดที่เป็น “คอขวด” ของการผลิตลูกหอยและหอยวัยอ่อนได้

ระบบประสาทและฮอร์โมนประสาทที่ควบคุมกระบวนการสืบพันธุ์ในหอย pulmonates และหอย opisthobranchs

ดังที่ได้กล่าวมาแล้วว่าองค์ความรู้ส่วนใหญ่ได้มาจากการศึกษาในหอยพวก pulmonates และ opisthobranchs เนื่องจากหอยพวก pulmonates มีระบบประสาทที่พัฒนามากที่สุดในกลุ่ม gastropods ด้วยกัน กล่าวคือเซลล์ประสาทและระบบประสาทมีการรวมศูนย์เป็นปมประสาท (ganglia) ขนาดใหญ่หลายปม ซึ่งติดต่อกันด้วยเส้นประสาท ทำหน้าที่คล้ายกับระบบประสาทกลางของสัตว์ชั้นสูง ปมประสาทเหล่านี้ มีอยู่เป็นคู่ ๆ ได้แก่ ปมประสาท tentacular, optic, cerebral, buccal, pleural, parietal และ pedal นอกจากนี้ยังมีปมประสาทเดี่ยวได้แก่ ปมประสาท abdominal หรือ visceral ganglia ปมประสาท 4 อันหลังมักเชื่อมกันเป็นปมเดี่ยว ปมประสาทเหล่านี้โยงต่อกันโดยเส้นประสาทซึ่งมีใยของเซลล์ประสาทที่มีตัวเซลล์อยู่ในปมประสาท

ในปมประสาทของหอยพวก pulmonate มีเซลล์ประสาท (neuron) ที่ปรับสภาพไปเป็น neurosecretory cells (NSC) ซึ่งทำหน้าที่สร้างและหลั่งฮอร์โมนประสาท (neurohormone) ที่ทำหน้าที่ควบคุมการเจริญเติบโตและกระบวนการสืบพันธุ์ต่าง ๆ NSC

เหล่านี้มักอยู่รวมกันเป็นกลุ่ม ๆ ในปมประสาท cerebral, pleural, parietal และ visceral (abdominal) ในปมประสาท cerebral มี NSC สองกลุ่มที่เกี่ยวข้องกับการสร้างฮอร์โมนประสาทที่กระตุ้นระบบสืบพันธุ์เพศเมีย คือ dorsal bodies (DB) และ caudo-dorsal cells (CDC) ในหอย *Lymnaea stagnalis* ซึ่งเป็นหอยทากน้ำ (basommatophoran pulmonate) DB แบ่งเป็น 2 กลุ่ม คือ lateral (LDB) และ medial (MDB) dorsal bodies นอกจากนั้นยังพบกลุ่ม NSC ซึ่งทำหน้าที่เช่นเดียวกันในเยื่อเกี่ยวพันที่หุ้มปมประสาท cerebral ของหอยทาก *Helix aspersa* ซึ่งเป็นหอยทากบก (stylommatophoran pulmonate) ที่เรียกว่า juxta-ganglionar cells DB ทำหน้าที่ผลิต dorsal body hormone (DBH) ซึ่งเป็น neuropeptide ที่มีน้ำหนักโมเลกุลประมาณ 4,000-7,000 dalton DBH ควบคุมกระบวนการสร้างเซลล์ไข่ (oogenesis) และยังกระตุ้นการพัฒนาของท่อนำไข่และต่อมต่าง ๆ ที่เกี่ยวข้องกับระบบสืบพันธุ์ และการสร้างสาร galactogen ในท่อสืบพันธุ์เพศเมีย อีกนัยหนึ่งฮอร์โมนชนิดนี้ทำหน้าที่คล้ายกับ follicle-stimulating hormone (FSH) ในสัตว์มีกระดูกสันหลังชั้นสูง การสร้างและหลั่ง DBH ถูกยับยั้งโดย growth-promoting factor (insulin-liked hormone-ILH) ซึ่งสร้างและหลั่งจากกลุ่ม NSC ที่มีชื่อว่า light green cells (LGC) ซึ่งเป็นกลุ่มเซลล์ส่วนใหญ่ในปมประสาท cerebral การสร้าง DBH ถูกกระตุ้นอีกทางหนึ่งโดยกลุ่ม NSC ใน lateral lobe (LL) ของปมประสาท cerebral ในเพศผู้ NSC ที่อยู่ใน LL สร้าง gonadal-stimulating hormone (GSH) ทำหน้าที่เสริมกับ optic ganglion hormone (OGH) ในการกระตุ้นการสร้างเซลล์อสุจิและระบบสืบพันธุ์เพศผู้ ฮอร์โมนประสาทจาก LL อาจจะยับยั้ง LGC ซึ่งมีผลทำให้ลดการหลั่ง ILH ลง ทั้งนี้เพื่อให้มีการควบคุมแบบย้อนกลับ (negative feedback loop) ระหว่างกลุ่ม NSC เหล่านี้ ทำให้เกิดการสลับช่วงและรักษาสมดุลย์ระหว่างกระบวนการเจริญเติบโต (somatic growth)และกระบวนการสืบพันธุ์ (reproductive growth) นอกจากนี้เซลล์ในกลุ่ม NSC ของ DB อาจเกี่ยวข้องกับการผลิต ecdysteroid ซึ่งทำหน้าที่ควบคุมการเจริญเติบโตและกระบวนการสืบพันธุ์แต่ยังมีหลักฐานสนับสนุนไม่ชัดเจนนัก

กลุ่ม caudo-dorsal cells (CDC) เป็นกลุ่ม NSC ที่อยู่ค่อนไปทางด้านหลังของปมประสาท cerebral NSC กลุ่มนี้เกี่ยวข้องกับการสร้าง gonadotropin อีกชนิดหนึ่งที่เรียกว่า caudo-dorsal cell hormone (CDCH) เชื่อว่า NSC กลุ่มนี้ส่งเส้นประสาทไปที่ขอบของ cerebral commissure และปล่อยฮอร์โมน CDCH เข้าสู่ neurohemal organ ที่อยู่ในบริเวณนั้น CDCHทำหน้าที่กระตุ้นการปล่อยไข่ (spawning) และมันอาจจะกระตุ้นระยะสุดท้ายของกระบวนการพัฒนาไข่ (oogenesis) เพื่อให้เซลล์ไข่พัฒนาเต็มที่เช่นการเกิด germinal vesicle breakdown (GVDB) ซึ่งทำให้ไข่สามารถปฏิสนธิกับเซลล์อสุจิได้ ฮอร์โมนนี้จึงทำหน้าที่คล้าย luteinizing hormone (LH) ในสัตว์ชั้นสูง

ในหอยพวก opisthobranch (*Aplysia californica*) พบว่ามีฮอร์โมนคล้ายกลับ CDCH อยู่ในปม ประสาท visceral หรือ abdominal NSC เหล่านี้สร้างฮอร์โมนที่เรียกว่า egg-laying hormone (ELH) NSC เหล่านี้มีเซลล์ขนาดใหญ่เรียกว่า “bag cells” เชื่อกันว่า bag cells บางตัวยังส่งเส้นประสาทตรงไปที่ต่อมสืบพันธุ์ โดยอาจมีการหลั่งฮอร์โมนชนิดนี้ที่ปลายประสาทที่แทรกอยู่ในเยื่อเกี่ยวพันของต่อมสืบพันธุ์ ELH มีปริมาณและลำดับกรดอะมิโนคล้ายกับ CDCH ยิ่งไปกว่านั้นมีการรายงานว่าการสร้าง ELH ถูกควบคุมโดยยีนชุดเดียวกับที่ควบคุมการสร้าง CDCH

นอกจากนี้ยังมีฮอร์โมนที่ไม่ได้อยู่ในกลุ่ม peptide ที่อาจมีบทบาทในการควบคุมระบบสืบพันธุ์ของหอย pulmonates ซึ่งได้แก่ฮอร์โมนเพศในกลุ่ม sex steroids โดยเฉพาะ 5α-dihydrotestosterone และ 17β -estradiol และฮอร์โมนในกลุ่ม icosanoid เช่น prostaglandin (PG) โดยเฉพาะ PG-E และ PG-F ฮอร์โมนเพศอาจทำหน้าที่กระตุ้นการพัฒนาเซลล์สืบพันธุ์และลักษณะเพศร่วมกับ DBH และ CDCH เช่นเดียวกับในสัตว์ชั้นสูงแต่ยังไม่มีหลักฐานที่ชี้บ่งแน่ชัดจึงน่าจะมีการวิจัยในประเด็นนี้ต่อไป

ความสัมพันธ์ระหว่างสารสื่อประสาท (neurotransmitters) สารขยายสัญญาณประสาท (neuromodulators) และฮอร์โมนประสาท (neurohormones)

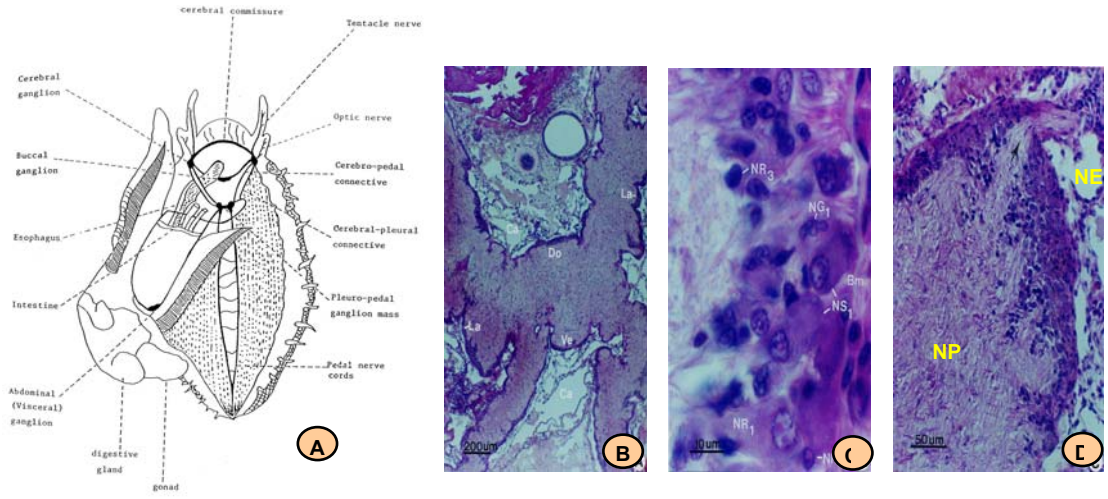
นอกจากฮอร์โมนประสาทและฮอร์โมนเพศที่กล่าวมาแล้ว ยังมีกลุ่มฮอร์โมนประสาทที่เป็นโมเลกุลขนาดเล็กอีกกลุ่มหนึ่งคือสารสื่อประสาท (neurotransmitters) ที่เกี่ยวข้องกับการควบคุมกระบวนการสืบพันธุ์ ได้แก่ serotonin (5-hydroxytryptamine, 5HT), dopamine (DA) octopamine (OA) gamma aminobutyric acid (GABA) และอีกกลุ่มหนึ่งคือสาร amides ขนาดเล็ก เช่น FMRF APGW และ GnRH ฯลฯ เป็นต้น พบว่ามี 5HT กระจายอยู่ทั่วไปในเซลล์ประสาทส่วนกลางของปมประสาทและเยื่อเกี่ยวพันรอบปมประสาท และในเยื่อเกี่ยวพันที่หุ้มต่อมสืบพันธุ์ของหอยพวก pulmonate และหอยสองฝา (bivalves) ได้มีการทดลองในหอยสองฝาพบว่าการฉีด 5HT สามารถกระตุ้นการหลั่งเซลล์สืบพันธุ์ได้ ซึ่งก็ยังไม่สามารถอธิบายให้กระจ่างได้ว่า 5HT ทำให้เกิดการหลั่งเซลล์สืบพันธุ์ได้อย่างไร คาดกันว่า 5HT อาจทำหน้าที่เป็นสารสื่อประสาทที่กระตุ้นให้เกิดการหลั่งฮอร์โมนตัวอื่นรวมทั้ง CDCH หรือ ELH และ PG ซึ่งอาจเป็น neurohormones ที่ทำหน้าที่เป็นตัวกระตุ้นสุดท้ายซึ่งทำให้เกิดการตกไข่และพฤติกรรมที่เกี่ยวข้อง ยิ่งไปกว่านั้น 5HT น่าจะทำหน้าที่เป็นสารสื่อประสาทขั้นต้น (first messenger) ในเซลล์ประสาทรับสัมผัสที่อยู่ในระบบประสาทส่วนกลางด้านหน้า ซึ่งทำหน้าที่รับสัญญาณจากสภาพแวดล้อมภายนอก เช่น สภาวะของ

อาหารที่เหมาะสม ช่วงความยาวของแสงสว่าง และอุณหภูมิของน้ำทะเล ฯลฯ สภาวะแวดล้อมเหล่านี้มีอิทธิพลต่อการพัฒนาและการทำงานของระบบสืบพันธุ์ ในทางตรงข้ามสาร DA และพวก amides ขนาดเล็กที่อาจเป็นทั้งสารสื่อประสาทหรือสารปรับสัญญาณประสาท เช่น FMRF และ APGW ซึ่งกระจายอยู่ทั่วไปในระบบประสาทมีการออกฤทธิ์ตรงกันข้ามกับ 5HT และสามารถยับยั้งการหลั่งฮอร์โมนจาก DB และ CDC

ส่วนในเพศผู้ พบว่า optic gland ซึ่งอยู่ที่ฐานของ optic tentacle เป็นกลุ่ม NSC ที่ขับเคลื่อนให้เกิดการจำแนกเป็นเพศผู้ optic gland ประกอบด้วย NSC ที่เรียก collar cell ซึ่งสร้างและหลั่ง optic gland hormone (OGH) ฮอร์โมนตัวนี้ทำหน้าที่กระตุ้นการสร้างเซลล์สืบพันธุ์เพศผู้ใน ovotestis โดยทำงานร่วมกับ GSH ที่ผลิตจาก LL ส่วนฮอร์โมนที่จำแนกเพศเมียอาจประกอบด้วย DBH และ CDCH ซึ่งกระตุ้นการสร้างเซลล์สืบพันธุ์เพศเมียใน ovotestis และลักษณะเพศเมีย ในอนาคตคงต้องมีการวิจัยว่ามีฮอร์โมนเพศกลุ่มสาร steroids ได้แก่ testosterone และ estradiol กับ progesterone มีอยู่ในต่อมสืบพันธุ์ของหอยหรือไม่ และถ้ามีจะเกี่ยวข้องกับการจำแนกเพศอย่างไร

ระบบประสาทและฮอร์โมนประสาทที่ควบคุมกระบวนการสืบพันธุ์ในหอยเป๋าฮื้อ

ระบบประสาทของหอยเป๋าฮื้อมีการรวมศูนย์และการพัฒนาส่วนหน้าของระบบประสาท (cephalization) น้อยกว่าในพวก pulmonate ดังได้กล่าวมาแล้ว Crofts (1922) เป็นคนแรกที่ได้ศึกษาและอธิบายมหกายวิภาคของระบบประสาทในหอยเป๋าฮื้อเขตอบอุ่นคือ *H. tuberculata* หอยเป๋าฮื้อ *H.asinina* ก็มีระบบประสาทที่มีลักษณะโครงสร้างคล้ายกันกับของ *H.tuberculata* กล่าวคือมีระบบประสาทกลาง ซึ่งประกอบด้วยปมประสาทที่มีอยู่เป็นคู่ได้แก่ ปมประสาท buccal และปมประสาท cerebral ซึ่งโยงต่อกับปมประสาท pleuropedal โดย nerve connectives จากปมประสาท pleuropedal มีคู่ของ pedal nerve cord (PNC) ทอดไปกลางลำตัวสู่ทางด้านหลังตลอดความยาวของตัว มีเส้นประสาทงอกออกจาก PNC เป็นระยะ ๆ เพื่อไปเลี้ยงกล้ามเนื้อเท้า (pedal muscle) นอกจากนี้ยังมีเส้นประสาทจากปมประสาทpleuropedalซึ่งมีลักษณะเป็นบ่วงคล้ายเลข 8 ทอดไปทางด้านหลังเพื่อเลี้ยงอวัยวะภายในรวมทั้งเส้นประสาทที่ไปเลี้ยงอวัยวะและต่อมสืบพันธุ์โดยตรง ที่ปลายสุดของบ่วงเส้นประสาทดังกล่าวมีปมประสาทขนาดเล็กที่เรียกว่าปมประสาท visceral หรือ abdominal (รูปที่ 3A)



รูปที่ 3 (A) ภาพวาดมหกายวิภาคระบบประสาทของหอยเป๋าฮื้อ H.asinina (B) ภาพปมประสาท pleuropedal (C) ภาพชั้น cortex ในปมประสาท pleuropedal ประกอบด้วยเซลล์ประสาท (neurons-NR) และเซลล์หลั่งฮอร์โมนประสาท (neurosecretory cells-NS) (D) ส่วนกลางของปมประสาท (neuropil)-NP ประกอบด้วยใยประสาทที่รวมตัวออกไปเป็น

คณะผู้วิจัยได้ศึกษาทั้งมหกายวิภาคและจุลกายวิภาคของระบบประสาทในหอยเป๋าฮื้อ *H. asinina* พบว่าปมประสาทแต่ละปมมีลักษณะทางจุลกายวิภาคคล้ายกัน กล่าวคือประกอบด้วยเปลือกนอก (cortex) (รูปที่ 3B, C) ที่มีตัวเซลล์ประสาท (neurons) 4 ชนิด เซลล์พี่เลี้ยง (neuroglia) 2 ชนิด และ NSC 3 ชนิดซึ่งกระจายอยู่ทั่วๆ ไปโดยไม่มีการรวมตัวเป็นกลุ่มชัดเจนเช่นเดียวกับ NSC ในปมประสาทของหอยพวก pulmonates ส่วนชั้นในของปมประสาท (medulla) มีกิ่งของเซลล์ประสาทและเซลล์พี่เลี้ยงสานกันอยู่ซึ่งเรียกว่า neuropil (รูปที่ 3D) ปมประสาท cerebral มีขนาดเล็กกว่าของหอย pulmonate และอาจทำหน้าที่หลักในการรับรู้สภาพแวดล้อมภายนอกโดยผ่านเส้นประสาทตา (optic tentacle) และหนวด (cephatic tentacle) และควบคุมการเจริญเติบโต มีการทดลองฉีดสารสกัดจากปมประสาท cerebral ให้แก่หอยเป๋าฮื้อพบว่าหอยมีน้ำหนักเพิ่มขึ้นและมีการสะสมน้ำในตัวมากขึ้น นอกจากนี้มีการทดลองฉีดสารสกัดจากปมประสาท pleuropedal รวมกับสารสกัดจากปมประสาท visceral พบว่า

สามารถกระตุ้นต่อมสืบพันธุ์และทำให้เกิดการตกไข่ได้ แสดงว่าปมประสาททั้งสองเมื่อนำมาสกัดและฉีดรวมกันจะเพิ่มประสิทธิภาพในการกระตุ้นการตกไข่ซึ่งเป็นหลักฐานที่ส่อว่ามีฮอร์โมนกระตุ้นระบบสืบพันธุ์ (gonadotropin) อยู่ในปมประสาททั้งสอง อย่างไรก็ตามการผลิต gonadotropin อาจจะไม่มีอยู่เฉพาะที่ปมประสาท pleuropedal และ visceral เท่านั้น เพราะเมื่อตัดปมประสาท cerebral ออกก็สามารถยับยั้งการพัฒนาของต่อมสืบพันธุ์และการจำแนกเพศ (sexual differentiation) ได้ที่ระดับหนึ่งด้วย นอกจากนี้ยังมีการรายงานว่ามี NSC อยู่เดี่ยว ๆ หรือเป็นกลุ่มตามขอบของปมประสาท cerebral ซึ่งอาจหลั่งฮอร์โมน gonadotropin กลุ่ม NSC ดังกล่าวนี้มีโครงสร้างเหมือนกับเซลล์ใน DB ของหอย pulmonate โดยสรุปแล้วจะเห็นได้ว่ามีการศึกษาค่อนข้างน้อยมากเกี่ยวกับโครงสร้างของระบบประสาทและ ฮอร์โมนประสาทที่เกี่ยวข้องในการควบคุมกระบวนการสืบพันธุ์ และการเจริญเติบโตของหอยเป๋าฮื้อ เมื่อเปรียบเทียบกับองค์ความรู้ในเรื่องเดียวกันที่ทราบแล้วในหอยพวกpulmonate และ opisthobranch ดังนั้นจึงมีความจำเป็นที่จะต้องศึกษาโครงสร้างและหน้าที่ของระบบประสาทและฮอร์โมนประสาทของหอยเป๋าฮื้อในขั้นพื้นฐานต่อไป

หัวข้อที่ 4 การศึกษาฮอร์โมนกระตุ้นการตกไข่ (egg-laying hormone-ELH) และยีนที่ควบคุม

การศึกษาระดับโมเลกุลและยีนของฮอร์โมนที่เกี่ยวข้องกับการสืบพันธุ์ของหอยส่วนใหญ่มุ่งไปที่ฮอร์โมนซึ่งควบคุมการตกไข่ คือ egg-laying hormone (ELH) ของหอยพวก Aplysia และ caudodorsal cell hormone (CDCH) ของหอยพวก Lymnaea ฮอร์โมนทั้งสองชนิดนี้เป็น neuropeptides มีรายงานว่าการตกไข่และพฤติกรรมที่เกี่ยวข้องถูกควบคุมโดยฮอร์โมนเหล่านี้ร่วมกับ neuropeptide ที่มีโมเลกุลขนาดเล็กหลายตัว ซึ่งเกิดจากการตัดส่วน N-terminal ของ preprohormone ที่เป็นตัวตั้งต้น (precursors) ของทั้ง ELH และ CDCH

การศึกษาใน *A. californica* พบว่า ELH preprohormone มีลักษณะเป็นสายโปรตีนประกอบด้วยกรดอะมิโน 271 ตัว ที่มี α-BCP, β-BC, δ-BCP, γ-BCP และ acidic peptide อยู่ทางด้าน amino end และตัว ELH อยู่ทางด้าน carboxy end ของ preprohormone ซึ่งถูกผลิตและหลั่งจาก bag cell (BC) ที่อยู่ในปมประสาท visceral นอกจากนั้นแล้วยังพบแบบ (isotype) อื่น ๆ ของ preprohormone ในตระกูล ELH ใน atrial gland ที่กระจายอยู่ตามท่อสืบพันธุ์ของเพศเมียซึ่งประกอบด้วยกรดอะมิโน 173 ตัว ฮอร์โมนดังกล่าวถูกหลั่งเข้าสู่ท่อนำไข่ของหอยและยังแตกตัวออกเป็น ELH กับ peptide A และ pepitde B ฮอร์โมนกลุ่มนี้จึงมีโครงสร้างและทำหน้าที่โดยรวมเหมือนกับ ELH preprohormone ของ bag cells

Caudodorsal cell (CDC) ในปมประสาท cerebral ของ *L. stagnalis* ก็สร้าง preprohormone อย่างน้อยสองชนิด คือ prepro-CDCH I, prepro-CDCH II ต่อมาพบว่ามี isotype เพิ่มอีกคือ prepro-CDCH III นอกจากในกลุ่มเซลล์ CDC แล้วยังพบการแสดงออกของ CDCH gene family ภายในเซลล์ประสาทที่อยู่ในระบบประสาทส่วนกลางและส่วนนอก CDCH I preprohormone ประกอบด้วยกรดอะมิโน 259 ตัว หลังจากถูกตัดออกเป็นส่วน ๆ แล้วมันจะให้ peptide สั้น ๆ หลายตัวเช่น α-CDCP, β-CDCP, δ-CDCP, calfluxin, ε-peptide, γ-peptide และเปปไทด์ที่เป็น CDCH I ประกอบด้วยกรดอะมิโน 36 ตัว ซึ่งควบคุมการตกไข่โดยตรง ส่วน CDCH II ประกอบด้วยกรดอะมิโน 44 ตัว ซึ่งมีรูปแบบการเรียงตัวเหมือนกัน CDCH I แต่ยังไม่มีใครทราบหน้าที่ของ CDCH II

ถึงแม้ว่า ELH preprohormone และ CDCH preprohormone มีความเหมือนกันน้อย (ประมาณ 28.2%) แต่ก็มีบริเวณเฉพาะที่ได้ถูกอนุรักษ์ไว้ถึง 51% คือส่วนที่เป็นฮอร์โมน ELH และ CDCH ที่อยู่ด้าน carboxyl terminal ซึ่งออกฤทธิ์เหมือนกัน คือสามารถกระตุ้นการตกไข่ในหอยทั้งสองกลุ่ม ส่วนเปปไทด์อื่นที่มาจาก N-terminal เช่น α-BCT และ α-CDCP ก็มีความเหมือนกัน 69% และมีหน้าที่กระตุ้น (auto excitation) ให้เซลล์ CDC หรือ bag cell ให้หลั่งฮอร์โมน ELH ออกมา

ฮอร์โมนกระตุ้นการตกไข่ในหอยเป๋าฮื้อ

การศึกษาฮอร์โมนประสาทที่ควบคุมการพัฒนาระบบสืบพันธุ์ในหอยพวก prosobranch รวมทั้งหอยเป๋าฮื้อมีน้อยมาก การศึกษาด้านพันธุกรรมระดับโมเลกุลของ ELH ในหอยพวก opisthobranch และ pulmonate แสดงให้เห็นว่า ELH ยีนของหอยทั้งสองพวกมีโครงสร้างและส่วนอนุรักษ์ที่เหมือนกันมาก ดังนั้นจึงคาดว่าหอยเป๋าฮื้อน่าจะมียีนที่เหมือนกันซึ่งทำหน้าที่ควบคุมการตกไข่รวมทั้งพฤติกรรมต่าง ๆ เมื่อไม่นานมานี้พบว่ามีสารคล้าย ELH และ CDCH อยู่ในปมประสาท cerebral ของหอยพวก prosobranch ซึ่งเป็นหลักฐานสนับสนุน การวิวัฒนาการที่มีการอนุรักษ์ของฮอร์โมนชนิดนี้ในหอย gastropods ทั้งหมด ได้มีการศึกษายีนที่กำกับ ELH ในหอยเป๋าฮื้อ *H. rubra* ที่อยู่ในเขตอบอุ่นพบว่ายีนที่กำกับ abalone egg-laying hormone (aELH) มีความเหมือนกับ ELH ของ Aplysia ถึง 56% และมีความเหมือนกับ Lymnaea CDCH ถึง 97% คณะวิจัยของเราได้พบว่า aELH ใน *H.asinina* มีความเหมือนกับ aELH ของ *H.rubra* ถึง 99% ซึ่งแสดงว่ามีการอนุรักษ์ของฮอร์โมนชนิดนี้สูงมากแม้ในหอยเป๋าฮื้อต่าง

species กัน นอกจากนั้นเราได้สังเคราะห์โปรตีน aELH แล้วผลิตแอนติบอดีในหนูทดลอง เมื่อนำแอนติบอดีต่อ aELH ไปย้อมหาตำแหน่ง aELH ในเนื้อเยื่อของ *H.asinina* พบว่ามีฮอร์โมนชนิดนี้กระจายอยู่ใน NSC ของปมประสาท cerebral pleuropedal และ visceral โดยมีจำนวน NSC ที่สร้าง aELH มากที่สุดในปมประสาท pleuropedal นอกจากนั้นยังพบ aELH ในรังไข่และอัณฑะของหอย *H.asinina* โดยเฉพาะในเยื่อเกี่ยวพันที่เป็นถุงหุ้ม (capsule) และแผ่น trabeculae โดยพบว่า aELH มีปริมาณสูงใน granular cells ที่กระจายอยู่ในโครงเยื่อเกี่ยวพัน เซลล์ดังกล่าวอาจเป็นแหล่งผลิต aELH ในรังไข่ ซึ่งอาจเป็น isotype ที่แตกต่างจากที่พบในปมประสาทก็ได้ นอกจากนั้นคณะวิจัยของเรายังพบว่ามี ELH-liked peptide อยู่ในปมประสาทโดยเฉพาะใน supraesophageal ganglion หรือสมองของกุ้งกุลาดำและกุ้งก้ามกราม ซึ่งแสดงว่าฮอร์โมนชนิดนี้มีอยู่ในสัตว์ไม่มีกระดูกสันหลังชนิดอื่นและมีการอนุรักษ์ของโมเลกุลอีกด้วย ดังนั้นจึงเป็นไปได้ว่า ELH อาจทำหน้าที่เช่นเดียวกันในสัตว์ไม่มีกระดูกสันหลังที่อยู่ใน phylum ต่าง ๆ

(ดูรายละเอียดในเอกสารหมายเลข 1.3, 1.4 ในภาคผนวก)

Serotonin (5-HT) และฮอร์โมนประสาทอื่น ๆ ที่เกี่ยวข้องกับกระบวนการสืบพันธุ์ในหอยเป๋าฮื้อ

มีรายงานจำนวนมากที่เกี่ยวกับการศึกษาบทบาทของ 5HT ในการควบคุมกระบวนการสืบพันธุ์ของหอยพวก pulmonate และหอยสองฝา แต่ในหอยเป๋าฮื้อมีงานวิจัยทางด้านนี้น้อยมาก เพียงแต่มีรายงานที่พบว่ามี 5HT กระจายอยู่ในเส้นประสาทและเยื่อเกี่ยวพันที่อยู่ระหว่างปมประสาทของหอยพวก prosobranch บางชนิด คณะวิจัยของเราพบว่ามี 5HT กระจายอยู่ในปมประสาท cerebral และ pleuropedal และในเยื่อเกี่ยวพันที่เป็นโครงและถุงหุ้มของต่อมสืบพันธุ์ซึ่งมีเส้นประสาทไปเลี้ยงเป็นจำนวนมาก มีรายงานว่าถ้านำหอยเป๋าฮื้อที่อยู่ในเขตอบอุ่นเช่น *H. discus hannai* แช่ในน้ำทะเลที่มี hydrogen peroxide หรือน้ำทะเลที่ถูกฉายโดยแสง UV พบว่าสามารถกระตุ้นให้หอยตกไข่ได้ การตกไข่ดังกล่าวอาจเป็นผลมาจากการกระตุ้นให้มีการหลั่งเซลล์ไข่อย่างรวดเร็วโดย prostaglandin และ aELH ที่สะสมอยู่ในเนื้อเยื่อรังไข่ที่ปริมาณสูง ฮอร์โมนดังกล่าวอาจไปกระตุ้นการหดตัวของเซลล์กล้ามเนื้อที่อยู่ในเยื่อเกี่ยวพันที่ทำหน้าที่เป็นโครงและเป็นถุงหุ้มของต่อมสืบพันธุ์ ทำให้มีการปล่อยที่ไม่เป็นธรรมชาติของไข่ทั้งที่เจริญเต็มที่และยังเจริญไม่เต็มที่ออกจากรังไข่ คณะวิจัยของเราได้พบว่า 5-HT เป็นโมเลกุลตัวกลางที่สามารถทำให้เกิดการตกไข่ในหอยเป๋าฮื้อได้ดังนั้น 5HT อาจเป็นตัวกระตุ้นระดับต้นในกระบวนการตกไข่ที่ควบคุมการปล่อย aELH และ prostaglandins อีกต่อหนึ่ง นอกจากนั้นแล้ว5HTอาจควบคุมการปรับสภาพ (differentiation) และการเจริญเติบโตในช่วงสุดท้ายของไข่ (oocyte maturation) เนื่องจากพบว่ามี 5HT อยู่ในไซโตปลาสซึมของเซลล์ไข่ขั้นสุดท้ายในปริมาณสูง การศึกษาในหอย opisthobranch และหอยสองฝาชี้บ่งว่า 5HT ก็มีอิทธิพลต่อการพัฒนาขั้นสุดท้ายของไข่ดังกล่าวแล้วเช่นกัน

นอกเหนือจาก aELH, 5HT และ prostaglandin แล้ว ยังมีฮอร์โมนประสาทตัวอื่น ๆ ที่อาจมีบทบาทเกี่ยวข้องกับการปรับสภาพและการพัฒนาของเซลล์สืบพันธุ์ และอวัยวะที่เกี่ยวข้องกับระบบสืบพันธุ์กับการตกไข่ เช่น octopamine, FMRF และ APGW amide คณะวิจัยของเราพบว่า FMRF และ APGW amides สามารถกระตุ้นการหลั่งอสุจิในพ่อพันธุ์ได้ถึง 100% ในขณะที่ amide ดังกล่าวไม่สามารถกระตุ้นการตกไข่ในแม่พันธุ์ได้ ดังนั้นในแง่ของการประยุกต์ใช้เราอาจนำ aELH และ 5HT ไปฉีดกระตุ้นหอยแม่พันธุ์ให้ตกไข่และใช้ APGW ฉีดกระตุ้นพ่อพันธุ์ให้ปล่อยอสุจิในช่วงเวลาที่ตรงกันได้ ซึ่งจะช่วยให้การเก็บเซลล์สืบพันธุ์สะดวกขึ้นและสามารถผลิตตัวอ่อนได้มากขึ้น

(ดูรายละเอียดในเอกสารหมายเลข 1.14, 1.24 ในภาคผนวก)

หัวข้อที่ 5 ฮอร์โมนที่ควบคุมการเจริญเติบโตและการพัฒนาของตัวอ่อน

ในสัตว์มีกระดูกสันหลัง การเจริญเติบโตและเมตาบอลิซึมที่เกี่ยวกับการเจริญเติบโตนั้นถูกควบคุมโดยฮอร์โมนเปปไทด์หลายชนิด ได้แก่ growth hormone กับ prolactin ที่ผลิตจากต่อมใต้สมองและ insulin ที่ผลิตจากตับอ่อน thyroid hormone และ androgen ก็มีส่วนในการกระตุ้นการเจริญเติบโตด้วย ในสัตว์ไม่มีกระดูกสันหลังก็พบว่าฮอร์โมนมีความสัมพันธ์ต่อกระบวนการเจริญเติบโตและกระบวนเมตาบอลิซึมเช่นเดียวกัน อาทิเช่นในสัตว์พวก arthropods และ crustaceans มีฮอร์โมน 2 ชนิด คือ juvenile hormone และ ecdysone ที่ควบคุมการเพิ่มน้ำหนักตัวของสัตว์ ในสัตว์ตระกูลหอยที่มีวิวัฒนาการต่ำสุดเช่น *Crepidula fornicata* พบว่าถ้าตัดปมประสาท cerebral ออกจะทำให้ฮอร์โมนกระตุ้นการเจริญเติบโตลดลงและส่งผลให้อัตราการเติบโตลดลงอย่างรวดเร็ว ฮอร์โมนนี้สามารถถูกกระตุ้นให้มีปริมาณเพิ่มขึ้นมาได้ใหม่ และสัตว์เองก็มีอัตราการเจริญเติบโต

เพิ่มขึ้นเมื่อมีการฝังปมประสาท cerebral กลับเข้าไปในตัวหอยตามเดิม จากผลการทดลองดังกล่าวสามารถสรุปได้ว่าภายในปมประสาท cerebral อาจจะมีเซลล์ประสาทที่สามารถผลิตฮอร์โมนที่ช่วยกระตุ้นการเจริญเติบโตในสัตว์ชนิดนี้ได้ ต่อมาได้มีการศึกษาโดยใช้วิธีการที่คล้ายกันในหอย *Lymnaea stagnalis* ซึ่งเป็นหอยที่มีวิวัฒนาการสูงสุดในพวก gastropod การตัด NSC กลุ่ม light green cell (LGC) ออกทำให้หอยทากเจริญเติบโตช้าลง แต่การเจริญเติบโตกลับสู่สภาวะปกติเมื่อมีการฝังเซลล์กลุ่มนี้กลับเข้าไปที่ตัวหอยตามเดิม จึงสรุปได้ว่าฮอร์โมนจาก LGC น่าจะเป็นฮอร์โมนที่ควบคุมการเจริญเติบโตของร่างกายซึ่งมีคุณสมบัติที่คล้ายกับ growth hormone ของสัตว์ชั้นสูง ได้มีการศึกษาการออกฤทธิ์ของสารในกลุ่มฮอร์โมนที่กระตุ้นการเจริญเติบโตของสัตว์มีกระดูกสันหลัง อาทิเช่น insulin, human insulin growth factor I (h-IGFI), human epidermal growth factor (h-EGF) และ fibroblast growth factor (FGF) ต่อกิจกรรมหรือการเคลื่อนไหวของเซลล์เม็ดเลือดที่นำมาเพาะเลี้ยงจากหอยเป๋าฮื้อ *H. tuberculata,* เซลล์เยื่อหุ้ม (mantle cells) และเซลล์บุผิวระบบย่อยอาหาร (digestive cells) จากหอยสองฝา *Pecten maximus* เมื่อวัดการนำเข้า thymidine และ leucine ที่ติดฉลากด้วยทริเทียม (^{3}H-thymidine, ^{3}H-leucine) ในเซลล์เพื่อติดตามการสังเคราะห์ DNA และโปรตีนตามลำดับ พบว่า insulin ทำให้เกิดการนำเข้าของทั้ง ^{3}H-thymidine และ ^{3}H-leucine ในเซลล์ทุกชนิดดังกล่าวแล้วในอัตราที่สูง ในขณะที่ฮอร์โมนชนิดอื่น ๆ ทำให้เกิดการนำเข้าของทั้ง ^{3}H-thymidine และ ^{3}H-leucine ในอัตราที่ต่ำกว่ามาก ข้อมูลเหล่านี้เป็นหลักฐานที่แสดงว่าฮอร์โมนในกลุ่ม growth hormones โดยเฉพาะ insulin มีประสิทธิภาพในการส่งเสริมการเจริญเติบโตของเซลล์จากหอย ต่อมาได้มีการศึกษาคุณลักษณะของฮอร์โมนในสกุล insulin ในสัตว์ไม่มีกระดูกสันหลังอื่น ๆ อีกหลายชนิด เช่น แมลง หนอนตัวกลม (nematodes) และหอยต่าง ๆ พบว่าฮอร์โมนกลุ่มนี้มีลักษณะคล้ายคลึงกันมากถูกจัดให้อยู่ในกลุ่ม "insulin-related peptides (IRP)" เมื่อศึกษาด้วยกรรมวิธี immunocytochemistry ในสัตว์สายพันธุ์ต่าง ๆ โดยเฉพาะในแมลง และหอย โดยใช้แอนติบอดีที่จำเพาะต่อ insulin ของสัตว์เลี้ยงลูกด้วยนม พบว่ามี IRP อยู่ในเซลล์ NSC ของ pars intercerebralis ของสมองแมลง และพบ IRP ทั้งในระบบประสาทและระบบย่อยอาหารของหอยสองฝาและหอยทาก *L.stagnalis* โดยเฉพาะที่กลุ่มเซลล์ LGC ดังนั้นจึงสรุปได้ว่าในสัตว์พวกหอย IRP เป็นฮอร์โมนหลักที่ควบคุมการเจริญเติบโต ซึ่งฮอร์โมนดังกล่าวส่วนใหญ่น่าจะถูกผลิตขึ้นจากเซลล์ LGC ในปมประสาท cerebral และเซลล์ในระบบย่อยอาหารที่ยังไม่สามารถบ่งชี้ตัวตนได้

จากการศึกษาโครงสร้างหลักระดับโมเลกุลของ insulin และยีนของ preproinsulin รวมถึงลำดับนิวคลีโอไทด์ของ cDNA ในสัตว์มีกระดูกสันหลังหลาย species พบว่า insulin จากระดับปลาไปจนถึงระดับสัตว์เลี้ยงลูกด้วยนม มีโครงสร้างที่มีการอนุรักษ์สูงมาก โครงสร้างของ insulin ประกอบด้วยสาย polypeptide 2 สาย ได้แก่ สาย A และ สาย B เชื่อมต่อกันด้วยพันธะไดซัลไฟด์ โปรตีนเบื้องต้น หรือ preproinsulin มีลักษณะเป็น polypeptide สายเดี่ยวที่ประกอบด้วยส่วนของลำดับกรดอะมิโน สาย A, สาย B, สาย C และสายเปปไทด์ที่เป็นตัวสัญญาณ (signal peptide) ซึ่งจะถูกตัดออกระหว่างกระบวนการขนถ่ายเปปไทด์นี้ผ่านendoplasmic reticulum (ER) และ Golgi complex ซึ่งเมื่อสายเปปไทด์ผ่านออแกนเนลดังกล่าวแล้วโมเลกุลก็จะถูกปรับเป็น proinsulin ซึ่งเป็นเปปไทด์ที่จะถูกปรับเป็น insulin ต่อไป

การศึกษาลักษณะโครงสร้างเต็มของ IRP ในสัตว์ไม่มีกระดูกสันหลังได้มีขึ้นครั้งแรกในตัวไหม ปรากฏว่าเปปไทด์ IRP มีลักษณะโครงสร้างคล้าย insulin ของสัตว์มีกระดูกสันหลังมาก ซึ่งต่อมาได้ถูกตั้งชื่อว่า "Bombyxin" โปรตีนชนิดนี้ผลิตโดยเซลล์ NSC 4 คู่ ที่อยู่ทางด้านหลังของส่วน pars intercerebralis ของสมองในตัวไหม และมีน้ำหนักโมเลกุล 5 kDa การศึกษาโครงสร้างของ IRP ในแมลงหวี่ Drosophila พบว่ามี IRP เปปไทด์อยู่ 7 ชนิด ซึ่งเรียกว่า *Drosophila* insulin like peptides 1-7 (DILP 1-7) สายเปปไทด์เหล่านี้มีโครงสร้างที่มีความคล้ายคลึงกับโปรตีนแม่แบบในกลุ่ม insulin ของสัตว์เลี้ยงลูกด้วยนมมาก

ในสัตว์ตระกูลหอยได้มีการศึกษาลักษณะโครงสร้างของเปปไทด์ IRP เช่นกัน โดยส่วนใหญ่มีการศึกษาในหอยทาก *Lymnaea stagnalis* ซึ่งผลของการศึกษาพบว่ามีเปปไทด์อยู่ 7 ตัว ที่มีลักษณะคล้ายกับ insulin ซึ่งเรียกว่า mollusc insulin-related peptides (MIP I-VII) ซึ่งมีเพียง 5 ตัวเท่านั้นที่มีการศึกษาลงลึกถึงระดับยีน ได้แก่ MIP I-III, V, VII ซึ่งสามารถพบและแยกได้จากเซลล์ประสาท LGC ในปมประสาท cerebral ส่วนเปปไทด์ MIP IV และ VI เป็นโปรตีนที่พบในเซลล์บุผิวของระบบย่อยอาหาร

ดังนั้นเปปไทด์ดังกล่าวอาจเป็น isotypeที่ต่างกัน ทั้งนี้แต่ละแบบอาจมีบทบาทและหน้าที่ในการควบคุมการเจริญเติบโตและกระบวนการเมตาบอลิซึมในเนื้อเยื่อเฉพาะอย่าง ในหอยเป๋าฮื้อ *H.asinina* คณะวิจัยของเราได้ทำการศึกษาเบื้องต้นและพบว่าสามารถใช้แอนติบอดีต่อ human growth hormone (GH) แสดงการกระจายตัวของฮอร์โมนที่เหมือน GH ใน NSC ของปมประสาท cerebral และ pleuropedal ซึ่งอาจเป็นปมประสาทหลักที่ควบคุมการเจริญเติบโตและการสืบพันธุ์ของหอยกลุ่มนี้ นอกจากนั้นยังพบฮอร์โมนที่เหมือน GH ในเซลล์เยื่อบุผิวลำไส้และเซลล์ของตับ-ตับอ่อน (hepatopancreas) ในขั้นต้นของเซลล์สืบพันธุ์ทั้งเพศผู้ (spermatocytes) และเพศเมีย (oocytes) จากการศึกษษด้วยวิธี immunoblotting พบว่าแถบโปรตีนที่ย้อมติดโดย Anti-GH จากเนื้อเยื่อต่างๆดังกล่าวแล้วอยู่ที่น้ำหนักโมเลกุล 45 และ 110 kDa ซึ่งอาจเป็น isoforms ของ GH ในหอยเป๋าฮื้อ

(ดูรายละเอียดในเอกสารหมายเลข 2.16 ในภาคผนวก)

หัวข้อที่ 6. การลงเกาะ (settlement) และเมตามอร์โฟซิส (metamorphosis) ในหอยเป๋าฮื้อ

หลังจากปฏิสนธิ ไซโกตของหอย *H.asinina* พัฒนาอย่างรวดเร็วจนกลายเป็นตัวอ่อนว่ายน้ำระยะ trochophore ภายใน 1.5-2 ชั่วโมง และระยะ veliger ภายใน 5-24 ชั่วโมง ซึ่งพร้อมจะลงเกาะภายใน 2-3 วัน เมื่อถึงจุดนี้ตัวอ่อนจะมีปฏิกิริยาตอบสนองต่อสัญญาณเคมีที่มาชักนำให้เกิดการลงเกาะ โดยตัวอ่อนจะหยุดว่ายน้ำแล้วลงเกาะบนผิวของพื้นที่ลงเกาะ (substrate) ซึ่งกระบวนการดังกล่าวเรียกว่าการลงเกาะ (settlement) (รูปที่ 4B) ต่อมาตัวอ่อนจะสลัดชิเลียออกไปแล้วค่อยๆ เปลี่ยนสภาพไปเป็นหอยตัวเล็กๆ ซึ่งเรียกว่าการเมตามอร์โฟซิส (metamorphosis) การลงเกาะเป็นพฤติกรรมที่ย้อนกลับได้ ถ้าหากตัวอ่อนพบว่าพื้นที่ที่มันลงเกาะไม่เหมาะสม แต่เมื่อตัวอ่อนลงเกาะแล้วกระบวนเมตามอร์โฟซิสต้องเกิดต่อไปโดยไม่สามารถย้อนกลับได้ เมื่อถึงระยะนี้หอยก็เริ่มเปลี่ยนวงจรชีวิตจากช่วงกินแพลงตอนเป็นอาหาร (planktonic phase) เข้าสู่ช่วงกินสาหร่ายเป็นอาหาร (benthic phase) ช่วงการลงเกาะและการเมตามอร์โฟซิสเป็นระยะ “คอขวด” ของกระบวนการผลิตหอยเป๋าฮื้อ โดยจะเห็นว่าจากระยะไซโกตมีตัวอ่อนเพียง 20% เท่านั้นที่ลงเกาะได้ และจากจำนวนนี้มีไม่เกิน 10% ที่ผ่านกระบวนเมตามอร์โฟซิส และในที่สุดมีเพียง 2-5% เท่านั้นที่จะกลายเป็นหอยวัยอ่อนที่พัฒนาต่อไปได้ (รูปที่ 1D) ดังนั้นการเข้าใจกลไกควบคุมกระบวนการลงเกาะและเมตามอร์โฟซิส ซึ่งเป็นกระบวนการที่ควบคุมด้วยสารสื่อประสาทและฮอร์โมน น่าจะนำไปประยุกต์ใช้เพื่อให้สามารถผลิตตัวอ่อนและลูกหอยให้มีอัตรารอดเพิ่มขึ้น

กลไกของการลงเกาะและการเมตามอร์โฟซิส

ในสภาพธรรมชาติปัจจัยหลักที่ชักนำให้เกิดการลงเกาะมีอยู่ 4 ปัจจัยคือ (1) สาหร่ายที่เคลือบอยู่บนพื้นที่ลงเกาะซึ่งอาจเป็นก้อนหินหรือปะการังที่ตายแล้วซึ่งเรียกว่าสาหร่ายคลุมปะการัง (coralline algae) (2) สารเมือก (mucus) ที่ขับออกจากพ่อ-แม่พันธุ์ขณะเคลื่อนไปบนพื้นที่ลงเกาะ (3) จุลินทรีย์ที่ปะปนอยู่กับสาหร่ายคลุมปะการัง โดยเฉพาะแผ่นสาหร่ายไดอะตอม (diatom) ที่เคลือบอยู่บนพื้นที่ลงเกาะ (4) สารเคมีที่ปล่อยออกมาจากกระบวนการเมตาบอลิซึม (metabolism) ของสาหร่ายและจุลินทรีย์ที่อาศัยอยู่ปะปนกันบนพื้นที่ลงเกาะ นอกจากปัจจัยภายนอกที่เป็นตัวชักนำแล้ว ปัจจัยภายในตัวอ่อนของหอยเองก็มีส่วนผลักดันให้ตัวอ่อนลงเกาะได้ เนื่องจากพบว่าอัตราการลงเกาะมีความสัมพันธ์โดยตรงกับอายุของตัวอ่อน veliger ทั้งนี้เป็นเพราะเมื่อตัวอ่อนมีอายุมากขึ้นสารไข่ที่สะสมไว้ในตัวอ่อนลดน้อยลงจึงเป็นปัจจัยที่ผลักดันให้ตัวอ่อนจำเป็นต้องลงเกาะ ดังนั้นอาจสรุปได้ว่าตัวอ่อนมีโปรแกรมทางพันธุกรรมที่บังคับให้มันลงเกาะอยู่แล้ว โดยสภาพแวดล้อมที่เหมาะสมดังกล่าวข้างต้นเป็นตัวชักนำให้มันลงเกาะเร็วขึ้น

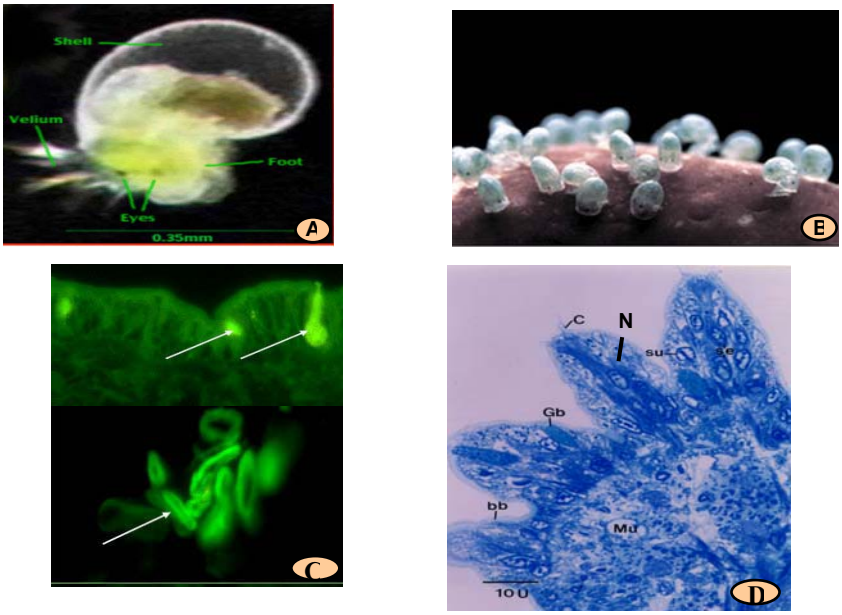
GABA เป็นสารชักนำการลงเกาะและเมตามอร์โฟซิส

GABA ซึ่งเป็นสารสื่อประสาทชนิดหนึ่งที่สามารถกระตุ้นให้ตัวอ่อน veliger (รูปที่ 4A) ลงเกาะได้ซึ่งเป็นปฏิกริยาจำเพาะ เนื่องจากสารสื่อประสาทชนิดอื่นไม่สามารถเลียนแบบ GABA ได้ GABAจึงเป็นตัวกระตุ้นจำเพาะสำหรับการลงเกาะ ส่วนการเมตามอร์โฟซิสอาจถูกกระตุ้นด้วยสัญญานต่อเนื่องที่มาจากแผ่นสาหร่ายที่เคลือบพื้นที่ลงเกาะซึ่งมีจุลินทรีย์ปะปนอยู่

และจากสารเมือกของตัวเต็มวัย สมมติฐานที่ได้ถูกนำเสนอก็คือ GABAเป็นสารที่มาจากกรดอะมิโนจึงน่าจะมีโครงสร้างคล้ายกับกรดอะมิโนที่ปล่อยออกมาจากแผ่นสาหร่ายปะการัง ซึ่งสามารถจับกับตัวรับ (chemo-receptor) ที่อยู่บนผิวของตัวอ่อน การจับกันระหว่าง GABAและตัวรับสามารถกระตุ้นสัญญานประสาทที่ควบคุมการว่ายน้ำของตัวอ่อน veliger ทำให้มันหยุดว่ายแล้วลงเกาะและสบัดซิเลียให้หลุดไป พบว่ามีสารสกัดจากสาหร่ายปะการังที่สามารถแข่งขันและขัดขวางการลงเกาะที่ชักนำด้วยสาร GABA ได้คือ gamma aminovaleric acid (5 AVA) ซึ่งถูกปล่อยออกมาจากสาหร่าย Hydrolithon samoense สาร 5 AVA สามารถกระตุ้นการลงเกาะของตัวอ่อนได้เช่นเดียวกับ GABA ที่ความเข้มข้น 1-2 เท่า พบว่ามีสาร 5 AVA อยู่ในสาหร่ายเคลือบปะการังสูงถึง 0.72 มก/ก.ของน้ำหนักแห้ง ถึงแม้ไม่พบ GABA ในสาหร่ายแต่การทดลองของกลุ่มวิจัยของเราพบว่ามี GABA อยู่ในสารเมือกจากหอยตัวเต็มวัยปริมาณสูงถึง 0.68 มก/ก สารเมือกที่น่าจะมี GABA อยู่นี้สามารถชักนำการลงเกาะของตัวอ่อน H.asinina ได้สูงถึง 30 เปอร์เซนต์ เมื่อเทียบกับกลุ่มควบคุมที่ระดับ 10 เปอร์เซ็นต์ นอกจากนั้นเรายังพบว่าการใช้ 5 AVA ที่ความเข้มข้น 1 μM สามารถชักนำการลงเกาะได้สูงถึง 60-70% เมื่อเวลาผ่านไป 72 ชั่วโมง ในขณะที่ GABA ที่ความเข้มข้น 1 μM สามารถชักนำการลงเกาะได้ 50-60% และผงชูรสซึ่งประกอบด้วย monosodium glutamate ก็สามารถชักนำการลงเกาะได้เช่นกันถึงแม้จะมีเปอร์เซนต์ต่ำกว่า (ประมาณ 50%) เมื่อเทียบกับ GABA ที่ความเข้มข้นเท่ากัน

แหล่งที่สร้างสาร GABA ในหอยตัวเต็มวัยน่าจะเป็นเซลล์ผลิตสารเมือก (mucus cells) ที่กระจายอยู่ในเยื่อบุผิวรอบตัวหอย (mantle layer) (รูปที่ 4C) และจากเซลล์บุผิวของหนวด (tentacle) ของหอย นอกจากนั้นยังพบว่ามีปริมาณ GABA สูงมากในเซลล์ประสาทบุผิว (neuroepitheliall cells) (รูปที่ 4D) ของ cephalic และ epipodial tentacles โดยเฉพาะบริเวณที่อยู่ในตุ่มรับสัญญาน (sensory papillae) เซลล์สร้างสารเมือกอาจเป็นแหล่งสร้างและปล่อย GABA เพื่อออกไปกระตุ้นตัวอ่อนและหอยตัวอื่นให้มีปฏิกริยาตอบสนอง ในขณะเดียวกัน GABA จากหอยตัวอื่นหรือจากแหล่งอาหารก็อาจจับกับตัวรับในเซลล์ประสาทบุผิวในตุ่มรับสัญญานเพื่อกระตุ้นให้หอยเคลื่อนเข้าสู่แหล่งอาหารและเข้าไปหากลุ่มหอยตัวอื่นๆ ดังนั้นจึงเป็นไปได้ว่านอกจากสามารถชักนำให้ตัวอ่อนลงเกาะได้แล้ว GABA อาจเป็นหนึ่งในฟีโรโมน (pheromone) ที่ทำหน้าที่ดึงดูดให้หอยเคลื่อนเข้าหาแหล่งอาหารและเข้าสู่สังคมหอยชนิดเดียวกัน เพื่อเกิดการปฏิสัมพันธ์ทางสังคมและการสืบพันธุ์ ซึ่งควรมีการศึกษาในประเด็นนี้ต่อไป

สารในกลุ่ม GABA ดังที่กล่าวสามารถออกฤทธิ์ได้โดยการจับกับตัวรับ (GABA receptor, GABA-R) ในสัตว์มีกระดูกสันหลังมี GABA-R อยู่ 2 ชนิด คือ GABA-R_a และ GABA-R_b ส่วนในสัตว์ประเภท mollusc พบว่า GABA-R แตกต่างจากตัวรับทั้งสองชนิดของสัตว์ชั้นสูงเนื่องจากตัวห้าม (inhibitors) ของ GABA-R ในสัตว์ชั้นสูง เช่น bisculline picrotoxin และ phaclofen ไม่สามารถห้าม GABA ในการออกฤทธิ์ชักนำการลงเกาะของตัวอ่อนทั้งๆ ที่ตัวห้ามทั้งสามตัวนี้สามารถขัดขวางการทำงานของ GABA-R ทั้งสองชนิดในสัตว์ชั้นสูงได้โดยสิ้นเชิง ดังนั้นการวิเคราะห์ชนิดของ GABA-R ของสัตว์พวก mollusc โดยเฉพาะในหอยเป๋าฮื้อ การศึกษาตำแหน่งและการกระจายของ GABA-R ในตัวอ่อนและในหอยตัวเต็มวัยเป็นโจทย์วิจัยที่ควรศึกษาอย่างยิ่ง สมมติฐานที่เราเชื่อว่าเป็นไปได้สูงคือน่าจะมี GABA-R อยู่ที่เซลล์ประสาทบุผิว (neuroepithelial cells) ในตุ่มรับความรู้สึกที่กระจายอยู่บนหนวดและผิวหนังของหอยตัวเต็มวัย และในผิวของตัวอ่อน veligers ซึ่งคณะวิจัยของเรากำลังทำการศึกษาอยู่ คาดว่าการวิจัยในเรื่องดังกล่าวนี้จะทำให้เกิดองค์ความรู้ขึ้นมากที่สามารถนำไปประยุกต์ใช้เพื่อเพิ่มผลผลิตของหอยเป๋าฮื้อทั้งในระดับเศรษฐกิจพอเพียงและระดับเชิงพาณิชย์ต่อไปได้



รูปที่ 4(A) ตัวอ่อนว่ายน้ำระยะ veliger (B) ตัวอ่อน veliger ลงเกาะ (C) สาร GABA ที่ปรากฏในเซลล์ผลิตสารเมือกในชั้น mantle ของตัวเต็มวัย (บน) และที่ปล่อยออกไปกับสารเมือก (ล่าง) (D) ตุ่มรับความรู้สึกที่มีเซลล์ประสาทบุผิว (neuroepithelial cell-NC) แทรกอยู่ ซึ่งเป็นแหล่งที่มี GABA อยู่ด้วย

(ดูรายละเอียดในเอกสารหมายเลข 1.13 และ 1.15 ในภาคผนวก)

หัวข้อที่ 7. การศึกษาบทบาทของฮอร์โมน aELH และ GnRH ที่มีผลต่อการเจริญเติบโต และพัฒนาการของต่อมเพศและเซลล์สืบพันธุ์ในหอยเป๋าฮื้อตัวอ่อน

การกระตุ้นการเจริญเติบโตและการพัฒนาของต่อมสืบพันธุ์และเซลล์สืบพันธุ์ในหอยเป๋าฮื้อตัวอ่อนด้วยฮอร์โมน aELH และ GnRH

การทดลองนี้ใช้หอยเป๋าฮื้ออายุประมาณ 4 เดือน มีความยาวของเปลือกหอยเฉลี่ย 1.18±0.062 เซนติเมตร และน้ำหนัก 0.33±0.08 กรัม โดยแบ่งสัตว์ทดลองออกเป็น 10 กลุ่ม กลุ่มละ 150 ตัว ดังนี้

กลุ่มที่ 1 เป็นกลุ่มควบคุมที่ไม่ฉีดสารละลาย

กลุ่มที่ 2 เป็นกลุ่มควบคุม ฉีดด้วยสารตัวทำละลายที่ไม่มีฮอร์โมน (normal saline solution)

กลุ่มที่ 3 และ 4 เป็นกลุ่มทดลอง ฉีดด้วยสารประสาทฮอร์โมน aELH ที่ ความเข้มข้น 20 และ 200 ng/g body weight (BW) ตามลำดับ

กลุ่มที่ 5 และ 6 เป็นกลุ่มทดลอง ฉีดด้วยสาร buserelin ซึ่งเป็น mammalian GnRH agonist ที่ ความเข้มข้น 20 และ 200 ng/g BW ตามลำดับ

กลุ่มที่ 7 และ 8 เป็นกลุ่มทดลอง ฉีดด้วยสาร octopus GnRH ที่ ความเข้มข้น 20 และ 200 ng/g BW ตามลำดับ

กลุ่มที่ 9 และ 10 เป็นกลุ่มทดลอง ฉีดด้วยสาร tunicate-I GnRH ที่ ความเข้มข้น 20 และ 200 ng/g BW ตามลำดับ

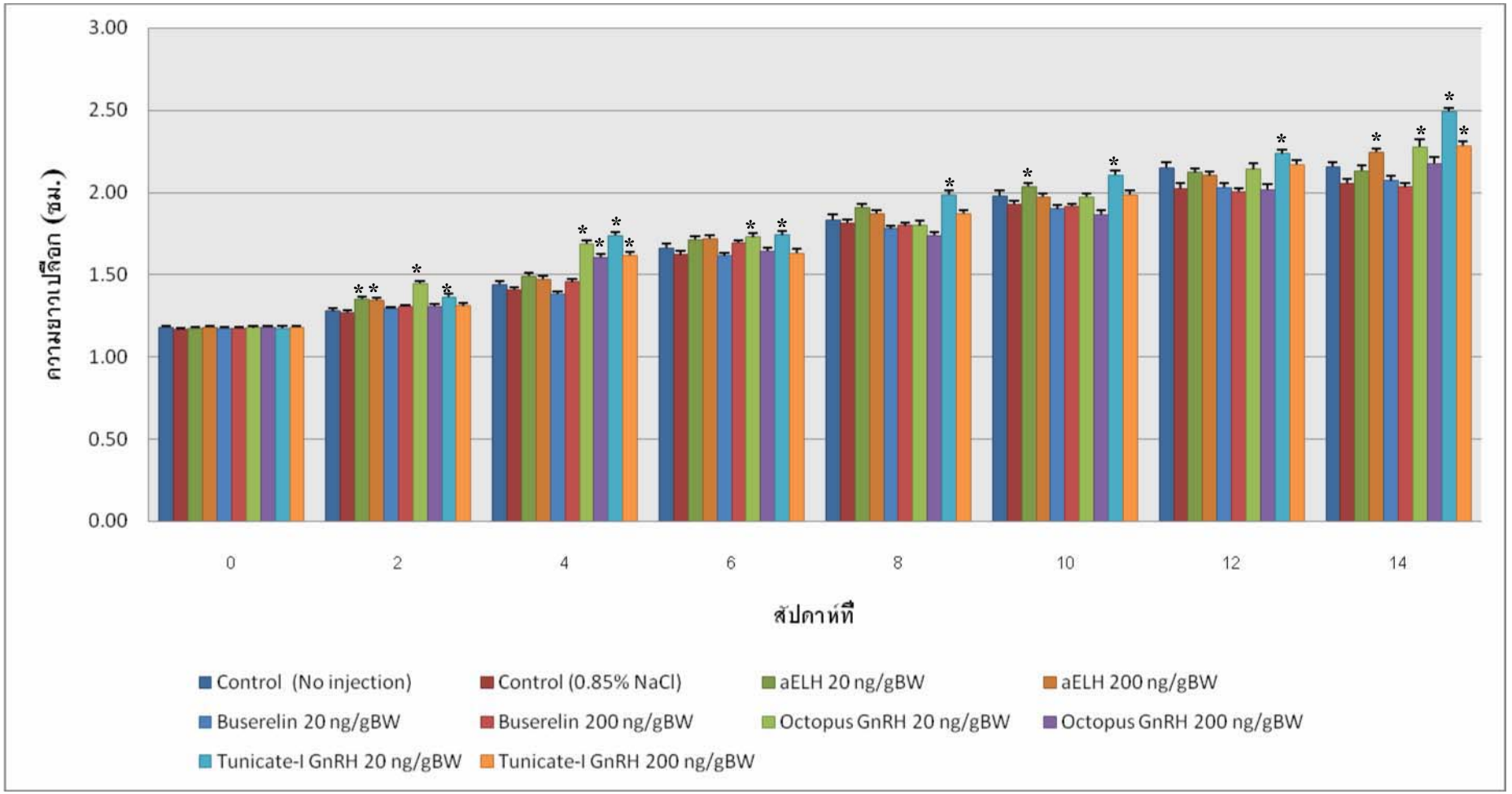
โดยที่สัตว์ทดลองจะถูกฉีดกระตุ้นทุก 7 วัน เป็นจำนวน 14 ครั้ง โดยฉีดเข้าไปตรงบริเวณกล้ามเนื้อเท้าของสัตว์ทดลอง การวัดผลการทดลองใช้ข้อมูล 2 ส่วน คือ 1. การวัดผลการกระตุ้นการเจริญเติบโต ซึ่งทำโดย การวัดความยาวของเปลือกหอย และการชั่งน้ำหนักตัวหอยจำนวน 50 ตัวทุก 2 สัปดาห์ ซึ่งค่าที่ได้จากการวัด จะถูกนำมาหาค่าทางสถิติและประเมินการเจริญเติบโตเทียบกับกลุ่มควบคุม 2. การวัดผลการกระตุ้นการพัฒนาของต่อมสืบพันธุ์ (รังไข่และอัณฑะ) ซึ่งทำโดยการเก็บตัวอย่างชิ้นเนื้อของตัวอ่อนหอยจำนวน 10 ตัวในทุก 2 สัปดาห์ จากนั้นนำมาศึกษาลักษณะทางจุลกายวิภาคของอัณฑะและรังไข่ และดูการพัฒนาของเซลล์สืบพันธุ์ ด้วยกล้องจุลทรรศน์ธรรมดา

ผลการทดลอง

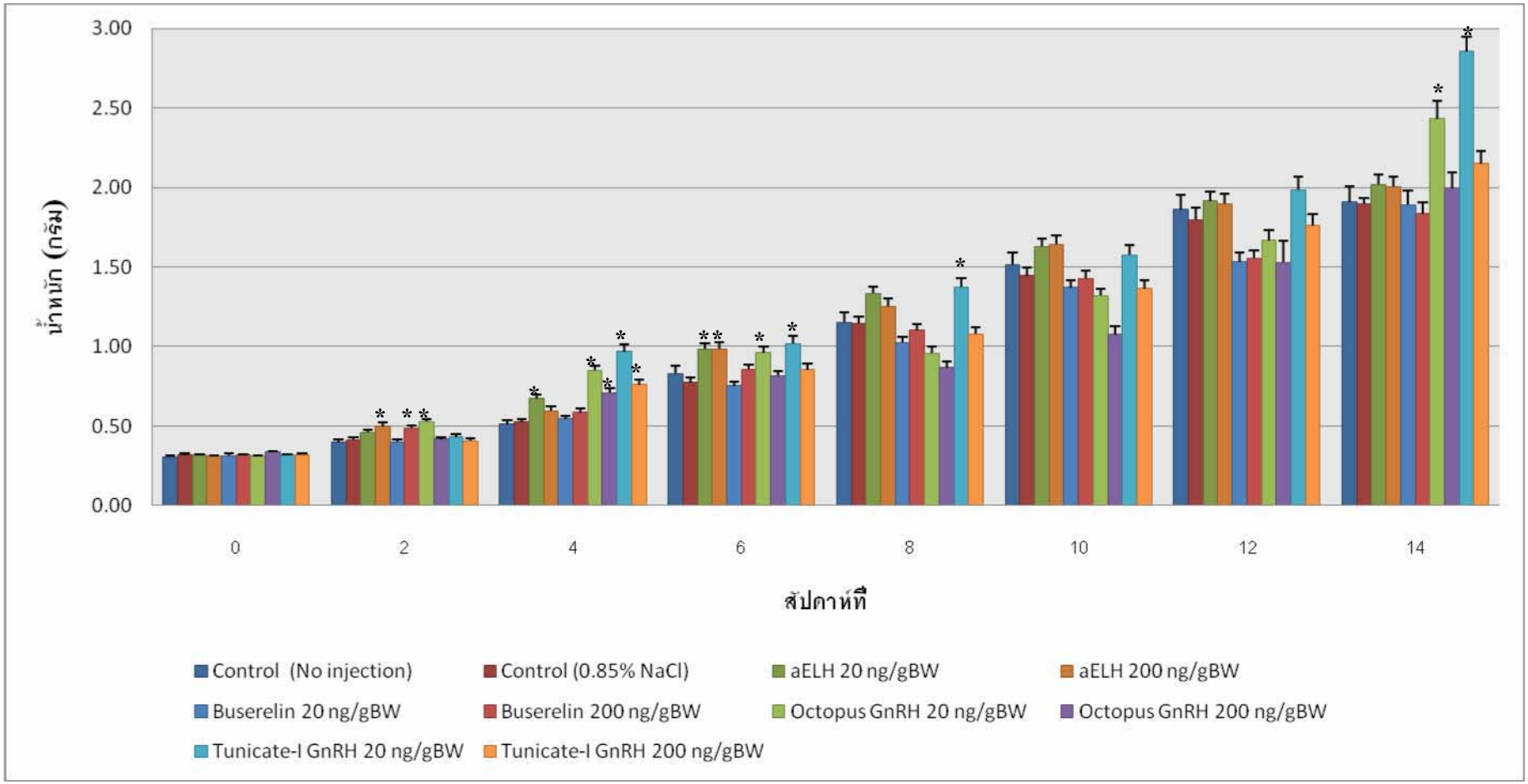
จากแผนภูมิแสดงผลการวัดความยาวเปลือกและชั่งน้ำหนักของหอยเป๋าฮื้อที่ถูกกระตุ้นด้วยสารชนิดต่างๆเป็นเวลา 14 สัปดาห์ (รูปที่ 5 และ 6) พบว่า กลุ่มทดลองที่ถูกฉีดกระตุ้นด้วยสาร aELH ในแต่ละสัปดาห์ ส่วนใหญ่มีการเจริญเติบโตไม่ต่างจากกลุ่มควบคุม ทั้งความยาวเปลือกและน้ำหนักตัวหอย ส่วนกลุ่มทดลองที่ฉีดด้วยสาร buserelin และ octopus GnRH ปริมาณ 20 และ 200 ng/g BW ในแต่ละสัปดาห์พบว่ามีการเจริญของความยาวเปลือกไม่แตกต่างกันมากนักเมื่อเปรียบเทียบกับกลุ่มควบคุม แต่มีผลทำให้น้ำหนักตัวหอยลดลงหลังจากถูกกระตุ้นไป 6 สัปดาห์ ซึ่งต่างจากกลุ่มทดลองที่ฉีดด้วย tunicate-I GnRH ปริมาณ 20 ng/g BW ในแต่ละสัปดาห์พบว่ามีผลทำให้เกิดการเจริญของความยาวเปลือกและน้ำหนักตัวเพิ่มมากขึ้นเมื่อเทียบกับกลุ่มควบคุม ส่วนในกลุ่มการทดลองที่ฉีดด้วย tunicate-I GnRH ที่ระดับ 200 ng/g BW พบว่ามีการเจริญของความยาวเปลือกไม่แตกต่างกันเมื่อเปรียบเทียบกับกลุ่มควบคุม แต่มีผลทำให้น้ำหนักตัวหอยลดลงหลังจากถูกกระตุ้นไป 6 สัปดาห์

จากการศึกษาลักษณะทางเนื้อเยื่อวิทยาของต่อมสืบพันธุ์ของหอยตัวอ่อนที่ถูกกระตุ้นด้วยสารชนิดต่างๆ เป็นเวลา 14 สัปดาห์ สามารถสรุปผลการพัฒนาของต่อมสืบพันธุ์และเซลล์สืบพันธุ์ได้ดังตารางที่ 2 และ 3 พบว่าก่อนการทดลอง หอยทุกกลุ่มยังไม่มีการพัฒนาของเซลล์สืบพันธุ์ พบแต่ช่องว่างที่จะบรรจุต่อมสืบพันธุ์ (gonadal cavity) บริเวณรอบ hepatopancreas และพบกลุ่มเซลล์ที่สร้างเนื้อเยื่อเกี่ยวพันรอบๆบริเวณช่องว่าง (รูปที่ 7B, D และ F) จากนั้นในสัปดาห์ที่ 6 (หอยมีอายุประมาณ 5 เดือนครึ่ง) เริ่มพบการพัฒนาของเซลล์สืบพันธุ์ระยะเริ่มแรก ในหอยกลุ่มควบคุมที่ฉีดด้วยสารตัวทำละลาย (normal saline solution) และ กลุ่มทดลองที่ฉีดด้วย tunicate-I GnRH ปริมาณ 20 ng/g BW ส่วนในหอยกลุ่มทดลองที่ฉีดด้วย aELH และ buserelin ที่ความเข้มข้น 20 และ 200 ng/gBW พบว่ามีการเจริญของเซลล์สืบพันธุ์ทั้งเพศผู้ และเพศเมียอย่างรวดเร็ว โดยพบว่ามีการพัฒนาของเซลล์สืบพันธุ์จำนวนมาก ในขณะที่กลุ่มควบคุมที่ไม่ฉีดสาร และกลุ่มทดลองที่ฉีดด้วยสาร octopus GnRH ปริมาณ 20 และ 200 ng/gBW และ tunicate-I GnRH ปริมาณ 200 ng/gBW เริ่มพบการพัฒนาของเซลล์สืบพันธุ์ในสัปดาห์ที่ 8 หลังจากการทดลอง แต่พบหอยจำนวนน้อยกว่ากลุ่มทดลองที่ฉีดด้วย aELH และ buserelin จากนั้นหอยในทุกกลุ่มการทดลองมีการพัฒนาต่อมสืบพันธุ์ และเซลล์สืบพันธุ์ทั้งเพศผู้และเพศเมียมากขึ้นเรื่อยๆ จนถึงในสัปดาห์ที่ 14 (รูปที่ 8 – 10) ซึ่งเป็นสัปดาห์สุดท้ายของการทดลอง พบว่ากลุ่มทดลองที่ฉีดด้วย aELH ทั้งสองความเข้มข้นคือ 20 และ 200 ng/gBW มีผลทำให้เกิดการพัฒนาของต่อมสืบพันธุ์และเซลล์สืบพันธุ์ไปเป็นเพศเมียในจำนวนที่มากกว่าเพศผู้เมื่อเปรียบเทียบกับทุกกลุ่มการทดลอง ส่วนการทดลองที่ฉีดด้วย buserelin, octopus GnRH และ tunicate-I GnRH พบว่าทำให้เกิดการพัฒนาของต่อมสืบพันธุ์ได้ทั้งเพศผู้และเพศเมียในจำนวนที่ไม่แตกต่างกันมากนักเมื่อเทียบกับกลุ่มควบคุม

ผลการทดลองดังกล่าวสรุปได้ว่าสาร aELH ที่ปริมาณเพียง 20 ng/gBW มีผลกระตุ้นการพัฒนาของอวัยวะสืบพันธุ์และเซลล์สืบพันธุ์ไปเป็นเพศเมียได้มากกว่าเพศผู้ และไม่มีผลกระทบต่อการเจริญเติบโตทั้งความยาวเปลือกและน้ำหนักตัวของหอย ส่วนสาร buserelin, octopus GnRH และ tunicate-I GnRH มีผลทำให้เกิดการพัฒนาของอวัยวะสืบพันธุ์ไปเป็นทั้งเพศผู้และเพศเมียได้เท่าๆกัน และมีผลทำให้การเจริญเติบโตโดยเฉพาะของน้ำหนักตัวหอยลดลง แต่เมื่อใช้สาร tunicate-I GnRH กระตุ้นในปริมาณน้อย คือ 20 ng/gBW สามารถเพิ่มการเจริญเติบโตได้ทั้งความยาวเปลือกและน้ำหนักตัวของหอย



รูปที่ 5 แผนภูมิแสดงความยาวเปลือกของหอยเป๋าฮื้อในช่วงอายุ 4 เดือน หลังจากที่ฉีดกระตุ้นด้วยสาร aELH, buserelin, octopus GnRH และ tunicate-I GnRH ที่ความเข้มข้น 20 และ 200 ng/gBW เป็นเวลา 14 สัปดาห์เปรียบเทียบกับกลุ่มควบคุม (เครื่องหมายดอกจันแสดงกลุ่มทดลองที่มีความแตกต่างอย่างมีนัยสำคัญทางสถิติ $P<0.05$, บาร์ แสดงค่าความคลาดเคลื่อนมาตรฐานเฉลี่ย; s.e.m.)



รูปที่ 6 แผนภูมิแสดงการเพิ่มน้ำหนักตัวหอยเป๋าฮื้อในช่วงอายุ 4 เดือน หลังจากที่ฉีดกระตุ้นด้วยสาร aELH, buserelin, octopus GnRH และ tunicate-I GnRH ที่ความเข้มข้น 20 และ 200 ng/gBW เป็นเวลา 14 สัปดาห์ เปรียบเทียบกับกลุ่มควบคุม (เครื่องหมายดอกจันแสดงกลุ่มทดลองที่มีความแตกต่างอย่างมีนัยสำคัญทางสถิติ $P<0.05$)

ตารางที่ 2 แสดงผลการกระตุ้นการพัฒนาของต่อมสืบพันธุ์ในหอยเป๋าฮื้อตัวอ่อนอายุ 4 เดือนที่ฉีดกระตุ้นด้วยสาร aELH เป็นเวลา 14 สัปดาห์

กลุ่ม	กลุ่มควบคุม						กลุ่มทดลอง					
	ไม่ฉีดสาร			ฉีดด้วยสารตัวทำละลาย (NaCl)			ELH 20 ng/gBW			ELH 200 ng/gBW		
สัปดาห์ที่	ไม่พัฒนา (ตัว)	เพศผู้ (ตัว)	เพศเมีย (ตัว)	ไม่พัฒนา (ตัว)	เพศผู้ (ตัว)	เพศเมีย (ตัว)	ไม่พัฒนา (ตัว)	เพศผู้ (ตัว)	เพศเมีย (ตัว)	ไม่พัฒนา (ตัว)	เพศผู้ (ตัว)	เพศเมีย (ตัว)
0	10	0	0	10	0	0	10	0	0	10	0	0
2	10	0	0	10	0	0	10	0	0	10	0	0
4	10	0	0	10	0	0	10	0	0	10	0	0
6	**10**	**0**	**0**	**8**	**1**	**1**	**5**	**1**	**4**	**6**	**1**	**3**
8	8	1	1	7	1	2	5	1	4	3	3	4
10	8	1	1	6	2	2	3	1	6	1	2	7
12	4	2	4	6	1	3	1	3	6	3	2	5
14	**4**	**4**	**2**	**2**	**6**	**2**	**3**	**1**	**6**	**1**	**2**	**7**

ตารางที่ 3 แสดงผลการกระตุ้นการพัฒนาของต่อมสืบพันธุ์ในหอยเป๋าฮื้อตัวอ่อนด้วยสาร buserelin, octopus GnRH และ tunicate-I GnRH

กลุ่ม /	กลุ่มทดลอง																	
	Buserelin 20 ng/gBW			Buserelin 200 ng/gBW			Octopus GnRH 20 ng/gBW			Octopus GnRH 200 ng/gBW			Tunicate-I GnRH 20 ng/gBW			Tunicate-I GnRH 200 ng/gBW		
สัปดาห์ที่	ไม่พัฒนา (ตัว)	เพศผู้ (ตัว)	เพศเมีย (ตัว)	ไม่พัฒนา (ตัว)	เพศผู้ (ตัว)	เพศเมีย (ตัว)	ไม่พัฒนา (ตัว)	เพศผู้ (ตัว)	เพศเมีย (ตัว)	ไม่พัฒนา (ตัว)	เพศผู้ (ตัว)	เพศเมีย (ตัว)	ไม่พัฒนา (ตัว)	เพศผู้ (ตัว)	เพศเมีย (ตัว)	ไม่พัฒนา (ตัว)	เพศผู้ (ตัว)	เพศเมีย (ตัว)
0	10	0	0	10	0	0	10	0	0	10	0	0	10	0	0	10	0	0
2	10	0	0	10	0	0	10	0	0	10	0	0	10	0	0	10	0	0
4	10	0	0	10	0	0	10	0	0	10	0	0	10	0	0	10	0	0
6	**6**	**2**	**2**	**5**	**3**	**2**	**10**	**0**	**0**	**10**	**0**	**0**	**8**	**0**	**2**	**10**	**0**	**0**
8	6	1	3	6	2	2	8	1	1	9	1	0	6	2	2	8	0	2
10	6	2	2	3	4	3	7	1	2	8	1	1	8	0	2	7	0	3
12	2	3	5	5	1	4	5	1	4	7	1	2	5	3	2	5	4	1
14	**2**	**4**	**4**	**3**	**2**	**5**	**6**	**3**	**1**	**4**	**2**	**4**	**3**	**6**	**1**	**5**	**2**	**3**

รูปที่ 7 ภาพจุลทรรศน์ธรรมดา ย้อมด้วยสี Haematoxylin และ Eosin แสดงต่อมสืบพันธุ์ของหอยเป๋าฮื้ออายุ 4 เดือน ก่อนการทดลอง

A-B) ต่อมสืบพันธุ์ของหอยเป๋าฮื้อตัวอ่อนในกลุ่มควบคุมที่ไม่ฉีดสาร แสดงตำแหน่ง gonadal cavity (GC) รอบ hepatopancreas และกลุ่มเซลล์ที่สร้างเนื้อเยื่อเกี่ยวพันบริเวณรอบๆช่องว่าง (ลูกศร)

C-D) ต่อมสืบพันธุ์ของหอยเป๋าฮื้อตัวอ่อนในกลุ่มควบคุมที่ฉีดด้วยสารตัวทำละลาย NaCl แสดงกลุ่มเซลล์ที่สร้างเนื้อเยื่อเกี่ยวพัน (หัวลูกศร) ล้อมรอบ hepatopancreas และภายใน gonadal cavity (GC)

E-F) ต่อมสืบพันธุ์ของหอยเป๋าฮื้อตัวอ่อนในกลุ่มทดลองที่ฉีดด้วย aELH 20 ng/g BW แสดงกลุ่มเซลล์ (หัวลูกศร) ที่เนื้อเยื่อเกี่ยวพันบริเวณเยื่อหุ้ม (Cp) รอบ hepatopancreas

รูปที่ 8 ภาพจุลทรรศน์ธรรมดา ย้อมด้วยสี Haematoxylin และ Eosin แสดงการพัฒนาของต่อมสืบพันธุ์ในหอยเป๋าฮื้ออายุ 4 เดือนภายหลังที่ฉีดกระตุ้นด้วย aELH เป็นเวลา 14 สัปดาห์

A-B) ต่อมสืบพันธุ์ของหอยเป๋าฮื้อตัวอ่อนในกลุ่มควบคุมที่ไม่ฉีดสาร แสดงการพัฒนาของอัณฑะ และเซลล์สืบพันธุ์เพศผู้ระยะเริ่มแรก (spermatogonia; Sg) เซลล์สืบพันธุ์ระยะต้น (spermatocytes; Sc) และเซลล์สืบพันธุ์ระยะ spermatid (St).

C-D) ต่อมสืบพันธุ์ของหอยเป๋าฮื้อตัวอ่อนในกลุ่มควบคุมที่ฉีดด้วยสารตัวทำละลาย NaCl แสดงการเจริญของเซลล์สืบพันธุ์เพศเมียจากระยะเริ่มแรกไปเป็น เซลล์สืบพันธุ์ระยะ stage II oocyte (Oc2) และระยะ stage III oocyte (Oc3) มากขึ้น

E-F) ต่อมสืบพันธุ์ของหอยเป๋าฮื้อตัวอ่อนในกลุ่มทดลองที่ฉีดด้วย aELH 20 ng/g BW แสดงการพัฒนาของอวัยวะสืบพันธุ์เพศเมียและมีการเจริญของเซลล์สืบพันธุ์เพศเมียระยะเริ่มแรก (Og) และเซลล์สืบพันธุ์เพศเมียระยะ stage I oocyte (Oc1)

รูปที่ 9 ภาพจุลทรรศน์ธรรมดา ย้อมด้วยสี Haematoxylin และ Eosin แสดงการพัฒนาของต่อมสืบพันธุ์ในหอยเป๋าฮื้ออายุ 4 เดือน หลังจากการฉีดกระตุ้นด้วย aELH และ buserelin เป็นเวลา 14 สัปดาห์

A-B) ต่อมสืบพันธุ์ของหอยเป๋าฮื้อตัวอ่อนในกลุ่มทดลองที่ฉีดด้วย aELH 200 ng/g BW แสดงการพัฒนาของรังไข่ขนาดใหญ่ขึ้น (Go) และมีการเจริญของเซลล์สืบพันธุ์เพศเมียระยะ stage I oocyte (ลูกศร) มากขึ้น

C-D) ต่อมสืบพันธุ์ของหอยเป๋าฮื้อตัวอ่อนในกลุ่มทดที่ฉีดลองที่ฉีดด้วย buserelin 20 ng/g BW แสดงการพัฒนาของรังไข่ และเซลล์สืบพันธุ์เพศเมียระยะ stage I oocyte (Oc1)

E-F) ต่อมสืบพันธุ์ของหอยเป๋าฮื้อตัวอ่อนในกลุ่มทดลองที่ฉีดด้วย buserelin 200 ng/g BW แสดงการพัฒนาของอัณฑะมีขนาดใหญ่ขึ้น (Go) และมีการเจริญของเซลล์สืบพันธุ์เพศผู้ระยะเริ่มแรก (spermatogonia; Sg), เซลล์สืบพันธุ์ระยะ spermatocytes (Sc) และเซลล์สืบพันธุ์ระยะ spermatid (St) จำนวนมาก

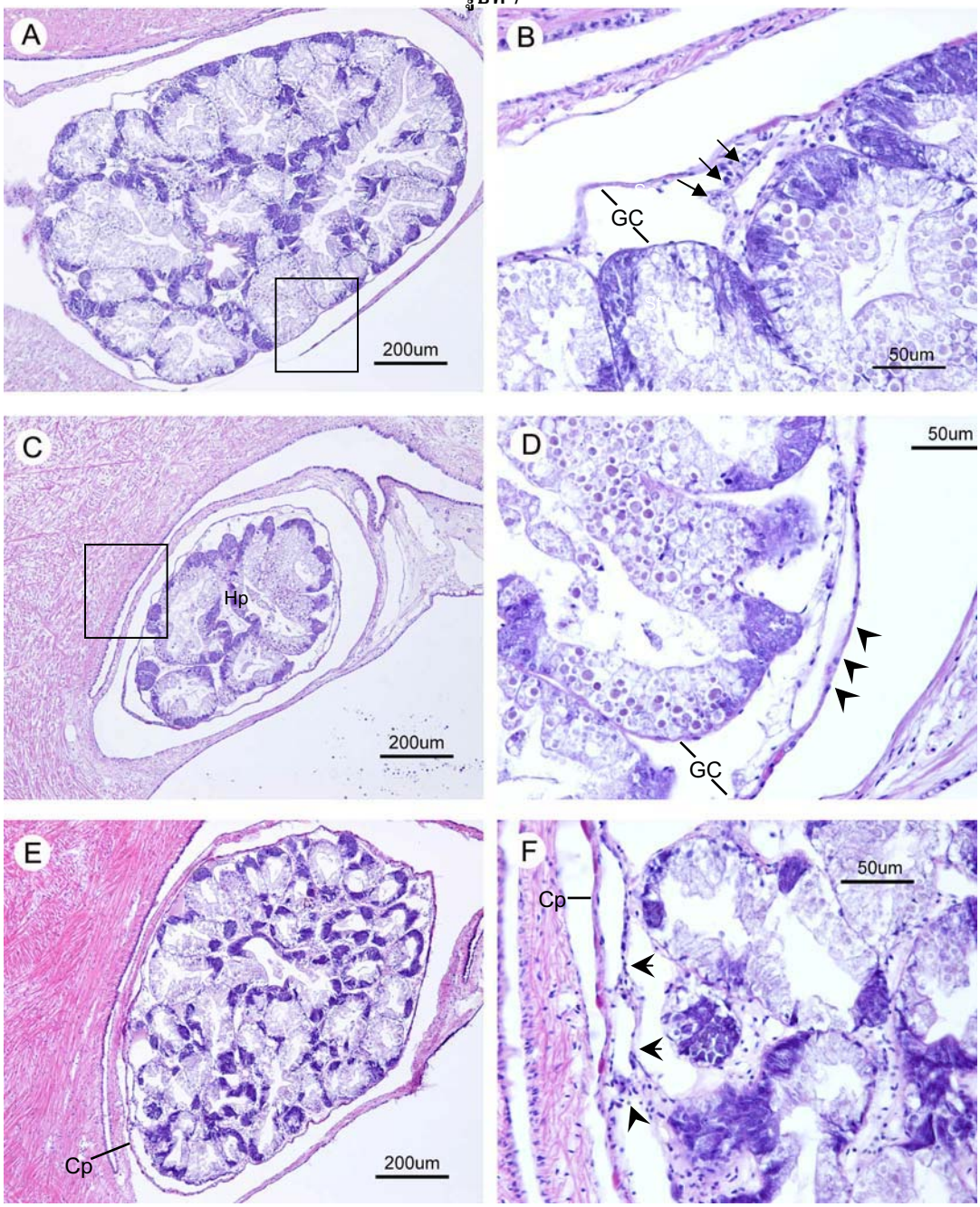
รูปที่ 10 ภาพจุลทรรศน์ธรรมดา ย้อมด้วยสี Haematoxylin และ Eosin แสดงการพัฒนาของอวัยวะสืบพันธุ์ในหอยเป๋าฮื้ออายุ 4 เดือน หลังจากการฉีดกระตุ้นด้วย octopus GnRH และ tunicate-I GnRH เป็นเวลา 14 สัปดาห์

A-B) ต่อมสืบพันธุ์ของหอยเป๋าฮื้อตัวอ่อนในกลุ่มทดลองที่ฉีดด้วย octopus GnRH 200 ng/g BW แสดงการพัฒนาของรังไข่ที่มีการเจริญของเซลล์สืบพันธุ์เพศเมียจากระยะเริ่มแรก (Og) ไปเป็น เซลล์สืบพันธุ์ระยะ stage I oocyte (Oc1) และระยะ stage II oocyte (Oc2) มากขึ้น

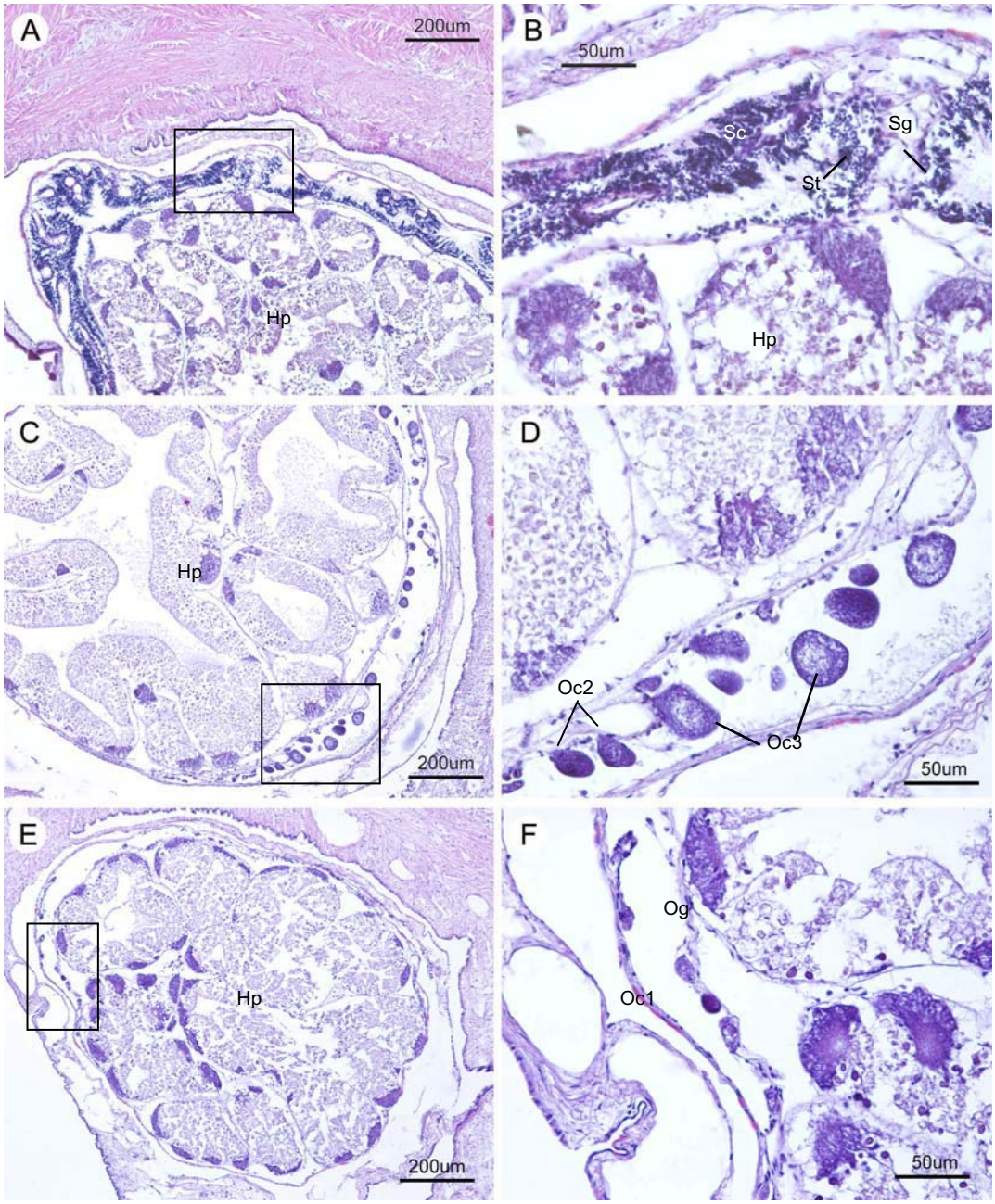
C-D) ต่อมสืบพันธุ์ของหอยเป๋าฮื้อตัวอ่อนในกลุ่มทดลองที่ฉีดด้วย tunicate-I GnRH 20 ng/g BW แสดงการเจริญของอัณฑะซึ่งมีเซลล์สืบพันธุ์เพศผู้ระยะเริ่มแรก (Sg; หัวลูกศร), เซลล์สืบพันธุ์ระยะ spermatocytes (Sc) และเซลล์สืบพันธุ์ระยะ spermatid (St) จำนวนมาก

E-F) ต่อมสืบพันธุ์ของหอยเป๋าฮื้อตัวอ่อนในกลุ่มทดลองที่ฉีดด้วย tunicate-I GnRH 200 ng/g BW แสดงการพัฒนาของรังไข่และเซลล์สืบพันธุ์เพศเมียระยะ stage I oocyte (Oc1) เพิ่มมากขึ้น

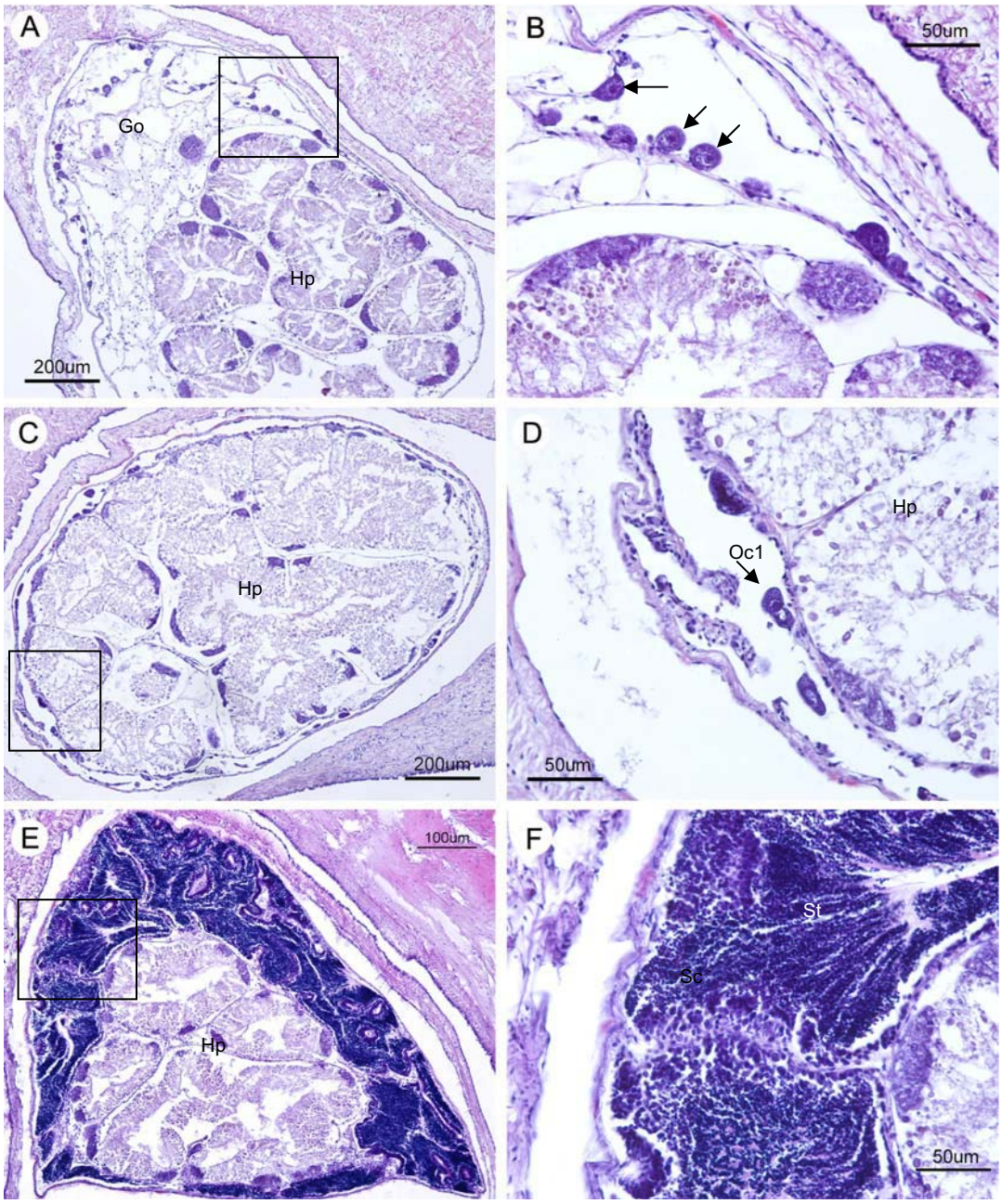
รูปที่ 7



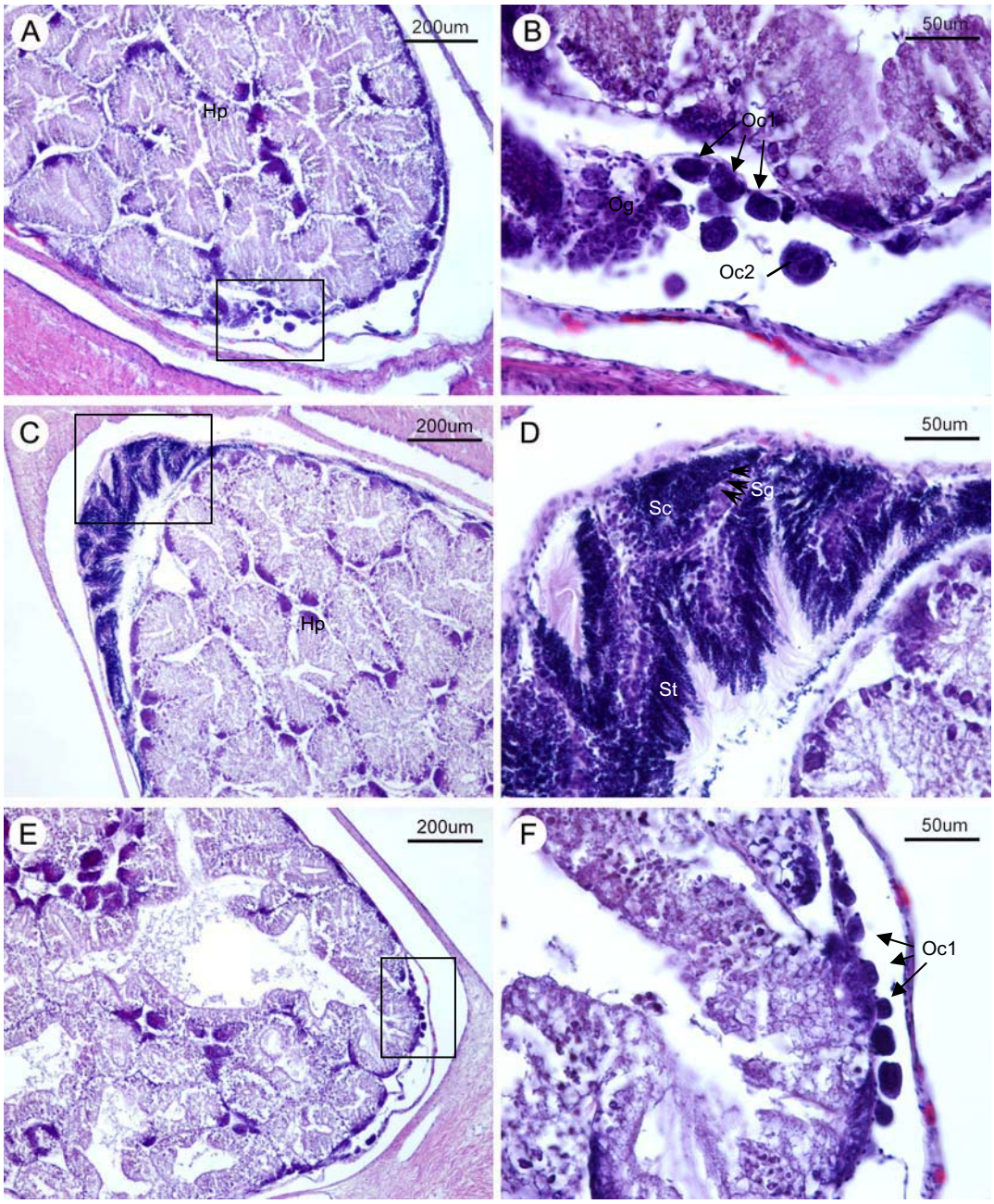
รูปที่ 8


A
200um
Hp
B
50um
Sc
Sg
St
Hp
C
Hp
200um
D
Oc2
Oc3
50um
E
Hp
200um
F
Og
Oc1
50um

รูปที่ 9


A
Go
Hp
200um
B
50um
C
Hp
200um
D
Hp
Oc1
50um
E
100um
Hp
F
St
Sc
50um

รูปที่ 10


A
200um
Hp
B
50um
Oc1
Og
Oc2
C
200um
Hp
D
50um
Sc
Sg
St
E
200um
F
50um
Oc1

หัวข้อที่ 8. การทดสอบการกระตุ้นการพัฒนาของต่อมสืบพันธุ์ในหอยเป๋าฮื้อตัวเต็มวัยด้วยฮอร์โมน aELH และ GnRH

การทดลองนี้จะใช้หอยเพศเมียตัวเต็มวัยอายุ 1 ปี น้ำหนักประมาณ 20 กรัม ความยาวเปลือกประมาณ 4 ซม. และมีต่อมสืบพันธุ์อยู่ในระยะ proliferative หรือ มีค่า visual gonad index (VGI) เท่ากับ 1 โดยการคำนวณ VGI ตามวิธีของ Kikuchi and Uki (1974) ซึ่งแบ่งออกเป็น 4 ระดับ คือ 0 = sex indistinguishable; 1 = sex distinguishable, thin gonad with pointed tip; 2 = gonad partially enlarged with pointed tip; 3 = gonad swollen with rounded tip โดยแบ่งสัตว์ทดลองออกเป็น 12 กลุ่ม กลุ่มละ 35 ตัว ดังนี้

กลุ่มที่ 1 เป็นกลุ่มควบคุมที่ไม่ฉีดสารละลาย

กลุ่มที่ 2 เป็นกลุ่มควบคุม ฉีดด้วยสารตัวทำละลายที่ไม่มีฮอร์โมน (normal saline solution)

กลุ่มที่ 3 และ 4 เป็นกลุ่มทดลอง ฉีดด้วยสารประสาทฮอร์โมน aELH ปริมาณ 500 และ 1000 ng/gBW

กลุ่มที่ 5 และ 6 เป็นกลุ่มทดลอง ฉีดด้วยสาร buserelin ปริมาณ 500 และ 1000 ng/gBW

กลุ่มที่ 7 และ 8 เป็นกลุ่มทดลอง ฉีดด้วยสาร lamprey-I GnRH ปริมาณ 500 และ 1000 ng/gBW

กลุ่มที่ 9 และ 10 เป็นกลุ่มทดลอง ฉีดด้วยสาร octopus GnRH ปริมาณ 500 และ 1000 ng/gBW

โดยที่สัตว์ทดลองถูกฉีดกระตุ้นทุก 7 วัน เป็นจำนวน 7 ครั้ง โดยฉีดเข้าไปตรงบริเวณกล้ามเนื้อเท้าของสัตว์ทดลอง จากนั้นจึงทำการบันทึก ค่า VGI ของแต่ละกลุ่ม ซึ่งค่าที่ได้ จะถูกนำมาหาค่าทางสถิติ และประเมินการเจริญของอวัยวะสืบพันธุ์เทียบกับกลุ่มควบคุม นอกจากนี้ยังเก็บตัวอย่างชิ้นเนื้อของหอยจำนวน 4 ตัวในแต่ละกลุ่มทุกสัปดาห์ เพื่อนำมาหาค่า Gonad index (GI) ซึ่งแสดงถึงการพัฒนาของอวัยวะสืบพันธุ์โดยใช้วิธีการวัดขนาดของเนื้อเยื่อซึ่งแสดงออกมาในรูปอัตราส่วนบริเวณอวัยวะสืบพันธุ์ต่อบริเวณ conical appendage โดยมีสูตรในการคำนวณดังนี้

$$I_G = 100 \times (L\text{-}L')/ L$$

โดยที่ I_G หรือ Gonad index (GI), L คือ เส้นผ่าศูนย์กลางของหน้าตัดตามขวางของ conical appendage ที่ห่างจากปลายสุดของอวัยวะ 0.5 ซม และ L′ คือ เส้นผ่าศูนย์กลางของหน้าตัดตามขวางของ hepatopancreas ที่ห่างจากปลายสุดของอวัยวะ 0.5 ซม (ดัดแปลงจาก Fukazawa และคณะ, 2007)

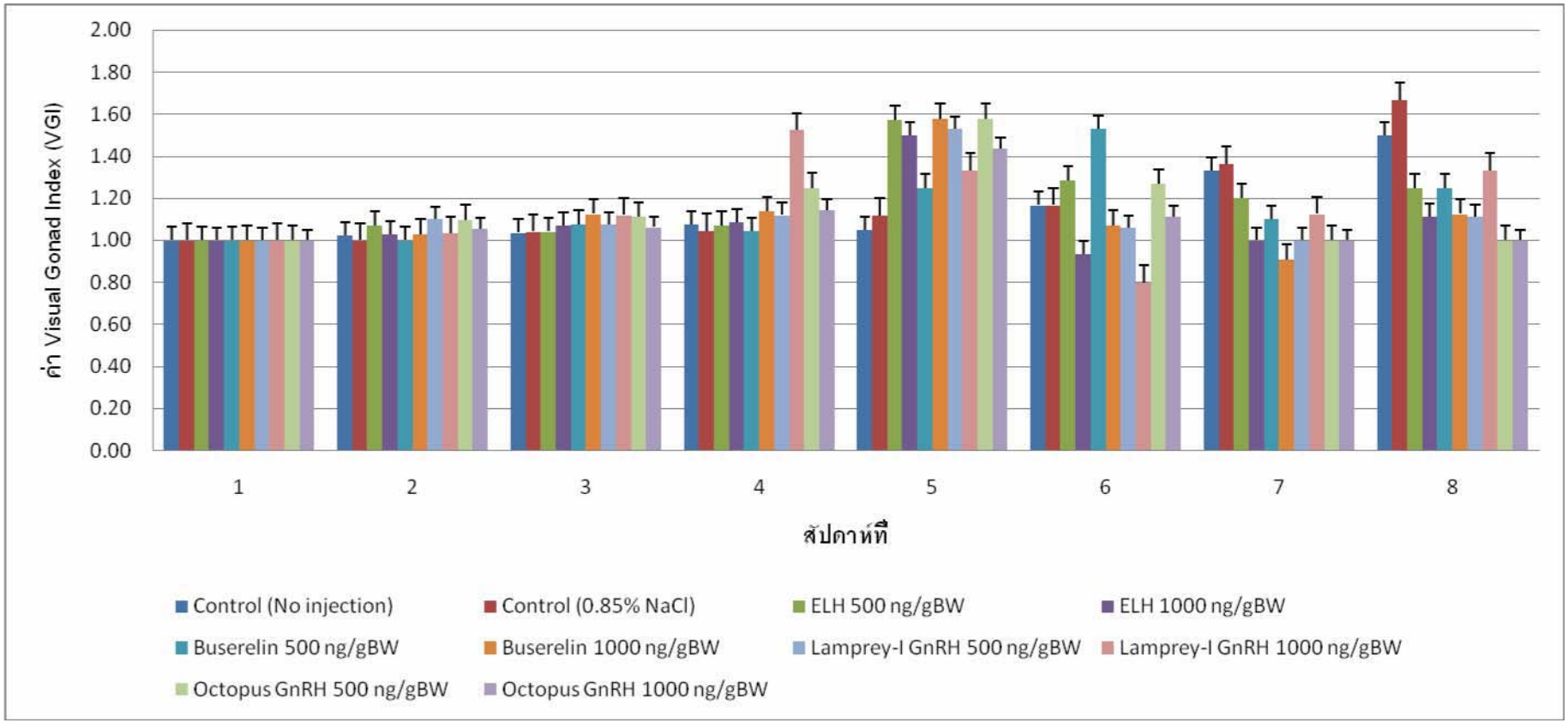
จากนั้นนำมาศึกษาลักษณะทางจุลกายวิภาคของรังไข่เพื่อดูระยะและการพัฒนาของเซลล์สืบพันธุ์ ด้วยกล้องจุลทรรศน์ธรรมดาตามวิธีการจำแนกของ Sobhon และคณะ (1997)

ผลการทดลอง

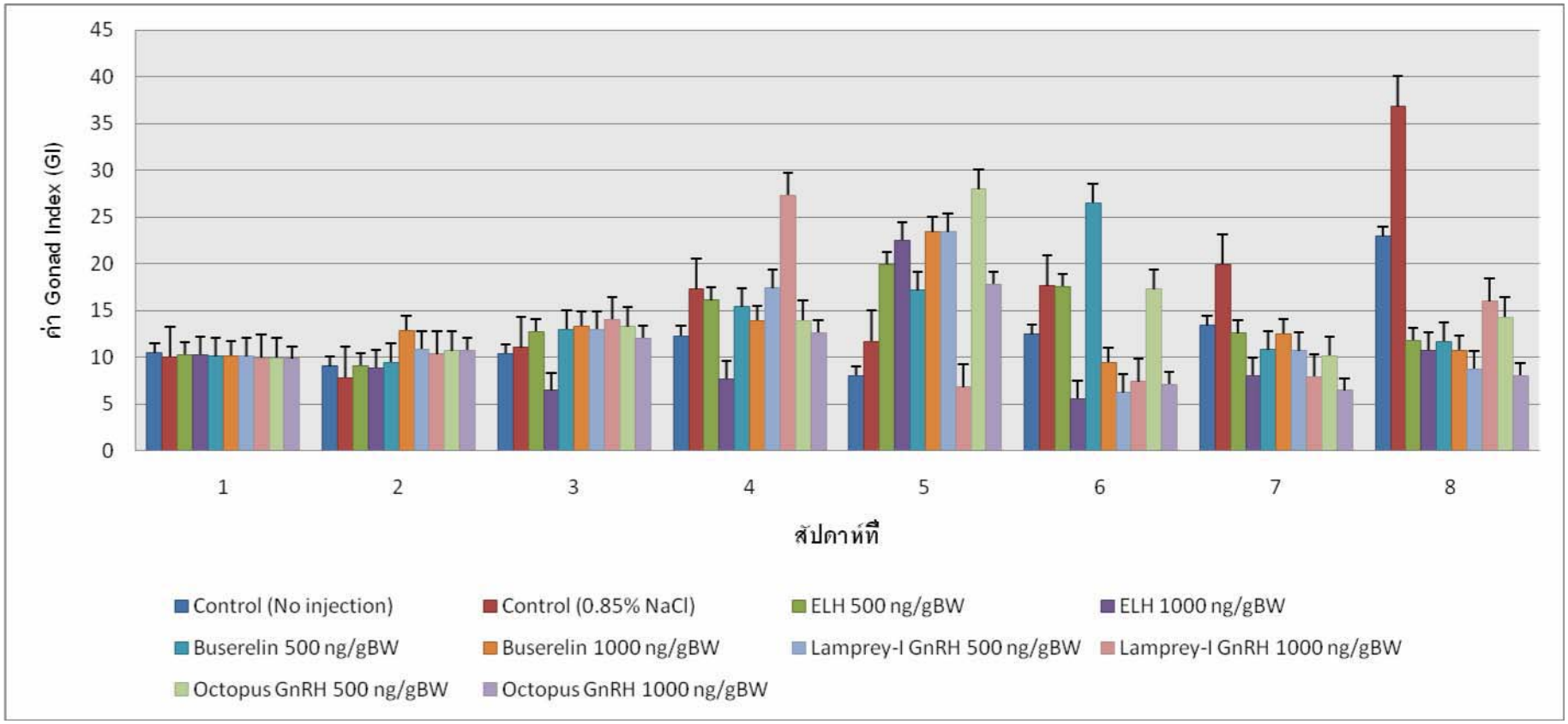
จากแผนภูมิแสดงค่าเฉลี่ยของ VGI และ GI ของหอยเป๋าฮื้อในแต่ละสัปดาห์หลังจากฉีดกระตุ้นด้วยสาร aELH, buserelin, lamprey-I GnRH และoctopus GnRH ที่ความเข้มข้น 500 และ 1000 ng/gBW (รูปที่ 11) เป็นเวลา 8 สัปดาห์ พบว่า ทุกกลุ่มการทดลองมีค่าเฉลี่ยของ VGI และ GI สัมพันธ์กัน กล่าวคือในสัปดาห์ที่ 1 ทุกกลุ่มการทดลองมีค่า VGI และ GI ต่ำ และมีแนวโน้มสูงขึ้นเรื่อยๆ เมื่อมีการพัฒนาของต่อมสืบพันธุ์มากขึ้นจนถึงระยะที่มีการพัฒนาของต่อมสืบพันธุ์เต็มที่ และมีการปล่อยเซลล์สืบพันธุ์ จากนั้นค่า VGI และ GI จะมีค่าลดลง และมีแนวโน้มเพิ่มขึ้นเรื่อยๆ ในสัปดาห์ถัดไป กลุ่มควบคุมที่ฉีดด้วยสารตัวทำละลาย และไม่ฉีดสาร พบว่าหอยมีการเจริญและพัฒนาของต่อมสืบพันธุ์จนถึงระยะที่ต่อมสืบพันธุ์เจริญเต็มที่ (mature) และมีการปล่อยเซลล์สืบพันธุ์บางส่วน (partial spawning) ซึ่งใช้เวลาประมาณ 8 สัปดาห์ ส่วนกลุ่มการทดลองที่ฉีดกระตุ้นด้วยสาร aELH ทั้งสองความเข้มข้น คือ 500 และ 1000 ng/gBW สามารถทำให้มีการเจริญและพัฒนาของต่อมสืบพันธุ์ถึงระยะเจริญเต็มที่จนกระทั่งมีการปล่อยเซลล์สืบพันธุ์ออกมาบางส่วนได้ภายใน 5 สัปดาห์ (รูปที่ 12) ส่วนกลุ่มทดลองที่ฉีดด้วยสาร buserelin ปริมาณ 500 และ 1000 ng/g BW พบว่าหอยมีการเจริญและพัฒนาของต่อมสืบพันธุ์จนถึงระยะเจริญเต็มที่ (รูปที่12) ในสัปดาห์ที่ 6 และ 5 ตามลำดับ ซึ่งต่างจากกลุ่มทดลองที่ฉีดด้วย Lamprey-I GnRH ปริมาณ 500 และ 1000 ng/g BW ในแต่ละสัปดาห์ พบว่าหอยมีการพัฒนาของต่อมสืบพันธุ์จนถึงระยะ

premature ในสัปดาห์ที่ 5 และ 4 ตามลำดับ ส่วนกลุ่มที่ฉีดด้วยสาร octopus GnRH ปริมาณ 500 และ 1000 ng/g BW พบว่าหอยมีการเจริญและพัฒนาของต่อมสืบพันธุ์จนถึงระยะเจริญเต็มที่ ภายในเวลา 5 สัปดาห์ นอกจากนี้สาร octopus GnRH ปริมาณ 500 ng/g BW มีผลทำให้มีการปล่อยเซลล์สืบพันธุ์ออกมาบางส่วนในสัปดาห์ที่ 6

จากผลการทดลองสรุปได้ว่าสาร aELH, buserelin, lamprey-I GnRH และoctopus GnRH ที่ความเข้มข้น 500 ng/gBW มีผลกระตุ้นการพัฒนาของรังไข่จากระยะ proliferative ไปจนถึงระยะ fully mature และมีการปล่อยเซลล์สืบพันธุ์ได้ โดยใช้เวลาเพียง 5 สัปดาห์ ซึ่งเร็วกว่ากลุ่มควบคุมที่ฉีดด้วยสารตัวทำละลาย และไม่ฉีดสารซึ่งต้องใช้เวลาถึง 8 สัปดาห์



รูปที่ 11 แผนภูมิแสดงค่าเฉลี่ยของ Visual Gonad Index (VG1) ของหอยเป๋าฮื้อในแต่ละสัปดาห์หลังจากฉีดกระตุ้นด้วยสาร aELH, buserelin, lamprey-I GnRH และoctopus GnRH ที่ความเข้มข้น 500 และ 1000 ng/gBW เปรียบเทียบกับกลุ่มควบคุม (เส้นตั้งฉากแสดงค่าความคลาดเคลื่อนมาตรฐาน; S.D.)



รูปที่ 12 แผนภูมิแสดงค่าเฉลี่ยของ Gonad Index (GI) ของหอยเป๋าฮื้อในแต่ละสัปดาห์หลังจากฉีดกระตุ้นด้วยสาร aELH, buserelin, lamprey-I GnRH และoctopus GnRH ที่ความเข้มข้น 500 และ 1000 ng/gBW เปรียบเทียบกับกลุ่มควบคุม (เส้นตั้งฉากแสดงค่าความคลาดเคลื่อนมาตรฐาน; S.D.)

หัวข้อที่ 9. การทดสอบการกระตุ้นการปล่อยเซลล์สืบพันธุ์ในหอยเป๋าฮื้อตัวเต็มวัยด้วยสาร aELH และ GnRH

การทดลองนี้เป็นการทดสอบการกระตุ้นการปล่อยเซลล์สืบพันธุ์ในหอยเป๋าฮื้อที่ถูกเลี้ยงเพื่อใช้เป็นพ่อพันธุ์ และแม่พันธุ์ที่มีอวัยวะสืบพันธุ์เจริญเต็มที่ โดยเพศผู้มีอวัยวะสืบพันธุ์สีเหลืองครีมชัดเจน ส่วนเพศเมียมีอวัยวะสืบพันธุ์สีเขียวชัดเจน โดยแบ่งสัตว์ทดลองออกเป็น 9 กลุ่ม กลุ่มละ 20 ตัว (เพศผู้ 10 ตัว เพศเมีย 10 ตัว) ดังนี้

กลุ่มที่ 1 เป็นกลุ่มควบคุม ฉีดด้วยสารตัวทำละลายที่ไม่มีฮอร์โมน (Normal saline solution)

กลุ่มที่ 2-4 เป็นกลุ่มทดลอง ฉีดด้วยสารประสาทฮอร์โมน aELH ปริมาณ 250, 500 และ 1000 ng/gBW

กลุ่มที่ 5 -7 เป็นกลุ่มทดลอง ฉีดด้วยสาร buserelin ปริมาณ 250, 500 และ 1000 ng/gBW

กลุ่มที่ 8 และ 9 เป็นกลุ่มทดลอง ฉีดด้วยสาร octopus GnRH ปริมาณ 500 และ 1000 ng/gBW

ก่อนทำการทดลองสัตว์ทดลองทั้ง 9 กลุ่มถูกนำมาพักไว้ในถังเลี้ยง ในห้องที่มีการควบคุมอุณหภูมิ ความเค็มของน้ำทะเล และการให้อาหารธรรมชาติ (สาหร่าย) การทดลองเริ่มขึ้นก่อนเวลาที่มีการปล่อยเซลล์สืบพันธุ์ตามธรรมชาติ 4 วัน โดยการทดลองเริ่มจากการแยกหอยเพศผู้ และเมียใส่ลงตู้กระจก ขนาด 16x20x20 ลูกบาศก์เซนติเมตร โดยใส่หอยจำนวน 1 ตัว ต่อ 1 ตู้ ในน้ำทะเล 2 ลิตร หลังจากการพักในตู้กระจกเป็นเวลา 30 นาที จึงทำการฉีดสารบริเวณกล้ามเนื้อเท้า จากนั้นบันทึกเวลาและจำนวนของสัตว์ทดลองที่ปล่อยเซลล์สืบพันธุ์ นับจำนวนและบันทึกคุณภาพของเซลล์ไข่และอสุจิที่ถูกปล่อยออกมา จากนั้นนำเซลล์ไข่และเซลล์อสุจิของแต่ละกลุ่มมาผสมพันธุ์กัน แล้วคำนวณอัตราส่วนของการปฏิสนธิตามวิธีการของ Pumtong และคณะ (1997) จากนั้นบันทึกเปอร์เซ็นต์ของการปฏิสนธิ และดูการพัฒนาของเซลล์จากระยะ 2 เซลล์ไปจนถึง ระยะ veliger larva

ผลการทดลอง

จากผลการทดลองดังแสดงในตารางที่ 4 พบว่า เมื่อฉีดสาร aELH ปริมาณ 250 ng/gBW หอยเพศผู้จำนวน 2 ตัว มีการปล่อยเซลล์อสุจิภายในเวลา 6-12 ชม. ส่วนกลุ่มที่ฉีดด้วย aELH ปริมาณ 500 ng/gBW หอยจำนวน 6 ตัว มีการปล่อยเซลล์อสุจิ และเพิ่มจำนวนมากขึ้นเมื่อกระตุ้นด้วย aELH ปริมาณมากขึ้นคือ 1000 ng/gBW พบจำนวน 7 ตัวที่ปล่อยเซลล์อสุจิ ส่วนกลุ่มควบคุมพบว่าหอยจำนวน 2 ตัว มีการปล่อยเซลล์อสุจิ นอกจากนี้ยังพบว่าปริมาณเซลล์อสุจิเฉลี่ยที่ปล่อยออกมาในแต่ละกลุ่มการทดลองมีปริมาณไม่แตกต่างกันมากนัก และเซลล์อสุจิที่ปล่อยออกมามีคุณภาพดีในทุกกลุ่มการทดลองคือ เคลื่อนไหวตลอดเวลาอย่างต่อเนื่อง สำหรับเพศเมียพบว่ามีการปล่อยเซลล์ไข่ในกลุ่มทดลองที่ถูกกระตุ้นด้วย aELH ปริมาณ 250 ng/gBW จำนวน 3 ตัว โดยเริ่มปล่อยไข่หลังจากฉีดสารไปแล้วประมาณ 6-12 ชม. และเพิ่มจำนวนมากขึ้นเมื่อกระตุ้นด้วย aELH ปริมาณมากขึ้นคือ 500 และ 1000 ng/gBW พบจำนวน 6 ตัว และ 8 ตัว ตามลำดับ ส่วนกลุ่มควบคุมพบว่าหอย 2 ตัวมีการปล่อยเซลล์ไข่ และมีคุณภาพของเซลล์ไข่ปกติในทุกกลุ่มการทดลองคือมีลักษณะกลม ขนาดเท่ากันและมี jelly coat หุ้ม ส่วนเปอร์เซ็นต์การ fertilization พบว่ามีเปอร์เซ็นต์เพิ่มขึ้นในกลุ่มที่ฉีดด้วยสาร aELH เมื่อเทียบกับกลุ่มควบคุม และเซลล์สามารถเจริญไปได้ถึง ระยะ veliger larva ได้ทุกกลุ่มการทดลอง ภายในเวลา 17 ชม หลังการ fertilization

ผลการฉีดกระตุ้นสารด้วย GnRH แสดงในตารางที่ 5 พบว่า เมื่อฉีดสาร buserelin ปริมาณ 250 ng/gBW พบว่าไม่สามารถกระตุ้นให้หอยทั้งเพศผู้และเพศเมียปล่อยเซลล์สืบพันธุ์ได้ ส่วนกลุ่มที่ฉีดด้วย buserelin ปริมาณ 500 ng/gBW หอยจำนวน 6 ตัว มีการปล่อยเซลล์อสุจิ และเมื่อกระตุ้นด้วย buserelin ปริมาณเพิ่มขึ้นคือ 1000 ng/gBW พบจำนวน 5 ตัวที่ปล่อยเซลล์อสุจิ ส่วนกลุ่มที่ฉีดด้วย octopus GnRH ปริมาณ 500 ng/gBW และ 1000 ng/gBW ไม่สามารถกระตุ้นให้หอย

เพศผู้ปล่อยเซลล์สืบพันธุ์ได้ ส่วนกลุ่มควบคุมพบว่าหอยจำนวน 2 ตัว มีการปล่อยเซลล์อสุจิ นอกจากนี้ยังพบว่าปริมาณเซลล์อสุจิเฉลี่ยที่ปล่อยออกมาในแต่ละกลุ่มการทดลองมีปริมาณไม่แตกต่างกันมากนัก และเซลล์อสุจิที่ปล่อยออกมามีคุณภาพดีในทุกกลุ่มการทดลอง

สำหรับเพศเมียพบว่ามีการปล่อยเซลล์ไข่ในกลุ่มทดลองที่ถูกกระตุ้นด้วย buserelin ปริมาณ 500 ng/gBW จำนวน 5 ตัว และลดลงเมื่อกระตุ้นด้วย buserelin ปริมาณมากขึ้นคือ 1000 ng/gBW พบจำนวน 2 ตัว ส่วนกลุ่มที่ฉีดด้วย octopus GnRH ปริมาณ 500 ng/gBW ไม่สามารถกระตุ้นให้หอยเพศเมียปล่อยเซลล์สืบพันธุ์ได้ แต่กลุ่มทดลองที่ฉีดด้วย octopus GnRH ปริมาณเพิ่มขึ้นคือ 1000 ng/gBW พบจำนวน 2 ตัวที่ปล่อยเซลล์ไข่ ส่วนกลุ่มควบคุมพบว่าหอย 2 ตัวมีการปล่อยเซลล์ไข่ และมีคุณภาพของเซลล์ไข่ปกติในทุกกลุ่มการทดลองคือมีลักษณะกลม ขนาดเท่ากันและมี jelly coat หุ้ม ส่วนเปอร์เซ็นต์การ fertilization พบว่ามีเปอร์เซ็นต์ไม่แตกต่างกันมากนักเมื่อเทียบกับกลุ่มควบคุม

ผลการทดลองดังกล่าวสรุปได้ว่าสาร aELH มีผลกระตุ้นโดยตรงในการปล่อยเซลล์สืบพันธุ์ทั้งเซลล์ไข่ และเซลล์อสุจิ ซึ่งปริมาณที่เหมาะสมคือ 500 ng/gBW และสามารถให้เปอร์เซ็นต์การ fertilization ได้ดี ส่วน buserelin และ octopus GnRH สามารถออกฤทธิ์ได้น้อยกว่า ELH และไม่สม่ำเสมอในการกระตุ้นการปล่อยเซลล์สืบพันธุ์ของทั้งสองเพศ

ตารางที่ 4 แสดงผลการทดสอบการกระตุ้นการปล่อยเซลล์อสุจิในหอยเป๋าฮื้อตัวเต็มวัยเพศผู้ด้วยสาร aELH

กลุ่มทดลอง	จำนวนสัตว์ทดลองที่ปล่อยเซลล์สืบพันธุ์ (n=10)		เปอร์เซ็นต์ของการปล่อยเซลล์สืบพันธุ์		ปริมาณเซลล์อสุจิเฉลี่ย (เซลล์/มล.)	คุณภาพเซลล์อสุจิ *	ปริมาณเซลล์ไข่เฉลี่ย (เซลล์)	คุณภาพเซลล์ไข่	เปอร์เซนต์ของการผสมพันธุ์
	เพศผู้	เพศเมีย	เพศผู้	เพศเมีย					
Control (NaCl)	2	2	20	20	$1.395x10^6$	+++	660,000	ลักษณะกลม มีขนาดเท่ากัน และมี jelly coat หุ้ม	67.58
ELH 250 ng/gBW	2	3	20	30	$6.825x10^6$	+++	147,500	ส่วนใหญ่มีลักษณะกลม ขนาดเท่ากัน และมีjelly coat หุ้ม	62.99
ELH 500 ng/gBW	6	6	60	60	$3.66x10^6$	+++	524,166	ลักษณะกลม มีขนาดเท่ากัน และมี jelly coat หุ้ม	86.94
ELH 1000 ng/gBW	7	8	70	80	$2.434x10^6$	+++	942,500	ลักษณะกลม มีขนาดเท่ากัน และมี jelly coat หุ้ม	84.14

* หมายเหตุ คุณภาพของเซลล์อสุจิแบ่งออกเป็น 3 ระดับคือ

+++ หมายถึง อสุจิทุกตัวเคลื่อนไหวตลอดเวลาอย่างต่อเนื่อง ++ หมายถึง อสุจิบางตัวเคลื่อนไหวช้า

\+ หมายถึง อสุจิไม่เคลื่อนไหว หรือเคลื่อนไหวช้ามาก

ตารางที่ 5 แสดงผลการทดสอบการกระตุ้นการปล่อยเซลล์สืบพันธุ์ในหอยเป๋าฮื้อตัวเต็มวัยด้วยสาร buserelin, และ octopus GnRH

กลุ่มทดลอง	จำนวนสัตว์ทดลองที่ปล่อยเซลล์สืบพันธุ์ (n=10)		เปอร์เซ็นต์ของการปล่อยเซลล์สืบพันธุ์		ปริมาณเซลล์อสุจิเฉลี่ย (เซลล์/มล.)	คุณภาพเซลล์อสุจิ *	ปริมาณเซลล์ไข่เฉลี่ย (เซลล์)	คุณภาพเซลล์ไข่	เปอร์เซนต์ของการผสมพันธุ์
	เพศผู้	เพศเมีย	เพศผู้	เพศเมีย					
Control (NaCl)	2	1	20	10	$1.275x10^6$	+++	90,000	ลักษณะกลม มีขนาดเท่ากัน และมีjelly coat หุ้ม	71.14
Buserelin 500 ng/gBW	6	5	60	50	$1.68x10^7$	++	341,875	มีลักษณะกลม ขนาดเท่ากัน และมีjelly coat หุ้ม	88.12
Buserelin 1000 ng/gBW	5	2	50	20	$3.97x10^6$	+++	319,000	ลักษณะกลม มีขนาดเท่ากัน และมีjelly coat หุ้ม	85.42
Octopus GnRH 1000 ng/gBW	-	2	-	20	-	-	107,500	ลักษณะกลม มีขนาดเท่ากัน และมีjelly coat หุ้ม	-

* หมายเหตุ คุณภาพของเซลล์อสุจิแบ่งออกเป็น 3 ระดับคือ

+++ หมายถึง อสุจิทุกตัวเคลื่อนไหวตลอดเวลาอย่างต่อเนื่อง ++ หมายถึง อสุจิบางตัวเคลื่อนไหวช้า

\+ หมายถึง อสุจิไม่เคลื่อนไหว หรือเคลื่อนไหวช้ามาก

โครงการที่ 2 กุ้งก้ามกราม

หัวข้อที่ 1 บทนำ

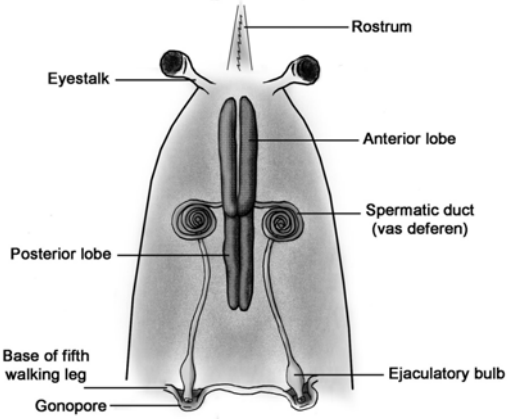
ในสภาพที่เลี้ยงแบบกักขังพ่อและแม่พันธุ์ของกุ้ง ลดประสิทธิภาพการสืบพันธุ์ลงมาก เนื่องจากต่อมสืบพันธุ์ไม่พัฒนาเท่าที่ควร ซึ่งเนื่องมาจากความเครียดที่ถูกเลี้ยงในสภาพที่ไม่เป็นธรรมชาติตามที่เคยอยู่ ทำให้ระดับสารสื่อประสาท (neurotransmitters) และฮอร์โมนที่กระตุ้นการสืบพันธุ์ลดปริมาณลง เนื่องจากถูกกดด้วยฮอร์โมนห้ามการพัฒนาต่อมสืบพันธุ์จากก้านตา (gonad inhibiting hormone-GIH) สำหรับกุ้งกุลาดำ (*P. monodon*) และกุ้งขาว (*P. vannamei*) ผู้เลี้ยงต้องทำการตัดตาเพื่อกำจัด GIH และทำให้ฮอร์โมนที่กระตุ้นการพัฒนาของต่อมสืบพันธุ์ได้แก่ gonad stimulating hormone (GSH), เมทิลฟาเนโซเอท (methyl farnesoate, MF) และฮอร์โมนที่กระตุ้นการตกไข่ (egg-laying hormone) เพิ่มขึ้น การตัดตานั้นทำให้อายุแม่กุ้งจำกัดและมีช่วงระยะการใช้งานสั้น ถ้าหากหลีกเลี่ยงการตัดตาได้ก็จะทำให้สามารถขยายอายุการใช้งานและประสิทธิภาพการสืบพันธุ์ของแม่กุ้งได้ดีขึ้น การที่จะกระทำเช่นนี้ได้ต้องเข้าใจถึงกลไกของฮอร์โมนประสาทที่ควบคุมการพัฒนาของต่อมสืบพันธุ์และการตกไข่ กับการหลั่งอสุจิจากแม่และพ่อพันธุ์ *สมมุติฐานที่คณะผู้วิจัยเสนอคือ สารสื่อประสาท 5-HT และ DA ที่ผลิตและหลั่งโดยเซลล์ประสาทในระบบประสาทกลาง (CNS) ของแม่พันธุ์ เป็นตัวสัญญาณรับรู้การเปลี่ยนแปลงสภาพแวดล้อมภายนอก ถ้าสภาพแวดล้อมเหมาะสม 5-HT จะกระตุ้น GnRH ซึ่งเป็นสารขยายสัญญาณประสาท (neuromodulator) ให้กระตุ้นการสร้างและการหลั่งฮอร์โมนกระตุ้นรังไข่ระดับสุดท้ายคือ GSH, ELH และ MF ซึ่งจะถูกปล่อยออกมาจากระบบประสาทกลาง และ/หรือต่อมสืบพันธุ์เพื่อกระตุ้นให้รังไข่พัฒนา มีเซลล์ไข่ที่สมบูรณ์มากขึ้น และสุดท้ายคือ มีไข่ที่ตกออกมาจำนวนมาก ทำให้ประสิทธิภาพการสืบพันธุ์ของแม่กุ้งดีขึ้น*

หัวข้อที่ 2. การศึกษาโครงสร้างของต่อมอัณฑะและการพัฒนาของเซลล์อสุจิในกุ้งก้ามกราม เปรียบเทียบกับกุ้งกุลาดำ

การจำแนกชนิดของเซลล์สืบพันธุ์เพศผู้ในกระบวนการ spermatogenesis ในกุ้งก้ามกราม

มหกายวิภาคระบบสืบพันธุ์เพศผู้ของกุ้งก้ามกราม(male reproductive system)

ระบบสืบพันธุ์เพศผู้ของกุ้งก้ามกรามประกอบด้วย อัณฑะ(testis) และท่อนำอสุจิ (vas deferen/spermatic duct) (รูปที่ 13) อัณฑะจะอยู่ในช่องอก โดยอยู่ระหว่าง hepatopancreas และหัวใจ (รูปที่ 14) อัณฑะของกุ้งชนิดนี้สามารถแบ่งได้เป็นสองส่วน คือ anterior lobe และ posterior lobe (รูปที่13 และ 14) ทั้งสองส่วนเชื่อมต่อกันตรงกลางและมีท่อนำอสุจิมาเปิดเข้าทั้งสองข้าง Anterior lobe มี 1 คู่และมีขนาดใหญ่กว่าทอดตัวขึ้นไปทางด้านส่วนหัวของกุ้ง ส่วน posterior lobe มีขนาดเล็กค่อนมาทางด้านหลังและทอดตัวอยู่ใต้หัวใจ ท่อนำอสุจิแบ่งได้เป็น 3 ส่วน คือ ส่วนต้น(proximal) ส่วนกลาง (middle) และส่วนปลาย(distal) ท่อนำอสุจิส่วนต้นมีลักษณะขดงอไปมา ท่อส่วนกลางจะทอดยาวลงมาทางด้านข้างของช่องอกท่อส่วนปลายมีลักษณะปลายท่อโป่งพองออกเป็นกระเปาะเรียกว่า ejaculatory bulb (รูปที่ 13, 14C) ซึ่งเป็นบริเวณที่เก็บเซลล์อสุจิชั่วคราวก่อนปล่อยออกเมื่อมีการผสมพันธุ์ เซลล์อสุจิจะถูกห่อหุ้มด้วยโครงสร้างที่เป็นเยื่อเมือกหลายชั้นเรียกว่า



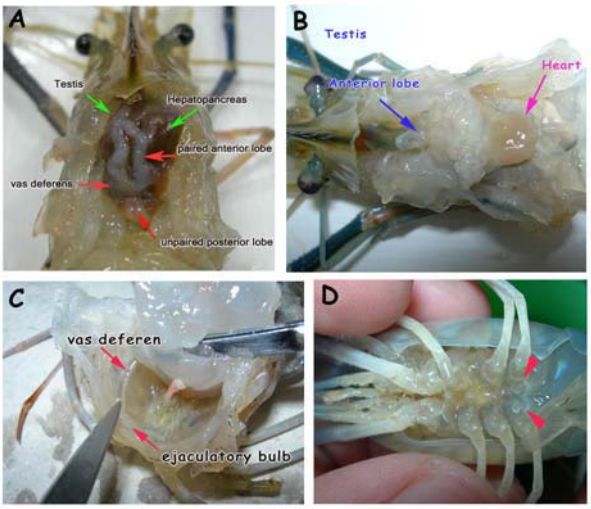
รูปที่ 13 แสดงภาพวาดตำแหน่งและส่วนต่างๆของอวัยวะสืบพันธุ์เพศผู้ของกุ้งก้ามกราม

spermatophore นอกจากนี้ยังมีต่อมสร้างฮอร์โมนเพศผู้(androgenic gland) ที่จำเป็นต่อการเจริญและพัฒนาเซลล์สืบพันธุ์เพศผู้ไปสู่ตัวเต็มวัย ทอดตัวขนาบอยู่กับ ejaculatory bulb จากนั้นท่อนำอสุจิส่วนปลายนี้จะมีขนาดเล็กลงที่ส่วนปลายสุด และเปิดออกสู่ภายนอกร่างกายตรงบริเวณที่เรียกว่า gonopore ซึ่งอยู่ที่ฐานของขาเดินคู่ที่ห้า(fifth walking leg) (รูปที่ 14D)

จุลกายวิภาคระบบสืบพันธุ์เพศผู้ของกุ้งก้ามกราม

อัณฑะ(Testis)

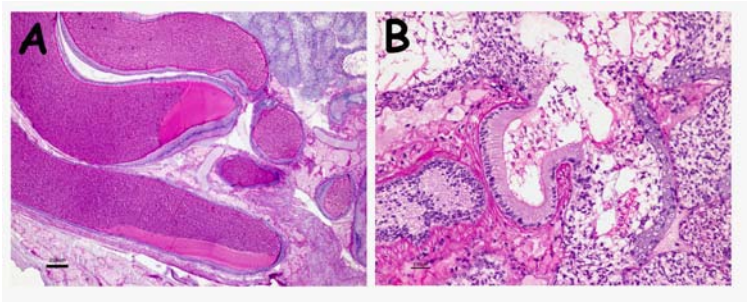
อัณฑะของกุ้งก้ามกรามถูกหุ้มด้วยเนื้อเยื่อเกี่ยวพันบางๆ เป็น capsule (รูปที่ 15A) ทั้ง anterior และ posterior lobe มีโครงสร้างภายในเหมือนกัน อัณฑะจะมีลักษณะเป็น acinus โดยเซลล์สืบพันธุ์ขั้นต้นจะอยู่ที่ขอบของ acinus และเซลล์ที่เจริญเต็มที่แล้วจะอยู่ตรงกลาง(รูปที่ 15B) นอกจากนี้ยังมีเซลล์พี่เลี้ยง (Sertoli/Nurse/Sustentacular cell) แทรกตัวอยู่ระหว่างเซลล์ระยะต้นอีกด้วย



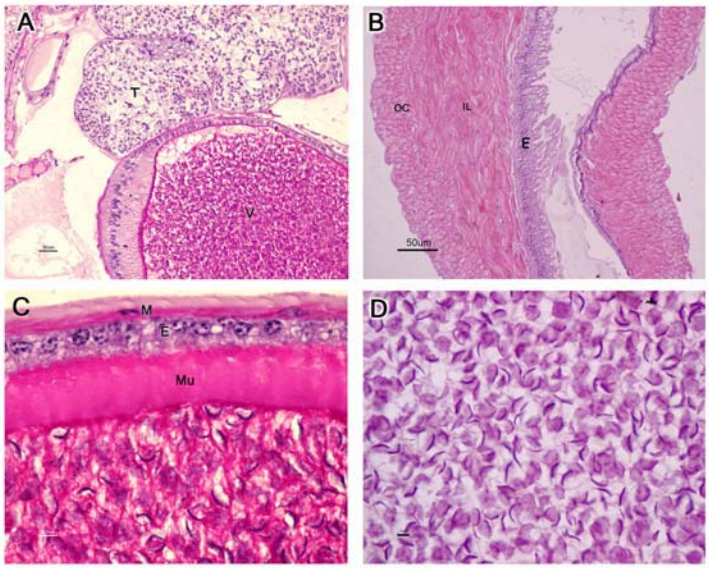
รูปที่ 14 แสดงมหกายวิภาคระบบสืบพันธุ์เพศผู้ในกุ้งก้ามกราม : ภาพ D = gonopore (หัวลูกศร)

ท่อนำอสุจิ (vas deferen/spermatic duct)

ท่อนำอสุจิสามารถแบ่งได้เป็น 3 ส่วน คือ ส่วนต้น (proximal) (รูปที่ 15) ส่วนกลาง (middle) (รูปที่ 16A) และส่วนปลาย (distal) (รูปที่ 16B) ท่อนำอสุจิในกุ้งก้ามกรามจะเชื่อมต่อกับอัณฑะในลักษณะเป็นแอ่งของเซลล์ (รูปที่ 15B) ท่อนำอสุจิจะทอดจากด้านข้างของอัณฑะลงไปตามแนวด้านข้างของช่องอก เยื่อบุผนังท่อเป็นแบบ pseudostratified columnar ด้านบนมี cilia นอกจากนี้พบว่าเยื่อบุผนังท่อนำอสุจิยกตัวสูงขึ้น (รูปที่ 16B) ใต้ต่อชั้นเยื่อบุผนังเป็นชั้นกล้ามเนื้อเรียบบางๆที่ช่วยในการหดตัวของท่อนำอสุจิ ภายในท่อจะประกอบด้วยเซลล์อสุจิที่เจริญเต็มวัยเป็นส่วนใหญ่ และมี mucus ปกคลุมเป็นจำนวนมากทำให้เห็นเป็นสีชมพูเข้มเมื่อย้อมด้วย Periodic Acid Schiff (PAS) (รูปที่ 15A และ15C) ท่อส่วนproximal ที่ใกล้กับอัณฑะจะมี mucus น้อยกว่าท่อส่วนอื่นๆ ท่อนำอสุจิในส่วนปลายบริเวณ ejaculatory bulb มีชั้นกล้ามเนื้อเรียบหนามากขึ้นจนสามารถแบ่งได้เป็น 2 ชั้นตามการทอดตัวของใยกล้ามเนื้อ คือ ชั้นในเรียงตามยาว (inner longitudinal) และชั้นนอกวนรอบท่อ (outer circular) (รูปที่ 16B) ท่อนำอสุจิมีหน้าที่บรรจุเซลล์สืบพันธุ์ให้เป็น spermatophore และพร้อมที่จะได้รับการปฏิสนธิต่อไป

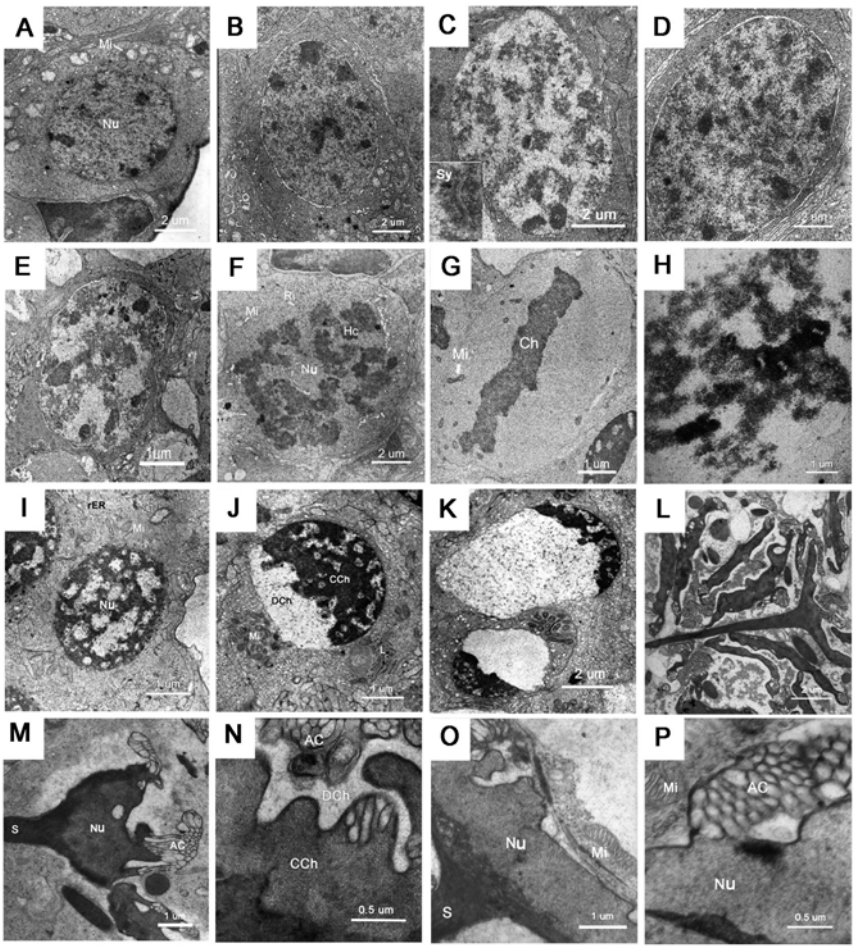


รูปที่ 15 แสดงจุลกายวิภาคของท่อนำอสุจิส่วนต้นในกุ้งก้ามกราม (ภาพ A) มีลักษณะขดไปมา และท่ออสุจิส่วนที่เชื่อมต่อกับอัณฑะ (ภาพ B) เทคนิค PAS กำลังขยาย 20X



รูปที่ 16 แสดงลักษณะจุลกายวิภาคของท่อนำอสุจิส่วนกลาง (ภาพ A), ส่วนปลาย (ภาพ B), ส่วนขยายบริเวณผนังท่ออสุจิ (ภาพ C): ภาพ A และ C ย้อมด้วยเทคนิค PAS ส่วนภาพ B และ D ย้อมด้วยสี H&E (T= Testis, V=Vas deferen, E=Epithelium lining, OC=Outer circular, IL=Inner longitudinal, M=Muscular layer และ Mu=Mucus กำลังขยายภาพ A-D= 20X, 10X และ 100X ตามลำดับ)

จากการศึกษาลักษณะโครงสร้างทางจุลทรรศอิเลคตรอนสามารถจำแนกการพัฒนาของเซลล์สืบพันธุ์เพศผู้ได้ 10 ขั้นดังนี้คือ 1. spermatogonia 2. primary spermatocytes ซึ่งสามารถแบ่งย่อยได้ 6 ขั้นย่อยได้แก่ leptotene, zygotene, pachytene, diplotene, diakinesis และ metaphase 3. secondary spermatocyte, 4. spermatids และ 5. mature sperm (รูปที่ 17). Spermatids สามารถแบ่งย่อยได้ 3 ระยะตามรูปแบบของการจัดเรียงตัวของโครมาตินภายในนิวเคลียส ได้แก่ spermatid ระยะต้น เซลล์ขั้นนี้มีนิวเคลียสรูปร่างกลม โครมาตินเรียงตัวกันแน่นจับกันเป็นแผ่นหนากระจายอยู่ทั่วนิวเคลียส. จากนั้นเซลล์จะพัฒนาเข้าสู่ขั้นกลาง(middle spermatid) ซึ่งใยโครมาตินจะเริ่มคลี่ออก decondense จากทางด้านใดด้านหนึ่งของนิวเคลียสไปจนกระทั่งคลุมเกือบทั้งนิวเคลียสในขั้นสุดท้าย (late spermatid) ซึ่งเซลล์ในระยะนี้ จะเห็น heterochromatin หลงเหลืออยู่เพียงเล็กน้อยที่ด้านหนึ่งของนิวเคลียสโดยมีลักษณะเป็นพระจันทร์เสี้ยว(crescent-shape). จากนั้น spermatid จะพัฒนาไปเป็นเซลล์อสุจิตัวเต็มวัย (mature sperm) ซึ่งมีรูปร่างคล้ายร่มกลับหัว (everted umbrella-shape) เซลล์อสุจิในกุ้งก้ามกรามไม่สามารถเคลื่อนที่ได้เหมือนในสัตว์เลี้ยงลูกด้วยนม แต่มีโครงสร้างคล้ายเรียวแหลมอยู่ด้านหน้าของเซลล์อสุจิเรียกว่า spike. โครมาตินมีลักษณะคลี่ออก (decondensed) อย่างสมบูรณ์เนื่องจากผลของการสูญเสียโปรตีน histone และที่ต่างจากเซลล์อสุจิของสัตว์เลี้ยงลูกด้วยนมที่ชัดเจนอีกประการหนึ่งคือ ไม่พบโปรตีนประจุบวก protamine ในนิวเคลียสเลย.

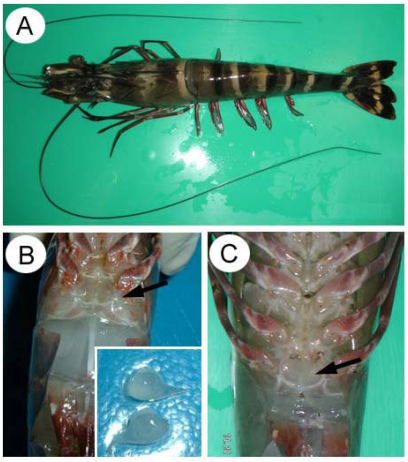


รูปที่ 17 Transmission electron micrographs showing various steps of male germ cells during spermatogenesis (A-H) and spermiogenesis (I-P) in *M. rosenbergii.* (A) Spermatogonia. (B-G) Primary spermatocyte in leptotene stage, zygotene stage, pachytene stage, diplotene stage, diakinesis stage and metaphase stage, respectively. (H) Secondary spermatocyte. (I) Early spermatid. (J) Mid spermatid. (K) Late spermatid. (L-M) Immature spermatozoa. (N) Sperm nucleus showing decondensed (DCh) and condensed chromatin (CCh). (O) Mature sperm showing highly decondensed nucleus. (P) High magnification of mature sperm showing the numerous acrosomal vesicles (AC) nucleus (Nu) and mitochondria (Mi). Nu: Nucleus, Mi: Mitochondria, Sy: Synaptonemal complex, Ri: Ribosome, Hc: Heterochromatin, Ch: Chromatin, rER: Rough endoplasmic reticulum, L: Lamella body, S: spike.

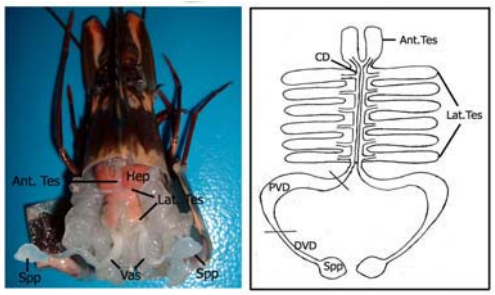
(ดูรายละเอียดในเอกสารหมายเลข 2.19 ในภาคผนวก)

กระบวนการสร้างเซลล์สืบพันธุ์เพศผู้ การเปลี่ยนแปลงโครงสร้างละเอียดของเซลล์อสุจิ และการเปลี่ยนแปลงของโปรตีนในนิวเคลียสที่สัมพันธ์กับการจัดระเบียบของเส้นใยโครมาตินในเซลล์อสุจิของกุ้งกุลาดำ

ระบบสืบพันธุ์ของกุ้งกุลาดำเพศผู้วางตัวอยู่ในส่วนหัวของกุ้ง ประกอบด้วย อัณฑะ (Testis) วางตัวอยู่บนตับ (Hepatopancreas) มีลักษณะแบนคล้ายนิ้วมือแผ่ยื่นออกไปเป็นพูโดยแบ่งออกเป็น พูคู่หน้า 1 คู่ และพูด้านข้าง 6 คู่ ด้านบนของอัณฑะมีหัวใจวางทับอยู่ ทางส่วนท้ายของอัณฑะติดต่อกับท่อนำอสุจิ (Vas deferens) เมื่อกุ้งโตจนถึงวัยเจริญพันธุ์ เซลล์อสุจิจะถูกพัฒนาขึ้นในอัณฑะและส่งผ่านมายังท่อเก็บและนำส่งเซลล์อสุจิ (Vas deferens) ณ ที่นี้ เซลล์อสุจิถูกเคลือบด้วยสารเมือกใสตลอดความยาวของท่อนำเซลล์อสุจิ ท่อนำอสุจินี้มี 1 คู่ซึ่งเป็นท่อยาววางตัวอ้อมไปทางด้านหน้าของตัวกุ้ง ที่ส่วนปลายสุดของท่อนี้พองออกเป็นกระเปาะที่เรียกว่า Spermatophore ซึ่งภายในบรรจุเซลล์อสุจิที่ถูกล้อมรอบด้วยสารเมือก Spermatophore มีสองข้างอยู่ที่บริเวณโคนขาเดินคู่ที่ 5 เมื่อเกิดการผสมพันธุ์ของกุ้งกุลาดำ กุ้งตัวผู้ทำการสอด spermatophore ซึ่งมีเซลล์อสุจิซึ่งถูกหุ้มด้วยสารเมือก (รูปที่ 18, 19) เข้าไปในกุ้งตัวเมียที่ลอกคราบใหม่และยังอยู่ในภาวะเปลือกอ่อน ถุงเซลล์อสุจินี้จะถูกเก็บไว้ระยะหนึ่งในอวัยวะสำหรับเก็บอสุจิของตัวเมียที่เรียกว่า Thelycum (รูปที่ 18) ซึ่งเป็นช่องที่มีฝาปิดที่อยู่บริเวณหน้าอกที่ระหว่างขาเดินคู่ที่ห้าของกุ้งตัวเมีย เมื่อกุ้งตัวเมียพัฒนารังไข่จนถึงระยะสมบูรณ์เต็มที่ แม่กุ้งจะวางไข่โดยปล่อยไข่และเซลล์อสุจิมาผสมกัน หลังจากการปฏิสนธิจะได้ตัวอ่อนของกุ้งในระยะที่เรียกว่า นอร์เพลียส (nauplius)

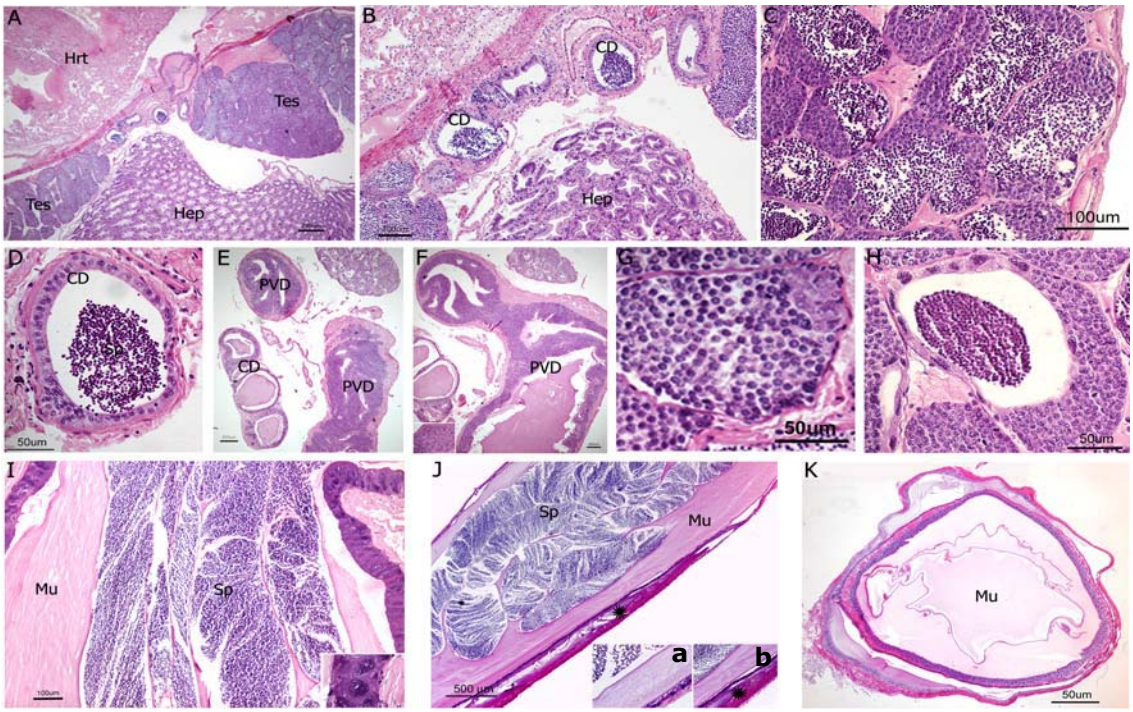


รูปที่ 18 (A) กุ้งกุลาดำ (dorsal view) (B) ตำแหน่งของถุงเก็บอสุจิส่วนปลายในกุ้งกุลาดำเพศผู้ (C) รูปแสดงตำแหน่งของอวัยวะสำหรับเก็บถุงอสุจิในกุ้งกุลาดำเพศเมีย (thelycum)

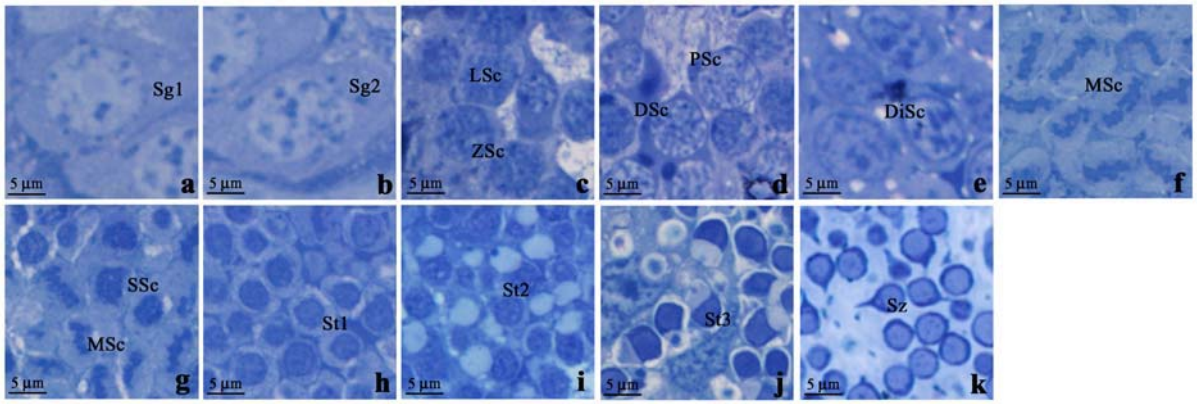


รูปที่ 19 ตำแหน่งและโครงสร้างจำลองของระบบสืบพันธุ์กุ้งกุลาดำเพศผู้ซึ่งอยู่ในส่วนหัวและวางตัวอยู่บนตับ (Hepatopancreas-Hep) อัณฑะ (testis-Tes) มีลักษณะเป็นพูคล้ายนิ้วมือยื่นไปทางด้านหน้า 1 คู่ (anterior lobe-Ant. Tes) และทางด้านข้าง 6 คู่ (lateral lobe-Lat. Tes) บริเวณทางส่วนท้ายของอัณฑะมีท่อนำอสุจิ (vas deferens-Vas) 1 คู่ ส่วนปลายของท่อพองออกเป็นถุงสำหรับเก็บอสุจิส่วนปลาย (spermatophore-Spp) อสุจิจะถูกสร้างจากภายในอัณฑะและส่งต่อมายังท่อนำอสุจิย่อย (collecting duct-CD) และส่งต่อไปยังท่อนำอสุจิ (vas deferens-Vas)

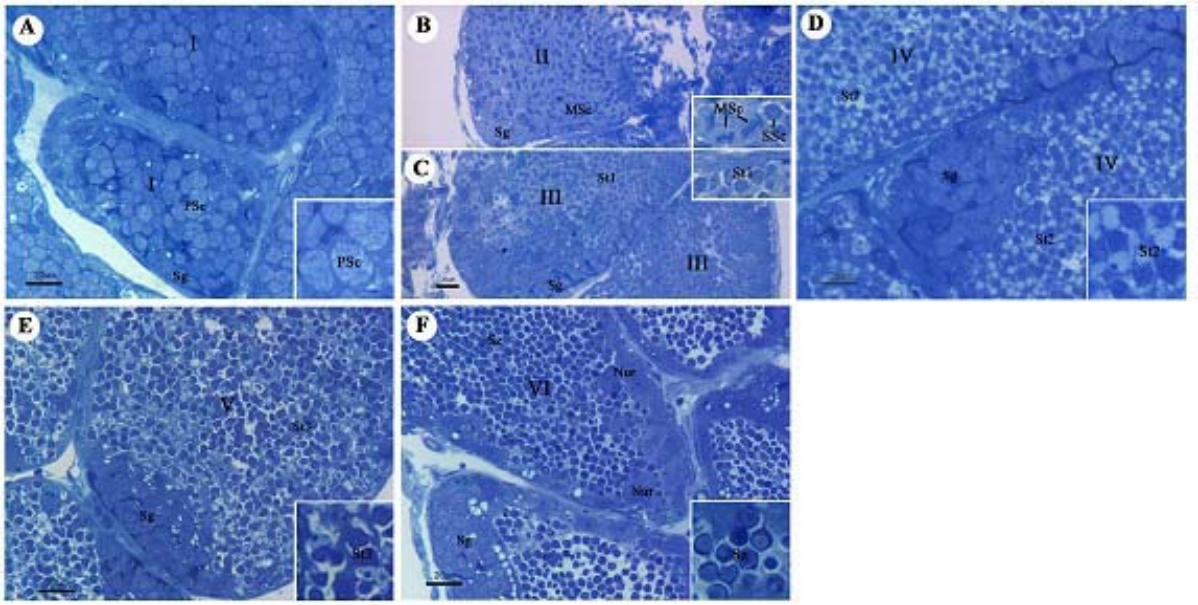
กระบวนการสร้างเซลล์สืบพันธ์เพศผู้นั้น เกิดในอัณฑะภายในท่อสร้างอสุจิ (Seminiferous tubules) ซึ่งมีอยู่มากมายในอัณฑะ เมื่อศึกษาทางจุลกายวิภาคของอัณฑะและท่อนำอสุจิพบว่าสามารถแบ่งเซลล์สืบพันธุ์เพศผู้ได้เป็นระยะต่างๆตามลำดับการพัฒนา โดยใช้ขนาดและลักษณะของเซลล์สืบพันธุ์ รวมถึงลักษณะการขดตัวของเส้นใยโครมาตินที่ปรากฏภายในเซลล์ระยะต่างๆเป็นเกณฑ์ ได้แก่ spermatogonia 2 ขั้น, spermatocyte 6 ขั้น (Leptotene, Zygotene, Pachytene, Diplotene, Diakinetic, Mataphase), spermatid 3 ขั้น, และ เซลล์อสุจิ (Spermatozoa) (รูปที่ 21) นอกจากนี้ยังสามารถแบ่งระยะของท่อสร้างเซลล์อสุจิออกได้เป็น 6 ระยะ ได้แก่ ระยะที่ 1 – ระยะที่ 6 (รูปที่ 22) โดยอาศัยลักษณะของกลุ่มเซลล์ที่ปรากฏอยู่รวมกันภายในท่อ (cellular association) ลักษณะของเซลล์ที่ปรากฏภายในท่อสร้างอสุจิระยะต่างๆนั้นแสดงถึงลักษณะการพัฒนาของเซลล์แบบพร้อมกันทั้งท่อ กล่าวคือภายในส่วนตัดขวางหนึ่งๆของท่อสร้างอสุจิจะพบเซลล์สืบพันธุ์เพศผู้ขั้นเดียวกันเกือบทั้งหมด โดยจะพบกลุ่มของเซลล์ spermatogonia รวมตัวกันอยู่ติดกับผนังท่อสร้างอสุจิ ในระยะที่ 6 ของท่อสร้างอสุจิเซลล์ส่วนใหญ่ที่พบคือเซลล์อสุจิ หลังจากนั้นเซลล์อสุจิจะถูกส่งออกไปยังท่อนำอสุจิย่อย (Collecting duct) ซึ่งจะรวมกันเป็นท่อนำอสุจิ (Vas deferens) ภายในท่อนำอสุจินี้พบว่าเซลล์อสุจิจะถูกล้อมรอบด้วยสารเมือกหนาที่ย้อมติดสีชมพู eosin ท่อนำอสุจินี้มีผนังค่อนข้างหนาในส่วนต้น และบางลงในส่วนปลาย ด้านนอกถูกล้อมรอบด้วยชั้นของกล้ามเนื้อ ที่ส่วนปลายของของท่อพองออกเป็นกระเปาะ spermatophore ซึ่งภายในบรรจุอสุจิที่ฝังอยู่ในสารเมือกที่ย้อมติดสีชมพู ผนังของ spermatophore มีหลายชั้น (รูปที่ 20)



รูปที่ 20 จุลกายวิภาคระบบสืบพันธุ์กุ้งกุลาดำเพศผู้ (A) เนื้อเยื่ออัณฑะ (testis-Tes) ซึ่งอยู่ระหว่างหัวใจ (heart-Hrt) และตับ (hepatopancreas-Hep) (B, D) ท่อนำอสุจิย่อย (collecting duct-CD) ที่อยู่ระหว่างพูซ้ายและขวาของอัณฑะ (C, G-H) ท่อสร้างอสุจิในอัณฑะ (seminiferous tubules) ซึ่งบรรจุด้วยเซลล์สืบพันธุ์เพศผู้ระยะต่างๆ (E, F) ส่วนปลายของท่อนำอสุจิย่อย (collecting duct-CD) และส่วนต้นของท่อนำอสุจิ (proximal vas deferens-PVD) (I) ส่วนต้นของท่อนำอสุจิ (proximal vas deferens-PVD) ภายในบรรจุอสุจิ (Sp) จำนวนมากซึ่งถูกล้อมรอบด้วยสารเมือกที่ย้อมติดสีชมพู (Mu) (J) ส่วนปลายของท่อนำอสุจิ (distal vas deferens-DVD) แสดงส่วนของท่อที่แบ่งออกเป็น primary และ secondary lumen ซึ่งเป็นช่องเล็กบรรจุสารที่ย้อมติดสีชมพูเข้ม (*) ส่วนprimary lumen นั้นบรรจุอสุจิและสารเมือกที่ล้อมรอบ (K) ส่วนตัดขวางของ spermatophore แสดงผนังที่มีหลายชั้น ภายในบรรจุสารเมือก (Mu) ที่ห่อหุ้มอสุจิอยู่ภายใน



รูปที่ 21 ระยะต่างๆของเซลล์สืบพันธุ์เพศผู้ใน semithin sections ของหลอดสร้างอสุจิเซลล์แบ่งเป็นระยะต่างๆ ตามขนาด, ลักษณะเฉพาะของเซลล์, และลักษณะโครมาตินในนิวเคลียส ออกเป็น ขั้นต่างๆคือ Spermatogonium 1-2 (Sg1-2), leptotene (LSc), Zygotene (ZSc), Pachytene (PSc), Diplotene (DSc), Diakinetic (DiSc), Mataphase (MSc), Spermatid 1-3 (St1-3), และ Spermatozoa (Sz).

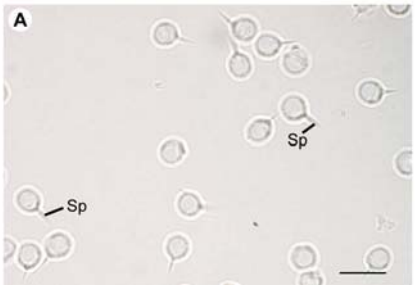


รูปที่ 22 ระยะที่ 1-6 (I-VI) ของท่อสร้างอสุจิ (seminiferous tubules) ใน semithin sections ของอัณฑะ ระยะที่ 1 เซลล์ส่วนใหญ่คือ Pachytene spermatocyte (PSc) ระยะที่ 2 เซลล์ส่วนใหญ่คือ Mataphase spermatocyte (MSc), ระยะที่ 3 เซลล์ส่วนใหญ่คือ spermatid 1 (St1), ระยะที่ 4 เซลล์ส่วนใหญ่คือ spermatid 2 *(St2), ระยะที่ 5 เซลล์ส่วนใหญ่คือ spermatid 3 (St3), และระยะที่ 6 เซลล์ส่วนใหญ่คือ เซลล์อสุจิ (spermatozoa-Sz) ในทุกระยะของท่อสร้างอสุจิจะพบกลุ่มของเซลล์ spermatogonia อยู่ทุกระยะ Nur = nurse cells*

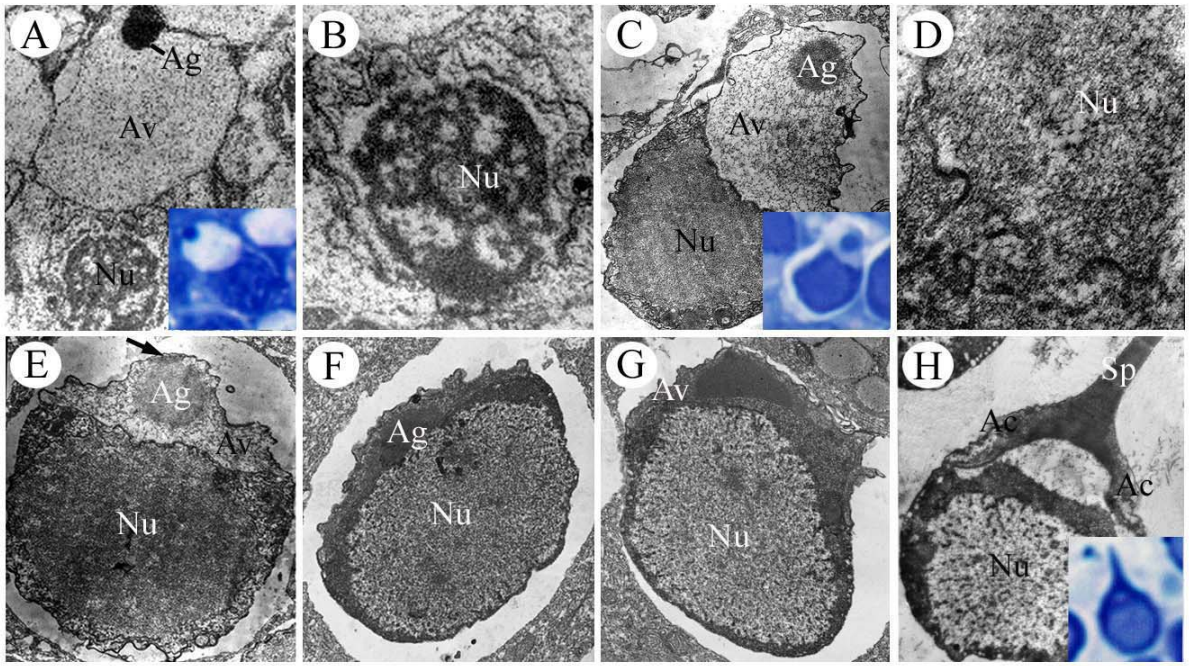
เมื่อศึกษาด้วยกล้องจุลทรรศน์อิเล็กตรอนแบบส่องผ่าน เซลล์อสุจิของกุ้งกุลาดำ มีรูปร่างกลม เส้นผ่านศูนย์กลางประมาณ 7-8 ไมโครเมตร มีส่วนปลายแหลมยื่นออกไปทางด้านหน้า 1 อันเรียกว่า Spike ส่วนตัวของเซลล์อสุจิที่มีลักษณะกลมนั้น ประกอบด้วย นิวเคลียส ที่มีขนาดใหญ่เกือบเต็มเซลล์ ซึ่งบรรจุเส้นใยโครมาตินที่คลี่กระจายออกเต็มนิวเคลียส ส่วนของไซโตรพลาสมที่อยู่โดยรอบนิวเคลียสมีเพียงเล็กน้อย เห็นเป็นเพียงแถบบางๆ เท่านั้น ทางด้านหน้าตรงบริเวณฐานของ spike นั้น มีโครงสร้างคล้ายถุงอยู่ 2 ข้างของ spike ซึ่งเชื่อว่าเป็นถุง acrosome นอกจากนั้น บริเวณใต้ acrosome หรือที่รอยต่อระหว่าง acrosome กับ nucleus มีส่วนของ subacrosome ในเซลล์อสุจิของกุ้งกุลาดำนี้ไม่พบเยื่อหุ้มนิวเคลียส (nuclear envelope) ซึ่งอาจเป็นเพราะเยื่อหุ้มนิวเคลียสได้สลายไปแล้ว เพื่อให้เซลล์อสุจิมีความพร้อม (capacitated) สำหรับการปฏิสนธิกับไข่ (รูปที่ 23-25)

สำหรับการพัฒนาโครงสร้างของเซลล์อสุจินั้น พบว่าในขั้น spermatid เซลล์อสุจิมีการพัฒนาถุง acosome โดยเริ่มต้นจาก acrosomal vesicle ที่บรรจุ acrosomal granule โดยถุง acrosomal vesicle นี้จะมีการวางตัวอยู่ที่ทางด้านหน้าของเซลล์ ที่ทางด้านหน้าสุดของ spermatid ขั้นท้ายๆ มีการพัฒนาส่วนของ spike เริ่มขึ้น นอกจากนี้ยังพบว่าเส้นใยโครมาตินภายในนิวเคลียส มีการคลี่และกระจายออกมากขึ้นจากใน spermatid ขั้นต้นๆ จนถึงขั้น spermatozoa (รูปที่ 24)

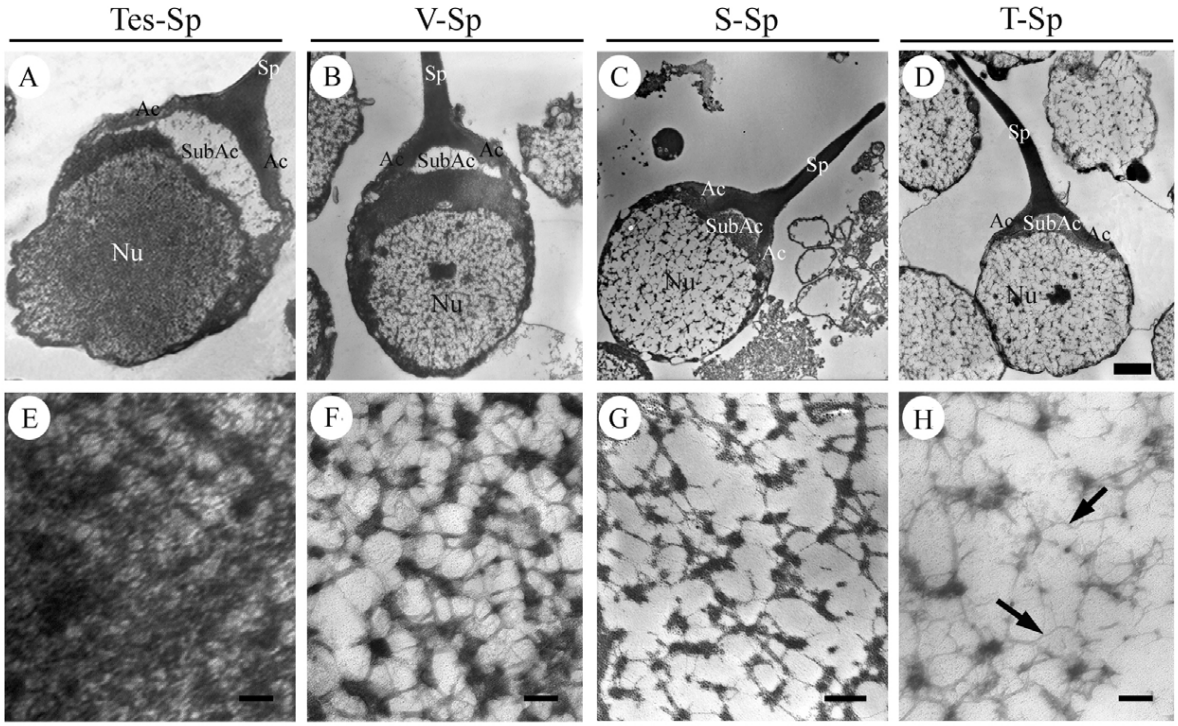
เซลล์อสุจิที่พบในท่อสร้างอสุจิ และภายในท่อนำอสุจิ รวมถึงอสุจิที่พบภายใน thelycum มีลักษณะโครงสร้างที่คล้ายคลึงกันโดยแบ่งได้เป็น 3 ส่วน ได้แก่ 1) ส่วนตัว (main body) มีลักษณะกลมขนาดประมาณ 7-8 ไมโครเมตรและประกอบด้วยนิวเคลียสเป็นส่วนใหญ่ 2) ส่วนอะโครโซม (acrosome) มีลักษณะเป็นถุงอยู่สองข้างของแท่ง spike, และ 3) ส่วนใต้อะโครโซม (subacrosomal) เป็นบริเวณที่อยู่ใต้ต่อถุง acrosome และอยู่เหนือต่อนิวเคลียส เมื่อพิจารณาอย่างละเอียดพบว่าเซลล์อสุจิมีการเปลี่ยนแปลงของโครงสร้างบางส่วนเมื่อเปรียบเทียบเซลล์อสุจิจากภายในท่อสร้างภายในอัณฑะ (testicular sperm), เซลล์อสุจิที่พบภายในท่อนำอสุจิ (vas deferens sperm), เซลล์อสุจิที่พบภายในถุงเก็บส่วนปลาย (spermatophore) และเซลล์อสุจิจากภายใน thelycum ของกุ้งเพศเมีย กล่าวคือ มีการเพิ่มระดับการคลี่และการกระจายของเส้นใยโครมาตินภายในนิวเคลียส นอกจากนี้ยังพบว่าบริเวณ subacrosome ของเซลล์อสุจิที่พบในอัณฑะ, ท่อนำอสุจิ และถุงเก็บส่วนปลาย ยังพัฒนาไม่สมบูรณ์ กล่าวคือยังคงสังเกตเห็นช่องว่างภายในอยู่บ้าง ขณะที่เซลล์อสุจิที่พบใน thelycum ไม่มีช่องว่างอยู่ในส่วน subacrosome (รูปที่ 25)



รูปที่ 23 ลักษณะของเซลล์อสุจิเมื่อดูใต้กล้องจุลทรรศน์ธรรมดา เซลล์มีลักษณะกลมและมี spike (Sp) ยื่นออกไปทางด้านหน้า Bar = 5 μm.



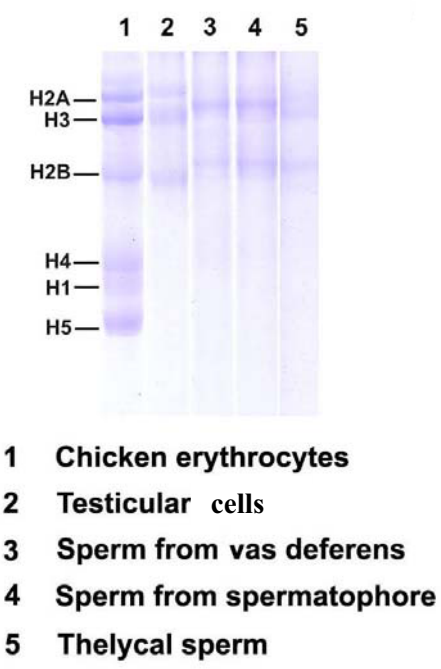
รูปที่ 24 เซลล์สืบพันธุ์เพศผู้ระยะต่างๆ เมื่อถ่ายด้วยกล้องจุลทรรศน์อิเล็กตรอนแบบส่องผ่าน (A-G) Spermatid ระยะต่างๆ (H) เซลล์อสุจิในท่อสร้างอสุจิในอัณฑะ (Testicular spermatozoa) Av = acrosomal vesicle; Ag = anterior granule; Nu = nucleus; SubAc = subacrosomal region; Ac = acrosome; Sp = anterior spike



รูปที่ 25 (A-D) เซลล์อสุจิจากภายในท่อสร้างในอัณฑะ (testicular sperm, Tes-sp), เซลล์อสุจิที่พบภายในท่อนำอสุจิ (vas deferens sperm, V-sp), เซลล์อสุจิที่พบภายในถุงเก็บส่วนปลาย (spermatophoric sperm, S-sp) และเซลล์อสุจิจากภายใน thelycum ของกุ้งเพศเมีย (Thelycal sperm, T-sp) เมื่อดูด้วยกล้องจุลทรรศน์อิเล็กตรอนแบบส่องผ่าน (E-H) รูปเปรียบเทียบเส้นใยโครมาตินของเซลล์อสุจิที่มาจากที่ต่างๆ ลูกศรในรูป H แสดงเส้นใยโครมาตินที่คลี่กระจายออกจนเป็นเส้นบางๆ Bar ในรูป D = 1 μm และ Bar in E-H = 0.1 μm.

จากการเปลี่ยนแปลงทางโครงสร้างละเอียดของเซลล์อสุจิที่พบในแต่ละส่วนของท่อสืบพันธุ์ทั้งในเพศผู้และเพศเมีย กล่าวคือ มีการเพิ่มขึ้นของระดับการคลี่กระจายของเส้นใยโครมาตินภายในนิวเคลียส จากขั้นอสุจิที่อยู่ภายในท่อสร้างเซลล์อสุจิภายในอัณฑะ (testicular sperm), เซลล์อสุจิที่พบภายในท่อนำอสุจิ (vas deferens sperm), เซลล์อสุจิที่พบภายในถุงเก็บส่วนปลาย (spermatophore) และเซลล์อสุจิจากภายใน thelycum ของกุ้งเพศเมีย ตามลำดับ โดยพบว่าในเซลล์อสุจิใน thelycum มีการคลี่กระจายของเส้นใยโครมาตินสูงสุด ดังนั้นจึงมีการศึกษาเพิ่มเติมถึงโปรตีนที่พบอยู่ภายในนิวเคลียสซึ่งสัมพันธ์อยู่กับเส้นใยโครมาตินและอาจอธิบายถึงกระบวนการเปลี่ยนแปลง ของการคลี่กระจายออกของเส้นใยโครมาตินได้ในระดับชีวโมเลกุล โดยการศึกษานี้ได้ใช้วิธีการแยกโปรตีนในนิวเคลียสซึ่งเป็นโปรตีนชนิดประจุบวกจากเซลล์ในอัณฑะ (testicular cells) และ อสุจิที่ได้จากแหล่งต่างๆของทางเดินสืบพันธุ์ของกุ้งกุลาดำทั้งเพศผู้และเพศเมีย คือจาก ท่อนำอสุจิ (vas deferens sperm), ถุงเก็บอสุจิส่วนปลาย (spermatophoric sperm) และจาก thelycum (thelycal sperm) โปรตีนที่สะกัดได้ถูกนำมาแยกในสนามไฟฟ้าบนแผ่นเจล acrylamide แบบ acid-urea acrylamide gel electrophoresis หลังจากนั้นจึงนำไปย้อมด้วยสีย้อมโปรตีน Coomassie blue R-250 และเปรียบเทียบแถบโปรตีนที่ได้กับโปรตีนที่สกัดจากโปรตีนในนิวเคลียสของเม็ดเลือดไก่ (chick erythrocyte) จากการทดลองแสดงว่า เซลล์อสุจิในอัณฑะมีโปรตีน

histone 3 ตัว ที่เทียบเท่ากับโปรตีน histone H2A, histone H2B, และ histone H3 ส่วนเซลล์อสุจิในท่อนำอสุจิ, ถุงเก็บอสุจิส่วนปลาย, และใน thelycum แสดงแถบโปรตีนเพียง 2 แถบที่เคลื่อนช้ากว่า histone H2B และ H3 ของโปรตีนจากเม็ดเลือดไก่ standard (รูปที่ 26) จะเห็นได้ว่าโปรตีน histone ภายในนิวเคลียสของเซลล์อสุจิที่พบในท่อนำอสุจิ, ถุงเก็บอสุจิส่วนปลาย, และใน thelycum มีการเปลี่ยนแปลงทั้งชนิดและมีปริมาณลดลง โดยแถบโปรตีนที่พบในอสุจิจากแหล่งต่างๆเหล่านี้อาจเป็นแค่อนุพันธ์ของโปรตีน histone H2B และ H3 ที่ยังหลงเหลืออยู่ การศึกษานี้แสดงให้เห็นว่าการเปลี่ยนแปลงของโปรตีนชนิดประจุบวกภายในนิวเคลียสของอสุจิอาจเกี่ยวข้องกับการคลี่กระจายออกของเส้นใยโครมาติน เนื่องจากมีโปรตีน histone ซึ่งมีประจุบวกลดลงมาก



รูปที่ 26 โปรตีนประจุบวกจากเซลล์ในอัณฑะ (testicular cells) และ อสุจิที่นำมาจากแหล่งต่างๆของท่อสืบพันธุ์ของกุ้งกุลาดำทั้งเพศผู้และเพศเมีย คือจากท่อนำอสุจิ (vas deferens sperm) ถุงเก็บอสุจิส่วนปลาย (spermatophoric sperm) และจาก thelycum (thelycal sperm)

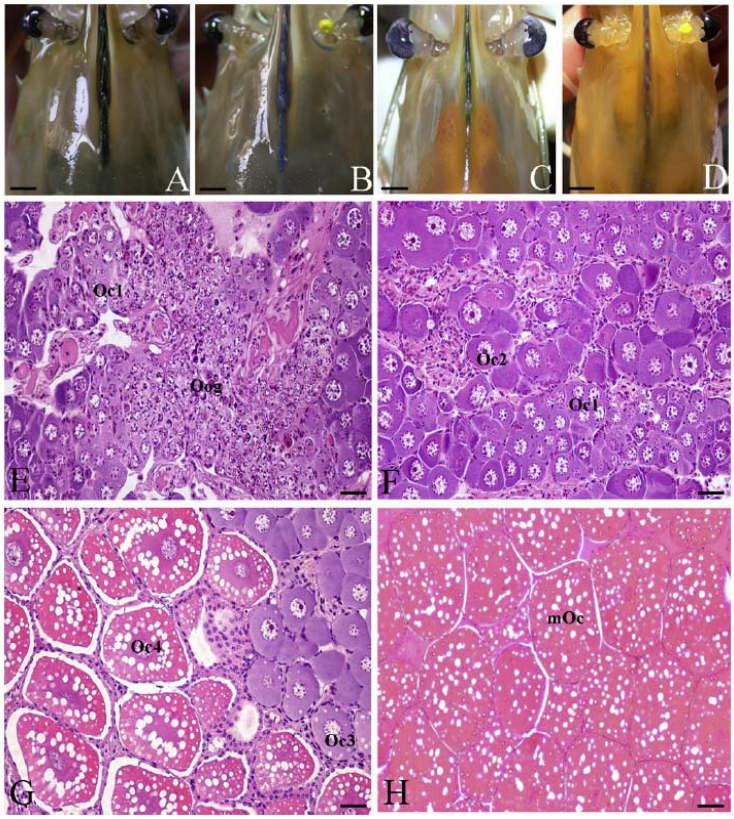
เราพบว่า อสุจิในถุง spermatophore ที่ถูกสอดเข้าไปใน thelycum ของเพศเมียต้องการระยะเวลาบ่มตัวเพื่อเตรียมความพร้อมในการปฏิสนธิกับเซลล์ไข่อย่างน้อย 3 วัน ในระหว่างระยะเวลาดังกล่าว มีการเปลี่ยนแปลงระดับโมเลกุลที่เกิดขึ้นข้างในนิวเคลียสดังที่กล่าวมาแล้วและในไซโทพลาสซึมโดยเฉพาะการเพิ่มปริมาณของ phosphorelated proteins ซึ่งปฏิกิริยาดังกล่าวเป็นส่วนของ sperm capacitation ซึ่งถูกชักนำโดยน้ำทะเลที่มีสารละลายจากเปลือกไข่

หัวข้อที่ 3. การศึกษาโครงสร้างของไข่และการพัฒนาของเซลล์ไข่ในกุ้งก้ามกรามเปรียบเทียบกับกุ้งกุลาดำและกระบวนการปฏิสนธิระหว่างไข่กับอสุจิ

เมื่อศึกษาการพัฒนาของรังไข่และเซลล์ไข่ของกุ้งด้วยวิธีจุลทรรศน์ธรรมดา พบว่ารังไข่ประกอบด้วยพู (lobe) ที่ห่อหุ้มด้วยเยื่อเกี่ยวพันที่แยกรังไข่ออกเป็นพูย่อย (lobules) แต่ละพูย่อยประกอบด้วย follicle ที่มีเซลล์ไข่

ขั้นต่างๆอัดอยู่ โดยเซลล์ไข่ที่กำลังพัฒนาแบ่งออกเป็น 5 ขั้นคือ oogonia (Og) primary oocytes 6 ขั้น และ secondary oocytes 4 ขั้น (Oc_1, Oc_2, Oc_3, Oc_4) วงจรของรังไข่แบ่งออกเป็น 4 ช่วงคือ spawn-spent (Stage I), proliferative (stage II), premature (stage III) และ mature (stage IV) แต่ละระยะมีกลุ่มเซลล์ Oc ที่พัฒนาในระดับขั้นต่างๆ stage I มี Og และ Oc_1 stage II มี Og, Oc_1, Oc_2 stage III มี Og, Oc_2, Oc_3 stage IV มี Oc_4 ส่วนใหญ่และ Og จำนวนน้อย

เซลล์ไข่กุ้งกุลาดำมีขั้นตอนต่างๆคล้ายคลึงกับเซลล์ไข่ของกุ้งก้ามกราม แต่ไข่กุ้งกุลาดำที่สมบูรณ์แล้วมีสารเคลือบไข่ที่มีลักษณะเป็นแท่งๆ (cortical rod) ซึ่งประกอบด้วย สารไกลโคโปรตีนที่มี molecular weight 35-250 kD ซึ่งมีปริมาณน้ำตาลเชิงเดี่ยว mannose สูง (เอกสารอ้างอิงหมายเลข 1) สารเคลือบไข่ดังกล่าวละลายในน้ำทะเลเมื่อไข่ตกออกจากตัวกุ้งซึ่งเรียกว่า egg water (EW) EW มีสารไกลโคโปรตีนและเอนไซน์ trypsin ที่สามารถกระตุ้นการเกิดปฏิกิริยา acrosome reaction ในเซลล์อสุจิได้

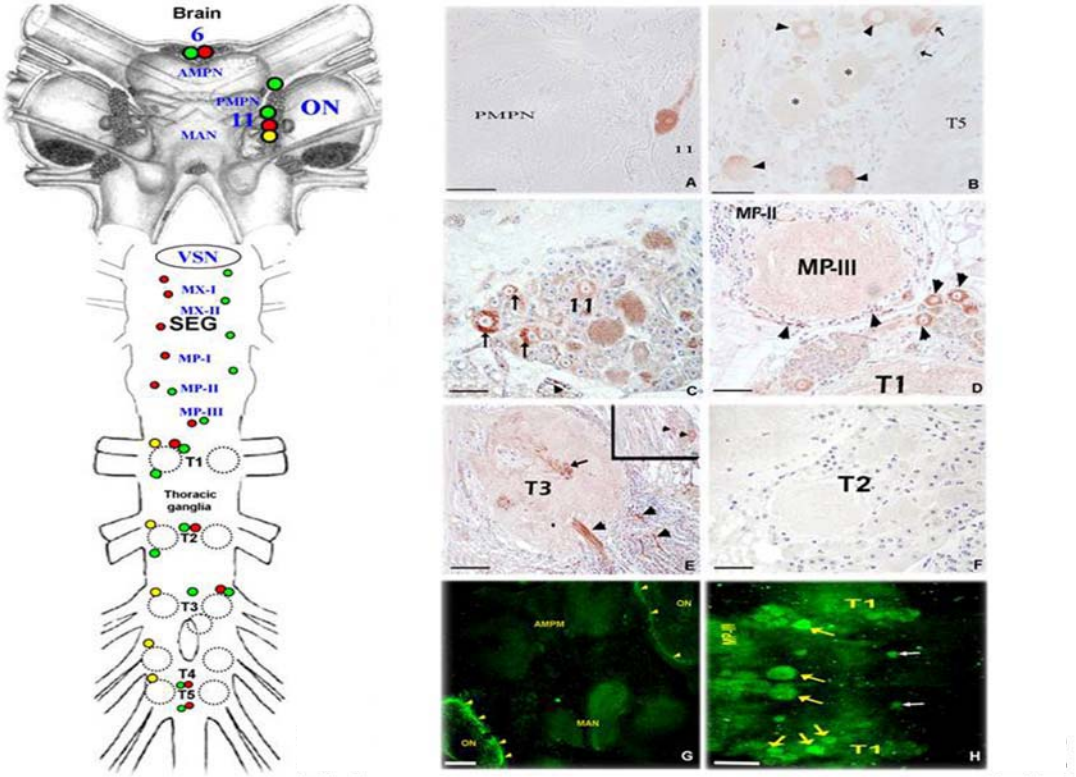


รูปที่ 27 Top views of female giant freshwater prawn, M. rosenbergii, showing ovary at various stages: (A) stage I, (B) stage II, (C) stage III, (D) stage IV. (E–H) Light micrographs of H&E-stained ovarian sections showing histology of various stages of ovarian cycle (I–IV) and steps of oocyte development. Oog, oogonia; Oc1, early previtellogenic oocyte; Oc2, late previtellogenic oocytes; Oc3, early vitellogenic oocytes; Oc4, late vitellogenic oocytes; mOc, mature oocytes (classified according to Meeratana and Sobhon 2007). Scale bars = 1 cm (A–D). Scale bars = 50 lm (E–H).

(ดูรายละเอียดในเอกสารหมายเลข 1.6, 1.7, 1.8 ในภาคผนวก)

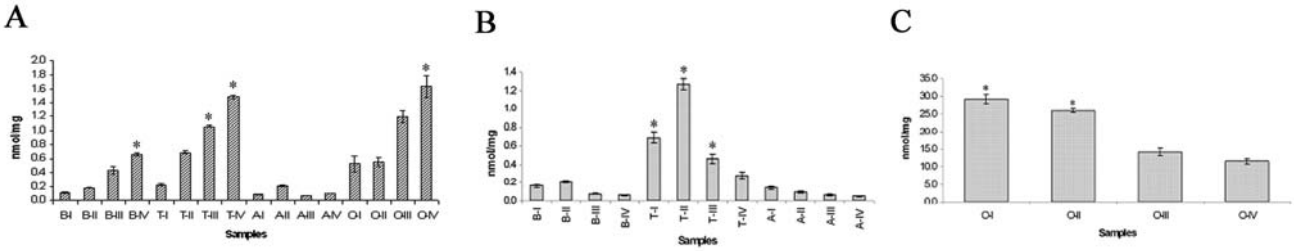
หัวข้อที่ 4 การวิเคราะห์การกระจายและวัดระดับของสารสื่อประสาทเซโรโทนิน (5-HT) โดปามีน (DA) ออกโตปามีน (OA) ในระบบประสาทและรังไข่กุ้งโดยวิธี immunocytochemistry (ICC) และ high performance liquid chromatography (HPLC)

จากการใช้กรรมวิธี ICC และ HPLC พบว่ามี 5-HT และ DA กระจายอยู่ในเซลล์ประสาทและใยประสาทที่อยู่ในปมประสาททั่วระบบประสาทส่วนกลางทุกอัน โดยมีจำนวนเซลล์ประสาทที่บรรจุ 5-HT และ DA มากเป็นพิเศษในสมอง (supraesophageal ganglion) และปมประสาทอก (thoracic ganglion) (รูปที่ 28 และ 29 และเมื่อทำการวัดปริมาณของสารสื่อประสาททั้งสองด้วยวิธี HPLC พบว่า 5-HT มีปริมาณเพิ่มขึ้นตามช่วงของการพัฒนาของรังไข่ ส่วน DA มีปริมาณลดลงสวนทางกับ 5-HT ทั้งในสมอง ปมประสาท thoracic และรังไข่ (รูปที่ 30)



รูปที่ 28 ภาพวาดแสดงการกระจายของเซลล์ที่บรรจุสารสื่อประสาท 5HT (สีเขียว) และ DA (สีแดง) และฮอร์โมน **GnRH (**สีเหลือง) ในปมประสาทต่างๆของระบบประสาทของกุ้ง AMPN-anterior medial protocerebral neuropil; PMPN-posterior medial protocerebral neuropil; MAN-medial antenna I neuropil; ON-olfactory neuropil**;** VSN-visceral sensory neuropil; MX-I-maxilla-I; MX-II-maxilla-II; MP-I, maxiliped-I; MP-II, maxiliped-II; MP-III, maxiliped-III.

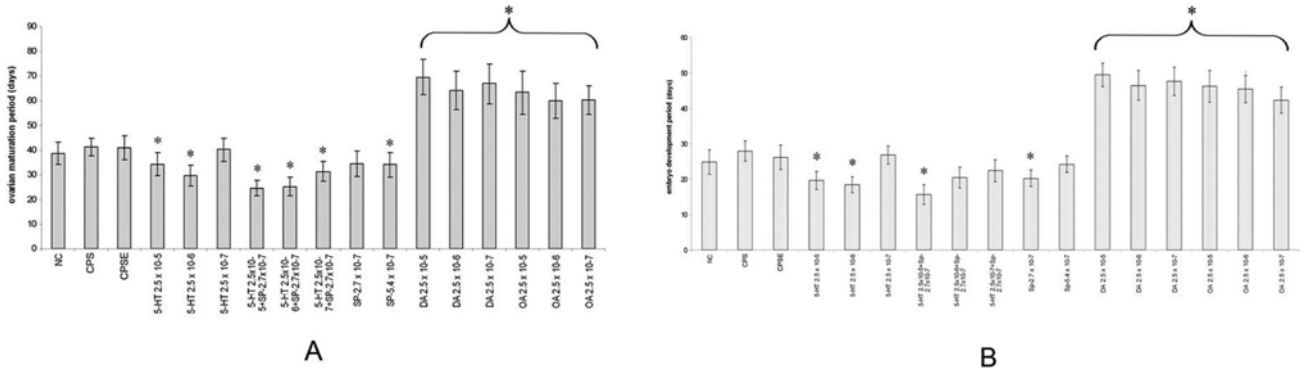
รูปที่ 29 Light micrographs of immunoperoxidase and immunofluorescence detections of 5-HT and DA in the CNS of mature female *M. rosenbergii* as illustrated in the diagram on the left (5-HT, green dot; DA, red dot; GnRH, yellow dot) **(A)** 5-HT-immunoreactive neuron in cluster 11 **(B)** 5-HT-immunoreactive neurons in T5 **(C)** DA-immunoreactive neurons in cluster 11 **(D)** DA-immunoreactive neurons in SEG and T1 **(E)** DA-immunoreactive fibers running out of T3 and DA-neurons in T3 (inset) **(F)** The negative control **(G)** Immunofluorescence detections of DA-immunoreactive fibers in olfactory neuropil **(H)** DA-immunoreactive neurons in SEG and T1



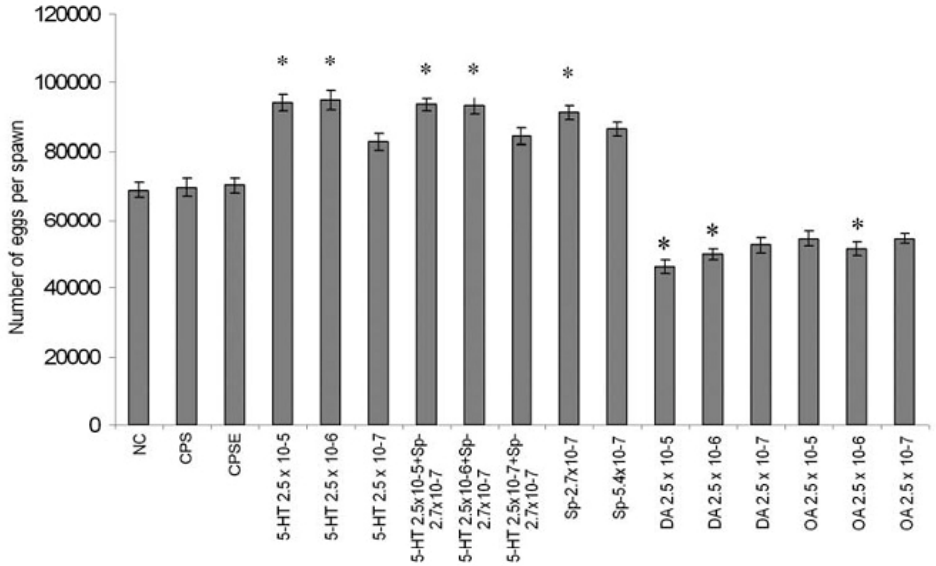
รูปที่ 30 Histogram illustrating the analysis of levels of 5-HT and DA in CNS of *M. rosenbergii* female by HPLC (A) the changing concentrations of 5-HT in the brain, thoracic ganglion, abdominal ganglion, and ovary. (B) the changing of concentrations of DA in the brain, thoracic ganglion, and abdominal ganglion. (C) the changing of concentrations of DA in the ovary. The concentration is expressed as nmol/mg of protein in the organ extract. Numbers are mean ± S.E.M. B-I to IV, T-I to IV, A-I to IV, and O-I to IV are the brain, thoracic ganglion, abdominal ganglion, and ovary at stages I to IV.

หัวข้อที่ 5. การศึกษาผลกระตุ้นการพัฒนาของรังไข่กุ้งด้วยสารสื่อประสาท 5-HT และ DA

เมื่อทำการฉีดแม่พันธุ์กุ้งด้วย 5-HT, DA antagonist (spiperone-SP) และออกโทพามีน (OA) ทำให้รังไข่พัฒนาเร็วขึ้นกว่าปกติมากเมื่อเทียบกับกลุ่มควบคุม (รูปที่ 31A) และมีการปล่อยไข่ออกมาซึ่งมีปริมาณและคุณภาพเหมือนสภาพปกติ (รูปที่ 32) นอกจากนั้นยังทำให้ระยะการพัฒนาของเอ็มบริโอลดลงด้วย (รูปที่ 31B)



รูปที่ 31 (A) Ovarian maturation period of *M. rosenbergii* (defined as the time for ovarian development from ovarian stage I to spawning). **(B)** Embryonic developmental period (defined as the time for egg development from spawning to black egg stage), after injections with various doses of 5-HT, DA, OA, SP, and 5-HT plus SP, when compared with the control groups (NC, CPS, CPSE). The numbers indicate doses of chemicals in various groups in mol/prawn for 5-HT, DA, OA, 5-HT plus SP, and SP alone. Asterisks indicate significant differences ($P<0.05$) with respect to the control groups; one asterisk indicates significantly shorter/longer OMP and EMP periods than control groups.

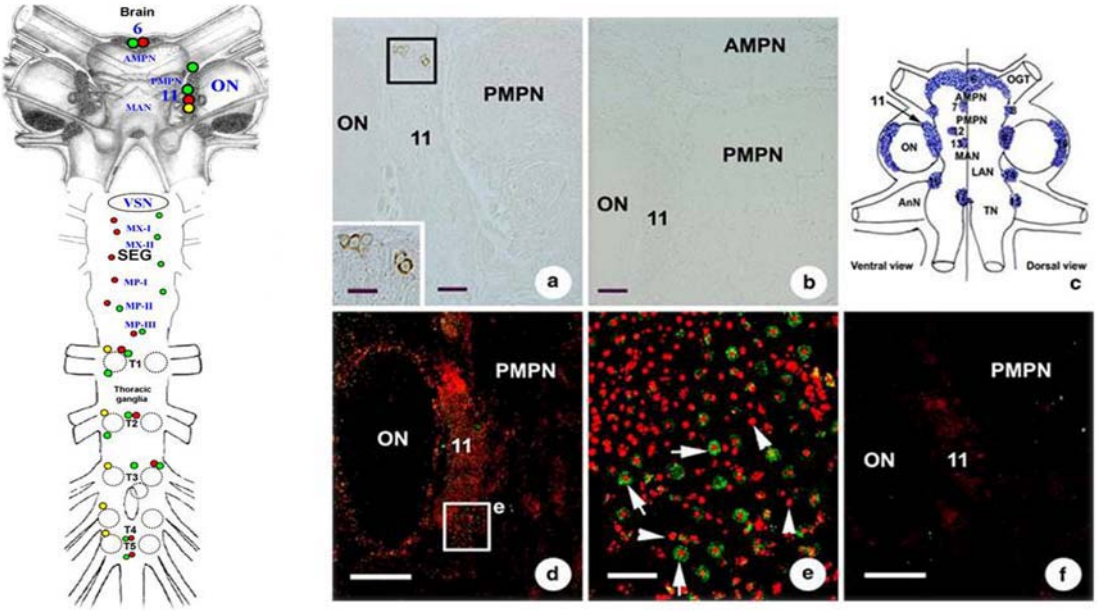


รูปที่ 32 Number of eggs per spawn, after injection with various doses of 5-HT, DA, OA, SP, and 5-HT plus SP, when compared to the control groups. Asterisks indicate significant differences ($P<0.05$) when compared to the control groups.

(ดูรายละเอียดในเอกสารหมายเลข 1.22 ในภาคผนวก)

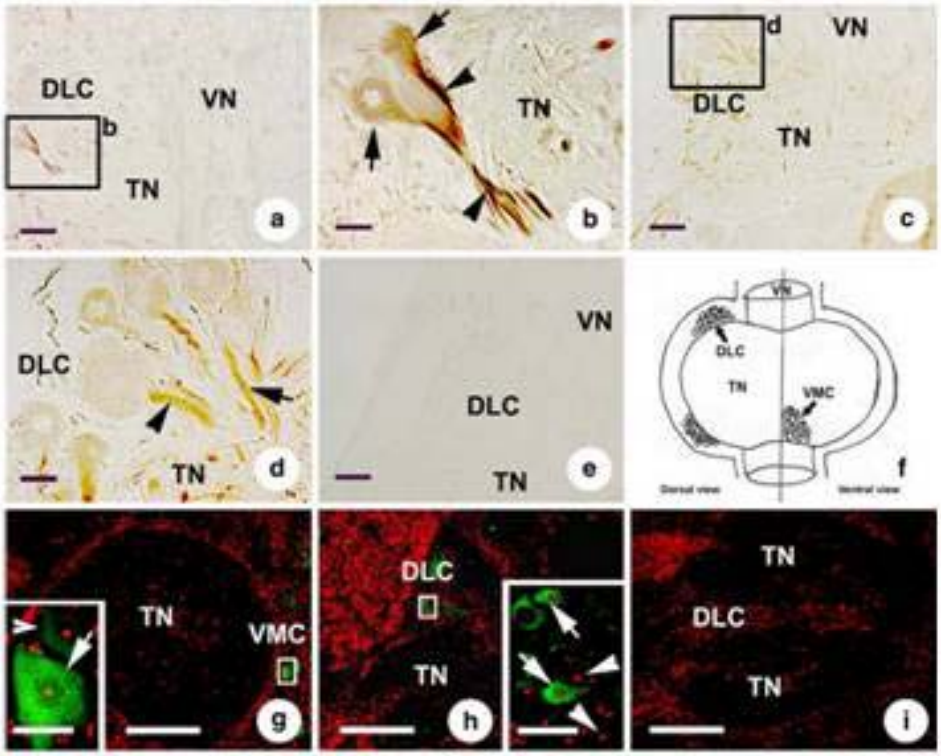
หัวข้อที่ 6. การวิเคราะห์การกระจายของฮอร์โมน gonadotropin-releasing hormone (GnRH) และ egg-laying hormone (ELH) โดยวิธี immunocytochemistry (ICC)

จากการใช้กรรมวิธี ICC พบว่า มี GnRH 3 isotypes ที่มีคุณลักษณะคล้าย lamprey GnRH III (lGnRHIII), octopusGnRH (OctGnRH) และ tunicateGnRH (tGnRH) ในปมประสาทต่างๆ ของระบบประสาทส่วนกลาง โดยในส่วน deutocerebrum ของปมประสาท supraesophageal ganglion หรือ brain มี isotype ที่คล้ายกับ lGnRHIII ในปมประสาท thoracic ganglion มี isotype ที่คล้ายกับ OctGnRH และ tGnRH (รูปที่ 33, 34, 35) ในขณะที่รังไข่มี isotype ที่คล้ายกับ lGnRHI (รูปที่ 36) ส่วนการใช้วิธี ICC วิเคราะห์หาการกระจายของฮอร์โมน ELH พบว่าฮอร์โมนชนิดนี้มีอยู่ทั้งในระบบประสาทกลางในส่วนสมองซึ่งมีจำนวนน้อย (รูปที่ 37) แต่มีจำนวน ELH เซลล์ในรังไข่จำนวนมาก (รูปที่ 36 และ 37)

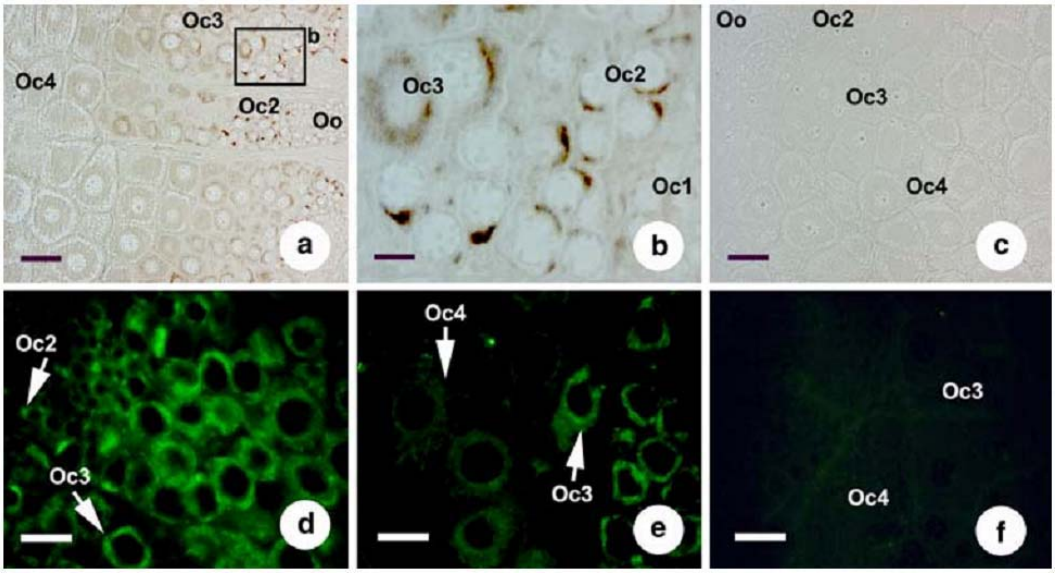


รูปที่ 33 Diagram illustrating the distribution of GnRH in the CNS of mature female freshwater prawn, *M. rosenbergii* (5-HT, green dot; DA, red dot; GnRH, yellow dot). AMPN-anterior medial protocerebral neuropil; PMPN-posterior medial protocerebral neuropil; MAN-medial antenna I neuropil; ON-olfactory neuropil**;** VSN-visceral sensory neuropil; MX-I-maxilla-I; MX-II-maxilla-II; MP-I, maxiliped-I; MP-II, maxiliped-II; MP-III, maxiliped-III.

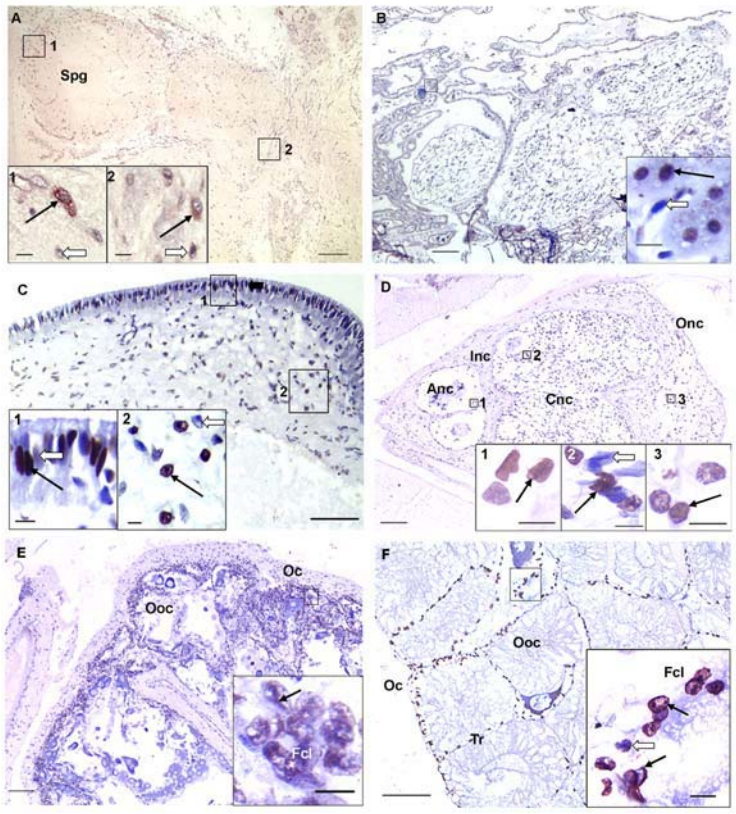
รูปที่ 34 Immunoperoxidase **(a-b)** and immunofluorescence **(d-f)**, showing the distribution of ir-lGnRH-III in the prawn supraesophageal ganglion. **(a)** The ir-lGnRH III is present in neuronal cell bodies within cluster11 of the deutocerebrum. (a, inset) Higher magnification of boxed area in (a), showing the ir-lGnRH-III in neuronal cell bodies of medium-sized neurons. **(b)** Negative control section of immunoperoxidase, using lGnRH-III-preabsorbed antiserum as a probe, showing no ir-lGnRH-III. **(c)** A diagram showing the locations of neuronal cell clusters as numbered in the supraesophageal ganglion (modified from Sandeman et al. 1992). **(d)** Immunofluorescence showing the ir-lGnRH-III neuronal cell bodies in cluster 11. **(e)** Higher magnification of the boxed area in (d), revealing the ir-lGnRH-III in medium-sized neuronal cell bodies (arrows). There was no ir-lGnRH-III in some neuronal cells within the same cluster (arrowheads). **(f)** Negative control section of immunofluorescence using lGnRH-III-preabsorbed antiserum as a probe, showing no immunoreactivity. AMPN anteriormedial protocerebral neuropil, AnN antenna II neuropil, LAN lateral antenna I neuropil, MAN medial antenna I neuropil, PMPN posterior medial protocerebral neuropil, OGT olfactory globular tract, ON olfactory neuropil, TN tegumental neuropil. Scale bars:100 µm(a and b);300 µm (d and f);30 lm (e);25 µm (a, inset)



รูปที่ 35 Immunoperoxidase **(a-e)** and immunfluorescence **(g-i)**, showing the distribution of ir-octGnRH in the prawn thoracic ganglia. **(a)** The ir-octGnRH is present in medium-sized neuronal cells in the dorsolateral neuronal cell cluster (DLC). **(b)** Higher magnification showing the ir-octGnRH in the soma of neuronal cells (arrows) and fibers (arrowheads) extending from the soma. **(c)** and **(d)** Light micrographs showing the ir-octGnRH positive fibers innervating medium-sized (d, arrow) and large-sized (d, arrowhead) neuronal locations of neuronal cell clusters in the thoracic ganglion. **(e)** Negative control using octGnRH-preabsorbed antiserum as a probe, revealing only background staining. **(f)** A diagram showing the locations of neuronal cell clusters in the thoracic ganglion. **(g)** and **(h)** showing the ir-octGnRH in the soma of some large-sized neuronal cells in ventromedial neuronal cell cluster (VMC) (g and inset, arrow) and in medium-sized neuronal cells in DLC (h and inset, arrows). However, some neuronal cells with in the same cluster show no ir-octGnRH (g and h, insets, arrowheads). **(i)** Negative control section of immunofluorescence using octGnRH-preabsorbed antiserum as a probe, showing only nuclear staining. TN thoracic neuropil, VN ventral nerve cord. Scale bars100 µm (a, c and e); 25 µm (b and d); 300 µm (g, h and i); 30 µm (g and h, insets) cells.



รูปที่ 36 Immunoperoxidase **(a-c)** and immmunofluorescence **(d-f)** showing the distribution of ir-lGnRH-I in the prawn ovary. Their- lGnRH-I is present in Oc2 and Oc3 oocytes (**a** and **d**). Higher magnification showing the ir-lGnRH-I localized at the perinuclear region of Oc2 and in the cytoplasm of Oc3 (**b**, **d**, and **e**).Negative control sections of immunoperoxidase **(c)** and immunofluorescence **(f)** using lGnRH-I-preabsorbed antiserum as a probe, showing only background staining. Oo oogonia, Oc2 oocyte stage 2 (late previtellogenic oocyte), Oc3 oocyte stage3 (early vitellogenic oocyte), Oc4 oocyte stage4 (late vitellogenic oocyte). Scale bars: 100 μm (**a** and **c**); 25 μm (b); 50 μm (**d**, **e** and **f**)



รูปที่ 37 Immunodetection of ELH in *P. monodon* cephalothoracic region and abdominal nerve tract. Detection used a primary antibody of polyclonal mouse anti-abalone ELH, a secondary of monoclonal biotinylated goat anti-mouse IgG, and visualisation using an avidin-HRP conjugate combined with a NovaRED substrate. Black arrows indicate positive cells under high magnification (insets of designated low power regions), whereas white arrows show negative cells. **A** is the cephalothoracic region showing the supraesophageal ganglion (Spg) and two locations of neurosecretory ELH positive cells. **B** is the antennal gland showing ELH positive cells. **C** is the dorsal cephalothoracic region posterior to the Spg, with high power insets showing ELH positive cells. **D** is the major abdominal nerve tract showing the appendage nerve cord (Anc), central nerve cord (Cnc), inner nerve capsule (Inc), and outer nerve capsule (Onc), with high power insets showing ELH positive cells. Scale bars 100 μm in A-C, 10 μm in insets. ELH immunodetection in female shrimp ovaries at different reproductive stages, using the same technique as used in Fig.37A-D. Arrows indicate positive cells. **E** is a Stage I shrimp ovary showing ovarian capsule (Oc) and oocytes (Ooc), with high magnification of ELH positive follicular cells (Fcl). **F** is a Stage IV shrimp ovary surrounded by a capsule (Oc) and showing fully mature oocytes (Ooc), and trabachulae (Tr), with high magnification of ELH positive Fcl. Scale bars 100 μm in A-C, 10 μm in insets.

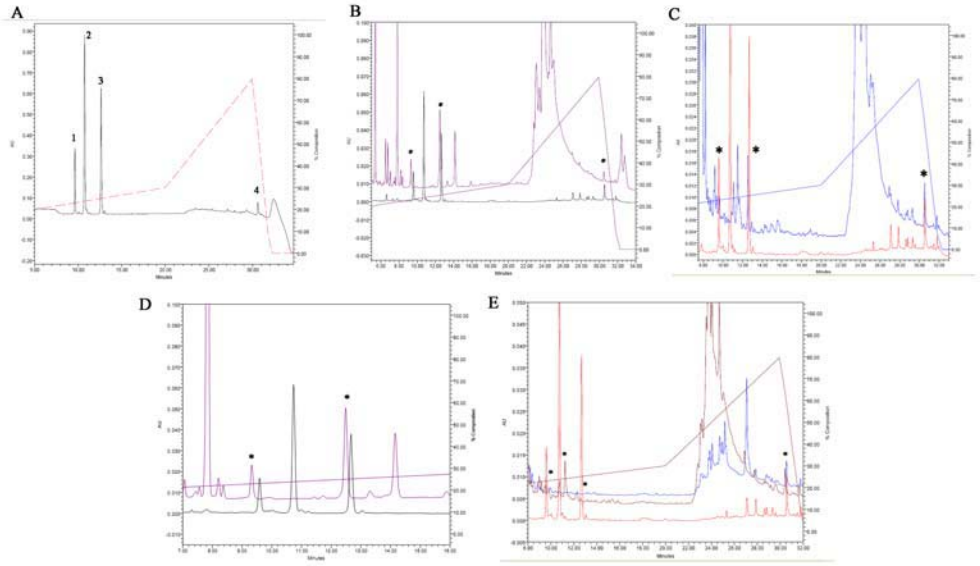
(ดูรายละเอียดในเอกสารหมายเลข 1.4, 1.10, 1.11, 1.12, 1.23 ในภาคผนวก)

หัวข้อที่ 7. วิเคราะห์คุณลักษณะของฮอร์โมน GnRH และ ELH โดยวิธี high performance liquid chromatography (HPLC)

เมื่อวิเคราะห์หาคุณลักษณะและปริมาณของฮอร์โมน GnRH และ ELHโดยวิธี HPLC พบว่า มี GnRH ถึง 3 isotypes ในปมประสาทและต่อมเพศเช่นกัน (รูปที่ 38) โดยมี lamprey I GnRH (lGnRHI) ใน brain และ thoracic ganglion ส่วน octopus GnRH (octGnRH) และ tunicate GnRH (tGnRH) พบมากในปมประสาท thoracic ganglion และนอกจากนี้ยังสามารถพบ octGnRH และ tGnRH ในต่อมเพศทั้งรังไข่และต่อมอัณฑะ ส่วน lGnRHI พบปริมาณเล็กน้อย ส่วน ELH สามารถพบได้ทั้งในระบบประสาทส่วนกลางและต่อมเพศของกุ้งทั้งเพศผู้และเพศเมีย (ตารางที่ 6)

ตารางที่ 6 แสดงการปรากฏของ GnRH และ ELH ในระบบประสาทส่วนกลางและต่อมเพศของกุ้งเพศผู้และเพศเมีย จากการตรวจหาปริมาณด้วยวิธี HPLC

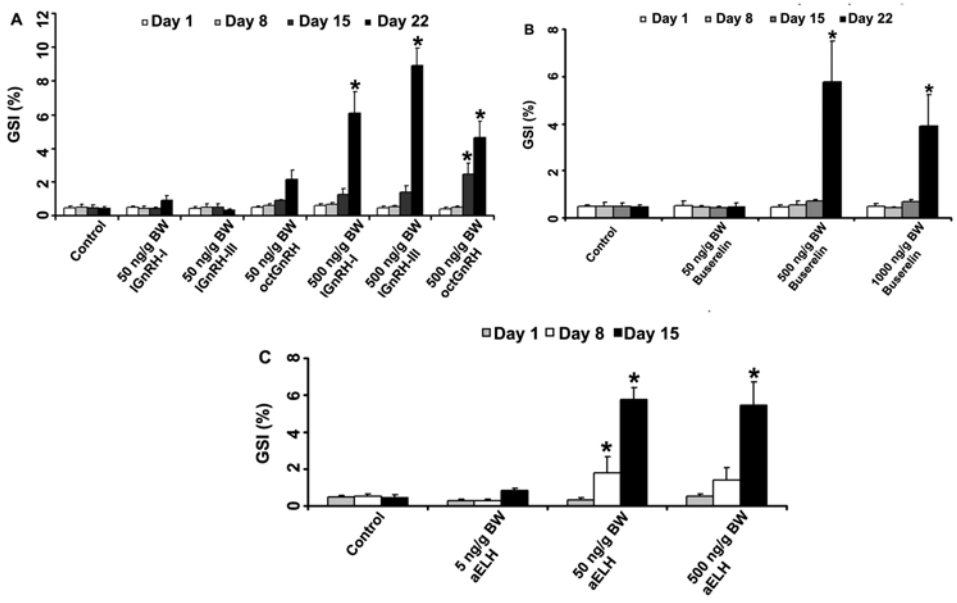
Neuropeptide & Neurohormone	Male				Female			
	Brain	Thoracic ganglion	Abdominal ganglion	Testis	Brain	Thoracic ganglion	Abdominal ganglion	Ovary
Octopus-GnRH	+	+++	+	+++	+	+++	-	++
Tunicate-GnRH	+	++	-	+++	+	++	-	++
Lamprey I GnRH	+++	+	+	-	++	+++	-	-
ELH	+	+++	++	++	+	+++	++	++



รูปที่ 38 (A) HPLC chromatograms of (A) standards at 1.0 ml/min flow rate. (1) Octopus GnRH ; (2) Lamprey I GnRH. ; (3) Tunicate GnRH; (4) abalone ELH extracts of brain **(B,** purple**)**, thoracic ganglion **(C,** dark blue**)**, and testis **(D,** purple**)** from mature male **(E)** The thoracic ganglion (brown) and ovary (blue) from female, *Macrobrachium rosenbergii*. Asterisks show the GnRH and ELH positive peaks.

หัวข้อที่ 8. ทดสอบการกระตุ้นพัฒนาการของรังไข่กุ้งด้วยฮอร์โมน GnRH, ELH และ methyl farnesoate (MF)

เมื่อทำการฉีดกระตุ้นพัฒนาการของรังไข่กุ้งแม่พันธุ์ทั้งกุ้งกุลาดำและกุ้งก้ามกรามด้วย GnRH, ELH และ MF ทำให้รังไข่พัฒนาเร็วขึ้นกว่าปกติมากเมื่อเทียบกับกลุ่มควบคุม อีกทั้งแม่กุ้งที่ได้รับฮอร์โมนมีการปล่อยไข่ออกมาซึ่งมีปริมาณและคุณภาพเหมือนสภาพปกติ (รูปที่ 39)



รูปที่ 39 GSI values at day 1, 8, 15 and 22 post-treatments. A: The prawns were treated with GnRHs (GnRH-I, lGnRH-III and octGnRH) at dose of 50 and 500 ng/g BW. B: The prawns were treated with GnRHa (buserelin) at doses of 50, 500 and 1,000 ng/g BW. C: The prawns were treated with aELH at doses of 5, 50 and 500 ng/g BW. Values were represented as mean ± S.D. Asterisks indicated significant differences *($p \leq 0.05$)* comparing to the control.

Groups	Treatments	Number of shrimp	Doses (ng/g BW)	Period of maturation (days)	% of spawners	Number of % eggs/spawn	% Fertilization
Eyestalk-ablated groups							
1	NS	7	–	7.43±0.98	100	$0.98\times10^6\pm4.59\times10^5$	84.53±3.55
2	sGnRH	7	10	6.00±0.82	100	$0.94\times10^6\pm2.26\times10^5$	-
3	sGnRH	7	50	4.29±1.38*	100	$0.95\times10^6\pm2.59\times10^5$	79.91±7.09
4	LHRH	7	10	6.14±1.21	100	$0.86\times10^6\pm1.53\times10^5$	-
5	LHRH	7	50	4.43±0.79*	100	$0.91\times10^6\pm4.24\times10^5$	81.57±4.51
6	lGnRH-I	7	50	4.00±0.82*	100	$0.89\times10^6\pm1.41\times10^5$	82.07±7.17
Eyestalk-intact groups							
7	NS	7	-	34.50±5.00	57.14	$1.15\times10^6\pm1.37\times10^5$	80.13±6.16
8	sGnRH	7	500	23.20±2.59*	71.43	$1.06\times10^6\pm2.81\times10^5$	81.26±4.78
9	lGnRH-I	7	500	22.80±2.17*	71.43	$1.01\times10^6\pm1.37\times10^5$	82.00±3.98

Note: * means statistically difference between control and GnRH-treated groups at $P<0.05$.
NS, normal saline.

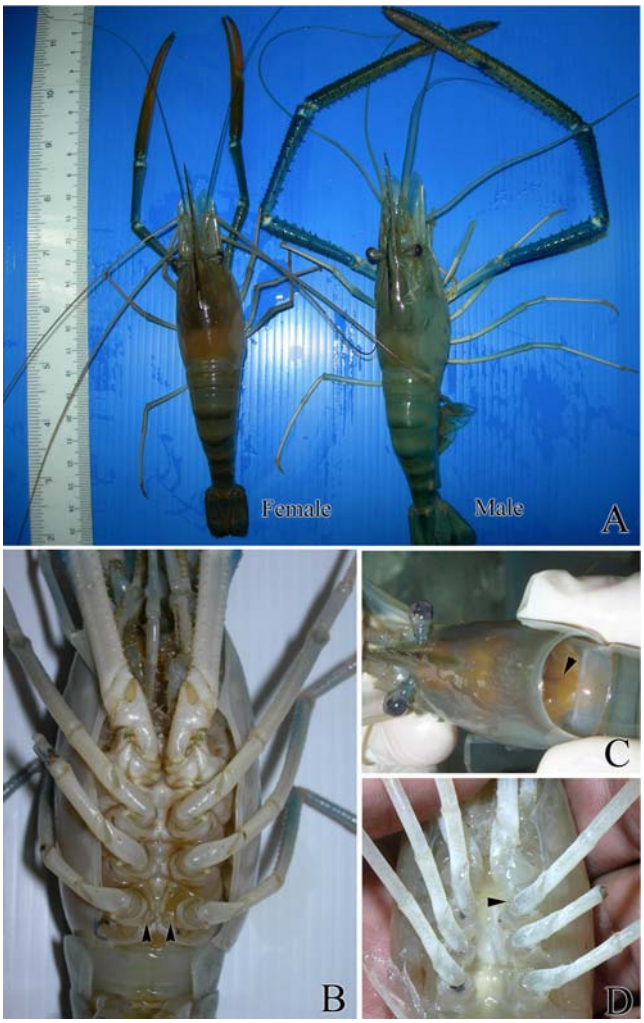
ตารางที่ 7 Effect of GnRHs on the period of ovarian maturation, quantity of spawned eggs, and fertilization

เมื่อทำการฉีดแม่กุ้งก้ามกรามด้วย methyl farnesoate ที่ 0.1 µg/gm น้ำหนักตัว พบว่า แม่กุ้งมีการพัฒนารังไข่เร็วขึ้นประมาณ 7 วัน แต่การออกฤทธิ์ของ MF ไม่มากเท่ากับการฉีด GnRH และ ELH

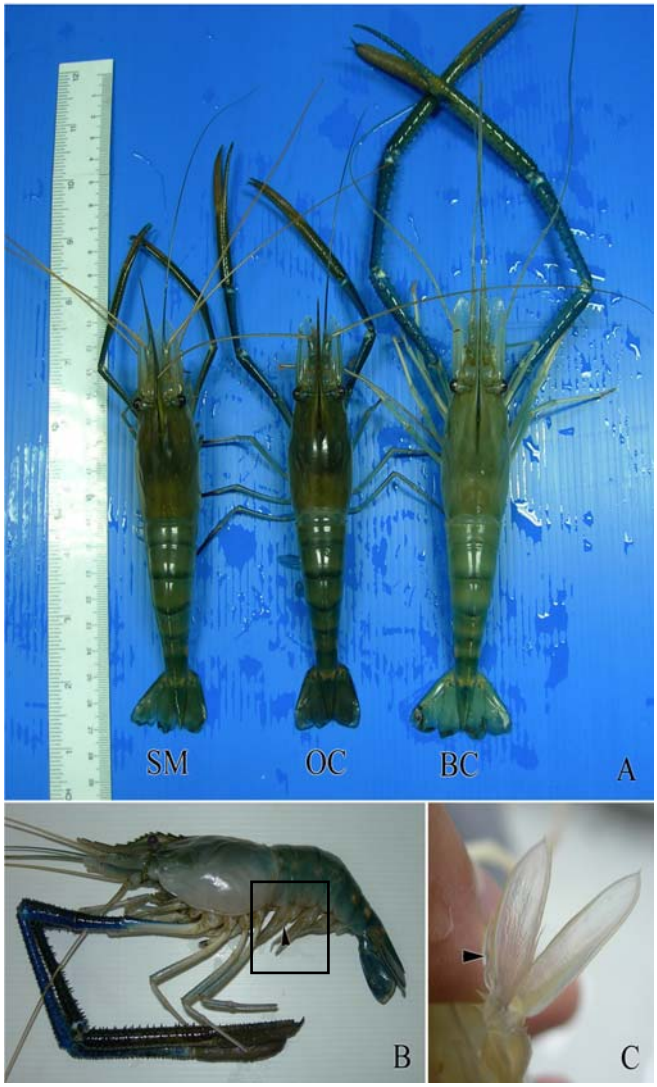
(ดูรายละเอียดในเอกสารหมายเลข 1.12 ในภาคผนวก)

หัวข้อที่ 9. การศึกษาโครงสร้างและเซลล์ในต่อมเพศผู้(Androgenic gland) ของกุ้งก้ามกราม

กุ้งก้ามกรามตัวผู้จะมีขนาดใหญ่กว่าเพศเมียและมีก้ามขนาดใหญ่สีฟ้า ในกุ้งก้ามกราม เพศเมียมีปลายเปิดของท่อนำไข่ที่โคนขาคู่ที่สาม ใน เพศผู้มีปลายเปิดของท่อนำสเปิร์ม(gonopore) อยู่ที่ด้านในโคนขาคู่ที่ห้า (รูปที่ 40) ด้านในของท่อเป็นทางเดินของสเปิร์มที่โป่งออก มีต่อมแอนโดรเจนนิดวางตัวอยู่ด้านบน ฮอร์โมนที่สร้างจากต่อมเพศนี้ กระตุ้นให้กุ้งเพศผู้สร้าง แอบเพนดิกมัสคูลิไน(Appendage masculine) บนขาว่ายน้ำคู่ที่สอง ซึ่งเป็นสิ่งแสดงออกลักษณะทางเพศชาย (รูปที่ 41) มีรายงานที่แสดงว่าต่อมแอนโดรเจนนิคเป็นต่อมที่สร้างฮอร์โมนเพศผู้ในสัตว์หลายประเภท รวมทั้ง ครัสตาเซียน แอมฟีพอด และไอโซพอด



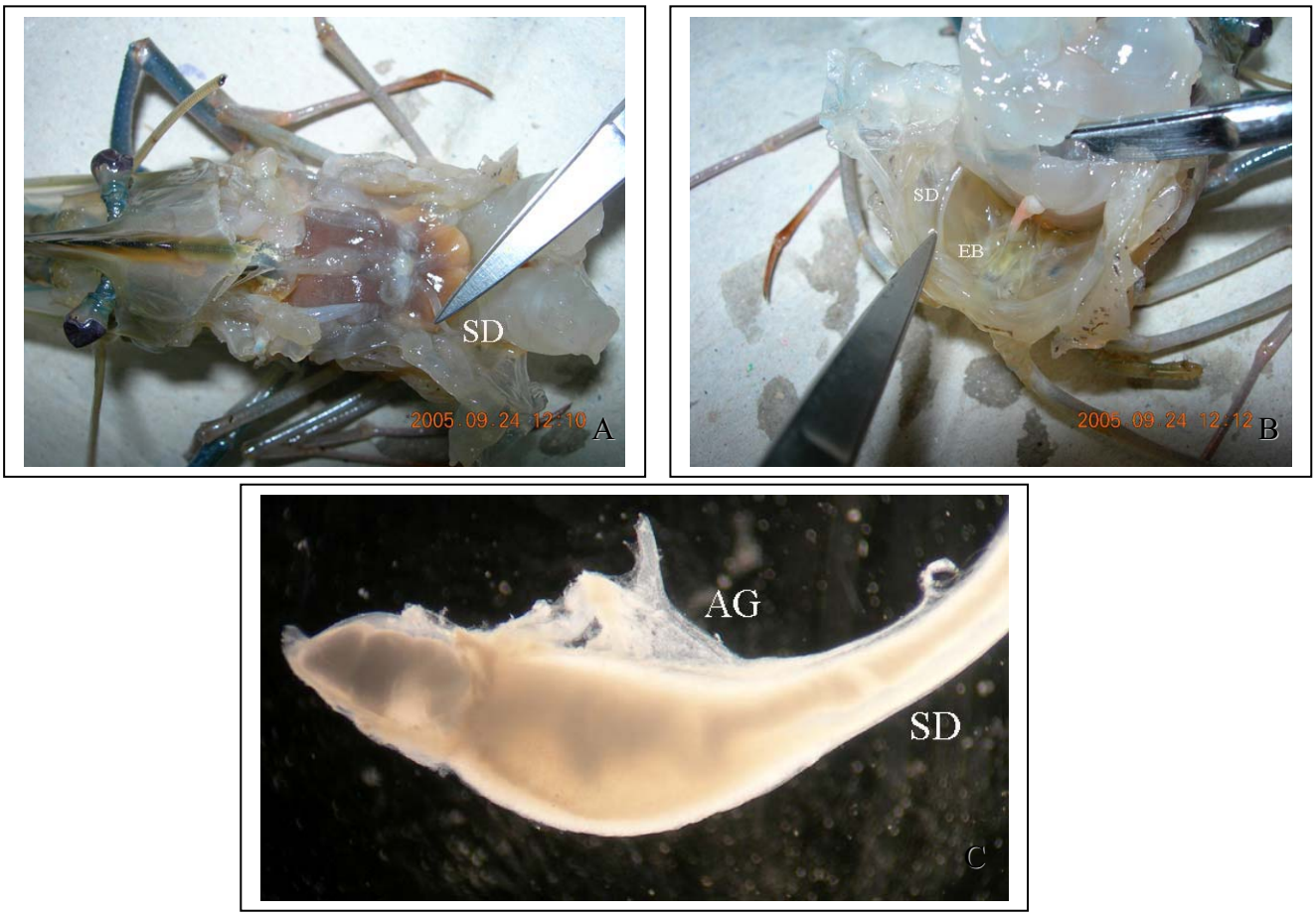
รูปที่ 40 แสดงเปรียบเทียบกุ้งเพศผู้กับเพศเมีย (A) โดยกุ้งเพศผู้มีขนาดใหญ่กว่าเพศเมียเมื่อเทียบกัน. (B) Gonopores ของกุ้งของเพศผู้ ที่โคนขาคู่ที่ห้า (ลูกศรชี้สีดำ). (C) กุ้งเพศเมียเมื่องอลำตัวดูด้านบนจะเห็น ovarian stage IV (ลูกศรชี้สีดำ). (D) รูเปิดของท่อนำไข่ที่โคนขาคู่ที่สามของเพศเมีย (ลูกศรชี้สีดำ).



รูปที่ 41 (A) เปรียบเทียบกุ้งก้ามกรามเพศผู้ 3 ขนาด ตามลำดับขนาด Small male (SM), orange-claw male (OC), and blue-claw male (BC) ซึ่งเป็นขนาดที่โตเต็มที่และสมบูรณ์เพศที่สุด. (B) ตำแหน่งของ Appendage masculine บนขาว่ายน้ำคู่ที่สอง (ลูกศรชี้สีดำ). (C) ภาพขยาย ของ Appendage masculine ซึ่งเป็นการแสดงออกของ secondary sex characteristic (ลูกศรชี้สีดำ).

ตำแหน่งของต่อมแอนโดรเจนนิคในกุ้งก้ามกราม

ต่อมแอนโดรเจนนิคเป็นกลุ่มเซลล์ที่วางตัวอยู่บนเนื้อเยื่อเกี่ยวพันรูปสามเหลี่ยม ตำแหน่งค่อนไปด้านข้างปลายของท่อนำน้ำเชื้อ (spermatic duct) ไปถึงส่วนที่โป่งออกเป็นกระเปาะ(ejaculatory bulb) ของท่อน้ำเชื้อด้านปลายสุด และทอดปลายด้านหนึ่งไปยึดเกาะกับกล้ามเนื้อด้านข้างลำตัวด้านใน

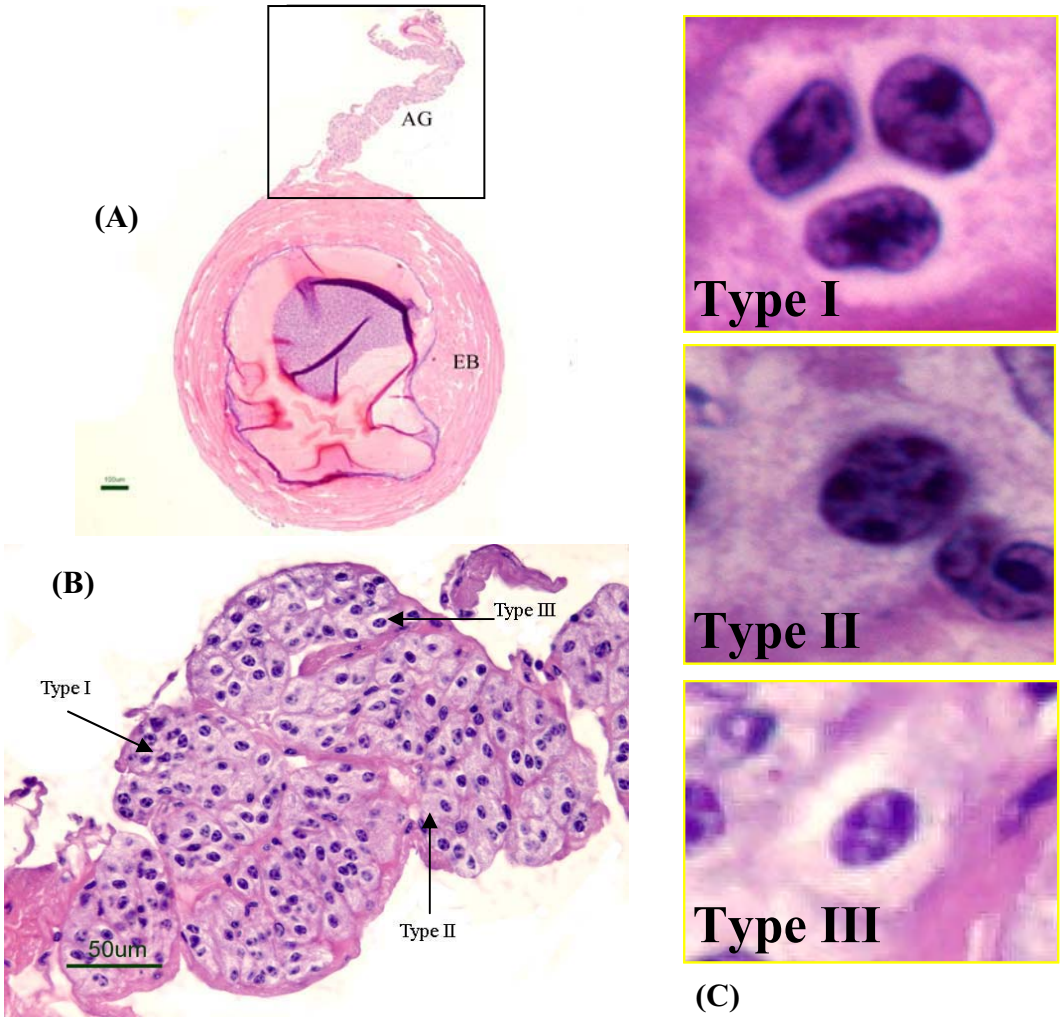


รูปที่ 42 แสดง ตำแหน่งของ androgenic gland ในกุ้งก้ามกรามเพศผู้ (SD; spermatic duct, EB; ejaculatory bulb, AG; androgenic gland)

ลักษณะทางจุลกายวิภาคของต่อมแอนโดรเจนนิค

ต่อมแอนโดรเจนนิดเป็นต่อมที่ประกอบด้วย เซลล์รูปทรงหลายเหลี่ยม(polygonal cells) รวมกันเป็นกลุ่ม และแทรกสอดด้วยเนื้อเยื่อเกี่ยวพันทำหน้าที่ยึดโยงกลุ่มเซลล์เข้าด้วยกัน เซลล์ของต่อมแอนโดรเจนนิค มี 3 ชนิด

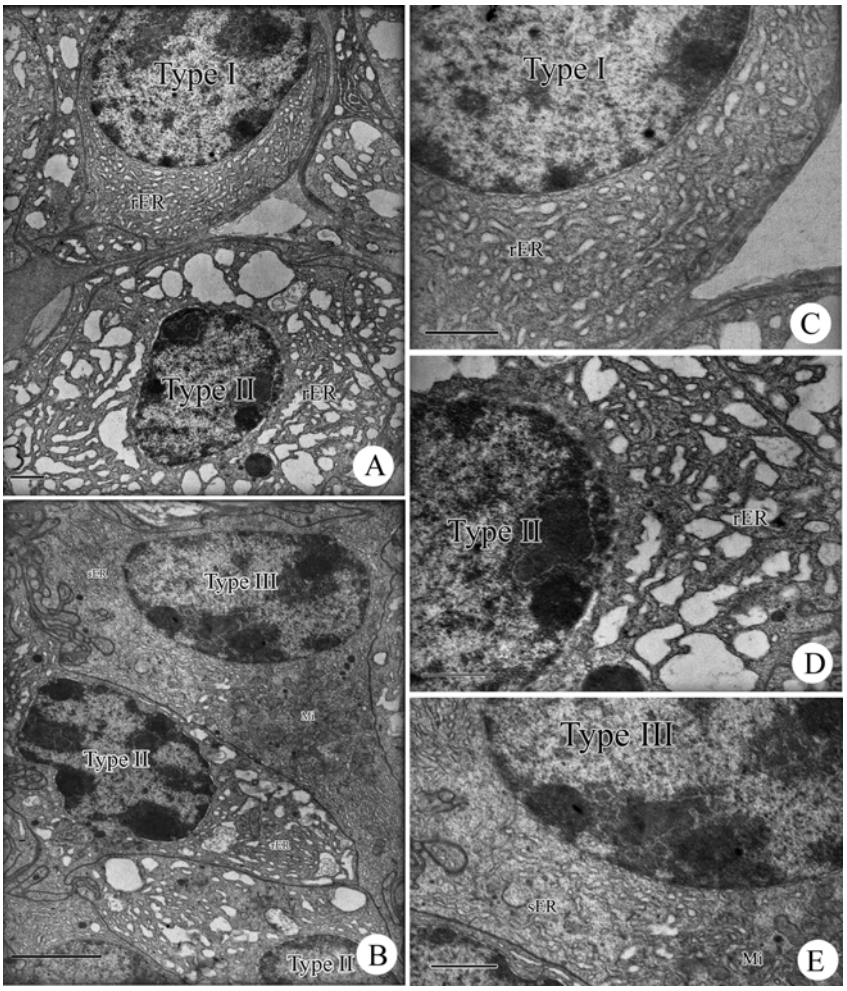
- เซลล์ชนิดที่ 1 (Type I) เป็นเซลล์ขนาดเล็ก เมื่อย้อมด้วย hematoxylin ไซโตพลาสซึมติดสีม่วงเข้ม
- เซลล์ชนิดที่ 2 (Type II) เป็นเซลล์ขนาดค่อนข้างใหญ่ เมื่อย้อมด้วย hematoxylin ไซโตพลาสซึมติดสีม่วงจางกว่า
- เซลล์ชนิดที่ 3 (Type III) เป็นเซลล์ขนาดเล็ก ไซโตพลาสซึมค่อนข้างใส ไม่ค่อยติดสี เมื่อย้อมด้วย hematoxylin



รูปที่ 43 แสดงภาพของต่อมแอนโดรเจนนิด (A) ตำแหน่งของ ต่อมแอนโดรเจนนิดบน ท่อนำสเปิร์ม (B) เซลล์ 3 ชนิด ของ ต่อมแอนโดรเจนนิด (C) ภาพขยายของเซลล์3 ชนิดในต่อมแอนโดรเจนนิด

โครงสร้างภายในแอนโดรเจนนิคเซลล์เมื่อดูด้วยกล้องจุลทรรศน์อิเลคตรอน แบบส่องผ่าน

ในเซลล์ของต่อม androgenic มีโครงสร้าง หลายชนิด ที่เห็นได้เด่นชัดคือ mitochondria และทั้ง rough endoplasmic reticulum (rER) เซลล์ชนิดที่ I มี rER จำนวนมาก โดยร่องของ rER มีลักษณะแคบและ rER เรียงซ้อนกันแน่น เซลล์ชนิดที่ II มี rER มากและส่วนใหญ่มีการโป่งขยายออก แสดงให้เห็นว่าเซลล์ชนิดนี้ทำหน้าที่สร้างและเก็บโปรตีนจำนวนมาก ในเซลล์ชนิดที่ III พบทั้ง sER และ rER ซึ่งอาจเป็นเซลล์ที่สร้าง steroid



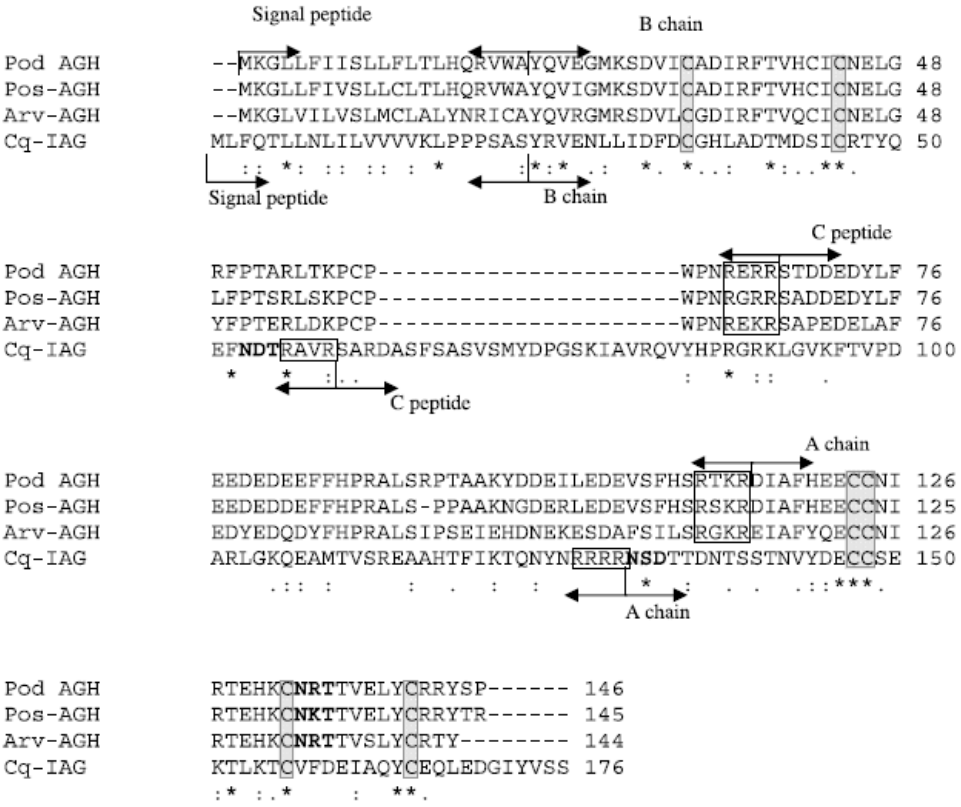
รูปที่ 44 ภาพจุลทรรศน์อิเลคตรอนแสดง แสดงเซลล์จำนวนมากของ ต่อมแอนโดรเจนนิคในกุ้งก้ามกราม (A) Type I, II ซึ่งมี rough endoplasmic reticulum (rER) จำนวนมาก. (B) Type II และ III cells ซึ่งมี smooth endoplasmic reticulum (sER). (C) Type I cell และแถว rER. (D) Type II cell และ rER ที่ขยายใหญ่. (E) Type III cell กับ sER และmitochondria (Mi). Bar = 1 μm

ขณะนี้เรายังทำการศึกษาต่อเนื่องโดยใช้วิธี immunocytochemistry เพื่อแสดงให้เห็นว่าเซลล์แต่ละชนิดสร้างฮอร์โมนเพศชนิดใด

หัวข้อที่ 10. การศึกษาคุณลักษณะของ Androgenic gland hormone (AGH) และ Insulin–like peptide hormone (ILP)

จากการศึกษาที่ผ่านมาของฮอร์โมน AGH ในสัตว์เพศผู้ของกลุ่ม ไอโซพอด (isopod) เช่น *Armadillidium vulgare, Porcellio scaber, Porcellio dilatatus* (Martin *et al.,* 1998, 1999; Okuno *et al*., 1999). AGH มีโครงสร้างคล้าย อินซูลิน โดยสามารถแบ่งออกเป็น 3 ส่วนย่อย A B และ C chains โดย ยีนของ AGH ของ *A. vulgare* มี 432 เบส แบ่งเป็น A chains ซึ่งมีกรดอะมิโน 29 ตัว C มีกรดอะมิโน 46 ตัว และ B มีกรด อะมิโน 44 ตัว *P. scaber* AGH ยีน มี 545 เบส (145 กรดอะมิโน) และ *P. dilatatus* AGH ยีนมี 544 เบส (146

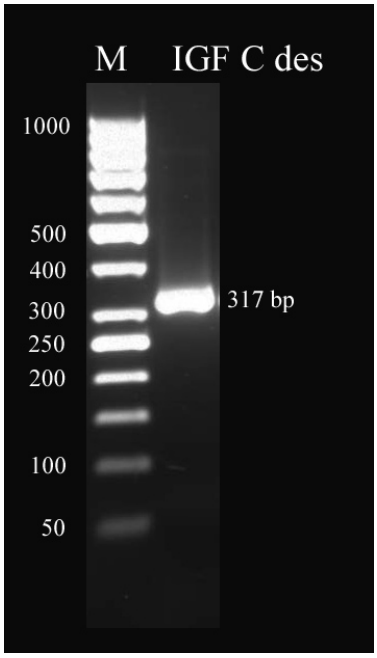
กรดอะมิโน) ยึดกันด้วยพันธะไดซันไฟต์ ในกุ้งก้ามกราม Sun et al., 2000 ได้รายงานว่าAGH ในกุ้งก้ามกราม น่าจะมีน้ำหนักโมเลกุลประมาณ 16 หรือ 18 kDa ซึ่งคล้ายคลึงกับ AGH ของ *A. vulgare* ต่อมาในปี 2007 Manor *et al.* พบ ยีนที่สร้างสารที่มีโครงสร้างคล้ายอินซูลิน ในต่อมแอนโดรเจนนิคของกุ้งเครฟิช (*Cherax quadricarinatus*) จึงให้ชื่อว่า insulin-like peptide (ILP) หรือ insulin-like growth factor (IGF) โดย IGF ที่พบนี้ มีความยาว 1445 นิวคริโอไทด์และแปรเป็นกรดอะมิโนได้ 176 ตัว เมื่อนำไปเปรียบเทียบกับ AGH จากไอโซพอด พบว่าแม้โครงสร้างจะคล้ายกันแต่ลำดับกรดอะมิโน ไม่เหมือนกัน (รูปที่ 45)



รูปที่ 45 แสดงการเปรียบเทียบทั้งสามส่วนของ แอนโดรเจนนิค (AGH) และอินซูลินไลค์ เปบไตด์ (ILP) ใน *A. Vulgar* (Arv -AGH), *P. scaber* (Pos-AGH), *P. dilatatus* (Pod-AGH) *และ C .quadricarinatus* (Cq-IAG)

ปัจจุบันนี้ยังไม่มีใครสามารถค้นหา AGH ในกุ้งก้ามกรามได้ ดังนั้นจึงมีความเชื่อว่า ILP อาจจะเป็น AGH ในกุ้งก้ามกราม คณะผู้วิจัยจึงใช้ลำดับนิวคลิโอไทด์ของ *Cherax quadricarinatus* เป็นแม่แบบในการสังเคราะห์ ไพรเมอร์เพื่อทำการโคลนยีน โดยใช้ RNA ของ *Cherax destructor* เป็น positive control สำหรับทดสอบไพรเมอร์ (รูปที่ 46) และนำมาโคลนยีนอินซูลินไลค์โกรทแฟกเตอร์ (IGF) ของกุ้งเครฟิช *Cherax destructor* และกุ้งก้ามกราม และสามารถโคลนยีนของอินซูลินไลค์นิวคลิโอไทด์ของกุ้งเครฟิช *Cherax destructor* โดยในตอนแรกได้ 317 เบสและสุดท้ายได้ 878 เบส รวมทั้ง signal sequence ของ ILP ยาว 176 กรดอะมิโน (รูปที่ 46, 47)

Manor R, Weil S, Oren S, Glazer L, Aflalo ED, Ventura T, Caspi VC, Lapidot M, and Sagi A. Gen. Comp. Endocrinol. 2007; 150: 326-336.



(A)

(B)

>IGF-Cdes

ATGCTGTCCCAAACATTACTCAACCTGATTTTGGTTGTGGTGGTGATGGTGCCTCTTCCCTCTGCCTCT
TACAGAGTGGATAACCTTCTGATTGACTTCGACTGTGGCCACCTGGCGGACACCATGGACAGTATTTGC
CGCACCTACAAGGAATTTAACGACACCCGAGCGGTGAGATCGGCCAGAGATACGTCACTTTCTGGCAGT
GTCTCCATGCAAGGCCCCGGGAGTGAGGTTGCTGTTAGTCAACTCTACCATCCAAGAGGCAGGAAGTTG
GGTGTCAGACTTACTGTCACTGATGCCAGGTTGGGTGAGCAGGAGGCGACGACAGTGAGTCGCGAGGCC
GCCAATACGTTTATTAAGACCCAGAACTACCACCGTCGCCGCCGTGACTCAGATACGACAGACAATACA
AGCAGTACTAACGTTTATGATGAGTGTTGCAGCGAGAAAACATTGAAGACTTGCGTCTTCGATGAGATT
GCCCAGTACTGTGAACAGTTGGAGGACGGAATCTACGTCAGTTCTTGAGGTGGGTGAGCTGGAGGCAGT
GACGGTGGTCTCCCCTAACATTGTCAAGACACTGACCCGTCACTGCCGATCTTACATTGTCAAGACACT
GACCCGTCACTGCCGATCTTACATTGTACTCACCAGTAACGGAATTACTGACCACTTTACATTCTGAAC
TGTTATCTATAATTCGTTTCATATTATCTTATGTTGGTGCATTAATTTCTGCCTTGTTTGACTCTGCGG
CGACTTGTTTGGTTAAGTACTTTCTGTATTAGTCCAAATTTGTTCTTTCTTCATCATGCCTTTCCAGCG
TCTTCCATTAAATAAATTCGTATTGACGTAAAAAAAAAAAAAAAAAAAA

Total length = 878 bp

รูปที่ 46 (A) Gel electrophoresis ของ PCR product แสดง แถบขนาด 317 bp ของ ILP ยีน จาก cDNA ของ *Cherax destructor*. (B) ลำดับนิวคลิโอไทด์ ของ ILP จากต่อมแอนโดรเจนิคของ *Cherax destructor*

เมื่อนำส่วน signal sequence ของอินซูลินไลค์เปปไตด์ที่ได้จาก *Cherax destructor* มาเปรียบเทียบกับ *Cherax quadricarinatus* พบว่ามีความใกล้เคียงกันมากถึง 87 % โดยแตกต่างกัน 13 % (รูปที่ 47) เราได้นำส่งลำดับเบสของ ILP ของกุ้งเครฟิช *Cherax destructor* ต่อฐานข้อมูลของ NCBI เมื่อวันที่ 9 กรกฎาคม 2551 โดยได้หมายเลขที่อ้างอิง EU718788

ในส่วนของ ILP และ AGH ยีน จากต่อมแอนโดรเจนนิคของกุ้งก้ามกรามกำลังอยู่ในช่วงโคลนยีน โดยอาศัยข้อมูลจากการโคลนยีนของ *Cherax destructor* ซึ่งคาดว่าลำดับเบสของยีน ILP ในกุ้งก้ามกรามจะคล้ายคลึงกับ ILP ของกุ้ง *C. destructor* มาก

```
SeqA Name          Len(aa)   SeqB Name          Len(aa)   Score
============================================================
1     Cquad        177       2     Cdes16208    177       87
============================================================

Cquad              MLFQTLLNLILVVVVKLPPPSASYRVENLLIDFDCGHLADTMDSICRTYQEFNDTRAVRS
60
Cdes               MLSQTLLNLILVVVVMVPLPSASYRVDNLLIDFDCGHLADTMDSICRTYKEFNDTRAVRS
60
                   ** ************ :* *******:**********************:**********

Cquad              ARDASFSASVSMYDPGSKIAVRQVYHPRGRKLGVKFTVPDARLGKQEAMTVSREAAHTFI
120
Cdes               ARDTSLSGSVSMQGPGSEVAVSQLYHPRGRKLGVRLTVTDARLGEQEATTVSREAANTFI
120
                   ***:*:*.**** .***::** *:**********::**.*****:*** *******:***

Cquad              KTQNYNRRRRNSDTTDNTSSTNVYDECCSEKTLKTCVFDEIAQYCEQLEDGIYVSSS
177
Cdes               KTQNYHRRRRDSDTTDNTSSTNVYDECCSEKTLKTCVFDEIAQYCEQLEDGIYVSSS
177
                   *****:****:**********************************************
```

Different = 23/177 = 12.99 = 13 %

Similarity = 87 %

รูปที่ 47 ตารางแสดงการเปรียบเทียบอินซูลินไลค์เปปไตด์ (IGF) ของ *Cherax destructor* กับ *Cherax quadricarinatus*

NCBI database 09-JUN-2008

```
LOCUS       EU718788     878 bp    mRNA    linear   INV 09-JUN-2008
DEFINITION  Cherax destructor insulin-like androgenic gland factor
mRNA,
            complete cds.
ACCESSION   EU718788
VERSION     EU718788.1  GI:189342953
KEYWORDS    .
SOURCE      Cherax destructor
  ORGANISM  Cherax destructor
            Eukaryota; Metazoa; Arthropoda; Crustacea; Malacostraca;
            Eumalacostraca; Eucarida; Decapoda; Pleocyemata;
Astacidea;
            Parastacoidea; Parastacidae; Cherax.
REFERENCE   1  (bases 1 to 878)
  AUTHORS   Phoungpetchara,I., Hanna,P.J. and Sobhon,P.
  TITLE     Identification of an insulin-like factor from Cherax
destructor
            androgenic gland mRNA
  JOURNAL   Unpublished
REFERENCE   2  (bases 1 to 878)
  AUTHORS   Phoungpetchara,I., Hanna,P.J. and Sobhon,P.
  TITLE     Direct Submission
  JOURNAL   Submitted (14-MAY-2008) Anatomy, Mahidol University,
            Rama 6 Road, Bangkok 10400, Thailand
FEATURES             Location/Qualifiers
     source          1..878
                     /organism="Cherax destructor"
                     /mol_type="mRNA"
                     /db_xref="taxon:6723"
     CDS             1..531
                     /note="IAG-Cd"
```

```
                     /codon_start=1
                     /product="insulin-like androgenic gland factor"
                     /protein_id="ACD91988.1"
                     /db_xref="GI:189342954"

/translation="MLSQTLLNLILVVVVMVPLPSASYRVDNLLIDFDCGHLADTMDS

ICRTYKEFNDTRAVRSARDTSLSGSVSMQGPGSEVAVSQLYHPRGRKLGVRLTVTDAR

LGEQEATTVSREAANTFIKTQNYHRRRRDSDTTDNTSSTNVYDECCSEKTLKTCVFDE

IAQYCEQLEDGIYVSS"

ORIGIN
        1 atgctgtccc aaacattact caacctgatt ttggttgtgg tggtgatggt
gcctcttccc
       61 tctgcctctt acagagtgga taaccttctg attgacttcg actgtggcca
cctggcggac
      121 accatggaca gtatttgccg cacctacaag gaatttaacg acacccgagc
ggtgagatcg
      181 gccagagata cgtcactttc tggcagtgtc tccatgcaag gccccgggag
tgaggttgct
      241 gttagtcaac tctaccatcc aagaggcagg aagttgggtg tcagacttac
tgtcactgat
      301 gccaggttgg gtgagcagga ggcgacgaca gtgagtcgcg aggccgccaa
tacgtttatt
      361 aagacccaga actaccaccg tcgccgccgt gactcagata cgacagacaa
tacaagcagt
      421 actaacgttt atgatgagtg ttgcagcgag aaaacattga agacttgcgt
cttcgatgag
      481 attgcccagt actgtgaaca gttggaggac ggaatctacg tcagttcttg
aggtgggtga
      541 gctggaggca gtgacggtgg tctcccctaa cattgtcaag acactgaccc
gtcactgccg
      601 atcttacatt gtcaagacac tgacccgtca ctgccgatct tacattgtac
tcaccagtaa
      661 cggaattact gaccacttta cattctgaac tgttatctat aattcgtttc
atattatctt
      721 atgttggtgc attaatttct gccttgtttg actctgcggc gacttgtttg
gttaagtact
      781 ttctgtatta gtccaaattt gttctttctt catcatgcct ttccagcgtc
ttccattaaa
      841 taaattcgta ttgacgtaaa aaaaaaaaaa aaaaaaaa //
```

หัวข้อที่ 11. การกระตุ้นการเปลี่ยนแปลงเพศกุ้งก้ามกรามด้วย 17 α methyltestosterone (17 αMT) และ สารสกัดรวมจาก androgenic gland

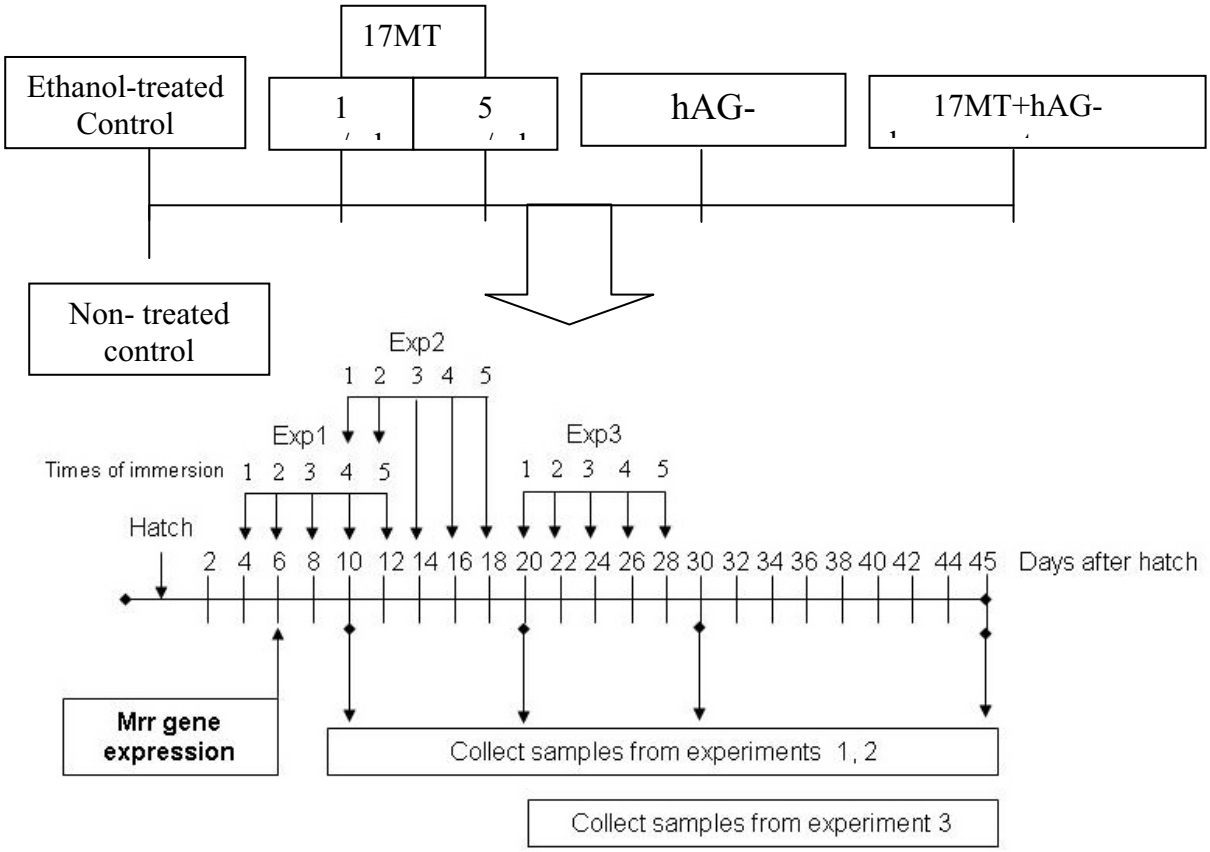
17 α methyltestosterone เป็นฮอร์โมนที่สามารถชักนำให้มีการเพิ่มประชากรเพศผู้ในสัตว์น้ำ จากการวิจัยของ Nam *et al.* (1998) พบว่าการใช้ 17 αMT สามารถเพิ่มปริมาณเพศผู้ในปลา mud loach (*Misgurnus mizolepis*) ได้ถึง 99.3 % Kitano *et al.* (2000) พบว่าฮอร์โมนนี้ สามารถชักนำให้เกิดการแปลงเพศของลูกปลา Japanese flounder, *Paralichthys olivaceus* เพศเมียให้กลายเป็นเพศผู้ได้ Arslan และ Phelps (2004) ยังพบว่าการจุ่มลูกปลา black crappie, *Pomoxis nigromaculatus* ในสารละลาย 17αMT 1 mg/l หลายๆครั้ง สามารถชักนำให้แปลงเพศเป็นเพศผู้ได้ถึง 96%

จากแนวคิดนี้คณะผู้วิจัยจึงนำ 17 αMT มาใช้ในการทดลองแปลงเพศลูกกุ้งก้ามกรามให้เป็นตัวผู้ โดยการจุ่มลูกกุ้งใน 17αMT ร่วมกับ สารสกัดรวมจาก hypertrophic androgenic gland ของกุ้งก้ามกรามที่ได้จากการตัดตาซึ่งคาดว่าจะมี AGH อยู่ในระดับสูง การทดลองแบ่งเป็น 3 กลุ่ม โดยกลุ่มแรกใช้ลูกกุ้งระยะ larvae อายุ 4 วันหลังจาก hatching (dah) กลุ่มที่สองใช้ลูกกุ้งระยะ larvae อายุ 10 วันหลังจาก hatching กลุ่มที่สามใช้ลูกกุ้งระยะ larvae อายุ 20 วันหลังจาก hatching โดยอ้างอิงจากการแสดงออกของยีนเพศผู้ได้ใน Mrr ยีน (Cao, et al., 2006) ซึ่งเริ่มแสดงออกวันที่ 5 หลัง hatching ซึ่งยีนนี้พบในเพศผู้เท่านั้น ลูกกุ้งแต่ละกลุ่มจะแบ่งย่อยเป็นกลุ่มเล็กๆ 6 กลุ่มๆละ 300 ตัว กลุ่มย่อยแรกเลี้ยงไว้โดยไม่แช่สาร กลุ่มย่อยที่สอง แช่ใน 95 % ethanol ซึ่งเป็นตัวทำละลาย 17 αMT กลุ่มย่อยที่สาม สี่ แช่ในสารละลาย 17 αMT ความเข้มข้น 1 mg/l และ 5 mg/l ที่ละลายใน ethanol ตามลำดับ กลุ่มย่อยที่ห้า แช่ในสารสกัดจาก hypertrophic androgenic gland (AG-homogenate) กลุ่มย่อยที่หก แช่ในสารละลาย ผสมของ 17 αMT รวมกับ AG-homogenate ลูกกุ้งถูกเลี้ยงในอ่างเรซิ่นขนาดความจุ 50 ลิตร อ่างละ 300 ตัว ด้วยน้ำกร่อย (15ppt) โดยควบคุมอุณหภูมิน้ำให้อยู่ระหว่าง 27-32 °C แสงสว่าง 12 ชั่วโมงและมืด 12 ชั่วโมง ให้อาหารลูกกุ้งด้วย commercial artemia วันละ 2 ครั้ง เปลี่ยนน้ำทุกๆ 4 วันขณะที่จะแช่สารละลาย น้ำในอ่างจะถ่ายออกให้เหลือ 2 ลิตร ในกลุ่มที่แช่ฮอร์โมน 17 αMT จะให้ความเข้มข้น 2 ระดับ คือ จำนวน 2 และ 10 mg 17 αMT (Sigma, USA) จะถูกละลายใน 95% ethanol 0.1 ml แล้วจึงนำไปละลายในน้ำ 2 ลิตร เพื่อให้ได้ความเข้มข้นสุดท้ายที่ 1 mg/l และ the 5 mg/l สารสกัด AG เตรียมโดยนำกุ้งตัวผู้ 10 ตัวมาตัดก้านตาสองข้าง ต่อม androgenic จะเกิดการ ขยายใหญ่ (hypertrophic) แล้วจะนำต่อมนี้มาบดใน crustacean physiological saline (CPS: NaCl 29 g, KCl 0.71 g, CaCl2.2H2O 2.38 g, MgSO4.7H2O 3.16 g, NaHCO3 0.5 g, MgCl2.6H2O 0.17 g, HEPES 4.76 g in 1 liter of distilled water) นำไปละลายในน้ำกร่อยให้ได้ความเข้มข้นที่ 1 mg protein/l กลุ่มที่แช่สารสกัดรวม จะเตรียมจากการผสมสาร 0.5 mg ของ 17 αMT รวมกับ 0.5 mg ของสารสกัด AG ให้ได้ความเข้มข้น 1 mg/l ในกลุ่มที่แช่ ethanol เตรียมโดยผสม 95 % ethanol 0.2 ml ในน้ำกร่อย 2 ลิตร. ลูกกุ้งแต่ละกลุ่มจะถูกแช่ในสารละลายวันเว้นวันนาน 4 ชั่วโมงต่อวัน ในกลุ่มแรก ลูกกุ้งอายุ 4 วัน จะถูกแช่ใน ฮอร์โมน วันที่ 4, 6, 8, 10 และ 12 ในกลุ่มที่สองจะแช่ลูกกุ้งอายุ 10 วัน ในวันที่ 10, 12, 14, 16, และ 18 ในกลุ่มที่สามลูกกุ้งอายุ 20 วันจะแช่วันที่ 20, 22, 24, 26 และ 28 (ดูแผนผังการทดลอง) หลังจุ่มครบตามเวลาแล้วนำลูกกุ้งมาเลี้ยงในน้ำกร่อยใหม่ ลูกกุ้งในกลุ่มแรกและกลุ่มที่สองจำนวน 30 ตัวต่อครั้งถูกเก็บในวันที่ 10, 20, 30 และ 45 ในกลุ่มที่สาม ลูกกุ้งถูกเก็บ วันที่ 20, 30 และ 45 ในการเก็บตัวอย่างแต่ละครั้งจะมีการวัดความยาวและชั่งน้ำหนักตัวเพื่อดูการเจริญเติบโต และแต่ละตัวอย่างจะดูการแสดงออกของยีน Mrr โดยใช้ RNA probe ที่จำเพาะในการวิเคราะห์แบบ northern blot เมื่อสิ้นสุดการทดลองในวันที่ 45 ตัวอย่างทั้งหมดจะถูกเก็บ วัดความยาว ชั่งน้ำหนักตัวและทดสอบหาอัตราส่วนเพศผู้และเพศเมีย โดยสามารถสังเกตดู gonopores และ appendix masculini (Arslan and Phelps, 2004) และค่าที่ได้จะนำไปคำนวณและเปรียบเทียบทางสถิติโดยโปรแกรม SPSS

Nam Y K, Noh C H, and Kim DS. Fish Sci. 1998;64:914-917.

Kitano T, Takamune K, Nagahama Y, and Abe S. Reprod. Dev. 2000; 56:1-5.

Arslan T, and Phelps, R. Aquaculture 2004; 234:561-573.



รูปที่ 48 แผนผังแสดงการทดลองเปลี่ยนเพศกุ้งก้ามกรามโดยวิธีแช่ตัวอ่อนกุ้งในสารละลายฮอร์โมน 17α methyltestosterone (17αMT)และสารสกัดรวมจากต่อม androgenic gland (hAG) และส่วนผสมระหว่าง 17αMT +hAG

ผลลัพธ์ที่ได้จากโครงการ

1. ผลงานที่ตีพิมพ์ในวารสารวิชาการนานาชาติ 26 เรื่อง

1.1. Vanichviriyakit R, Kruevaisayawan H, Weerachatyanukul W, Tawipreeda P, Withyachumnarnkul B, Pratoomchat B, Chavadej J, **Sobhon P**. 2004. Molecular modification of *Penaeus monodon* sperm in female thelycum and its consequent responses. *Molecular Reproduction and Development* 69:356-363.

1.2. Suphamungmee W, Apisawetakan S, Wanichanon C, Sretarugsa P, Poomtong T, **Sobhon P**. 2005. Basic nuclear protein pattern and chromatin condensation in sperm of a tropical abalone, *Haliotis asinina* Linnaeus. *Molecular Reproduction and Development* 70:211-221.

1.3. Saitongdee P, Apisawetakan S, Anunruang N, Poomthong T, Hanna P**, Sobhon P**. 2005. Egg-laying-hormone immunoreactivity in the neural ganglia and ovary of *Haliotis asinine* Linnaeus. *Invertebrate Neuroscience* 5:165-172.

1.4. Lui Z, **Sobhon P**, Withyachunarnkul B, Hanna P. 2006. Identification of a putative egg-laying hormone in neural and gonadal tissues of the black tiger prawn*, Penaeus monodon*, using immunocytochemistry. *Invertebrate Neuroscience* 6:41-46.

1.5. Meeratana P, Withyachumnarnkul B, Damrongphol P,Wongprasert K,Suseangtham A,and **Sobhon P**. 2006. Serotonin induced ovarian maturation in giant fresh water prawn broodstock, *Macrobrachium rosnbergi*i de Man*. Aquaculture* 260:315-325.

1.6. Meeratana P, **Sobhon P**. 2007. Classification of differentiating oocytes during ovarian cycle in the giant freshwater prawn *Macrobrachium rosenbergii*. *Aquaculture* 270:249-258.

1.7. Kruevaisayawan H, Vanichviriyakit R, Weerachatyanukul W, Withyachumnarnkul B, **Sobhon P**. 2007. Biochemical characterization and physiological role of cortical rods in black tiger shrimp, *Penaeus monodon*. *Aquaculture* 270:289-298.

1.8. Pongtippatee P, Vanichviriyakit R, Chavadej J, Plodpai P, Pratoomchat B, **Sobhon P**, Withyachumnarnkul B. 2007. Acrosome reaction in the sperm of the black tiger shrimp *Penaeus monodon* (Decapoda, Penaeidae). *Aquaculture Research*, 38:1635-1644.

1.9. Suphamungmee W, Wanichanon C, Vanichviriyakit R, **Sobhon P**. 2008. Spermiogenesis and chromatin condensation in the common tree shrew, *Tupaia glis. Cell and Tiss Research* 331:687-699.

1.10. Ngernsoungnern P, Ngernsoungnern A, Kavanaugh S, **Sobhon P**, Sower SA, Sretarugsa P. 2008. The presence and distribution of gonadotropin-releasing hormone-liked factor in the central nervous system of the black tiger shrimp, *Penaeus monodon*. *General Comparative Endocrinology* 155:613-22.

1.11. Ngernsoungnern A, Ngernsoungnern P, Kavanaugh S, Sower SA, **Sobhon P**, Sretarugsa P. 2008. The identification and distribution of gonadotropin-releasing hormone-like peptides in the central nervous system and ovary of the giant freshwater prawn, *Macrobrachium rosenbergii. Invertebrate Neuroscience* 8:49-57.

1.12. Ngernsoungnern A, Ngernsoungnern P, Weerachatyanukul W, Chavadej J, **Sobhon P**, Sretarugsa P. 2008. The existence of gonadotropin-releasing hormone (GnRH) immunoreactivity in the ovary and the effects of GnRHs on the ovarian maturation in the black tiger shrimp *Penaeus monodon*. *Aquaculture 279:*197-203.

1.13. Laimek P, Clark S, Stewart M, Pfeffer F, Wanichanon C, Hanna P, **Sobhon P**. 2008. The presence of GABA in gastropod mucus and its role in inducing larval settlement*. Journal of Experimental Marine Biology and Ecology* 354:182-191.

1.14. Chansela P, Saitongdee P, Stewart P, Soonklang N, Stewart M, Suphamungmee W, Poomtong T, **Sobhon P**. 2008. Existence of APGWamide in the testis and it's induction of spermiation in *Haliotis asinina* Linnaeus. *Aquaculture* 279:142-149.

1.15. Stewart P, Soonklang N, Stewart MJ, Wanichanon C, Hanna P, **Sobhon P.** 2008. Larval settlement of the tropical abalone, *Haliotis asinina* Linnaeus, using natural and artificial chemical inducers. *Aquaculture Research*. 39: 1181-1189.

1.16. Suphamungmee W, Weerachatyanukul W, Poomtong T, Hanna P, **Sobhon P**. 2008. Morphological and biochemical alterations of abalone testicular germ cells and spawned sperm and their fertilizing ability. *Marine Biotechnology* 10: 593-601.

1.17. Kruevaisayawan K, Vanichviriyakit R, Weerachatyanukul W, Iamsaard S, Withyachumnarnkul W, Basak A, Tanphaichitr N, **Sobhon P**. 2008. Induction of the acrosome reaction in black tiger shrimp, *Penaeus monodon*, requires sperm trypsin-like enzyme activity. *Biology of Reproduction* 79: 134–141.

1.18. Tinikul Y**,** Mercier AJ, Soonklang N, **Sobhon P.** 2008. Changes in the levels of serotonin and dopamine in the central nervous system and ovary, and their possible roles in the ovarian development in the giant freshwater prawn, *Macrobrachium rosenbergii*. *Gen Comp Endocrinol.* 158:250-258.

1.19. Worawittayawong P, Leigh C, Weerachatyanukul W, Monochantr S, **Sobhon P**, Breed W, Sretarugsa P. 2008. Changes in distribution of basic nuclear proteins and chromatin organization during spermiogenesis in the greater bandicoot rat, *Bandicota indica*. *Cell and Tissue Research.* 334: 135-144.

1.20. Duangsuwan P, Phoungpetchara I, Tinikul Y, Poljaroen J, Wanichanon C, **Sobhon P.** 2008. Histological and three dimensional organizations of lymphoid tubules in normal lymphoid organ of *Penaeus monodon. Fish & Shellfish Immunology* 24: 426-435.

1.21. Duangsuwan P, Tinikul Y, Chotwiwatthanakun C, Vanichviriyakit R, **Sobhon P.** 2008. Changes in the histological organization and spheroid formation in lymphoid organ of *Penaeus monodon* infected with yellow head virus. *Fish Shellfish Immunol* 25: 560-569.

1.22. Tinikul Y, Mercier AJ, Soonthornsumrith B, Phoungpetchara I, Poljareon J, Meeratana P, Duangsuwan P, Soonklang N, **Sobhon P.** 2008. Effects of serotonin, dopamine, octopamine, and spiperone on ovarian maturation and embryonic development in the giant freshwater prawn, *Macrobrachium rosenbergii*. *Crustaceana* (in press).

1.23. Liu Z, Donald J, Hanna P, Nuurai P, **Sobhon P**. 2009. Comparative distribution of a putative egg-laying hormone in neural and reproductive tissues of four Decapoda crustaceans. *Invertebrate Neuroscience.* (in press).

1.24. Panasophonkul S., Apisawetakan S., Cummin S., York P.S., Degnan B.M., Hanna P., Saitongdee P., **Sobhon P**., Sretarugsa P. 2009. Molecular characterization and analysis of a truncated serotonin receptor gene expressed in neural and reproductive tissues of abalone. *Histochemistry and Cell Biology*. *(accepted).*

1.25. Suphamungmee, W., Weerachatyanukul, W., Poomtong, T., Vanichviriyakit, R., **Sobhon, P**. 2009. Ultrastructure, compositions and possible roles of the egg coats in *Haliotis asinina*. *Journal of Shelfish Research(submitted).*

1.26. Suphamungmee, W., Vanichviriyakit, R., Sretarugsa, P., Chavadej, J., Poomtong, T., **Sobhon, P.** 2009. The sequence of interaction and optional proportion of sperm and egg number that yields maximal *in vitro* fertilization in a tropical abalone, *Haliotis asinine*. *Journal of Shelfish Research(submitted).*

2. การเสนอผลงานในที่ประชุมระดับนานาชาติ 19 เรื่อง

2.1. Saitongdee, P., Pisetpaisan, K., Apisawetakan, S., Anunruang, N., Poomthong, T., Hanna P.J. and **Sobhon, P**. 2004 Immunolocalization of egg-laying hormone, growth hormone, and insulin-liked hormone in the neural ganglia and gonads of *Haliotis asinina* (Linnaeus). The 8th Asia-Pacific Conference on Electron Microscopy (8 APEM) in conjuction with the 60th Annual Meeting of the Japanese Society of Microscopy, 7-11 June, 2004 Kanazawa, Japan. pp. 74.

2.2. Vanichviriyakit, R., Kruevaisayawan, H., Weerachatyanukul, W., Ngernsoungnern, P., Taweepreda, P., Chavadej, J., Sretarugsa, P., Withayachumnarnkul, B. and **Sobhon, P**. 2004 Production and changes of intra- and post-testicular sperm of *Penaeus monodon.* The 8th Asia-Pacific Conference on Electron Microscopy (8 APEM) in conjuction with the 60th Annual Meeting of the Japanese Society of Microscopy, 7-11 June, 2004 Kanazawa, Japan. pp. 95

2.3. Kruevaisayawan, H., Vanichviriyakit, R., Weerachatyanukul, W., Ngernsoungnern, P., Taweepreda, P., Chavadej, J., Sretarugsa, P., Withayachumnarnkul, B. and **Sobhon, P**. 2004 Oocyte ultrastructure and synthesis of oocyte's cortical rod proteins in *Penaeus monodon.* The 8th Asia-Pacific Conference on Electron Microscopy (8 APEM) in conjuction with the 60th Annual Meeting of the Japanese Society of Microscopy, 7-11 June, 2004 Kanazawa, Japan. pp. 95.

2.4. Tourtip, S., Poulpanich, N., Chavadej, J., **Sobhon, P**. and Withayachumnarnkul, B. 2004 Morphology and molecular biology of microsporidian spp. Infecting the black tiger shrimp *Penaeus monodon.* The 8th Asia-Pacific Conference on Electron Microscopy (8 APEM) in conjuction with the 60th Annual Meeting of the Japanese Society of Microscopy, 7-11 June, 2004 Kanazawa, Japan. pp. 98.

2.5. Wanichanon, C., Laimek, P., Chitchulanon, N., Linthong, V., Kruatrachue, M., Poomtong, T. and **Sobhon, P**. 2004 Distribution of GABAergic neurons and fibers in nervous system of *Haliotis asinina* Linnaeus. The 8th Asia-Pacific Conference on Electron Microscopy (8 APEM) in conjuction with the 60th Annual Meeting of the Japanese Society of Microscopy, 7-11 June, 2004 Kanazawa, Japan. pp. 119.

2.6. Sretarugsa, P., Panasophonkul, S., Anunruang, N., Apisawetakan, S., Saitongdee, P., Upathum, E.S., Poomtong, T., Hanna, P.J. and **Sobhon, P**. 2004 Serotonergic and FMRF-amidergic neurons in the nerve ganglia of *Haliotis asinina* Linnaeus. The 8th Asia-Pacific Conference on Electron Microscopy

(8 APEM) in conjuction with the 60th Annual Meeting of the Japanese Society of Microscopy, 7-11 June, 2004 Kanazawa, Japan. pp. 120.

2.7. Duangsuwan, P., and **Sobhon, P.** 2006. Classification of lymphoid cells in Black Tiger Shrimp, *Penaeus monodon*. The 16th International Microscopy Congress (IMC16), 3-8 Sep, 2006, Sapporo Japan. pp. 150.

2.8. Vanichviriyakit, R., Suphamungmee, W., Kruevaisayawan, H., Weerachatyanukul, W., Chavadej, J., Sretarugsa, P., Withyachumnarnkul, B., and **Sobhon, P**. 2006. Changes in basic nuclear proteins and chromatin structure during sperm maturation in Black Tiger Shrimp, *Penaeus monodon*. The 16th International Microscopy Congress (IMC16), 3-8 Sep, 2006, Sapporo Japan. pp. 151.

2.9. Suphamungmee, W., Weerachatyanukul, W., Poomtong, T., and **Sobhon, P**. 2006. Protein modifications in testicular and spawned sperm of the tropical abalone, *Haliotis asinina*, as related to sperm fertilizability**.** The 16th International Microscopy Congress (IMC16), 3-8 Sep, 2006, Sapporo Japan. pp. 151.

2.10. Panasophonkul, S., Sretarugsa, P., Hanna, P., Poomtong, T., and **Sobhon, P.** 2006. Expression of serotonin and its receptor in thecentral nervous tissues and gonads of the tropical abalone, *Haliotis asinina* Linnaeus. The 16th International Microscopy Congress (IMC16), 3-8 Sep, 2006, Sapporo Japan. pp. 167.

2.11. Saitongdee, P., Chansela, P., Taworntawat, S., Wanichanon, C., Poomtong, T., and **Sobhon P**. 2006. Presence of APGWamide and octopamine in the neural ganglia and gonadal tissues of the tropical abalone *Haliotis asinina* Linnaeus: Immunolocalization. The 16th International Microscopy Congress (IMC16), 3-8 Sep, 2006, Sapporo Japan. pp. 168.

2.12. Palasoon, R., Ngernsoungnern, A., Sretasugsa, P., **Sobhon, P**. and Chavadej, J. 2008. Distribution of FMRF and APGW amides in the central nervous system and ovary and their effects on ovarian maturation of *Macrobrachium rosenbergii*. The 9th Asia-Pacific Microscopy Conference (APMC9), 2-7 Nov, 2008, Jeju, Korea. pp. 49.

2.13. Ngernsoungnern, A., Ngernsoungnern, P., Weerachatyanukul, W., Kavanaugh, S., Sower, S.A., Chavadej, J., **Sobhon, P**., and Sretarugsa, P. 2008. The existence and distribution of gonadotropin-releasing hormone-like factor in the neural and gonadal tissues and their effects on reproductive processes of female *Macrobrachium rosenbergii*. The 9th Asia-Pacific Microscopy Conference (APMC9), 2-7 Nov, 2008, Jeju, Korea. pp. 114.

2.14. Ngernsoungnern, P., Ngernsoungnern, A., Weerachatyanukul, W., Chavadej, J., **Sobhon, P**., Sretarugsa, P. 2008. The existence of gonadotropin-releasing hormone (GnRH) immunoreactivity in the central nervous system and ovary and the effects of GnRHs on the ovarian maturation in the Black Tiger Shrimp *Penaeus monodon*. The 9th Asia-Pacific Microscopy Conference (APMC9), 2-7 Nov, 2008, Jeju, Korea. pp. 115.

2.15. Sretarugsa, P., Nakiem, J., Chavadej, J., Kruatrachue, M., and **Sobhon, P**. 2008. Expression of serotonin (5-HT) and dopamine (DA) in the central nervous system (CNS) and ovary of the blue swimming crab, *Portunus pelagicus*. The 9th Asia-Pacific Microscopy Conference (APMC9), 2-7 Nov, 2008, Jeju, Korea. pp. 115.

2.16. Saitongdee, P., Apisawetakan, S., Hanna, P., Poomthong, T., and **Sobhon, P**. 2008. Existence of growth hormone in neural tissue of *Haliotis asinina* (Linnaeus). The 9th Asia-Pacific Microscopy Conference (APMC9), 2-7 Nov, 2008, Jeju, Korea. pp. 115.

2.17. Nuurai, P., Engsusophon, A. Kuanpradit, C., Poomtong, T., Wanichanon, C., and **Sobhon, P**. 2008. Distribution of gonadotropin releasing hormone and its role in controlling ovarian maturation of *Haliotis asinina* Linnaeus. The 9th Asia-Pacific Microscopy Conference (APMC9), 2-7 Nov, 2008, Jeju, Korea. pp. 116.

2.18. Vanichviriyakit R., Weerachatyanukul, W., Chavadej, J., Withyachumnarnkul, B., and **Sobhon, P**. 2008. Dynamics of cytoskeletal and tyrosine phosphorylated proteins in sperm of the Black Tiger Shrimp, *Penaeus monodon*. The 9th Asia-Pacific Microscopy Conference (APMC9), 2-7 Nov, 2008, Jeju, Korea. pp. 117.

2.19. Poljaroen, J., Vanichviriyakit, R., Tinikul, Y., Phoungpetchara, I., Weerachatyanukul, W., and **Sobhon, P**. 2008. Classification of the male germ cells during spermatogenesis in the giant freshwater prawn, *Macrobrachium rosenbergii*. The 9th Asia-Pacific Microscopy Conference (APMC9), 2-7 Nov, 2008, Jeju, Korea. pp. 118.

3. บทความวิชาการภาษาไทยสำหรับบุคคลทั่วไป

3.1. เรื่อง "จากองค์ความรู้พื้นฐานในเรื่องของฮอร์โมนของระบบประสาทไปสู่การเพิ่มผลผลิตของหอยเป๋าฮื้อ สัตว์น้ำชนิดใหม่ที่มีศักยภาพสูง" ในหนังสืองานวิจัยพื้นฐาน ฐานรากของการพัฒนาประเทศตามปรัชญาเศรษฐกิจพอเพียง การวิจัยพื้นฐานเพื่อพัฒนาการเกษตร" สำนักงานกองทุนสนับสนุนการวิจัย (สกว.), ปี พ.ศ. 2551, หน้า 185-205

3.2. เรื่อง "การพัฒนาเซลล์สืบพันธุ์ และกระบวนการปฏิสนธิในกุ้งกุลาดำ (Gamete development and fertilization in Black Tiger Shrimp)" ในหนังสือรวมบทความวิชาการเนื่องในวาระเฉลิมฉลองครบรอบ 50 ปี แห่งการสถาปนาคณะวิทยาศาสตร์, ปี พ.ศ. 2551

4. รหัสพันธุกรรมของฮอร์โมนประสาทของกุ้งในฐานข้อมูล NCBI

NCBI database 09-JUN-2008

```
LOCUS       EU718788     878 bp    mRNA    linear   INV 09-JUN-2008
DEFINITION  Cherax destructor insulin-like androgenic gland factor
mRNA,
            complete cds.
ACCESSION   EU718788
VERSION     EU718788.1  GI:189342953
KEYWORDS    .
SOURCE      Cherax destructor
  ORGANISM  Cherax destructor
            Eukaryota; Metazoa; Arthropoda; Crustacea; Malacostraca;
            Eumalacostraca; Eucarida; Decapoda; Pleocyemata;
Astacidea;
```

```
            Parastacoidea; Parastacidae; Cherax.
REFERENCE   1  (bases 1 to 878)
  AUTHORS   Phoungpetchara,I., Hanna,P.J. and Sobhon,P.
  TITLE     Identification of an insulin-like factor from Cherax
destructor
            androgenic gland mRNA
  JOURNAL   Unpublished
REFERENCE   2  (bases 1 to 878)
  AUTHORS   Phoungpetchara,I., Hanna,P.J. and Sobhon,P.
  TITLE     Direct Submission
  JOURNAL   Submitted (14-MAY-2008) Anatomy, Mahidol University,
            Rama 6 Road, Bangkok 10400, Thailand
FEATURES             Location/Qualifiers
     source          1..878
                     /organism="Cherax destructor"
                     /mol_type="mRNA"
                     /db_xref="taxon:6723"
     CDS             1..531
                     /note="IAG-Cd"
                     /codon_start=1
                     /product="insulin-like androgenic gland factor"
                     /protein_id="ACD91988.1"
                     /db_xref="GI:189342954"

/translation="MLSQTLLNLILVVVVMVPLPSASYRVDNLLIDFDCGHLADTMDS

ICRTYKEFNDTRAVRSARDTSLSGSVSMQGPGSEVAVSQLYHPRGRKLGVRLTVTDAR

LGEQEATTVSREAANTFIKTQNYHRRRRDSDTTDNTSSTNVYDECCSEKTLKTCVFDE

IAQYCEQLEDGIYVSS"
```

5. นักวิจัยในโครงการที่ได้รับทุนอื่นในระหว่างรับทุนส่งเสริมกลุ่มวิจัย (ปี 2547-2550)

รศ.ดร.ชัยทิพย์ วนิชานนท์ ทุนผู้ช่วยวิจัยโครงการ คปก.ประจำปี 2547 และ 2548 จำนวน 2 ทุน

รศ.ดร.ประพีร์ เศรษฐรักษ์ ทุนผู้ช่วยวิจัยโครงการ คปก.ประจำปี 2546 จำนวน 1 ทุน

รศ. ดร. จิตติพันธุ์ ชวเดช ทุนผู้ช่วยวิจัยโครงการ คปก.ประจำปี 2548 จำนวน 1 ทุน

6. การผลิตบุคลากรและนักวิจัย

6.1. นักวิจัยรุ่นใหม่ที่ได้รับทุนพัฒนาศักยภาพการทำงานของอาจารย์รุ่นใหม่และรุ่นกลางของ สกว.-สกอ. ที่อยู่ภายใต้การดูแล (mentorship) ของหัวหน้าโครงการ จำนวน 2 คน (ปี 2547-2550)

6.1.1. นายประเสริฐ มีรัตน์ ทุนนักวิจัยรุ่นใหม่ประจำปี 2546 และทุนนักวิจัยรุ่นกลาง สกว. ประจำปี 2550

6.1.2. นายวัฒนา วีรชาติยานุกูล ทุนนักวิจัยรุ่นใหม่ประจำปี 2546 และทุนนักวิจัยรุ่นกลาง สกว.-สกอ. ประจำปี 2548

6.2. นักวิจัยรุ่นใหม่ที่ได้รับตำแหน่งวิชาการสูงขึ้น

6.2.1. นายประเสริฐ มีรัตน์ อาจารย์ **เลื่อนตำแหน่งจากอาจารย์เป็น** ผู้ช่วยศาสตราจารย์

6.2.2. นายวัฒนา วีรชาติยานุกูล อาจารย์ **เลื่อนตำแหน่งจากอาจารย์เป็น** รองศาสตราจารย์

6.2.3. น.ส.พรจันทร์ สายทองดี ผู้ช่วยศาสตราจารย์ **เลื่อนตำแหน่งผู้ช่วยศาตราจารย์เป็น** รองศาสตราจารย์

6.3. นักศึกษาบัณฑิตที่จบการศึกษาจากโครงการ

6.3.1. **นักศึกษาปริญญาโท 2 คน**

6.3.1.1. **น.ส. ปิยฉัตร จันทร์เสละ** จบปีการศึกษา 2550 หัวข้อวิทยานิพนธ์ "Localization of APGWamide and its effect on growth and spawning induction in *Haliotis asinina* Linaeus"

6.3.1.2. **นายอัตถกร เอ็งสุโสภณ** คาดว่าจะจบปีการศึกษา 2552 หัวข้อวิทยานิพนธ์ "The cryopreservation of sperm of the Dongkey's ear abalone (*Haliotis asinina*)"

6.3.2. **นักศึกษาปริญญาเอก 12 คน**

6.3.2.1. **น.ส.ศศิพร พนโสภณกุล** จบปีการศึกษา 2549 หัวข้อวิทยานิพนธ์ "Distribution and characterization of serotonin (5-HT) and its receptor in the neural and gonadal tissues and the role of 5-HT I the reproduction of *Haliotis asinina* Linaeus"

6.3.2.2. **นายวรวิทย์ ศุภมั่งมี** จบปีการศึกษา 2549 หัวข้อวิทยานิพนธ์ "Structure of the spawned gametes and the process of sperm-egg interaction in the tropical abalone, *Haliotis asinina*"

6.3.2.3. **นางประภาพร สจ๊วต** จบปีการศึกษา 2550 หัวข้อวิทยานิพนธ์ "Investigation of GABA and $GABA_A$ receptor in *Haliotis asinina* and their roles on growth development and larval settlement"

6.3.2.4. **นางปิยะดา เงินสูงเนิน** จบปีการศึกษา 2550 หัวข้อวิทยานิพนธ์ "The existence of gonadotropin-releasing hormone (GnRH)-liked factor in the nervous and gonadal tissues of *Penaeus nonodon* and the role of GnRH in reproductive processes."

6.3.2.5. **นายอภิชาติ เงินสูงเนิน** จบปีการศึกษา 2551 หัวข้อวิทยานิพนธ์ "The existence and distribution of gonadotropin-releasing hormone- and egg-laying nerrmone-like factors in the neural and gonadal tissues and their effects on reproductive processes of female *Macrobrachium rosenbergii*"

6.3.2.6. **นายยสวันต์ ตินิกุล** จบปีการศึกษา 2551 หัวข้อวิทยานิพนธ์ "The levels and distribution of serotonin and dopamine in the central nervous system and ovary of *Macrobrachium rosenbergii*, and their roles in ovarian maturation and spawning"

6.3.2.7. **น.ส.ปริญญาพร หนูอุไร** คาดว่าจะจบปีการศึกษา 2552 หัวข้อวิทยานิพนธ์ "Characterization and expression of egg-laying hormone (ELH) and gonadotropin-releasing hormone (GnRH), and their roles in the reproduction of *Haliotis asinina* Linnaeus"

6.3.2.8. **น.ส.จิตราภรณ์ ควรประดิษฐ์** คาดว่าจะจบปีการศึกษา 2553 หัวข้อวิทยานิพนธ์ "Identification and characterization of peptide pheromones with mate-attracting effects in *Haliotis asinina*"

6.3.2.9. **น.ส.จารุวรรณ ผลเจริญ** คาดว่าจะจบปีการศึกษา 2552 หัวข้อวิทยานิพนธ์ "Development of male germ cells and stimulation of testicular maturation and sperm production in

giant freshwater prawn, *Macrobrachium rosenbergii*, with serotonin (5-HT), dopamine (DA), and gonadotropin-releasing hormone (GnRH)"

6.3.2.10. **นายอิทธิพล พวงเพชร** คาดว่าจะจบปีการศึกษา 2552 หัวข้อวิทยานิพนธ์ "Morphology of androgenic gland and associated male reproductive tract, and characterizations of male-sex determining factors in *Macrobrachium rosenbergii*"

6.3.2.11. **นายรณรงค์ พละศูนย์** คาดว่าจะจบปีการศึกษา 2552 หัวข้อวิทยานิพนธ์ "Distribution of FMRFamide and APGWamide in central nervous system and ovary of giant freshwater prawn, *Macrobrachium rosenbergii*, and their effects on ovarian maturation and growth"

6.3.2.12. **น.ส. นันทวรรณ ศูนย์กลาง** คาดว่าจะจบปีการศึกษา 2552 หัวข้อวิทยานิพนธ์ "Morphology of differentiating oocytes and the effects of 17β-estradiol and prostaglandin-E2 on ovarian maturation and spawning in the giant freshwater prawn, *Macrobrachium rosenbergii*"

7. ผลิตภัณฑ์ที่ได้ซึ่งมีโอกาสนำไปประยุกต์ใช้ในเชิงพาณิชย์หรือเชิงสาธารณะ

หอยเป๋าฮื้อ

7.1. พิสูจน์ได้ว่า การใช้ GnRH และ ELH สามารถกระตุ้นการพัฒนาของรังไข่ของแม่พันธุ์ได้เร็วขึ้น

7.2. พิสูจน์ได้ว่าการฉีด APGW สามารถกระตุ้นการหลั่งเซลล์อสุจิ (spermiation) จากเพศผู้ที่มีความสมบูรณ์เพศได้ 100% ในขณะที่การฉีด ELH สามารถกระตุ้นการปล่อยไข่ (spawning) จากเพศเมียที่พร้อมได้ 60 % ดังนั้นจึงอาจปรับใช้สารทั้งสองชนิดเพื่อให้เกิดการหลั่งอสุจิและตกไข่จากพ่อ-แม่พันธุ์ในเวลาพร้อมกันหรือใกล้เคียงกันมากขึ้น ทำให้โอกาสในการเกิดปฏิสนธิและการได้ตัวอ่อนปริมาณมากขึ้น

7.3. พิสูจน์ได้ว่าการใช้สาร GABA, 5-AVA และ MSG ทำให้มีการลงเกาะ (settlement) ของตัวอ่อนได้มากขึ้นและมีอัตราการเกิด metamorphosis กับการรอดตายของตัวอ่อนมากขึ้น การใช้ผงชูรสที่มี MSG (monosodium glutamate) อยู่ ซึ่งเป็นสารราคาถูกและหาได้ง่าย สามารถนำไปใช้โดยเกษตรกรโดยมีค่าใช้จ่ายถูกมาก

กุ้งก้ามกราม

7.4. พิสูจน์ได้ว่าการใช้สารสื่อประสาท 5-HT, 5-HT+SP (spiperone), GnRH, ELH แบบเดี่ยวหรือแบบรวมสามารถกระตุ้นให้รังไข่ของแม่กุ้งพัฒนาเร็วขึ้น มีการตกไข่เร็วขึ้นและ จำนวนไข่ที่ได้ก็มีปริมาณและคุณภาพปกติ ทั้งนี้อาจต้องมีการทดลองใช้ doses ที่ต่ำที่สุดของแต่ละสารที่สามารถออกฤทธิ์ได้ทั้งแบบเดี่ยวและแบบที่รวมกัน เพื่อให้ได้โปรแกรมการฉีดกระตุ้นที่มีประสิทธิภาพสูงสุด และมีการรบกวนต่อสภาพสรีรวิทยาและสุขภาพของแม่กุ้งน้อยที่สุด อีกทั้งอาจใช้โปรแกรมการฉีดสารดังกล่าวในกุ้งกุลาดำและกุ้งขาว เพื่อกระตุ้นให้เกิดการพัฒนาของรังไข่โดยไม่ต้องตัดตาแม่พันธุ์

7.5. สามารถพัฒนาวิธีตรวจสอบความสามารถในการผลิตเซลล์อสุจิที่มีคุณภาพของพ่อพันธุ์ และความพร้อมของเซลล์อสุจิ (sperm maturation and capacitation) ในการปฏิสนธิกับไข่ โดยตรวจดูระดับ tyrosine phosphorylation และ/หรือ การกระจายของ cytoskeletal protein โดยเฉพาะ actin ไปอยู่ที่บริเวณ subacrosomal space

ภาคผนวก

- บทความที่ตีพิมพ์ในวารสารวิชาการนานาชาติ
  (เอกสารหมายเลข 1.1-1.26)
- บทคัดย่อผลงานวิจัยที่นำเสนอในการประชุมวิชาการนานาชาติ
  (เอกสารหมายเลข 2.1-2.19)

MOLECULAR REPRODUCTION AND DEVELOPMENT 69:356–363 (2004)

Molecular Modification of *Penaeus monodon* Sperm in Female Thelycum and Its Consequent Responses

RAPEEPUN VANICHVIRIYAKIT,[1] HATHAIRAT KRUEVAISAYAWAN,[1]
WATTANA WEERACHATYANUKUL,[1]* PATTIRA TAWIPREEDA,[1,2]
BOONSIRM WITHYACHUMNARNKUL,[1,2] BOONYARATH PRATOOMCHAT,[3]
JITTIPAN CHAVADEJ,[1] AND PRASERT SOBHON[1]

[1]*Department of Anatomy, Mahidol University, Bangkok, Thailand*
[2]*Research Center of Excellence (Centex Shrimp), Faculty of Science, Mahidol University, Bangkok, Thailand*
[3]*Department of Aquatic Science, Faculty of Science, Buraphar University, Chonburi, Thailand*

ABSTRACT Using *Penaeus monodon* as the model, we demonstrated the molecular changes and the mechanism of thelycal-dependent sperm modification resulting in an enhanced acrosome reaction (AR) response. Attention was paid to the modification of the sperm plasma membrane which was mediated through an adsorption or removal of sperm peripheral and integral membrane proteins as indicated by the different profiles of these proteins in spermatophore (S) and thelycal (T) sperm. In vitro adsorption of Alexa-488 conjugated T proteins onto the entire S-sperm surface confirmed protein transfer in a time–dependent manner. Specific anchoring of 83 and 140 kDa proteins to sperm peripheral proteins as well as 53/55 and 60 kDa proteins to sperm lipids was demonstrated. Apart from membrane modification, a substantial increase in protein tyrosine phosphorylation was shown to be closely associated with T-dependent sperm modification event. The physiological significance of this sperm modification in enhancing sperm AR response, which required at least 3 days of T residence in order for the sperm to gain a complete AR response, was also elucidated. *Mol. Reprod. Dev. 69: 356–363, 2004.* © 2004 Wiley-Liss, Inc.

Key Words: *Penaeus monodon*; sperm; thelycum; tyrosine phosphorylation; capacitation; acrosome reaction

INTRODUCTION

Upon their synthesis and release from the testis, the sperm of most marine invertebrates, including crustaceans, do not need post-testicular modification to acquire their fertilizing ability. They are readily capable of fertilization after a "broadcasting" release from males into the surrounding seawater where fertilization takes place (Clark and Griffin, 1988; Ohlendieck and Lennarz, 1996; Vacquier, 1998). However, this event does not occur throughout all species of marine invertebrates, particularly in certain species of penaeid shrimp possessing a close-typed-thelycum or sperm receptacle whose function or mechanism is still poorly understood. In *Sicyonia ingentis*, spermatophores (or sperm sacs) from a male shrimp need to be translocated into the female thelycum during mating (Wikramanayake et al., 1992; Clark et al., 1994). Post-insemination changes of the sperm, both morphological and functional [gauged from their ability to undergo the acrosome reaction (AR)], have been addressed (Clark and Griffin, 1988; Wikramanayake et al., 1992). Nevertheless, biochemical data for this sperm modification event are still scarce. Supporting the essence of post-testicular modification in penaeid sperm is very low (~10%) in vitro fertilization rate, compared to that occurs naturally where sperm in the thelycum are released to fertilize the spawned eggs (Clark et al., 1973). In addition, the ability to undergo an egg–water-induced AR, a prerequisite step in fertilization, of spermatophore (S) sperm is far inferior (~1–3%) to that of thelycal (T) sperm (>93%) (Clark et al., 1981).

Sperm molecular modification has been extensively reported in mammals. This process is accomplished through both sperm maturation and capacitation in male and female reproductive tracts, respectively, by which the sperm achieve their fertilizing capacity (Yanagimachi, 1994; Cooper, 1998). Similar information in the sperm of marine invertebrates, however, is less readily available. Attention has been paid to sperm plasma membrane modification. Structural reorganization of sperm surface proteins can happen through an adsorption of epididymal proteins, some of which are relevant to the egg interaction, onto the sperm surface during epididymal maturation (Cooper, 1998; Jones, 1998; Frenette and Sullivan, 2001). It can also be mediated through the removal of nonfunctional or marking molecules, so called "decapacitating" factors,

Grant sponsor: National Science and Technology Development Agency of Thailand (to BW); Grant number: BT-B-06-SG-14-4505; Grant sponsor: Thailand Research Fund (to WW); Grant number: MRG4680054.

*Correspondence to: Wattana Weerachatyanukul, Department of Anatomy, Faculty of Science, Mahidol University, Rama 6 Rd., Payathai, Bangkok, Thailand 10400. E-mail: scwwy@mahidol.ac.th

Received 11 March 2004; Accepted 1 June 2004
Published online in Wiley InterScience (www.interscience.wiley.com).
DOI 10.1002/mrd.20138

© 2004 WILEY-LISS, INC.

to fully expose the egg binding ligands during sperm capacitation (Hunter and Nornes, 1969; Oliphant et al., 1985). Modification and redistribution of sperm membrane lipids, both correlated with egg binding, for example, sulfogalactosylglycerolipid (SGG) in the case of higher mammals (White et al., 2000; Weerachatyanukul et al., 2001), and with regulation of membrane fluidity through the efflux of cholesterol or reorganization of phospholipids (Cross, 1998; Flesch and Gadella, 2000; Manjunath and Therian; 2002) are also well documented. Interestingly, a well defined signal transduction pathway, a cAMP-dependent protein tyrosine phophorylation, has been reported to be a consequence of this membrane cholesterol removal (Galantino-Homer et al., 1997; Visconti and Kopf, 1998; Visconti et al., 1999). Furthermore, sperm plasma membrane modification during maturation/capacitation also leads to at least two physiological responses, that is, the activation of sperm motility from nonmotile to hypermotile and the enhanced ability of sperm to undergo AR (Yanagimachi, 1994; Suarez, 1996).

In this study, we provided the evidence regarding the molecular modification of *P. monodon* sperm membrane through both peripheral proteins and lipids by female T components. As a consequence, the sequential increases of protein tyrosine phosphorylation coupled with an enhanced response of the sperm AR (the only physiological endpoint that can be monitored in *P. monodon* sperm since they are immotile) are of particular interest, and are suggestive of the significance of the T-dependent modification of *P. monodon* sperm prior to fertilization.

MATERIALS AND METHODS

Sample Collection

Broodstock shrimp were caught from the Andaman sea and maintained at the Department of Aquatic Science, Faculty of Science, Buraphar University, or at BAFCO farm, Nakhon Si Thammaraj, Thailand. Female shrimp were anesthetized under ice and then cut through the thoracoabdominal segment just below the 5th pair of walking legs where thelycum is situated. The gelatinous sperm masses were physically isolated from the dissected thelycums into 0.22-μm-filtered sea water (SW) containing 2 mM PMSF and 1 mM EDTA. Subsequently, these masses were segregated by vigorous shaking and pipetting. The sperm suspension was then filtered through a 212-μm-filter to remove any gross debris. T-sperm in the suspension were pelleted (500*g*, 5 min), leaving T fluid as a supernatant (S1). T-sperm were resuspended in SW at a final concentration of 1×10^7 sperm/ml before use. The S1-supernatant was centrifuged (12,000*g*, 10 min, 4°C) to clean any gross debris and the resulting supernatant (S2), termed "thelycal proteins," was kept frozen until use. Protein concentration of the T proteins was determined by Bradford's protein assay at the wavelength of 595 nm.

Spermatophores, located at the 5th pair of walking legs of male shrimp, were retrieved by the application of an electrostimulation (square wave, frequency = 100 cps, pulse duration = 0.1–0.5 sec, and voltage = 25 mV) to the ventral abdominal wall or by deep compression close to the location of the spermatophores, without sacrificing the shrimp. These spermatophores were processed to obtain sperm, so called S sperm, following the methods described for T-sperm.

Extraction of Sperm Peripheral and Integral Membrane Proteins

Peripheral membrane proteins were extracted according to the method described by Frenette and Sullivan (2001). Briefly, the sperm pellets were resuspended with 3 ml of 1 M NaCl and incubated with gentle agitation (30 min, 4°C). Thereafter, the sperm were pelleted (500*g*, 4°C, 5 min) and the supernatant containing peripheral membrane proteins were collected and cleaned (10,000*g*, 4°C, 10 min). The proteins were concentrated using a MicroCon centrifugation device (Millipore, Bedford, MA) and the protein concentration was determined by Bradford's protein assay. The viability of the sperm after being subjected to high salt treatment was examined by propidium iodide (PI) staining, according to manufacturer's protocol (Molecular Probes, Eugene, OR). The remaining sperm pellets were washed and resuspended in Tris buffered saline (TBS: 10 mM Tris-HCl, 150 mM NaCl, pH 7.4) for further extraction of sperm plasma membrane by a phase separation of Triton X-114, according to the method described by Bordier (1981). In brief, sperm were reconstituted in a final 1% Triton X-114 solution, thoroughly vortexed and centrifuged (5,000*g*, 4°C, 10 min) to get rid of the nuclear and cellular debris. The obtained supernatant was overlaid on top of a sucrose cushion (6% sucrose, 10 mM Tris-HCl, pH 7.4, 150 mM NaCl, 0.06% Triton X-114) and allowed to stand at room temperature until a cloudiness was observed in the suspension. The gradient was then subjected to low-speed centrifugation (300*g*, room temperature, 3 min). The upper aqueous and lower detergent phases were gently collected and reconstituted in final 1% Triton X-114 and TBS, respectively. Subsequently, the phase separation steps and collection of both phases were repeated. The detergent phase containing mainly integral membrane proteins (Bordier, 1981) was pooled and diluted with TBS before being subjected to protein quantification and SDS–PAGE. A modified method of Lowry's assay using a Dc Protein assay kit (Bio-Rad, Hercules, CA) was applied because of its compatibility with the detergent containing protein samples. The colored reaction product was measured at a wavelength of 750 nm.

Delipidation of Integral Proteins and Protein Profiling by SDS–PAGE

To obtain a pure fraction of integral proteins, contaminated lipids in detergent extracts were eliminated according to the delipidation method described by Mastro and Hall (1999). An ice-cold tri-*n*-butylphosphate:acetone:methanol (1:12:1) was added to the diluted detergent extracts to obtain a final 80% acetone concentration, and incubated at 4°C for 2–3 hr. At this

concentration, the integral proteins were readily precipitated leaving membrane lipids still dissolved in the organic solvent. The protein precipitate was pelleted (2,800*g*, 4°C, 10 min) and the supernatant containing lipids and detergent was discarded. The delipidated proteins were washed with acetone twice and finally resuspended in TBS. Protein concentration was determined by Bradford's protein assay.

Approximately 4 μg of total peripheral and integral membrane proteins isolated from S- and T-sperm as well as T proteins were resolved with 10% SDS–PAGE under a reducing condition (Laemmli, 1970) and further subjected to a silver staining method, as described by the manufacturer (Bio-Rad).

In Vitro Adsorption of Alexa-488 Conjugated Thelycal Proteins to Spermatophore Sperm

T proteins were conjugated to Alexa-488 fluorescent reactive dye (Molecular Probes) or biotinylated (Pierce, Rockford, IL) according to the procedure described by the manufacturers. Approximately, one million S-sperm were fixed with 4% paraformaldehyde for 1 hr and washed (500*g*, 5 min) with SW. Subsequently, the sperm were exposed to 5 mg/ml Alexa-488-conjugated T proteins at various time intervals, that is, 6, 12, and 24 hr, and washed twice (500*g*, 5 min) with SW to eliminate unbound conjugates prior to viewing under a Nikon Eclipse epifluorescent microscope equipped with a Nikon DXM 1200 CCD camera using a set of fluorescein filters (excitation/emission wavelength = 488/520 nm). A competition assay was performed by the addition of 50 mg/ml nonlabeled T proteins (10 fold) to compete with the labeled proteins. S-sperm incubated with Alexa-488- conjugated BSA or T-sperm incubated with Alexa-488-conjugated T proteins served as controls.

In an alternative experiment, aldehyde-fixed S-sperm were exposed to biotinylated T proteins under the same conditions described above. After extensive washing, sperm were treated either with 1 M NaCl in PBS to extract peripheral proteins or with SDS–PAGE loading buffer. They were then subjected to Western streptavidin blotting as described below.

Solid Phase Binding Assay of Labeled Thelycal Proteins With Sperm Membrane

Proteins and lipids. For the sperm protein binding assay, ~2–500 ng of each sample, including NaCl and Triton X-114 (with and without delipidation) protein extracts of S-sperm, was dotted onto a nitrocellulose membrane. The membrane was submersed in 4% BSA in TBS (1 hr, 4°C) to block any nonspecific binding. Then, dotted proteins were incubated (3 hr, 4°C) with biotinylated T proteins at various concentrations (1:250, 1:500, and 1:1,000) and extensively washed with TBS containing 0.1% Tween-20 (TBS-T). Thereafter, the samples were exposed (30 min, 4°C) to horseradish peroxidase (HRP) conjugated streptavidin (KPL, Gaithersburg, MD) (1:2,500) and visualized by means of an enhanced chemiluminescent method using an ECL kit (Amersham Pharmacia, Buckinghamshire, England). The competition assay was performed by the addition of an excessive amount of nonlabeled T proteins (10× that of labeled proteins) to interfere with the binding of labeled proteins.

For the sperm lipid binding assay, total sperm lipids were obtained following the chloroform/methanol extraction method described by Bligh and Dyer (1959). Dried lipids were resuspended in TBS, pH 7.4 and coated overnight onto a 96-well-plate. Unbound lipids were washed extensively with washing buffer (0.15 M PBS, pH 7.2). Nonspecific binding was eliminated with 1% BSA in washing buffer. Subsequently, the samples were incubated (3 hr, room temperature) with 0.1 mg/ml of biotinylated T proteins. After successive washes to remove unbound proteins, SDS–PAGE loading buffer was added to recover bound biotinylated T proteins followed by streptavidin blotting as described below.

Western Streptavidin Blotting

Bound biotinylated T proteins stripped either from whole sperm (by 1 M NaCl in PBS or SDS–PAGE loading buffer) or from micro-wells coated with sperm lipids as described above were resolved with 10% SDS–PAGE under a reducing condition (Laemmli, 1970). Thereafter, the protein samples on the gels were electrotransfered (Towbin et al., 1979) onto a Hybond N-ECL 0.45 μm nitrocellulose membrane (Amersham Pharmacia) and further exposed to streptavidin-HRP (1:2,500). Visualization of the streptavidin–biotin complexes was performed by an enhanced chemiluminescent method using an ECL kit.

Detection of Protein Tyrosine Phosphorylation

Two of the freshly retrieved spermatophores were artificially inseminated (AI) into the thelycum of an individual molting female shrimp. After 1, 2, and 3 days post-AI, the sperm were mechanically isolated and washed, according to the method described above. The total proteins of the whole sperm were quantified by Bradford's protein assay.

Approximately, 3 μg of total proteins taken from the S-sperm (Day 0) and Day 1, 2, and 3 post-AI sperm were resolved by 10% SDS–PAGE and transferred to a nitrocellulose membrane. The membrane was then subjected to Western immunoblotting using a monoclonal anti-protein tyrosine phosphate IgG (clone P-Try-102, Cell Signaling, Beverly, MA) (1:10,000) followed by a goat anti-mouse IgG-HRP (1:2,500) (Zymed, San Francisco, CA). Antigen–antibody complexes were detected by an enhanced chemiluminescent method using an ECL kit. In control experiments, retrieved spermatophores were incubated with SW for 1 day at 4°C and processed likewise as described for experimental samples.

Induction of the Acrosome Reaction of Artificially Inseminated Spermatophore Sperm

To investigate the physiological change in *P. monodon* sperm after translocation into the female thelycum at

different time points, the ability of AI sperm to undergo AR was monitored using a natural inducer, egg water (EW; collected as described previously by Griffin et al. (1987) with some modifications). Shrimp was allowed to spawn into a container containing 500 ml SW. After a gentle shaking for 5 min, eggs were settled at the bottom of the container and the flocculent SW or "egg water" was collected without disturbing the eggs. This EW was centrifuged (10,000*g*, 15 min) to remove any debris and the protein concentration was measured by Bradford protein assay.

S-sperm (Day 0) or Days 1, 2, and 3 post-AI sperm were isolated into filtered SW without protease inhibitors (known to block AR induction). These sperm were treated for 5 min with 40 and 100 μg/ml EW and without EW (control). Thereafter, a final concentration of 4% paraformaldehyde in SW was added to the sperm suspension. The status of the acrosome was checked under a Nikon phase contrast microscope and >200 sperm were counted for each data point. The acrosome intact sperm exhibited a long anterior spike while the acrosome reacted sperm showed a shortened spike. Differences among the samples tested were analysed statistically using ANOVA.

RESULTS

Comparison Between the Protein Profiles of S- and T-Sperm and the Profile of Thelycal Proteins

Profiles of NaCl- and detergent-extracted proteins of S- and T-sperm representing peripheral and integral proteins were compared in Figure 1. For peripheral proteins, the 72, 83, and 140 kDa proteins are more predominant in T-sperm than S-sperm; however, the 25, 45, and 70 kDa appeared to be more pronounced in S-sperm than T-sperm (Lane S_{Na} and T_{Na}, arrow heads). Some differences were also be notable in the integral proteins. A set of fast-mobility proteins with the M_r ranging from 35 to 43 kDa were clearly apparent in S-sperm while they were barely visible in T-sperm. On the other hand, the 53/55, 60, 72, and 83 kDa were more prominent in T-sperm than S-sperm (lane S_{De} and T_{De}, arrow heads). The 72 and 83 kDa proteins might be the traces of peripheral proteins that were abundantly present on the T-sperm surface. These results reflect both the adsorption of additional sperm peripheral and integral proteins as well as the removal of such proteins during sperm membrane modification. T proteins contained major protein bands with the molecular mass ranged from 50 to 200 kDa.

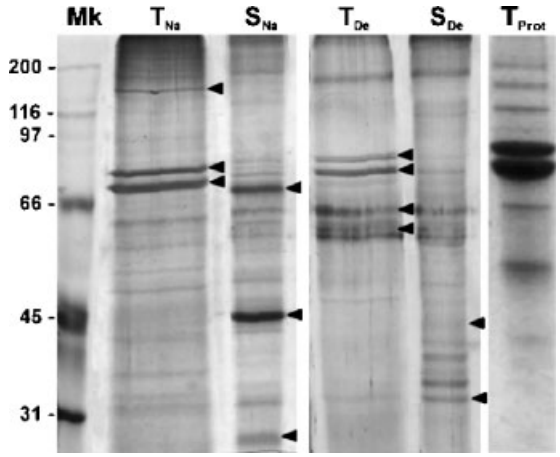


Fig. 1. Protein profiles of membrane extracts from thelycal (T) and spermatophore (S) sperm using NaCl (Na) and Triton X-114 (De) treatment, as well as thelycal proteins. Mk denotes standard markers.

In Vitro Transfer of Labeled Thelycal Proteins to the Surface of Spermatophore Sperm

We mimicked the adsorption of T components onto the sperm surface by incubating S-sperm in vitro with Alex-488 conjugated T proteins. The results in Figure 2 revealed an intense ring-like fluorescent staining around the entire sperm as well as on the anterior spikes (panels a and c). Interestingly, the longer the exposure to T proteins, the higher the number of positively stained sperm detected. The percentages of the stained sperm after 6-, 12-, and 24-hr incubation were 25, 40, and 95%, respectively. Moreover, the staining intensity of an individual sperm in all samples studied also varied from sperm to sperm (panels a and c, arrow heads). These results indicated a time-dependent adsorption of T proteins onto the surface of S-sperm. When an excess amount of nonlabeled T proteins was added to interfere with the binding of labeled proteins in the 24 hr incubating group, a minimal binding of labeled T proteins was achieved (panel e). Control sperm exposed to labeled BSA showed only background staining (data not shown). In addition, T-sperm exposed to labeled T proteins did not show positive staining, suggesting that these sperm were saturated with T components (data not shown).

Sperm Peripheral Proteins and Lipids Served as the Targets for Thelycal Protein Anchoring

Dot blot analysis as shown in Figure 3a revealed that NaCl extracts of S-sperm (S_{Na} represents peripheral proteins) had the highest adsorption activity with labeled T proteins, whereas the delipidated detergent extracts (S_{De}-delipid represents pure integral proteins) showed only background adsorption. Sperm detergent extracts (S_{De}) containing both membrane lipids and integral proteins revealed a moderate adsorption activity with T proteins. The control, where biotinylated BSA was used in place of labeled T proteins, showed minimal adsorption. A complete inhibition of the adsorption of labeled T proteins onto sperm peripheral proteins was demonstrated when an excess amount of nonlabeled proteins was added to compete with the binding (Fig. 3B, lower panel). These results indicate that, to a greater extent, T proteins were selectively directed to sperm peripheral proteins, and, to a lesser extent, to membrane lipids of S-sperm, but they did not interact with the integral proteins.

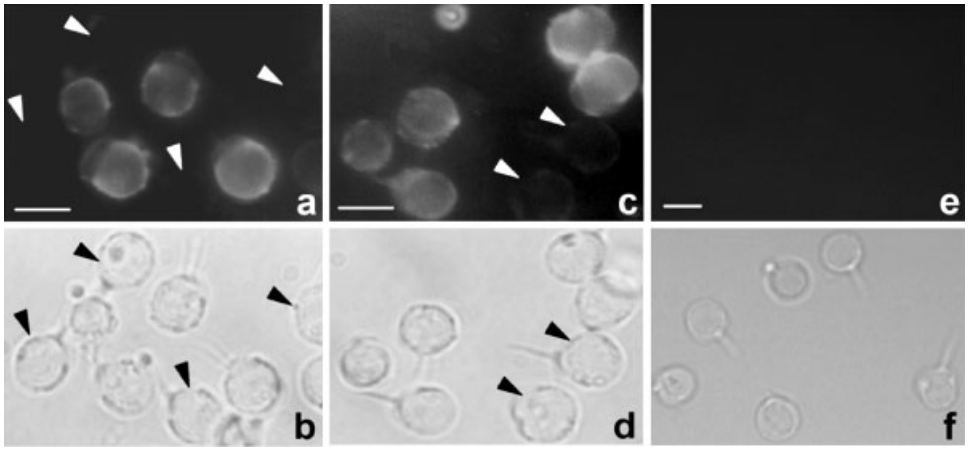


Fig. 2. In vitro adsorption of Alexa-488 labeled T proteins onto S-sperm surface. Note the increasing number of heterogeneously-stained sperm population after 12 hr (**a**) and 24 hr (**c**) incubation period. Arrow heads indicate unstained (a) or lightly stained (c) sperm. Background staining was observed when the 10-fold nonlabeled proteins were added to interfere with the binding (**e**). Above, a, c, and e are fluorescent micrographs; **b**, **d**, and **f** below are corresponding phase contrast micrographs. Bars = 10 μm.

Specific Thelycal Proteins Adsorbed Onto Sperm Membrane Acceptors

Labeled T proteins stripped from the whole sperm by SDS–PAGE loading buffer (which extracted the entire membrane components) revealed three distinct protein bands, that is, 60, 83, and 140 kDa (Fig. 4, lane 2). Alternatively, T proteins stripped from the entire sperm using 1 M NaCl in PBS (which extracted all peripheral proteins) revealed the 83 and 140 kDa T proteins (Fig. 4, lane 3). Furthermore, it appeared that the 60 kDa and, to the lesser extent, 53/55 kDa T proteins bound specifically to membrane lipids (Fig. 4, lane 4). Control sperm incubated in SW in place of labeled T proteins showed background staining (Fig. 4, lane 1).

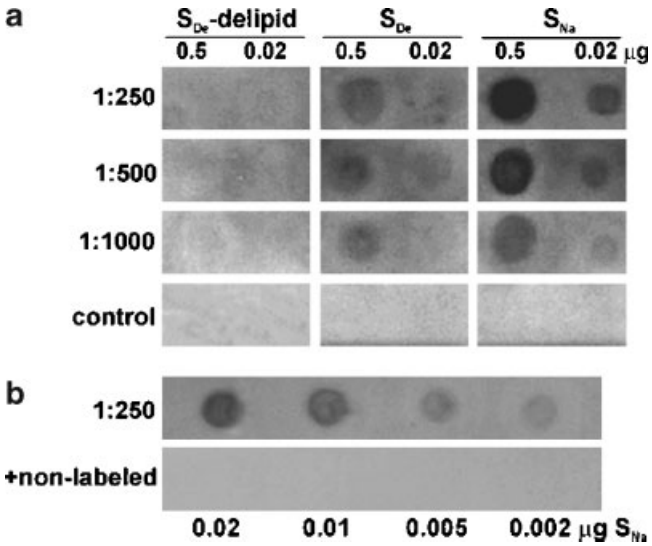


Fig. 3. Dot blot analysis of T protein binding to the sperm membrane acceptors. **a**: S-sperm membrane protein extracted by NaCl (SNa) or Triton X-114 with and without delipidation (SDe-delipid and SDe, respectively) were dotted onto a nitrocellulose membrane and exposed to various concentrations (1:250–1:1,000) of biotinylated T proteins. The control was those exposed to biotinylated BSA in place of labeled T proteins. **b**: NaCl extracts of S-sperm incubated with 1:250 labeled T proteins with the presence (**lower panel**) or absence (**upper panel**) of nonlabeled T proteins.

Sequential Increase of Sperm Protein Tyrosine Phosphorylation in Relation to the Duration of Thelycal Residence

A relatively low level of protein tyrosine phosphorylation was detected in the sperm directly isolated from the spermatophores (comparable to Day 0) (Fig. 5, lane 1). A step-wise increase of protein tyrosine phosphorylation was clearly apparent in the sperm taken from Day 1 and 2 post-AI and its level was relatively constant in Day 3 post-AI (Fig. 5, lanes 1–3). A drastic increase of 72 and 83 kDa phosphorylated proteins was observed on Days 2 and 3 post-AI, while proteins with the M_r ranging between 45 and 60 kDa also showed higher phosphorylated levels, compared to Day 0 and 1 post-AI (Fig. 5, arrow heads). Sperm isolated from spermatophores that were exposed to SW for 1 day revealed a background level of protein tyrosine phosphorylation similar to that of Day 0 sperm. The results suggest the significant role of T components in the sperm modification process, which in turn, results in an increased level of protein tyrosine phosphorylation.

Enhanced Response of Sperm Acrosome Reaction in Various Timings of Thelycal Storage

Since the sperm of *P. monodon* are immotile, we measured the ability of sperm to undergo an EW-induced AR as the only physiological endpoint. When Days 1, 2, and 3 post-AI sperm were treated with 40 μg/ml EW, the percentages of the AR responses were 23 ± 5.7, 55 ± 2.6, and $91 \pm 4.6\%$, respectively, while that of the S-sperm (Day 0) was $13 \pm 1.8\%$ (Fig. 6, solid bars). At 100 μg/ml EW, there was a slight increase in the AR response when

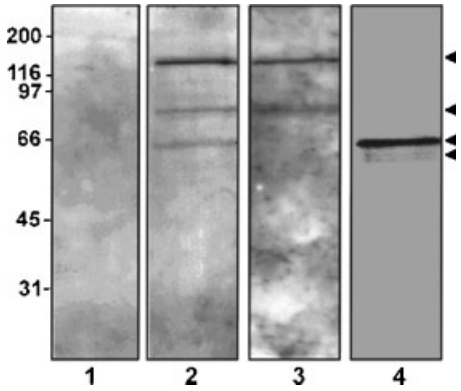


Fig. 4. Specific T proteins anchored to S-sperm peripheral proteins or lipids. S-sperm incubated with biotinylated T proteins were treated with SDS–PAGE loading buffer (**lane 2**) or 1 M NaCl in PBS (**lane 3**). The sperm extracted lipids were coated onto micro-well plate and subsequently incubated with labeled T proteins (**lane 4**). S-sperm from which labeled T proteins were omitted serve as negative control (**lane 1**).

compared to 40 μg/ml on Days 1 and 3 post-AI (Fig. 6, gray bars). A significant difference ($P < 0.01$) in the AR response between 100 μg/ml EW (75 ± 6.2) and 40 μg/ml EW (55 ± 2.6) was observed on Day 2 post-AI (Fig. 6, *). These results suggest that S-sperm have to be stored in the female thelycum for at least 3 days in order to gain a full response of sperm AR, thus increasing the fertilizing capacity.

DISCUSSION

Although a post-testicular modification of the close-thelycum penaeid shrimp has long been suggested to be crucial prior to fertilization (Clark and Griffin, 1988; Wikramanayake et al., 1992), the molecular mechanism

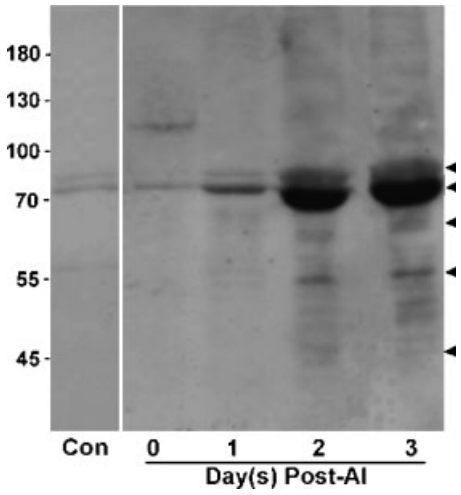


Fig. 5. Increase of protein tyrosine phosphorylation in relation to the duration of T residence. Spermatophores from male shrimp were artificially inseminated into thelycums of molting female shrimp in periods of 1, 2, and 3 days. The level of phosphorylation was detected in the total proteins of whole sperm by a monoclonal anti-tyrosine phosphate antibody. Proteins of S-sperm were also loaded as Day 0 before insemination for comparison. Protein extracts of sperm isolated from spermatophores which were exposed to SW for 1 day served as negative control.

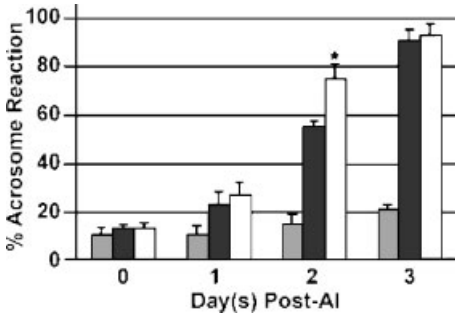


Fig. 6. Enhanced ability of inseminated sperm to undergo the acrosome reaction (AR). Day 0–3 post-artificial insemination (AI) sperm were tested for their ability to undergo AR with 40 μg/ml (solid bars) and 100 μg/ml (empty bars) egg water or without egg water (gray bars). Significant difference ($P < 0.01$) is denoted by *.

of this modification is still poorly understood. In this communication, we thus provided the information of the molecular modification of S-sperm by T components in another close-typed thelycum shrimp, *P. monodon*. The molecular basis of this modification was, to a certain extent, comparable to the mammalian sperm maturation and capacitation process (Yanagimachi, 1994; Cooper, 1998). Our silver staining profiles of both peripheral and integral membrane proteins, which revealed a relative difference between the extracted proteins of S- and T-sperm (Fig. 1), strongly indicated sperm plasma membrane modification. This process could have been accomplished through an adsorption of the T components onto the sperm plasma membrane or a removal of originally existing molecules from the sperm surface. Our following experimental evidence confirmed T protein adsorption: (1) the more pronounced 72, 83, and 140 kDa peripheral proteins, as well as 53/55 and 60 kDa integral proteins that were detected in T-sperm but were sparse in S-sperm; (2) the in vitro adsorption of Alexa-488-labeled T proteins onto the surface of S-sperm, but not T-sperm, which were saturated with T components (Fig. 2). This adsorption was a time-dependent process as indicated by a gradual increase in sperm population positively stained with labeled T proteins as well as the heterogeneity of sperm staining in all experimental groups (Fig. 2, a and c). The removal of certain protein species originally existing on S-sperm, for instance, the 25, 45, and 70 kDa peripheral proteins and 35–43 kDa integral proteins, were also revealed (Fig. 1). Mobilization of the sperm proteins that have less physiological relevance (so called "masking" molecules) in order to expose the buried egg-binding ligands, or the sperm proteins that serve more purposes during fertilization, is also crucial for the sperm to achieve maximum fertilizing ability (Hunter and Nornes, 1969; Oliphant et al., 1985).

The transfer of proteins from an epididymal source towards the sperm surface during mammalian sperm maturation has been extensively reported. One of the most well-studied examples is the adsorption of the epididymal carbonylreductases [i.e., hamster P26h (Legare et al., 1999); bull P25b (Frenette and Sullivan,

2001); monkey P31m (Lamontagne et al., 2001); human P34H (Boue et al., 1996)]. These proteins are transported to the sperm surface via multilamellar lipid vesicles known as prostasomes and become glycosylphosphatidylinositol (GPI)-linked proteins (Legare et al., 1999; Frenette and Sullivan, 2001). Other proteins, on the other hand, have been shown to be peripherally adhered to the existing sperm surface molecules and can thus be dissociated from their anchoring sperm ligands by a highly concentrated salt treatment. Some examples are β-galactosidase conjugated via fructose-6-phosphate (Grimalt et al., 1995), β-glucuronidase via mannose-6-phosphate (Barbieri et al., 1995), and our recently described arylsulfatase-A (AS-A) presumably via an interaction with the sulfated moiety of its existing substrate on the sperm surface, sulfogalactosylglycerolipid (SGG) (Carmona et al., 2002; Weerachatyanukul et al., 2003). Our findings in this article that the adsorbed 83 and 140 kDa T proteins which were extractable from the sperm surface by a high-strength NaCl treatment (Fig. 4) corresponded with the sperm peripheral membrane modification model.

Apart from the modification of peripheral molecules, we also reported here the interaction between the 53/55 and 60 kDa T proteins and the sperm membrane lipid extracts (Figs. 3 and 4), which was a part of the membrane lipid modification. The interaction was presumably mediated via hydrophobic conjugation or via direct incorporation of a prostasome-like carrier, as in the case of the carbonylreductases mentioned above. Modification and reorganization of sperm membrane lipids, particularly during sperm capacitation can drastically influence sperm physiological functions. It has been suggested that a decrease in cholesterol/phospholipid ratio of capacitated sperm up-regulates membrane fluidity, thus facilitating the fusion of the sperm plasma membrane and the outer acrosomal membrane during AR (Davis, 1981; Cross, 1998; Gadella and Harrison, 2000). A massive efflux of cholesterol during sperm capacitation seems to be a key point of membrane fluidity alteration (Wolf and Cardullo, 1991; Benoff, 1993; Cross, 1998). Reorganization of membrane phospholipids via many mediators has also been reported (Gadella et al., 2001; Rathi et al., 2001; Manjunath and Therien, 2002). While albumin, an enriched component of female reproductive tract and its functional agonistic compound, β-cyclodextrin, have been shown to play a crucial role in cholesterol sequestering (Davis et al., 1979; Cross, 1999; Visconti et al., 1999), a series of bovine seminal proteins (BSPs) and a scramblase enzyme have also been demonstrated to interact with phophatidylcholine and nonspecific phospholipid species, respectively, thus removing/reorganizing membrane phospholipids during capacitation (Gadella and Harrison, 2000; Manjunath and Therien, 2002). Cholesterol removal has recently been shown to trigger a cAMP-dependent protein tyrosine phosphorylation, a keynote event marking mammalian sperm capacitation (Galantino-Homer et al., 1997; Visconti and Kopf, 1998; Visconti et al., 1999). Among all marine invertebrates, we have demonstrated here, for the first time, a sequential increase of protein tyrosine phosphorylation during the T residence of shrimp sperm (Fig. 5). In fact, the results also indicate the conservation of this well-defined signal transduction pathway, at least from crustaceans to mammals. Furthermore, the increased response in the sperm AR, which required at least 3 days of T residence to achieve the maximum response (Fig. 6), added more fundamental detail to that previously reported in *S. ingentis* (Griffin et al., 1987). This would conclusively indicate the essence of T-dependent sperm modification as an indispensable process before gamete fertilization in this species.

Sets of experiments are being conducted in our laboratory to explore the molecular mechanism, how the membrane modification initiates a signal transduction and protein tyrosine phosphorylation in the sperm of penaeid species.

ACKNOWLEDGMENTS

The authors thank Ms. Penchan Meechonkit for the administrative help.

REFERENCES

Barbieri AM, Sosa MA, Grimalt P, Mayorga LS, Bertini F. 1995. Phosphomannosyl receptors on the surface of spermatozoa from the cauda epididymis of the rat. Int J Androl 18:113–119.

Benoff S. 1993. Preliminaries to fertilization. The role of cholesterol during capacitation of human spermatozoa. Hum Reprod 8:2001–2006.

Bligh GE, Dyer WJ. 1959. A rapid method of total lipid extraction and purification. Can J Biochem Physiol 37:911–917.

Bordier C. 1981. Phase separation of integral membrane proteins in Triton X-114 solution. J Biol Chem 256:1604–1607.

Boue F, Blais J, Sullivan R. 1996. Surface localization of P34H an epididymal protein, during maturation, capacitation, and acrosome reaction of human spermatozoa. Biol Reprod 54:1009–1017.

Carmona E, Weerachatyanukul W, Soboloff T, Fluharty AL, White D, Promdee L, Ekker M, Berger T, Buhr M, Tanphaichitr N. 2002. Arylsulfatase is present on the pig sperm surface and is involved in sperm–zona pellucida binding. Dev Biol 247:182–196.

Clark WH, Jr., Griffin FJ. 1988. The morphology and physiology of the acrosome reaction in the sperm of the decapod, *Sicyonia ingentis*. Dev Growth Differ 30:451–462.

Clark WH, Jr., Talbot P, Neal RA, Mick CR, Salser BR. 1973. In vitro fertilization with nonmotile spermatozoa of the brown shrimp *Penaeus aztecus*. Mar Biol 22:353–354.

Clark WH, Jr., Kleve MG, Yudin AI. 1981. An acrosome reaction in natantian sperm. J Exp Zool 218:279–291.

Clark WH, Jr., Griffin FJ, Witkramanayake AW. 1994. Prefusion events of sperm–oocyte interaction in the marine shrimp, *Sicyonia ingentis*. Dev Biol 5:225–231.

Cooper TG. 1998. Interactions between epididymal secretions and spermatozoa. J Reprod Fertil Suppl 53:119–136.

Cross NL. 1998. Role of cholesterol in sperm capacitation. Biol Reprod 59:7–11.

Cross NL. 1999. Effect of methyl-beta-cyclodextrin on the acrosomal responsiveness of human sperm. Mol Reprod Dev 53:92–98.

Davis BK. 1981. Timing of fertilization in mammals: Sperm cholesterol/phospho lipid ratio as a determinant of the capacitation interval. Proc Natl Acad Sci USA 78:7560–7564.

Davis BK, Byrne R, Hangund B. 1979. Studies on the mechanism of capacitation II. Evidence for lipid transfer between plasma membrane of rat sperm and serum albumin during capacitation in vitro. Biochim Biophys Acta 558:257–266.

Flesch FM, Gadella BM. 2000. Dynamics of the mammalian sperm plasma membrane in the process of fertilization. Biochim Biophys Acta 1469:197–235.

Frenette G, Sullivan R. 2001. Prostasome-like particles are involved in the transfer of P25b from the bovine epididymal fluid to the sperm surface. Mol Reprod Dev 59:115–121.

Gadella BM, Harrison RA. 2000. The capacitating agent bicarbonate induces protein kinase A-dependent changes in phospholipid transbilayer behavior in the sperm plasma membrane. Development 127:2407–2420.

Gadella BM, Rathi R, Brouwers JF, Stout TA, Colenbrander B. 2001. Capacitation and the acrosome reaction in equine sperm. Anim Reprod Sci 68:249–265.

Galantino-Homer H, Visconti PE, Kopf GS. 1997. Regulation of protein tyrosine phosphorylation during bovine sperm capacitation by a cyclic adenosine 39,59-monophosphate-dependent pathway. Biol Reprod 56:707–719.

Griffin FJ, Clark WH, Jr., Crowe JH, Crowe LM. 1987. Intracellular pH decreases during the in vitro induction of the acrosome reaction in the sperm of *Sicyonia ingentis*. Biol Bull 173:311–323.

Grimalt P, Barbieri MA, Sosa MA, Bertini F. 1995. Organ-specific binding system for beta-galactosidase in the male reproductive tract. Int J Androl 18:243–247.

Hunter AG, Nornes HO. 1969. Characterization and isolation of a sperm-coating antigen from rabbit seminal plasma with capacity to block fertilization. J Reprod Fertil 20:419–427.

Jones R. 1998. Plasma membrane structure and remodelling during sperm maturation in the epididymis. J Reprod Fertil Suppl 53:73–84.

Laemmli UK. 1970. Cleavage of structural proteins during the assembly of the head of bacteriophage T4. Nature 227:680–685.

Lamontagne N, Legare C, Gaudreault C, Sullivan R. 2001. Identification and characterization of P31m, a novel sperm protein in cynomolgus monkey (*Macaca fascicularis*). Mol Reprod Dev 59: 431–441.

Legare C, Berube B, Boue F, Lefievre L, Morales CR, El-Alfy M, Sullivan R. 1999. Hamster sperm antigen P26h is a phosphatidylinositol-anchored protein. Mol Reprod Dev 52:225–233.

Manjunath P, Therien I. 2002. Role of seminal plasma phospholipid-binding proteins in sperm membrane lipid modification that occurs during capacitation. J Reprod Immunol 53:109–119.

Mastro R, Hall M. 1999. Protein delipidation and precipitation by tri-*n*-butylphosphate, acetone, and methanol treatment for isoelectric focusing and two-dimensional gel electrophoresis. Anal Biochem 273: 313–315.

Ohlendieck K, Lennarz WJ. 1996. Molecular mechanisms of gamete recognition in sea urchin fertilization. Curr Top Dev Biol 32:39–58.

Oliphant G, Reynolds AB, Thomas TS. 1985. Sperm surface components involved in the control of the acrosome reaction. Am J Anat 174:269–283.

Rathi R, Colenbrander B, Bevers MM, Gadella BM. 2001. Evaluation of in vitro capacitation of stallion spermatozoa. Biol Reprod 65: 462–470.

Suarez SS. 1996. Hyperactivated motility in sperm. J Androl 17:331–335.

Towbin H, Staehelin T, Gordon J. 1979. Electrophoresis transfer of proteins from polyacrylamide gels to nitrocellulose sheets: Procedures and some applications. Proc Natl Acad Sci USA 76:4350.

Vacquier VD. 1998. Evolution of gamete recognition proteins. Science 281:1995–1998.

Visconti PE, Kopf GS. 1998. Regulation of protein phosphorylation during sperm capacitation. Biol Reprod 59:1–6.

Visconti PE, Galantino-Homer H, Ning X, Moore GD, Valenzuela JP, Jorgez CJ, Alvarez JG, Kopf GS. 1999. Cholesterol efflux-mediated signal transduction in mammalian sperm. beta-cyclodextrins initiate transmembrane signaling leading to an increase in protein tyrosine phosphorylation and capacitation. J Biol Chem 274:3235–3242.

Weerachatyanukul W, Rattanachaiyanont M, Carmona E, Furimsky A, Mai A, Shoushtarian A, Sirichotiyakul S, Ballakier H, Leader A, Tanphaichitr N. 2001. Sulfogalactosylglycerolipid is involved in human gamete interaction. Mol Reprod Dev 60:569–578.

Weerachatyanukul W, Xu H, Anupriwan A, Carmona E, Wade M, Hermo L, da Silva SM, Rippstein P, Sobhon P, Sretarugsa P, Tanphaichitr N. 2003. Acquisition of arylsulfatase A onto the mouse sperm surface during epididymal transit. Biol Reprod 69:1183–1192.

White D, Weerachatyanukul W, Gadella B, Kamolvarin N, Attar M, Tanphaichitr N. 2000. Role of sperm sulfogalactosylglycerolipid in mouse sperm–zona pellucida binding. Biol Reprod 63:147–155.

Wikramanayake AH, Uhlinger KR, Griffin FJ, Clark WH, Jr.. 1992. Sperm of the shrimp *Sicyonia ingentis* undergo a bi-phasic capacitation accompanied by morphological changes. Dev Growth Differ 34: 347–355.

Wolf DE, Cardullo RA. 1991. Physiological properties of the mammalian sperm plasma membrane. In: Baccetti B, editor. Comparative spermatology 20 years after. New York: Raven Press. pp 599–604.

Yanagimachi R. 1994. Mammalian fertilization. In: Knobil E, Neill JD, editors. The physiology of reproduction. New York: Raven Press. pp 189–317.

MOLECULAR REPRODUCTION AND DEVELOPMENT 70:211–221 (2005)

Basic Nuclear Protein Pattern and Chromatin Condensation in the Male Germ Cells of a Tropical Abalone, *Haliotis asinina*

WORAWIT SUPHAMUNGMEE,[1] SOMJAI APISAWETAKAN,[1] WATTANA WEERACHATYANUKUL,[1] CHAITIP WANICHANON,[1] PRAPEE SRETARUGSA,[1] TANES POOMTONG,[2] AND PRASERT SOBHON[1]*

[1]*Department of Anatomy, Faculty of Science, Mahidol University, Rama VI Road, Bangkok, Thailand*
[2]*The Coastal Aquaculture Development Center, Department of Fisheries, Klong-wan, Prachuabkirikhun Province, Thailand*

ABSTRACT The basic nuclear proteins (BNPs) in spermatozoa of a tropical abalone, *Haliotis asinina*, were composed of a majority of protamine-like (PL) protein and a small amount of histones H1 and H4. Abalone H1 and PL proteins exhibited strong immunological cross reactivities among themselves as well as with chick H5 and calf thymus H1. Thus, all these proteins may belong to the same family. Immunolocalization by indirect immunofluorescence and immunoelectron microscopy indicated that H1 and H4 were present in all steps of the male germ cells, however, with decreasing amount in late stage cells, particularly spermatids and spermatozoa. On the other hand, PL was present in middle step cells (secondary spermatocytes) with increasing amount in spermatids and spermatozoa when the chromatin became tightly packed. Thus, PL may be involved in the condensation of chromatin in the spermatozoa of this species. *Mol. Reprod. Dev. 70: 211–221, 2005.*
© 2005 Wiley-Liss, Inc.

Key Words: *Haliotis asinina*; sperm; basic nuclear proteins; protamine-like protein; chromatin condensation

INTRODUCTION

A high degree of condensation of the chromatin in mollusc sperm has been observed in many marine species, such as a prosobranch gastropod *Helcion pellucidus* (Sousa and Oliveira, 1994), a neogastropod *Murex brandaris* (Caceres et al., 1999), a cenogastropod *Thais hemostoma* (Ribes et al., 2001), and a cephalopod *Eledone cirrhosa* (Gimenez-Bonafe et al., 2002). However, the exact mechanism causing the condensation of the chromatin has not yet been elucidated. Biochemical studies showed that the basic protein components within the sperm nuclei of these molluscs contain protamine-like proteins (PL), which are rich in lysine and arginine, with a very low content of hydrophobic amino acids, whereas varying amount of histones still exist depending on species (Ausio and Van Holde, 1987; Galindo et al., 1992). PL has a trypsin-resistance globular core with a high sequence similarity to histone H5 present in the nuclei of chicken erythrocytes, which is a member of the histone H1 family (Ausio et al., 1987). H1-like and PL proteins were also demonstrated in the bivalve sperm of *Mytilus* and *Spisula* spp. (Giancotti et al., 1992), and are believed to originate from the common evolutionary origin as H1. Recently, our group has shown that in frog (*Rana tigerina*), H1 variant (H1V) is also related to H5 and may be instrumental in causing the condensation of chromatin in the sperm of this species, which incidentally lack both protamine and PL proteins (Manochantr et al., 2005).

So far in *Haliotis* spp., the pattern of basic proteins in the sperm nuclei has been studied only in *Haliotis tuberculata* (Subirana et al., 1973), and *Haliotis crackeroidii* (Balhorn et al., 1979). The latter authors suggested that protamine is the only component of the basic nuclear protein (BNP) in sperm of these temperate abalone species, while the histone fractions are totally absent. They have shown further that the abalone protamine contains very high amount of arginine, lysine, and serine, whereas it lacks cysteine. This protamine molecule has a higher molecular weight than salmon and mammalian protamines, but smaller than that of histones. In the present study, we have attempted to study the pattern of the basic proteins in the nuclei of sperm and testicular nuclei of a tropical abalone, *Haliotis asinina*, and localized the appearance of histones and PL protein in various steps of the male germ cells.

MATERIALS AND METHODS

Specimens

Adult male *Haliotis asinina*, aged more than 24 months, were obtained from the land-based aquaculture system operated by the Coastal Aquaculture Development Center, Department of Fisheries, Ministry

Grant sponsor: Thailand Research Fund.

*Correspondence to: Prof. Dr. Prasert Sobhon, Department of Anatomy, Faculty of Science, Mahidol University, Rama VI Road, Bangkok 10400, Thailand. E-mail: scpso@mahidol.ac.th

Received 26 April 2004; Accepted 24 May 2004
Published online in Wiley InterScience (www.interscience.wiley.com).
DOI 10.1002/mrd.20199

© 2005 WILEY-LISS, INC.

of Agriculture and Cooperatives, Klong-Wan, Prachuabkirikhun. The maturity of the male gonad was determined by the appearance as its creamy white or yellowish surface (Singhagraiwan and Doi, 1993). The mature sperm were collected from the abalone that spawn into seawater. These sperm were filtered through 45 μm nylon mesh and washed in the filtered seawater.

Preparation of the Nuclei From Sperm and Testicular Germ Cells

The mature abalone sperm were centrifuged at 500*g*, 4°C, for 10 min. The pellet was resuspended and centrifuged twice in an ice-cold buffer A (2 mM $MgCl_2$, 250 mM sucrose, 10 mM Tris, pH 7.4). It was then incubated in a solution containing 0.15M NaCl, 1% Triton X-100, 10 mM Tris-HCl, pH 8.0, and 1 mM phenylmethylsulfonyl fluoride (PMSF) at 4°C. The suspension was sonicated 10 times with a 15 sec burst. After centrifugation, the pellet containing only sperm nuclei, devoiding of the tails and acrosomes as judged by viewing under a light microscope, was washed twice in buffer A at 4°C. In addition to the abalone sperm, the rat sperm nuclei were prepared by the same protocol and used for comparison.

To isolate nuclei from the abalone testicular cells, the whole testis, dissected free from the hepatopancreas, was teased and homogenized in an ice-cold buffer B (3 mM $MgCl_2$, 0.31M sucrose, 0.05% Triton X-100, 10 mM KH_2PO_4, pH 6.0, and 1 mM PMSF). The homogenate was centrifuged at 600*g*, 4°C, for 10 min, and the supernatant was discarded. The pellet was rehomogenized and recentrifuged by the same procedure. Testicular cells were then incubated in a solution containing 0.15M NaCl, 1% Triton X-100, 10 mM Tris-HCl, pH 8.0, and 1 mM PMSF at 4°C. The suspension was sonicated 10 times with a 15 sec burst. The pure testicular cells' nuclei, as judged by viewing under a light microscope, were washed twice in the washing buffer (5 mM $MgCl_2$, 5 mM NaH_2PO_4, pH 6.5) at 4°C.

Extraction of the BNPs

The isolated nuclei from sperm and testicular cells were treated in a reducing solution (0.15M NaCl, 10 mM dithiothreitol, 50 mM Tris-HCl, pH 8.0) at 4°C, for 1 hr (for abalone nuclei) and 3 hr (for rat sperm nuclei). Thereafter, the nuclei were dissolved in 0.4N hydrochloric acid (HCl) and left at 4°C, for 2 hr. The supernatant was removed after centrifugation at 12,000*g*, 4°C, for 10 min, and the BNP were precipitated by 20% trichloroacetic acid (TCA). The precipitated proteins were then centrifuged at 12,000*g*, 4°C, for 10 min. The pellet was washed twice in cold acidified acetone, and in several changes of cold acetone. Finally, the protein pellet was dried in a vacuum dessicator for 1 hr and stored at −20°C until used.

For comparison, BNPs from chicken erythrocytes' nuclei were also prepared. The collected chicken blood was immediately mixed with 10 mM ethylenediamine tetraacetic acid (EDTA) and then spun at 600*g*, 4°C, for 10 min. The pellet of erythrocytes was resuspended in a hypotonic solution (0.5% Triton X-100 in an ice-cold buffer A), 4°C, for 5 min. After centrifugation at 1,000*g*, 4°C, for 10 min, the pellet which contained pure erythrocytes' nuclei was resuspended in a washing buffer (5 mM $MgCl_2$, 5 mM NaH_2PO_4, pH 6.5) at 4°C, and then recentrifuged at the same condition. The washing steps were repeated until the pellet was colorless. Finally, the pellet was resuspended in buffer A and stored at 4°C. Basic proteins were extracted by 0.4N HCl and precipitated by 20% TCA as described above. Furthermore, for comparison, salmon protamine sulfate and calf thymus histone H1 were purchased from Sigma-Aldrich Chemical Co., Saint Louis, MO.

Protein Purification

The BNPs extract from the abalone sperm's nuclei were fractionated into individual components by reverse phase HPLC on a NOVAPAK C_{18} column (15 × 0.39 cm in size with 4 μm in slit diameter). Each sample was dissolved in 1N Tris buffer, pH 8.0 and then carefully pushed through 0.22 μm nylon filter in order to get rid of contaminants. The purification was performed using a linear gradient of acetronitrile (0%–20%) in 0.1% trifluoroacetic acid, at a flow rate of 1 ml/min, for 115 min. The eluent of protamine-like (PL) protein was collected and freeze-dried overnight. Molecular weight of the purified PL protein was determined by mass spectrometry.

Gel Electrophoresis

Extracted BNPs from all specimens mentioned above were dissolved in the sample buffer containing 1 ml glacial acetic acid, 5.4 g urea, 0.5 ml β-mercaptoethanol, 0.1% pyronin-G in 4.5 ml deionized water. Each protein fraction was carefully loaded into wells (at 10 μg per well) of acetic acid–urea–Triton X-100 (AUT) polyacrylamide gels (resolving gel: 15% acrylamide, 2.5M urea, 6 mM Triton X-100, 5% acetic acid; stacking gel: 7.5% acrylamide, 2.5M urea, 4 mM Triton X-100, 1.5% acetic acid) in a 10 × 10 cm Hoefer vertical slab gel electrophoretic apparatus with 0.75 mm spacers (Amersham Biosciences, Buckinghamshire, UK). The separation was done in an electrophoretic buffer (0.9N acetic acid) at a constant voltage (120 V), for 2 hr. Bands of the BNPs were detected by Coomassie blue stain.

For the production of polyclonal antibodies, bands of histones H1 and H4 and PL protein were directly excised from AUT gels, ground with Tris buffer, pH 8.0, and then stored at −20°C until used for immunization.

Antibody Production

Six-week old female mice (strain ICR) were immunized by subcutaneous injection with the selected abalone testicular BNP, i.e., H1, H4, and PL prepared as mentioned above. Each protein (∼100 μg) was mixed with an equal volume of Freund's complete adjuvant (Sigma-Aldrich Co.). Boosting injections, each containing the same amount of protein with Freund's incomplete adjuvant, were given twice at 2-week intervals. Immune sera were collected by the tail bleeding and

tested by Western blotting with preimmune sera as the control. The animals, whose antisera were found to be reacting exclusively with the targeted antigens, were sacrificed at 7th day after the second boosting, and blood was collected from the heart. After centrifugation, the antisera were kept at −20°C until used.

Western Blot Analysis

BNPs separated in AUT gel were electrophoretically transferred onto nitrocellulose membrane (Amersham Pharmacia Biotech) in an electrophoretic transfer chamber (LKB Bromma, Hoefer Scientific Instruments, San Francisco, CA), using the current set at 400 mA, for 4 hr, in a cold transfer buffer (0.9N acetic acid). Nonspecific bindings were blocked with 5% skimmed milk in 10 mM Tris buffer saline, pH 7.4, 0.1% Tween-20 (TBST), and then the membranes were incubated in mouse antiserum to H1 or PL protein (at 1:500 dilution for anti-H1 and at a serial dilution of 1:100, 1:250, 1:500, 1:1,000 for anti-PL), for 1 hr at room temperature. For the negative control, the membrane strips were incubated with preimmune serum instead of primary antibodies. Then, the membranes were incubated in goat anti-mouse IgG conjugated to horseradish peroxidase (Zymed Labolatories Inc., San Francisco, CA) in TBST at 1:4,000 dilution, for 30 min at room temperature, and visualized by the color reaction between diaminobenzidine (Sigma-Aldrich Co.) and 0.013% H_2O_2, enhanced with 0.03% $NiCl_2$.

Indirect Immunofluorescence

For localizing histones H1, H4, and PL proteins in various steps of the abalone male germ cells, the spawned spermatozoa and blocks of testicular tissue were immersed in a fixative solution of 0.5% glutaraldehyde, 4% paraformaldehyde in 0.1M phosphate buffer, pH 7.8 at 4°C, for 3 hr. After washing, specimens were dehydrated in an increasing concentration of ethanol (50%–100%), and embedded in LR White resin (London Resin Co., Thule, England). Semithin sections, about 1 μm thick, were cut using MT-2 Porter-Blum ultramicrotome fitted with glass knives. Indirect immunofluorescence was performed by washing semithin sections in 10 mM Tris buffer saline (TBS), pH 7.4 and then incubating them in the blocking solution containing 0.15M glycine, and in 4% bovine serum albumin (BSA) (Sigma-Aldrich Co.) in TBS, respectively. The sections were incubated further in mouse anti-H1 (dilution 1:500), anti-H4 (dilution 1:500), and anti-PL (dilution 1:200) antisera or preimmune sera (for the control) in TBST, for 1 hr at 37°C, and then washed in the same buffer. Immunofluorescence signal was detected by incubating the sections in biotinylated rabbit anti-mouse IgG (Zymed Labolatories Inc.) in TBST at 1:100 dilution, and then with fluorescein isothiocyanate (FITC)-conjugated streptavidin (Amersham Pharmacia Biotech) in TBST at 1:100 dilution, 37°C, for 30 min. After the third wash, the sections were mounted with cover glasses, using Vectashield mounting medium (Vector Laboratories Inc., Burlingame CA), observed and photographed under a Nikon epifluorescence microscope.

Immunoelectron Microscopy

LR White embedded tissue samples used for localization of H1 and PL proteins by immunoelectron microscopy were prepared as described above. Ultrathin sections were cut and placed on 300-mesh nickle grids. The sections were then washed in 50 mM TBS, pH 7.4 and then incubated in the blocking solutions containing 0.15M glycine, and in 4% BSA in TBS, respectively. Then, they were incubated in mouse anti-H1 (dilution 1:50), anti-PL (dilution 1:100), or preimmune serum (as the control) in 50 mM TBS at 37°C for 2 hr. After washing five times in the same buffer, the sections were incubated with protein A conjugated to 20 nm colloidal gold (Sigma-Aldrich Co.) in TBS at the dilution of 1:100. The sections were then washed with TBS, fixed in 1% glutaraldehyde. After washing in deionized distilled water, they were stained with uranyl acetate and observed in a Hitachi H-300 TEM set at 75 kV.

RESULTS

BNP Profile in the Male Germ Cells of *H. asinina*

BNPs from the abalone testicular nuclei (Fig. 1A, lane 2) separated in AUT gel exhibited bands which were equivalent to histones from chick erythrocytes' nuclei, which were used as the references (Fig. 1A, lane 1), i.e., H2A, H3, H2B, H4, and H1. However, these bands were weakly stained compared to chick histones. There was no band equivalent to H5 as present in the chick erythrocytes' nuclei. BNPs from the abalone sperm showed a substantial amount of H4, detectable amount of H1, while H2A, H2B were very weakly stained and H3 were lost (Fig. 1A, lane 3). Furthermore, abalone H4 appeared to have slightly higher electrophoretic mobility than that of the chick's equivalent, while the remaining histone bands showed identical mobility. In addition to H1 and H4 histones, there was a fast moving band, which appeared broad and intensely stained, whose mobility was only slightly less than protamine from rat sperm ($M_r \cong 7{,}000$; Fig. 1A, lane 4), and much less compared to salmon protamine ($M_r \cong 4{,}000$; Fig. 1A, lane 5). Judging from its similar electrophoretic mobilities with those found in other mollusc species (Ausio, 1992; Rocchini et al., 1995), this fast moving band should be protamine-like (PL) protein. Chromatogram of BNPs of *H. asinina* sperm showed the dominant peak of PL, which was well separated from other histones (Fig. 2). The molecular mass (M_r) of the eluted PL, as determined by mass spectrometry, was at 10,015 Da. In addition to PL, there was an intermediate protein band (IP) in both testicular and sperm nuclei, whose mobility was halfway between H1 and PL protein (Fig. 1A, lanes 2 and 3). Both IP and PL proteins were more prominent in sperm than in the testicular nuclei. There was no equivalent to this IP band in chick or rat sperm BNPs (Fig. 1A, lanes 1 and 4).

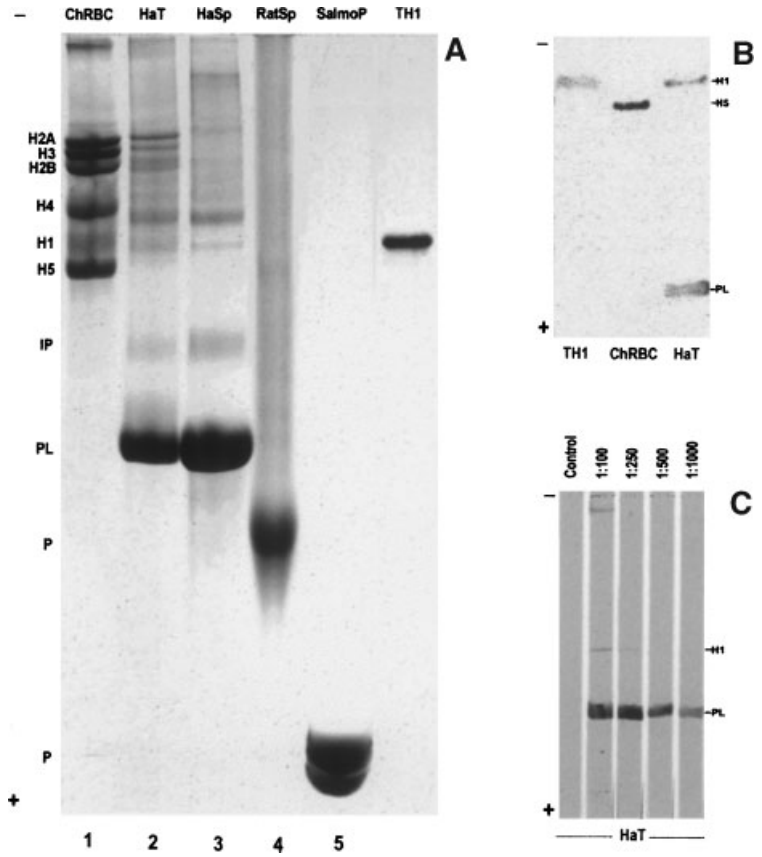


Fig. 1. A: Electrophoretic pattern of the basic nuclear proteins (BNPs) separated on 15% AUT-PAGE. BNPs extracted from chick erythrocytes' nuclei (ChRBC) are used as referenced histones (**lane 1**). BNPs extracted from *H.asinina* testicular cells (HaT) and spawned spermatozoa (HaSp) are run in **lanes 2** and **3**, respectively. The rat sperm BNPs (**lane 4**, RatSp), salmon protamine sulfate (**lane 5**, SalmoP), and calf thymus histone H1 (**lane 6**, TH1) are used as the references. **B**: Calf thymus histone H1 (**lane 1**,-TH1), BNPs from the nuclei of chicken erythrocytes (**lane 2**, ChRBC), and *H. asinina* testicular cells (**lane 3**, HaT) are electrophoresed in 15% AUT-PAGE, transferred onto nitrocellulose membrane, and probed with mouse anti-H1. The positive bands (H1, H5, PL) are exhibited by staining with secondary antibody conjugated to horseradish peroxidase. **C**: The mouse antiserum against PL protein (at various dilutions 1:100–1:1,000) is used as probed to stain nitrocellulose membrane strips containing BNPs extracted from the nuclei of *H. asinina* testicular cells (HaT). There is strong reaction of the antibody to PL band and weak reaction with H1 band (**lane 2**).

Characterization of Antisera to *H. asinina* H1 and PL Protein

Electrophoretically separated abalone testicular BNPs, chicken erythrocytes BNPs, and calf thymus histone H1 were transferred onto nitrocellulose membrane sheets as described in "Materials and Methods." Mouse antibody against histone H1 was used as a probe in the Western blot analysis. The immunoblotting pattern indicated that both abalone H1 and PL, chick H5 and calf thymus H1 cross-reacted with anti-H1, while other histones in both chick erythrocytes' and abalone testicular nuclei did not (Fig. 1B). In a similar experiment where the BNPs from the abalone testicular nuclei were probed with anti-PL, only H1 and PL bands exhibited cross-reactivity (Fig. 1C). These data implicated that anti-H1 serum cross-reacted with the calf thymus histone H1, chick histone H5, as well as abalone PL protein. Whist anti-PL serum cross-reacted with H1 and PL bands, especially at the high concentration of the antiserum and the reactivity diminished when anti-PL serum concentration was decreased (Fig. 1C).

Localization of Histones H1, H4, and PL Protein in the Male Germ Cells of *H. asinina* by Indirect Immunofluorescence

Immunoblotting as shown above indicated that antibodies against H1 and PL were quite specific, and could be used for immunolocalization of histone H1 and PL in the abalone testicular cells and sperm. Similarly, mouse antiserum against histone H4 fractionated from AUT-PAGE, was also tested to be quite specific and used as primary antibody. Semithin LR White sections were stained with each antibody followed by FITC-conjugated goat anti-mouse IgG as secondary antibody.

Localization of H1. Anti-histone H1 showed strong fluorescence over the nuclei of spermatogonia (Sg) and primary spermatocytes (PSc), which were located close to the connective tissue trabeculae of the testis (Fig. 3B) (also see Sobhon et al., 2001 for detailed histology and male germ cell classification). Moderate staining was observed in the nuclei of middle steps germ cells, including secondary spermatocytes (SSc), which were located further away from the trabeculae. The fluorescence was

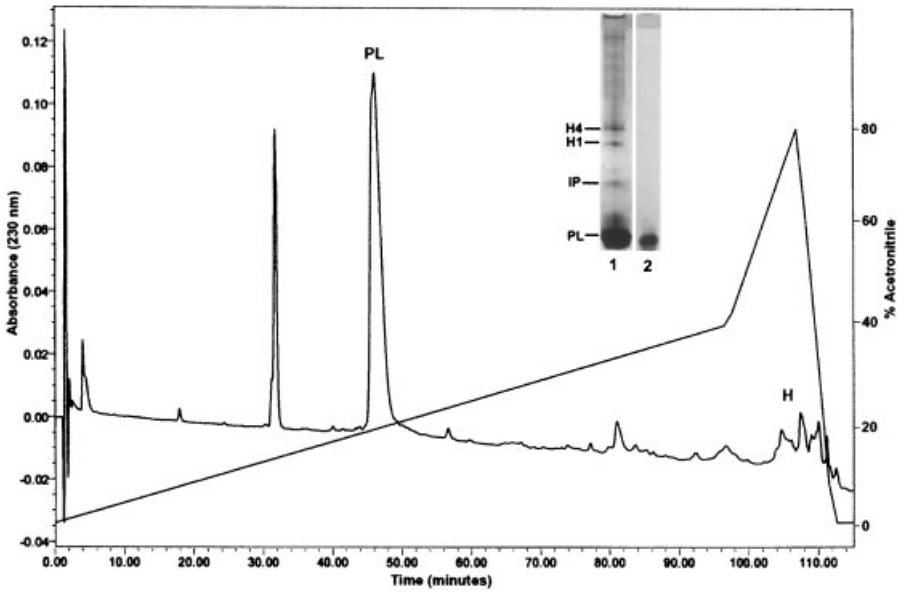


Fig. 2. HPLC fractionated *H. asinina* sperm BNPs using a linear gradient of acetronitrile (0%–20%). Protamine-like (PL) fraction is eluted at 38–40 min as shown in the chromatogram. A dominant band of an eluted PL fraction (**lane 2**) is shown after analysis on Coomassie blue stained 15% AUT-PAGE, in comparison to the whole sperm BNPs in a similar gel (**lane 1**). H, histones; PL, protamine-like protein.

progressively decreased over the nuclei of spermatids (St) and spermatozoa (Sz), which were located at the outermost layer some distance away from the trabecular axis (Fig. 3B)

Localization of H4. Intense fluorescence due to the staining by anti-H4, which is the nucleosomal core histone, was observed over the nuclei of PSc and SSc, which were located close to the trabecular axis (Fig. 3C). Decreasing fluorescence was expressed over the nuclei of spermatids, particularly steps three (St_3) and four (St_4), and mature sperm. In these late step cells, the fluorescence still remained strong at the nuclear rim, while in the central area of the nuclei the fluorescence was weak or absent (Fig. 3D). Only a very weak non-specific fluorescence was observed in the control section (Fig. 3A).

Localization of PL protein. The fluorescence was absent or very weak in the early step cells (Sg, PSc). Intense fluorescence was, however, observed in the nuclei of middle and final step cells, including SSc, St_1–St_4 spermatids, and Sz (Fig. 4B,E). No fluorescence was observed over the acrosomal cap and tail regions of the mature spermatozoa (Fig. 4D,E). The control section showed very faint background fluorescence (Fig. 4A).

Localization of H1 and PL by Immunoelectron Microscopy

Localization of H1. Immunogold labels from staining with anti-histone H1 were found over the nuclei of all steps of spermatogenic and spermiogenic cells (Fig. 5). The gold particles were especially abundant in a spermatogonium, whose chromatin was loosely packed (Fig. 5A,B), and gradually diminished in the nuclei of St_1 (Fig. 5C,D). In the early step cells and St_1, the gold particles were deposited specifically over the 30 nm chromatin fibers (Fig. 5B,D), with only few gold particles observed over the heterochromatin. The amount of gold labels decreased in late spermatids, i.e., St_3 (Fig. 5E), St_4 (Fig. 5F), and was hardly detected in Sz (Fig. 5G). No labeling was observed in the control group (data not shown).

Localization of PL protein. Immunogold labels from staining with anti-PL serum were observed over the nuclei of secondary spermatocytes through to spermatozoa, while the labels were very few or absent in the earlier step germ cells. Unlike anti-H1, the gold labels from anti-PL were present directly over the area of heterochromatin in SSc, while only few gold particles were present over the euchromatic area (Fig. 6A and inset). The number of gold particles was gradually increased in St_1 (Fig. 6B) and St_2 (Fig. 6C), correlating well with the increased condensation of their chromatin. The maximum number of gold labels was observed over the 40 nm chromatin fibers found in St_3 (Fig. 6D), and over the 60 nm fibers in St_4 (Fig. 6E) (see Sobhon et al., 2001 for chromatin fiber sizes and condensation pattern). The gold particles were also detected in the nuclei of mature spermatozoa, though the number was usually fewer than in spermatid nuclei (Fig. 6F). No gold labels were observed in the acrosomes and tails of the mature spermatozoa and in the control sections (data not shown).

DISCUSSION

BNP Profile in the Male Germ Cells and the Relatedness of Histone H1 and PL Protein

In the present study, we could define components of the BNPs existing in the testicular cells of *H. asinina* as H1, H2A, H3, H2B, and H4, including the fastest

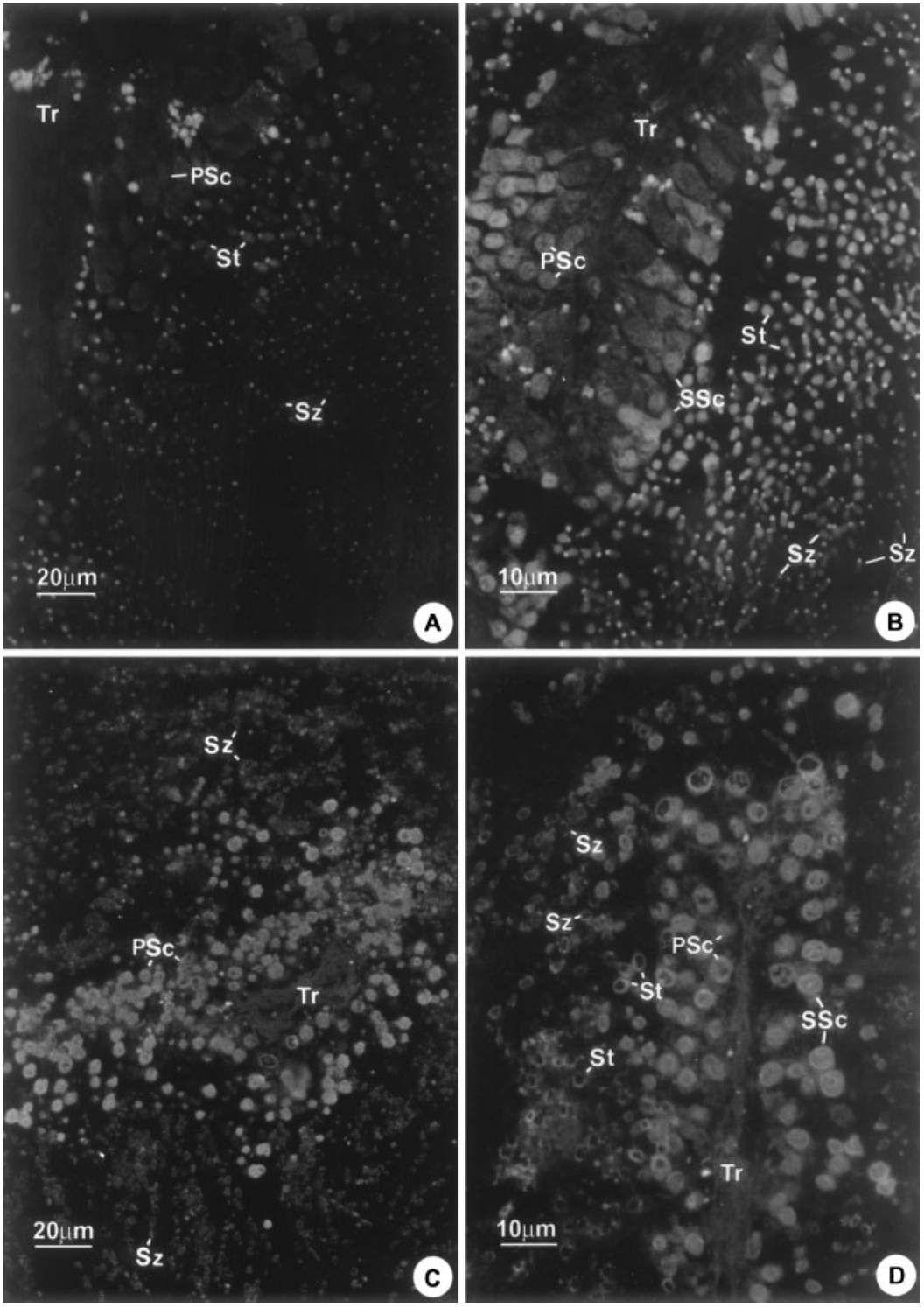


Fig. 3. Immunofluorescence micrographs of LR White semithin sections of *H. asinina* testes stained with mouse anti-H1 (**B**), mouse anti-H4 sera (**C**, **D**). **A**: A control section of the testis incubated with mouse preimmune serum, minimal background staining is observed in various steps of the male germ cells. B: Anti-H1 serum exhibits strong immunofluorescence over the nuclei of primary spermatocytes (PSc), moderate fluorescence over the nuclei of secondary spermatocytes (SSc), and weak fluorescence over the nuclei of mature spermatozoa (Sz). C, D: The anti-H4 serum shows strong fluorescence over the nuclei of PSc and SSc which are located around the trabeculae (Tr) (in C and D). Strong fluorescence is present around nuclear rim of spermatids (St) and spermatozoa (Sz) (in D).

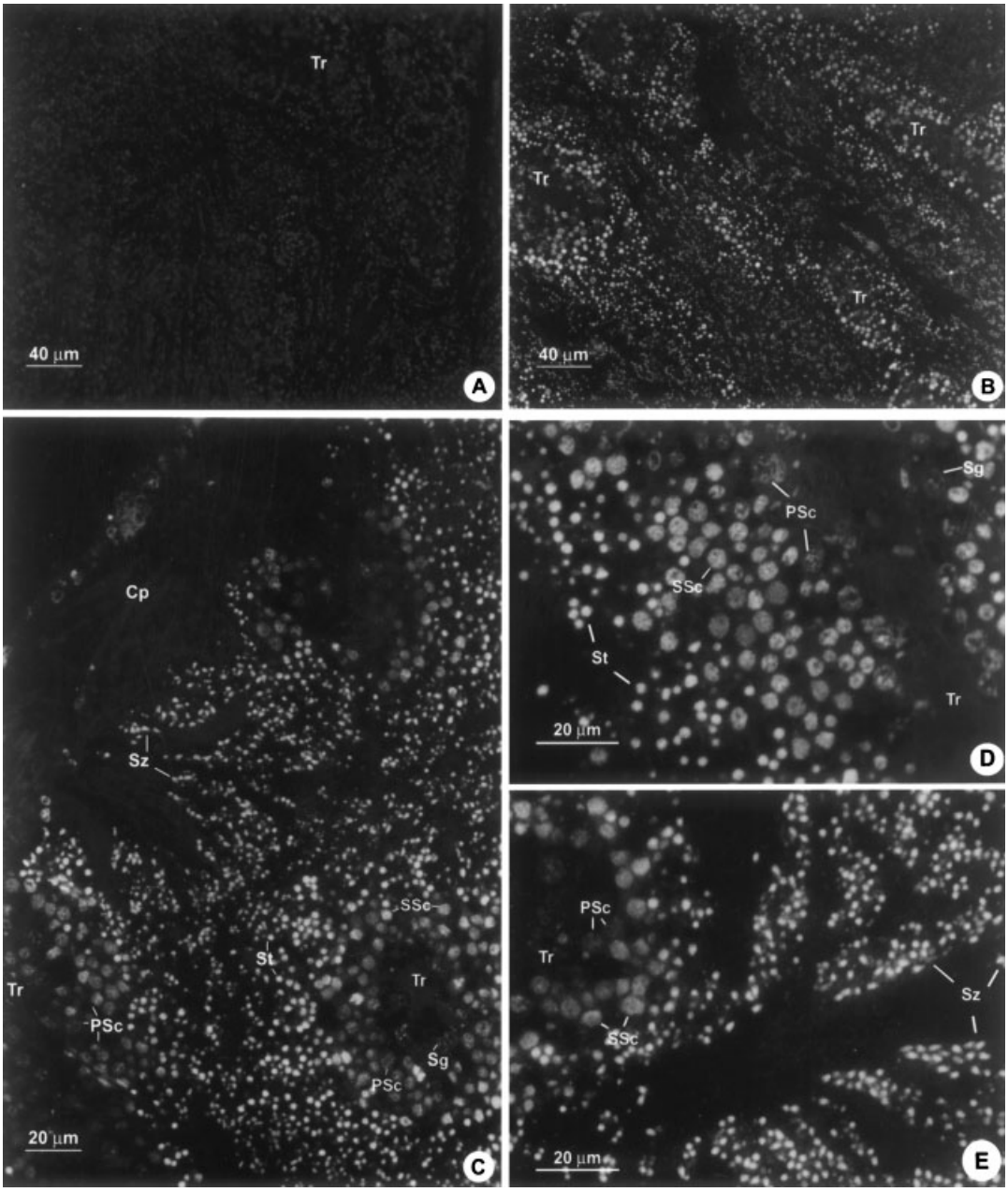


Fig. 4. Immunofluorescence micrographs of LR White semithin sections of *H. asinina* testes stained with mouse anti-PL. **A**: A control section incubated with mouse preimmune serum, showing very faint background fluorescence. **B**–**E**: Intense fluorescence is present over the nuclei of spermatids (St) and spermatozoa (Sz), whereas secondary spermatocytes (SSc) are moderately fluoresce. Spermatogonia (Sg) and primary spermatocytes (PSc) exhibit very faint fluorescence. Tr, trabeculae.

moving band, a protamine-like (PL) protein, as shown in bivalves (Subirana et al., 1973; Daban et al., 1991; Ausio, 1992). Extensive studies of mollusc sperm BNPs have been done on the PL family from the bivalves, which exhibited the highest degree of structural heterogeneity (Galindo et al., 1992; Giancotti et al., 1992; Rocchini et al., 1995; Caceres et al., 1999). From these studies, it was shown that PL consisted of at least four major components: PL-I ($M_r = 50{,}000$), PL-II ($M_r = 15{,}600$), PL-III ($M_r = 11{,}300$), and PL-IV ($M_r = 6{,}500$), all of which are related to the histone H1 (Ausio, 1999). The smaller size PL proteins, i.e., PL II–IV, usually existed together, such as in a mussel, *Mytilus*, which contained PL-II, III, and IV (Ausio, 1992, 1999), and in a razor clam, *Ensis minor*, which contained PL-II and PL-III (Bandiera et al., 1995). In this study, only one discrete though rather broad protamine-like (PL) band was found in *H. asinina*. Based on the data published to date and the similar electrophoretic mobility, PL protein found in *H.asinina* is very similar to PL-III described in

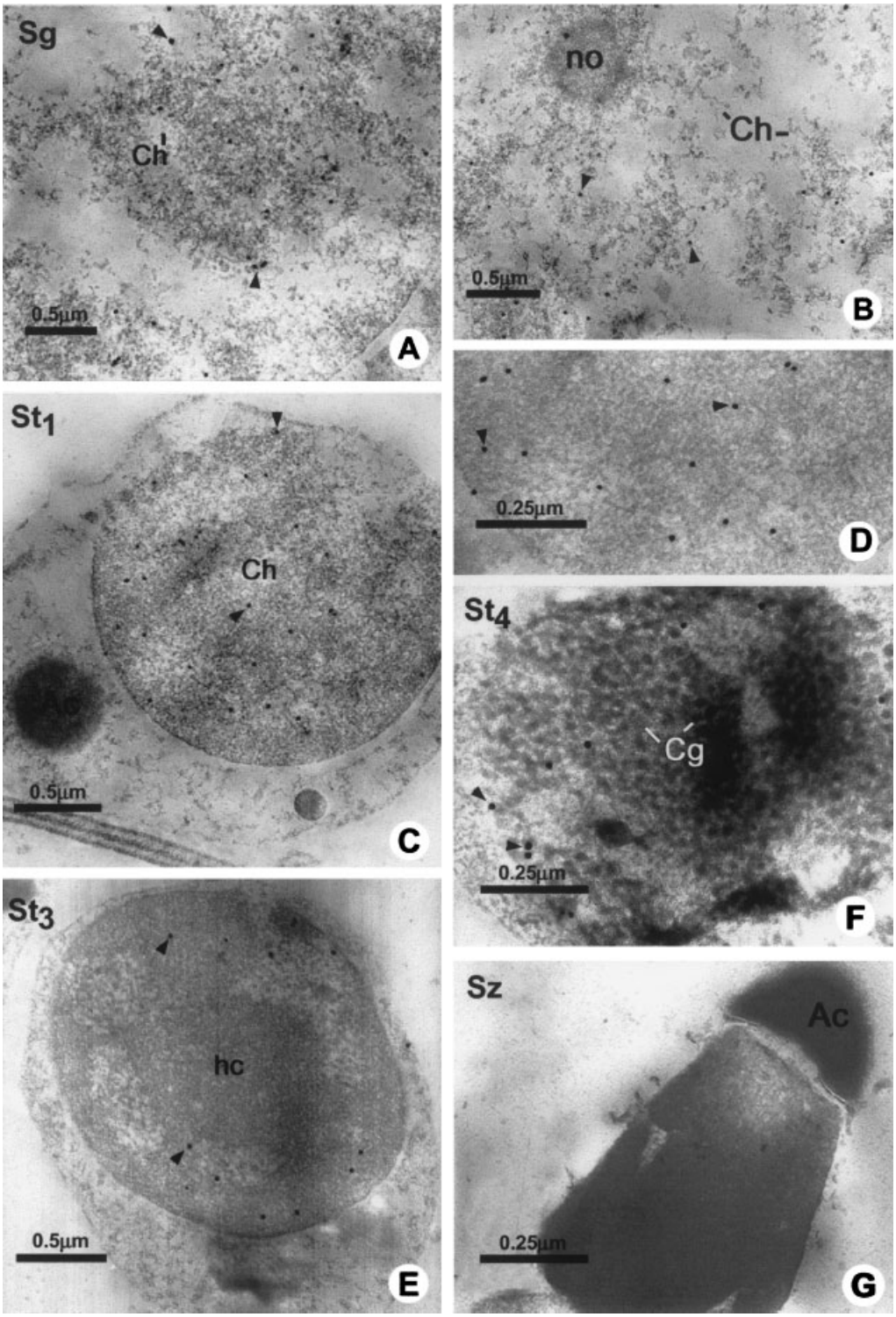


Fig. 5. TEM micrographs of LR White ultrathin sections, showing various steps of male germ cells of *H. asinina* labeled with mouse anti-H1 and immunogold particles. **A, B**: The gold particles (arrow heads) are present on the 30 nm chromatin fibers (Ch) in a spermatogonium (Sg). no, nucleolus. **C–E**: In late step germ cells, especially spermatids, the gold particles deposit over the 30 nm chromatin fibers (Ch) in spermatid step 1 (St_1) (arrow heads, in C, D) and step 3 (St_3) (E). **F, G**: The number of gold labels is low in the late spermatid (St_4 in F) and spermatozoa (G). In St_4, only occasional gold particles are present over the 60 nm chromatin granules (Cg), whereas spermatozoa (Sz) show a minimal amount of gold deposition (G). No gold particles are found over the acrosome (Ac) and tail regions.

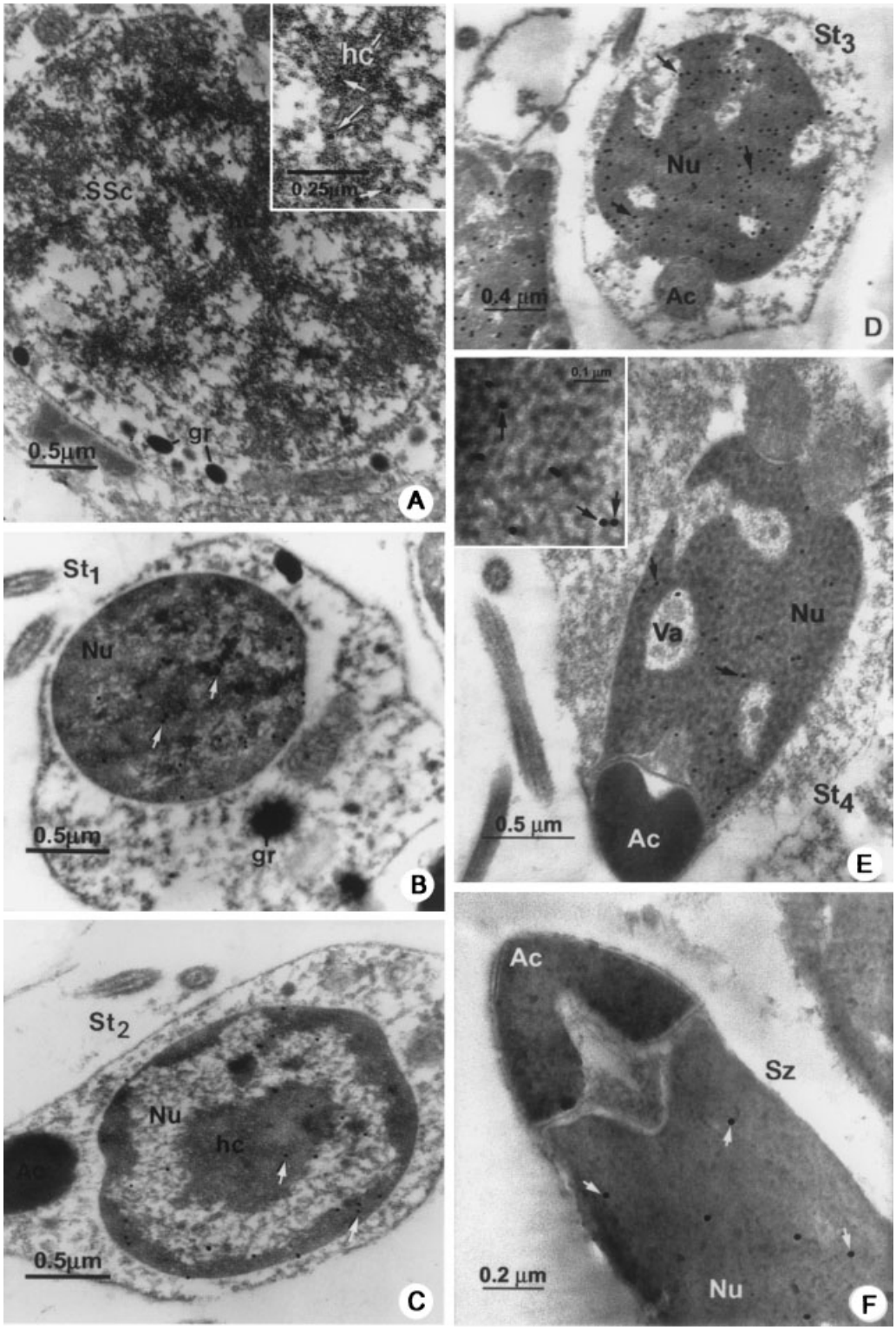


Fig. 6. TEM micrographs of LR White ultrathin sections of *H. asinina* testes stained with mouse anti-PL. **A**: The gold particles are moderate in number over the nucleus of a secondary spermatocyte (SSc); inset shows the gold labels (arrows) on the heterochromatin (hc) in the nucleus. gr, granules. **B**–**D**: In steps 1 (St_1 in B), 2 (St_2 in C), and 3 (St_3 in D) spermatids, there are more numerous gold particles (arrows) throughout the condensing heterochromatin (hc) in the nuclei (Nu). The number of gold particles is increasing from early (B, C) to late steps of spermatids (D). gr, acrosomal granules; Ac, acrosome. **E**: Gold particles (arrows) are deposited in the nucleus of step 4 spermatids (St_4). Inset shows gold labels (arrows) on the compact 60 nm chromatin fibers. Ac, acrosome; Nu, nucleus; Va, vacuole. **F**: A mature spermatozoon (Sz) exhibits fewer gold particles (arrows) on its highly condensed chromatin (**G**). Ac, acrosome; Nu, nucleus.

the cephalopods (Martin-Ponthieu et al., 1991) and the *Mytilus* (Rocchini et al., 1995), though comparison of the complete amino acid sequences awaits further study. It is notable that in mature (spawned) *H.asinina* sperm, only H4 and H1 remained, while PL fraction appeared to be markedly increased. Furthermore, the intermediate protein (IP) also became more prominent. This is in contrast to the temperate species (*H. crackeroidii*) in which histones were entirely absent (Balhorn et al., 1979).

The relatedness of H1 and PL were analyzed by their cross reactivities to antibodies against H1 and PL in Western blot. The immunoblotting pattern indicated that anti-H1 and anti-PL antisera each reacted specifically to its corresponding antigen as well as showing high cross-reactivity with the other antigen. This implicates that histone H1 may share a certain common determinant with PL protein. In addition, anti-H1 also reacted with the calf thymus histone H1 and histone H5 of chick erythrocytes. Thus, all these proteins (abalone H1, PL, and chick H5) may belong to the same family, and share a common ancestral gene. The relatedness of H1 and PL have also been demonstrated in other mollusc species, particularly in bivalves (Jutglar et al., 1991; Carlos et al., 1993; Ausio, 1999). In fact, it was suggested that PL proteins and protamine may arise from the same ancestral H1 gene, and protamine may emerge relatively later in the chordates as a result of the conversion of a lysine-rich histone H1 to an arginine-rich protamine (Wouters-Tyrou et al., 1998; Lewis et al., 2004).

Immunolocalization of Histone H1, H4, and PL in the Male Germ Cells

The attempt to clarify the process of chromatin condensation during spermatogenesis and spermiogenesis in relationship to the BNPs pattern have not been considered in molluscs, eventhough the species-specific chromatin organization have been well illustrated (Hodgson, 1986; Hodgson and Bernard, 1986; Sousa and Oliveira, 1994). In addition, information on the sequence of change and the replacement of histones by PL protein during the differentiation of the male germ cells, which may results in chromatin condensation during spermiogenesis, have not yet been available.

In the present study, we attempt to correlate the appearance of the H1, H4, and PL proteins found in the nuclei of testicular cells and spermatozoa with the precise steps of the male germ cells using immunocytochemical approaches. Immunolocalization of histone H1 by indirect immunofluorescence showed immunoreactivity appearing in the nuclei of all steps of the malegerm cells. The strong immunofluorescence was detected over the nuclei of early to middle step cells (spermatogonia and primary spermatocytes), while moderate to weak fluorescence was observed over the nuclei of secondary spermatocytes, spermatids, and spermatozoa, respectively. Immunostaining of H4 showed strong immunoreactivity over the nuclei of spermatogonia, primary and secondary spermatocytes. The fluorescence signal was decreased gradually until it was found concentrated only at the periphery of the nuclei of spermatids step 3 (St_3) and 4 (St_4), and spermatozoa. This is expected since H4 was the only major histones observed in the mature abalone sperm. Since H4 is a nucleosomal core protein (Luger et al., 1997), it is possible, though not yet proven, that part of the abalone sperm chromatin may still have nucleosomal structure. In contrast to histone H1, anti-PL showed strong immunoreactivity over the nuclei of the late step cells, beginning in the nuclei of secondary spermatocytes, and the fluorescence became very intense in the nuclei of spermatids and spermatozoa. This informative finding was consistent with the distribution of histone H1 and PL protein using immunogold labeling method as observed under TEM. Immunogold labels of H1 sites were observed in the nuclei of all steps of spermatogenic and spermiogenic cells, where the gold particles deposited specifically over the 30 nm chromatin fibers, with only occasional particles observed over the heterochromatin. The number of gold particles was comparatively low in St_3, St_4, and spermatozoa. On the other hand, immunogold labels attached to PL sites were found in the nuclei of secondary spermatocytes through to spermatozoa, particularly in the areas of the highly condensed heterchromatin. The gold particles were gradually increased in number in St_1 and St_2, correlating well with the increased condensation of their chromatin, and the labeling was specifically localized over the 40 nm chromatin fibers found in St_3 and over the 60 nm in St_4. Finally, the gold particles were observed in the nuclei of mature spermatozoa, though the number of particles was usually lower than in the nuclei of spermatids. This may be due to the extreme condensation of the sperm chromatin, thus fewer sites were accessible for the antibody-binding. Therefore, we believe that in *H. asinina*, PL protein expressed in all stages of spermatids could play a major role in replacing most of the nucleosomal histones and causes the chromatin condensation, by transforming the 30 nm nucleosomal type fibers in St_3 to 40 nm fibers in St_4, which eventually transform to the large 60 nm beaded fibers that become tightly packed in spermatozoa, as observed earlier by our group (Apisawetakan et al., 2000; Sobhon et al., 2001).

ACKNOWLEDGMENTS

This study was supported by grants form the Thailand Research Fund (Senior Research Scholar Fellowship to Prasert Sobhon and the Royal Golden Jubilee PhD Scholarship to Worawit Suphamungmee).

REFERENCES

Apisawetakan S, Sobhon P, Wanichanon C, Linthong V, Upatham ES, Kruatrachue M, Jarayabhand P, Poomtong T. 2000. Ultrastructure of spermatozoa in the testis of *Haliotis asinina* Linnaeus. J Med Appl Malacol 10:101–109.

Ausio J. 1992. Purification and biochemical characterization of the nuclear sperm-specific proteins of the bivalve mollusks *Agriodesma saxicola* and *Mytilimeria nuttalli*. Biol Bull 182:31–40.

Ausio J. 1999. Histone H1 and the evolution of the sperm nuclear basic proteins. J Biol Chem 274:31115–31118.

Ausio J, Van Holde KE. 1987. A dual chromatin organization in the sperm of the bivalve mollusc *Spisula solidissima*. Eur J Biochem 165: 363–371.

Ausio J, Toumadje A, McParland R, Becker RR, Johnson WC, Jr., van Holde KE. 1987. Structural characterization of the trypsin-resistant core in the nuclear sperm-specific protein from *Spisula solidissima*. Biochemistry 26:975–982.

Balhorn R, Lake S, Gledhill BL. 1979. Electrophoretic analysis of nuclear proteins isolated from sperm of the black abalone *Haliotis crackeroidii*. Exp Cell Res 123:414–417.

Bandiera A, Patel UA, Manfioletti G, Rustighi A, Giancotti V, Crane-Robinson C. 1995. A precursor-product relationship in molluscan sperm proteins from *Ensis minor*. Eur J Biochem 233:744–749.

Caceres C, Gimenez-Bonafe P, Ribes E, Wouters-Tyrou D, Martinage A, Kouach M, Sautiere P, Muller S, Palau J, Subirana JA, Cornudella L, Chiva M. 1999. DNA-interacting proteins in the spermiogenesis of the mollusc *Murex brandaris*. J Biol Chem 274:649–656.

Carlos S, Jutglar L, Borrell I, Hunt DF, Ausio J. 1993. Sequence and characterization of a sperm-specific histone H1-like protein of *Mytilus californianus*. J Biol Chem 268:185–194.

Daban M, Chiva M, Rosenberg E, Kasinsky HE, Subirana JA. 1991. Protamine in prosobranchia gastropods (Mollusca) vary with different modes of reproduction. J Exp Zool 257:265–283.

Galindo M, Rodriguez H, Olivares C. 1992. Sperm basic nuclear proteins in the bivalve mollusc *Mesodesma donacium*: Characterization and comparison with histone-like and protamine-like proteins of other molluscs. Comp Biochem Physiol Part B 102:643–965.

Giancotti V, Buratti E, Santucci A, Neri P, Crane-Robinson C. 1992. Molluscan sperm proteins: *Ensis minor*. Biochim Biophys Acta 1119:296–302.

Gimenez-Bonafe P, Ribes E, Sautiere P, Gonzalez A, Kasinsky H, Kouach M, Sautiere PE, Ausio J, Chiva M. 2002. Chromatin condensation, cysteine-rich protamine, and establishment of disulphide interprotamine bonds during spermiogenesis of *Eledone cirrhosa* (Cephalopoda). Eur J Cell Biol 81:341–349.

Hodgson AN. 1986. Invertebrate spermatozoa—Structure and spermatogenesis. Arch Androl 17:105–114.

Hodgson AN, Bernard RTF. 1986. Ultrastructure of the sperm and spermatogenesis of three species of Mytilidae (Mollusca, Bivalvia). Gamete Res 15:123–135.

Jutglar L, Borrell J, Ausio J. 1991. Primary, secondary, and tertiary structure of the core of a histone H1-like protein from the sperm of *Mytilus*. J Biol Chem 266:8184–8194.

Lewis JD, Saperas N, Song Y, Zamora MJ, Chiva M, Ausio J. 2004. Histone H1 and the origin of protamines. PNAS 101:4148–4152.

Luger K, Mader AW, Richmond RK, Sargent DF, Richmond TJ. 1997. Crystal structure of the nucleosome core particle at 2.8 Å resolution. Nature 389:251–260.

Manochantr S, Sretarugsa P, Chavadej J, Sobhon P. 2005. Chromatin organization and basic nuclear proteins in the male germ cells of *Rana tigerina*. Mol Reprod Dev 70:184–197.

Martin-Ponthieu A, Wouters-Tyrou D, Belaiche D, Sautiere P, Schindler P, Van Dorsselaer A. 1991. Cuttlefish sperm protamines. I. Amino acid sequences of two distinct variants. Eur J Biochem 195: 611–619.

Ribes E, Sanchez De Romero LD, Kasinsky HE, del Valle L, Gimenez-Bonafe P, Chiva M. 2001. Chromatin reorganization during spermiogenesis of the mollusc *Thais hemostoma* (Muricidae): Implications for sperm nuclear morphogenesis in cenogastropods. J Exp Zool 289: 304–316.

Rocchini C, Rice P, Ausio J. 1995. Complete sequence and characterization of the major sperm nuclear basic protein from *Mytilus trossulus*. FEBS 36:37–40.

Singhagraiwan T, Doi M. 1993. Seed production and culture of a tropical abalone, *Haliotis asinina* Linné. The Research Project of Fishery Resource Development in the Kingdom of Thailand. The Eastern Marine Fisheries Development Center (EMDEC), Department of Fisheries, Ministry of Agriculture and Cooperatives, Thailand. 32 p.

Sobhon P, Apisawetakan S, Linthong V, Pankao V, Wanichanon C, Meepool A, Kruatrachue M, Upatham ES, Poomtong T. 2001. Ultrastructure of differentiating male germ cells of *Haliotis asinina* Linnaeus. Invert Reprod Dev 39:55–66.

Sousa M, Oliveira E. 1994. An ultrastructural study of spermatogenesis in *Helcion pellucidus* (Gastropoda, Prosobranchia). Invert Reprod Dev 26:119–126.

Subirana JA, Cozcolluela C, Palau J, Unzeta M. 1973. Protamines and other basic proteins from spermatozoa of molluscs. Biochim Biophys Acta 317:364–379.

Wouters-Tyrou D, Martinage A, Chevaillier P, Sautiere P. 1998. Nuclear basic proteins in spermiogenesis. Biochimie 80:117–128.

Invert Neurosci (2005) 5: 165–172
DOI 10.1007/s10158-005-0032-5

ORIGINAL ARTICLE

P. Saitongdee · S. Apisawetakan · N. Anunruang
T. Poomthong · P. Hanna · P. Sobhon

Egg-laying-hormone immunoreactivity in the neural ganglia and ovary of *Haliotis asinina* Linnaeus

Accepted: 19 February 2005 / Published online: 1 April 2005
© Springer-Verlag 2005

Abstract Immunoreactivity against the abalone egg-laying hormone (aELH) was detected in the fine granules of type 1 and 2 neurosecretory (NS) cells, neurites in the neuropil, and blood sinuses in the connective tissue sheath of the cerebral, pleuropedal, and visceral ganglia of the tropical abalone, *Haliotis asinina* Linnaeus. The number of positive NS cells, and the intensity of staining in the ganglia, varied and might be related to the stage of ovarian cycle. At any stage, positive cells were most numerous in the pleuropedal, and least numerous in the visceral ganglion. In addition, several cells of the statocyst and associated nerves also exhibited the immunoreactivity. In the ovary, the most intense reactivity was detected in the follicular and granular cells adjacent to mature oocytes, in the trabeculae and the ovarian capsule. The cytoplasm of mature oocytes was also moderately stained. The results indicate that the cerebral, pleuropedal, and visceral ganglia are the main sites of aELH-producing cells. The ovary may also produce aELH locally.

Keywords Egg-laying hormone · Neural ganglia · Ovary · Immunolocalization · *Haliotis*

P. Saitongdee · S. Apisawetakan · N. Anunruang · P. Sobhon (✉)
Anatomy Department, Faculty of Science, Mahidol University,
Rama VI Road, Bangkok, 10400, Thailand
E-mail: scpso@mahidol.ac.th
Tel.: +61-662-2015406
Fax: +61-662-3547168

T. Poomthong
The Coastal Aquaculture Research and Development Centre,
Department of Fisheries, Ministry of Agriculture
and Cooperatives, Klong Wan, Prachaubkirikhan,
77000, Thailand

P. Hanna
School of Biological and Chemical Sciences,
Deakin University, Geelong, Victoria, 3217, Australia

Introduction

Egg-laying hormone (ELH) plays a crucial role in the induction of spawning activity of gastropod mollusks. The effects of ELH on the reproductive behaviour of gastropods have been well documented in *Aplysia californica* (an opisthobranch) and *Lymnaea stagnalis* (a pulmonate) (Conn and Kaczmarek 1989; Geraerts and Bohlken 1976). In *Aplysia*, ELH has been shown by molecular and immunocytochemical studies to be synthesized and released by the neurosecretory (NS) bag cells of the abdominal ganglion (Nambu and Scheller 1986). In addition, ELH-containing neurons have also been detected in the cerebral and pleuropedal ganglia of *A. californica* (Chiu and Strumwasser 1984; Painter et al. 1989). In *L. stagnalis* a similar hormone was detected in the caudo-dorsal cells of cerebral ganglia, and has therefore been called caudo-dorsal cell hormone (CDCH) (Van Minnen et al. 1989). A molecular study of ELH indicated that it has 36 amino acids and a molecular weight of 4.5 kDa (Ebberink et al. 1985). Injection of an abdominal ganglion extract from *A. californica* induced egg laying and associated behaviours in several other *Aplysia* spp. (Bernheim and Mayeri 1995). The administration of cerebral ganglion extract from *L. stagnalis* also caused spawning of snails of the same genus (Geraerts and Bohlken 1976). In *Haliotis discus hannai*, injection of crude homogenates of visceral or pleuropedal ganglion alone could cause spawning, but a combination of pleuropedal and visceral ganglia caused spawning of an even larger number of eggs (Yahata 1973).

Recently, immunoreactivity to ELH has been detected in neurons of the cerebral and pleuropedal ganglia, and in the ovary of *Haliotis rubra* (blacklip abalone), but specific cells types were not clearly identified (Cummins et al. 2001). Using the same antibody, ELH-immunoreactivity has also been found in the gonad of *Haliotis asinina* Linnaeus (Chanpoo et al. 2001). However, the types of immunoreactive neurons and

structures in the gonad were not detailed. The present study aimed to identify and localize the ELH-immunoreactive neurons in the cerebral, pleuropedal, and visceral ganglia, and positive cells in the ovary of *H. asinina*, using immunohistochemical techniques.

Materials and methods

Animal used and tissue preparation

Specimens of adult female *H. asinina*, with an average body weight of 35–45 g, were obtained from the Coastal Aquaculture Research and Development Centre, Department of Fisheries, Prachuabkirikhan Province, Thailand. Most of the animals were at stage V (mature stage of the ovarian cycle). The cerebral, pleuropedal, and visceral ganglia were dissected out and immediately fixed in Bouin's fixative for 16 h at 4°C. The specimens were then dehydrated and embedded in paraffin, sectioned at 3–5 μm, and placed on chrome-alum-coated glass slides for immunostaining.

Expression of abalone ELH as a fusion protein

A recombinant pGEX/abalone ELH (aELH) clone of *H. rubra* was kindly provided by P. Hanna, Deakin University, Geelong, Australia. The glutathione-*S*-transferase (GST) gene fusion system (Sigma) was used for the expression and purification of the recombinant fusion protein (GST–aELH) according to the directions supplied with the kit. The expression and identification of the recombinant fusion protein was analysed by SDS–PAGE.

Polyclonal antibody production

Mice (ICR strain) were obtained from the Animal Care Unit, Mahidol University, and used with the approval of the Animal Ethics Committee to produce antiserum. The immunization procedure was carried out as described by Harlow and Lane (1988), with some modifications. Briefly, 6-week-old female mice were immunized by subcutaneous injection of 100 μg aELH–GST in phosphate buffered saline (PBS), mixed with an equal volume of Freund's complete adjuvant (Sigma–Aldrich, St. Louis, Mo.). Another injection, containing the same amount of the protein but with Freund's incomplete adjuvant, was administered 3 times, at 2-week intervals. A final booster injection containing 50 μg pure protein was administered 2 weeks later. Finally, the antiserum was obtained by venal tail bleeds. The antiserum against aELH was then tested for antibody titer and specificity by enzyme-linked immunosorbent assay, following the standard protocol as described by Harlow and Lane (1988). Polyclonal antibodies in the antiserum were preabsorbed with GST and the specificity of the antiserum to only aELH was ascertained by immunoblotting (data not shown). The preabsorbed antiserum was then stored at −20°C until used in the immunohistochemical study.

Immunohistochemistry

Prepared sections were deparaffinized, rehydrated, and endogenous peroxidase activity inactivated by treatment with 0.3% H_2O_2 in 30% methanol for 30 min, followed by washing in PBS containing 0.4% Triton X-100 (PBST). Non-specific binding was blocked by incubating the sections in 2% normal goat serum and 4% bovine serum albumin in PBST, for 2 h. The sections were then incubated in the primary antibody (diluted 1:200) overnight in a moist chamber. The sections were washed 3 times for 10 min each in PBS and then incubated in the secondary antibody, i.e. biotinylated anti-mouse Ig (Sigma–Aldrich), diluted 1:200 in the blocking solution, for 45 min. After rinsing in PBS, the sections were incubated in streptavidin-HRP (diluted 1:200 in PBST), for 45 min. The sections were finally exposed to substrate solution, NovaRED (Vector, Burlingame, Calif.), containing H_2O_2 for 2–5 min. Finally, they were washed with tap water, counterstained with hematoxylin, washed in water, dehydrated and then mounted with Permount. For controls, sections were processed by the same protocol but preimmune mouse serum or blocking solution was used instead of the primary antibody.

Results

Immunoreactivity in the cerebral ganglia

The technique used in this study showed positively stained structures as red, and, in contrast, there was no staining in any of the controls. A summary of the distribution pattern of aELH-containing cells in the cerebral, pleuropedal, and visceral ganglia, is shown in Fig.1.

The ELH-immunoreactivity was found in NS cells located at the peripheral region of each disc-shaped cerebral ganglion (Figs. 1a; 2a, c), in the neurites within the neuropil of the ganglion, in the commissure between the ganglia and in the nerve bundles (data not shown). The immunoreactive cells were localized principally in the upper lateral edge, lower lateral and medial edges of the cerebral ganglion (Figs. 1a, 2a), and there were 266 positive cells per 1,386 total cells counted (i.e. 16.3%) at the midsection of the ganglion. Furthermore, the immunoreactivity was also detected in the blood sinus within the connective tissue capsule of the ganglion (Fig. 2a, inset). No immunoreactivity was detected in the control section (Fig. 2b).

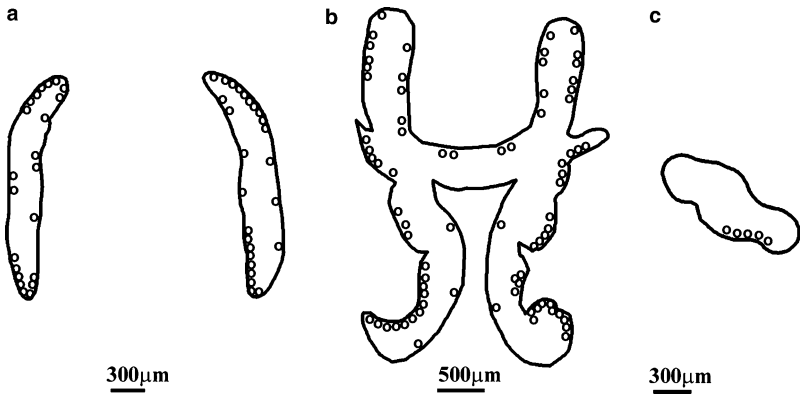


Fig. 1 Schematic representation of the distribution of abalone egg-laying hormone (aELH) immunoreactive neurosecretory (NS) cells in the cerebral (**a**), pleuropedal (**b**) and visceral (**c**) ganglia of *Haliotis asinina*. The immunoreactive cells were found to be concentrated in the upper lateral edge, lower lateral, and medial edges of the cerebral ganglion, the medial and lateral edge of the dorsal horns (Dh), as well as the lateral edge of the ventral horns (Vh) of the pleuropedal ganglion, and the lower medial edge of the visceral ganglion

The labelled ovoid NS cells had an approximate size of 9×16 μm and contained positively stained clusters of small granules in their cytoplasm (Fig. 2d, e). These positive cells had eccentric euchromatic nuclei with prominent nucleoli, and have been classified as NS type 1 (NS1) cells (Upatham et al. 1998). The other labelled NS cells had a round to ovoid shape with an approximate size of 7×10 μm and contained some small granules in the cytoplasm. These positive cells had smaller nuclei with a thick heterochromatic rim and have been classified as NS2 cells (Upatham et al. 1998).

Immunoreactivity in the pleuropedal ganglion

The H-shaped pleuropedal ganglion has bilateral dorsal and ventral horns, connected by a central body (Figs. 1b, 3a). Intense immunoreactivity was observed in the NS cells located at the periphery of the ganglion (Fig. 3a, c–f), and in the neurites within the neuropil (Fig. 3c). Positive NS1 cells were more numerous than NS2 cells, with immunoreactivity shown in small granules in the cytoplasm of cell soma (Fig. 3e, f). The labelled NS cells were distributed throughout the peripheral part of the ganglion (Figs. 1b; 3c–f). Most of the positive NS cells were concentrated along the lateral edges of the dorsal and ventral horns (Figs. 1b; 3a, c–f). There were 530 positive NS cells per 4,760 total cells counted (i.e. 11.1%) at the midsection of the ganglion. In addition, immunoreactivity was also observed in the cytoplasm of the epithelial cells of statocysts, located between the right and left dorsal horns of the pleuropedal ganglia (Fig. 3a, g, inset), and in the associated nerve situated in the connective tissue surrounding the statocysts (data not shown). The NS cells and statocyst epithelial cells in the control sections appeared negative except for a few spots resulting from endogenous peroxidase reactions which could not be totally suppressed (Fig. 3b).

Immunoreactivity in the visceral ganglion

The visceral ganglion has a dumbbell shape (Figs. 1c; 4a, b), and is connected to both cerebral and pleuropedal ganglia by long nerve bundles (data not shown). ELH immunoreactivity was detected principally in the NS2 cells, neurites (Fig. 4c), as well as the nerve bundles connected to the other ganglia (data not shown). The immunoreactive cells were concentrated in the lower medial edge of the ganglion (Figs. 1c; 4a, c), and there were 33 positive cells per 175 total cells counted (i.e. 18.8%) in the midsection of the ganglion. The control showed no immunoreactivity in the section (Fig. 4b).

Immunoreactivity in the ovary

The ovary surrounds the hepatopancreas (Fig. 5a). Light immunostaining was detected in the outer capsule (Fig. 5d), which contained layers of muscles, alternated with collagen bundles, and cuboidal epithelial cells lining the outer surface (data not shown). More intense staining appeared in trabeculae (parts of the capsule extending inwards to form the connective tissue sheets dividing the ovary into many compartments) (Fig. 5c, d, f), particularly those located adjacent to mature oocytes (Fig. 5e, f). The immunoreactive products in the trabeculae were located in the cytoplasm of the follicular cells situated close to the basal and peripheral areas of the oocytes (Fig. 5e, f), and in granulated cells which were distributed at regular intervals in the trabecula (Fig. 5e). The cytoplasm of the stage IV and V oocytes also appeared to be moderately stained (Fig. 5c–f), whilst the jelly coat was not stained (Fig. 5c, d). There was no immunoreactivity detected in the control section (Fig. 5b).

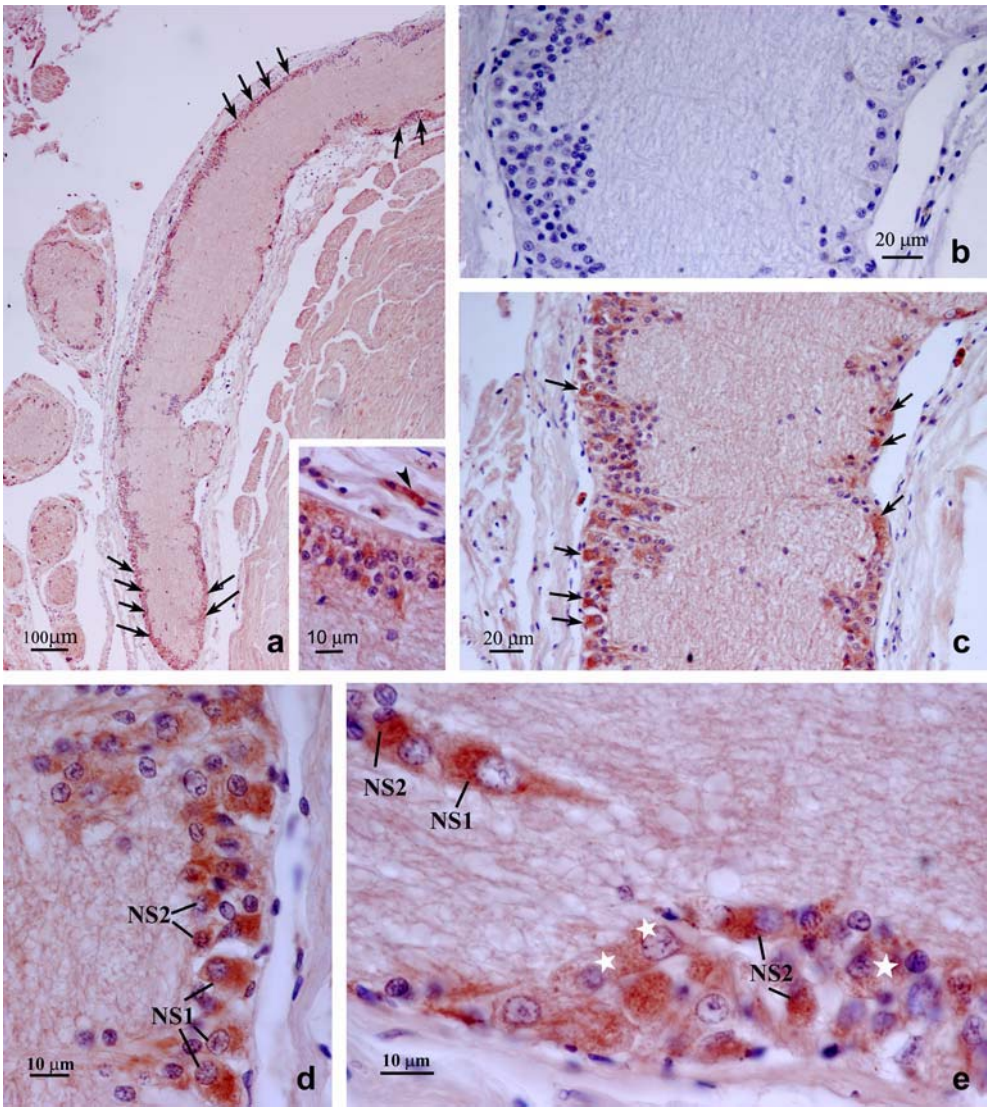


Fig. 2a–e Light micrographs of the cerebral ganglion of a female *H. asinina* stained for aELH. **a**, **c** Sections showing immunoreactivity in NS cells (*arrows*) at the peripheral region of the ganglion. **a** *Inset* showing the aELH immunoreaction (*arrowhead*) in the blood sinus of the ganglion capsule. **b** Medium power negative control section showing no immunoreactive staining. **d**, **e** High power micrographs showing intense reactions in small granules within the cytoplasm of NS type 1 (NS1) and NS2 cells. The ovoid NS1 cell has an eccentric nucleus with euchromatin and a prominent nucleolus, whereas the smaller, round NS2 cell has a thick rim of nuclear heterochromatin. For other abbreviations, see Fig. 1

Discussion

The immunoreactivity to aELH was detected in the large NS cells in specific regions of the cortex of cerebral, pleuropedal, and visceral ganglia. It was estimated from the cell size, the chromatin pattern, the presence of a prominent nucleolus, and the clusters of positively stained granules, that these cells were likely to be NS1, according to the classification of cell types in the cerebral, pluropedal, and visceral ganglia (Thongkukiatkul et al. 2001; Upatham et al. 1998). In addition, some smaller NS2 cells were also stained in all three ganglia. In contrast, the smallest NS cell (NS3), the large size neuron (NR1) and small size neurons (NR2–4) appeared unstained. We estimated that there were considerably more cells with aELH in the pleuropedal than cerebral ganglion, in a ratio of approximately 2:1, even though the percentage of positive cells is higher in the cerebral and visceral ganglia. Furthermore, positive neurites were also detected in the neuropils of the cerebral and pleuropedal ganglia. This indicated that aELH might be produced in the NS cells and transported to target organs located elsewhere. Some aELH might be secreted directly into the hemal sinuses surrounding the ganglia as intense immunoreactivity was detected in the sinus wall. A similar pattern of distribution of aELH immunoreactive structures was also reported in *H. rubra*, another abalone species which has been investigated so far (Cummins et al. 2001), though the visceral ganglion was not studied. In a study by Hahn (1994), using nonspecific histochemical stain it was found that there were four cell types (A, B, C, and D) in the cerebral ganglia of *H. discus hannai*, and only types A and B were believed to be NS. Only cell type A showed correlation with vitellogenesis and gametogenesis in the ovary. Another study by Yahata (1973) indirectly showed the existence of an ELH mainly in the pleuropedal and visceral ganglia through the successful induction of spawning in

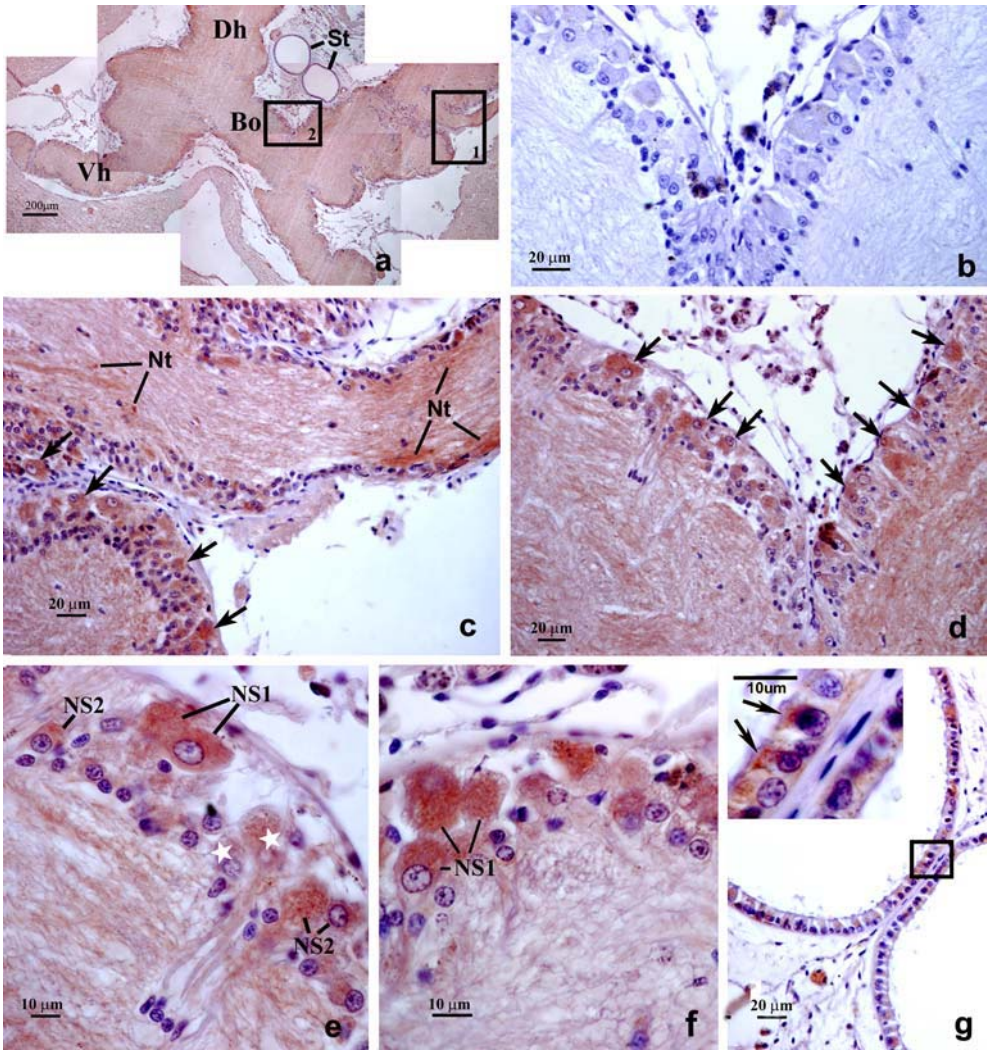


Fig. 3a–g Light micrographs of the pleuropedal ganglion of a female *H. asinina* stained for aELH. **a** Low power micrograph of the H-shaped ganglion, with adjacent statocysts (*St*) located between the lower parts of Dh. **b** Medium power negative control section showing no immunoreactivity. **c**, **d** Higher power micrographs of the area of the Dh in the *boxed areas 1* and *2* in **a**, respectively, showing immunostaining in the NS cells (*arrows*), and in the neurites (*Nt*). **e**, **f** High power micrographs showing the intense immunoreactivity within the numerous small granules of the NS1 and NS2 cells. Some NS cells show negative staining (*white stars*). **g** Immunoreactivity of epithelial cells of the statocysts at lower power, with the *inset* (high power) showing immunoreactivity in the columnar epithelial cells (*arrows*). *Bo* Body; for other abbreviations, see Fig. 1

mature female *Nordotis discus*, by injecting a suspension of either ganglion and a mixture of both. Interestingly, it was noted that the combination of suspensions of the two ganglia produced an enhanced reaction. Taken together these studies and ours indicated that the ELH hormone producing NS cells is widely distributed throughout the three chief ganglia of the abalone nervous system. This is in contrast to the findings in higher gastropods where the ELH NS cells tend to be concentrated in specific areas (nuclei) of the central nervous system. For example, in *Lymnaea* the so-called CDCH, equivalent to aELH, was produced mainly by a group of caudo-dorsal cells arranged in two clusters at the posterior end of the cerebral ganglia (Van Minnen et al. 1992). On the other hand in the less advanced gastropod, *Aplysia*, the ELH-producing cells, the so-called bag cells, were concentrated in the visceral ganglia (Nambu and Scheller 1986).

In the ovary, the most intense staining appeared in the connective tissue of the trabeculae, as reported earlier by Chanpoo et al. (2001). There were also some intensely stained spots in the granulated cells, which could be aELH-producing cells in the trabeculae. Apisawetakan et al. (2001) have reported the presence of these endocrine-like cells, the so-called granular cells, which contained specific granules distributed at regular intervals throughout the connective tissue of the trabeculae. These cells were also observed to be more numerous in the inner (ovarian hepatopancreatic) capsule than in the outer capsule of the ovary. The intensity of immunostaining appeared to reflect this. It is possible that the ovarian tissue might partly receive aELH from extramural sources, possibly cerebral and pleuropedal ganglia which could send axons to innervate the capsule and connective tissue scaffold of the gonad. At the same time the ovary might also have the capability to produce aELH intramurally, possibly in the granular cells. The immunoreactivity that occurred in the cytoplasm of mature oocytes at stages IV and V raises the question as to whether aELH and/or associated neuropeptides might play some role in stimulating the maturation of oocytes in addition to causing spawning. aELH was also detected in the connective tissue trabeculae of the ovary of *H. rubra* (Cummins et al. 2001) as in that of *H. asinina* (Chanpoo

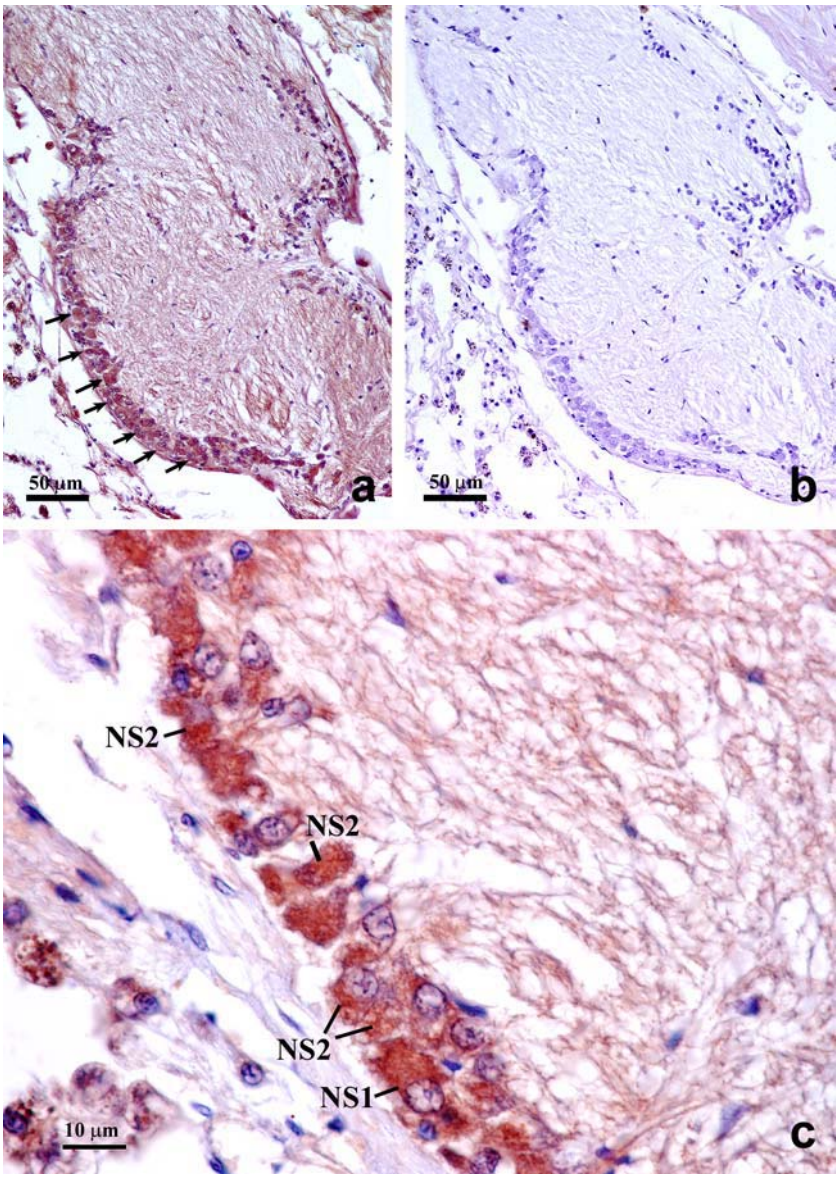


Fig. 4a–c Light micrographs of the visceral ganglion of a female *H. asinina* stained for aELH. **a** Low power micrograph showing immunoreactivity in NS cells at the medial border (*arrows*). **b** Low power negative control section showing no reactivity. **c** High power micrograph showing immunoreactivity in clusters of granules within NS1 and NS2 cells. For abbreviations, see Fig. 1

et al. 2001). However, the specific structures and cell type that were positive have not been identified in these studies. In the present study granular cells as identified by Apisawetakan et al. (2001) could be the major source of intra-ovarian aELH, judging from the strong immunoreactivity associated with them (Fig. 5e). In higher gastropods (*Lymnaea* and *Aplysia*) the ELHs were also detected in the female reproductive tract (the oothecal gland, muciparous gland, pars contorta, and ovotestis, respectively) but none have been reported in the ovarian tissue (Choate et al. 1993; Van Minnen et al. 1989). It was suggested that ELH expressed in the reproductive tissues of these higher gastropods might belong to a different isotype from that expressed in the neural tissues (Fisher et al. 1988). In the case of abalone it was demonstrated that aELH of *H. rubra* exhibited very high nucleotide homology with CDCH of *L. stagnalis* and only 56% homology to ELH of *A. californica* (Wang and Hanna 1998). It was demonstrated further that aELHs from several species of abalone, including *H. asinina*, were nearly identical (Hanna et al. 2000). However, all the cDNA sequences obtained so far are from the neural tissue. It will be interesting to investigate whether the ovarian aELH detected by antibody against neural aELH exhibits any difference which could indicate the expression of the hormone from the same gene but with a different isotype in the reproductive tissue. Recent findings in a paper co-authored by one of us seem to indicate that this might be the case, as the Western blot analysis of proteins extracted from cerebral, pleuropedal, and mature female gonad by the antibody against neural aELH, as used in the present experiment, exhibited a slightly different pattern of immunogenic bands (Cummins et al. 2001). This may be due to a difference in isotypes of aELH, or the cellular processing of the preprohormones. Further study, particularly a comparison of cDNA cloned from these two tissue sources, is needed to substantiate either of these notions.

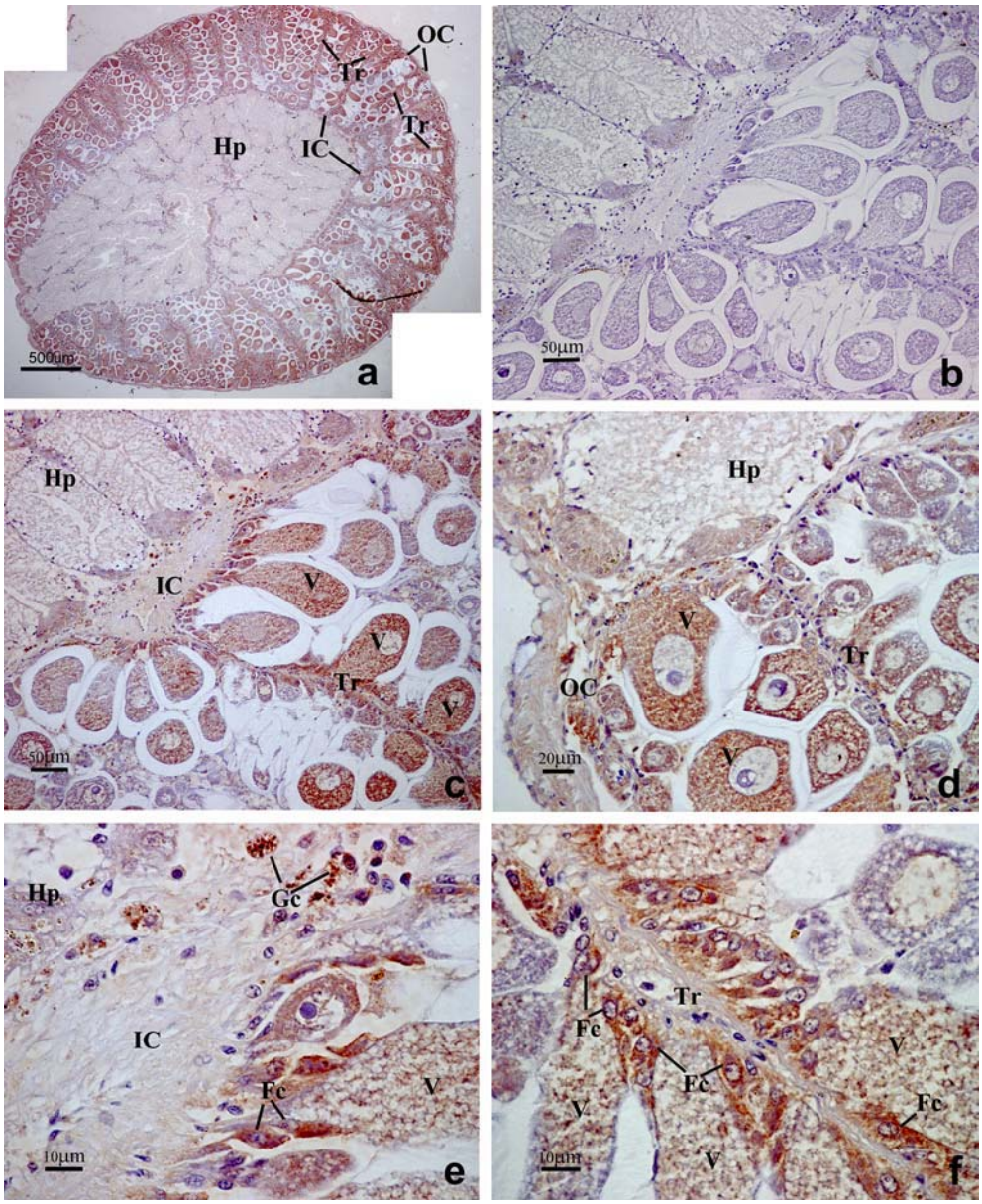


Fig. 5a–f Light micrographs of the ovary of *H. asinina* stained for aELH. **a** Low power micrograph showing immunoreactivity in the outer capsule (*OC*), inner capsule (*IC*), and trabeculae (*Tr*). **b** Medium power micrographs showing no immunoreactivity in a negative control. **c** Positive staining was present in trabeculae and stage V oocytes (*V*). **d–f** High power micrographs showing immunoreactivity within granulated cells (*Gc*), follicular cells (*Fc*) of the trabeculae, and the cytoplasm of stage V mature oocytes. *Hp* Hepatopancreas

Acknowledgement This research was supported financially by the Thailand Research Fund.

References

Apisawetakan S, Chanpoo M, Wanichanon C, Linthong V, Kruatrachue M, Upatham ES, Pumthong T, Sobhon P (2001) Characterization of trabecular cells in the gonad of *Haliotis asinina* Linnaeus. J Shellfish Res 20:717–724

Bernheim SM, Mayeri E (1995) Complex behavior induced by egg-laying hormone in *Aplysia*. J Comp Physiol 176:131–136

Chanpoo M, Apisawetakan S, Thongkukiatkul A, Wanichanon C, Linthong V, Kruatrachue M, Upatham ES, Pumthong T, Hanna PJ, Sobhon P (2001) Localization of egg-laying hormone in the gonads of a tropical abalone, *Haliotis asinina* Linnaeus. J Shellfish Res 20:725–731

Chiu AY, Strumwasser F (1984) Two neuronal populations in the head ganglia of *Aplysia californica* with egg-laying hormone-like immunoreactivity. Brain Res 294:83–93

Choate JV, Kruger TE, Micci MA, Blankenship JE (1993) Isolation of an egg-laying hormone-binding protein from the gonad of *Aplysia californica* and its localization in oocytes. J Comp Physiol 173:475–483

Conn PJ, Kaczmarek LK (1989) The bag cell neurons of *Aplysia*. A model for the study of the molecular mechanisms involved in the control of prolonged animal behaviors. Mol Neurobiol 3:237–273

Cummins S, Thongkukiatkul A, Hanna PJ (2001) Location of egg-laying hormone in reproductive structures and neurons of *Haliotis rubra* (Leach) using antibodies raised against recombinant fusion proteins. J Shellfish Res 20:705–710

Ebberink RH, Van Loenhout WP, Geraerts WP, Joose J (1985) Purification and amino acid sequence of the ovulation neurohormone of *Lymnaea stagnalis*. Proc Natl Acad Sci USA 82:7767–7771

Fisher JM, Sossin W, Newcomb R, Scheller RH (1998) Multiple neuropeptides derived from a common precursor are differentially packaged and transported. Cell 54:813–822

Geraerts WP, Bohlken S (1976) The control of ovulation in the hermaphroditic freshwater snail *Lymnaea stagnalis* by the neurohormone of the caudodorsal cells. Gen Comp Endocrinol 28:350–357

Hahn KO (1994) The neurosecretory staining in the cerebral ganglia of the Japanese abalone (ezoawabi), *Haliotis discus hannai*, and its relationship to reproduction. Gen Comp Endocrinol 93:295–303

Hanna PJ, Chai Z, Cummins SF, Huang B (2000) Application of molecular biology to abalone fisheries and aquaculture. J Med Appl Malacol 10:133–144

Harlow E, Lane D (1988) Antibodies: a laboratory manual. Cold Spring Harbor Laboratory Press, Cold Spring Harbor, N.Y.

Nambu JR, Scheller RH (1986) Egg-laying hormone genes of *Aplysia*: evolution of the ELH gene family. J Neurosci 6:2026–2036

Painter SD, Kalman VK, Nagle GT, Blankenship JE (1989) Localization of immunoreactive alpha-bag-cell peptide in the central nervous system of *Aplysia*. J Comp Neurol 287:515–530

Thongkukiatkul A, Sobhon P, Upatham ES, Kruatrachue M, Wanichanon C, Chitramvong YP, Pumthong T (2001) Ultrastructure of neurosecretory cells in the cerebral and pleuropedal ganglia of *Haliotis asinina* Linnaeus. J Shellfish Res 20:33–741

Upatham ES, Thongkukiatkul A, Kruatrachue M, Wanichanon C, Chitramvong YP, Sahavacharin S, Sobhon P (1998) Classification of neurosecretory cell, neuron, and neuroglia in the cerebral ganglia of *Haliotis asinina* Linnaeus by light microscopy. J Shellfish Res17:737–742

Van Minnen J, Dirks RW, Vreugdenhil E, Van Diepen J (1989) Expression of the egg-laying hormone genes in peripheral neurons and exocrine cells in the reproductive tract of the mollusk, *Lymnaea stagnalis*. Neuroscience 33:35–46

Van Minnen J, Schallig HD, Ramkema MD (1992) Identification of putative egg-laying hormone containing neuronal systems in gastropod molluscs. Gen Comp Endocrinol 86:96–102

Wang L, Hanna PJ (1998) Isolation, cloning and expression of a gene encoding an egg-laying hormone of the blacklip abalone (*Haliotis rubra* Leach). J Shellfish Res 17:785–793

Yahata T (1973) Induced spawning of abalone (*Nordotis discus* Reeve) injected with ganglional suspensions. Bull Jpn Soc Sci Fish 39:1117–1122

Invert Neurosci (2006) 6: 41–46
DOI 10.1007/s10158-006-0016-0

ORIGINAL PAPER

Zhipeng Liu · Prasert Sobhon
Boonsirm Withyachumnarnkul · Peter Hanna

Identification of a putative egg-laying hormone in neural and ovarian tissues of the black tiger shrimp, *Penaeus monodon*, using immunocytochemistry

Received: 8 February 2006 / Accepted: 13 February 2006 / Published online: 17 March 2006
© Springer-Verlag 2006

Abstract The existence of an egg-laying hormone (ELH) was identified for the first time in the black tiger shrimp, *Penaeus monodon*, by means of immunoenzyme and immunofluorescence techniques. This was achieved using a polyclonal antibody produced against expressed recombinant ELH of the female Australian blacklip abalone, *Haliotis rubra*. The shrimp ELH reactive material was found to be localised within female neurosecretory tissues and the secretory tissue of the antennal gland, but was not identified in the X-organ sinus gland within the eyestalk. It was also present in the ovary, where the amount of ELH present was observed to be greatest in the period prior to spawning. These findings implied that the induction of *P. monodon* spawning might be involved with humoral regulation relating to ELH expression.

Keywords Egg-laying hormone · *Penaeus monodon* · Neurosecretory cells · Ovary · Immunocytochemistry

Introduction

Several marine shrimp species make up a very large seafood industry, of which the black tiger shrimp, *Penaeus monodon*, is very popular worldwide. This is because it has well distinguished banded stripes on the back entitling it "black tiger", and its large size (i.e. common harvested adult body weight is approximately 150 g, while the maximum total length has been reported to be 336 mm) (Dall 1957; Jones and Morgan 1994). For these reasons, the culture of *P. monodon* has advanced rapidly. Cultured *P. monodon* in the global shrimp production increased from 33% in 1989, to 47% in 1992 (Klinbunga et al. 1999), and has dominated the global market at 57% (Bray and Lawrence 1998).

However, the *P. monodon* industry has been restricted by some serious problems, i.e. widespread infectious diseases (Boonyaratpalin et al. 2001), wild broodstock depletion, and limited success in breeding culture broodstock due to gonad maturation and spawning difficulties in pond-reared systems. The last of these issues cross-relates to the other two (Hoang et al. 2002), particularly in the current practice in farming as the oogenesis is artificially induced and spawning taking place through eyestalk ablation of wild female broodstock (Primavera 1978). Supplies of the wild broodstock are not reliable (Arena et al. 2003), and the harvesting of wild female broodstock at an industrial scale inflicts on the sustainability of the natural resource. Introduction of wild broodstock shrimps into culture facilities poses a risk of introducing infectious diseases from the natural environment, as well as bringing uncertainty to the shrimp offspring (i.e. the genetics are unknown and could include such traits as, slow growth and disease sensitivity).

It is known that homologous egg-laying hormone (ELH) genes and peptides, play critical roles in reproduction, and have been identified in a wide range of invertebrates using genetic and immunocytochemistry techniques. Molluscan examples include *Aplysia californica* (California sea hare), *Haliotis rubra* (blacklip abalone), *H. asinina* (tropical abalone), *Biomphalaria glabrata* (bloodfluke planorb), *Limax maximus* (giant garden slug), *Helix aspersa* (brown garden snail), *Lymnaea stagnalis* (great pond snail), and several basommatophoran snails (i.e. *Listera ovata*, *Bulinus*

Z. Liu · P. Hanna (✉)
School of Life & Environmental Sciences, Deakin University,
3217 Geelong, VIC, Australia
E-mail: peter.hanna@deakin.edu.au
Tel.: +61-3-52271394

P. Sobhon
Department of Anatomy, Faculty of Science, Mahidol University,
10400 Bangkok Thailand

B. Withyachumnarnkul
Centex Shrimp, Faculty of Science, Mahidol University,
10400 Bangkok Thailand

truncates, B. glabrata, Planorbis planorbis, P. vortex and Planorbarius corneus) (Vreugdenhil et al. 1988; Van Minnen et al. 1992; Cummins et al. 2001; Saitongdee et al. 2005). Other examples include the annelid *Theromyzon tessulatum* (rhyonobdellid leech) (Salzet et al. 1997), and the arthropods *Sarcophaga bullata* (flesh fly), *Leptinotarsa decemlineata* (Colorado potato beetle), *Locusta migratoria* (migratory locust), *Periplaneta americana* (American cockroach), and *Drosophila melanogaster* (fruit fly) (Theunis et al. 1990; Herndon and Wolfner 1995).

Due to the diverse taxa possessing ELH homologues, and particularly the arthropods, we decided to acquire evidence for the existence of a similar hormone in *P. monodon*. Identification and production of a hormone of this nature might lead to the controlling of the reproductive cycle and spawning of *P. monodon*, without having to perform eyestalk ablations of female broodstock.

Materials and methods

Animals and tissue preparations

Paraffin embedded specimens of ripe, Stage IV, female *P. monodon* gonadal tissue were obtained from the Centex Shrimp, Mahidol University, Bangkok, Thailand. Live 9-month-old female *P. monodon* (~100 g each) with undeveloped gonads was supplied by the Commonwealth Scientific and Industrial Research Organisation, Marine Research Laboratory Cleveland, Queensland, Australia, and immediately used for histological purposes.

Live shrimps were injected with freshly prepared Davison's fixative (330 ml of 95% v/v ethanol, 220 ml of 4% w/v paraformaldehyde, 115 ml of glacial acetic acid with dH_2O made up to 1,000 ml), at 10% of the body weight (~10 ml). A 4 ml volume was injected into the cephalothorax and 1 ml into each abdominal segment, and after 5 min at room temperature, samples were dissected and shell removed. The longitudinally divided cephalothoric tissues, entire gonads, transversely divided abdominal tissues, and the eyestalks were dissected out and immediately transferred to 20 volumes of the same fixative, which were then stored at room temperature for 24 h, after which the fixative was replaced with fresh one for another 24 h. The samples were then transferred to 1% w/v phosphate buffer for 24 h to remove excessive fixative and prevent over-fixation, and then paraffin-embedded in a histokinette (Lecia), using a 24 h cycling program. After that, the paraffin blocks were cooled at room temperature for 12 h, and serial sections cut with a Reichert-Jung microtome, mounted onto gelatin-coated slides, and then stored until required.

Immunostaining

The primary antibody was produced in mouse against expressed recombinant abalone egg-laying hormone (aELH), at Mahidol University (Bangkok), as reported by Saitongdee et al. (2005).

Immunoenzyme studies utilised horse raddish peroxidase (HRP) with a prior avidin–biotin amplification step. Prepared sections were firstly dewaxed in three changes of fresh 100% xylene, then rehydrated in a descending concentrations of ethanol (i.e. 100, 90 and 70%), for 2 min each. Following this, the sections were immersed in 70% ethanol containing 1% saturated lithium carbonate ($LiCO_3$) to remove residual picric acid and placed into running tap water for 5 min. The sections were then treated with 10% v/v H_2O_2 in 80% v/v methanol (in dH_2O) to quench endogenous HRP activity, and the highest antigenicity of tissue was retrieved following microwaving three times for approximately 5 min each in 0.1 M phosphate buffer saline (PBS) at 80 W, without boiling. The sections were then placed into prewarmed PBS to prevent the glass from breaking. After soaking in PBS for 2 min, they were blocked with 1% w/v gelatin in PBS for 30 min, and then 4% bovine serum albumin (BSA) and 2% goat serum w/v in PBS for another 30 min. Following this, the blocking solution was removed and primary antibody applied after being diluted 1:500 in PBS. Sections were incubated at 4°C overnight, then washed and soaked three times in PBS for 5 min. Secondary antibody (i.e. biotinylated monoclonal goat anti mouse IgG (Sigma), diluted 1:800 in PBS), was added to the sections and they were then incubated at room temperature for 45 min. Following another series of washes and soaks in PBS, as above, they were incubated with HRP–avidin conjugate (Sigma), diluted 1:800 from a stock solution of 10 mg/ml, for another 45 min. This was followed by another series of washes and soaks in PBS as above, and a freshly prepared NovaRED™ (Vector Laboratory) substrate, was applied to develop a colour reaction. This colour reaction was stopped by rinsing in dH_2O as soon as a light red colour was observed in the sections (~10 s). The sections were then counterstained in 0.1% haematoxylin (Mayer) for 45 s, rinsed in dH_2O for 30 s, and soaked in formulated tap water (i.e. 0.35% w/v $NaHCO_3$, 2% w/v $MgSO_4$) for 30 s and rinsed again in dH_2O as above. The sections were then mounted in aqueous mounting medium (DAKO) and examined under a Zeiss Axioskop MC 80 microscope, and images captured with a Spot cooled CCD camera.

Immunofluorescence studies utilised fluorescein isothiocyanate (FITC). Before the application of primary antibody, sections were prepared as described previously, except that the quenching step was omitted. In these studies the primary antibody was diluted 1:100 in PBS and incubation conditions were the same. After being washed and soaked three times in PBS as performed in immunoenzyme technique, the sections were incubated in secondary antibody [i.e. FITC-conjugated monoclonal sheep anti-mouse IgG (Sigma), and diluted 1:100 in PBS], in the dark for 45 min. After further washes and soaks in PBS in the dark, the sections were mounted in FITC mounting medium (50% glycerol in

PBS), then examined and images captured under a fluorescence microscope (Leica).

Positive controls for the two methods were performed using the primary antibody on sections of known immunoreactive abalone tissues, i.e. cerebral ganglia, pleuropedal ganglia, and gonad, of reproductively mature female abalones, i.e. *H. rubra*, as previously identified by Chanpoo et al. (2001) and Cummins et al. (2001). Negative controls were made by omitting the primary antibody incubation step in the protocols, and substituting it with pre-immune mouse serum.

Results

In this study the positive controls using abalone tissue sections all showed that the primary antibody was effective with both immuno-detection systems described in this paper, i.e. immunoenzyme using standard secondary HRP-conjugated antibodies for detection and FITC-immunofluorescence (data not shown). Some weak backgrounds were detected in the negative controls of the shrimp brain sections but the ELH positive cells, detected in our experimental sections, did not show immunoreactive signals.

Overall, ELH immunoreactive material was clearly identified in neural, antennal gland, and reproductive tissues of the black tiger shrimp, *P. monodon*, by both immunoenzyme and immunofluorescence techniques (Figs. 1, 3, 4). However, ELH immunoreactivity was absent in the X-organ sinus gland situated in the eyestalk (Fig. 2). In the cephalothoracic region, ELH was detected in the supraesophageal ganglia (Spg), i.e. brain, and the antennal nerve, and surrounding tissue

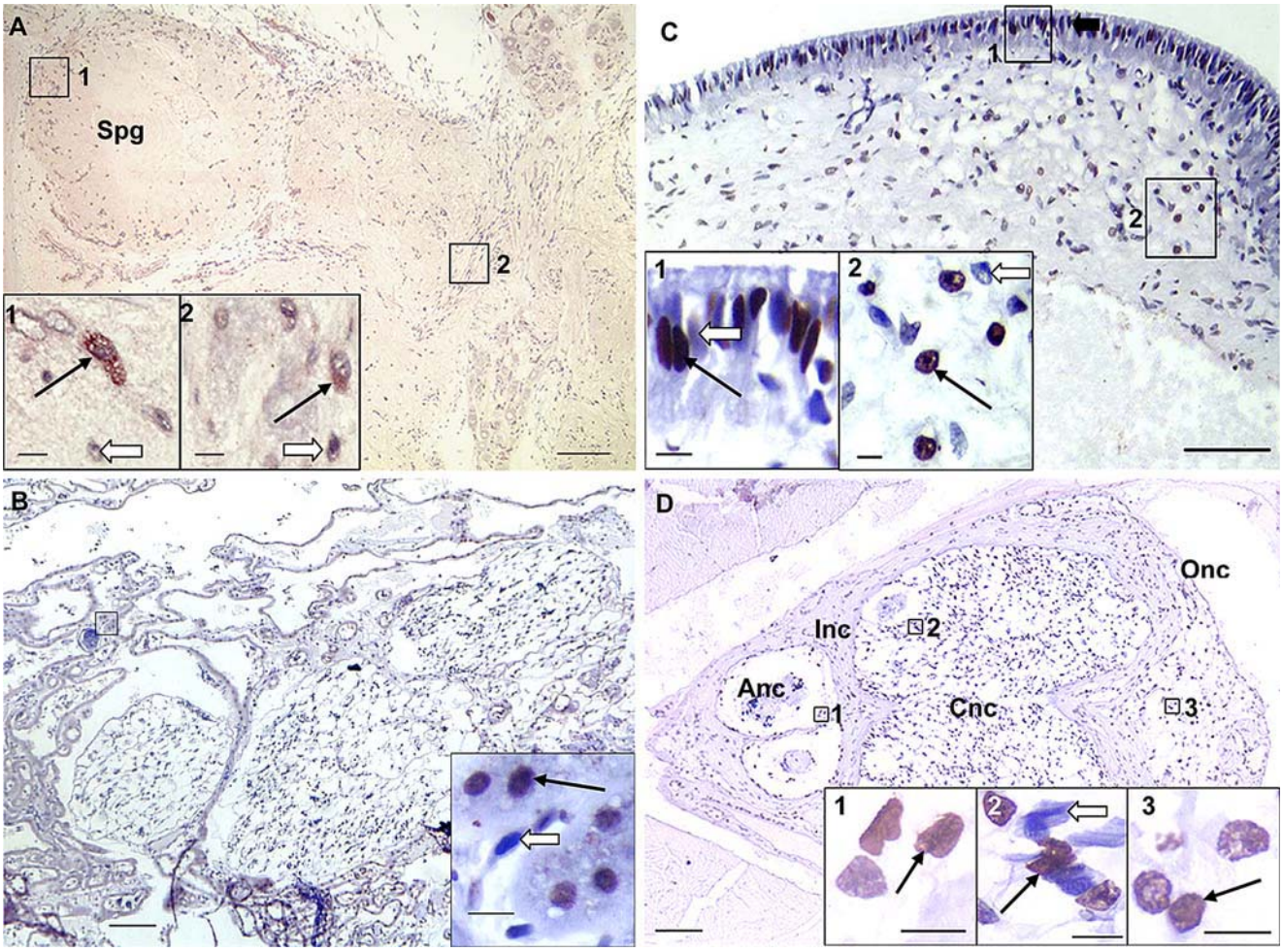


Fig. 1 Immunodetection of ELH in *P. monodon* cephalothoracic region and abdominal nerve tract. Detection used a primary antibody of polyclonal mouse anti-abalone ELH, a secondary of monoclonal biotinylated goat anti-mouse IgG, and visualisation using an avidin–HRP conjugate combined with a NovaRED substrate. *Black arrows* indicate positive cells under high magnification (*insets* of designated low power regions), whereas *white arrows* show negative cells. **a** The cephalothoracic region showing the supraesophageal ganglion (*Spg*) and two locations of neurosecretory ELH positive cells. **b** The antennal gland showing ELH positive cells. **c** The dorsal cephalothoracic region posterior to the Spg, with high power *insets* showing ELH positive cells. **d** The major abdominal nerve tract showing the appendage nerve cord (*Anc*), central nerve cord (*Cnc*), inner nerve capsule (*Inc*), and outer nerve capsule (*Onc*), with high power *insets* showing ELH positive cells. *Scale bars* 100 μm in **a**–**c**, 10 μm in *insets*

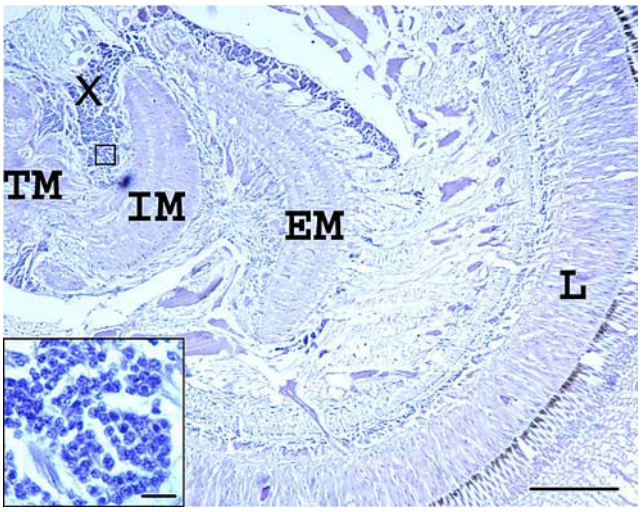


Fig. 2 Absence of ELH in the mature eyestalk tissues, particularly the X-organ sinus gland, following immunostaining with primary antibody of polyclonal mouse anti-abalone ELH. Staining methods were the same as used for Fig. 1. *L* Laminar ganglionaris, *EM* external medulla, *IM* internal medulla, *TM* terminal medulla, and *X* X-organ sinus gland including *inset*. *Scale bars* 100 μm in low magnification and 10 μm in the *inset*

(Fig. 1a). Under high magnification, the ELH was found to be located in the cytoplasm around the nuclei of some neurosecretory cells (Fig. 1a, insets 1 and 2). Cells within the antennal gland were also positive (Fig. 1b). Strong immuno-staining was also detected in cells within two types of tissues of the dorsal cephalothoracic region posterior to the Spg within (Fig. 1c). The positive cells of the cephalothorax epithelial tissue were distinctly elongated in comparison to those of the underlying stromal tissue (Fig. 1c, insets 1 and 2). In the major abdominal nerve trunk linking abdominal ganglia, ELH was detected around the nuclei of cells within the inner nerve capsule separating the nerve cords, around the nuclei of the neurons in the central nerve cord, and around the nuclei of cells within the outer nerve capsule (Fig. 1d, insets 1–3, respectively). These results were obtained from a nine months old female *P. monodon* whose gonad had not yet matured.

The amount and distribution of ELH immunostaining varied with each reproductive stage (Fig. 3a–c). Within the developing shrimp gonad a medium density of staining for ELH was found around the nuclei of the follicular cells (Fcl) situated close to the ovarian capsule and connective tissue trabaculae (Fig. 3a, inset). In comparison, a very strong density of staining for ELH was observed in the cytoplasm of Fcl surrounding each mature oocyte within the ripe shrimp gonad (Fig. 3b, inset). However, a very weak ELH staining density was found in the Fc1 and connective tissue of the post-spawned shrimp gonad (Fig. 3c, inset).

Endogenous enzyme was sometimes difficult to quench when identifying positive cells using immunoenzyme detection. All results were confirmed by

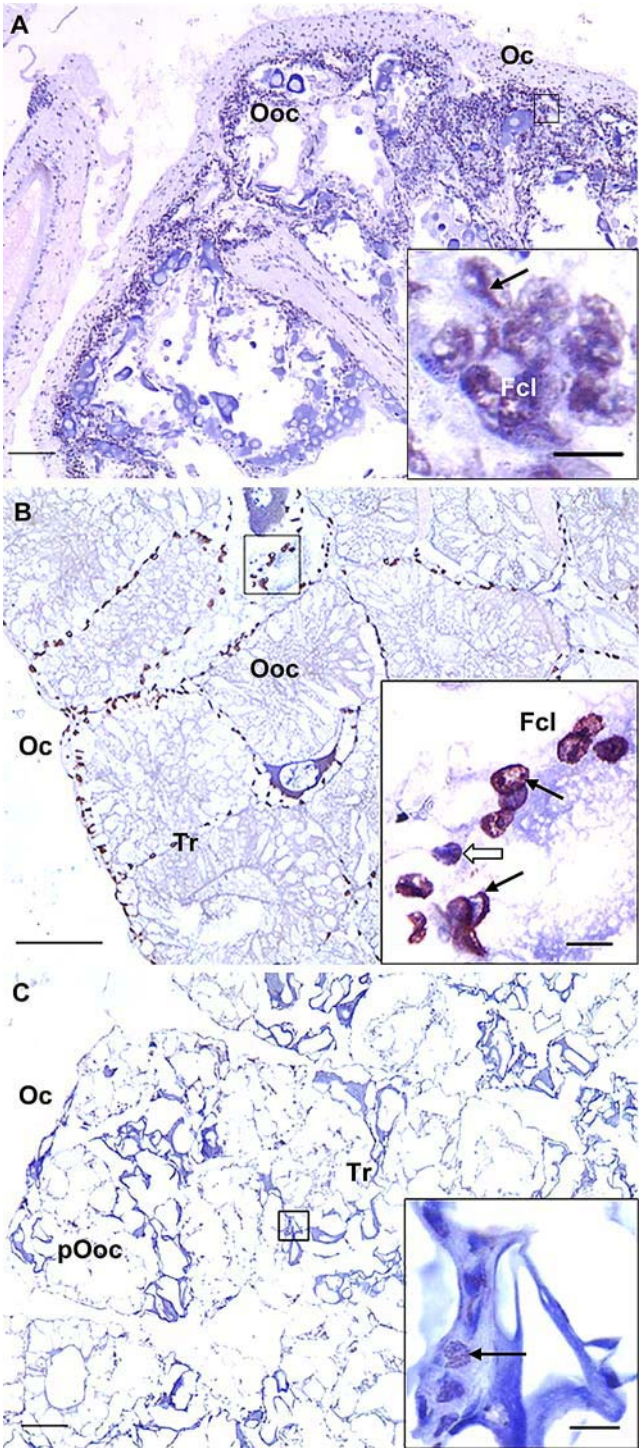


Fig. 3 ELH immunodetection in female shrimp ovaries at different reproductive stages, using the same technique as used in Fig. 1. *Arrows* indicate positive cells. **a** Stage I shrimp ovary showing ovarian capsule (*Oc*) and oocytes (*Ooc*), with high magnification of ELH positive follicular cells (*Fcl*). **b** Stage IV shrimp ovary surrounded by a capsule (*Oc*) and showing fully mature oocytes (*Ooc*), and trabachulae (*Tr*), with high magnification of ELH positive Fcl. **c** Post-spawned shrimp ovary showing the structures of Oc, Tr and post oocyte area (*pOoc*), with high magnification of a few very weak ELH positive Fcl. *Scale bars* 100 μm in **a**–**c**, 10 μm in *insets*

immunofluorescence in which endogenous enzymes were not involved (see Fig. 4 for representative data).

Discussion

Our immunocytochemistry studies have indicated the presence of a putative ELH in the brain, neural, and reproductive tissues of *P. monodon*. These were based on indirect immunoenzyme techniques, with the confirmation using immunofluorescence. The presence of ELH within the *P. monodon* neurosecretory cells of the supraesophageal ganglia, nerve tract and gonads, is consistent with the findings in molluscs (Kupferman 1967; Van Minnen et al. 1992; Ram et al. 1998; Cummins et al. 2001; Saitongdee et al. 2005), an annelid (Salzet et al. 1997), and insects (Theunis et al. 1990). It is of particular interest that the cells of the antennal gland exhibited immunoreactivity, since this type of tissue in shrimp is involved in the excretion of organic compounds, resorption of body fluid, amino acids and sugars from the primary urine filtrate; the control of hemolymph volumes, and is associated with regulations of osmolarity between hemolymph and urine (Lin et al. 2000). Another distinctive feature is that the immunoreactivity in positive reacting cells of *P. monodon* were located in the cytoplasm around the nucleus, and this is consistent with the location of aELH in *H. asinina* ganglia and gonad (Saitongdee et al. 2005).

The immunoreactivity to the abalone ELH also occurred within the shrimp gonad, and particularly follicular cells adjacent to developing and mature oocytes. This observation is the same as that in abalone where the follicular cells around the mature oocytes, located close to the ovarian trabeculae, contain aELH (Cummins et al. 2001; Chanpoo et al. 2001; Saitongdee et al. 2005). There was a positive correlation of the abundance of ELH in the female shrimp ovary with the female spawning cycle, and this was also consistent with the variation found in abalone (S. Cummins, personal communication). This variation commenced with a low immunoreactivity at stage I oocyte development, and culminated in a peak level at stage IV, corresponding to the ripe pre-spawn gonad. Following eye ablation, female gonads showed an almost undetectable level of immunoreactivity, indicating a remarkable release of ELH.

It has been postulated that the ovarian follicle development of female mosquitoes, *Aedes aegypti*, is activated by neurohormones originating from the brain, after which follicle cells in the gonad secrete ecdysteroids which are responsible for ovarian development (Claeys et al. 2003). Molluscan ELH and associated peptides are know to be cleaved from a preprohormone in ganglia, then secreted by the nervous system and transferred to associated target organs triggering egg-laying related activities, such as cessation of locomotion, feeding inhibition, increased respiratory pumping and head weaving, as well as the release of eggs (Scheller et al. 1982; Vreugdenhil et al. 1988). A similar mechanism may exist in mature shrimp in which activation of the neural cells containing ELH results in secretion of ELH and then induction of spawning. The location of ELH in follicular cells of the female gonad may be the result of localised expression of a member of a gene family (Scheller et al. 1982), which is different to the one expressed in neural ganglia, which is an uncleaved prohormone.

Molluscs have been successfully spawned by injection of ganglion extracts into ripe females (Ram et al. 1998; Yahata 1973), and more recently ELHs produced by expression of cloned aELH's, have been used to spawn ripe females (unpublished). However, cultured *P. monodon* females require eye ablation to successfully undergo ovarian maturation and spawning. This dependence on eye ablation has resulted in considerable research on the molecular and physiological aspects of a family of crustacean neuropeptides within the X-organ situated in the medulla terminalis and the associated neurohaemal organ, sinus gland (Nanthika et al. 2005). It contains crustacean hyerglycaemic hormones (CHH), moult inhibiting hormone (MIH), and vitellogenesis or gonad inhibiting hormone (VIH or GIH), which play negative inhibitory roles in the

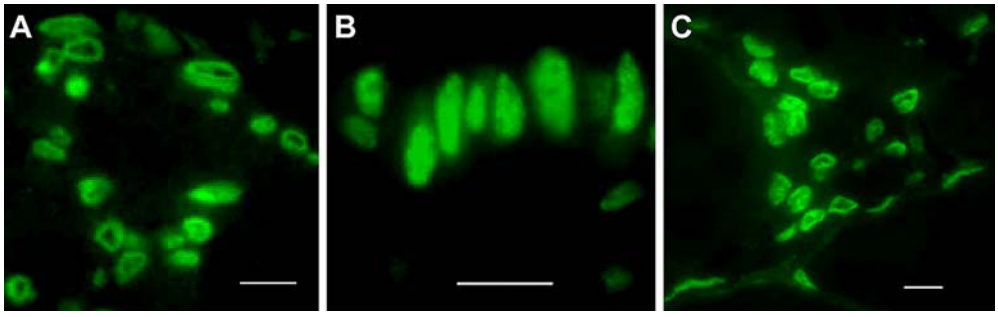


Fig. 4 FITC immunofluorescence confirming the presence of ELH positive cells detected by immunoenzyme technique, in tissues of *P. monodon*. The primary antibody was the same as that used for immunoenzyme detection, but the secondary antibody was FITC-conjugated monoclonal sheep anti-mouse IgG. Positive cells shown are high magnifications of **a** supraesophageal neurosecretory cells (see Fig. 1a), **b** positive cells tissue posterior to the supraesophageal ganglia (see Fig. 1b), and **c** follicular cells in a Stage IV ovary (see Fig. 2b). *Scale bars* 10 μm

female reproductive performance, such as molting and gonad development (Keller 1992). The effect of VIH/GIH is removed during eye ablation, but little is known about the inducer molecules involved in shrimp spawning. Furthermore, the absence of ELH in the X-organ sinus gland also suggests that the separation of locations between inhibiting and inducing groups of neuropeptides, and that the shrimp ELH is a functional peptide acting within defined organs. We postulate that shrimp ELH located in neural and gonad tissues may be responsible for the induction of spawning. Current research aims to identify and characterise the gene encoding the ELH described in this shrimp study.

Acknowledgements We wish to thank Nigel Preston and Melony Sellar, CSIRO Marine Laboratory, for supplying specimen of live shrimp. The assistance provided by Apichart Nernsoungnern was most appreciated. We thank the Thailand Research Fund and National Center for Genetic Engineering and Biotechnology of Thailand for providing financial support.

References

Arena L, Montalvan M, Espinosa G, Gaxiola G, Sanchez A, Wormhoudt AV, Hernandez D, Diaz T, Rosa C (2003) Genetic relationship between *Litopenaeus setiferus* (L.) and *L. schmitti* (Burkenroad) determined by using 16S mitochondrial sequences and enzymatic analysis. Aquac Res 34:981–990

Boonyaratpalin M, Supamattaya K, Verakunpiriya V, Suprasert D (2001) Effects of aflatoxin B1 on growth performance, blood components, immune function and histopathological changes in black tiger shrimp (*Penaeus monodon* Fabricius). Aquac Res 32:388

Bray WA, Lawrence AL (1998) Successful reproduction of *Penaeus monodon* following hypersaline culture. Aquaculture 159:275–282

Chanpoo M, Apisawetakan S, Thongkukiatkul A, Wanichanon C, Linthong V, Kruatrachue M, Upatham ES, Pumthong T, Hanna PJ, Sobhon P (2001) Localization of egg-laying hormone in the gonads of a tropical abalone, *Haliotis asinina* Linnaeus. J Shellfish Res 20:725–731

Claeys I, Simonet G, Van Loy T, De Loof A, Vanden Broeck J (2003) cDNA cloning and transcript distribution of two novel members of the neuroparsin family in the desert locust, *Schistocerca gregaria*. Insect Mol Biol 12:473–481

Cummins S, Thongkukiatkul A, Hanna PJ (2001) Location of egg-laying hormone in reproductive structures and neurons of *Haliotis rubra* (Leach) using antibodies raised against recombinant fusion proteins. J Shellfish Res 20:705–710

Dall W (1957) A revision of the Australian species of Penaeinae (Crustacea: Decapoda: Penaeidae). Aust J Mar Fresh Res 1:136–230

Herndon L, Wolfner M (1995) A Drosophila seminal fluid protein, Acp26Aa, stimulates egg laying in females for 1 day after mating. Proc Natl Acad Sci USA 92:10114–10118

Hoang T, Lee ST, Keenan CP, Marsden GE (2002) Observations on growth, sexual maturity and spawning performance of pond-reared *Penaeus merguiensis*. Aquac Res 33:863

Jones DS, Morgan GJ (1994) A field guide to crustaceans of Australian waters. Reed, Chatswood

Keller R (1992) Crustacean neuropeptides: structures, functions and comparative aspects. Experientia 48:439–449

Klinbunga S, Penman DJ, McAndrew BJ, Tassanakajon A (1999) Mitochondrial DNA diversity in three populations of giant tiger shrimp *Penaeus monodon*. Mar Biotechnol 1:113–121

Kupferman I (1967) Stimulation of egg laying: possible neuroendocrine function of bag cells of abdominal ganglion of *Aplysia californica*. Nature 216:814–815

Lin SC, Liou CH, Cheng JH (2000) The role of the antennal glands in ion and body volume regulation of cannulated *Penaeus monodon* reared in various salinity conditions. Comp Biochem Physiol 127:121–129

Nanthika P, Paisarn S, Parin C, Siwaporn L, Weerawan S, Amorn P (2005) Production of monoclonal antibodies specific to eyestalk neuropeptides of *Penaeus monodon* using sinus gland section and immunosuppression technique. Sci Asia 31:29–35

Primavera JH (1978) Induced mauration and spawning in five-month-old *Penaeus monodon* Fabricius by eyestalk ablation. Aquaculture 13:355–359

Ram JL, Gallardo CS, Ram ML, Croll RP (1998) Reproduction-associated immunoreactive peptides in the nervous systems of prosobranch gastroods. Bio Bull 195:308–318

Saitongdee P, Apisawetakan S, Anunruang N, Poomthong T, Hanna JP, Sobhon P (2005) Egg-laying-hormone immunoreactivity in the neural ganglia and ovary of *Haliotis asinina* Linnaeus. Invert Neurosci 5:165–172

Salzet M, Verger-Bocquet M, Vanderbulcke F, Van Minnen J (1997) Leech egg-laying-like hormone: structure, neuronal distribution and phylogeny. Mol Brain Res 49:211–221

Scheller RH, Jackson JF, McAllister LB, Schwarts JH, Kandel ER, Axel R (1982) A family of genes that codes for ELH, a neuropeptide eliciting a stereotyped pattern of behavior in *Aplysia*. Cell 28:707–710

Theunis W, Van Minnen J, De Loof A (1990) Immunocytochemical localization in the central nervous system of four different insect species of molecules immunoreactive against peptides present in the caudodorsal cells of *Lymnaea stagnalis*. Gen Comp Endocrinol 79:415–422

Van Minnen J, Schallin HDFH, Ramkema MD (1992) Identification of putative egg-laying hormone containing neuronal systems in gastropod molluscs. Gen Comp Endocrinol 86:96–102

Vreugdenhil E, Jackson JF, Bouwmeester T, Smit AB, Van Minnen J, Van Heerikhuizen H, Klootwijk J, Joosse H (1988) Isolation, characterization, and evolutionary aspects of a cDNA clone encoding multiple neuropeptides involved in the stereotyped egg-laying behavior of the fresh water snail *Lymnaea stagnalis*. J Neurosci 8:4184–4191

Yahata T (1973) Induced spawning of abalone (Nordotis discus REEVE) injected with ganglional suspensions. Bull Jpn Soc Sci Fish 39:1117–1122

Available online at www.sciencedirect.com
ScienceDirect
Aquaculture 260 (2006) 315–325
Aquaculture
www.elsevier.com/locate/aqua-online

Serotonin induces ovarian maturation in giant freshwater prawn broodstock, *Macrobrachium rosenbergii* de Man

Prasert Meeratana [a,*], Boonsirm Withyachumnarnkul [b], Praneet Damrongphol [c], Kanokphan Wongprasert [b], Anchalee Suseangtham [b], Prasert Sobhon [b]

[a] *Department of Medical Science, Faculty of Science, Burapha University, Chonburi, 20131, Thailand*
[b] *Department of Anatomy, Faculty of Science, Mahidol University, Rama VI Road, Bangkok, 10400, Thailand*
[c] *Department of Biology, Faculty of Science, Mahidol University, Rama VI Road, Bangkok, 10400, Thailand*

Received 16 December 2005; received in revised form 8 June 2006; accepted 9 June 2006

Abstract

This study investigated the effects of serotonin (5-hydroxytryptamine or 5HT) on ovarian development in *Macrobrachium rosenbergii* de Man. Adult female prawns at the ovarian stage I (spent) were injected with 5HT at 1, 5, 10, 20 and 50 μg g^{-1} body weight (BW) intramuscularly on days 0, 5 and 10, and sacrificed on day 15. The doses as related to the effect could be categorized into three levels: low (1 and 5 μg g^{-1} BW of 5HT), medium (10 and 20 μg g^{-1} BW of 5HT) and high (50 μg g^{-1} BW of 5HT). The low-dose, especially at 1 μg g^{-1} BW, caused prawns to exhibit a significant increase in ovarian index (ovarian weight/body weight × 100) (5.79 ± 0.09%) as compared to the control (1.49%). The ovaries of most of these prawns could develop to stage IV (mature) and contained synchronously mature oocytes while most of the control ovaries remained at stage I and II (proliferative), and contained only oogonia to previtellogenic (Oc1, Oc2) and early vitellogenic oocytes (Oc3). The medium- and high-dose treated prawns exhibited ovaries that could reach stages III and IV and contained various types of oocytes of different maturity. Pretreatment with 5HT receptor antagonist, cyproheptadine (CYP), at 10 μg g^{-1} BW before 5HT injection significantly suppressed the effect of 5HT. Intramuscular injection of the 5HT-primed thoracic ganglion culture medium into CYP-pretreated prawns resulted in the increase of ovarian index about 5–6 times more than in the control, and in the groups injected with 5HT-primed media from muscle strip, eyestalk and brain. The ovaries of most prawn could develop up to stage IV and contained synchronously developed vitellogenic (Oc4) and mature oocytes (Oc5). These findings suggest that 5HT indirectly induces ovarian development and oocytes maturation in *M. rosenbergii*, probably via a putative ovarian stimulating factor released from the thoracic ganglia.
© 2006 Elsevier B.V. All rights reserved.

Keywords: *Macrobrachium rosenbergii*; Broodstock; Serotonin; Oocyte; Ovarian maturation

1. Introduction

The giant freshwater prawns, *Macrobrachium rosenbergii* de Man are found in fresh as well as brackish water of the tropical area, including Southeast Asia. It is considered to be one of the crustacean species with increasing potential for aquaculture, and thus was

* Corresponding author. Tel.: +662 745900x3167; fax: +662 38 393497.
E-mail address: g3936465@yahoo.com (P. Meeratana).

0044-8486/$ - see front matter © 2006 Elsevier B.V. All rights reserved.
doi:10.1016/j.aquaculture.2006.06.010

introduced worldwide (Sandifer and Smith, 1985). The female prawns become sexually mature at 4–6 months, when mating occurs between hard-shelled males and soft-shelled females, which have just completed molting. A premating molted female could be distinguished by the presence of the large reddish-orange ovarian mass on the dorsal side of cephalothorax beneath the carapace. The male deposits spermatophore, a gelatinous mass containing spermatozoa, between the walking legs of the female. Egg laying occurs within a few hours and the eggs are fertilized externally. The number of eggs produced by each female is directly proportional to its size. A fully mature female may lays between 80,000 and 100,000 eggs per spawning, but at the first brood it may lay only about 5,000–20,000 eggs (New, 2002). The fertilized eggs remain attached to the brood chamber between the swimming legs for about 18–23 days after spawning. The newly spawned eggs are characterized by bright yellow to orange color, which gradually change to brown and finally grey color at about 2–3 days before hatching.

The hormonal control of decapods' reproduction was extensively studied in crayfish, *Procambarus clakii*, and lobster, *Homarus americanus*, in which a number of hormones from several neuroendocrine and endocrine organs play key roles in controlling the gonad development and secondary sexual characteristics (Van Herp and Soyez, 1997; Chen et al., 2003). At least two antagonistic neurohormones regulate the gonadal maturation: gonad inhibiting hormone (GIH), released from the sinus gland in the eyestalk optic lobes of both sexes inhibits the gonadal maturation; whilst gonad stimulating hormone (GSH), believed to be secreted by the supraesophageal and thoracic ganglia, stimulates the gonadal maturation. Several neurotransmitters have been shown to affect the release of these reproductive hormones. For instance, dopamine (DA) stimulates GIH in eyestalk (Fingerman, 1997) and inhibit GSH in thoracic ganglia (Chen et al., 2003), whereas serotonin (5HT) stimulates GSH release (Fingerman, 1997). 5HT also stimulates the releases of other hormones, including crustacean hyperglycemic hormone (CHH) (Keller and Beyer, 1968), red pigment dispersing hormone (RPDH) (Rao and Fingerman, 1970), molt inhibiting hormone (MIH) (Chang, 1985; Mattson and Spazaini, 1985) and black pigment dispersing hormone (BPDH) (Bauchau and Mangeot, 1966). In addition, it was reported that female crayfish, *Procambarus clarkii*, given 5HT exhibited a significant increase in ovarian index and oocyte size (Sarojini et al., 1995). This study aims to investigate whether 5HT could also stimulate ovarian maturation in *M. rosenbergii*, one of the most economically important prawns in Thailand. If the result is positive, the endocrine manipulation by 5HT may be one way that could be used to enhance the fecundity of female broodstock in captivity.

2. Materials and methods

2.1. Experimental animals

Adult females *M. rosenbergii* de Man were obtained from a commercial farm and they were used in the experiment as soon as they exhibited stage I (spent) of the ovarian cycle. The animals were kept in ten outdoor circular concrete tanks (1.5 m in diameter) containing water at depth 0.80 m, with adequate aeration, and 20% of water being changed daily. Commercial prawn feed was provided at 3% body weight daily. They were acclimatized under the natural light–dark cycle for 2 weeks before the experiments. To allow mating, blue-claw males were stocked in the same tank at a ratio of 1 male to 5 females.

2.2. In vivo effect of 5HT on ovarian maturation

The female animals were randomly divided into seven groups of 10 animals per group: the non-injected control, vehicle-injected control and five 5HT-injected groups. Seven female prawns with two male prawns were reared in the same tank but identified by tying different color plastic loops around their eyestalks. 5HT was dissolved in crustacean physiological saline (CPS: NaCl 29 g, KCl 0.71 g, $CaCl_2 2H_2O$ 2.38 g, $MgSO_4$ $7H_2O$ 3.16 g, $NaHCO_3$ 0.5 g, $MgCl_2 6H_2O$ 0.17 g, HEPES 4.76 g) at 10 mg ml^{-1} as the stock solution. 5HT was injected at the dosage of 1, 5, 10, 20 and 50 μg 5HT g^{-1} BW in 0.05 ml volume on the stage I of ovarian cycle. These experimental groups were designated as 5HT-1, 5HT-5, 5HT-10, 5HT-20, 5HT-50, respectively. Subsequent injections were repeated on days 5 and 10 after the first injection. Animals from each group were sacrificed on day 15. The body weight was measured on the first day, and again with the ovarian weight at the end of the experiment. Average ovarian index (OI = ovarian weight / body weight × 100) of the prawns in each group were determined. The ovaries were fixed with Davidson's fixative, and prepared for LM studies.

2.3. In vivo effect of 5HT antagonist on ovarian maturation

The other set of 70 females were divided into seven groups as in the preceding experiment. The same

protocol was employed, except that the 5HT injection was preceded at 30 min by the administration of 10 μg/g^{-1} BW of cyproheptadine (CYP), which is a 5HT antagonist. All animals were sacrificed on day 15 and the body weight, ovarian weight was measured, and ovarian index was determined. The ovaries were immediately fixed and prepared for histological examination.

2.4. In vivo effect of organ media on the ovarian maturation

This study was performed based on the hypothesis that 5HT may stimulate the release of a putative ovarian stimulating factor (OSF) from the brain or thoracic ganglia or other parts of the nervous system, and that OSF would subsequently stimulate ovarian maturation. The following organs were isolated from the adult female broodstock at stage IV (mature) of the ovarian cycle: eyestalk containing optic lobes, brains (supraesophageal ganglion), thoracic ganglia, and muscle strips. All organs were obtained from prawns with complete ovarian maturation to ensure that OSF was present. Each organ was washed with CPS containing 60 mg in 100 ml streptomycin and 100 units ml^{-1} penicillin G and 0.1% glucose. The organs were then incubated with 1 μg ml^{-1} of 5HT (the effective dose as proven in the first experiment) in 2 ml of Medium 199 (Gibco BRL, Life Technologies, New York, USA) in a CO_2 incubator set at 27–28 °C, in total darkness for 30 min. The media were collected and immediately kept in a deep freezer (Forma Scientific, USA) at −70 °C and

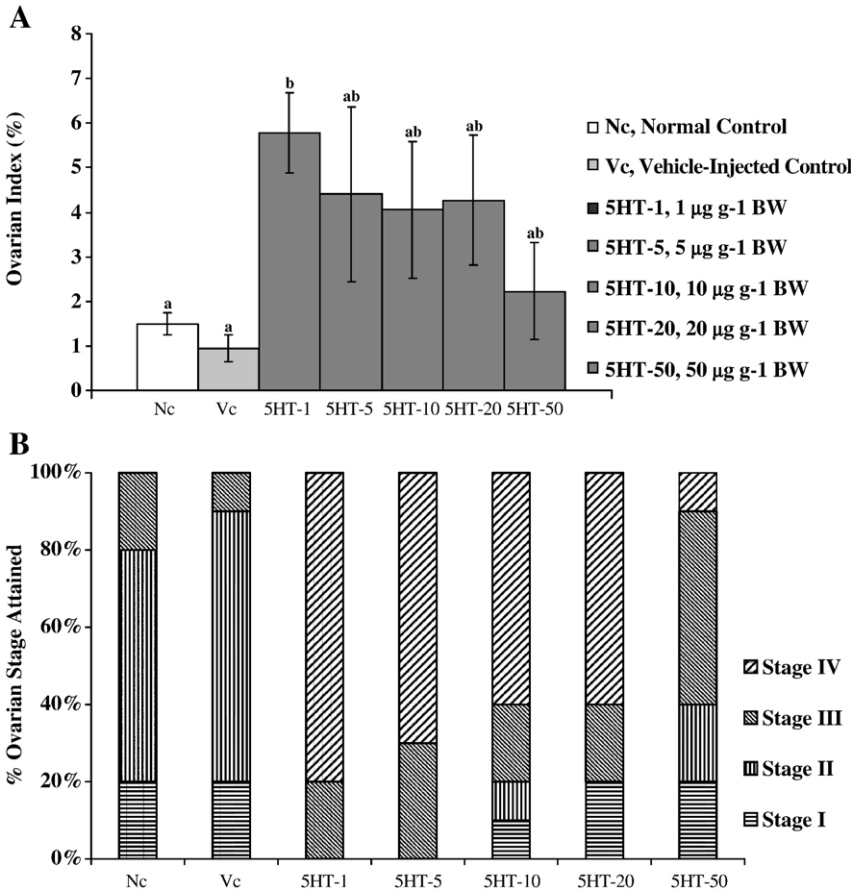


Fig. 1. (A) Ovarian index (OI) of the giant freshwater prawn, *M. rosenbergii*, at day 15th after multiple injections of 5HT at 1, 5, 10, 20, 50 μg g^{-1} BW on day 0, 5th and 10th. Nc—normal control, Vc—vehicle-injected control, 5HT-1, 5HT-5, 5HT-10, 5HT-20 and 5HT-50; prawns injected with 1, 5, 10, 20 and 50 μg of 5HT g^{-1} BW, respectively. The number of prawns in each group is ten. Each bar represents the mean value from ten samples with the standard error. Bars with different letter superscripts are significantly different ($p<0.05$). (B) Percentage of ovarian stages that the prawns attained 15 days after the first injection as described in (A). Stage I—spent, stage II—proliferative, stage III—premature, stage IV—mature.

later lyophylized (Lyovac GT2, Cologne, Germany) for 5 h and stored at −70 °C. These lyophylized media were made in three replicates, and each replicate was tested for the presence of OSF. Each replicate of the culture medium was dissolved in 0.05 ml of CPS and injected into a mature adult female prawn appearing in

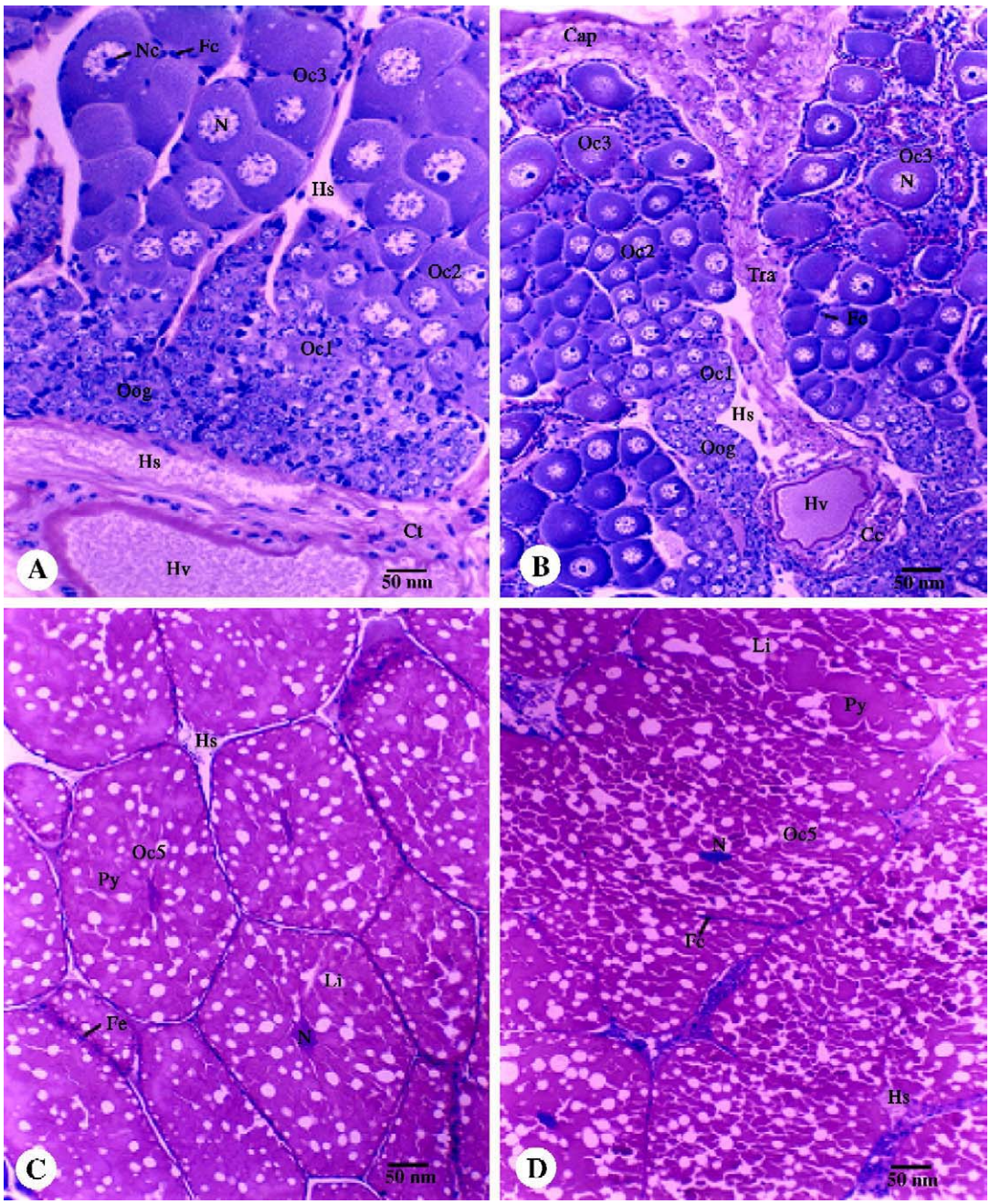


Fig. 2. Light micrographs of H&E-stained 5 μm thickness paraffin sections, showing ovarian development of control and 5HT-injected prawns. A and B—ovaries of the control prawns, C and D—ovaries of 1 and 5 μg 5HT g^{-1} BW injected prawns, Oc1, Oc2—previtellogenic oocytes, Oc3—vitellogenic oocytes, Oc5—mature oocytes, Cap—ovarian capsule, Cc—central ovarian core, Ct—connective tissue, Fc—follicular cells, Oz—oogenic zone, Hs—hemolymph sinus, Hv-hemolymph vessel, N—nucleus, No—nucleolus, Oog—oogonia, Oc1—early previtellogenic oocyte Oc2—late previtellogenic oocyte, Oc3—early vitellogenic oocyte, Oc4—late vitellogenic oocyte, Oc5—mature oocyte, Li—lipid droplets, Py—proteinaceous yolk plaques, Tra—trabeculae.

stage I ovarian development, at days 0, 5 and 10. Since the medium also contained 5HT, it was therefore necessary to negate the effect of 5HT by injecting the prawn first with CYP at the dose of 10 μg g^{-1} BW, 30 min before the injection of the medium. A total of 25 prawns were divided into 5 groups of 5 animals per group, each of the experimental groups was injected with medium of 5HT-primed muscle strip, eyestalk, brain and thoracic ganglia. The control group was injected with the same volume of CPS.

At the end of the experiment, the body weight, ovarian weight and ovarian index were determined. The ovaries were fixed and processed for LM examination.

2.5. Observation of ovarian stages and histological examination of the ovarian tissues

The ovarian cycle in female broodstock was classified into five stages based on their size and color as reported by Chang and Shih (1995). Stages 0 and I were spawned and spent phases when the ovaries appeared white. In stage II (proliferative) a small yellow mass of ovary could be observed dorsally in the carapace. In stage III (premature) the ovaries became orange, and in stage IV the reddish-orange ovaries extended from behind the eye down to the first abdominal segment.

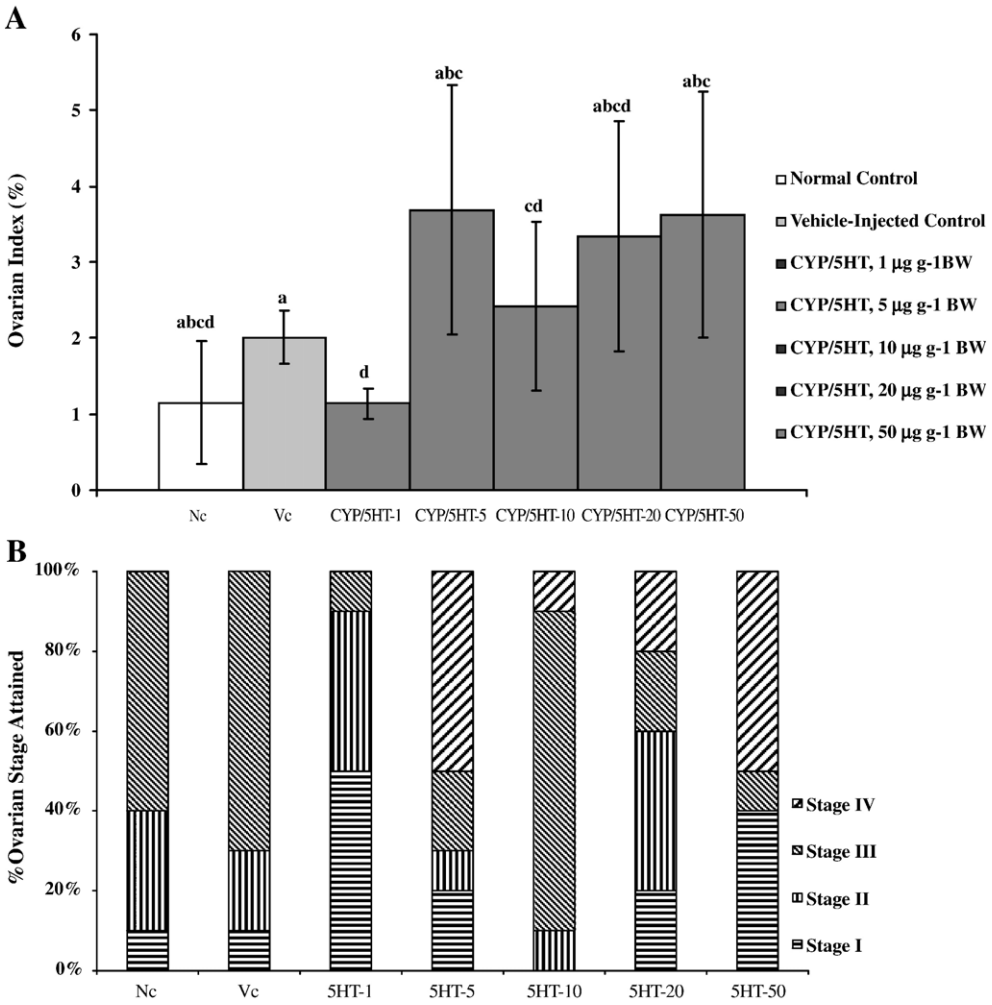


Fig. 3. (A) Ovarian index of the cyproheptadine-5HT treated prawns at day 15 after the first injection. Nc—normal control, Vc—vehicle-injected control, CYP/5HT-1, CYP/5HT-5, CYP/5HT-10, CYP/5HT-20 and CYP/5HT-50; prawns injected with CYP followed by 1, 5, 10, 20 and 50 μg of 5HT g^{-1} BW, respectively. Each bar represents the mean value from ten samples with the standard error. Bars with different letter superscripts are significantly different ($p<0.05$). (B) Percentage of ovarian stages that the CYP-5HT treated prawns attained at 15 days after the first injection.

For histological examination, blocks of ovaries from experimental and control animals were fixed in Davidson's fixative and embedded in paraffin using standard technique. Changes of the ovarian histology were examined in 7 μm thick paraffin sections stained with Harris's hematoxylin and counter-stained with eosin

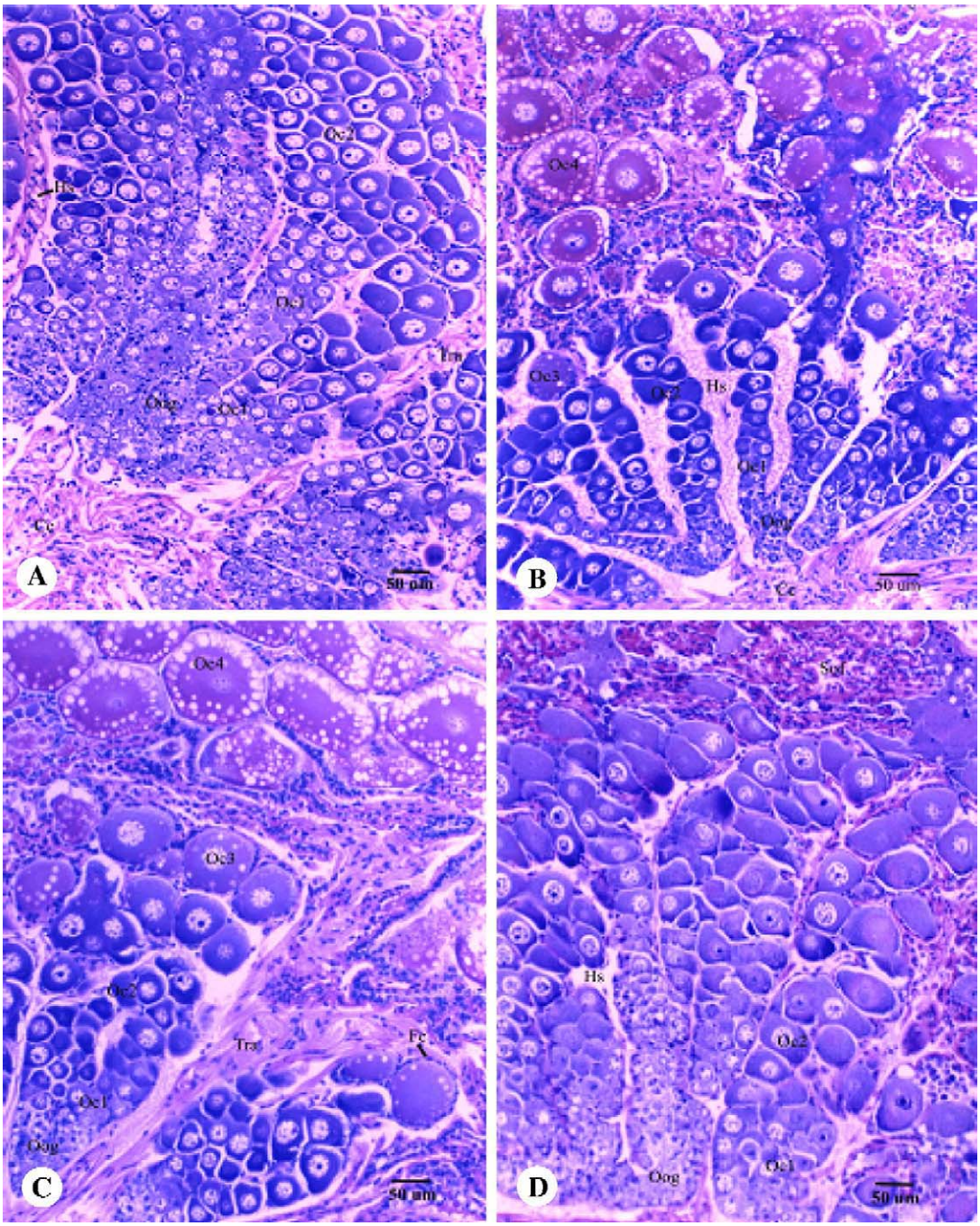


Fig. 4. Light micrographs of H&E-stained paraffin sections, showing ovarian development in the experimental groups: CYP/5HT-1 (A), CYP/5HT-5 (B), CYP/5HT-20 (C) and CYP/5HT-50 (D)-treated prawns. Cc—central ovarian core, Fc—follicular cell, Hs—hemolymph sinus, Oog—oogonia, Oz—oogenic zone, Oc1, Oc2—previtellogenic oocytes, Oc3—early vitellogenic oocytes, Oc4—vitellogenic oocytes, Oc5—mature oocytes, Sof—spent oogenic follicle, Tra—trabeculae.

(H&E stain) by light microscopy (Olympus BX50 equipped with digital camera DP12).

2.6. Statistical analysis

The data were expressed as means and standard errors of means (mean±SE). Statistical significance differences were tested by one-way ANOVA followed by Least-Significant Difference (LSD) ($p<0.05$).

3. Results

3.1. Effect of 5HT on the ovarian maturation

At 1 μg g^{-1} BW, 5HT induced a significant increase in the ovarian index (5.79±0.9%) as compared to that of the non-injected control (NC) (1.59±0.3%) and vehicle-injected control (VC) (0.94±0.3%), with significant different at $p<0.05$. Smaller increase of OI was observed in other groups of 5HT-treated animals, and the increase was generally lower when the dose of 5HT was higher (Fig. 1A). However, no statistical difference was observed in the OI of prawns receiving these higher doses of 5HT when compared to those of the control.

The ovarian maturation was judged by observing the histology at day 15 after the first 5HT injection. The ovaries of NC and VC prawns mostly developed to stage II (60% and 70%) and stage III (20% and 10%) while the rest remained at stage I. Eighty percent of the 5HT-1 and 70% 5HT-5 prawns reached stage IV, while 60% of the 5HT-10 and 5HT-20 prawns reached stage IV, but only 10% of 5HT-50 prawns reached stage IV. No 5HT-1 and 5HT-5 prawns remained at ovarian stage I and II (Fig. 1B).

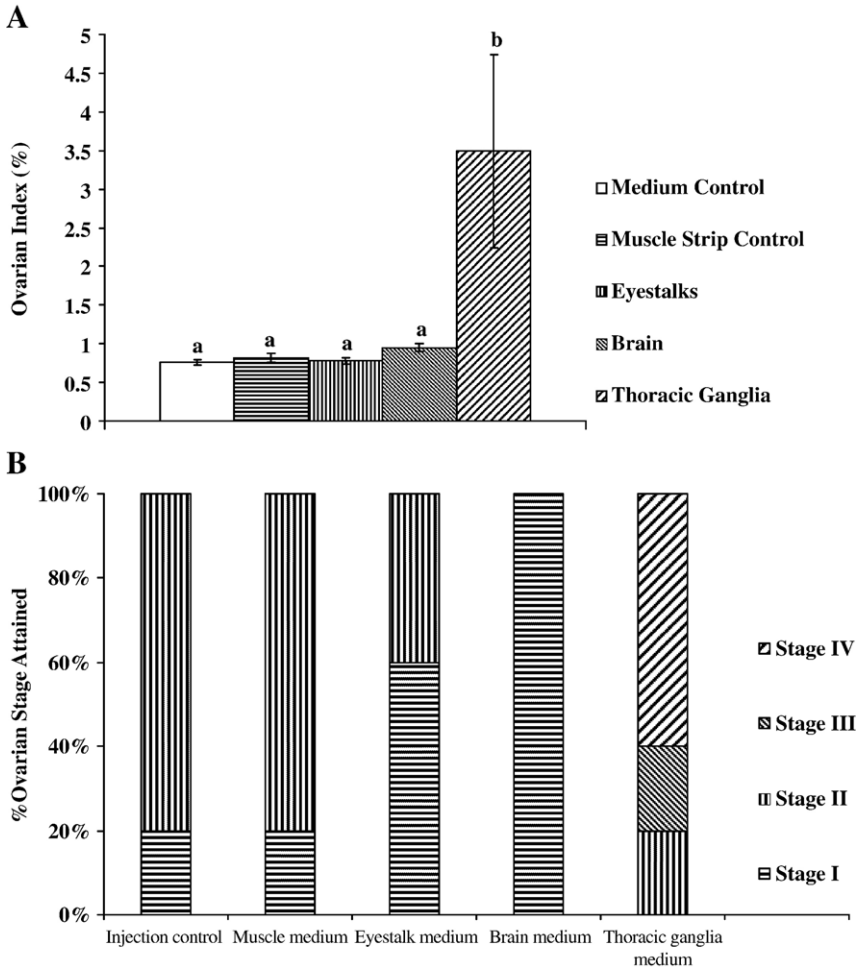


Fig. 5. (A) Ovarian index of prawns injected with culture medium of 5HT-primed organs. The number of prawns in each group is five. Each bar represents the mean value from ten samples with the standard error. Bars with different letter superscripts are significantly different ($p<0.05$). (B) Percentage of ovarian stages attained by the prawns injected with culture medium of organ culture media as described in (A).

Histologically, the ovaries of most NC and VC prawns, which reached stage II, contained mainly previtellogenic oocytes (Oc1, Oc2) (Fig. 2A, B). In contrast ovaries of 5HT-1 and 5HT-5 prawns which were in stage IV, contained fully mature oocytes (Oc5) that were synchronously developed (Fig. 2C, D). Ovaries of the 5HT-10, 5HT-20 and 5HT-50 prawns also contained mostly mature oocytes, and various stages of immature oocytes, which indicated that the development was not complete nor as synchronous as in the first two groups.

3.2. Effect of 5HT when preceded by cyproheptadine (CYP)

In most the treated groups, OI was not significantly higher when compared to the control groups, whilst OI of

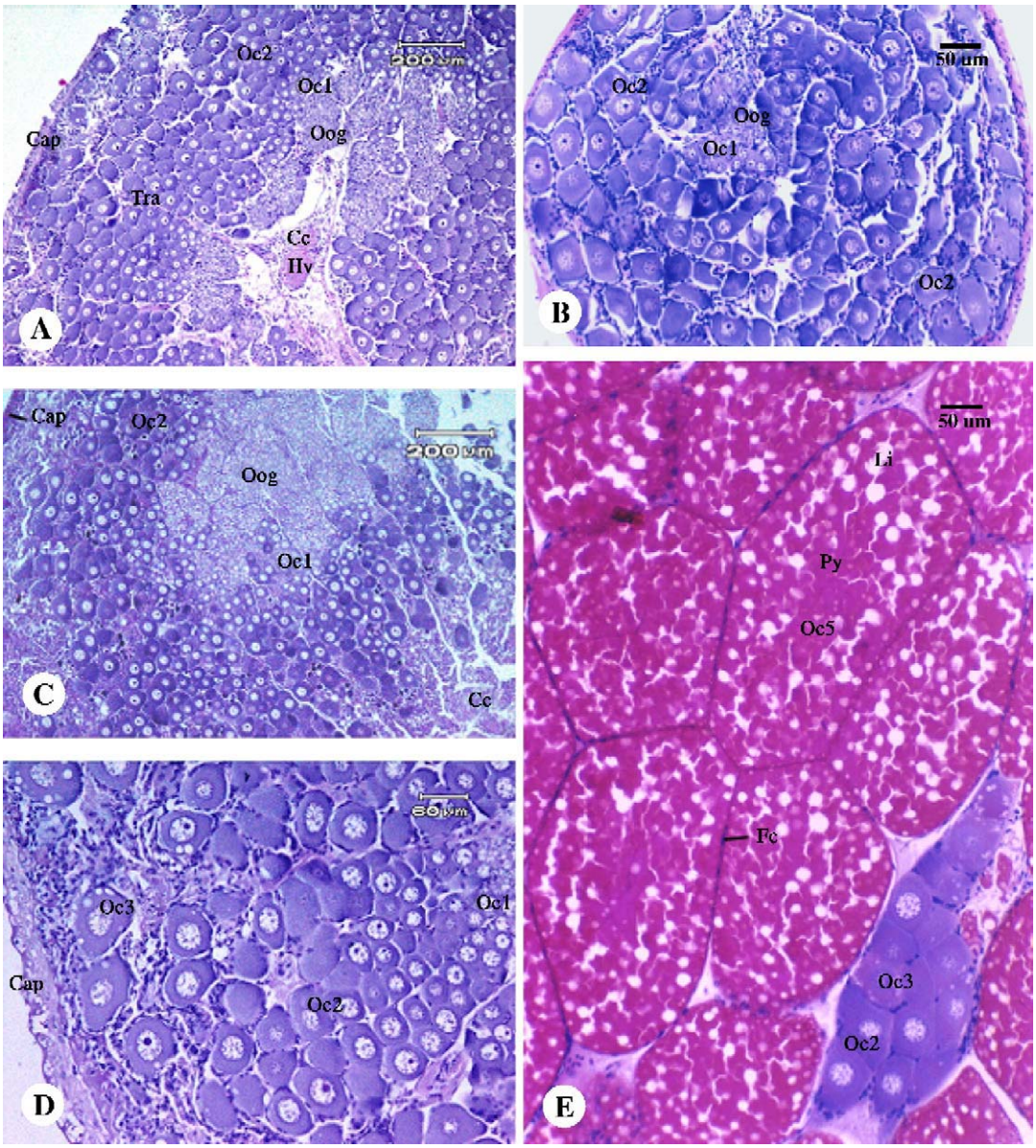


Fig. 6. Light micrograph of paraffin sections stained with H&E, showing the ovarian development of the prawns injected with culture media (M199) of organs primed with 1 μg ml^{-1} 5HT. The prawns were given 5HT-receptor antagonist, cyproheptadine (CYP) at 10 μg g^{-1} BW for 30 min before 5HT injection. A—with control medium, B—medium from muscle strip, C—eyestalk, D—brain, E—thoracic ganglion. Cap—ovarian capsule, Cc—central ovarian core, Fc—follicular cell, Hs—hemolymph sinus, Hv—hemolymph vessel, Li—lipid droplet, Py—proteinatious yolk plaque.

CYP/5HT-1 treated prawns (1.14±0.2%) was significantly lower than that of the VC (2.01±0.35%) prawns ($p<0.05$) (Fig. 3A). The OI of CYP/5HT-1 prawns was also significantly lower than that of the CYP/5HT-5 (3.69±1.64%) and CYP/5HT-50 (3.62±1.2%) groups.

In most NC and VC prawns the ovaries were still at stages I, II or III of the ovarian cycle (Fig. 3B). The ovaries of most CYP/5HT-1 prawns developed only to stage I (50%), and the rest to stage II (40%) and stage III (10%), while none reached stage IV. The ovaries of CYP/5HT-5, CYP/5HT-10 and CYP/5HT-20 developed to stage IV at 50%, 10% and 20%, respectively. Most of the CYP/5HT-50 prawns (40%) remained at stage I and 10% in stage III and 50% in stage IV, and none in stage II. Thus the attainment of mature ovarian stage (stage IV) by low dose 5HT treatment was clearly negated by pretreatment with CYP.

Histologically, the ovary of CYP/5HT-1 prawns contained mostly previtellogenic oocytes (Oc1, Oc2) (Fig. 4A), while the ovaries of CYP/5HT-5, CYP/5HT-10, CYP/5HT-20 and CYP/5HT-50 prawns contained previtellogenic oocytes (Oc1, Oc2) as well as vitellogenic oocytes (Oc3, Oc4) which occupied the periphery of the ovary (Fig. 4B–D).

3.3. Effect of organ culture media on ovarian maturation

As 5HT injection could stimulate the ovarian development, the question is whether this was due to the direct effect of 5HT, or that 5HT may act through other putative ovarian stimulating factor (OSF). The injection of culture medium from the 5HT-primed thoracic ganglia in the prawn pretreated with CYP resulted in significantly increased OI (3.49±1.25%) ($p<0.05$) compared to the control (0.76±0.04%), while OI of other groups of prawns injected with media from other 5HT-primed tissues (muscle, eyestalk, brain) showed no significant difference from the control (Fig. 5A). The increase of OI by treatment with the thoracic ganglia medium was 4.5 times more than that of the control group and 3 times more than the stimulation by other media. Since the effect of thoracic ganglion medium was not negated by CYP pretreatment, the increased OI could be due to the action of some mediator (OSF) released from the thoracic ganglia.

The percentages of ovarian stages attained by 5HT-primed organ media were shown in Fig. 5B. The prawns injected with the control and the muscle strip media displayed mostly ovarian stage II (80%) and the rest remained in stage I (20%). The ovaries of prawns injected with the eyestalk medium remained mostly in stage I (60%) and the rest developed only to stage II (40%). All the ovaries of prawns injected with the brain medium developed to ovarian stage I. Sixty percent of the ovaries of prawns injected with the thoracic ganglia medium advanced to ovarian stage IV, with the rest remaining at stage II (20%) and stage III (20%).

Histologically, the ovarian tissues of the prawns injected with the control media and muscle strip medium showed ovaries at stages I and II, containing mainly oogonia (Oog) and previtellogenic oocyte (Oc1, Oc2) and rarely vitellogenic oocytes (Oc3) (Fig. 6A, B). The prawn injected with medium from 5HT-primed eyestalk culture had their ovaries containing mostly previtellogenic oocytes at Oc2 (Fig 6C). In contrast, the ovaries of prawns injected with medium from the 5HT-primed thoracic ganglion contained mostly vitellogenic oocytes (Oc3, Oc4) and mature oocytes (Oc5), with only few previtellogenic oocytes (Oc2) (Fig. 6E).

4. Discussion

In this study, 5HT at the dosage 1 μg g^{-1} BW is the most effective dose in increasing the ovarian index of *M. rosenbergii* female broodstock to about 5 times that of the control. It also shortened the period for ovarian maturation to 15 days, which usually needs 30–35 days for the development from stages I to IV (New, 2000). Several studies show that 5HT and the nervous tissue extract could stimulate ovarian maturation and spawning in some crustaceans including the freshwater shrimp, *Paratya compressa* (Mattson and Spazaini, 1985) and the red swamp crayfish, *P. clarkii* (Bauchau and Mangeot, 1966). Crayfish given 5HT showed a significant increase in the ovarian index and oocytes diameter (Kullkarni et al., 1992). In fiddler crab, *Uca pugilator*, 5HT and 5HT agonists, fenfluramine and fluoxetine, stimulated ovarian development, while 5,6-dihydroxytryptamine, an antagonist, inhibited it (Matsutani and Nomura, 1987; Krantic et al., 1993). 5HT had been found to be distributed widely in the crayfish central nervous system (Fong et al., 1994), eyestalk (Martinez, 1991), brain (Barley, 1985), subesophageal, thoracic, and abdominal ganglia (Matsutani, 1990). The amount of 5HT per wet weight of the nervous tissue was determined to be between 54 and 168 pg mg^{-1} (Eloffson et al., 1982). Administration of 5HT at 15 and 50 μg g^{-1} BW to the white shrimp *Penaeus vannamei* also induced ovarian maturation and spawning (Vaca and Alfaro, 2000). All prawns injected with 5HT have their ovaries developed to full maturation, and underwent successful spawning, hatching and increased larva survival. Recently, Alfaro et al. (2004)induced ovarian maturation and spawning in *Liptopenaeus stylirostris* and *Liptopenaeus vannamei* by combined treatment of 5HT and Dopamine antagonist, spiperone. Furthermore, 5HT

shortened the latency period of GVBD in spawning oocytes in bivalves, *Chlamys (Mmachllamys) asperima*, both *in vivo* and *in vitro* (O'Connor and Heasman, 1995). In marine and freshwater bivalves, 5HT exists in neural ganglia, germinal epithelium and gonoduct (Matsutani and Nomura, 1987), and has been shown to stimulate reproductive process by initiating meiotic division (Krantic et al., 1993), germinal vesicle breakdown (GVBD) (Fong et al., 1994, Martinez, 1991) and spawning (Barley, 1985). 5HT content in the testes and nervous ganglia was increased at the time of spawning and decreased after spawning in the bivalve *Chlamys farreri nipponensis* (Matsutani, 1990). Recently, it was demonstrated that 5HT raised hemolymph vitellogenin 15–26 times from the normal levels within 16 days in eyestalk-ablated broodstock of *M. rosenbergii* (Chen et al., 2003). Taken together it seems that 5HT plays an important role in gametogenesis and spawning process of bivalves and decapods crustaceans. In bivalve, it was proposed that 5HT regulated gametogenic process directly by acting via 5HT surface receptor on the gonadal cells resulting in activation of adenyl cyclase and cAMP production, and subsequently enhanced glycogen phosphorylase leading to the mobilization of trophic materials for gametogenesis (Khotimchenko and Deridovich, 1991). The action of 5HT via the inositol trisphosphate (IP3) and phospholipase C pathway on the induction of GVBD and spawning in marine bivalve mollusc and echinoderms have also been confirmed (Chang, 1985).

In crustaceans, 5HT may act directly on the gonads or indirectly by stimulating the release of other putative gonadotrophic factor, such as, gonad stimulating hormone (GSH) from the thoracic ganglion, and by inhibiting the release of gonad inhibiting hormone (GIH) from the optic lobe as proposed in crayfish (Kullkarni et al., 1992). Evidence suggesting the direct action of 5HT on the gonads is scarce, while the indirect actions seem to be more plausible. In supporting this suggestion, it was found that the extract of the brain and thoracic ganglia could stimulate the ovarian vitellogenin synthesis and the development of secondary oocytes in crayfish, *Pacifastacus leniusculus* (Eloffson et al., 1982; Eloffson, 1983), crab, *U. pugilator* (Chang, 1985), and shrimp, *P. compressa* (Takayanagi et al., 1986), whereas the extract of the muscle did not (Kravitz, 1988). Several lines of evidence suggest that in crustaceans putative GSH is present in the thoracic ganglion and is released by 5HT, which is distributed widely in the central nervous system, eyestalk optic lobe, brain, subesophageal ganglion, thoracic ganglia and abdominal ganglia (Laxmyr, 1984; Chang, 1985; Kravitz, 1988; Kadam and Kodie, 1989; Arechiga et al., 1990). The thoracic ganglion GSH activity was also found to be increased by 5HT administration in the crab *U. pugilator* (Ridchardson et al., 1991) and freshwater crayfish *P. clarkii* (Kullkarni et al., 1991). Under *in vivo*, but not *in vitro* preparation, 5HT could increase ^{14}C leucine incorporation into the ovarian proteins in the freshwater crayfish, *P. clarkii* (Sarojini et al., 1995; Fingerman, 1997). Moreover, the eyestalk extract from *P. clarkii* inhibited ^{14}C leucine incorporation into ovarian protein, but the extract from the brain, subesophageal ganglia and thoracic ganglia stimulated the incorporation (Kullkarni et al., 1991). Similar action was also accomplished by 5HT agonists: while serotonergic neurotoxin, 5,6-DHT, block the 5HT effect *in vivo*, but not *in vitro* (Sarojini et al., 1995). *P. clarkii* receiving media of brain or thoracic ganglia developed their ovaries to the more advance stages than those injected with muscle strip and eyestalk medium (Sarojini et al., 1995). In this study, the ovaries of prawns injected with medium from 5HT-primed thoracic ganglion exhibited the increasing number of oocytes that developed to the vitellogenic and mature stages. Such increased in oocytes' development could be attained despite the pretreatment of the broodstock with CYP. The findings, therefore, strongly suggest that 5HT did not induce ovarian maturation directly, but through its action on the thoracic ganglion. Unlike other decapods as mentioned above, the medium of brain could not stimulate the ovarian development as the thoracic ganglion medium did. It might be possible that in *M. rosenbergii* the putative OSF is contained only in the thoracic ganglion. Similarly, the medium from the eyestalk bearing optic lobe could not stimulate the ovarian development beyond stage II. It is possible that a release of a GIH like factor from the optic lobe might be responsible for this inhibition.

Acknowledgements

This research was supported by the grants from Thailand Research Fund (TRF) to P.M. and P.S., Mahidol University, Burapha University and Chareon Pokphand Feedmill Co. Ltd., Thailand.

References

Alfaro, J., Zunica, G., Komen, J., 2004. Induction of ovarian maturation and spawning by combined treatment of serotonin and a dopamine antagonist, spiperone in *Liptopenaeus stylirostris* and *Liptopenaeus vannamei*. Aquaculture 236, 511–522.

Arechiga, H., Banueols, E., Frixione, E., Picones, A., Rodriguez, S.L., 1990. Modulation of crayfish internal sensitivity by 5-hydroxytryptamine. J. Exp. Biol. 150, 123–143.

Barley, R.D., 1985. Serotonin induced spawning in giant clams, *Bivalvia tridanidae*. Aquaculture 47, 321–325.

Bauchau, A.G., Mangeot, J.C., 1966. Serotonin et glycenic chez le crustacea. Experimentia 92, 238–259.

Chang, E.S., 1985. Hormonal control of molting in decapod crustacea. Am. Zool. 25, 179–185.

Chang, C.F., Shih, T.W., 1995. Reproductive cycle of ovarian development and vitellogenin profiles in the freshwater prawns, *Macrobrachium rosenbergii*. Invertebr. Reprod. Dev. 27, 11–20.

Chen, Y.N., Fanm, H.F., Hsiehm, S.L., Kuom, C.M., 2003. Physiological involvement of DA in ovarian development of the freshwater giant prawn, *Macrobrachium rosenbergii*. Aquaculture 228, 383–395.

Eloffson, R., 1983. 5HT like immunoreactivity in central nervous system of crayfish, *Pacifastacus leniusculus*. Cell Tissue Res. 232, 221–236.

Eloffson, R., Laxmyr, L., Rosengren, E., Hasson, C., 1982. Identification and quantitative measurements of biogenic amines and DOPA in the central nervous system and hemolymph of the crayfish, *Pacifastacus leniusculus* (Crustacea). Comp. Biochem. Physiol. 71C, 195–201.

Fong, P.P., Kyosuka, K., Abdelghani, H., Hardege, J.D., Ram, J.L., 1994. In vivo and in vitro induction of germinal vesicle breakdown in freshwater bivalve, the zebra mussel, *Dreissena polymorpha* (Pallas). J. Exp. Zool. 269, 467–474.

Fingerman, M., 1997. Roles of neurotransmitters in regulating reproductive hormone release and gonadal maturation in decapod crustaceans. Invertebr. Reprod. Dev. 31, 47–54.

Kadam, A.L., Kodie, S.S., 1989. Serotonin analog and spisula oocyte maturation. Invertebr. Reprod. Dev. 15, 225–227.

Keller, R., Beyer, J., 1968. Zur hyperglykamischen wirkung von serotonin und augenstiel extrakt beim flusskrebs, *Orconectes limosus*. Z. Vgl. Physiol. 59, 78–85.

Khotimchenko, Y.S., Deridovich, I.I., 1991. Monoaminergic mechanism of reproduction control in the marine bivalve mollusc and echinoderms: a review. Com. Biochem. Physiol. 100C, 311–317.

Krantic, S., Guerrier, P., Dube, F., 1993. Meiosis re-initiation in surf clam oocytes is mediated via 5-hydroxytryptamine, serotonin membrane receptor and a vitelline envelope associated high affinity binding site. J. Biol. Chem. 268, 7983–7989.

Kravitz, E.A., 1988. Hormonal control of behavior: Amines and the biasing of behavioral output in lobsters. Science 241, 1775–1781.

Kullkarni, G.K., Glade, L., Fingerman, M., 1991. Oogenesis and effects of neuroendocrine tissues on in vitro synthesis of protein by the ovary of the red swamp crayfish *Procambarus clarkii* (Girard). J. Crustac. Biol. 11, 513–522.

Kullkarni, G.K., Nagebhushanam, R., Amaldoss, G., Jaiswal, R.G., Fingerman, M., 1992. In vitro stimulation of ovarian development in the red swamp crayfish, *Procambarus clarkii* (Girard), by 5-hydroxytryptamine. Invertebr. Reprod. Dev. 21, 231–240.

Laxmyr, L., 1984. Biogenic amines and DOPA in the central nervous system of crustaceans. Comp. Biochem. Physiol. 77C, 139–143.

Matsutani, T., 1990. Endogenous factors controlling spawning in marine bivalves: Advance in invertebrate reproduction. In: Hochima, M., Yamashita, O. (Eds.), Publishes BV Biomedical Division, Elsevier Science, Amsterdam, pp. 231–237.

Matsutani, T., Nomura, T., 1987. *In vitro* effect of serotonin and prostaglandins on release of eggs from the ovary of the scallop, *Patinipecten yessoensis*. Gen. Comp. Endocrinol. 67, 111–118.

Mattson, M.P., Spazaini, E., 1985. 5-hydroxytryptamine mediates release of molt inhibiting hormone activity from isolated crab eyestalk ganglia. Biol. Bull. 36, 347–358.

Martinez, A., 1991. Seasonal variation in biochemical composition of three size classes of the chilean scallop, *Agropecten purpuratus* Larmark 1819. Veliger 34, 335–343.

New, M.B., 2002. Farming freshwater prawns: A manual for the culture of the giant river prawn (*Macrobrachium rosenbergii*). FAO Fisheries Technical Paper, vol. 428. A network of Aquaculture Centers in Asia Pacific, Rome, Italy, pp. 1–10.

O'Connor, W.A., Heasman, M.P., 1995. Spawning induction and fertilization in the dogboy scallop, *Chlamys (Mmachllamys) asperima*. Aquaculture 136, 117–129.

Rao, K.R., Fingerman, M., 1970. Action of biogenic amines on chromatophores: II. Analysis of the response of erythrophores in fiddler crab, *Uca pugilator,* to indolealkyl amines and eyestalk hormone. Comp. Gen. Pharmacol. 11, 117–126.

Ridchardson, H.G.D., Decaraman, M., Fingerman, M., 1991. The effect of biogenic amines on ovarian development in fiddler crab, *Uca pugilator*. Comp. Biochem. Physiol. C, Comp. Pharmacol. Toxicol. 99, 53–56.

Sandifer, P.A., Smith, T.J., 1985. Freshwater prawn: Crustacean and mollusk aquaculture in the United States. A Publishing Company Inc., West port, USA, pp. 1–15.

Sarojini, R., Nagabhushanam, R., Fingerman, M., 1995. Mode of action of the neurotransmitter 5-hydroxytryptamine in stimulating ovarian maturation in the red swamp crayfish, *Procambarus clarkii*: An in vivo and in vitro study. J. Exp. Zool. 271, 395–400.

Takayanagi, H., Yamamoto, Y., Takeda, N., 1986. An ovary stimulating pheromone in the freshwater shrimp, *Paratya compressa*. J. Exp. Zool. 240, 397–400.

Vaca, A.A., Alfaro, J., 2000. Ovarian maturation and spawning in white shrimp, *Peneaus vannamei*, by serotonin injection. Aquaculture 182, 373–385.

Van Herp, F., Soyez, D., 1997. Arthropoda-Crustacea. In: Adiyodi, R.G., Adiyodi, K.G., Adams, T.S. (Eds.), Reproductive biology of invertebrates, vol. III. John Wiley & Sons, New York, pp. 247–275.

Available online at www.sciencedirect.com
ScienceDirect
Aquaculture
Aquaculture 270 (2007) 249–258
www.elsevier.com/locate/aqua-online

Classification of differentiating oocytes during ovarian cycle in the giant freshwater prawn, *Macrobrachium rosenbergii* de man

Prasert Meeratana [a,*], Prasert Sobhon [b]

[a] *Department of Medical Sciences, Faculty of Science, Burapha University, Chonburi, 20131, Thailand*
[b] *Department of Anatomy, Faculty of Science, Mahidol University, Rama 6 Rd., Bangkok, 10400, Thailand*

Received 9 August 2006; received in revised form 1 March 2007; accepted 7 March 2007

Abstract

Based on the light microscopic observations of cells' sizes, chromatin patterns, amount of lipid droplets and yolk granules, the female germ cells could be classified into four different phases, which include 1) oogonia (Oog), 2) primary oocytes (pOc), 3) secondary oocytes (sOc), and 4) mature oocyte (mOc). Oog are small oval-shaped cells with irregular-shaped nuclei sizing 4–6 μm in diameter. They rest on the connective tissue germinal cord at the tip of each ovarian pouch (lobule). Oogonia increase their number through mitotic division, and the daughter cells move into ovarian pouch where they undergo first meiotic division to become primary oocytes, which have various steps of 1st meiotic prophase accumulating at the innermost zone of the ovarian pouch. The primary oocytes are small oval-shaped cells (8.5–10 μm in diameter) with large nuclei containing chromatin in various states of condensation that finally transform into chromatids. Their nuclei are surrounded by thin rim of faint blue-stained cytoplasm. The secondary oocytes derived from 2nd meiosis and comprise five steps: Oc1 and Oc2, classified as previtellogenic oocytes, Oc3 and Oc4, classified as vitellogenic oocytes, and mature oocyte (mOc) The zones of ovarian pouch are defined based on the accumulation of various steps of developing oocytes, namely, oogenic, previtellogenic, vitellogenic and mature zones, respectively. The ovarian cycle is divided into five stages based on the number and types of oocytes present in each stage. Stage 0 and I are spawn and spent stages. Stage II and III are proliferative and premature stages, while stage IV is mature stage. During ovarian stage I, each ovarian pouch contains primarily oogonia, primary oocytes, Oc1 and a few Oc2. In stage II, the pouch contains mainly Oc2 and Oc3, while in stage III the predominant cells are Oc4. Mature oocytes appear synchronously, in stage IV. The ovulating mature oocytes pass through the thin disrupted wall of ovarian pouch into subcapsular space, that leads into the oviduct situated on the ventro-lateral side of the ovarian lobe. At spawning, the ovarian pouches break down and only connective sheaths and hemolymph sinuses remain. The germinal cords and islets of oogonia remain in the central area of stage 0 ovary. The ovarian capsule, including the muscular layer, becomes attenuated as the ovary progresses from stage 0 to IV. The hemolymph vessels become highly convoluted in the central area of the ovary, and they branch radially into smaller hemolymph sinuses around each oogenic pouch.
© 2007 Elsevier B.V. All rights reserved.

Keywords: Differentiating oocytes; Ovarian pouch; Ovarian cycle; *Macrobrachium rosenbergii*

1. Introduction

The gonads of female crustaceans undergo a sequence of morphological transformation during each reproductive cycle. Such changes exhibit a number and classes of oocytes that are undergoing various steps of cellular differentiation. The cycle of ovarian and oocyte

* Corresponding author. Tel.: +66 2 745900x3167; fax: +66 2 393497.
E-mail address: g3936465@yahoo.com (P. Meeratana).

0044-8486/$ - see front matter © 2007 Elsevier B.V. All rights reserved.
doi:10.1016/j.aquaculture.2007.03.009

development in *Macrobrachium rosenbergii* have been studied by a few groups of investigators (O'Donovan et al., 1984; Charniaux-Cotton, 1985; Chang and Shih, 1995). In 1984, O'Donovan et al. divided the developing ovary of *M. rosenbergii* during intermolt period into six stages based on timing of embryogenesis, premating molt and oviposition, while the developing oocytes were divided into five stages based on size, yolk accumulation and follicular cell stage. The steps of oogenesis were also classified according to the accumulation of a yolk protein, vitellogenin, into previtellogenic and vitellogenic stages (Charniaux-Cotton, 1985). Recently, Chang and Shih (1995) classified five stages of ovarian cycle according to the changes in gross morphology and coloration as observed through the carapace, in correlation with oocytes' diameters. However, detailed classification and variation in oocyte numbers and steps remaining in each stage of the ovarian cycle are still not clearly defined. In the present study we attempted to identify all steps of differentiating oocytes and their accumulation pattern in various stages of each ovarian cycle.

2. Materials and methods

2.1. Experimental animals

Adult females, *M. rosenbergii*, weighing 35–40 gm were obtained from a commercial farm in Panasnikom district of Chonburi province, Thailand. The stages of ovarian development were determined by visual observation through the carapace as ordinarily used in hatcheries (O'Donovan et al., 1984; Charniaux-Cotton, 1985; Chang and Shih, 1995). The animals were kept in in-door concrete tanks, each with 1.5 m in diameter and 1 m in height, containing 0.80 m water with adequate aeration, and 20% of water volume changed daily. The prawns were acclimated under the light–dark cycle of 12:12 for two weeks before the experiment. The water temperature was maintained at 27–28 °C. Commercial prawn feed was provided daily at 3% of the body weight. To allow mating, blue-claw males were stocked in the same tank at the ratio of 1 male to 5 females. The prawns were anesthetized by placing on ice and the ovaries were dissected out and cut into small blocks about 1 mm^3 size. They were immediately washed in isotonic physiological saline (IPS) (Meeratana et al., 2006), and fixed in Davidson's fixative for 72 h.

2.2. Tissue preparation for histological observation

The ovarian tissue blocks were dehydrated through a series of increasing concentrations of ethanol, cleared in xylene, infiltrated with liquid paraffin at 58 °C, and finally embedded in paraffin blocks. The blocks were trimmed and sectioned at 5–7 μm thick and stained with Harris' Hematoxylin and counter-stained with Eosin (H&E stain). Periodic Acid Schiff (PAS) was also used to stain ovarian sections for determining the presence of carbohydrate components in the ovarian structures and oocytes. Mallory stain was used to outline the connective tissue scaffolds.

3. Results

3.1. Histology of the developing ovary and oviduct

The ovary of the mature giant freshwater prawn has two lobes situated underneath the carapace dorsal to the hepatopancreas and ventral to the heart. Histologically, the developing ovary is invested by ovarian capsule made of fibromuscular tissue. Parts of the capsule extended as sheet-like structures into the interior of the ovary. These sheets divide the ovarian tissue of each lobe into cone-shaped ovarian pouches or lobules, each containing various steps of oocytes according to the stages of ovarian development. The core of each ovarian lobe contains the main convoluted hemolymph vessel surrounded by connective and muscular tissues. This hemolymph vessel branches radially into hemolymph sinuses, which pass into trabeculae to form a network around each pouch, and finally drained into the subcapsular hemolymph sinus (Fig. 1A–C).

The oviduct is a delicate translucent fibromuscular sac continuing from the ovarian capsule on ventrolateral side of each ovarian lobe (Fig. 1D). Its luminal surface is lined by a simple cuboidal epithelium resting on the basement membrane (Fig. 1E). The cuboidal epithelial cells possess prominent spherical nuclei with granular heterochromatin, which are centrally located. Proximally, the lining of the oviduct is thickened as it becomes stratified cuboidal epithelium, which is also folded. Numerous long fibrillar network of mucin-like coating appears on the surface of apical epithelial cells (Fig. 1F). Transitions to low cuboidal and squamous type epithelium occur gradually towards the distal part of the oviduct (Fig. 1G). Connective tissue and smooth muscle lie underneath the basement membrane of the epithelium.

Within 48 h after spawning, the ovarian tissue appears loose, and contains large subcapsular space and dilated hemolymph sinuses. The germinal cords holding germinal cells appear in the central area of the ovary (Fig. 2A, B). Islets of new clones of growing oocytes are

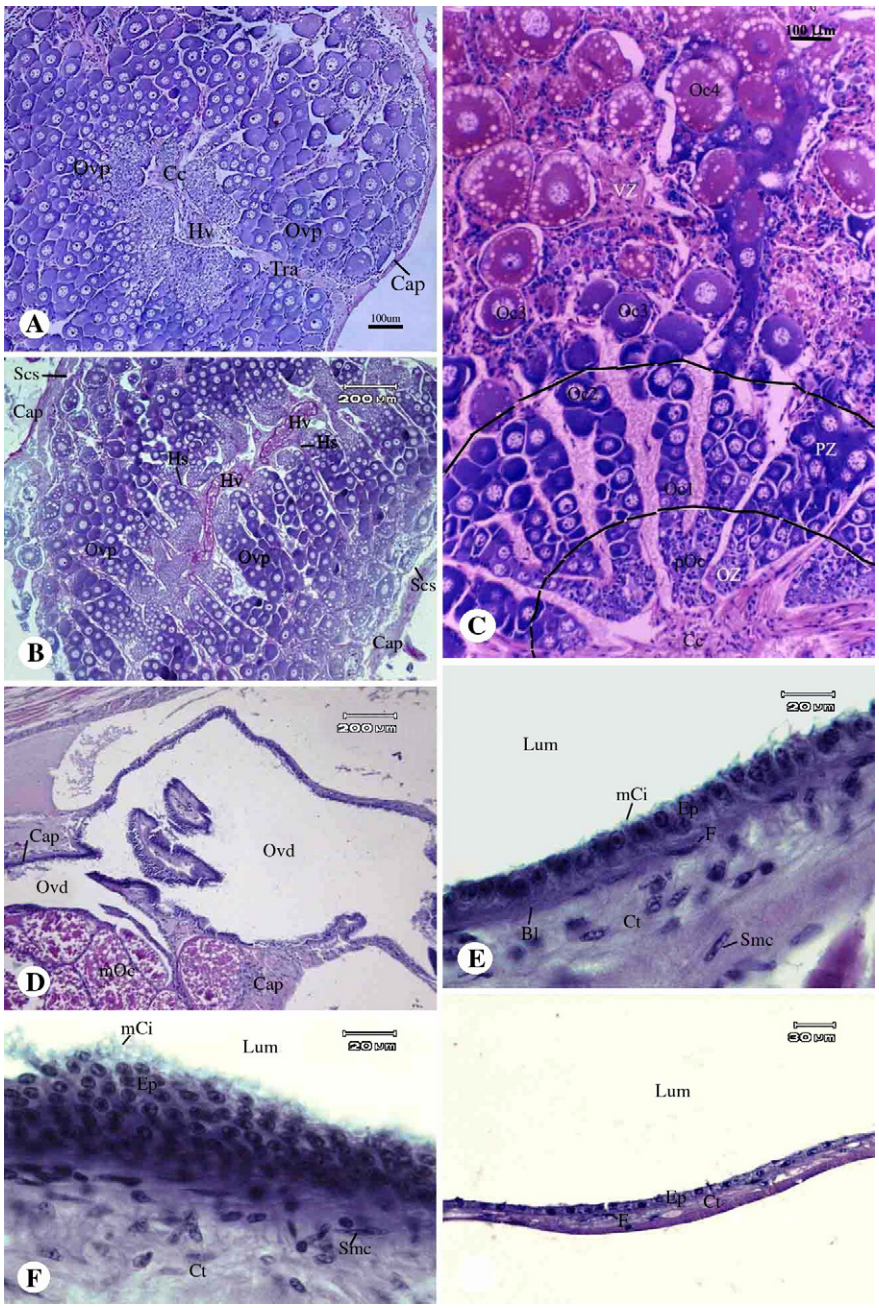


Fig. 1. Light micrographs of paraffin sections stained with PAS, showing the general histology of giant freshwater prawn ovary. A, B. Cross and longitudinal sections of stage II ovaries, showing fibromuscular ovarian capsule (Cap), trabeculae (Tra), ovarian pouches (Ovp), central ovarian core (Cg), hemolymph vessel (Hv), hemolymph sinuses (Hs), and subcapsular space (Scs). C. Cross section of stage III ovary: oogenic zone (OZ) containing primary oocytes (pOc), previtellogenic zone (PZ) containing previtellogenic oocytes (Oc1, Oc2), vitellogenic zone (VZ) containing vitellogenic oocytes (Oc3, Oc4). D. The fully mature ovary in premating broodstock showing oviduct (Ovd) and fibromuscular ovarian capsule (Cap). E. The proximal and middle parts of oviductal wall are lined by simple cuboidal epithelium. Bl—basal lamina, Ct—loose connective tissue, Smc—smooth muscle cells, Ep—epithelium, mCi —Mucin-like coating, Lum—luminal surface. F. Tangential section of the epithelial lining of the proximal part of oviduct showing accumulation of mucin-like coating (mCi) on the luminal surface. The epithelial cells possess a prominent central spherical nuclei with granular heterochromatin. Ct—loose connective tissue, Smc—smooth muscle cells, Ep—epithelium, mc—mucin-like coating, Lum—luminal surface. G. Transition of epithelial lining from simple cuboidal to simple squamous on the distal part of the oviduct.

clearly visible among the germinal cords. Based on the number and steps of differentiating oocytes the growing ovarian pouches can be divided into four zones: oogenic, previtellogenic, vitellogenic and mature zones. The oogenic zone is the inner most region facing the central ovarian core. This zone contains dividing oogonia and primary oocytes, which predominate in ovarian stage I (Fig. 2C). The previtellogenic zone is located next to the oogenic zone and contains previtellogenic secondary oocytes (Oc1 and Oc2). This zone predominates in the ovarian stage II (Fig. 1A, B, D). The vitellogenic zone is located in peripheral area of the ovary and contains vitellogenic secondary oocytes (Oc3 and Oc4). This zone predominates in stage III ovary (Figs. 1C, 2E). In ovarian stage IV, the maturation zone contains fully mature oocytes (mOc) which are distinguished by deep acidophilic (reddish) stain, and the zone expands throughout the ovarian tissue of mature ovary (Fig. 2F).

The follicular cells are classified into two types. Type I follicular cells (Fc1) exhibits ellipsoid shape, and surround Oc2, Oc3 and Oc4. They become more elongated and flattened around the mOc stage, and exhibit prominent spindle-shaped nuclei with deeply

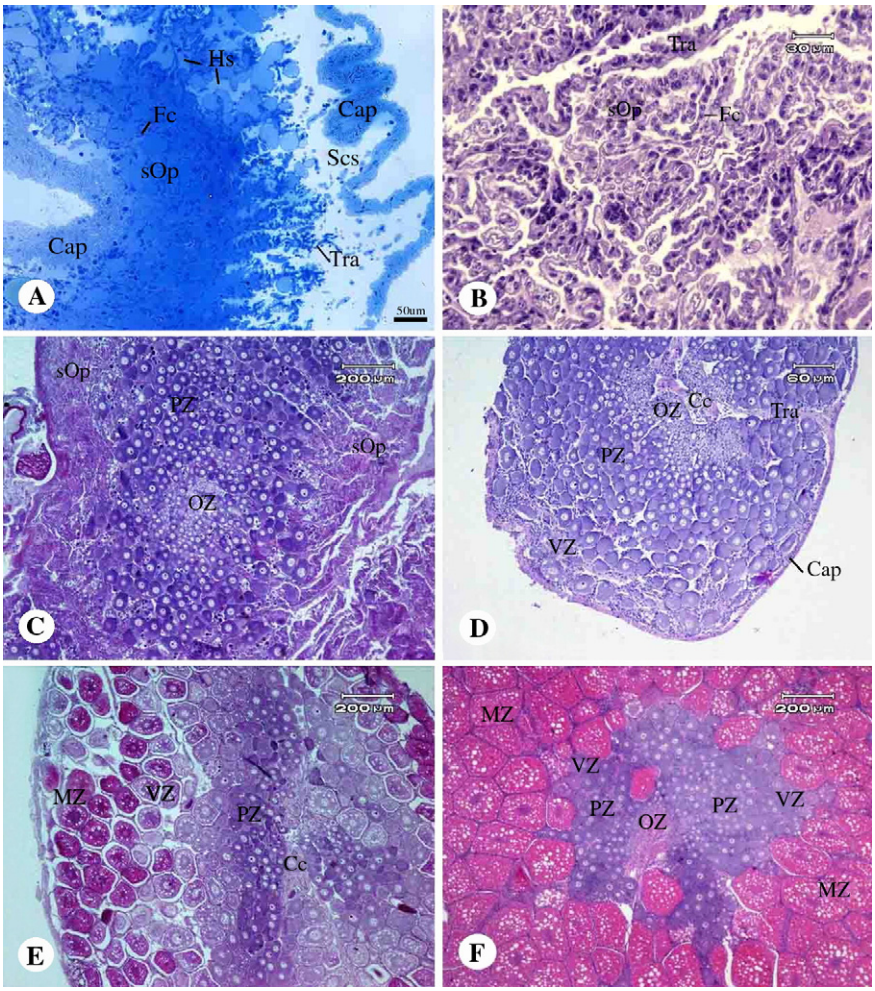


Fig. 2. Light micrographs of semithin section stained with toludine blue (A) and paraffin sections stained with H&E (B–F), showing different ovarian stages. A, B. The ovary following spawn (stage 0): Ovp—ovarian pouch, sOp—spent ovarian pouch, Scs—subcapsular space, Hs—hemolymph sinus, Tra—trabeculae, Fc—follicular cells, Cap—fibromuscular ovarian capsule. Stage I (spent) at 2 days after spawning: Oz—oogenic zone, Pz—previtellogenic zone, sOp—spent ovarian pouch. Stage II (proliferation) ovary: The oocytes in this ovarian stage advance to early vitellogenic oocytes(Oc3). This stage occurs about one week following spent period. Cap—fibromuscular ovarian capsule. Stage III (premature) ovary containing mainly Oc4. Cc—central ovarian core, PZ—previtellogenic zone, VZ—vitellogenic zone, MZ—mature zone. F. The ovarian stage IV (mature) is mostly occupied by the fully mature oocytes appearing in deep eosinophilia in the maturation zone (MZ). Islets of primary and previtellogenic oocytes still remain in the central ovarian core (Cc). This stage of ovary usually occurs at 3 to 8 weeks after spawn period.

stained chromatin. Fc1 adhere closely to oocytes' surface (Fig. 3E). Type II follicular cells (Fc2) first appear during Oc2 step. They exhibit less change in shape and size from Oc2 to Oc4 steps. Fc2 have lighter stained and more ovoid nuclei, and they form an outer layer next to Fc1 (Figs. 3E, F, 4D–F). They proliferate and aggregate in the spaces between oocytes during Oc3 and Oc4 steps. During the mOc step, the nuclei of both types of follicular cells are quite similar. However, the Fc1 nucleus is more flattened into spindle shape and the Fc2 nucleoplasm becomes darker.

3.2. Steps of differentiating oocytes

3.2.1. Oogonia (Oog)

The Oog are located in the germinal epithelium that lies along the trabeculae and connective tissue scaffold. The Oog is an ovoid cell that contains an irregularly shaped nucleus (4–6 μm in diameter) with deep blue-stained heterochromatin. It is notable that the nucleolus is not noticeable in this stage (Fig. 3A–C), while the cytoplasm is stained faint blue with H&E. Oog are frequently seen in groups, each with 2–4 cells in a row at the tip of the ovarian pouch. The Oog are dividing

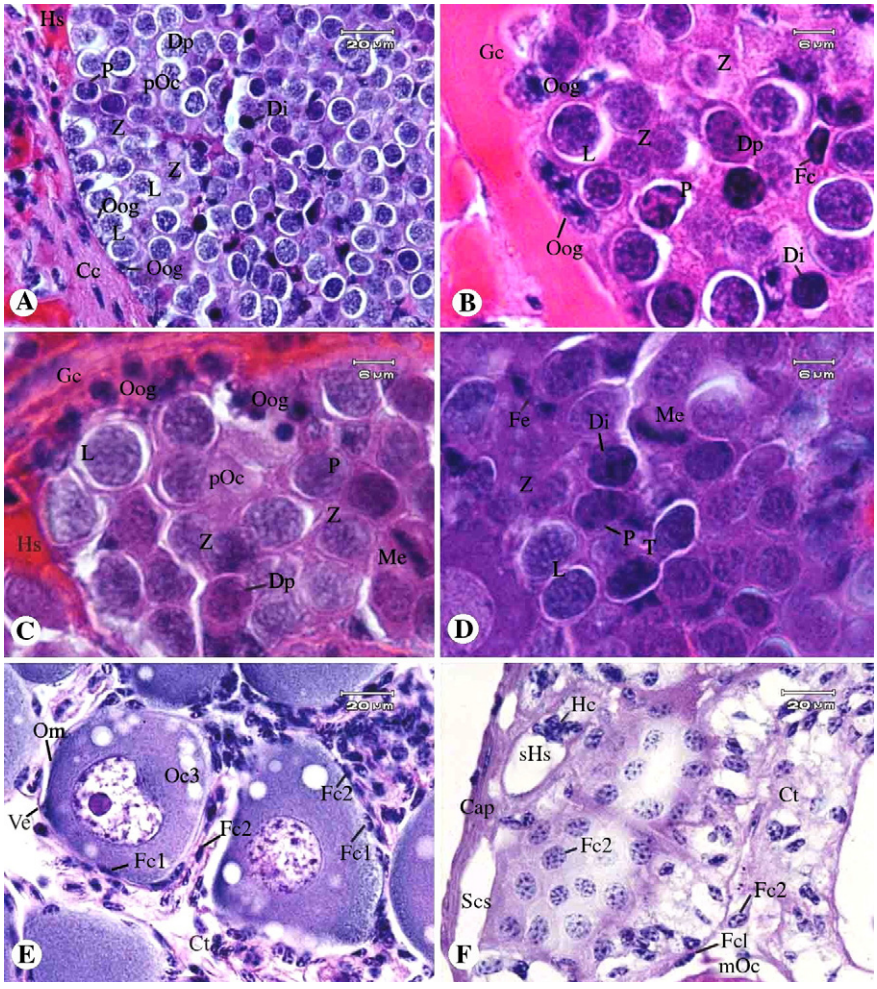


Fig. 3. Light micrographs of paraffin section stained with PAS, showing various stages of developing germ cells and oocytes. Oog (oogonia) aggregate at the tip of the ovarian pouch near the central ovarian core (Cc). All stages of primary oocytes including leptotene (L), zygotene (Z), pachytene (P), diplotene (Dp) and diakinesis (Di) of 1st meiotic prophase are also present. Higher magnification of A showing oogonia appearing in rows of 2–4 cells on the connective tissue trabeculae of an ovarian pouch. C, D. Primary oocytes in various prophase I stage including metaphase (Me) and telophase (T) of 1st meiotic prophase. Follicular cells (Fc) during Oc3 and Oc4 stages that surround the oocytes. Tangential section of mature oocyte (mOc) in ovarian stage IV, showing extremely thin follicular cells around its surface. Other abbreviations: Cap—ovarian capsule, Fc1— type I follicular cell, Fc2— type II follicular cell, Gc— germinal cord, Hc—hemocytes, N— nucleus, No— nucleolus, Om—oocyte membrane, Scs—subcapsular space, sHs—subcapsular hemolymph sinus.

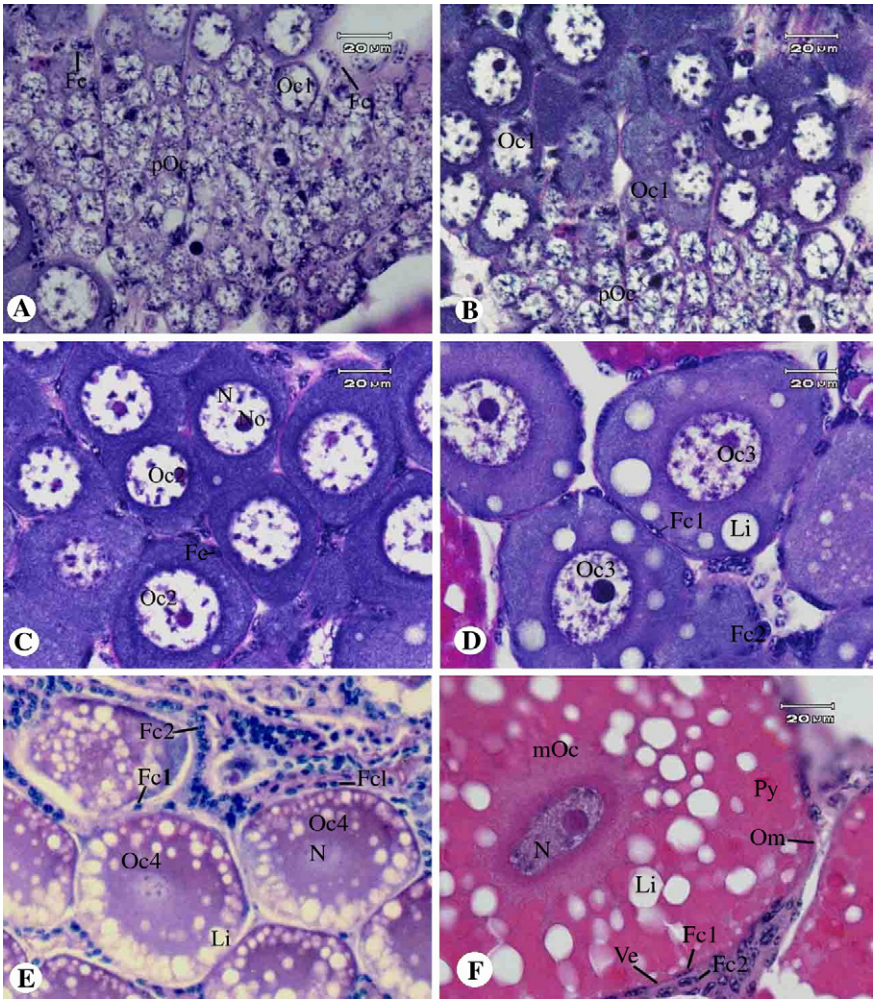


Fig. 4. Micrographs of the developing oocytes taken from paraffin sections stained with H&E, showing different steps of oocytes from primary oocyte (pOc) to mature oocyte (mOc). Primary oocytes (pOc) at the tip of an ovarian pouch. Fc—follicular cell. Early previtellogenic oocyte (Oc1). N—nuclei. Late previtellogenic oocyte (Oc2). Follicular cells with ovoid profile appear more distinct. No—nucleolus. Early vitellogenic oocyte (Oc3) containing lipid droplet (Li). Two types of follicular cells, type I (Fc1) and type II (Fc II), could be identified at this stage. Late vitellogenic oocyte (Oc4). Follicular cells with elongated shape are prominent. F. Mature oocyte (mOc) containing proteinatious yolk plaques (Py). Type I follicular cell is more flattened and in close apposition to the oocyte surface, while type II is more prominent and more frequently seen. The vitelline envelope (Ve) appears as a very thin line closes to the oocyte membrane (Om).

mitotically, and their daughter cells progress into the pouch and increase in size while entering the 1st meiosis.

3.2.2. Primary oocyte (pOc)

Primary oocytes accumulate at the oogenic zone next to the germinal cord, at the tip of a conical-shaped ovarian pouch. These cells are undergoing 1st meiosis, and are characterized by the nuclei containing dense small cords of heterochromatin with variable sizes which are intertwined within the nuclear boundaries. Primary oocytes appear in various steps of prophase, including leptotene, zygotene, pachytene, diplotene, diakinesis, metaphase and telophase (Fig. 3A–D). Their very thin rim of cytoplasm appear blue with H&E stain, and their sizes range from 8.5–10 µm in diameter. The oogonia and pOc are predominantly in the ovarian stage I (Fig. 2C).

3.2.3. Secondary oocytes (sOc)

This phase of developing oocytes is undergoing 2nd meiosis and they are classified into five steps, which include Oc1, Oc2, Oc3, Oc4, and mOc.

3.2.4. Early previtellogenic oocyte (Oc1)

Oc1 is characterized by a substantial increase in size (ranging from 10–30 µm in diameter) when compared

to the primary oocytes. The cytoplasm is large and appears deep blue with H&E stain. The nucleus is characterized by the presence of the intensely blue-stained small blocks of heterochromatin, while the rest of the nucleoplasm appears very light. The nucleolus is small and not always clearly visible. Oc1 occupy a zone external to the oogonia and primary oocytes, which is termed previtellogenic zone (Fig. 4B). They are surrounded by spindle-shaped follicular cells.

3.2.5. Late previtellogenic oocyte (Oc2)

Oc2 is characterized by the increase in cell size (ranging from 30–100 μm in diameter) and the decrease of nucleo-cytoplasmic ratio. The cytoplasm is enlarged and exhibits more intensely blue staining with H&E. The nucleus is characterized by the presence of dense blocks of heterochromatin scattering throughout. The centrally located nucleolus becomes prominent with densely packed materials. The follicular cells surrounding Oc2 are more elongated as well as increased in number and size (Fig. 4C). Oc2, like Oc1, are located in the previtellogenic zone next to the oogenic zone of the developing ovary, and this zone occupies most of the oogenic pouch in the ovarian stage II (Fig. 2D).

3.2.6. Early vitellogenic oocyte (Oc3)

Oc3 is characterized by the decrease of bluish stain (basophilia) and the increase of reddish stain (eosinophilia) in the cytoplasm. The cytoplasm also contains some lipid droplets, which are distributed randomly at the periphery (Figs. 3E and 4D). The cell size is about 100 to 200 μm in diameter. The round nucleus is enlarged and still centrally located, and exhibits numerous and variable size heterochromatin blocks scattering throughout. This step of oocyte has increasing number of type II follicular cells with oval nuclei. Meanwhile, type I follicular cells are tightly adhered to the surface of each oocyte and remain unchanged from their previous stage.

3.2.7. Late vitellogenic oocyte (Oc4)

Oc4 displays violet-stained acidophilic cytoplasm with increasing amount of lipid droplets and reddish proteinaceous yolk plaques. The acidophilia at the periphery is more intense in comparison to the area surrounding nucleus. The cell size ranges from 150–250 μm in diameter. At this stage of oocyte, the lipid droplets apparently increase in size and become located along the cytoplasmic rim. The follicular cells type I and II are more apparent and more elongated in shape (Fig 4E). Oc4 and Oc3 are located in the vitellogenic zone peripheral to the previtellogenic zone of the developing ovary, and this zone occupies most of the oogenic pouch in the ovarian stage III (Fig. 2E).

3.2.8. Mature oocyte (mOc)

The mOc is characterized by a remarkable increase in cell size, more than ten times the early previtellogenic oocytes. Most of them are around 300–550 μm in diameter and have a hexagonal shape. The cytoplasm becomes highly acidophilic and filled with large lipid droplets and proteinaceous yolk plaques. Accumulation of a deep purple-stained material could be noticed underneath the perivitelline space. The nucleus contains almost entirely euchromatin and a prominent nucleolus (Fig. 4F). The nuclear membrane is not apparent and frequently disappears, which may be the result from germinal vesicle breakdown. Type I and type II follicular cells surrounding mOc are fully elongated, and they are tightly attached to the cell surface. Unlike *Penaeus* shrimp, no cortical rod is observed in mature oocytes.

3.3. Stages of the ovarian cycle

Histologically, the ovarian cycle could be classified into five stages: stage 0 (spawn), I (spent), II (proliferative), III (premature) and IV (mature), respectively.

In stage 0, the ovary right after spawning appears loose and empty. It contains collapsed ovarian pouches with only strands of follicular cells and connective tissue remaining. Most of the follicular cells return to their original ovoid shape. The main hemolymph vessel in the central ovarian area is still present and appears intact. However, the small hemolymph sinuses are dispersed throughout ovarian tissue, but their boundaries are not clearly defined. Groups of oogonia at the central ovarian core are frequently seen. Thickening and folding of the ovarian capsule is apparent around the ovary (Fig. 2A, B).

During stage I (spent), the ovary is filled with primary oocytes occupying the oogenic zone, and previtellogenic oocytes (Oc1 to Oc2) occupying the previtellogenic zone. Follicular cells are rarely seen at this stage of the oocytes. The hemolymph vessels and sinuses reconvert to the more intact form (Fig. 2C).

In stage II (proliferative), the ovary exhibits faint orange color. The oocytes are mainly the late previtellogenic (Oc2) and the early vitellogenesis (Oc3) steps. The division between oogenic and previtellogenic zone becomes clearly visible. Follicular cells increase in number and become more apparent (Fig. 2D).

In stage III (premature), the ovary is bright orange in color and increases in size. Most of the oocytes are in late vitellogenesis (Oc4). The follicular cells

elongate to spindle shape and are less frequently seen (Fig. 2E).

In stage IV (mature), the ovary appears in deep orange color and it size increases remarkably when compared to earlier stages. The ovary contains mostly mature oocytes (mOc), while islets of oogonia and primary oocytes are frequently seen in the central ovarian core, and other oocytes (Oc1–Oc4) are absent. Follicular cells are decreasing in number, while those remaining appear as thin spindle shapes closely surrounding each oocyte (Fig. 2F). The ovarian capsule and trabeculae are very thin and the ovarian pouch boundaries are hardly discernible. The oviducts are seen on the ventro-lateral side of each ovarian lobe. Their walls continue with the extremely thin ovarian capsule (Fig. 1D).

4. Discussion

4.1. General histology and origin of oogonia

The capsule of the ovary is made of relatively thick connective and muscular tissues. In turn, the capsule forms trabecular sheets, from which the germinal cells appear to generate. The trabecular sheets divided the ovary into a number of conical-shaped ovarian lobules called ovarian pouches, which are similar in structure to ovarian subunits in *Penaeus vannamei* (Krol et al., 1992) and oogenic pouches in crayfish (Holdich, 2002) and freshwater crab *Potamon dehaani* (Ando and Makioka, 1999). Each ovarian pouch contains various stages of differentiating oocytes surrounded by follicular cells. The germinal cells, from which the oogonia are derived, aggregate at the tip of the ovarian pouch facing the central ovarian core. In lobster, *Homarus americanus*, the germinal cells aggregates between ovarian pouches and serve as oogonial reserve (Talbot, 1981). The oogonia undergo mitotic division with successive karyokinesis and incomplete cytokinesis within the germinal layer in the same way as reported in another species of crustacea, *Eoleptestherita ticinensis* (Scanabissi and Tommasini, 1990). The daughter oogonia then separate from the germinal cord and enter the oogenic zone, where they undergo 1st meiotic division. The aggregation of oogonia at the tip of the ovarian pouch is different from other decapods, and factors contributing to the migration and aggregation of oogonia at this location have not yet been elucidated. In any case, oocytes, which are their daughter cells, develop, enter the previtellogenic zone and move to periphery, while the ovarian pouches become expanded. Depending on ovarian stages, each ovarian pouch of *M. rosenbergii* may contain combinations of various steps of developing germ cells, including Oog, pOc, Oc1, Oc2, Oc3, Oc4 and mOc. Each step of developing oocytes is aggregated in the same zone. Thus the oocytes differentiate while they also move from the central core to the periphery of the ovary.

The central core of the ovary is made of connective and muscular tissues running along its longitudinal axis. The main hemolymph vessel is highly convoluted and runs within the central core. It branches radially, and the branches run in the trabeculae between ovarian pouches and terminate as hemolymph capillary plexus surrounding each pouch. Muscle cells in the capsule, trabeculae and central ovarian core are not striated type as reported in the lobster's, *Homarus americanus* ovary (Harrison and Humes, 1992; Talbot and Helluy, 1995). In this prawn, the ovarian muscle cells exhibit corkscrew nuclei and indistinct striation, thus resembling vertebrate smooth muscles. Such muscle cells are believed to be the contractile part that squeeze oocytes into the oviduct and broodchamber during oviposition. In crayfish, *Procambarus paeninsulanus*, such contraction of the ovarian muscle during oviposition is reportedly induced by prostaglandins (Spaziani et al., 1993). Unlike in *Penaeus* shrimps, the oviduct of this prawn is not present in the central ovarian core (Bell and Lightner, 1988). In stead the oviduct is the receptacle that is continuous with the subcapsular space lying underneath the capsule. Mature oocytes at periphery of the ovarian pouch move into the space and then pass into the oviduct, perhaps by contraction of the muscle cells as mentioned above.

4.2. Classification of differentiating oocytes

In this species, Oog differentiate into primary oocytes which enter 1st meiotic division within the oogenic zone. All steps of prophase I, including leptotene, zygotene, pachytene, diplotene, metaphase, and telophase could be observed in the oogenic zone. The previtellogenic and vitellogenic oocytes (Oc1, Oc2, Oc3 and Oc4) are, most likely secondary oocytes, undergoing differentiation during 2nd meiotic prophase. The differentiation process stops at mOc step, waiting for ovulation to occur. The developmental process of oocytes in the giant freshwater prawn is comparable to those reported in other crustaceans (Van Herp and Soyes, 1997), which is characterized by a long 1st meiotic prophase during which DNA replication and the first phase of cell division are taking place; and also relatively long period of 2nd meiotic prophase, during which the oocytes accumulate ribosomes, glycogen, lipid, yolk and mRNAs (Kleckner et al., 1994). The deposition of yolk in the Oc3 is slow while the oocytes undergo gradual increase in size. At this stage, yolk

protein probably is produced endogenously (Van Herp, 1992; Tsutsui, 2000). In contrast, Oc4 and mOc rapidly increases in size and acidophilia due to accumulation of yolk protein which could be derived from extra-ovarian sources (Chang and Shih, 1995; Sagi et al., 1995). The hepatopancreas and adipose tissue were proposed as exogenous sources of yolk proteins (Lee and Chang, 1999; Tsutsui et al., 2000; Yang et al., 2000; Jasmani et al., 2004). Once the oocytes reach maturation they become highly enlarged, and they probably exert strong pressure in the ovary, so much that the thin connective tissue surrounding oogenic pouches are broken, allowing the oocytes to be released into the subcapsular space and pass into the oviduct.

4.3. Stages of the ovarian cycle

O'Donovan et al. (1984) divided developing ovary of the giant freshwater prawn during intermolt period in captivity, into six stages, while Damrongphol et al. (1991) proposed only four stages. More recently, Chang and Shih (1995) divided ovarian stages of this prawn, by observing the gross morphology and coloration through carapace, into five stages. Using histological criteria we also divide the ovarian cycle into five stages. The spawn ovary (stage 0) has enlarged in size more than the spent one (stage I). The stromal and connective tissues from collapsed and empty ovarian pouches become loosened and flaccid, while those of the spent ovary is firm and starts to have more oogonia and previtellogenic oocytes. The accumulation in significant numbers of previtellogenic oocytes (Oc1, Oc2) is the distinguishing characteristic of proliferative ovary (stage II). Progressive increase in size of premature (stage III) and mature (stage IV) ovaries is due to the increased numbers of vitellogenic oocytes (Oc3, Oc4, mOc), whose sizes are enlarged significantly due to the uptake of yolk protein from exogenous sources. The islets of oogonia and previtellogenic oocytes among fully mature oocytes in stage IV reflect the reserve capacity of the ovary of the multiple spawning species and it's readiness to start a new cycle.

Acknowledgements

This research was supported by the grants from Thailand Research Fund (TRF) to P.M. and P.S., Burapha and Mahidol Universities, Thailand.

References

Ando, H., Makioka, T., 1999. Structure of the ovary and mode of oogenesis in a freshwater crab *Potamon dehaani*. J. Morphol. 239, 107–114.

Bell, T.A., Lightner, D.V., 1988. A Handbook of Normal Penaeid Shrimp Histology. World Aquaculture Society, Baton Rouge, LA.

Chang, C.F., Shih, T.W., 1995. Reproductive cycle of ovarian development and vitellogenin profiles in the freshwater prawns, *Macrobrachium rosenbergii*. Invertebr. Reprod. Dev. 27, 11–20.

Charniaux-Cotton, H., 1985. Vitellogenesis and its control in malacostracan crustacea. Amer. Zool. 25, 197–206.

Damrongphol, P., Eangchuan, N., Poolsanguan, B., 1991. Spawning cycle and oocyte maturation in laboratory maintained giant freshwater prawn (*Macrobrachium rosenbergii*). Aquaculture 95, 347–357.

Harrison, F.W., Humes, A.G., 1992. Microscopic Anatomy of Invertebrates, vol. 9. John Wiley&Sons Inc., New York. 652pp.

Holdich, D.M., 2002. Biology of Freshwater Crayfish. Blackwell Science, England. 702pp.

Jasmani, S., Ohira, T., Jayasankar, V., Tsutsui, N., Aida, K., Wilder, M.N., 2004. Localization of vitellogenin mRNA expression and vitellogenin uptake during ovarian maturation in the giant freshwater prawn *Macrobrachiun rosenbergii*. J. Exp. Zool. A Comp. Exp. Biol. 301, 334–343.

Kleckner, N., Szollosi, D., Wassarman, P., Willison, K., 1994. Germ cells and fertilization, In: Alberts, B., Bray, D., Lawis, J., Raff, M., Roberts, K., Watson, J.D. (Eds.), Molecular Biology of the Cell, 3rd ed. Garland Publishing Inc., New York, pp. 1011–1035.

Krol, R.M., Hawkins, W.E., Overstreey, R.M., 1992. Reproductive components. In: Harrison, F.W., Humes, A.G. (Eds.), Microscopic Anatomy of Invertebrates, vol. 10. Wiley-Liss Inc., New York, pp. 295–343.

Lee, F.Y., Chang, C.F., 1999. Hepatopancreas is the likely organ of vitellogenin synthesis in the freshwater prawn, *Macrobrachium rosenbergii*. J. Exp. Zool. 284, 798–806.

Meeratana, Prasert, Withyachumnarnkul, Boonsirm, Damrongphol, Praneet, Wongprasert, Kanokphan, Seuseangthum, Anchalee, Sobhon, Prasert, 2006. Serotonin induces ovarian maturation in giant freshwater prawn broodstock, *Macrobrachium rosenbergii* de Man. Aquaculture 260, 315–325.

O'Donovan, P., Abraham, M., Cohen, D., 1984. The ovarian cycle during the intermolt in ovigerous *Macrobrachium rosenbergii*. Aquaculture. 36, 347–358.

Scanabissi, S.F., Tommasini, S., 1990. Origin and early development of female germ cells in *Eoleptestheria ticinensis* Balsamo-Crivelli, 1859 (Crustaeaa, Branchiopoda, Conchostraca). Mol. Reprod. Dev. 26, 47–52.

Sagi, A., Soroka, Y., Snyr, E., Chomsky, O., Calderon, J., Milner, Y., 1995. Ovarian protein synthesis in the prawn *Macrobrachium rosenbergii*: does ovarian vitellin synthesis exist? Invertebr. Reprod. Dev. 27, 41–47.

Spaziani, E.P., Hinsch, G.W., Edwards, S.C., 1993. Changes in prostaglandin E2 and F2α during vitellogenesis in the Florida crayfish *Procambarus paeninsulanus*. J. Com. Physiol. B. 163, 541–545.

Talbot, P., 1981. The ovary of the lobster, *Homarus americanus*.I. Architecture of mature ovary. J. Ultrastruct. Res. 76, 235–248.

Tabolt, P., Helluy, S., 1995. Reproduction and embryonic development. In: Factor, J.R. (Ed.), Biology of the Lobster *Homarus americanus*. Academic press, San Diego, pp. 177–216.

Tsutsui, N., 2000. Molecular characterization of a cDNA encoding vitellogenin and its expression in the hepatopancreas and ovary during vitellogenin synthesis in the kuruma prawn, *Penaeus japonicus*. Zool. Sci. 17, 651–660.

Van Herp, F., 1992. Inhibiting and stimulating neuropeptides controlling reproduction in crustacea. Invertebr. Reprod. Dev. 22, 21–30.

Van Herp, F., Soyes, D., 1997. Arthropoda–Crustacea. In: Adiyodi, K.G., Adiyodi, R.G., Adams, T.S. (Eds.), Reproductive Biology of Invertebrates, vol. VIII. John Wiley & Sons, New York, pp. 247–275.

Yang, W.J., et al., 2000. Determination of amino acid sequence and site of mRNA expression of four vitellin in giant freshwater prawn, *Macrobrachium rosenbergii*. J. Exp. Zool. 287, 413–422.

Provided for non-commercial research and education use.
Not for reproduction, distribution or commercial use.



This article was published in an Elsevier journal. The attached copy is furnished to the author for non-commercial research and education use, including for instruction at the author's institution, sharing with colleagues and providing to institution administration.

Other uses, including reproduction and distribution, or selling or licensing copies, or posting to personal, institutional or third party websites are prohibited.

In most cases authors are permitted to post their version of the article (e.g. in Word or Tex form) to their personal website or institutional repository. Authors requiring further information regarding Elsevier's archiving and manuscript policies are encouraged to visit:

http://www.elsevier.com/copyright

Author's personal copy

Available online at www.sciencedirect.com
ScienceDirect
Aquaculture
Aquaculture 270 (2007) 289–298
www.elsevier.com/locate/aqua-online

Biochemical characterization and physiological role of cortical rods in black tiger shrimp, *Penaeus monodon*

Hathairat Kruevaisayawan [a,c], Rapeepun Vanichviriyakit [a], Wattana Weerachatyanukul [a,*], Sirilug Magerd [a], Boonsirm Withyachumnarnkul [a,b], Prasert Sobhon [a]

[a] *Department of Anatomy, Faculty of Science, Mahidol University, Rama VI Road, Bangkok 10400, Thailand*
[b] *The Center of Excellence in Shrimp Biotechnology, Faculty of Science, Mahidol University, Bangkok 10400, Thailand*
[c] *Department of Anatomy, Faculty of Medical Science, Naresuan University, Phitsanulok 65000, Thailand*

Received 28 December 2006; received in revised form 15 March 2007; accepted 3 April 2007

Abstract

Cortical rods (CRs), precursors of egg jelly investment in many penaeoid shrimp, are composed of different proportions of proteins and carbohydrates, the physiological role of which still requires extensive investigation. In this study, we demonstrated the biochemical properties of the CRs and their role in the induction of the acrosome reaction (AR). Profiles of the isolated CRs revealed a number of major protein bands ranging from 35 to 230 kDa. These CR proteins were extensively glycosylated and sulfated. Lectin-based carbohydrate analysis further revealed the highest reactivity of concanavalin A (Con A) among other lectins used. In addition, the selective interference of Con A binding with mannose but not glucose indicated that CR glycoproteins were of high-mannose type. Using immunoblotting with anti-CR antibody, we further demonstrated that part of egg water (EW, a natural AR inducer) was derived from miscible components of the CRs. Physiological tests of water-soluble CR (wsCR) revealed its high AR inducing competency comparable to that of EW, which was far superior to that of acid-urea treated CR (auCR). Furthermore, the wsCR-induced AR was selectively inhibited by Con A, suggesting the significance of the exposing mannose residues in regulating *P. monodon* sperm AR response.
© 2007 Elsevier B.V. All rights reserved.

Keywords: Cortical rod; Egg jelly; Carbohydrate; Acrosome reaction

1. Introduction

By the end of vitellogenesis in penaeiod shrimp, the developing eggs reach the final stage of oocyte maturation which is characterized by the appearance of rod-like bodies, called cortical rods (CRs), arranged radially around the periphery of the oocyte plasma membranes (Anderson et al., 1984; Lynn and Clark, 1987; Pongtippatee-Taweepreda et al., 2004; Rankin and Davis, 1990; Yano, 1988). These CRs are located in the extracellular crypts formed by the invagination of the oolemma into the egg cortex. During spawning, CRs are released upon contact of the eggs with seawater and form a jelly investment around the eggs in many penaeiod shrimp species (Clark et al., 1990; Pongtippatee-Taweepreda et al., 2004; Rankin and Davis, 1990; Yano, 1995). Thereafter, the jelly substances gradually fall off from the spawned egg surface and become the

* Corresponding author. Tel.: +66 02 201 5422; fax: +66 02 354 7168.
E-mail address: scwwy@mahidol.ac.th (W. Weerachatyanukul).

0044-8486/$ - see front matter © 2007 Elsevier B.V. All rights reserved.
doi:10.1016/j.aquaculture.2007.04.004

Author's personal copy

flocculent materials referred to as "egg water" (EW), the property of which is recognized as a natural inducer of sperm acrosome reaction (AR) (Clark et al., 1990; Pillai and Clark, 1990). Biochemical characterization of the isolated CR from mature ovaries of *P. aztecus* has revealed that CRs contain approximately 25–30% carbohydrates and 70–75% proteins by weight (Lynn and Clark, 1987). Histochemical evidence in *P. monodon* has also consistently demonstrated that CRs are glycoprotein-based materials (Tan-Fermin and Pudadera, 1989). In *Sicyonia ingentis*, amino acid analysis of the crude CR proteins has indicated a predominance of aspartic acid and glycine with a relatively high ratio of cysteine (Lynn and Clark, 1987).

To date, many shrimp CR proteins have been characterized. In *P. semisulcatus*, one of the CR proteins has high sequence homology to insect peritrophins (intestinal chitin-binding proteins) (Elvin et al., 1996; Tellam et al., 1999), hence the term "shrimp ovarian peritrophin (SOP)" is introduced (Khayat et al., 2001; Avarre et al., 2001). The other protein termed "cortical rod protein (CRP)" is also biochemically characterized in *Marsupenaeus japonicus* (Kim et al., 2004; Kim et al., 2005). SOP and CRP share many common characteristics: 1) their mobility on SDS-PAGE (~33 kDa) is relatively similar; 2) both SOP and CRP are highly glycosylated; and importantly, 3) amino acid sequence of CRP shares the identities of 29 residues in the N-terminus to that of peritrophins or SOP, suggesting that these two proteins might be transcriptional products of the same gene. The other high molecular weight (>130 kDa) CR protein having sequence similarities to thrombospondin (TSP, the extracellular matrix protein in a cartilage oligomeric protein family) is characterized in *M. japonicus* and *Fennerpenaeus chinensis* and termed *mj*TSP and Fc-TSP, respectively (Sun et al., 2006; Yamano et al., 2004). Interestingly, the N-terminal domain of *mj*TSP peptide baring no significant homology to TSP family reveals a high sequence similarity to SOP (Yamano et al., 2004). These findings indicate that SOP is a considerably large extracellular protein family found in the CR glycoproteins. Nevertheless, the known functions of this insect peritrophin-related SOP as chitin-binding and antimicrobial proteins are not correlated to the fertilization-related function of egg jelly that is derived directly from the CRs. In this study, we therefore aimed to study the physiological significance of CR derived materials in regards to fertilization along with the biochemical characterization of the CR glycoprotein compositions.

2. Materials and methods

2.1. Sample preparation

2.1.1. Cortical rod isolation

Mature female shrimp containing fully mature ovaries were cold-anesthetized under ice. The carapace and shell were carefully dissected away and the mature ovaries (exhibiting dark green color on the dorsal region throughout the body length) were collected. Isolation of CRs was performed following the previously described protocol (Lynn and Clark, 1987). Briefly, pieces of ovaries were homogenized in the isolation medium (IM: 500 mM NaCl, 9 mM $CaCl_2$, 14 mM KCl, 15 mM $MgCl_2$, and 10 mM Tris, pH 7.6) containing 30% sucrose until no visible fragments were left in the suspension. This suspension was subjected to centrifugation (1000 ×*g*, 4 °C, 5 min). The pellet was resuspended in IM, and the suspension was overlaid onto 60% sucrose in IM and centrifuged (8000 ×*g*, 4 °C, 60 min). The green supernatant containing chiefly yolk granules was discarded, while the white pellet containing mainly CRs was extensively washed (1000 ×*g*, 4 °C, 5 min) with IM to get rid of contaminating yolk granules and used immediately or stored at −80 °C until use. Protein concentration was determined by Bradford's protein assay (Bradford, 1976) using Sigma Bradford reagents (Sigma, St. Louis, MO, USA).

To prepare the water-soluble materials of CRs (wsCR), isolated CRs were left overnight at 4 °C in IM solution. The suspension was centrifuged (1000 ×*g*, 4 °C, 10 min) to pellet CR materials. The supernatant assigned as "wsCR" was collected and re-centrifuged (12,000 ×*g*, 4 °C, 15 min) to eliminate contaminants. The insoluble CR materials in the pellet were further subjected to acid-urea treatment with 7 M urea in 0.1 N HCl (4 °C, overnight) followed by brief sonications at 100 W output (4×30 s). After centrifugation to pellet the remaining CR fragments, the supernatant was collected and designated as "acid-urea treated CRs (auCR)". Both wsCR and auCR were extensively dialysed against artificial seawater (ASW: 423 mM NaCl, 9 mM KCl, 9.3 mM $CaCl_2$, 23 mM $MgCl_2$, 9.3 mM $MgSO_4$, 2.1 mM $NaHCO_3$, pH 7.8) and the protein concentration was determined following the aforementioned method.

2.1.2. Collection of thelycal sperm and egg water

Since thelycal (T-) sperm have been known to possess higher fertilizing ability than spermatophoric sperm due to their higher maturation/capacitation status (Alfaro et al., 2003; Vanichviriyakit et al.,

Author's personal copy

2004), we thus used T-sperm for all the following experiments. To collect T-sperm, inseminated females were anesthetized under ice and the thelyca located at the 5th-pair walking legs were carefully removed and placed in calcium-free artificial seawater (CFASW: 423 mM NaCl, 9 mM KCl, 23 mM $MgCl_2$, 9.3 mM $MgSO_4$, 2.1 mM $NaHCO_3$, pH 7.8). Subsequently, the sperm masses and contents inside the thelycum were physically isolated using dissecting forceps. T-sperm suspension was filtered through a 212-μm-metal sieve (Endecotts, London, UK) to remove aggregates, washed (500 ×*g*, 5 min) and resuspended in CFASW at the final concentration of 1×10^7 sperm/ml before use.

Collection of egg water (EW) was carried out at the Bangkok Aquaculture Farm Company, Nakhon Si Thammarat, Thailand. Uninseminated mature females with mature ovaries were individually placed in a 500-l plastic tank. Upon spawning, the shrimp was held firmly over a 500-ml container and allowed to spawn their eggs into filtered seawater. After gentle swirling to settle the eggs to the bottom, seawater without spawned eggs was collected and assigned as "EW". This EW was centrifuged (12,000 ×*g*, 15 min, 4 °C) to remove particulates and kept in −80 °C until use. Protein concentration of the EW was determined by Bradford's protein assay.

2.2. Production of polyclonal antibody against CR proteins

Polyclonal antibody directed against the entire CR isolates was prepared in BALB/c mice according to the method described previously (Harlow and Lane, 1999). The animal handling procedures strictly followed the guidelines of The Animal Care Committee, Mahidol University. Briefly, the animals were given an intraperitoneal injection with ~2 mg of the CR proteins emulsified with Freund's complete adjuvant (1:1, v/v). Booster injections with the same amount of immunogens mixed with Freund's incomplete adjuvant were administered 2 and 4 weeks after the first injection. One week after every immunization, the blood was collected for titer determination. The collected blood was allowed to clot (37 °C, 1 h) and the sera were obtained after centrifugation (3000 ×*g*, 10 min). These sera were further subjected to decomplimentation (56 °C, 1 h) prior to any applications. Titers of the antisera were checked by immunoblotting (see below). Antisera with titers >1:1000 were pooled and further subjected to ammonium sulfate precipitation and stored at −20 °C until use.

2.3. SDS-PAGE and detection of the sulfated glycans

Isolated CRs were homogenized in 10 mM PBS, pH 7.4 containing 2% SDS and sonicated at 100 W output (4 × 30 s). The non-solubilized fraction was discarded by centrifugation (12,000 ×*g*, 15 min, 4 °C). Approximately 20 μg of CR isolates, wsCR, auCR, or EW was solubilized in loading buffer and resolved by 10% SDS-PAGE under a reducing condition (Laemmli, 1970). The separated proteins on the gel were stained with 0.025% Coomassie Brilliant blue R 250. In order to analyze glycosulfated compositions in the CR glycoproteins, separated proteins on the duplicated gels were stained with periodic acid Schiff (PAS) or with 0.1% toluidine blue in 7% acetic acid and 20% methanol (Hirohashi and Vacquier, 2002).

2.4. Western immuno- and lectin blottings

For immunoblotting, approximately 3 μg of each sample was separated by 10% SDS-PAGE and was electrotransferred (Towbin et al., 1979) to a Hybond N-ECL 0.45 μm nitrocellulose membrane (Amersham Biosciences, UK). Non-specific binding of antibodies was blocked with 5% skim milk in Tris-buffered saline (TBS) containing 0.1% Tween 20 (TBS-T) (room temperature, 1 h). The transferred proteins were exposed to 1:1000 anti-CR antiserum (room temperature, 2 h) and subsequently to 1:2000 horse radish peroxidase (HRP)-conjugated goat anti-mouse IgG. Antigen–antibody complexes were visualized by an enhanced chemiluminescent method using ECL detection kit (Amersham Biosciences).

For lectin blotting (Bar-Nun and Gershoni, 1998), the transferred proteins were blocked with 4% bovine serum albumin (BSA) in TBS-T and further exposed to various biotinylated lectins (Vector laboratories, Burlingame, CA, USA) at a final concentration of 4 μg/ml (room temperature, 2 h). Lectins used in this study included concanavalin A (Con A), wheat germ agglutinin (WGA), *Ricinus communis* agglutinin I (RCA-I), *Ulex europeaus* agglutinin I (UEA-I) and *Griffonia* (*bandeiraea*) *simplicifolia* agglutinin I (BSL-I). After washing with TBS-T, the proteins were incubated with 1:5000 HRP-conjugated streptavidin and the lectin reactivity was detected by an enhanced chemiluminescent method as described above. In order to determine the binding specificity of biotinylated Con A (which was shown to be the major bound lectin to the CR glycoproteins: see Fig. 3) to either mannose or glucose residues, the final concentration of 0.4 M of these complimentary sugars

Author's personal copy

were added and pre-incubated (4 °C, 1 h) with Con A before exposing to the resolved CR proteins.

2.5. Enzyme-linked lectin assay (ELLA)

Quantitative analysis of lectin binding was performed using ELLA (Hirohashi and Lennarz, 2001). One hundred microlitres of 20 μg/ml CR proteins diluted in coating buffer, pH 9.0, were coated onto a 96-well plate at 4 °C for overnight. After extensive washes with TBS-T, the coated CR proteins were blocked with 3% BSA in TBS, washed and subsequently incubated in various concentrations (0.02–1 μg/ml) of biotinylated lectins in 1% BSA–TBS (room temperature, 1 h). After three washes with TBS-T, the proteins were exposed to HRP-conjugated streptavidin (1:5000 dilution, 1 h). Binding of lectins was detected by tetramethyl benzidine (TMB) peroxidase substrate (KPL, Gaithersburg, MD, USA). The reaction was stopped by adding 1 N HCl and the developing color was quantified at the wavelength of 450 nm using a VERSAmax microplate reader (Molecular Devices, Sunnyvale, CA, USA). Coated CR proteins exposed to HRP-conjugated streptavidin served as a blank control, the obtained value of which was used to eliminate the background staining of the experimental samples.

2.6. Induction of sperm acrosome reaction

To determine the possible physiological function of CR in an induction of sperm acrosome reaction (AR), isolated T-sperm were treated with 4–64 μg/ml of wsCR, auCR or EW for 5 min to initiate AR response. Treated sperm were fixed with 4% paraformaldehyde and the percentages of unreacted (with an intact long spike) and reacted (without the anterior spike) sperm (Vanichviriyakit et al., 2004) were scored under a phase contrast microscope. The percentage of spontaneous AR, as a control, was assessed from sperm treated with ASW. Approximately 200 sperm were counted for each data point. Each experiment was triplicated using different sperm samples.

To investigate the significance of specific sugar moieties of the CR glycoproteins in the AR induction, wsCR was pre-incubated with 50 μg/ml of each the following: Con A, UEA-I, WGA, BSL-I and RCA-I or with the additional 100 μg/ml Con A (the only lectin that showed inhibitory effect on the wsCR-induced AR: see Fig. 5B). These pre-incubated mixtures were then used to treat sperm and the assessment of the AR response was performed according to the aforementioned method. Sperm treated with 100 μg/ml Con A served as a negative control.

3. Results

3.1. Profiles of the isolated CRs and their glycosulfated compositions

Protein profiles of the entire CR isolates determined by Coomassie blue staining were shown in Fig. 1. It was revealed that CRs consisted of a broad spectrum of the protein bands ranging from ~25 kDa to more than 200 kDa (Fig. 1, lane 2). Among these CR glycoproteins, the protein bands with M_r of 230, 180, 140, 100, 84, 80, 73, 58, 54, 50/51, 47, 44, 36 and 34 kDa (Fig. 1, lane 2) were intensely stained with Coomassie blue and considered as the major CR proteins. Some of these CR proteins with the M_r of 230, 180, 140, 120, 47 and 36 kDa were also reactive with PAS (Fig. 1, lane 3, arrowheads). Notably, the 36 kDa protein band appeared to be more intensely reactive than the other PAS-positive protein bands. This indicated that CR proteins were post-translationally modified by an extensive glycosylation. The details of sugar termini that were enriched in the CR glycoproteins were also studied and described below.

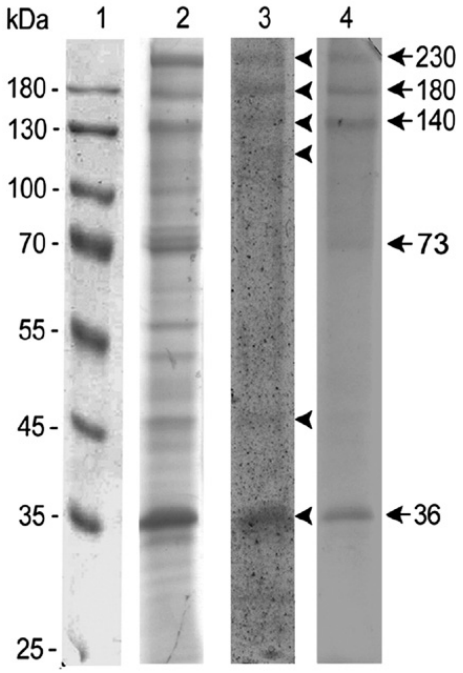


Fig. 1. Profiles of the isolated CR glyproteins subjected to Coomassie blue (lane 2), PAS (lane 3) and toluidine blue (lane 4) staining. Arrowheads and arrows indicate major bands of CR proteins that are intensely reactive with PAS and toluidine blue, respectively. Lane 1 = protein molecular weight marker.

Author's personal copy

We also investigated the sulfated moieties on the CR glycoproteins using metachromatic reaction of toluidine blue staining (Hirohashi and Vacquier, 2002). The result revealed that three slowly migrating (230, 180 and 140 kDa) and fast-medium migrating (36 and 73 kDa) CR glycoproteins showed the positive metachromatic reactivity, as visualized by a pinkish-purple staining on the protein bands (Fig. 1, lane 4, arrows). It was thus suggestive from this result that some CR glycosylated proteins were additionally sulfated at the *N*-linked sugar residues.

3.2. Determination of sugar moieties in the CR glycoproteins

To elucidate the specific types of sugar moieties that made up carbohydrate compositions of the CR glycoproteins, lectin blotting was performed with various biotinylated lectins. It was demonstrated that Con A (recognizing both mannose and glucose residues) appeared to have the broadest spectrum of reactivity (ranging from 28 to 180 kDa) and the highest reactive intensity with the isolated CR glycoproteins (Fig. 2A). To further rule out whether the reactivity of Con A indicated high-mannose or high-glucose type in the CR glycoproteins, a competitive assay of Con A binding with the complimentary sugars was performed. Inclusion of mannose monosaccharides into biotinylated Con A showed a much pronounced inhibition of Con A binding to the resolved CRs than that of glucose (Fig. 2B), indicating the selective enrichment of mannose over glucose residues in the CR glycoproteins. Reactive intensity of other lectins (WGA, UEA-I, RCA-I and BSL-I), however, was to a lesser extent than that of Con A. Notably, among all lectins used, UEA-I was the only lectin that specifically recognized the ~36 kDa protein band, suggesting the selective modification of this 36-kDa protein with L-fucose residues (Fig. 2A, asterisk). A trace amount of reactivity was observed at the 180, 32 and 29 kDa protein bands in negative controls in which the biotinylated lectins were omitted.

We also investigated lectin reactivity on the wsCR and EW glycoproteins using Con A and RCA (as a representative of the four lectins having a minimal reactivity with the isolated CR glycoproteins). Reactivity of Con A on the wsCR samples was fairly different from the isolated CR samples (Fig. 2C). While wsCR protein bands ranging from 36 to 60 kDa were more prominently reactive (particularly the 60 kDa band) than those of the isolated CRs, the fast migrating wsCR proteins (27–33 kDa) were less reactive. This suggests that the intermediate migrating proteins (i.e., 36–60 kDa) in the CRs possess higher solubilizing property than the fast migrating ones, rendering them a higher proportion in the total wsCR proteins when compared to the total isolated CR proteins. Reactivity of Con A to the

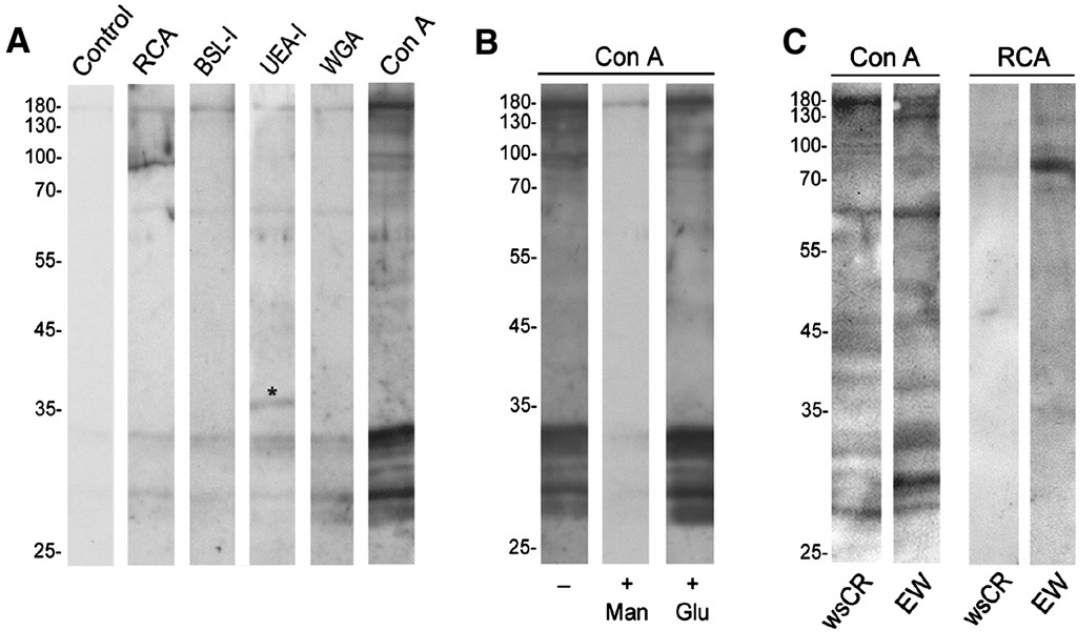


Fig. 2. Lectin blotting of the isolated CR, wsCR and EW glycoproteins. Panels A and C: The isolated CRs (panel A), wsCR and EW (panel C) were resolved by 12.5% SDS-PAGE and subjected to various biotinylated lectin staining. Types of lectins used are indicated on top of each lane. Control represents isolated CRs exposed to HRP–streptavidin. *Indicates the specific reactivity of the 36-kDa CR protein band with UEA-I. Panel B: Competition assay of Con A binding to the isolated CR proteins with mannose (+Man) and glucose (+Glu) monosaccharides. Note the interference of mannose but not glucose with Con A binding.

Author's personal copy

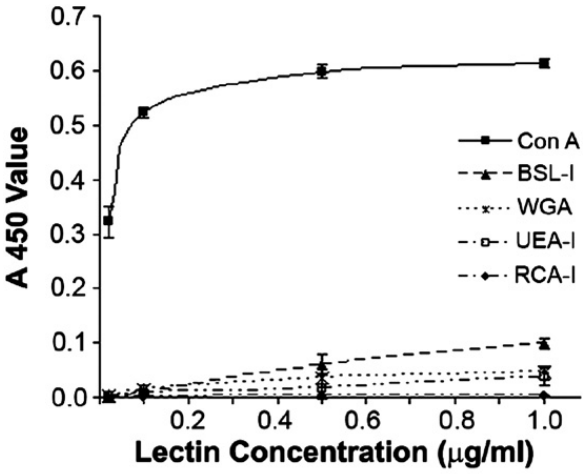


Fig. 3. Enzyme-linked lectin assay (ELLA) of the isolated CRs with various lectins. The CR proteins were coated onto micro-well plates and subsequently exposed to various concentrations of biotinylated lectins followed by TMB substrate. Bound lectins were measured as the absorbance of the developed color products at 450 nm (A450). The data were from four replicates and expressed as mean ± S.D.

slow migrating proteins (100–180 kDa) was relatively similar in both samples. In EW, some common Con A-reactive protein bands with wsCR could be observed, namely, the 180, 60, 47 and a set of 27–33 kDa proteins (Fig. 2C). However, it might not be able to claim at this state that these Con A-reactive proteins in EW were parts of wsCR proteins. RCA was minimally reactive with soluble proteins in both wsCR and EW with the exception of the 84-kDa EW protein. Therefore, this RCA-reactive protein in EW should be derived from the alternative sources apart from the CRs.

Quantitative analysis of the individual sugar moiety in the isolated CR glycoproteins using ELLA (Fig. 3) generally supported the lectin blotting findings. It was found that the A450 value of Con A reactivity with the coated CR proteins was over 0.6. The binding level of Con A was concentration-dependent and the binding plateau was approached at the concentration of 0.5 μg/ml. At this concentration, the reactivity of Con A was >10 folds higher than the other lectins. BSL-I, WGA and UEA-I at 0.5 μg/ml revealed minimal reactivities with their A450 value ranging from 0.01 to 0.06 while RCA-I showed a negligible level of lectin reactivity.

3.3. Components of CRs that made up egg water

Two components of CRs, wsCR and auCR, were isolated and their protein profiles and physiological properties were compared with a natural AR inducer, EW. The protein pattern of wsCR was to some extent similar to that of EW. Both wsCR and EW shared at least 5 common protein bands including 230, 84, 73, 60 and 28 kDa (Fig. 4A). On the other hand, the pattern of

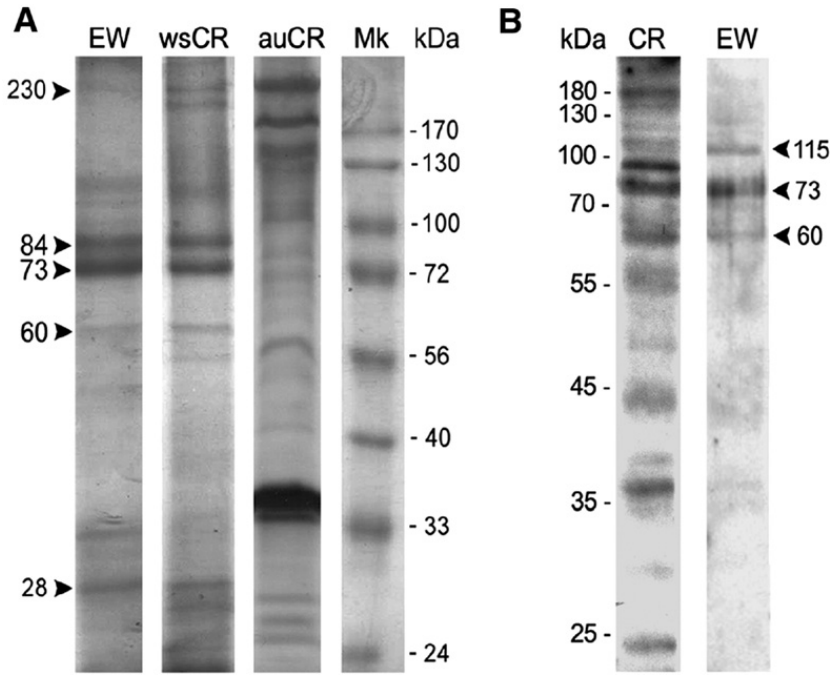


Fig. 4. Panel A: Protein profiles of two components of CRs, water-soluble (wsCR) and acid-urea treated (auCR), in comparison with that of egg water (EW). Arrowheads denote major CR glycoproteins that are resembled in both wsCR and EW. Panel B: Western immunoblotting of the isolated CRs and EW with anti-CR antibody. The immunoreactive protein bands of EW with the anti-CR antibody are indicated by arrowheads.

Author's personal copy

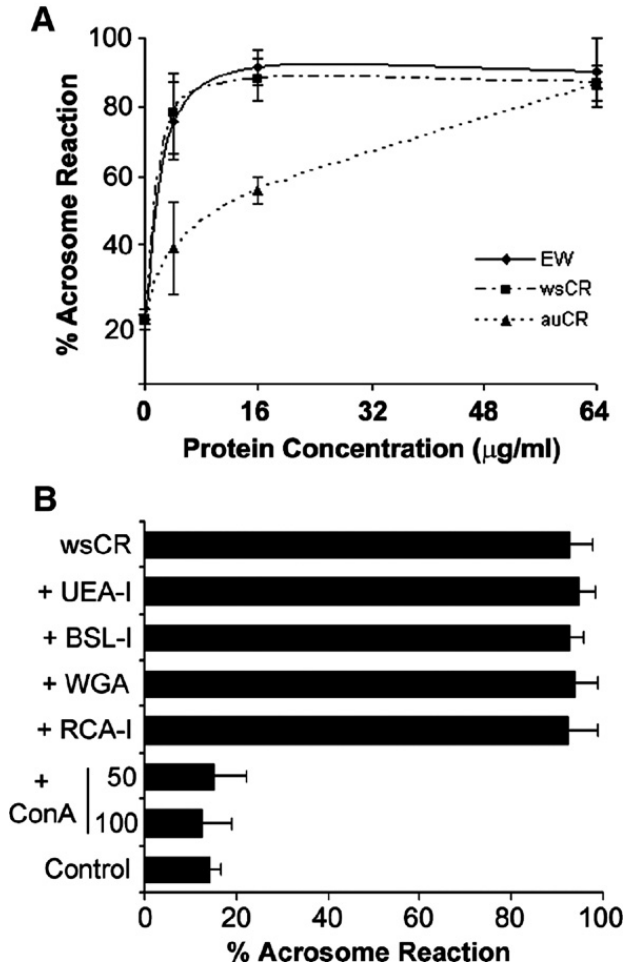


Fig. 5. Induction of the AR responses with various concentrations of EW, wsCR, and auCR (panel A) or with 16 μg/ml wsCR in the presence of 50 μg/ml of all studied lectins as well as in the presence of the additional 100 μg/ml of Con A (panel B). Sperm exposed to 100 μg/ml Con A (Control) served as a negative control for lectin competition assay. At least 200 sperm-cells were counted for each data point. Data were expressed as means±S.D. of four replicates performed on different sperm samples.

auCR containing many fast and slowly migrating proteins (Fig. 4A) drastically differed from those of EW and wsCR. The major protein bands of the auCR extracts were 36, 56 kDa and a set of slowly migrating proteins with the M_r>110 kDa.

In order to detect the components of EW that were derived from part of CRs during egg spawning, Western immunoblotting using antibody against the entire CR proteins was performed. Fig. 4B revealed that anti-CR antibody reacting with a broad range of the isolated CR proteins (lane 1), immunoreacted with some EW proteins including the 115, 73 and 60 kDa bands (lane 2, arrowheads). This result suggested that at least three protein components of CRs were highly solubilized and were readily dispersed into seawater upon spawning to form part of EW ingredients.

3.4. Ability of CR glycoproteins in initiating sperm acrosome reaction

We further tested the physiological role of wsCR and auCR in initiating sperm AR response. The result in Fig. 5A demonstrated that wsCR was able to induce sperm AR in a comparable manner as with the ability of EW. The AR inducing ability of both EW and wsCR was relatively similar. The percentages of wsCR-induced AR were 78.4±11.5, 88.0±6.1 and 86.9±4.9 at 4, 16 and 64 μg/ml, respectively. On the other hand, at the low concentrations of auCR (4 and 16 μg/ml), the AR response was far inferior to those initiated by the corresponding concentrations of wsCR and EW. However, with 64 μg/ml auCR, sperm AR response approached the plateau of the AR induction (86.3±0.8%) which was comparable to that of wsCR (86.9±4.9%) or EW (90.1±9.9%).

When wsCR was pretreated with 50 μg/ml of various lectins and tested for the ability to induce AR, it was found that Con A drastically inhibited the wsCR-induced AR to the background level (17.2±9.2%) (Fig. 5B). Pretreatment of wsCR with 100 μg/ml Con A slightly decreased the AR response to be 15.7±1.0%. Percentage of the AR response inhibited by Con A was relatively comparable to that of negative control in which sperm were exposed to 100 μg/ml Con A (13.3±8.2%). Other lectins, in contrast, did not show any notable inhibitory effect on the wsCR-induced AR. The percentages of the AR responses were >90% when other lectins were included, similar to that observed for wsCR (Fig. 5B).

4. Discussion

In penaeiod shrimp including *P. monodon*, CR materials embedded in the egg's extracellular crypts have long been known to be glycoprotein-based constituents (Lynn and Clark, 1987; Tan-Fermin and Pudadera, 1989). Analysis of CR glycoproteins in kuruma prawn, *M. japonicus* has revealed five major glycoproteins with the apparent M_r of ~210, 150, 140, 130 and 30 kDa (Yamano et al., 2003). Based on the mobility on SDS-PAGE, the profile of the isolated CRs in *P. monodon* was also composed of many large (230, 180, 140 kDa), intermediate (73 and 58 kDa) and small (47 and 36 kDa) major glycoproteins. These CR glycoproteins represented extracellular matrices of the eggs which generally exhibited the bottle brush-like feature at the ultrastructural level in some shrimp species including *S. ingentis* (Clark et al., 1990) and *P. monodon* (Pongtippatee-Taweepreda et al., 2004). To date, the

Author's personal copy

characterization of these extracellular proteins in penaeiod shrimp has classified shrimp CR proteins into 2 major groups, SOP and TSP (Avarre et al., 2001; Khayat et al., 2001; Sun et al., 2006; Yamano et al., 2004). Whether the CR glycoproteins of *P. monodon* fall into these 2 protein categories is still unknown. While SOP, an insect peritrophin-related protein, has been shown to possess a chitin-binding property and anti-microbial activity (Khayat et al., 2001), the function of shrimp TSP has not yet been discovered and has been proposed to act as a physical barrier to prevent polyspermy and egg damage (Yamano et al., 2004). As CRs serve as the precursors for egg jelly (Clark et al., 1990; Lynn and Clark, 1987; Yano, 1995), the aforementioned functions of SOP and the proposed function of TSP do not correspond to the fertilization-related function of the egg jelly. In this study, we have provided, for the first time, the fertilization-related function of the CR materials in shrimp sperm AR induction (Fig. 5A). Specifically, the wsCR components could generate a superior AR response compared to the corresponding concentration of the auCR components. In addition, this AR inducing ability of wsCR was comparable to that of EW. Taken together, these results implicated that shrimp sperm AR inducing elements were derived at least partly from the highly miscible components of CRs. This postulation was, in fact, supported by immunoblotting results demonstrating the positive immunoreactivity of some EW proteins with the anti-CR antibody (Fig. 4B).

Carbohydrates have been known to play significant roles in many steps of fertilization in invertebrates (Mengerink and Vacquier, 2001; Mulloy, 2005). The importance of the carbohydrate moieties for fertilization also holds true towards higher mammals including humans as was evident by the essence of carbohydrate moieties in the zona pellucida (ZP) glycoproteins in sperm-ZP binding (Shalgi and Raz, 1997; Wassarman, 2005; Zara and Naz, 1998). Using a number of lectins to analyze the specific sugar compositions of *P. monodon* CR glycoproteins, it was found that the reactivity of Con A to the isolated CR proteins was more predominant than the other lectins used in this study (Figs. 2 and 3). However, interpretation of Con A reactivity could be two fold: high-mannose or high-glucose CR glycoproteins. We substantiated the findings to explore that mannoses rather than glucoses were the enriched sugar termini in the CR's carbohydrates (Fig. 2B). In this regard, two well-characterized major CR proteins, SOP and CRP, have also been reported to be highly reactive with Con A (Khayat et al., 2001; Kim et al., 2004), and interpreted as the high-mannose type CR glycoproteins. Apart from mannoses, a minor proportion of the CR carbohydrates also contained other sugars such as fucose (reactive with UEA-I), *N*-acetylglucosamine (GlcNAc) and sialic acid (both of which were reactive with WGA). Interestingly, the 36-kDa CR protein band reactive with UEA-I also developed a metachromatic reaction with toluidine blue staining, suggesting the presence of fucose and sulfated moieties in shrimp CR glycoproteins, although it is still unknown whether sulfation of CR glycoproteins takes place on carbohydrates or proteins and whether it is involved in the AR induction. In echinoderms, these fucose sulfate polymers (FSP) have been extensively studied in the egg jelly (Alves et al., 1998; Mulloy et al., 1994; Vilela-Silva et al., 1999) and reported to serve their pivotal role in the species-specific AR induction (Alves et al., 1997; Vacquier and Moy, 1997; Vilela-Silva et al., 2002). According to the glycoprotein rich property of the jelly materials in both sea urchins and shrimp, one would expect that shrimp's jelly substances, particularly sulfated glycans, may also be involved in the AR induction. We provided evidence herein that shrimp CRs, the jelly precursors, were involved in modulating the AR response. However, it was mannose rather than (sulfated) fucose residues that played a central role in the carbohydrate-mediated AR, which was a unique characteristic for this shrimp species. Further extensive experiments are required to address whether the carbohydrate termini or protein cores of the active CR glycoprotein(s) or both are responsible for modulating AR response in shrimp sperm.

Conclusively, we have shown in this study that CR materials in *P. monodon* are of high-mannose type glycoproteins. These CR glycoproteins also contain a minor proportion of GlcNAc, sialic acid and fucose residues, some of which are additionally sulfated. Upon solubilized into seawater, they form part of EW ingredients. These CR glycoproteins, especially their exposing mannose residues, play a key role in modulating shrimp sperm AR response. Our finding on the novel role of CR proteins in the AR induction may lead to an established method for detecting sperm quality which will be advantageous for improving artificial fertilization in the penaeid shrimp aquaculture.

Acknowledgements

This work was supported by the National Science and Technology Development Agency of Thailand (to BW), Thailand Research Fund (to PS, WW and RV) and Commission of Higher Education (to HK). The authors would like to thank Ms. Chor Hoon Poh for her

Author's personal copy

thorough proof-reading of this manuscript and Dr. Boonyarath Pratoomchat, Department of Aquatic Science, Faculty of Science, Buraphar University for kindly providing shrimp samples.

References

Alfaro, J., Munoz, N., Vargas, M., Komen, J., 2003. Induction of sperm activation in open and closed thelycum penaeoid shrimps. Aquaculture 216, 371–381.

Alves, A.P., Mulloy, B., Diniz, J.A., Mourao, P.A., 1997. Sulfated polysaccharides from the egg jelly layer are species-specific inducers of acrosomal reaction in sperms of sea urchins. J. Biol. Chem. 272, 6965–6971.

Alves, A.P., Mulloy, B., Moy, G.W., Vacquier, V.D., Mourao, P.A., 1998. Females of the sea urchin *Strongylocentrotus purpuratus* differ in the structures of their egg jelly sulfated fucans. Glycobiology 8, 939–946.

Anderson, S.L., Chang, E.S., Clark Jr., W.H., 1984. Timing of postvitellogenic ovarian changes in the ridgeback prawn *Sicyonia ingentis* (Penaeidae) determined by ovarian biopsy. Aquaculture 42, 257–271.

Avarre, J.C., Khayat, M., Michelis, R., Nagasawa, H., Tietz, A., Lubzens, E., 2001. Inhibition of de novo synthesis of a jelly layer precursor protein by crustacean hyperglycemic hormone family peptides and posttranscriptional regulation by sinus gland extracts in *Penaeus semisulcatus* ovaries. Gen. Comp. Endocrinol. 124, 257–268.

Bar-Nun, S., Gershoni, J.M., 1998. Protein-blot analysis of glycoproteins and lectin overlays. Cell Biology: A Laboratory Handbook. Harcourt Publishers, New York, pp. 458–466.

Bradford, M.M., 1976. A rapid and sensitive method for the quantitation of microgram quantities of protein utilizing the principle of protein-dye binding. Anal. Biochem. 72, 248–254.

Clark Jr., W.H., Yudin, A.I., Lynn, J.W., Griffin, F.J., Pillai, M.C., 1990. Jelly layer formation in Penaeoidean shrimp eggs. Biol. Bull. 178, 295–299.

Elvin, C.M., Vuocolo, T., Pearson, R.D., East, I.J., Riding, G.A., Eisemann, C.H., Tellam, R.L., 1996. Characterization of a major peritrophic membrane protein, peritrophin-44, from the larvae of *Lucilia cuprina*. cDNA and deduced amino acid sequences. J. Biol. Chem. 271, 8925–8935.

Harlow, E., Lane, D., 1999. Using Antibodies: a Laboratory Manual. Cold Spring Harbor Laboratory Press, New York.

Hirohashi, N., Lennarz, W.J., 2001. Role of a vitelline layer-associated 350 kDa glycoprotein in controlling species-specific gamete interaction in the sea urchin. Dev. Growth Differ. 43, 247–255.

Hirohashi, N., Vacquier, V.D., 2002. Egg sialoglycans increase intracellular pH and potentiate the acrosome reaction of sea urchin sperm. J. Biol. Chem. 277, 8041–8047.

Khayat, M., Babin, P.J., Funkenstein, B., Sammar, M., Nagasawa, H., Tietz, A., Lubzens, E., 2001. Molecular characterization and high expression during oocyte development of a shrimp ovarian cortical rod protein homologous to insect intestinal peritrophins. Biol. Reprod. 64, 1090–1099.

Kim, Y.K., Kawazoe, I., Tsutsui, N., Jasmani, S., Wilder, M.N., Aida, K., 2004. Isolation and cDNA cloning of ovarian cortical rod protein in kuruma prawn *Marsupenaeus japonicus* (Crustacea: Decapoda: Penaeidae). Zool. Sci. 21, 1109–1119.

Kim, Y.K., Tsutsui, N., Kawazoe, I., Okumura, T., Kaneko, T., Aida, K., 2005. Localization and developmental expression of mRNA for cortical rod protein in kuruma prawn *Marsupenaeus japonicus*. Zool. Sci. 22, 675–680.

Laemmli, U.K., 1970. Cleavage of structural proteins during the assembly of the head of bacteriophage T4. Nature 227, 680–685.

Lynn, J.W., Clark Jr., W.H., 1987. Physiological and biochemical investigations of the egg jelly release in *Penaeus aztecus*. Biol. Bull. 173, 451–460.

Mengerink, K.J., Vacquier, V.D., 2001. Glycobiology of sperm–egg interactions in deuterostomes. Glycobiology 11, 37R–43R.

Mulloy, B., 2005. The specificity of interactions between proteins and sulfated polysaccharides. An. Acad. Bras. Cienc. 77, 651–664.

Mulloy, B., Ribeiro, A.C., Alves, A.P., Vieira, R.P., Mourao, P.A., 1994. Sulfated fucans from echinoderms have a regular tetrasaccharide repeating unit defined by specific patterns of sulfation at the 0–2 and 0–4 positions. J. Biol. Chem. 269, 22113–22123.

Pillai, M.C., Clark Jr., W.H., 1990. Development of cortical vesicles in *Sicyonia ingentis* ova: their heterogeneity and role in elaboration of the hatching envelope. Mol. Reprod. Dev. 26, 78–89.

Pongtippatee-Taweepreda, P., Chavadej, J., Plodpai, P., Pratoomchart, B., Sobhon, P., Weerachatyanukul, W., Withyachumnarnkul, B., 2004. Egg activation in the black tiger shrimp *Penaeus monodon*. Aquaculture 234, 183–198.

Rankin, S.M., Davis, R.W., 1990. Ultrastructure of oocytes of the shrimp, *Penaeus vannamei*: cortical specialization formation. Tissue Cell 22, 879–893.

Shalgi, R., Raz, T., 1997. The role of carbohydrate residues in mammalian fertilization. Histol. Histopath. 12, 813–822.

Sun, Y.D., Zhao, X.F., Kang, C.J., Wang, J.X., 2006. Molecular cloning and characterization of Fc-TSP from the Chinese shrimp *Fennerpenaeus chinensis*. Mol. Immunol. 43, 1202–1210.

Tan-Fermin, J.D., Pudadera, R.A., 1989. Ovarian maturation stages of the wild giant tiger prawn, *Penaeus monodon* Fabricius. Aquaculture 77, 229–242.

Tellam, R.L., Wijffels, G., Willadsen, P., 1999. Peritrophic matrix proteins. Insect Biochem. Mol. Biol. 29, 87–101.

Towbin, H., Staehelin, T., Gordon, J., 1979. Electrophoresis transfer of proteins from polyacrylamide gels to nitrocellulose sheets: procedures and some applications. Proc. Natl. Acad. Sci. U. S. A. 76, 4350.

Vacquier, V.D., Moy, G.W., 1997. The fucose sulfate polymer of egg jelly binds to sperm REJ and is the inducer of the sea urchin sperm acrosome reaction. Dev. Biol. 192, 125–135.

Vanichviriyakit, R., Kruevaisayawan, H., Weerachatyanukul, W., Tawipreeda, P., Withyachumnarnkul, B., Pratoomchat, B., Chavadej, J., Sobhon, P., 2004. Molecular modification of *Penaeus monodon* sperm in female thelycum and its consequent responses. Mol. Reprod. Dev. 69, 356–363.

Vilela-Silva, A.C., Alves, A.P., Valente, A.P., Vacquier, V.D., Mourao, P.A., 1999. Structure of the sulfated alpha-L-fucan from the egg jelly coat of the sea urchin *Strongylocentrotus franciscanus*: patterns of preferential 2-*O*- and 4-*O*-sulfation determine sperm cell recognition. Glycobiology 9, 927–933.

Vilela-Silva, A.C., Castro, M.O., Valente, A.P., Biermann, C.H., Mourao, P.A., 2002. Sulfated fucans from the egg jellies of the closely related sea urchins *Strongylocentrotus droebachiensis* and *Strongylocentrotus pallidus* ensure species-specific fertilization. J. Biol. Chem. 277, 379–387.

Wassarman, P.M., 2005. Contribution of mouse egg zona pellucida glycoproteins to gamete recognition during fertilization. J. Cell. Physiol. 204, 388–391.

Yamano, K., Seto, H., Qiu, G.F., Unuma, T., 2003. Immunological characterization of cortical rod proteins of kuruma prawn,

Author's personal copy

Marsupenaeus japonicus. Comp. Biochem. Physiol., Part A Mol. Integr. Physiol. 136, 371–377.

Yamano, K., Qiu, G.F., Unuma, T., 2004. Molecular cloning and ovarian expression profiles of thrombospondin, a major component of cortical rods in mature oocytes of penaeid shrimp, *Marsupenaeus japonicus*. Biol. Reprod. 70, 1670–1678.

Yano, I., 1988. Oocyte development in the kuruma prawn *Penaeus japonicus*. Mar. Biol. 99, 547–553.

Yano, I., 1995. Final oocyte maturation, spawning and mating in penaeid shrimp. J. Exp. Mar. Biol. Ecol. 193, 113–118.

Zara, J., Naz, R.K., 1998. The role of carbohydrates in mammalian sperm–egg interactions: how important are carbohydrate epitopes? Front. Biosci. 3, D1028–D1038.

Aquaculture Research, 2007, **38,** 1635–1644 doi: 10.1111/j.1365-2109.2007.01824.x

Acrosome reaction in the sperm of the black tiger shrimp *Penaeus monodon* (Decapoda, Penaeidae)

Pattira Pongtippatee[1], Rapeepan Vanichviriyakit[2], Jittipan Chavadej[2], Pornthep Plodpai[3], Boonyarath Pratoomchart[4], Prasert Sobhon[2] & Boonsirm Withyachumnarnkul[2,5]

[1]Department of Anatomy, Faculty of Science, Prince of Songkla University, Songkla 90110, Thailand

[2]Department of Anatomy, Faculty of Science, Mahidol University, Bangkok 10400, Thailand

[3]Shrimp Culture Research Center, Charoen Pokphand Foods Company (Public), Nakorn Srithamaraj 80170, Thailand

[4]Department of Marine Biology, Faculty of Science, Burapha University, Cholburi 20131, Thailand

[5]Centex Shrimp, Faculty of Science, Mahidol University, Bangkok 10400, Thailand

Correspondence: B Withyachumnarnkul, Centex Shrimp, Chalerm Prakiat Building, 4th Floor, Faculty of Science, Mahidol University, 272 Rama 6 Rd., Bangkok 10400, Thailand. E-mail: boonsirm@yahoo.com

Abstract

Owing to the problem of male infertility in the domesticated shrimp *Penaeus monodon*, this study was conducted to reveal the morphological events of an acrosome reaction (AR) of sperm of this highly valuable species. The AR observed in an *in vitro* incubation of sperm with egg water (EW) and that during actual spawning was compared. Under transmission and scanning electron microscopy, sperm taken from the female thelycum was composed of a posterior main body, a central cap and an anterior single spike. Upon contact with EW, the sperm underwent two phases of AR: acrosomal exocytosis and spherical mass formation. The former was composed of a degeneration of the spike, swelling of the cap region and rupture of the acrosomal pouch. The latter began with polymerization of materials within the subacrosomal region and ended with re-configuration of the subacrosomal region into an electron-dense spherical mass. The AR of the sperm observed during spawning revealed similar morphological events, with degeneration of the spike upon contact with the vitelline envelope and formation of the spherical mass while penetrating into jelly material produced by protruding cortical rods. The results suggest the presence of AR inducers derived from the vitelline envelope and cortical rods of the egg. This study forms the basis for an evaluation of infertility regarding to AR in the domesticated *P. monodon* male.

Keywords: acrosome reaction, sperm, thelycum, fertilization, *Penaeus monodon*, broodstock

Introduction

The black tiger shrimp *Penaeus monodon* is one of the two most important cultured shrimp species in the world; the other one is the Pacific white shrimp *Penaeus vannamei*. In the cultivation of both species, the main problems being faced by the industry are disease outbreaks, slow growth and fluctuating shrimp price. One problem that has not been adequately addressed is male fertility. Hatchery operators know that, occasionally, male shrimp of both species have fertilization problems, especially the domesticated ones. The problem could be due to a low sperm count in the spermatophore (Pratoomchat, Piyatiratitivorakul & Menasveta 1993) or the low capacity of individual sperm to fertilize the eggs or both. At the time of fertilization, sperm of the penaeid shrimp need to undergo a morphological transformation termed an acrosome reaction (AR) before penetrating the eggs (Leung-Trujillo & Lawrence 1987; Griffin & Clark Jr. 1990). Because the AR process has never been explored in *P. monodon*, the purpose of this study was to study the morphological events of the sperm of *P. monodon* before and at the time of fertilization. The results of this study can serve as a basis for

Journal Compilation © 2007 Blackwell Publishing Ltd. No Claim to original Government works

future research on the problem of male infertility in this species.

Penaeus monodon is a closed thelycum species and the male inserts spermatophores or sperm sacs into the female thelycum during mating. After being inserted into the female thelycum, the sperm are stored for several weeks or longer, during which time they undergo morphological and biochemical changes that render them ready for fertilization (Clark Jr., Kleve & Yudin 1981; Hall, Young & Kenway 1999; Vanichviriyakit, Kruevaisayawan, Weerachatyanukul, Pongtippatee-Tawipreeda, Withyachumnarnkul, Pratoomchat, Chavadej & Sobhon 2004). It is generally believed that sperm are extruded from the thelycum to mix externally with the eggs that are released from gonopores during spawning. At spawning, the sperm undergoes AR, which is composed of two phases in most marine invertebrates: the acrosomal exocytosis, which is a release of the contents of the acrosomal vesicle onto the egg surface, and the acrosomal process formation (Colwin & Colwin 1963; Fa, Lin, Wei & Shuai 2004). The acrosomal process is a structure that extends from the sperm to make contact with the egg membrane and probably serves as a way to facilitate the entry of the sperm DNA into the egg. The mechanisms underlying the acrosomal exocytosis and acrosomal process formation are poorly understood. In the sea urchin *Lytechinus pictus* and *Strongylocentrotus purpuratus*, it has been known that acrosomal exocytosis requires a Ca^{2+} influx from the external environment (Collins & Epel 1977; SeGall & Lennarz 1979; Gonzalez-Martinez, Guerrero, Morales, de Ja Torre & Darszon 1992). In *S. purpuratus*, the acrosomal process formation is probably caused by polymerization of globular actin molecules in the subacrosomal region and depends on the release of hydrogen ions from the sperm head (Schackmann, Eddy & Shapiro 1978). In the marine shrimp *Sicyonia ingentis*, acrosomal exocytosis is induced when the sperm contact the vitelline envelope of the egg and the acrosomal process formation is induced by a proteolytic enzyme released from the egg (Clark Jr. *et al.* 1981; Griffin, Clark Jr., Crowe & Crowe 1987; Pillai & Clark Jr. 1987; Griffin & Clark Jr. 1990; Wikramanayake & Clark Jr. 1994).

In this study, the morphological events of *P. monodon* AR during an *in vitro* incubation with egg water (EW) and during spawning were examined under light microscopy (LM), transmission electron microscopy (TEM) and scanning electron microscopy (SEM). The study covered events from the beginning, or before the sperm underwent morphological changes, to the end of AR.

Materials and methods

Animals and EW collection

Wild-caught *P. monodon* broodstock (15 females and 15 males) from the Andaman Sea were kept in hatchery maturation tanks (4 m × 2 m), and maintained under continuous darkness, 30 °C and 30 g L^{-1} seawater, at 0.5 m depth. Mating usually occurred in the tank, and sperm were taken from the female thelycum for observation of AR upon contact with EW. One female was used for EW preparation and three females for AR observation of the sperm during spawning. The females were unilaterally eyestalk ablated and maintained in maturation tanks until their ovaries had become mature (Tan-Fermin & Pudadera 1989). To prepare EW, females that were ready to spawn were transferred to a 500 L tank and continuously observed for spawning behaviour, which was swimming in a circle on the water surface. Just before spawning, the shrimp was manually held and allowed to spawn into 200 mL artificial seawater (ASW) at 4 °C in a 500 mL bucket, and placed back in the 500 L tank. The eggs and ASW in the bucket were transferred to a 250 mL beaker.

The protocol for EW isolation was based on the original technique developed by Griffin *et al.* (1987). The eggs were allowed to settle to the bottom of the beaker, which was usually complete within 2 min. Water from the top devoid of eggs (ca. 200 mL) was drawn off and transferred to a new 250 mL beaker. It was then centrifuged at 10 000 *g* for 15 min at 4 °C and clear EW supernatant was prepared in 1 mL aliquots, and then stored in liquid nitrogen.

Thelycal sperm collection, EW incubation and morphological observations

To extract sperm from the thelycum, the gelatinous sperm mass was gently withdrawn from the thelycum by a 1 mL syringe, placed in a tube containing 1 mL ASW, gently homogenized by a glass grinder to release the sperm and the tissue debris was allowed to settle. The supernatant was withdrawn and centrifuged at 200 *g* for 5 min to pellet the sperm. The supernatant was then removed and sperm were re-suspended by aspiration in 1 mL ASW. Five hundred microlitre of the sperm suspension was incubated

with 500 μL of EW for 15, 30, 45, 60 s, 2, 5, 10 min and 1 h.

At each incubation period, 75 μL aliquot of the suspension was pipetted and fixed for 1 h in ASW-buffered 2.5% glutaraldehyde. Then, 15 μL aliquot of the fixed sperm was also pipetted, placed on glass slides and viewed under differential interference contrast light microscopy (LM) (Nikon ECLIPSE E-600, Kanagawa, Japan). At the same time, the remaining fixed sperm were processed for TEM and SEM. For TEM, the sperm were washed in buffer, postfixed for 30 min in 1% buffered OsO_4, rinsed in ASWand dehydrated through an ethanol series. The samples were embedded in a low-viscosity resin, thin sectioned on an ultramicrotome (MT-XL RMC, Boeckeler Instruments, Inc., Tucson, AZ, USA), stained with uranyl acetate and lead citrate and observed under TEM (JEOL, JEM-100 CXII, Tokyo, Japan).

For SEM, the fixed sperm were affixed to glass coverslips coated with 1% poly-L-lysine, washed in seawater, postfixed for 30 min in seawater-buffered 1% OsO_4, critical-point dried, mounted on stubs and coated with 25 nm of gold and examined under SEM (Hitachi, S-2500, Tokyo, Japan).

Observation of AR of the sperm in the spawning tank

The AR of the sperm that had been released from a female during spawning was also observed in a spawning tank under the hatchery conditions. The eggs and sperm released from the female broodstock at the time of spawning were immediately collected and fixed as soon as the eggs came out from the gonopores (approximately 5 s). The samples were fixed and processed for TEM and SEM as described above, and also for LM with haematoxylin and eosin and fluorescent chromosome staining. Bisbenzimide Hoechst 33258 (Sigma-Aldrich Pte., Ltd, Singapore) was used as a fluorescent chromosome stain to allow visualization of the sperm nucleus. A stock solution of Hoechst 33258 (0.005%), dissolved in sterile-distilled water containing 0.1% thimerosal, was filtered through 0.22 μm millipore membrane filters, protected from light and stored at 4 °C. The Hoechst stock solution was stirred for 30 min at room temperature and diluted 1:200 in sterile-distilled water, which was stirred for another 30 min at room temperature. Fertilized eggs were fixed for 10 min in 98% acetic acid and absolute methanol at 1:3 v/v, and air dried. Diluted Hoechst solution (50 μL) was added to fixed samples, which were incubated for 30 min in the dark at room temperature. After the incubation time had lapsed, the samples were rinsed three times with 500 μL distilled water, air dried and mounted for fluorescent microscopy.

Statistical analysis for numerical data was determined by Student's *t*-test.

Results

In vitro induction of AR

The AR took place within 1–2 min after incubation of the sperm with EW. Approximately 82 ± 12% of sperm had undergone AR, while the other 18 ± 12% remained unreacted (Fig. 1a); the percentage of reacted sperm was significantly higher than the unreacted ones ($P < 0.01$). The unreacted sperm were composed of a posterior spherical main body, a central cap and an anterior single spike extending from the cap (Fig. 1b). The main body contains a nucleus that houses a mixture of fibrous and globular chromatin, but the nuclear envelope was not observed (Fig. 1c). In contrast to mammalian sperm, which are highly motile, *P. monodon* sperm are non-motile and contain no mitochondria. The central cap region contains two main parts: the acrosome and subacrosome. The acrosome is composed of a high-density outer layer and a low-density inner layer (Fig. 1c). The subacrosomal region contains flocculent electron-lucent materials. The most anterior comprises a long single, electron-dense spike, which extends from its base located between the acrosome and subacrosomal region (Fig. 1c). The base of the spike extends into the central cap region and becomes a dense limiting membrane, separating the low-density inner layer of the acrosome and the subacrosomal region.

The AR began with curling, shortening and disappearance of the spike (Fig. 2a, b and c, respectively). The spike base existed for < 1 min after the onset of the AR and then disappeared (Fig. 2c and e). During the shortening and disappearance of the spike, the cap became markedly swollen (Fig. 2e), which was caused by the swelling of the acrosome (Fig. 2e and f). While the acrosome appeared to be swollen, the distinction between the high-density outer and low-density inner layers was not observed and the structures inside became flocculent (Fig. 2d and f). After complete disappearance of the spike, the outer limiting membrane of the acrosome was ruptured and the acrosomal content was released (Fig. 3a and b). The posterior part of the subacrosomal region began to condense, or polymerize, resulting in the subacrosomal region comprising the electron-dense and

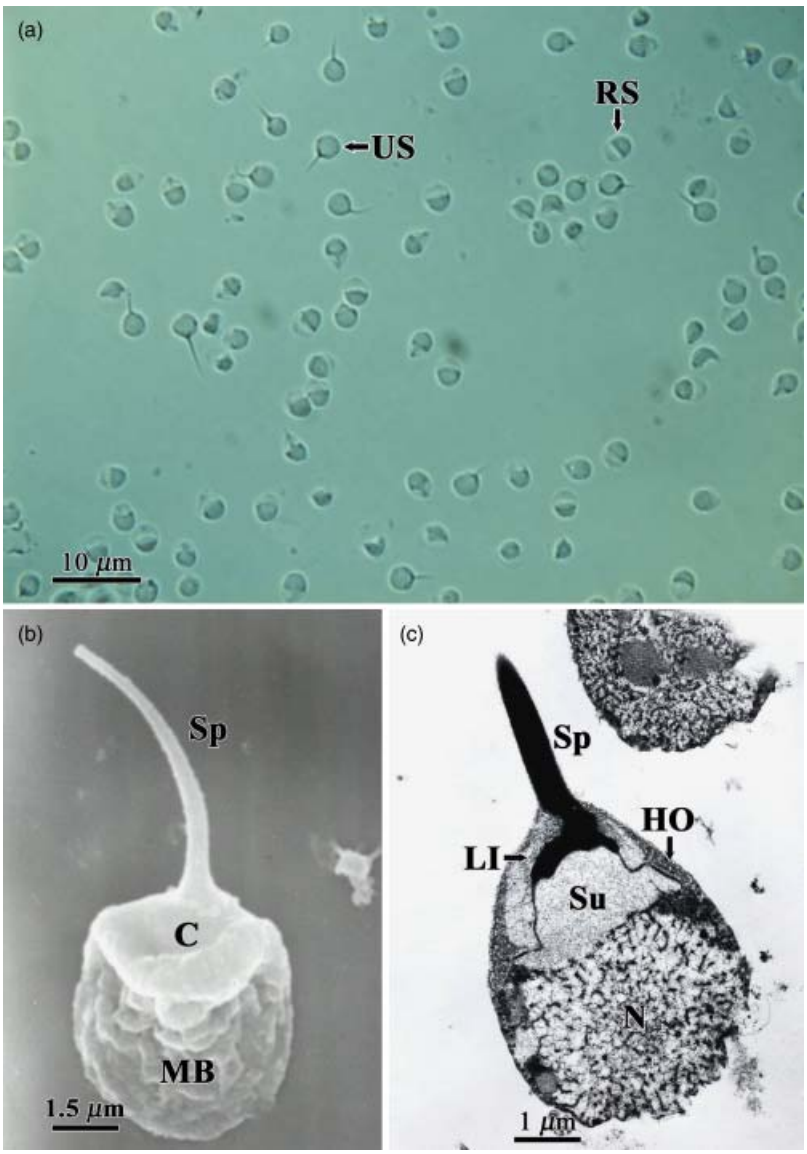


Figure 1 Light (a), scanning electron (b) and transmission electron (c) micrographs of *P. monodon* sperm. Using light microscopy, it was observed that most of the sperm become reactive after incubating with egg water, and few remain unreacted. Using scanning electron microscopy, it was observed that the unreacted sperm is composed of a posterior main body, a central cap region a and anterior spike. Using transmission electron microscopy, it was observed that the posterior main body contains a nucleus, the cap region consists of three parts: a high-density outer layer, a low-density inner layer and a subacrosomal region. The anterior spike extends its base towards an area between the low-density inner layer and the subacrosomal region. C, cap; HO, high-density outer layer; LI, low-density inner layer; MB, main body; N, nucleus; RS, reacted sperm; Sp, spike; Su, subacrosomal region; US, unreacted sperm.

electron-lucent areas when observed under TEM (Fig. 3a and c). Under SEM, the electron-lucent area appeared as a spherical knob at the anterior end of the sperm (Fig. 3d). Without the acrosome, the subacrosomal region became the most anterior part of the sperm, with the remaining outer limiting membrane of the acrosome hanging on the side of the subacrosomal region (Fig. 3c). Subsequently, the subacrosomal polymerization expanded throughout the region, and was re-configured to be a spherical mass on the anterior end of the sperm (Fig. 3e). These morphological changes made the sperm appear spherical, with a condensed knob at its anterior end when visualized under LM and SEM (Fig. 3e and f).

During morphological development of the AR, the ultrastructure of nucleoplasm, especially the ratio between the fibrous and globular chromatin that reflects the degree of chromatin decondensation, did not reveal any remarkable change (comparing Figs 1c–3e).

AR in the spawning tank

Immediately after spawning, within 5 s, most of the sperm that contacted the eggs did not undergo AR (Fig. 4a). The sperm approached the egg by touching its spike on the egg surface (Fig. 4b), which was the

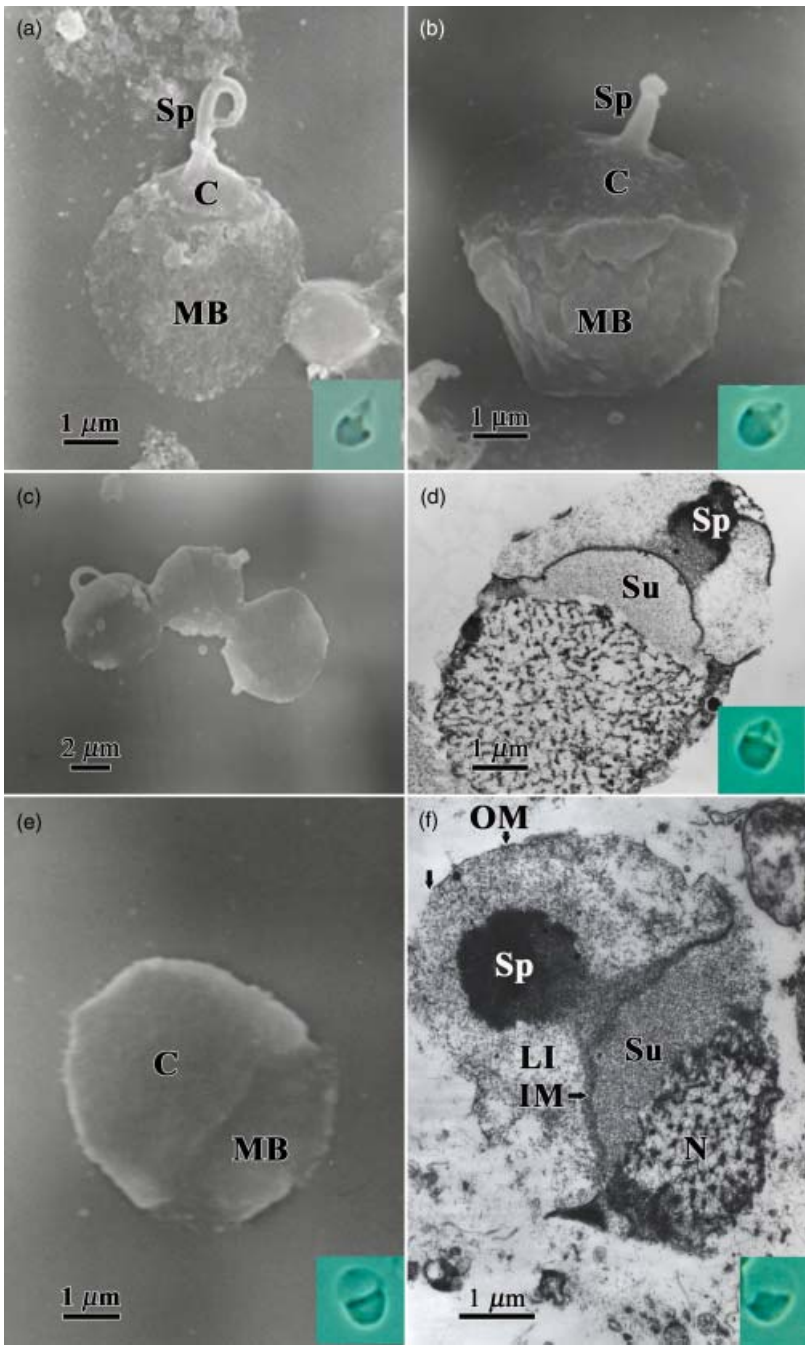


Figure 2 Scanning (a, b, c, e) and transmission (d, f) electron micrographs of the reacted sperm at 15 s after incubation with egg water. The insets correspond to LM pictures. The reaction begins with curling (a) and shortening (b, c, d) of the spike, followed by swelling of the cap (e). Using transmission electron microscopy, it was observed that the spike is reduced in length and shows only a stump in the cap region, which is markedly swollen (f). C, cap; IM, inner limiting membrane; LI, low-density inner layer; MB, main body; N, nucleus; OM, outer limiting membrane; Sp, spike; Su, subacrosomal region.

vitelline envelope. It then began the first phase of AR as it passed through the vitelline envelope (Fig. 4c and d) and was in contact with the cortical rod (Fig. 5a). Curling and degeneration of the sperm spike took place on the cortical rod surface (Fig. 5a), followed by penetration of the sperm into the substance of the cortical rod (Fig 5b). As the cortical rod was protruding, its content dispersed out and formed a jelly material surrounding the egg surface (Fig. 5c). The reacted sperm on the surface of the jelly material developed the spherical mass only after being immersed in the jelly material (Fig. 5d). A clear zone was observed in the jelly material surrounding the spherical mass (Fig. 5e), which might suggest that the sperm excreted enzymes that digest its way through the jelly material. The ultrastructural features of this

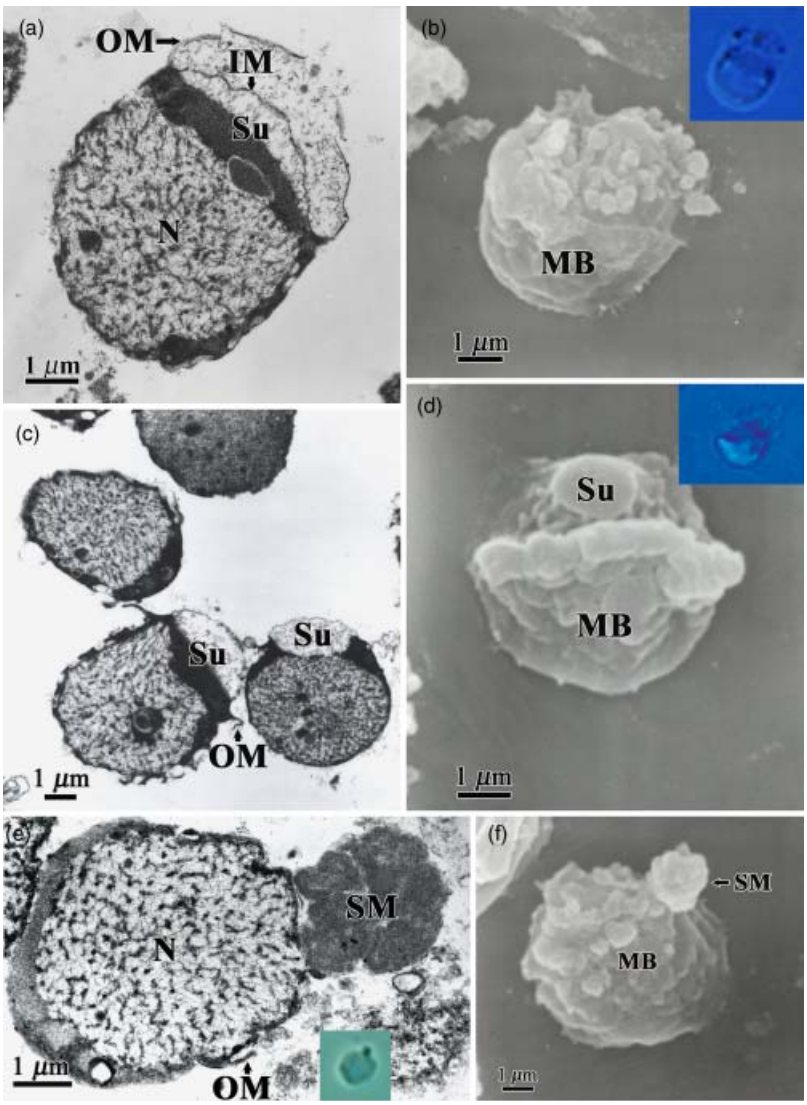


Figure 3 Transmission (a, c, e) and scanning (b, d, f) electron micrographs of the reacted sperm at exocytosis and formation of the spherical mass stage. The insets correspond to LM pictures. Following the disappearance of the spike, the outer limiting membrane is ruptured and the subacrosomal region begins to polymerize (a, b). Following the release of acrosomal content, the subacrosomal region becomes the most anterior part of the sperm (c, d) and becomes the spherical mass after complete polymerization (e, f). IM, inner limiting membrane; MB, main body; OM, outer limiting membrane; N, nucleus; Su, subacrosomal region; SM, spherical mass.

last stage of AR were identical to those of the *in vitro* sperm and the whole event was completed within 1 min post-spawning.

Discussion

This study reveals that *P. monodon* sperm are a usual form of natantian sperm that have been reported in various shrimp species (Brown Jr., Kleve & Clark Jr. 1976; Kleve, Yudin & Clark Jr. 1980; Clark Jr. *et al.* 1981; Leung-Trujillo & Lawrence 1987; Pratoomchat *et al.* 1993; Rios & Barros 1997; Hall *et al.* 1999). They are non-motile, and composed of a single spike originating from the acrosomal region, a central cap with an acrosome and a subacrosomal region and a nucleus of decondensed chromatin structures. In reptantian (crayfish, lobsters and crabs) sperm, the spikes are multiple, project from the nucleus and contain microtubules. The significant function of these nuclear extended spikes has not been explained, however (Yasuzumi 1960; Yasuzumi, Kaye, Pappas, Yamamoto & Tsubo 1961; Talbot & Summers 1978). The electron-dense content of the spike may be a kind of contractile protein such as actin or other cytoskeletal proteins having depolymerizing or repolymerizing ability. The mechanism behind the curling and shortening of the spike is probably by depolarization of the cytoskeletal proteins.

In *P. monodon* sperm, the spherical main body contains the decondensed chromatin structure but the nuclear envelope was not observed. It is possible that

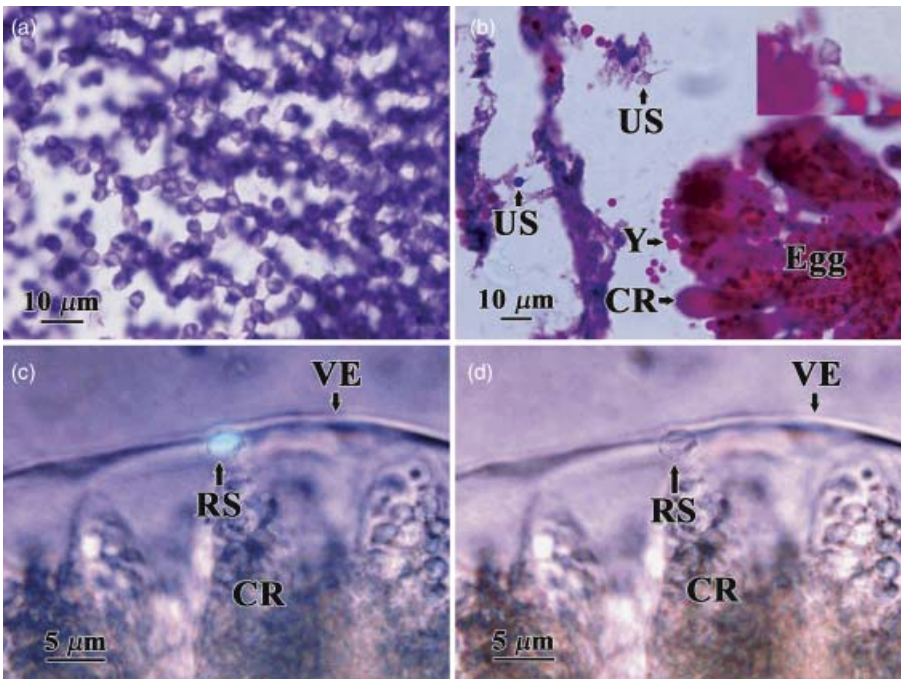


Figure 4 Light micrographs of the ejected sperm in the water at spawning stained with haematoxylin and eosin (a, b) and with Hoechst staining observed under fluorescent (c) and differential interference contrast microscopy (d). Immediately after spawning, several unreacted sperm are observed (a) and some orient their spikes towards the egg surface (b, inset). Sperm located on the vitelline envelope (c, d) lacks a spike, suggesting that it could be a reacted one. CR, cortical rod; RS, reacted sperm; US, unreacted sperm; VE, vitelline envelope; Y, yolk granule.

breakdown of the nuclear envelope had occurred; the phenomenon was observed in natantian decapod crustaceans in concomitant with chromatin decondensation (Kleve *et al.* 1980). This phenomenon is believed to be important in preparing the sperm for fertilization.

The significance behind the different density layers (high and low) of the acrosome is not known at present. The low-density inner layer of the acrosomal content in *P. monodon* may be analogous to a similar structure of *S. ingentis* sperm that are in the AR process, which is arranged in a number of small pouches (Kleve *et al.* 1980). During exocytosis in *P. monodon*, the high-density outer and the low-density inner layers became enlarged, lightened and blended as a single layer. This phenomenon may be due to water influx from the external environment, which interacts with hydratable proteins, e.g. glycoproteins; the mechanism has been suggested for *S. ingentis* sperm and results in swelling and rupture of the pouch (Clark Jr. *et al.* 1981). In the lobster *Homarus americanus*, the acrosome contains a hydrolytic enzyme; the swelling of the cap is caused by this hydrolase and rapid hydration pulls the sperm forward to the hatching envelope of the egg (Talbot & Chanmanon 1980). In mammals and sea urchins, the acrosomal exocytosis is usually accompanied by Ca^{2+}-mediated fusion of membrane-enclosed acrosomal vesicle with the plasma membrane (Florman, Corron, Kim & Babcock 1992; Gonzalez-Martinez *et al.* 1992).

The subacrosomal region of *P. monodon* sperm taken from the female thelycum contained flocculent electron-lucent materials. These materials were found to be highly concentrated and more opaque than that of the subacrosomal region of sperm taken from the vas deferens and testes in the male (R. Vanichviriyakit, pers. comm.). The difference could be due to the higher degree of molecular cross linkages or molecular modifications of the subacrosomal contents, which is to prepare for the second phase of AR during fertilization. In *S. ingentis* and sea urchin, the formation of acrosomal process also originated from the subacrosomal region and, in sea urchin, the extension of the acrosomal process involves polymerization of subacrosome globular actin molecules (Schackmann *et al.* 1978; Tilney, Kiehart, Sardet & Tilney 1978; Griffin, Shigekawa & Clark Jr. 1988).

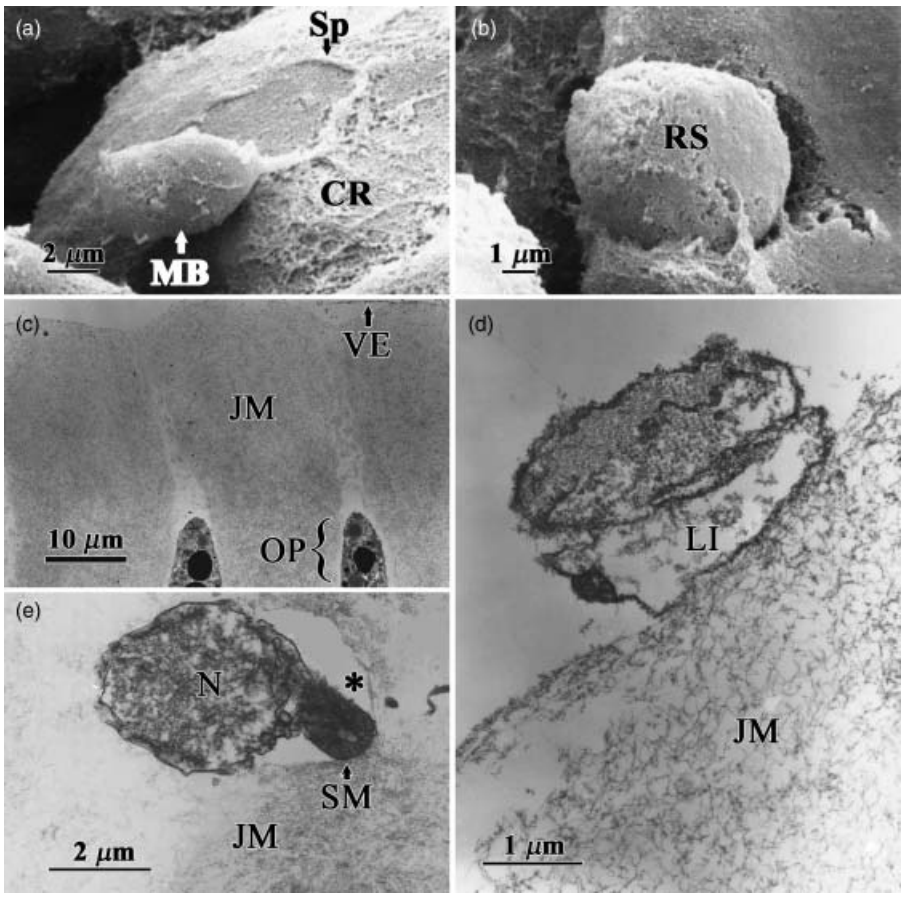


Figure 5 Scanning (a, b) and transmission (c, d, e) electron micrographs of the sperm on the egg surface at actual spawning. A sperm on the surface of the protruding cortical rod shows a curled and degenerative spike (a) before sinking into the protruding cortical rod (b), which forms a jelly material surrounding the egg (c). The sperm attached to the jelly material shows a subacrosomal change (d) while penetrating into the material, with a clear space (*) surrounding the spherical mass (e). CR, cortical rod; JM, jelly material; LI, low-density inner layer; MB, main body; N, nucleus; OP, ooplasm; RS, reacted sperm; Sp, spike; SM, spherical mass; VE, vitelline envelope.

This study shows that *P. monodon* sperm also has two phases of AR, similar to those of other marine species. The main point of interest here is what induces the first and the second phases of AR of the sperm. In *S. ingentis*, the first phase of AR occurs when the sperm is in contact the vitelline envelope of the egg (Wikramanayake & Clark Jr. 1994); a similar event occurs in *P. monodon* sperm as shown in this study. The acrosome of *P. monodon* sperm presumably contains enzymes that digest the vitelline envelope and allow the sperm to move forward; this mechanism has been shown in other species as well (Clark Jr. *et al.* 1981; Griffin *et al.* 1988; Wikramanayake & Clark Jr. 1994).

In the second phase, *P. monodon* sperm underwent this stage only after coming in contact with the jelly material released from the egg cortical rod. In sea urchin, AR occurs when the sperm contacts a jelly material surrounding the egg and causes an ion influx into the sperm (Neill & Vacquier 2004; Darszon, Nishigaki, Wood, Trevino, Felix & Beltran 2005). The substance in the jelly material of the sea urchin that could induce AR is sulfated fucan (Hirohashi, Ana-Cristina, Vilela-Silva, Mourao & Vacquier 2002). It is likely that similar substances in the jelly material of *P. monodon* egg induces AR of the sperm, probably with a similar mechanism; an ongoing study also suggests that the cortical rod of *P. monodon* contains sulphated fucan (Kruevaisayawan, pers. comm.).

Most of the *P. monodon* sperm under the *in vitro* and under actual spawning conditions had AR within 1–2 min upon contact with seawater, compared with

several minutes to more than an hour in other penaeoid shrimps, like *Trachypenaeus byrdi* and *Xiphopenaeus riveti* (Alfaro, Munoz, Vargas & Komen 2003). In those species, as well as in *P. monodon*, evidence has shown that capacitation of the sperm is accomplished while being in the thelycum (Alfaro *et al.* 2003; Vanichviriyakit *et al.* 2004). The fact that *P. monodon* sperm requires less time to complete AR suggests that their sperm is more reactive than sperm of other penaeids, which implies that the capacitation process in *P. monodon* may be more efficient than that of other species.

The results of this study form a basis for future evaluation of sperm quality in *P. monodon*, especially the domesticated ones. Besides the total sperm count, the ratio of reacted and unreacted sperm upon contacting EW and the morphological changes during AR could provide a reliable and better assessment of the sperm maturation in this highly economic species.

Acknowledgments

This study was supported by the Center for Molecular Biology and Biotechnology of the National Science and Technology Development Agency (NSTDA), Thailand, Grant No. BT-B-06-SG-14-4505.

References

Alfaro J., Munoz N., Vargas M. & Komen J. (2003) Induction of sperm activation in open and closed thelycum penaeoid shrimps. *Aquaculture* **216**, 371–381.

Brown A. Jr., Kleve M.G. & Clark W.H. Jr. (1976) Evidence for the presence of actin in natantian sperm. *American Zoology* **16**, 180.

Clark W.H. Jr., Kleve M.G. & Yudin A.I. (1981) An acrosome reaction in natantian sperm. *Journal of Experimental Zoology* **218**, 279–291.

Collins F. & Epel D. (1977) The role of calcium ions in the acrosome reaction of sea urchin sperm. *Experimental Cell Research* **106**, 211–222.

Colwin A.L. & Colwin L.H. (1963) Role of the gamete membrane in fertilization in *Saccoglossus kowalevskii* (Enteropneustra) I. The acrosome reaction and its changes in early stages of fertilization. *Journal of Cell Biology* **19**, 477–500.

Darszon A., Nishigaki T., Wood C., Trevino C.L., Felix R. & Beltran C. (2005) Calcium channels and Ca^{2+} fluctuations in sperm physiology. *International Review of Cytology* **243**, 79–172.

Fa Z.D., Lin W.G.C., Wei Y.H. & Shuai Z. (2004) Morphological and structural changes of sperm during the acrosome reaction in the swimming crab *Portunus trituberculatus*. *Acta Zoologica Sinica* **50**, 800–807.

Florman H.M., Corron M.E., Kim T.D.-H. & Babcock D.F. (1992) Activation of voltage-dependent calcium channels of mammalian sperm in required for zona pellucida-induced acrosomal exocytosis. *Developmental Biology* **152**, 304–314.

Gonzalez-Martinez M.T., Guerrero A., Morales E., de Ja Torre L. & Darszon A. (1992) A depolarization can trigger Ca^{2+} uptake and the acrosome reaction when preceded by a hyperpolarization in *L. pictus* sea urchin sperm. *Developmental Biology* **150**, 193–202.

Griffin F.J. & Clark W.H. Jr. (1990) Induction of acrosomal filament formation in the sperm of *Sicyonia ingentis*. *Journal of Experimental Zoology* **254**, 296–304.

Griffin F.J., Clark W.H. Jr., Crowe J.H. & Crowe L.M. (1987) Intracellular pH decrease during the in vitro induction of the acrosome reaction in the sperm of *Sicyonia ingentis*. *Biological Bulletin* **173**, 311–323.

Griffin F.J., Shigekawa K. & Clark W.H. Jr. (1988) Formation and structure of the acrosomal filament in the sperm of *Sicyonia ingentis*. *Journal of Experimental Zoology* **246**, 94–102.

Hall M.R., Young N. & Kenway M. (1999) *Manual for the determination of egg fertility in Penaeus monodon*. AIMS. Research. Australia, Available: http://www.aims.gov.au/pages/research/mdef/mdef-oo.html. [Accessed Aug 04 1999].

Hirohashi N., Ana-Cristina E.S., Vilela-Silva P., Mourao A.S. & Vacquier V.D. (2002) Structural requirements for species-specific induction of the sperm acrosome reaction by sea urchin egg sulfated fucan. *Biochemical and Biophysical Research Communications* **298**, 403–407.

Kleve M.G., Yudin A.I. & Clark W.H. Jr. (1980) Fine structure of the unistellate sperm of the shrimp, *Sicyonia ingentis* (Natantia). *Tissue and Cell* **12**, 29–45.

Leung-Trujillo J.R. & Lawrence A.L. (1987) Observation on the decline in sperm quality of *Penaeus setiferus* under laboratory conditions. *Aquaculture* **65**, 363–370.

Neill A.T. & Vacquier V.D. (2004) Ligands and receptors mediating signal transduction in sea urchin spermatozoa. *Reproduction* **127**, 141–149.

Pillai M.C. & Clark W.H. Jr. (1987) Egg activation in the marine shrimp, *Sicyonia ingentis*. *Journal of Experimental Zoology* **244**, 325–329.

Pratoomchat B., Piyatiratitivorakul S. & Menasveta P. (1993) Sperm quality of pond-reared and wild-caught *Penaeus monodon* in Thailand. *Journal of World Aquaculture Society* **24**, 530–540.

Rios M. & Barros C. (1997) Trypsin-like enzymes during fertilization in the shrimp *Rhynchocinetes typus*. *Molecular Reproduction and Development* **46**, 581–586.

Schackmann R.W., Eddy E.M. & Shapiro B.M. (1978) The acrosome reaction of *Strongylocentrotus purpuratus* sperm: ion requirements and movements. *Developmental Biology* **65**, 483–495.

SeGall G.K. & Lennarz W.J. (1979) Chemical characterization of the component of the jelly coat from sea urchin eggs responsible for induction of the acrosome reaction. *Developmental Biology* **71**, 33–48.

Talbot P. & Chanmanon P. (1980) Morphological features of the acrosome reaction of lobster (*Homarus*) sperm and the role of the reaction in generating forward sperm movement. *Journal of Ultrastructure Research* **70**, 287–297.

Talbot P. & Summers R.G. (1978) The structure of sperm from *Panulirus*, the spiny lobster, with special regard to the acrosome. *Journal of Ultrastructure Research* **64**, 341–351.

Tan-Fermin J.D. & Pudadera R.A. (1989) Ovarian maturation stages of the wild giant tiger prawn *Penaeus monodon* Fabricius. *Aquaculture* **77**, 229–242.

Tilney L.G., Kiehart D.P., Sardet C. & Tilney M. (1978) Polymerization of actin. IV. Role of Ca^{2+} and H^{+} in the assembly of actin and in membrane fusion in the acrosomal reaction of echinoderm sperm. *Journal of Cell Biology* **77**, 536–560.

Vanichviriyakit R., Kruevaisayawan H., Weerachatyanukul W., Pongtippatee-Tawipreeda P., Withyachumnarnkul B., Pratoomchat B., Chavadej J. & Sobhon P. (2004) Molecular modification of *Penaeus monodon* sperm in female thelycum and its consequent responses. *Molecular Reproduction and Development* **69**, 356–363.

Wikramanayake A.H. & Clark W.H. Jr. (1994) Two extracellular matrices from oocytes of the marine shrimp *Sicyonia ingentis* that independently mediate only primary or secondary sperm binding. *Development, Growth and Differentiation* **36**, 89–101.

Yasuzumi G. (1960) Spermatogenesis in animals as revealed by electron microscopy. VII. Spermatid differentiation in the crab, *Eriocher japonicus*. *Journal of Biophysical and Biochemical Cytology* **7**, 73–78.

Yasuzumi G., Kaye G.I., Pappas G.D., Yamamoto H. & Tsubo I. (1961) Nuclear and cytoplasmic differentiation in developing sperm of the crayfish *Cambaroides japonicus*. *Zeitschrift fuer Zellforschung und Mikroskopische Anatomie* **53**, 141–158.

Cell Tissue Res (2008) 331:687–699
DOI 10.1007/s00441-007-0557-5

REGULAR ARTICLE

Spermiogenesis and chromatin condensation in the common tree shrew, *Tupaia glis*

Worawit Suphamungmee · Chaitip Wanichanon · Rapeepun Vanichviriyakit · Prasert Sobhon

Received: 25 May 2007 / Accepted: 13 November 2007 / Published online: 19 December 2007
© Springer-Verlag 2007

Abstract We have investigated the cellular characteristics, especially chromatin condensation and the basic nuclear protein profile, during spermiogenesis in the common tree shrew, *Tupaia glis*. Spermatids could be classified into Golgi phase, cap phase, acrosome phase, and maturation phase. During the Golgi phase, chromatin was composed of 10-nm and 30-nm fibers with few 50-nm to 60-nm knobby fibers. The latter were then transformed into 70-nm knobby fibers during the cap phase. In the acrosome phase, all fibers were packed into the highest-order knobby fibers, each about 80–100 nm in width. These chromatin fibers became tightly packed in the maturation phase. In a mature spermatozoon, the discoid-shaped head was occupied by the acrosome and completely condensed chromatin. H3, the core histone, was detected by immunostaining in all nuclei of germ cell stages, except in spermatid steps 15–16 and spermatozoa. Protamine, the basic nuclear protein causing the tight packing of sperm chromatin, was detected by immunofluorescence in the nuclei of spermatids at steps 12–16 and spermatozoa. Cross-immunoreactivity of *T. glis* H3 and protamine to those of primates suggests the evolutionary resemblance of these nuclear basic proteins in primate germ cells.

Keywords Spermiogenesis · Sperm · Chromatin condensation · Histone · Protamine · Tree shrew, *Tupaia glis* (Scandentia)

This work was supported by the Thailand Research Fund (Senior Research Fellowship to Prof. Prasert Sobhon).

W. Suphamungmee · C. Wanichanon (✉) · R. Vanichviriyakit · P. Sobhon
Department of Anatomy, Faculty of Science, Mahidol University, Rama VI Road,
Bangkok 10400, Thailand
e-mail: sccwn@mahidol.ac.th

Introduction

The process of spermatogenesis in mammals involves the mitotic division of spermatogonia; the first meiotic division yields spermatocytes, and the second meiotic division gives rise to spermatids that differentiate into spermatozoa (Clermont 1972; Kerr 1992; Johnson 1995; De Kretser et al. 1998; Lombardi 1998). During the last step, which is called spermiogenesis, unique events take place that comprise the condensation of the nuclear chromatin (Lalli and Clermont 1981), formation of the acrosome (Leblond and Clermont 1952a; Clermont and Leblond 1955; Bernstein and Teichman 1972), virtual elimination of the cytoplasm, and development of the tail with the arrangement of mitochondria into a helical formation in the midpiece (Oko and Clermont 1991; Turner 2006).

During spermiogenesis in mammals, the somatic-type basic nuclear proteins (histones) are partly replaced by testis-specific lysine-rich histones, which consist of H1t, TH2A, TH2B, and TH3 (Oko et al. 1996; Steger et al. 1998; Ausio 1999). These proteins are then replaced by the more basic nuclear proteins enriched in arginines, termed transitional proteins (Moneisi 1971; Martinage et al. 1990). Finally, transitional proteins are replaced by protamines, which are proteins relatively rich in arginine and cysteine (Balhorn 1982; Roux et al. 1988; Le Lannic et al. 1993; Kistler et al. 1996). Protamines are believed to be the major factor that results in the final condensation and tight packaging of the chromatin, events that partly lead to the formation of a variety of shapes of sperm heads in several mammalian species (Calvin and Bedford 1971; Calvin 1976; Chevaillier 1983; Dadoune and Alfonsi 1986; Auger and Dadoune 1993; Brewer et al. 1999). In human sperm, protamines induce the coiling of the DNA molecules into a doughnut structure called a toroid. Each toroidal loop

contains about 500 bp of DNA, and the torus grows in size as subsequent loops bind to previous loops (Balhorn et al. 1999). In addition to nucleoprotamines, approximately 15% of the DNA in human sperm is still packaged by histones in the form of nucleosomal type fibers (Tanphaichitr et al. 1978). Apart from the toroidal model, which is believed to occur in human sperm, other patterns of packaging are also possible in other mammalian species. For example, the nucleoprotamine fibers may be packed laterally into a bundle-type structure as appears in rat sperm (Wanichanon et al. 2001).

Evolutionarily, the common tree shrew (*Tupaia glis*) is considered to be a primitive primate with many similar characteristics to those possessed by the ancestor of the present day primates (Poonkhum et al. 2000). Spermatogenesis and the stages of seminiferous epithelium have been studied by Maeda et al. (1996). However, to date, no data are available concerning the ultrastructure of differentiating male germ cells of the common tree shrew, particularly during spermiogenesis. Therefore, the objectives of this work have been to study the ultrastructural characteristics of spermiogenic cells of the common tree shrew, especially with regard to their chromatin organization and the profile of their basic nuclear proteins.

Materials and methods

Specimen collection

Adult common tree shrews (*Tupaia glis*) were captured in a tropical forest area in Thailand. A total of 10 animals (120–180 g body weight) were studied. They were anesthetized with ether, and then their testes were removed, fixed, and prepared for light- and electron-microscopic observations. Alternatively, pieces of tissues were prepared for immunohistochemical localization and profiling of basic nuclear proteins.

Histological and ultrastructural observations

Testes were fixed in Bouin's fixative overnight, after which they were dehydrated in graded ethanol and embedded in paraffin blocks. Sections were cut at a thickness of 5 μm and stained with hematoxylin and eosin. In order to investigate the ultrastructure of the germ cells, pieces of testes were fixed immediately in 4% glutaraldehyde and 2% paraformaldehyde in 0.1 M phosphate-buffered saline (PBS), pH 7.4 at 4°C, overnight, and then washed several times with PBS. Specimens were postfixed in 1% osmium tetroxide in 0.1 M PBS, at 4°C for 1 h, washed with the same buffer, dehydrated in increasing concentrations of ethanol, and embedded in Araldite 502 resin (Electron Microscopy Sciences, Fort Washington, PA). Semithin and thin sections were cut by using a MT-2 Porter-Blum ultramicrotome and then mounted on glass slides and copper grids, respectively. Semithin sections were stained with 1% methylene blue and observed by a Nikon Eclipse E600 light microscope (LM). Thin sections were stained with uranyl acetate and lead citrate and then observed by a Hitachi H-300 transmission electron microscope (TEM), operating at 75 kV.

The size of the chromatin fibers in each step of germ cell development was measured from electron-microscopic negatives in a Nikon Profile Projector and compared with the lattice intervals (~0.232 Å) of catalase crystals (Agar Aids, Stansted, UK) at the same magnifications. At least 10 cells at each stage were used for chromatin fiber measurements.

Extraction of basic nuclear proteins from nuclei of testicular cells

Fresh testes from adult animals were dissected, and the basic nuclear proteins were extracted according to Suphamungmee et al. (2005). Briefly, testes were homogenized in cold incubation buffer consisting of 3 mM $MgCl_2$, 0.31 M sucrose, 0.01% Triton X-100, 10 mM KH_2PO_4, pH 6.0, and 1 mM phenylmethane sulfonyl-fluoride (PMSF). The homogenate was centrifuged at 600*g*, at 4°C, for 10 min, and the supernatant was then discarded. The pellet was resuspended in a solution containing 0.15 M NaCl, 1% Triton X-100, 10 mM TRIS-HCl, pH 8.0, and 1 mM PMSF at 4°C. The suspension was placed on ice and sonicated six times for 15 s each, with a 15-s interval. Separation of the nuclei of the testicular cells from the tail debris was confirmed by viewing under a microscope. The nuclear suspension was washed twice in the washing buffer (5 mM $MgCl_2$, 5 mM NaH_2PO_4, pH 6.5) followed by centrifugation at 8,000*g*, at 4°C. The pellet was treated in a reducing solution (0.15 M NaCl, 10 mM dithiothreitol, 50 mM TRIS-HCl, pH 8.0) at 4°C, for 1 h. Thereafter, the nuclei were dissolved in 0.4 N hydrochloric acid and maintained at 4°C, for 2 h. The supernatant was removed after centrifugation at 12,000*g*, at 4°C, for 10 min, and the basic nuclear proteins were precipitated by 20% trichloroacetic acid. The precipitated proteins were then centrifuged at 12,000*g*, at 4°C, for 10 min. The pellet was washed twice in cold acidified acetone and in several changes of cold acetone. Finally, the protein pellet was dried in vacuum desiccators for 1 h and stored at −20°C until used.

Acid-urea-Triton X-100 polyacrylamide gel electrophoresis

Extracted basic nuclear proteins from the testes were dissolved in sample buffer (1 ml glacial acetic acid, 5.4 g urea,

0.5 ml β-mercaptoethanol, 0.1% pyronin-G in 4.5 ml deionized water). The protein concentration was determined by using bovine serum albumin as the standard (Lowry et al. 1951). The protein sample (15 μg per well) was carefully loaded onto acid-urea-Triton X-100 polyacrylamide gel (AUT gel; resolving gel: 15% acrylamide, 2.5 M urea, 6 mM Triton X-100, 5% acetic acid; stacking gel: 7.5% acrylamide, 2.5 M urea, 4 mM Triton X-100, 1.5% acetic

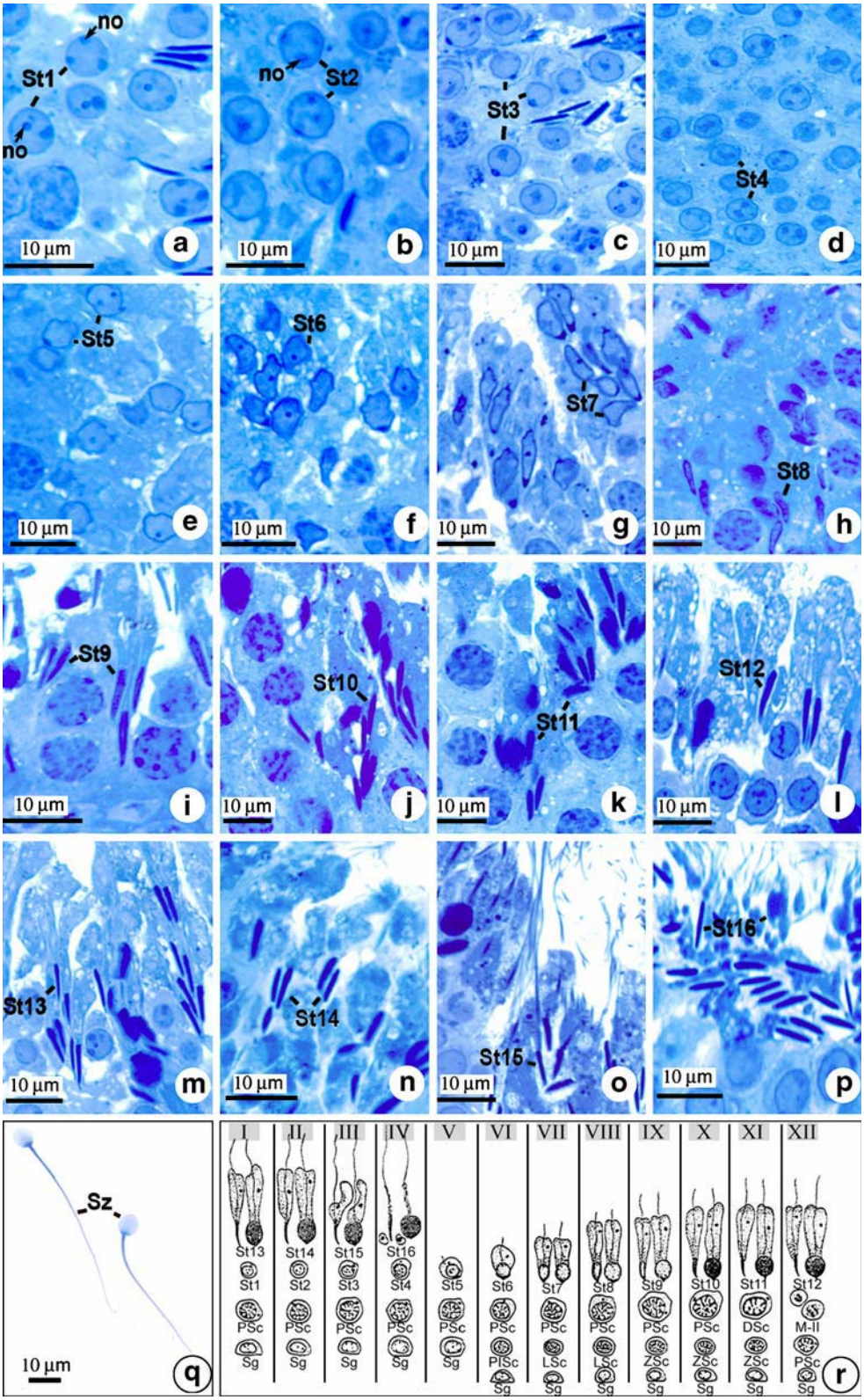


Fig. 1 Semithin sections stained with methylene blue showing the stages of seminiferous epithelium based on acrosome development and chromatin condensation during spermiogenesis. Developing spermatids (*St*) partly embedded in the cytoplasm of Sertoli cells are classified into the Golgi phase (*St1-St2* in **a**, **b**), cap phase (*St3-St5*in **c**–**e**), early acrosome phase (*St6-St8* in **f**–**h**), mid acrosome phase (*St9-St11* in **i**–**k**), late acrosome phase (*St12-St14* in **l**–**n**), and maturation phase (*St15-St16* in **o**, **p**). Whole-mounts of mature spermatozoa (*Sz* in **q**) demonstrate the discoid shape of the head. The 12 stages of cellular association of seminiferous epithelium in the *T. glis* testis, as modified from Maeda et al. 1996, are also shown in **r**

acid) in a 8×10 cm Hoefer vertical slab gel electrophoretic apparatus fitted with 0.75-mm spacers (Amersham Biosciences, USA; as modified from Panyim and Chalkley 1969). The separation was carried out in an electrophoretic buffer (0.9 N acetic acid) at 120 V, for 1.5 h. The bands of basic nuclear proteins were detected by Coomassie blue staining. Basic nuclear proteins similarly prepared from chick erythrocyte nuclei and human testicular nuclei were run under the same conditions and used for comparison.

Western blot analysis of basic nuclear proteins

Basic nuclear proteins separated in AUT gel were electrophoretically transferred onto nitrocellulose membrane (Amersham Biosciences, Buckinghamshire, UK) in an electrophoretic transfer chamber (LKB Bromma, Hoefer Scientific Instruments, San Francisco, Calif.) with the current set at 400 mA, for 4 h, in cold transfer buffer (0.9 N acetic acid). Non-specific binding was blocked with

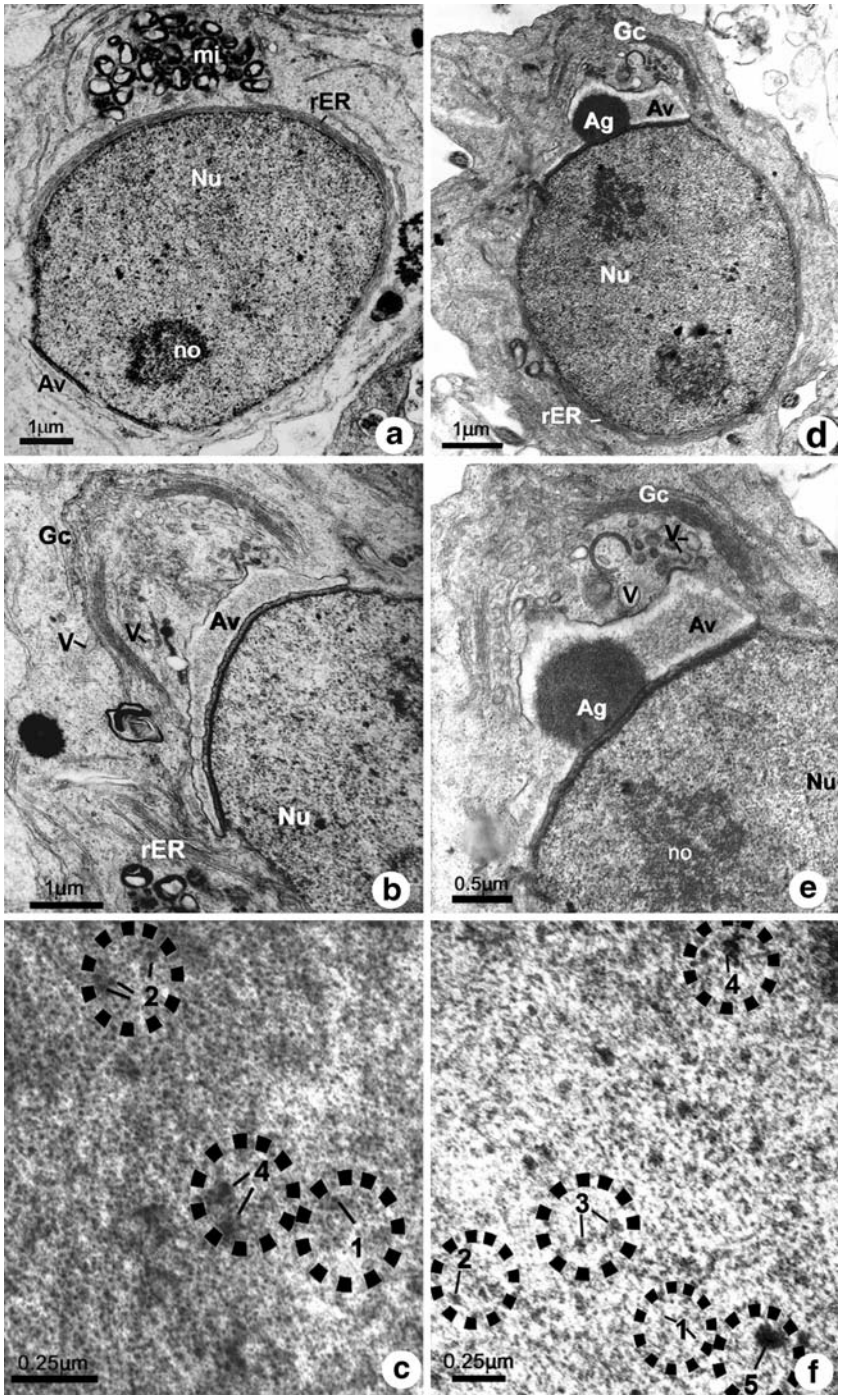


Fig. 2 **a–c** Ultrastructure of the early round spermatids in the Golgi phase (steps 1–2) showing many mitochondria (*mi*) and the nucleus (*Nu*) with a prominent nucleolus (*no*). The Golgi complex (*Gc*) is a conspicuous structure in close association with proacrosomal vesicles (*V*). The nucleus contains chromatin fibers (**c**) with diameters of 10 nm (*circle 1*), 30 nm (*circle 2*), and 50–60 nm (*circle 4*). **d–f** Longitudinal sections of the cap phase spermatids (steps 3–5) showing the round nucleus (*Nu*) surrounded by rough endoplasmic reticulum (*rER*). The Golgi complex (*Gc*) is prominent and shows many proacrosomal vesicles (*V*). These vesicles fuse together to form the large cap of the acrosomal vesicle (*Av*), which contains a large acrosomal granule (*Ag*) attached to the inner acrosomal membrane. A higher magnification (**f**) shows five types (levels) of chromatin fibers dispersed throughout the nucleus: the 10-nm (*circle 1*) and the 30-nm (*circle 2*) fibers are most abundant, whereas fewer 40–45 nm (*circle 3*), 50–60 nm (*circle 4*), and 70-nm (*circle 5*) fibers are seen

5% skim milk in 10 mM TRIS-buffered saline, pH 7.4, containing 0.1% Tween-20 (TBST), and then the membranes were incubated in mouse monoclonal antibody raised against human protamine P1N (1:500 dilution) or rabbit polyclonal antibody to chick-histone H3 (1:500 dilution) for 1 h at room temperature. For the negative control, the membrane strips were incubated with preimmune sera instead of the primary antibody. After being washed with TBST, the membranes were incubated in goat anti-mouse IgG or mouse anti-rabbit IgG conjugated to horseradish peroxidase (Zymed laboratories, San Francisco, Calif.) in TBST (1:2,000 dilution), for 30 min at room temperature. The color reaction was visualized by using diaminobenzidine as a chromogenic substrate (Sigma-Aldrich, Saint Louis, Mo.) and 0.013% H_2O_2.

Indirect immunofluorescence staining of basic nuclear proteins in testicular cells

Testes were dissected and fixed in a solution containing 0.5% glutaraldehyde, 4% paraformaldehyde in 0.1 M phosphate buffer, pH 7.4, at 4°C, for 2 h. Following a washing step in the same buffer, the specimens were dehydrated in an ethanol series and embedded in LR white resin (Electron Microscopy Sciences). Semithin sections were cut by using a MT-2 Porter-Blum ultramicrotome fitted with glass knives, picked up, and placed on the gelatin-coated glass slides. Non-specific binding was blocked by incubating the tissue sections with 0.15 M glycine and with 4% bovine serum albumin (Sigma-Aldrich). The sections were then incubated with rabbit polyclonal antibody against chicken-H3 (1:50 dilution) or mouse monoclonal antibody against human-protamine, P1N fraction (1:100 dilution) for 1 h, at 37°C, and then treated with fluorescein-isothiocyanate (FITC)-conjugated goat anti-rabbit IgG or rabbit anti-mouse IgG (Zymed laboratories) as secondary antibodies, for 30 min, at 37°C, followed by observation under a fluorescence microscope. Negative control sections were processed similarly but were incubated with preimmune sera in place of the primary antibodies.

Results

Testes of the common tree shrew were oval in shape and covered by a layer of tunica vaginalis on the anterior surface. The seminiferous tubules with the interstitial (Leydig's) cells were covered by a layer of tunica albuginea, a dense fibrous connective tissue capsule that was thickened on the posterior surface of the testes, whereas a layer of tunica vasculosa was not observed in any sections. In contrast to other mammals, the tunica albuginea did not extend inward to form the connective tissue septae dividing the testis into lobules.

The cycle of seminiferous epithelium in the common tree shrew was classified into 12 stages (Fig. 1r) as reported earlier by Maeda et al. (1996), and each cross section of the seminiferous tubule represented a single stage of cellular association. As in other mammals, the basal compartment of the epithelium contained the preleptotene and leptotene steps of primary spermatocytes, whereas the adluminal compartment contained the middle steps of differentiating cells from the zygotene and pachytene steps of primary spermatocytes up to spermatids.

Table 1 Summary of six orders of chromatin organization (*Levels 1–6*), as appearing in various stages of spermatids of the common tree shrew (*SE* standard error of mean, − absent)

Spermiogenic cells	Chromatin fibers (diameter±SE)					
	Level 1 (10 nm)	Level 2 (30 nm)	Level 3 (40–45 nm)	Level 4 (50–60 nm)	Level 5 (70 nm)	Level 6 (80–100 nm)
Golgi phase spermatids (steps 1–2)	10.14±0.11	29.60±0.12	–	54.04±1.59	–	–
Cap phase spermatids (steps 3–5)	10.19±0.09	29.75±0.16	41.13±1.84	–	70.02±0.08	–
Early acrosome phase spermatids (steps 6–8)	10.03±0.07	29.60±0.31	–	56.97±2.95	69.92±0.11	–
Mid acrosome phase spermatids (steps 9–11)	–	–	41.12±2.31	–	69.65±0.18	–
Late acrosome phase spermatids (steps 12–14)	–	–	–	–	–	88.49±4.19
Maturation phase spermatids (steps 15–16)	Complete condensation					

Histological and ultrastructural characteristics of spermiogenic cells

As in other mammals, four phases of spermatid differentiation could be distinguished according to acrosome development and the pattern of chromatin condensation in the nucleus, i.e., Golgi phase, cap phase, acrosome phase, and maturation phase. Based on observations at the LM and TEM levels, these four phases of spermatids of the common tree shrew could be subdivided into 16 steps (Fig. 1).

Golgi phase (steps 1–2) These spermatids were characterized by the presence of spherical nuclei (~7 μm in diameter) with prominent nucleoli (Figs. 1a,b, 2a). Golgi apparatus was conspicuous and associated with small membrane-bound vesicles that were possible precursors of

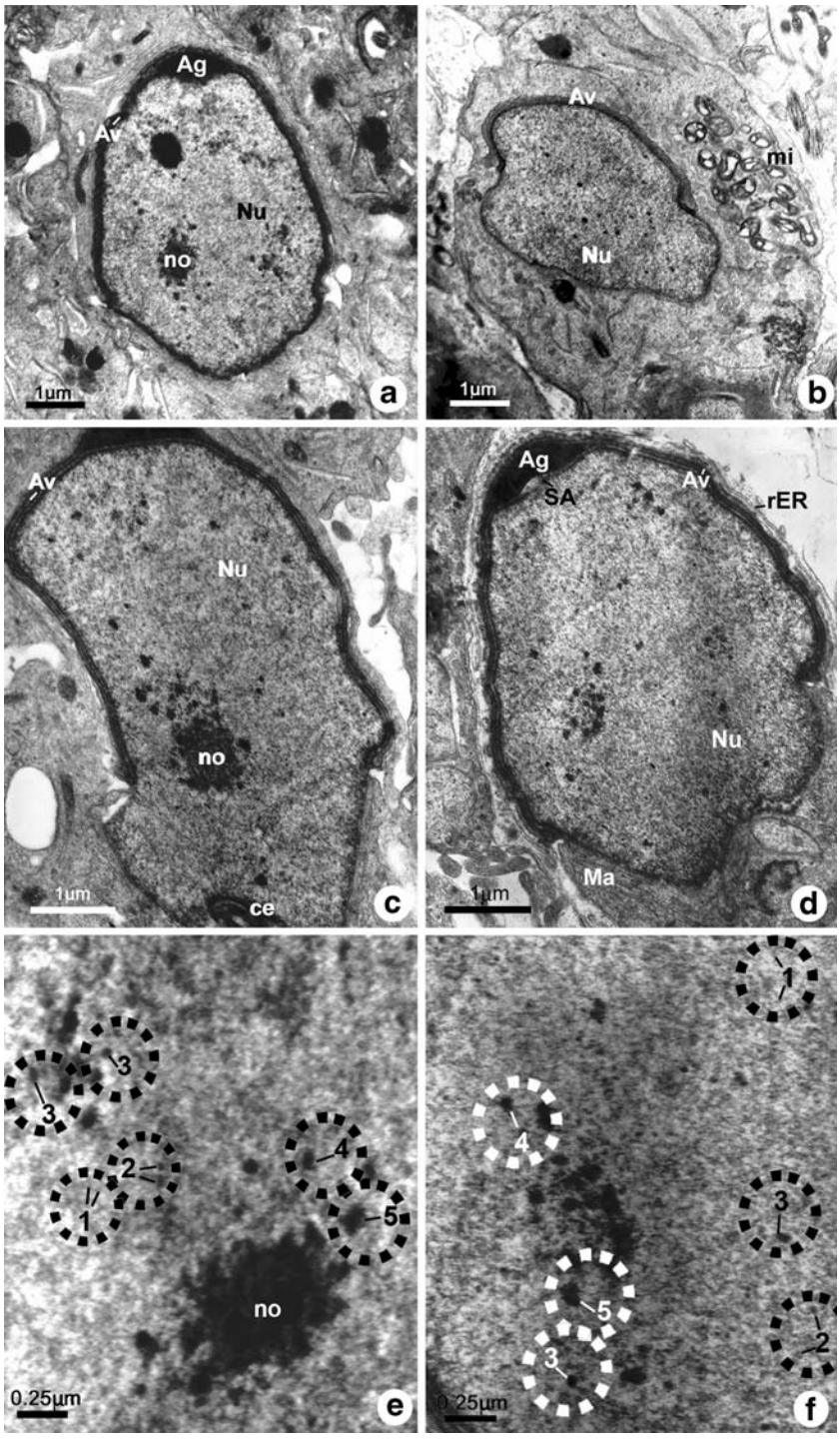


Fig. 3 **a**, **b** Early acrosome phase spermatids (steps 6–8) demonstrating nuclear elongation (*Nu*). The acrosomal cap (*Av*) extends backward to the sides of the nucleus, and mitochondria (*mi*) still aggregate adjacent to one pole of the nucleus. **c**, **d** During caudal extension of the acrosomal cap, the subacrosomal space (*SA*) is observed beneath the entire acrosome. Microtubular manchettes (*Ma*) first appear at the caudal end of nucleus, and the proximal centriole (*ce*) is attached at the distal end of the nucleus. **e**, **f** The nuclear chromatin in this phase shows five levels of chromatin fibers: the 10-nm (*circle 1*) and 30-nm (*circle 2*) fibers are numerous, whereas the 40–nm to 45-nm (*circle 3*), 50–nm to 60-nm (*circle 4*), and 70-nm (*circle 5*) fibers are more sparse (*no* nucleolus)

the proacrosomal vesicles (Fig. 2b). Mitochondrial clusters were located near the Golgi apparatus. Rough endoplasmic reticulum was present throughout the cytoplasm (Fig. 2a,b). Within the nucleus, chromatin was dispersed homogeneously and showed dense circular masses possibly representing the reappearing nucleoli (Figs. 1a,b, 2a). The chromatin fibers could be classified into three groups (levels): (1) the fine 10-nm fibers that were the major component of euchromatin in the nucleus, (2) the 30-nm fibers, which were dispersed throughout the nucleoplasm and appeared in smaller quantities, amd (3) the largest fibers (50–60 nm in diameter) surrounding the heterochromatin mass, which was composed of clusters of the 30-nm fibers (Fig. 2c, Table 1). At step 2 of this phase, the membrane-bound vesicles from the Golgi apparatus began to fuse together forming a large acrosomal vesicle (Fig. 2b). The chromatin appeared denser, especially along the inner surface of the nuclear envelope, whereas the nucleolus became less prominent (Figs. 1b, 2b).

Cap phase (steps 3–5) Cells in this phase were characterized by the presence of acrosomal vesicles that increased further in size and covered the apical pole of their nuclei (Figs. 1c-e, 2d-f). A layer of electron-dense material was attached to the inner surface of the acrosomal vesicle. An acrosomal granule was produced and appeared as a large dense body associated with the center of the inner acrosomal membrane (Fig. 2d–f). The enlarged acrosome with the acrosomal granule finally formed a cap-like structure covering the anterior pole of the nucleus, and only a narrow subacrosomal space was present between the inner acrosomal membrane and the nuclear membrane (Fig. 2f). The nucleus itself remained spherical (7–8 μm in diameter) and contained chromatin fibers that became thicker. The majority of fibers were at the levels of 10 nm and 30 nm and were dispersed throughout the nucleus (Fig. 2f). Thicker chromatin fibers with diameter of 40–45 nm and fewer fibers at 50–60 nm and 70 nm started to appear (Fig. 2f, Table 1).

Early acrosome phase (steps 6–8) The cell and nucleus began to elongate (Fig. 1f–h). The narrow electron-dense acrosome expanded over the anterior half of the nucleus (Fig. 3a–c). The proximal centriole was located in the depression at the caudal end of the nucleus (Fig. 3c). A microtubular manchette appeared in the cytoplasm adjacent to the nuclear membrane (Fig. 3d). The mass of cytoplasm, containing mitochondria, began to move caudally. At the

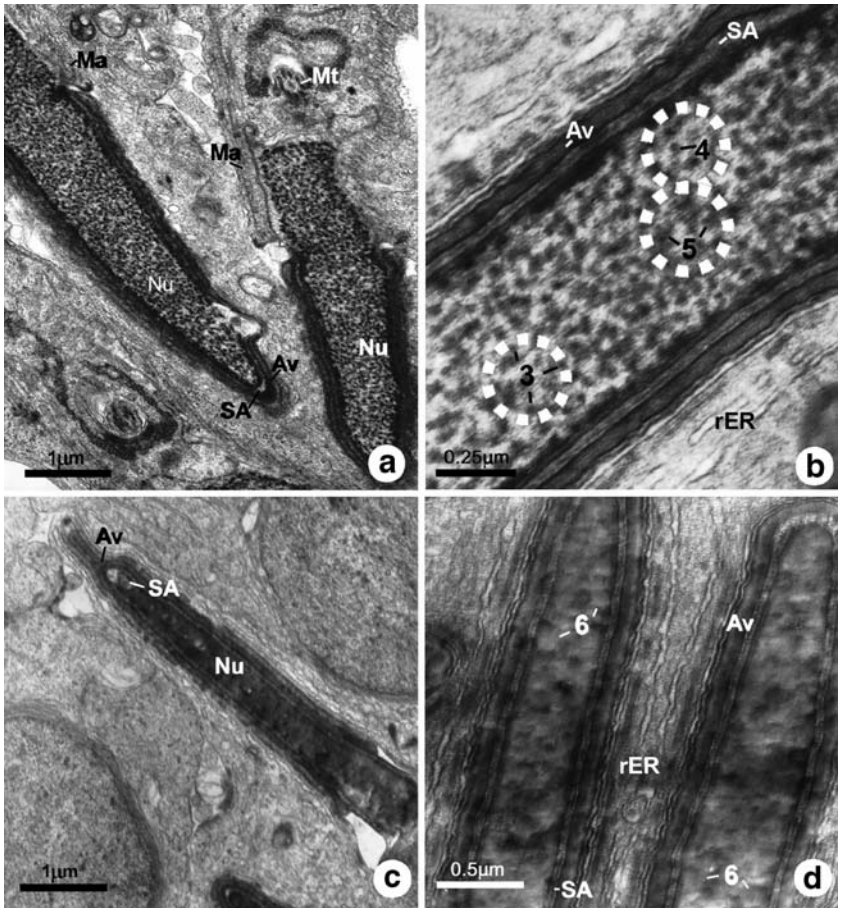


Fig. 4 **a**, **b** Mid acrosome phase spermatids (steps 9–11) showing the acrosome (*Av*) covering the apical pole of the nucleus (*Nu*), which becomes progressively elongated and highly condensed. Microtubular manchettes (*Ma*) are seen adjacent to the caudal half of the nucleus (*Mt* microtubular axoneme, *SA* subacrosomal space). The nucleus contains chromatin fibers with thicknesses of 40–45 nm (*circle 3*), 50–60 nm (*circle 4*), and 70 nm (*circle 5*). **c**, **d** Longitudinal sections of late acrosome phase spermatids (steps 12–14) displaying the more elongating and condensing nucleus covered by an acrosome (*Av*). Chromatin fibers in the nucleus (*Nu*) become larger at 80–100 nm (*6*) in thickness. Rough endoplasmic reticulum (*rER*) still appears to surround the acrosome and nucleus

LM level, the nuclear material appeared to become increasingly denser (Fig. 1f–h); as revealed by TEM, the chromatin fibers appeared in five levels, i.e., with the majority still at 10 nm and 30 nm, but with thicker fibers at 50 nm, 60 nm, and 70 nm increasing in number (Fig. 3e,f, Table 1), and 40-nm to 45-nm fibers being present in smaller quantities.

Mid acrosome phase (steps 9–11) The nucleus and acrosome continued to elongate to such an extent that the nucleus assumed a distinctive wedge shape (Fig. 1i–k). The acrosome became condensed and assumed an arrow-shape that extended over the entire rostral end of the nucleus (Fig. 4a,b). At the last step of this phase, nuclear elongation reached its greatest length (Fig. 1k). At the LM level, the nuclear material appeared dense (Fig. 1i–k), and as revealed by TEM, the chromatin consisted of 70-nm knobby fibers disposed along the nuclear membrane, whereas the 10-nm and 30-nm fibers had disappeared. However, the majority of chromatin was made up of 40–45 nm fibers and a smaller amount of 50–60 nm fibers, most of which appeared as dense cords distributed throughout the nucleus (Fig. 4b, Table 1). Some rough endoplasmic reticulum surrounded the acrosome and nuclear membrane (Fig. 4b). The microtubular manchette continued to extend from the posterior end of the acrosome to the caudal end of the nucleus (Fig. 4a). The cytoplasmic mass containing the mitochondria continued to move to the caudal end of the cell (Fig. 5a).

Late acrosome phase (steps 12–14) The spermatids in this phase were characterized by highly elongated heads that became slimmer than those of the earlier steps (Fig. 1l–n, 4c,d). The cytoplasmic mass continued to move caudally, leaving only a small amount over the acrosome (Fig. 4c). The main body of the acrosome remained at the rostral end of the nucleus, but its lateral margins extended over the caudal end of the nucleus (Fig. 4c–d). At the LM level, the nuclear material appeared to be completely dense (Fig. 1l–n); TEM revealed that most chromatin fibers occurred as large 80-nm to 100-nm knobby fibers that became closely packed (Fig. 4d, Table 1).

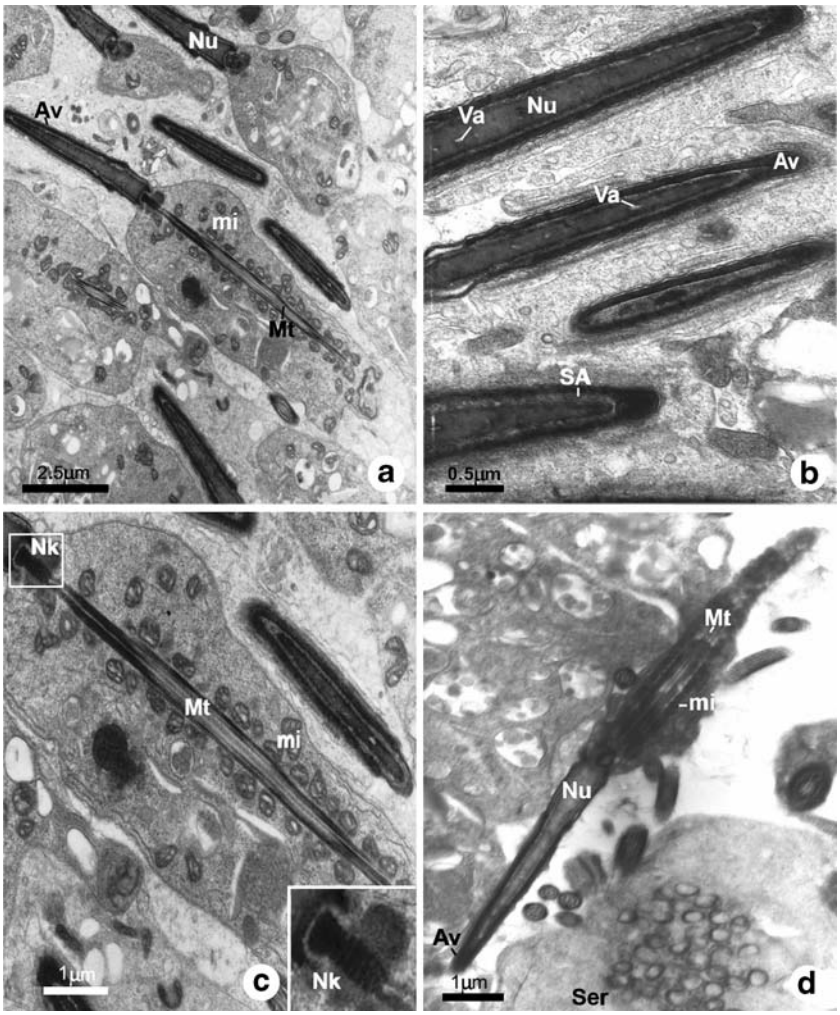


Fig. 5 **a**, **b** Maturation phase spermatids (steps 15–16) demonstrating the complete condensation of chromatin within the nucleus (*Nu*). The acrosome (*Av*) is clearly visible with its underlying subacrosomal space (*SA*). The nucleus contains a few vacuoles (*Va*). **c** Higher magnification of the tail showing the small amount of intact cytoplasm that moves caudally. The neck (*Nk*) is located at the caudal end of the nucleus and attached to the tail axoneme. Numerous mitochondria (*mi*) are present around the microtubular axoneme (*Mt*) of the tail. *Inset* Detail of the neck region in the *boxed area*. **d** Longitudinal section of a spermatozoon released from the cytoplasm of a Sertoli cell (*Ser*). The head contains completely condensed chromatin and only a few vacuoles in the nucleus (*Nu*). At the midpiece, mitochondria (*mi*) are packed as a mitochondrial sheath around an axoneme (*Mt*)

Maturation phase (steps 15–16) The spermatids in this phase showed similar ultrastructural characteristics to those of mature spermatozoa (Figs. 1o-p, 5a-c). Chromatin fibers coalesced into a dense mass, but the nucleus still contained small electron-lucent vacuoles within the increasingly compact chromatin (Fig. 5b). All the cytoplasmic mass was relocated to the posterior end of the nucleus and became the residual body (Figs. 1o-p, 5a,c). The fully formed tail showed the helically arranged mitochondria surrounding a column of the outer dense fibers and an axoneme (Fig. 5a,c).

Mature spermatozoa The spermatozoa were freely distributed in the lumen of the seminiferous tubule after shedding their residual cytoplasm and being released from the apical cytoplasm of the Sertoli cells (Fig. 5d). In whole-mounts, the head had a discoidal shape of approximately 6×9 μm (Fig. 1q), whereas in side view, the head was a thin wedge-shaped structure (Fig. 5d). The nucleus contained electron-opaque chromatin covered with the fully developed acrosome. Only a few small vacuoles remained in the completely condensed chromatin. The tail was approximately 95–98 μm in length (Fig. 1q) and comprised the neck with the proximal centriole, the connecting piece, and the midpiece containing a sheath of mitochondria surrounding the outer dense fibers and the 9+2 microtubular doublets (Fig. 5d). In the principal piece, the fibrous sheath, instead of the mitochondrial sheath, covered the outer dense fibers and the axoneme, whereas the end piece had the same structure as the principal piece but lacked the fibrous sheath.

Characterization of the basic nuclear proteins

Profile of basic nuclear proteins

Basic nuclear proteins from the nuclei of the testicular cells of the tree shrew were separated in 15% AUT gel (Fig. 6, lane 3). Most bands, i.e., H2A, H3, H2B, H4, and H1, exhibited identical mobilities to those from chick erythrocyte nuclei (Fig. 6, lane 1) and human testicular nuclei (Fig. 6, lane 2), which were used as references. No equivalent band to chick-H5 was present. However, a band with high basicity was seen at the bottom of the gel with slightly slower mobility than human protamine (Fig. 6, lane 3), implying that the protamines of the tree shrew had a smaller amount of basic amino acids.

Western blotting of histone H3 and protamine

When tree shrew basic nuclear proteins from the nuclei of testicular cells were blotted and probed with anti-chick-H3, only the H3 band exhibited positive immunoreactivity

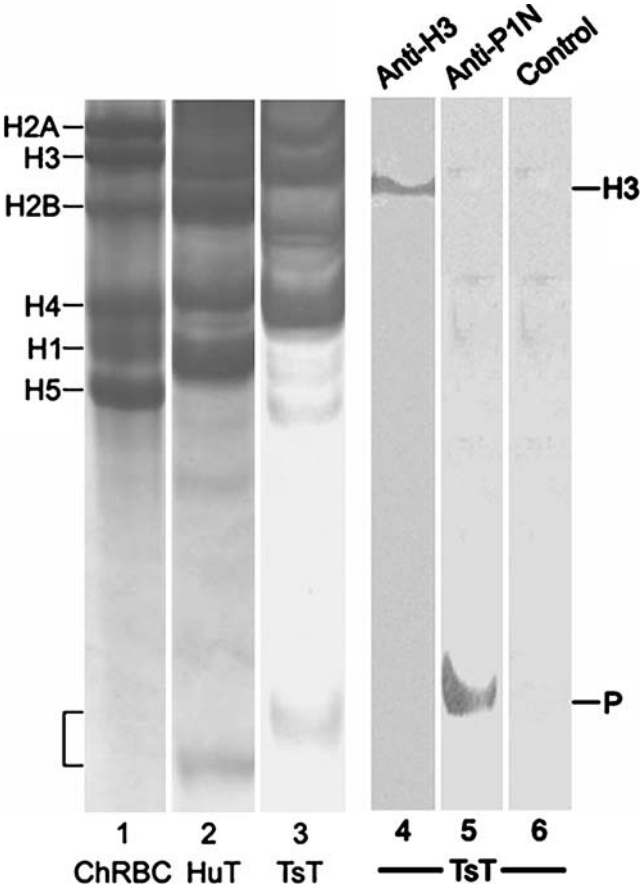


Fig. 6 Acid-urea-Triton X-100 polyacrylamide gel electrophoresis (15%) of basic nuclear proteins: basic nuclear proteins extracted from chick erythrocyte nuclei (*ChRBC*, reference histones; *lane 1*), from human testis (*HuT*; *lane 2*), and *T. glis* testis (*TsT*; *lane 3*). *Lanes 4–6* Western blotting of extracted proteins from the tree shrew testis (*TsT*) probed with rabbit antiserum against chick H3 (*lane 4*) and mouse antiserum against human protamine P1N (*lane 5*). Strong reactions of the anti-H3 (*Anti-H3*) and anti-P1N (*Anti-P1N*) antibodies are detected at the *H3* and protamine (*P*) bands of the tree shrew testis, respectively. The negative control (*lane 6*) shows no immunoreactivity

(Fig. 6, lane 4). The band at the bottom also showed positive immunoreactivity to the anti-human-protamine probe (Fig. 6, lane 5). In the negative control, no positive band was detected (Fig. 6, lane 6). These results indicated the presence of homologous basic nuclear proteins in human, chick, and tree shrew.

Immunofluorescence staining for histone-H3 and protamine in testicular cells

Immunostaining with the anti-H3 antiserum resulted in intense fluorescence in the nuclei of Sertoli cells and spermatogonia lining the basement membrane of the seminiferous tubules (Fig. 7b,c). Primary spermatocytes, especially those at the pachytene stage, also exhibited fluorescence in their nuclei (Fig. 7d–f). A uniformly intense immunofluorescence was present in the early round

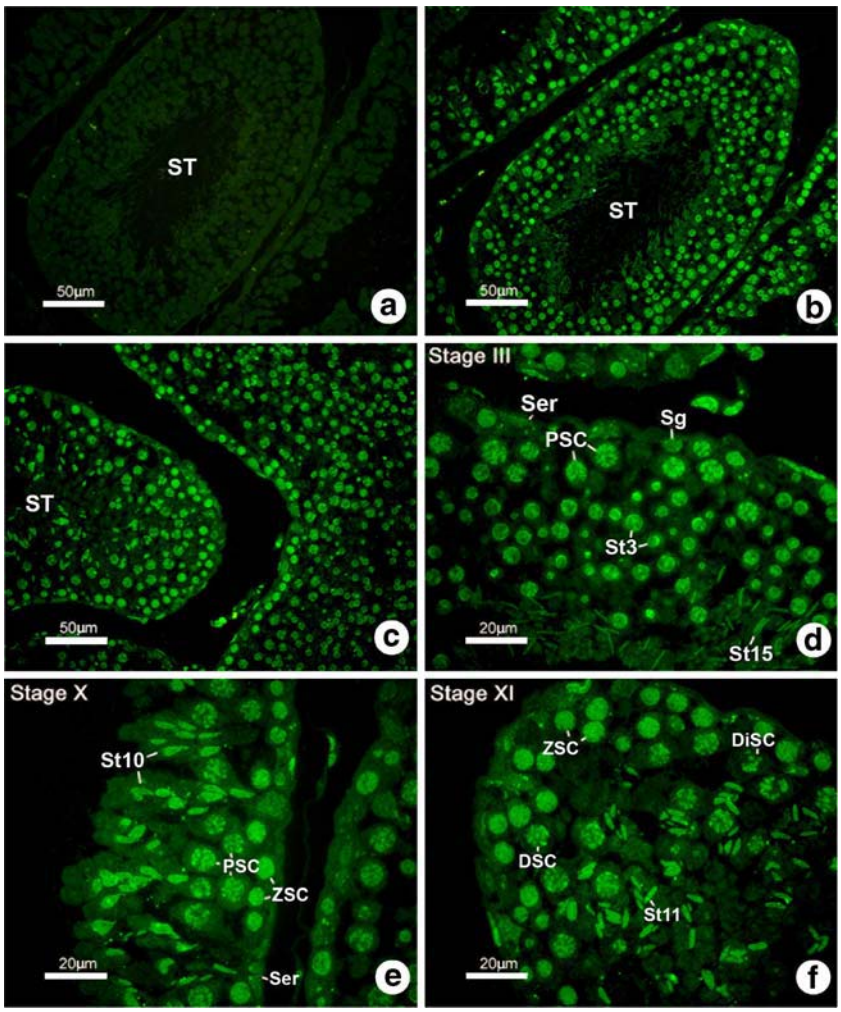


Fig. 7 **a–f** Immunofluorescence images of *T. glis* seminiferous tubules (*ST*) stained with anti-H3 serum. **a** Negative control showing no immunoreactivity. **b–f** Immunoreactivity is found in all spermatogenic cells. Positive fluorescence decreases in the nuclei of mature spermatids (*Ser* Sertoli cell, *Sg* spermatogonia, *ZSC* zygotene spermatocyte, *PSC* pachytene spermatocyte, *DSC* diplotene spermatocyte, *DiSC* diakinetic spermatocyte, *St* spermatid, *numbers* steps)

spermatid nuclei (steps 1–5) and elongating spermatids (steps 6–14; Fig. 7e,f). In the late stages of spermatids (steps 15–16), anti-H3 immunofluorescence decreased (Fig. 7d) and almost disappeared in the last step of spermatids and mature spermatozoa. No immunofluorescence was found in the nuclei of any of the germ cells or Sertoli cells in the negative control (Fig. 7a).

When the anti-protamine antiserum was used for immunostaining, intense fluorescence was detected only in steps 12–16 of spermatids, whereas nuclei of all spermatogenic cells and early spermatids were not stained (Fig. 8b–f). In the negative control, no immunoreactivity was seen in the nuclei of any of the germ cells or somatic cells (Fig. 8a).

Discussion

General histology of the testes of the common tree shrew

The testes of the tree shrew lie in a prepenial position, which differs from that of other primates whose testes are in a postpenial position (Collins et al. 1982). The general histology of the tree shrew testes and stages of the cycle of seminiferous epithelium are similar to those described for other mammals (Kerr 1992). Each cross section of the seminiferous tubule shows only one stage of the cycle of seminiferous epithelium as found in the rat (Clermont 1972; Kerr 1992). However, the cycle is divided into 12 stages, whereas eight stages have been described in human (Clermont 1963), 14 stages in the rat (Leblond and Clermont 1952b), and 13 stages in the hamster (Mething 1998).

The process of spermiogenesis in the tree shrew is, in general, similar to that of other mammals (Clermont and Leblond 1955; Lalli and Clermont 1981). The four phases are based on acrosomal formation and the degree of chromatin condensation, i.e., Golgi, cap, acrosome, and maturation phases. The proacrosomal vesicles are synthesized and released from the Golgi complex in the Golgi phase spermatids and later fuse together to form a large acrosomal vesicle at the apical pole of the nucleus. Concurrent with the formation of the acrosomal vesicle,

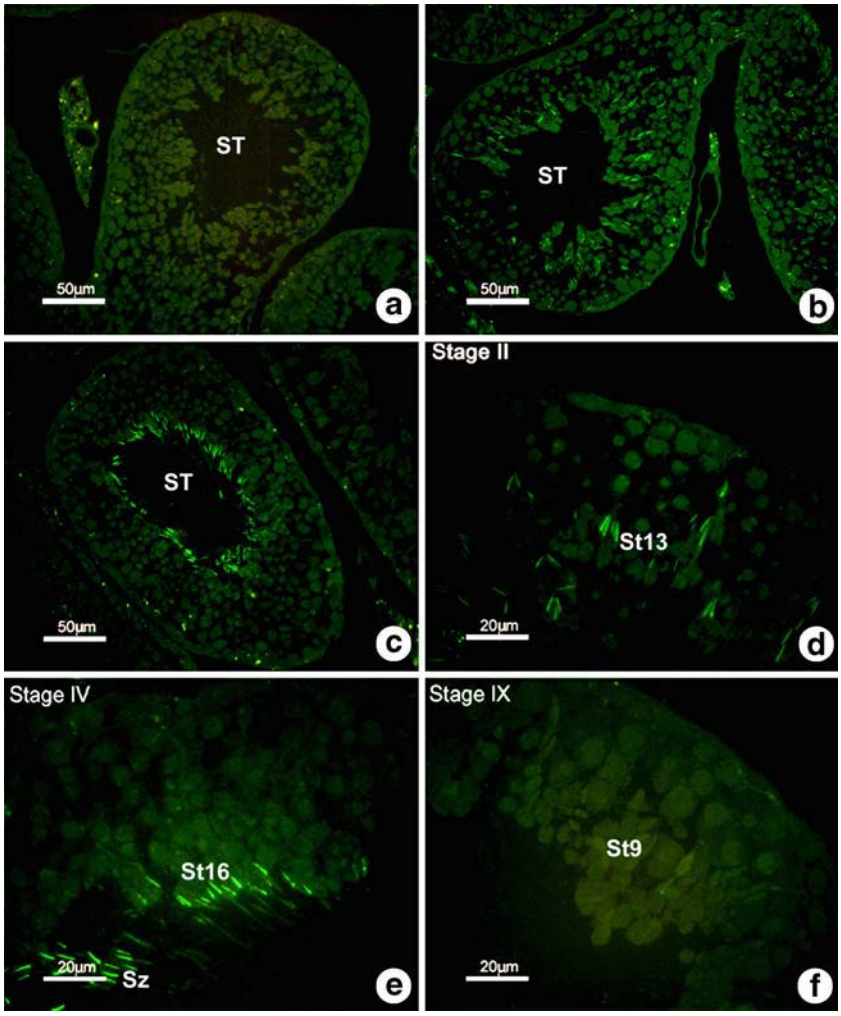


Fig. 8 **a–f** Immunofluorescence staining in seminiferous tubules (*ST*) with the anti-protamine serum reveals intense immunoreactivities only in late spermatid steps (*St* spermatid, *Sz* spermatozoa, *numbers* steps). No immunoreactivity is observed in the negative control (**a**)

electron-dense materials inside the vesicle coalesce to form a large acrosomal granule, which is a characteristic of step 1 spermatids of the common tree shrew. The acrosomal vesicles then transform into a large cap that extends backward to cover the side of the nucleus; this characteristic is consistent with other mammalian sperm, including those of man, boar, and rabbit (Fawcett 1965). In the common tree shrew, early spermatids possess a small subacrosomal space, which lies between the inner acrosomal membrane and the outermost membrane of the nuclear envelope, as seen in the sperm of primates and human. In contrast, in rodents, a relatively large pyramidal subacrosomal space extends backward along the side of nucleus. This space contains perithecal materials that form a structure called the perforatorium (Lalli and Clermont 1981; Oko and Clermont 1990, 1991; Fornes and Bustos-Obregon 1994).

The nuclear chromatin in the spermatogonia and all spermatocytes of the common tree shrew exhibits fundamental fibers of 10 nm and 30 nm. Condensation into large heterochromatin blocks in these cellular stages is accomplished by the winding of the 30-nm fibers. This pattern of chromatin condensation appears to be universal in early germ cells of all mammalian species including the common tree shrew. In contrast, the patterns of chromatin organization and packaging during spermiogenesis are unique to each species (Chevaillier 1983). In *T. glis*, condensation starts by the transformation of the 10-nm and 30-nm fibers in the Golgi phase spermatid (steps 1) into the highly compact and knobby 50-nm to 60-nm fibers in the late Golgi phase (step 2). In the cap phase (steps 3–5), 10-nm and 30-nm fibers are still present, although most fibers have been transformed into higher ordered fibers of 40–45 nm and 50–60 nm, the larger knobby fibers being 70 nm (possibly transformed from the 50–nm to 60-nm fibers in earlier steps). The subsequent transformation of chromatin fibers continues in the early acrosome phase (steps 6–8) as is evident by both the presence of small 10-nm and 30-nm fibers and the increasing number of the larger sized 40–nm to 45-nm, 50–nm to 60-nm, and 70-nm fibers. Eventually, all chromatin appears in the form of the 40–nm to 45-nm, 50–nm to 60-nm, and 70-nm fibers in the mid acrosome

phase (steps 9–11). The 70-nm fibers might be transformed into the largest ordered fibers with a thickness about 80–100 nm in the late acrosome phase (steps 12–14). In addition, the condensation of the chromatin begins at the rim of the nuclear envelope and at the subacrosome region, later progressing toward the central part of the nucleus. In the maturation phase, especially the last two steps of spermatid development (steps 15–16), the highest ordered fibers (80–100 nm) become completely condensed and coalesce with each other, with only a few small vacuoles remaining in between them. These structures have also been observed in the nuclei of mature spermatozoa. The transformation from 30-nm to the multi-step, higher ordered, knobby fibers, which appear granulo-fibrillar in cross sections, is similar to that found in human spermatids in which toroids of 50–100 nm form after protamines replace histones in the 30-nm fibers (Brewer et al. 1999; Balhorn et al. 1999, 2000). These toroids are actually parts of the knobby fibers that become tightly packed in the maturation phase spermatids and spermatozoa (Holstein 1976). Whether the final higher order of chromatin in the spermatids and spermatozoa of the tree shew contain toroidal structures remains to be established.

Profiling and immunolocalization of the basic nuclear proteins

Analysis by AUT electrophoresis has shown that the histone-protamine compositions in the nuclei of the testicular cells of the tree shrew are similar to those of human (Prigent et al. 1996; Van Roijen et al. 1998) but probably with a smaller amount of protamines. Immunostaining with anti-H3 has revealed that H3 is present in the nuclei of spermatogonia, spermatocytes, most steps of spermatids, and Sertoli cells. Immunoblotting with anti-chick-H3 has detected immunoreactive H3 proteins in the tree shrew suggesting that H3, which is one of the nucleosomal core histones, is highly conserved. However, the amount of this histone, as reflected by the intensity of the fluorescence, decreases in the final steps of spermatids (steps 15–16) and almost completely disappears in spermatozoa. In contrast, immunostaining with anti-human protamine is intense in late spermatids and spermatozoa, whereas earlier stages of the germ cells are not stained. This result indicates the high degree of homology to human protamine; the presence of this protein in late stage spermatids and mature spermatozoa of the tree shrew is also similar to that reported in rat and human (Le Lannic et al. 1993; Kistler et al. 1996; Prigent et al. 1996; Steger 1999). Hence, in tree shrew, protamines are believed to be amongst the major nucleoproteins that play a role in the final condensation of chromatin in the nuclei from late spermatids to mature spermatozoa, as is the case in human and other mammals.

Acknowledgements We are grateful to Prof. Rod Balhorn, Lawrence Livermore National Laboratory, California, for kindly providing the monoclonal antibody against human-protamine, HuP1N fraction, and to Dr. Sirikul Manochantr, Thammasat University, Thailand, for providing the polyclonal antibody to chick-H3.

References

Auger J, Dadoune JP (1993) Nuclear status of human sperm cells by transmission electron microscopy and image cytometry: changes in nuclear shape and chromatin texture during spermiogenesis and epididymal transit. Biol Reprod 49:166–175

Ausio J (1999) Histone H1 and evolution of sperm nuclear basic proteins. J Biol Chem 274:31115–31118

Balhorn R (1982) A model for the structure of chromatin in mammalian sperm. J Cell Biol 93:298–305

Balhorn R, Cosman M, Thornton K, Krishnan VV, Corzett M, Bench G, Kramer C, Lee JD IV, Hud NV, Allen MJ, Prieto M, Meyer-Iese W, Brown JT, Kirz J, Zhang X, Bradbury EM, Maki G, Braun RE, Breed W (1999) Protamine mediated condensation of DNA in mammalian sperm. In: Gagnon C (ed) The male gamete: from basic science to clinical applications. Cache River, Vienna, pp 55–70

Balhorn R, Brewer L, Corzett M (2000) DNA condensation by protamine and arginine-rich peptides: analysis of toroid stability using single DNA molecules. Mol Reprod Dev 56:230–234

Bernstein MH, Teichman RJ (1972) Regional differentiation in the heads of spermatozoa of rabbit, man and bull. Am J Anat 133:165–178

Brewer LR, Corzett M, Balhorn R (1999) Protamine-induced condensation and decondensation of the same DNA molecule. Science 286:120–123

Calvin HI (1976) Comparative analysis of the nuclear basic proteins in rat, human, guinea pig, mouse and rabbit spermatozoa. Biochim Biophys Acta 434:377–389

Calvin HI, Bedford JM (1971) Formation of disulfide bonds in the nucleus and accessory structures of mammalian spermatozoa during maturation in the epididymis. J Reprod Fertil 13:65–75

Chevaillier P (1983) Some aspects of chromatin organization in sperm nuclei. In: Andre J (ed) The sperm cell: fertilizing power, surface properties, motility, nucleus and acrosome, evolutionary aspects. Nijhoff, London, pp 179–196

Clermont Y (1963) The cycle of the seminiferous epithelium in man. Am J Anat 112:35–51

Clermont Y (1972) Kinetics of spermatogenesis in mammals: seminiferous epithelium cycle and spermatogonial renewal. Physiol Rev 52:198–236

Clermont Y, Leblond CP (1955) Spermiogenesis of man, monkey, ram and other mammals as shown by the periodic acid-Schiff technique. Am J Anat 96:229–253

Collins PM, Thang WN, Lofts B (1982) Anatomy and function of the reproductive tract in the captive male tree shrew (*Tupaia belangeri*). Biol Reprod 26:169–182

Dadoune JP, Alfonsi MF (1986) Ultrastructural and cytochemical changes of the head components of human spermatids and spermatozoa. Gamete Res 14:33–46

De Kretser DM, Loveland KL, Meinhardt A, Simorangkir D, Wreford N (1998) Spermatogenesis. Hum Reprod 13:1–8

Fawcett DW (1965) The anatomy of the mammalian spermatozoon with particular reference to the guinea pig. Z Zellforsch 67:279–296

Fornes MW, Bustos-Obregon E (1994) Study of nuclear decondensation of the rat spermatozoa by reducing agents during epididymal transit. Andrologia 26:87–92

Holstein AF (1976) Ultrastructural observations on the differentiation of spermatids in man. Andrologia 8:157–165

Johnson L (1995) Efficiency of spermatogenesis. Microsc Res Tech 32:385–422

Kerr JB (1992) Functional cytology of the human testis. Baillieres Clin Endocrinol Metab 6:235–250

Kistler WS, Henriksen K, Mali P, Parvinen M (1996) Sequential expression of nucleoproteins during rat spermiogenesis. Exp Cell Res 225:374–381

Lalli M, Clermont Y (1981) Structural changes of the head components on the rat spermatid during late spermiogenesis. Am J Anat 160:419–434

Le Lannic G, Arkhis A, Vendrely E, Chevaillier P, Dadoune JP (1993) Production, characterization, and immunocytochemical applications of monoclonal antibodies to human sperm protamines. Mol Reprod Dev 36:106–112

Leblond CP, Clermont Y (1952a) Spermiogenesis of rat, mouse, hamster and guinea pig as revealed by the "Periodic acid-Fuchsin sulfurous acid" technique. Am J Anat 90:167–206

Leblond CP, Clermont Y (1952b) Definition of the stages of the cycle of seminiferous epithelium in the rat. Ann N Y Acad Sci 55:548–573

Lombardi J (1998) Gamete and their reproduction. In: Lombardi J (ed) Comparative vertebrate reproduction. Kluwer Academic, London, pp 109–130

Lowry OH, Rosebrough NJ, Farr AL, Randall RJ (1951) Protein measurement with the Folin phenol reagent. J Biol Chem 193:265–275

Maeda S, Endo H, Kimura J, Rerkamnuaychoke W, Chungsamarnyart N, Yamada J, Kurohmarum, Hayashi Y, Nishida T (1996) Classification of the cycle of the seminiferous epithelium in the common tree shrew (*Tupaia glis*). J Vet Med Sci 58:481–484

Martinage A, Arkhis A, Alimi E, Sautiere P, Chevaillier P (1990) Molecular characterization of nuclear basic protein HPI1, a putative precursor of human sperm protamines HP2 and HP3. Eur J Biochem 191:449–451

Mething A (1998) The establishment of spermatogenesis in the seminiferous epithelium of the pubertal golden hamster (*Mesocricetus auratus*). Adv Anat Embryol Cell Biol 140:1–92

Moneisi V (1971) Chromosome activities during meiosis and spermiogenesis. J Reprod Fertil 13:1–14

Oko RJ, Clermont Y (1990) Mammalian spermatozoa: structure and assembly of the tail. In: Gagnon C (ed) Control of sperm mobility: biological and clinical aspects. CRC Press, Florida, pp 4–21

Oko R, Clermont Y (1991) Origin and distribution of perforatorial proteins during spermatogenesis of the rat: an immunocytochemical study. Anat Rec 230:489–501

Oko RJ, Jando V, Wagner CL, Kistler WS, Hermo LS (1996) Chromatin reorganization in rat spermatids during the disappearance of testis-specific histone, H1t, and the appearance of transition proteins TP1 and TP2. Biol Reprod 54:1141–1157

Panyim S, Chalkley R (1969) High resolution acrylamide gel electrophoresis of histones. Arch Biochem Biophys 130:337

Poonkhum R, Pongmayteegul S, Meeratana W, Pradidarcheep W, Thongpila S, Mingsakul T, Somana R (2000) Cerebral microvascular architecture in the common tree shrew (*Tupaia glis*) revealed by plastic corrosion casts. Microsc Res Tech 50:411–418

Prigent Y, Muller S, Dadoune JP (1996) Immunoelectron microscopical distribution of histones H2B and H3 and protamines during human spermiogenesis. Mol Hum Reprod 2:929–935

Roux C, Gusse M, Chevaillier P, Dadoune JP (1988) An antiserum against protamines for immunohistochemical studies of histone to protamine transition during human spermiogenesis. J Reprod Fertil 82:35–42

Steger K (1999) Transcriptional and translational regulation of gene expression in haploid spermatids. Anat Embryol (Berl) 199:471–487

Steger K, Klonisch T, Gavenis K, Drabent B, Doenecke D, Bergmann M (1998) Expression of mRNA and protein of nucleoproteins during human spermiogenesis. Mol Hum Reprod 4:939–945

Suphamungmee W, Apisawetakan S, Weerachatyanukul W, Wanichanon C, Sretarugsa P, Poomtong T, Sobhon P (2005) Basic nuclear protein pattern and chromatin condensation in the male germ cells of a tropical abalone, *Haliotis asinina*. Mol Reprod Dev 70:211–221

Tanphaichitr N, Sobhon P, Taluppeth N, Chalermisarachai P (1978) Basic nuclear proteins in testicular cells and ejaculated spermatozoa in man. Exp Cell Res 117:347–356

Turner RM (2006) Moving to the beat: a review of mammalian sperm motility regulation. Reprod Fertil Dev 18:25–38

Van Roijen JH, Ooms MP, Spaargaren MC, Baarends WM, Weber RFA, Grootegoed JA, Vreeburg JTM (1998) Immunoexpression of testis-specific histone2B in human spermatozoa and testis tissue. Hum Reprod 13:1559–1566

Wanichanon C, Weerachatyanukul W, Suphamungmee W, Meepool A, Apisawetakan S, Linthong V, Sretarugsa P, Chavadej J, Sobhon P (2001) Chromatin condensation during spermiogenesis in rats. Sci Asia 27:211–220

Available online at www.sciencedirect.com
ScienceDirect
General and Comparative Endocrinology 155 (2008) 613–622
GENERAL AND COMPARATIVE ENDOCRINOLOGY
www.elsevier.com/locate/ygcen

The presence and distribution of gonadotropin-releasing hormone-liked factor in the central nervous system of the black tiger shrimp, *Penaeus monodon*

Piyada Ngernsoungnern [a,b], Apichart Ngernsoungnern [a,b], Scott Kavanaugh [b], Prasert Sobhon [a], Stacia A. Sower [b], Prapee Sretarugsa [a,*]

[a] *Department of Anatomy, Faculty of Science, Mahidol University, Bangkok 10400, Thailand*
[b] *Department of Biochemistry and Molecular Biology, University of New Hampshire, Durham, NH 03824, USA*

Received 4 April 2007; revised 5 July 2007; accepted 10 August 2007
Available online 26 August 2007

Abstract

The distribution and presence of gonadotropin-releasing hormone (GnRH) in the central nervous system (CNS) of *Penaeus monodon* were examined by immunocytochemistry, high performance liquid chromatography (HPLC), and radioimmunoassay (RIA). We demonstrated the existence of octopus (oct)GnRH-liked immunoreactivity (ir-octGnRH) and lamprey (l)GnRH-III-liked immunoreactivity (ir-lGnRH-III) in cell bodies of medium-sized neurons of the anterior part (protocerebrum) of the supraesophageal ganglion (brain). In addition, only the ir-octGnRH was detected in the nerve fibers located in the brain and segmental ganglia (subesophageal, thoracic, and abdominal ganglia). Moreover, some branches of these fibers also innervated the neurons in the middle (deutrocerebrum), posterior (tritocerebrum) brain and segmental ganglia. There was no ir-lGnRH-I and ir-salmon (s)GnRH detected in the shrimp CNS. The results from HPLC and RIA showed ir-GnRH in the CNS using anti-lGnRH-III, but not with anti-mammalian (m)GnRH. The data from immunocytochemistry, HPLC and RIA suggest that ir-GnRH in shrimp may be more similar to octGnRH and lGnRH-III than the other forms. These findings support the hypothesis that GnRH-liked factor(s) may be an ancient peptide that also exists in this decapod crustacean.
© 2007 Elsevier Inc. All rights reserved.

Keywords: GnRH; Immunocytochemistry; Nervous system; Crustacean; *Penaeus monodon*

1. Introduction

GnRH is a well-known decapeptide that is a major mediator in the brain–pituitary–gonadal axis in vertebrates (Fernald and White, 1999; Morgan and Millar, 2004; Millar, 2005). Fourteen isoforms of GnRH have been reported in vertebrates and have been classified into three groups: GnRH1, 2, and 3 (Fernald and White, 1999; Tsai, 2006). Silver et al. (2004) proposed that there is the fourth group of vertebrate GnRH based on phylogenetic analysis, function, neuronal distribution, and developmental origin. In tetrapods, GnRH1 is synthesized in neurons of forebrain, transported to median eminence, and finally released into hypothalamo-hypophyseal portal circulation to stimulate the release of gonadotropins, i.e., follicle stimulating hormone (FSH) and luteinizing hormone (LH) from the pituitary. GnRH2 is localized in the midbrain, and is speculated to serve as neurotransmitter/neuromodulator (Tsai, 2006). GnRH3 which is present in the telencephalon and the terminal nerves could be involved in sex-associated behaviors (Fernald and White, 1999). The lamprey GnRHs (lGnRH-I and -III) form the fourth group, GnRH4, which are both hypothalamic neurohormone and are derived from diencephalon/ventricular origin (Silver et al., 2004). In addition, GnRH is also detected in extra-pituitary tissues such as gonad, liver, kidney, placenta, breast, and prostate gland (González-Martínez et al., 2004).

* Corresponding author.
E-mail address: scpsr@mahidol.ac.th (P. Sretarugsa).

0016-6480/$ - see front matter © 2007 Elsevier Inc. All rights reserved.
doi:10.1016/j.ygcen.2007.08.012

Recently, many studies have reported the presence of GnRH in several invertebrates, which implies that this peptide could be conserved structurally as well as functionally throughout animal phyla (Young et al., 1999; Anctil, 2000; Tsai et al., 2003; Gorbman and Sower, 2003). Ten GnRH isoforms have been isolated and their primary structures determined in invertebrates, i.e., nine in tunicates and one in octopus (Powell et al., 1996; Iwakoshi et al., 2002; Adams et al., 2003; Kavanaugh et al., 2005). GnRH-like immunoreactivities have also been reported in an ascidian (Tsutsui et al., 1998), mollusks (Goldberg et al., 1993; Di Cosmo and Di Cristo, 1998; Young et al., 1999; Zhang et al., 2000; Di Cristo et al., 2002; Iwakoshi et al., 2002; Tsai et al., 2003; Iwakoshi-Ukena et al., 2004), a cnidarian (Anctil, 2000), a platyhelminthes (Anctil and Tekaya, 2005), and a coral (Twan et al., 2006). Although the structures have not yet been identified, the existence of the ir-GnRH in a variety of invertebrates suggests the ancestral GnRH has predated the emergence of vertebrate, and that GnRH is an ancient peptide that exists throughout vertebrate and invertebrate phyla (Rastogi et al., 2002; Gorbman and Sower, 2003; Tsai, 2006). GnRH has been reported to be functionally conserved as a reproduction-regulating factor in a few invertebrate species (Fang et al., 1991; Young et al., 1999; Di Fiore et al., 2000; Zhang et al., 2000; Adams et al., 2003; Gorbman et al., 2003; Iwakoshi-Ukena et al., 2004; Twan et al., 2006). In this report, we demonstrated ir-GnRH present in the CNS of the black tiger shrimp, *Penaeus monodon*, which may suggest the involvement of GnRH in the shrimp reproduction.

2. Materials and methods

2.1. Animals

Sexually mature female shrimp, with average weight of 180–250 g were caught from the Gulf of Thailand, and maintained at the Department of Aquatic Science, Faculty of Science, Burapha University, Chonburi, Thailand. The shrimp were maintained in a cement tank filled with seawater, at a temperature of about 25–28 °C, salinity at 30 ppt, with continuous aeration. They were fed with minced squid and kept under a normal day/light cycle (12/12 h). Approximately 70% of the seawater was replaced once a day. The shrimp were acclimatized for at least 7 days before being sacrificed. For chromatographic and radioimmunological studies, 30 whole CNS (supraesophageal and segmental ganglia) were dissected, and immediately frozen in liquid nitrogen and stored at −80 °C until use.

2.2. Antibodies and GnRH peptides

For immunocytochemitry, four available antibodies against GnRHs were used. The first was antibody against octGnRH (anti-octGnRH, Lot 9779, generously provided by Dr. Pei-San Tsai). This antibody was selected since octopus is considered to be more related to shrimp as both are protostomes. The other three antibodies were generated from one basal vertebrate (lamprey) and one basal teleost (salmon) which included anti-sGnRH, Lot 1667 (a kind gift of Dr. Judy King), anti-lGnRH-I, Lot 1467, and anti-lGnRH-III, Lot 3952 (produced in the laboratory of Dr. Stacia A. Sower, Sower et al., 1993). The lamprey as a basal vertebrate may have retained ancentral characteristics found in invertebrate GnRHs. The sGnRH is considered as GnRH3, whereas the lGnRHs are classified as GnRH4. Antibody against mGnRH (GnRH1, Lot R1245) was also used for determining the existence of a mGnRH-liked peptide in the RIA. The RIA using anti-mGnRH showed no immunoreactivity (see Section 3), thus this antibody was excluded from further use in immunocytochemistry. For peptides used in preabsorption study, octGnRH peptide (a gift from Dr. Hiroyuki Minakata and Dr. Pei-San Tsai), lGnRH-I, and lGnRH-III peptides (from the laboratory of Dr. Stacia A. Sower, purchased from American Peptide at 95% purity) were used.

2.3. Immunocytochemistry

The eyestalk, supraesophageal ganglion, and segmental ganglia were removed from non-gravid female shrimps. They were fixed in Bouin's fixative overnight, dehydrated, embedded in paraffin blocks, and then sectioned at 7 μm thick. The sections were deparaffinized with xylene, rehydrated through a graded series of ethanol (100–70%). The sections were immersed in 1% H_2O_2 in 70% ethanol for 15 min to eliminate endogenous peroxidase, then covered with 0.1% glycine and 4% BSA in 0.1 M phosphate buffer saline (PBS), pH 7.4, for 15 min for blocking free-aldehyde and non-specific binding, respectively. The sections were then incubated with the primary antisera including anti-octGnRH (1:500), anti-sGnRH (1:500), anti-lGnRH-I (1:1000), and anti-lGnRH-III (1:4000), at 4 °C for overnight. Negative controls were performed by incubating the sections in PBS or in primary antisera which were preabsorbed with GnRH peptides (50 μg/0.1 ml antisera at working dilution). Thereafter, sections were rinsed in several baths of PBS containing 0.1% Tween-20, and subsequently incubated with peroxidase-conjugated goat anti-rabbit IgG (Sigma, St. Louis, MO) diluted at 1:1500 for 1 h. The presence of ir-GnRH in the tissues was enhanced and visualized by DAB enhanced liquid substrate system (Sigma). The sections were then dehydrated, cleared, mounted, and observed under a light microscope. The experiments were repeated for at least three times for each tissue. In addition, some sections were processed by conventional method, and then stained with hematoxylin (H) and eosin (E) dyes for histological characterization of the tissues being studied.

In order to compare the staining intensity of ir-GnRH in experimental and controlled sections which were probed with preabsorbed anti-GnRHs, densitometric analysis of stained neurons was performed using ImageJ software. A box of 50×50 pixels was generated and placed over the positively-stained areas. On the same section, the areas which showed negative staining were also measured and considered as background staining. These background values were then used to subtract from the values measured from the positively-stained areas. At least 10 areas from both positive and negative immunoreactive areas were randomly measured in one section, and three sections from each experiment were analyzed.

2.4. GnRH peptide extraction and HPLC analysis

The shrimp CNS were extracted according to the methods described by Fahien and Sower (1990) at the Faculty of Science, Mahidol University, Thailand. Briefly, the CNS parts were weighed, and then homogenized at 4 °C with a polytron in 2.0 M ice-cold acetic acid. The homogenate was centrifuged at 10,000*g* for 45 min. The supernatant was subsequently dried in Speed Vac Concentrator, and then kept at −80 °C. Further processing of the extracts was performed at the Department of Biochemistry and Molecular Biology, University of New Hampshire, USA. The extract was resuspended with Milli-Q water, and purified by a Sep-Pak C18 cartridge column pretreated with 100% methanol. The peptide was eluted from the column with 70% acetronitrile. The elute was then dried on Speed Vac Concentrator followed by resuspension in Milli-Q water. Insoluble material was filtered using an ARCO LC 13 (0.45 μm). The filtrate was subsequently injected into a 20 μl the injection loop of a Perkin–Elmer HPLC system filled with a Percosphere 3CR C18 (0.46×8.3 cm) reverse-phase column. The isocratic mobile phase consisted of 7.4 g ammonium acetate and 3.04 g citric acid in 1000 ml of 19% acetronitrile with flow rate of 2 ml/min. The fractions were collected every 18 s.

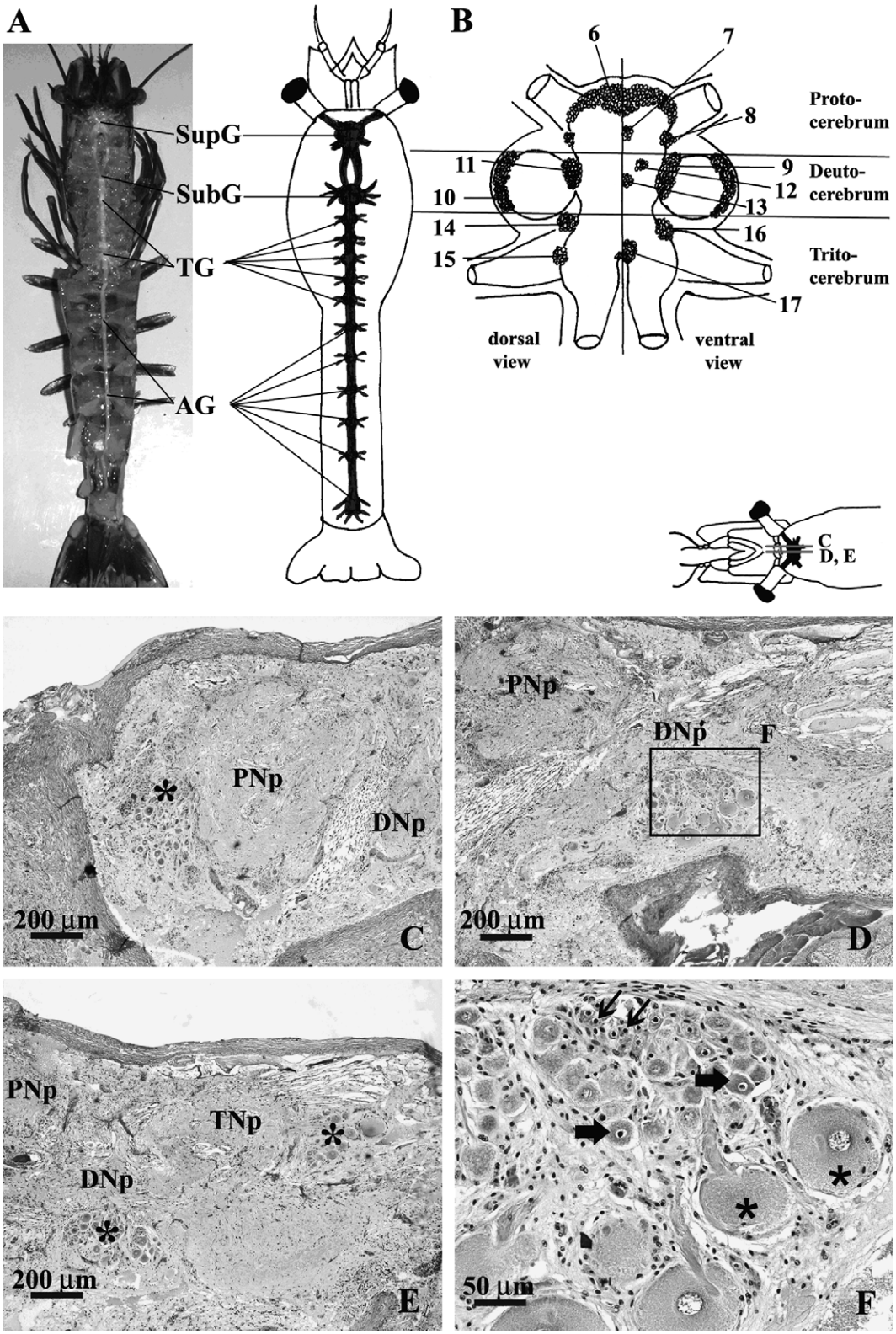


Fig. 1. (A) A photo of a dissected shrimp and a corresponding diagram illustrating the organization of the shrimp CNS which is comprised of the supraesophageal ganglion (SupG) and segmental ganglia (subesophageal ganglion, SubG; thoracic ganglia, TG; and abdominal ganglia, AG). The segmental ganglia are connected by a ventral nerve cord which runs along the ventral axis of the shrimp body. (B) A diagram showing the locations of various neuronal clusters as numbered in the supraesophageal ganglion (modified from Sandeman et al., 1992). (C–E) Sagittal sections of the supraesophageal ganglion stained with H&E, demonstrating neuropils and neuronal cell clusters (asterisks) in protocerebrum (C), deutocerebrum (D), and tritocerebrum (E). (F) Three types of neurons: large-sized neurons (asterisks), medium-sized neurons (large arrows), and small-sized neurons (small arrows) are revealed in cluster 13. PNp, protocerebrum neuropil; DNp, deutocerebral neuropil; TNp, tritocerebral neuropil.

Mammalian GnRH, chicken (c)GnRH-I and II, octGnRH, sGnRH, and lGnRH-I and III standards were chromatographed in parallel in the same HPLC system.

2.5. Radioimmunoassay

The eluted HPLC fractions were dried on Speed Vac Concentrator and then resuspended in phosphate gelatin buffer before measuring the concentrations of GnRH-liked factor using RIA as previously described by Fahien and Sower (1990). The HPLC fractions were assayed in duplicate. The synthetic mGnRH or lGnRH-I was used as the radio-iodinated tracer and standard. The anti-mGnRH and anti-lGnRH-III were used at dilutions of 1:30,000 for mGnRH RIA and 1:16,000 for lGnRH-III RIA, respectively. The antibody binding ranged between 26–32% for anti-mGnRH of ^{125}I-mGnRH and 50–59% for anti-lGnRH-III of ^{125}I-lGnRH. Anti-mGnRH has a specificity with cross-reactivities of 100%, 65%, 19.5%, 4.16%, and <0.00001% for mGnRH, cGnRH-I, sGnRH, cGnRH-II, and lGnRH-I, respectively (Calvin et al., 1993; Sower et al., 1995). The anti-lGnRH-III has cross-reactivities of 100% with lGnRH-I and III, <0.01% with mGnRH, cGnRH-I, cGnRH-II, and sGnRH (Robinson et al., 2000), and 0.1% with octGnRH (unpublished data). Standard curves were constructed by assaying the standard GnRHs that ranged from 0 to 2500 pg for lGnRH-III assay and 0 to 1250 pg for mGnRH assay. Lower limit of detection in each assay was 9.8 pg/0.1 ml. A RIA for anti-octGnRH has not yet been developed.

3. Results

3.1. Immunocytochemistry

The shrimp CNS comprised of supraesophageal ganglion and segmental ganglia, and the latter were divided into subesophageal, thoracic, and abdominal ganglia (Fig. 1A). The shrimp supraesophageal ganglion (comprising of protocerebrum, deutocerebrum, and tritocerebrum) is organized as the neuropils and clusters of neuronal cells (Fig. 1B–E). Neuronal cells in each cluster were classified into three types based on their sizes: small-, medium-, and large-sized neurons which ranged about 7–15, 20–40, and 50–150 μm, respectively (Fig. 1F). Four antisera as mentioned in Section 2 were applied as probes to determine the presence of ir-GnRH in this part of the shrimp CNS. Anti-octGnRH exhibited the most intense staining. There was no ir-octGnRH observed in neuronal cell bodies, fibers, or neuropils of the eyestalk (Fig. 2A and B). However, ir-octGnRH was detected in cell bodies of medium-sized neurons located in the anterior part of the brain, the protocerebrum, and in fibers distributed in the protocerebrum (Fig. 3A and B). There was no ir-octGnRH observed in cell bodies of neurons located in the deutocerebrum, tritocerebrum and segmental ganglia. In contrast, intense ir-octGnRH was detected in the fibers surrounding the neuropils of deutocerebrum and tritocerebrum, and also in the fibers that innervated neuronal cell bodies in these two parts of brain (Fig. 3C–F). The fibers innervated neuronal cell bodies in segmental ganglia also exhibited intense ir-octGnRH (Fig. 4). There was no ir-octGnRH observed in the sections incubated with preabsorbed anti-octGnRH (Fig. 3G).

The ir-lGnRH-III was found only in the cell bodies of medium-sized neurons located in protocerebrum (Fig. 5A). However, the immunostaining was less intense, and there were fewer immunoreactive neuronal cell bodies when compared to the ir-octGnRH positive neurons. In addition, neither neuronal cell bodies nor fibers in eyestalk and segmental ganglia exhibited ir-lGnRH-III. Interestingly, ir-octGnRH and ir-lGnRH-III were detected in neuronal cell bodies of neuronal cluster number 6 only, while the closely associated neuronal clusters numbered 7 and 8 were not stained. There was no ir-lGnRH-I or ir-sGnRH were detected in any other parts of the shrimp CNS. The presence of each ir-GnRH isoform in each section of the shrimp CNS is summarized in Table 1. There was no ir-lGnRH-III observed in the sections incubated with preabsorbed anti-lGnRH-III (Fig. 5B).

The specificities and intensities of anti-octGnRH and anti-lGnRH-III staining were compared, and the results are summarized in Table 2. Anti-octGnRH exhibited intense staining in the shrimp CNS with the intensity of 76.00 ± 1.73 U. After preabsorption of this antibody with octGnRH peptide, the intensity was reduced to 3.70 ± 0.82 U, suggesting that this antibody was highly specific to octGnRH. However, approximately 50% reduction in the intensity (39.10 ± 4.06 U) was observed after

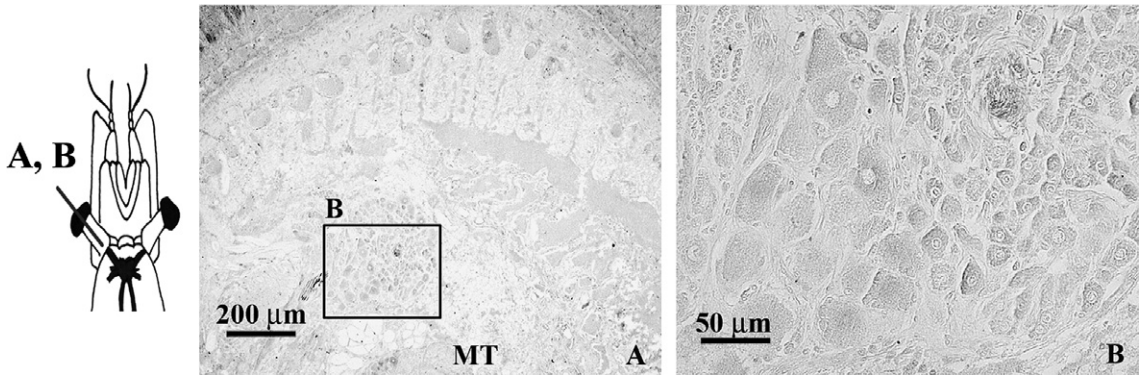


Fig. 2. Immunocytochemical localization of ir-octGnRH in the shrimp eyestalk. No ir-octGnRH is detected in neurons and neuropils of the optic lobe (A and B). MT, medulla terminalis.

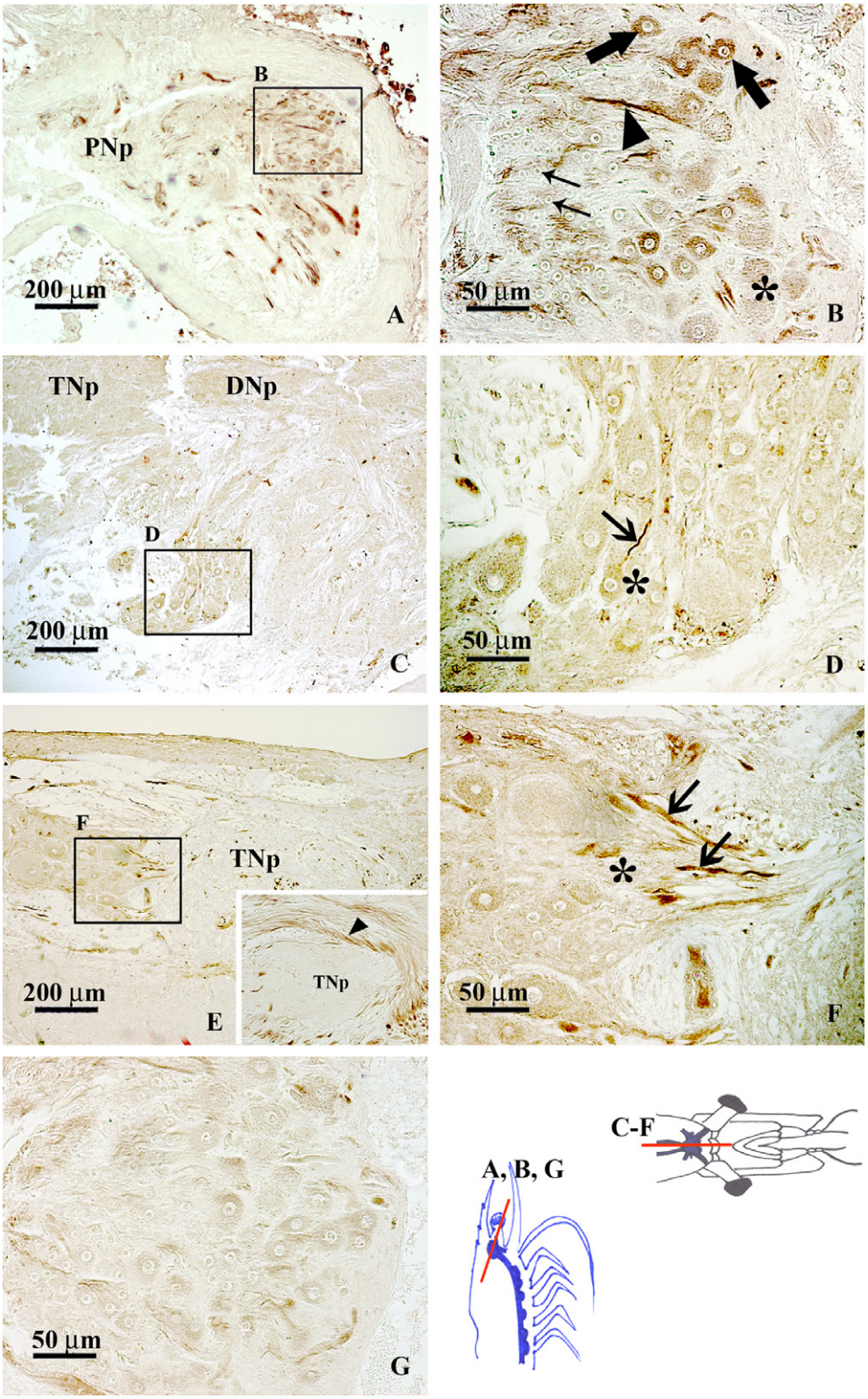


Fig. 3. Immunocytochemical localization of ir-octGnRH in the shrimp supraesophageal ganglion. Intense immunoreactivity is detected in some medium-sized neurons located in protocerebrum (A and B, large arrows) and in the neuronal fibers (arrow head). Other medium-sized neurons (asterisk) and all of the small-sized neurons (small arrows) in this part of the ganglion show no immunoreactivity. The ir-octGnRH is also detected in the fibers (C–F, arrows) that innervated neurons (asterisks), as well as the fibers surrounded the neuropils of deutocerebrum and tritocerebrums (E, inset, arrow head). (G) The section incubated with preabsorbed anti-octGnRH shows only background staining. DNp, deutocerebral neuropil; PNp, protocerebral neuropil; TNp, tritocerebral neuropil.

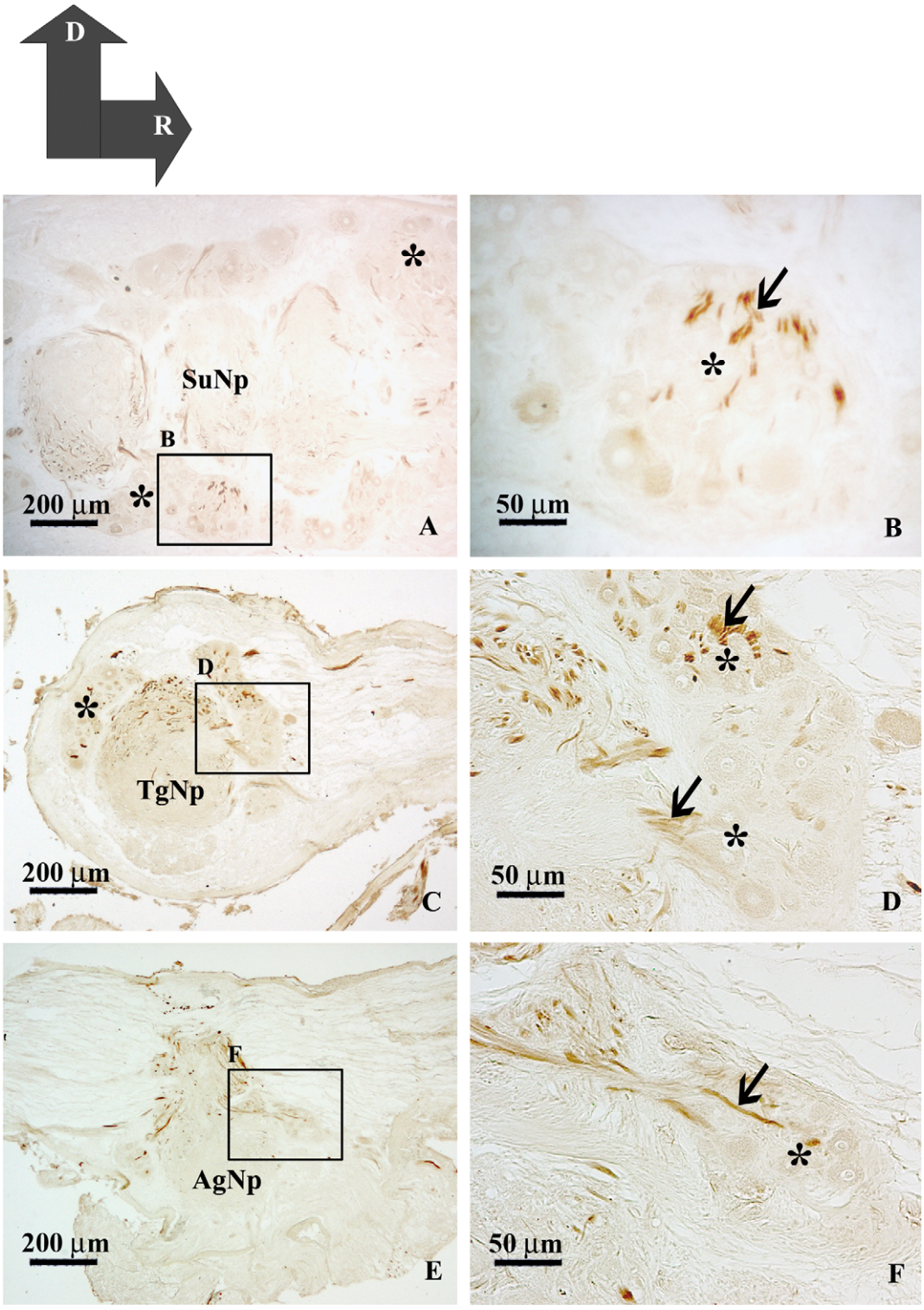


Fig. 4. Immunocytochemical localization of ir-octGnRH in subesophageal (A and B), thoracic (C and D), and abdominal ganglia (E and F). The ir-octGnRH is observed in the subesophageal neuropil (SuNp), thoracic ganglion neuropil (TgNp), abdominal ganglion neuropil (AgNp), and in fibers (arrows) innervating the neurons (asterisks) located in the segmental ganglia. D, dorsal; R, rostal.

preabsorbing the antibody with lGnRH-III peptide. Without preabsorption, the anti-lGnRH-III exhibited moderate staining in the shrimp CNS with the intensity of 55.60 ± 1.18 U. After preabsorption with lGnRH-I and lGnRH-III peptides, this antibody was totally blocked resulting in background staining only (3.17 ± 0.60 and 1.47 ± 0.38 U, respectively). In contrast, when the anti-lGnRH-III was preabsorbed with octGnRH, there were

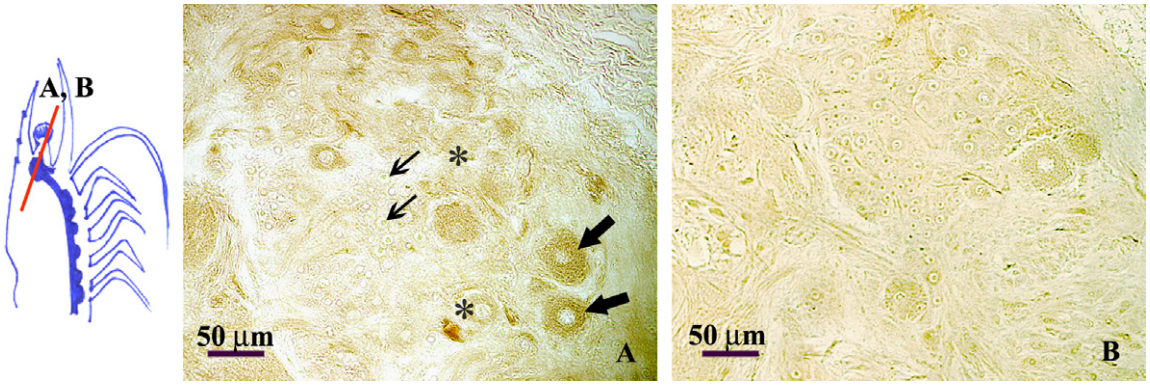


Fig. 5. Immunocytochemical localization of ir-lGnRH-III in the shrimp supraesophageal ganglion. (A) Immunoreactivity is seen in some medium-sized neurons of protocerebrum (large arrows). Other medium-sized neurons (asterisks) and all small-sized neurons (small arrows) show no immunoreactivity. (B) The section incubated with preabsorbed anti-lGnRH-III shows only background staining.

Table 1
Distribution of four GnRH isoforms in the black tiger shrimp CNS as determined by relative intensities of immunostaining with antibodies against octGnRH, lGnRH-I, lGnRH-III, and sGnRH

Antisera against	Part of CNS									
	Eyestalk		Supraesophageal ganglion						Segmental ganglia	
			Protocerebrum		Deutocerebrum		Tritocerebrum			
	Soma	Fibers	Soma	Fibers	Soma	Fibers	Soma	Fibers	Soma	Fibers
octGnRH	–	–	+++	+++	–	+++	–	+++	–	+++
lGnRH-III	–	–	++	–	–	–	–	–	–	–
lGnRH-I	–	–	–	–	–	–	–	–	–	–
sGnRH	–	–	–	–	–	–	–	–	–	–

Note. +++, intense immunostaining; ++, moderate immunostaining; +, faint immunostaining; –, no immunostaining.

Table 2
The staining intensities and specificities of antibodies before and after preabsorption with GnRH peptides exhibiting ir-GnRH in the black tiger shrimp supraesophageal ganglion

Antibodies	Lot No.	Without preabsorption	Preabsorbtion with		
			OctGnRH	lGnRH-I	lGnRH-III
αoct-GnRH	9779	76.00 ± 1.73	3.70 ± 0.82	74.93 ± 1.06	39.10 ± 4.06
αlGnRH-III	3952	55.60 ± 1.18	51.80 ± 1.48	3.17 ± 0.60	1.47 ± 0.38

The numbers represent the units of staining intensities obtained by subtracting values of background staining from positive one.

very low cross-reactivity with octGnRH (51.80 ± 1.48 U), and the antibody still exhibited the usual staining.

3.2. HPLC and RIA

In the HPLC and RIA analyses from CNS extract using the anti-lGnRH-III, there was only one major peak of ir-GnRH (Fig. 6). The elution time of this fraction was compared to the elution times of seven different synthetic GnRH standards run in parallel on the same HPLC system. It was shown that the elution position of the ir-GnRH peak was about 18 and 54 s earlier than those of lGnRH-III and octGnRH standards, respectively. This suggested that the shrimp CNS contained at least one GnRH-liked factor that may be closely related to lGnRH-III.

4. Discussion

In this study, we demonstrated the existence of GnRH-liked factor(s) in a penaeid shrimp CNS by immunocytochemistry using four different types of GnRH antibodies. Ir-octGnRH and ir-lGnRH-III were detected in the neuronal cell bodies located in protocerebrum. Considering that anti-lGnRH-III and anti-octGnRH showed about 0.1% cross-reactivity (unpublished data), we propose that there may be at least two isoforms of GnRH in the shrimp CNS. These findings were supported by the results obtained from the RIA assay of individual HPLC fractions which revealed the existence of at least one GnRH-liked factor that is closely related to lGnRH-III in the shrimp CNS. Unfortunately, the RIA system for ir-octGnRH has not yet been developed, thus we could not confirm

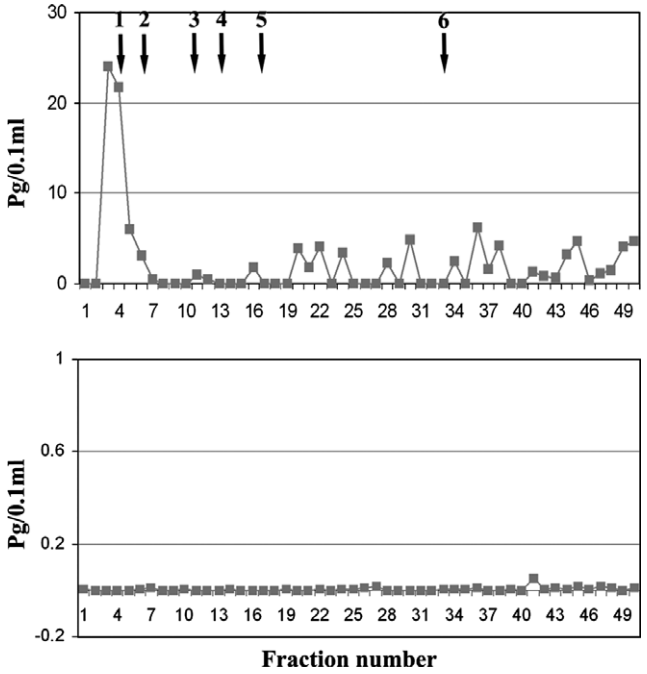


Fig. 6. RIA of HPLC fractions using anti-lGnRH-III (top) and anti-mGnRH (bottom). Arrows indicate elution times of standard GnRHs in the following order: 1, lGnRH-III; 2, octGnRH; 3, mGnRH/cGnRH-I; 4, lGnRH-I; 5, cGnRH-II; 6, sGnRH. The elution position of the shrimp ir-GnRH is about 18 and 54 s earlier than the positions of lGnRH-III and octGnRH standards, respectively.

the presence of octGnRH-liked factor in the shrimp CNS by this method.

Immunocytochemistry showed stronger intensity of ir-octGnRH in both neuronal cell bodies and fibers than that exhibited by ir-lGnRH-III. This implies the presence of more octGnRH-liked factor in the shrimp CNS than that of lGnRH-III-liked factor. In contrast to the presence of ir-octGnRH and ir-lGnRH-III, there was no ir-lGnRH-I or ir-sGnRH in any part of the shrimp CNS as determined by immunocytochemistry. This was consistent with the results from the HPLC and RIA studies, which did not show any ir-peaks corresponding to the peaks of the standards of lGnRH-I or sGnRH. The specificity of both ir-octGnRH and ir-lGnRH-III in the shrimp CNS was shown by preabsorption of the antisera with corresponding synthetic octGnRH and lGnRH-III peptides. In both cases, only a background level of the immunoreactivity was detected, thus confirming that these antibodies were highly specific to their corresponding GnRH-liked factors. Thus, it is suggested that there are at least two GnRH-liked peptides present in the shrimp CNS.

Interestingly, no ir-GnRH was detected in either the neuronal cell bodies or fibers of the shrimp eyestalk, especially in the optic lobe that is connected to the protocerebrum, and is considered to play an important role in the regulation of molting and reproduction. The protocerebrum is the site where a number of reproduction-regulating neurohormones including molt-inhibiting hormone (MIH), gonad-inhibiting hormone (GIH), and mandibular organ-inhibiting hormone (MOIH) are synthesized (Huberman, 2000). Functionally, MIH inhibits secretion of a molting hormone, ecdysone produced by the Y-organ. GIH is shown to inhibit ovarian development and vitellogenin synthesis, whereas MOIH acts on mandibular organ by inhibiting the secretion of methyl-farnesoate (MF), which is believed to stimulate vitellogenesis and ecdysteroid synthesis in Y-organ (Okumura and Aida, 2001). Since we have shown that there is no apparent ir-GnRH in the eyestalk, we postulate that GnRH may be confined to the distal part of the shrimp nervous system and subjected to the regulation by the inhibiting factors present in the eyestalk. However, the identification of the primary structures of shrimp GnRH and the possible interrelationships of GnRH and the eyestalk inhibiting factors will need to be studied before any firm conclusion can be reached.

In vertebrates, GnRH neurons are neuroendocrine cells that release their contents to affect a large number of target cells (Goldberg et al., 1993). The significance of GnRH in regulating reproduction has been well defined in all vertebrates and suggested for some invertebrates (Fang et al., 1991; Young et al., 1999; Di Fiore et al., 2000; Zhang et al., 2000; Adams et al., 2003; Gorbman and Sower, 2003; Gorbman et al., 2003; Iwakoshi-Ukena et al., 2004; Twan et al., 2006). Although the protocerebrum contains many neuronal cell clusters (Sandeman et al., 1992), our present study demonstrated ir-octGnRH and ir-lGnRH-III only in cell bodies of medium-sized neurons of neuronal cluster 6 that is located in the most anterior part of the shrimp brain. In decapod crustaceans, these neurons are also considered to be "neurosecretory cells" (Bell and Lightner, 1988). Similarly in a mollusk, *Halisoma trivolvis*, the neuronal cells involved in controlling reproduction were shown to be located in the anterior part of the nervous system especially in the cerebral ganglia, and that this ganglion was shown to be the site for ir-GnRH neurons (Goldberg et al., 1993). By contrast, it is well known that deutocerebrum and tritocerebrum are mainly involved in olfaction and mechanosensory functions, respectively (Sandeman et al., 1992). In *Aplysia californica*, prior to spawning, stimulatory signals originating from the head ganglia are transmitted to the bag cells (neurons) in the abdominal ganglion to trigger the release of egg-laying hormone (ELH), thus initiating egg-laying behavior and spawning (Wayne, 2001). In shrimp, these functions are known to be controlled in part by gonad-stimulating hormone (GSH) secreted from brain and/or thoracic ganglia (Huberman, 2000). The GSH was suggested to be regulated by an increased level of serotonin (Meeratana et al., 2006; Wongprasert et al., 2006). It is also possible that GnRH may be involved in this pathway. However, the interrelationships of GnRH and GSH will need further study.

Our immunocytochemical results showed that the ir-GnRH(s) were detected exclusively in the cell bodies of neurons located in the protocerebrum, while neuronal fibers with ir-GnRH were observed to innervate neurons

in the deutocerebrum, tritocerebrum, and segmental ganglia. This suggests that GnRH produced in protocerebrum may be passed caudally to exercise its reproductive control on the more distally located neurons that may be involved in the production and release of final effector neurohormone such as GSH. We have started initial investigations on the potential role of GnRH-liked factor in mediating reproductive function in this species of shrimp. Results from these ongoing studies and future structural–functional studies will provide much needed information on GnRH in an invertebrate. In summary, we have detected ir-GnRH in the CNS of shrimp, whether these GnRH(s) are directly involved in reproduction has yet to be determined.

Acknowledgments

This study was supported by the Thailand Research Fund (Royal Golden Jubilee Ph.D. Program (Grant No. PHD/0162/2544) to P. Ngernsoungnern and P. Sretarugsa, and Senior Research Scholar Fellowship to P. Sobhon), and NSF0421923 to Stacia A. Sower. The authors thank Dr. Pei-San Tsai, Dr. Judy King, Dr. Hiroyuki Minakata for generously providing GnRH antibodies and peptides, Dr. Wattana Weerachatyanukul for useful suggestions, Mr. Boworn Soonthornsumrith, Mr. Yotsawan Tinikul, and Mrs. Pornsawan Duangsuwan for preparing samples for HPLC, and Dr. Boonyarath Pratoomchat for providing shrimp samples.

References

Adams, B.A., Tello, J.A., Erchegyi, J., Warby, C., Hong, D.J., Akinsanya, K.O., Mackie, G.O., Vale, W., Rivier, J.E., Sherwood, N.M., 2003. Six novel gonadotropin-releasing hormones are encoded as triplets on each of two genes in the protochordate, *Ciona intestinalis*. Endocrinology 144, 1907–1919.

Anctil, M., 2000. Evidence for gonadotropin-releasing hormone-like peptides in a Cnidarian nervous system. Gen. Comp. Endocrinol. 119, 317–328.

Anctil, M., Tekaya, S., 2005. Gonadotropin-releasing hormone-like immunoreactivity in the planarian *Bdelloura candida* (Platyhelminthes, Tricladida). Invertebr. Biol. 124, 11–17.

Bell, T.A., Lightner, D.V., 1988. A Handbook of Normal *Penaeid shrimp* Histology. World Aquaculture Society, Baton Rouge, LA, USA.

Calvin, J.L., Slater, C.H., Bolduc, T.G., Laudano, A.P., Sower, S.A., 1993. Multiple molecular forms of gonadotropin-releasing hormone in the brain of an elasmobranch: evidence for IR-lamprey GnRH. Peptides 14, 725–729.

Di Cosmo, A., Di Cristo, C., 1998. Neuropeptidergic control of the optic gland of *Octopus valgaris*: FMRF-amide and GnRH immunoreactivity. J. Comp. Neurol. 398, 1–12.

Di Cristo, C., Paolucci, M., Iglesias, J., Sanchez, J., Di Cosmo, A., 2002. Presence of two neuropeptides in the fusiform ganglion and reproductive ducts of *Octopus vulgaris*: FMRFamide and gonadotropin-releasing hormone (GnRH). J. Exp. Zool. 292, 267–276.

Di Fiore, M.M., Rastogi, R.K., Ceciliani, F., Messi, E., Botte, V., Botte, L., Pinelli, C., D'Aniello, B., D'Aniello, A., 2000. Mammalian and chicken I forms of gonadotropin-releasing hormone in the gonads of a protochordate, *Ciona intestinalis*. Proc. Natl. Acad. Sci. USA 97, 2343–2348.

Fahien, C.M., Sower, S.A., 1990. Relationship between brain gonadotropin-releasing hormone and final reproductive period of the adult male sea lamprey, *Petromyzon marinus*. Gen. Comp. Endocrinol. 80, 427–437.

Fang, Y.-Q., Wang, H., Zhang, C.-L., 1991. Correlation of annual change of luteinizing hormone–releasing hormone (LH–RH) with gonadal development in amphioxus. Sci. China 34, 814–822.

Fernald, R.D., White, R.B., 1999. Gonadotropin-releasing hormone genes: phylogeny, structure, and functions. Front. Neuroendocrin. 20, 224–240.

Goldberg, J.I., Garofalo, R., Price, C.J., Chang, J.P., 1993. Presence and biological activity of a GnRH-like factor in the nervous system of *Helisoma trivolvis*. J. Comp. Neurol. 336, 571–582.

González-Martínez, D., Madigou, T., Mañanos, E., Cerdá-Reverter, J.M., Zanuy, S., Kah, O., Muñoz-Cueto, J.A., 2004. Cloning and expression of gonadotropin-releasing hormone receptor in the brain and pituitary of the European sea bass: an in situ hybridization study. Biol. Reprod. 70, 1380–1391.

Gorbman, A., Sower, S.A., 2003. Evolution of the role of GnRH in animal (Metazoan) biology. Gen. Comp. Endocrinol. 134, 207–213.

Gorbman, A., Whiteley, A., Kavanaugh, S., 2003. Pheromonal stimulation of spawning release of gametes by gonadotropin releasing hormone in the chiton, *Mopalia* sp. Gen. Comp. Endocrinol. 131, 62–65.

Huberman, A., 2000. Shrimp endocrinology. A review. Aquaculture 191, 191–208.

Iwakoshi, E., Takuwa-Kuroda, K., Fujisawa, Y., Hisada, M., Ukena, K., Tsutsui, K., Minakata, H., 2002. Isolation and characterization of a GnRH-like peptide from *Octopus valgaris*. Biochem. Biophy. Res. Commun. 291, 1187–1193.

Iwakoshi-Ukena, E., Ukena, K., Takuwa-Kuroda, K., Kanda, A., Tsutsui, K., Minakata, H., 2004. Expression and distribution of octopus gonadotropin-releasing hormone in the central nervous system and peripheral organs of the octopus (*Octopus valgaris*) by in situ hybridization and immunohistochemistry. J. Comp. Neurol. 477, 310–323.

Kavanaugh, S.I., Root, A.R., Sower, S.A., 2005. Distribution of gonadotropin-releasing hormone (GnRH) by in situ hybridization in the tunicate *Ciona intestinalis*. Gen. Comp. Endocrinol. 141, 76–83.

Meeratana, P., Withyachumnarnkul, B., Damrongphol, P., Wongprasert, K., Suseangtham, A., Sobhon, P., 2006. Serotonin induces ovarian maturation in giant freshwater prawn broodstock, *Macrobrachium rosenbergii* de man. Aquaculture 260, 315–325.

Millar, R.P., 2005. GnRHs and GnRH receptors. Anim. Reprod. Sci. 88, 5–28.

Morgan, K., Millar, R.P., 2004. Evolution of GnRH ligand precursors and GnRH receptors in protochordate and vertebrate species. Gen. Comp. Endocrinol. 139, 191–197.

Okumura, T., Aida, K., 2001. Effects of bilateral eyestalk ablation on molting and ovarian development in the giant freshwater prawn, *Macrobrachium rosenbergii*. Fish. Sci. 67, 1125–1135.

Powell, J.F.F., Reska-Skinner, S.M., Prakash, M.O., Fischer, W.H., Park, M., Rivier, J.E., Craig, A.G., Mackie, G.O., Sherwood, N.M., 1996. Two new forms of gonadrotropin-releasing hormone in a protochordate and the evolutionary implications. Proc. Natl. Acad. Sci. USA 93, 10461–10464.

Rastogi, R.K., Di Fiore, M.M., D'Aniello, A.D., Iela, L., Fiorentino, M., 2002. GnRH in the invertebrates: an overview. Prog. Brain. Res. 141, 19–29.

Robinson, C.T., Tobet, S.A., Chase, C., Waldron, T., Sower, S.A., 2000. Gonadotropin-releasing hormones in the brain and pituitary of the teleost, the white sucker. Gen. Comp. Endocrinol. 117, 381–394.

Sandeman, D., Sandeman, R., Derby, C., Schmidt, M., 1992. Morphology of the brain of crayfish, crabs, and spiny lobsters: a common nomenclature for homologous structures. Biol. Bull. 183, 304–326.

Silver, M.R., Kawauchi, H., Nozaki, M., Sower, S.A., 2004. Cloning and analysis of the lamprey GnRH-III cDNA from eight species of

lamprey representing the three families of Petromyzoniformes. Gen. Comp. Endocrinol. 139, 85–94.

Sower, S.A., Chiang, Y.C., Lovas, S., Conlon, J.M., 1993. Primary structure and biological activity of a third gonadotropin-releasing hormone from lamprey brain. Endocrinology 132, 1125–1131.

Sower, S.A., Nozaki, M., Knox, C.J., Gorbman, A., 1995. The occurrence and distribution of GnRH in the brain of Atlantic hagfish, an Agnatha, determined by chromatography and immunocytochemistry. Gen. Comp. Endocrinol. 97, 300–307.

Tsai, P.-S., Maldonado, T.A., Lunden, J.B., 2003. Localization of gonadotropin-releasing hormone in the central nervous system and a peripheral chemosensory organ of *Aplysia californica*. Gen. Comp. Endocrinol. 130, 20–28.

Tsai, P.-S., 2006. Gonadotropin-releasing hormone in invertebrates: structure, function, and evolution. Gen. Comp. Endocrinol. 148, 48–53.

Tsutsui, H., Yamamoto, N., Ito, H., Oka, Y., 1998. GnRH-immunoreactive neuronal system in the presumptive ancestral Chordate *Ciona intestinalis* (Ascidian). Gen. Comp. Endocrinol. 112, 426–432.

Twan, W.-H., Hwang, J.-S., Lee, Y.-H., Jeng, S.-R., Yueh, W.-S., Tung, Y.-H., Wu, H.-F., Dufour, S., Chang, C.-F., 2006. The presence and ancestral role of gonadotropin-releasing hormone in the reproduction of scleractinian coral, *Euphyllia ancora*. Endocrinology 147, 397–406.

Wayne, N.L., 2001. Regulation of seasonal reproduction in mollusks. J. Biol. Rhythms 16, 391–402.

Wongprasert, K., Asuvapongpatana, S., Poltana, P., Tiensuwan, M., Withyachumnarnkul, B., 2006. Serotonin stimulates ovarian maturation and spawning in the black tiger shrimp *Penaeus monodon*. Aquaculture 261, 1447–1454.

Young, K.G., Chang, J.P., Goldberg, J.I., 1999. Gonadotropin-releasing hormone neuronal system of the fresh water snails *Helisoma trivolvis* and *Lymnaea stagnalis*: possible involvement in reproduction. J. Comp. Neurol. 404, 427–437.

Zhang, L., Wayne, N.L., Sherwood, N.M., Postigo, H.R., Tsai, P.-S., 2000. Biological and immunological characterization of multiple GnRH in an opisthobranch mollusk, *Aplysia californica*. Gen. Comp. Endocrinol. 118, 77–89.

Invert Neurosci (2008) 8:49–57
DOI 10.1007/s10158-008-0067-5

ORIGINAL PAPER

The identification and distribution of gonadotropin-releasing hormone-like peptides in the central nervous system and ovary of the giant freshwater prawn, *Macrobrachium rosenbergii*

Apichart Ngernsoungnern · Piyada Ngernsoungnern · Scott Kavanaugh · Stacia A. Sower · Prasert Sobhon · Prapee Sretarugsa

Received: 20 December 2007 / Accepted: 6 February 2008 / Published online: 21 February 2008
© Springer-Verlag 2008

Abstract In the present study, we demonstrated the existence of GnRH-like peptides in the central nervous system (CNS) and ovary of the giant freshwater prawn, *Macrobrachium rosenbergii* using immunocytochemistry. The immunoreactivity (ir) of lamprey (l) GnRH-III was detected in the soma of medium-sized neurons located in neuronal cluster number 11 in the middle part of supraesophageal ganglion (deutocerebrum), whereas ir-octopus (oct) GnRH was observed in the soma of both medium-sized and large-sized neurons in thoracic ganglia, as well as in the fibers innervating the other medium-sized and large-sized neuronal cell bodies in the thoracic ganglia. In addition, ir-lGnRH-I was observed in the cytoplasm of late previtellogenic oocyte and early vitellogenic oocyte. These data suggest that *M. rosenbergii* contain at least three isoforms of GnRH: two GnRH isoforms closely related to lGnRH-III and octGnRH in the CNS, whereas another isoform, closely related to lGnRH-I, was localized in the ovary. This finding provides supporting data that ir-GnRH-like peptide(s) may exist in this decapod crustacean.

A. Ngernsoungnern · P. Ngernsoungnern · P. Sobhon · P. Sretarugsa (✉)
Department of Anatomy, Faculty of Science, Mahidol University, Rama 6 Road, Rajathevi, Bangkok 10400, Thailand
e-mail: scpsr@mahidol.ac.th

A. Ngernsoungnern · P. Ngernsoungnern · S. Kavanaugh · S. A. Sower
Department of Biochemistry and Molecular Biology, University of New Hampshire, Durham, NH 03824, USA

Keywords GnRH · Immunoreactivity · Central nervous system · Ovary · *Macrobrachium rosenbergii*

Introduction

In vertebrates, gonadotropin-releasing hormone (GnRH), a decapeptide, plays a critical role in regulating reproduction (Gorbman and Sower 2003; Morgan and Millar 2004; Tsai 2006). The major reproductive-regulating pathway of GnRH is known as the hypothalamo-pituitary-gonadal axis. GnRH is synthesized in the hypothalamic neurosecretory cells and then transported to the anterior pituitary gland via the hypophyseal portal vessels (in tetrapods) or direct innervation (in teleosts) to regulate the secretion of gonadotropins, i.e., follicle stimulating hormone (FSH) and luteinizing hormone (LH). The gonadotropins are then released into blood stream and act on the gonads to stimulate gametogenesis and steroidogenesis (Fernald and White 1999). To date, the primary structures of 14 and 11 GnRHs have been identified in vertebrates and invertebrates, respectively (Gorbman and Sower 2003; Tsai 2006; Kah et al. 2007; Zhang et al. 2007). Among invertebrate GnRHs, nine isoforms identified in the tunicates are decapeptides, whereas two isoforms discovered in the octopus and aplysia are dodecapeptides (Powell et al. 1996; Iwakoshi et al. 2002; Adams et al. 2003; Kavanaugh et al. 2005; Zhang et al. 2007).

Within the last decade, GnRH or immunoreactive GnRH-like peptides have been shown in a number of invertebrate species, which indicates that this peptide or variant exists throughout vertebrate and invertebrate phyla (Gorbman and Sower 2003; Tsai 2006; Kah et al. 2007). In mollusks, the existence of immunoreactivity (ir)-GnRH

was reported in gastropods, *Halisoma trivolvis, Lymnaea stagnalis*, and *Aplysia californica* (Goldberg et al. 1993; Pazos and Mathieu 1999; Young et al. 1999; Zhang et al. 2000, 2007; Tsai et al. 2003), and a cephalopod, *Octopus vulgaris* (Di Cosmo and Di Cristo 1998; Di Cristo et al. 2002; Iwakoshi et al. 2002; Iwakoshi-Ukena et al. 2004). Ir-GnRH was also observed in a cnidarian (Anctil 2000), a platyhelminthes (Anctil and Tekaya 2005) and a coral (Twan et al. 2006). As in vertebrates, it was demonstrated that GnRH serves multiple functions in reproduction or reproductive related activities, such as induction of spawning in a tunicate, *Ciona intestinalis* (Terakado 2001; Adams et al. 2003); a coral, *Euphyllia ancora* (Twan et al. 2006), and a chiton, *Mopalia* sp. (Gorbman et al. 2003); regulating gamete transport in an octopus, *O. vulgaris* (Di Cristo et al. 2002); stimulating rhythmic contraction of the octopus oviduct (Iwakoshi-Ukena et al. 2004); and acting as a pheromone in hemichordates, *Saccoglossus* and *Ptychodera* (Cameron et al. 1999) and *Mopalia* sp. (Gorbman et al. 2003). GnRH may also have a role in mediating neuronal signals not associated with reproduction, as a neurotransmitter and/or neuromodulator (Tsai 2006).

Recently, our group has demonstrated the presence of two GnRH-like peptides in CNS of the black tiger shrimp, *Penaeus monodon* (Ngernsoungnern et al. 2008). Both *M. rosenbergii* and *P. monodon* belong to the class Malacostraca and order Decapoda. However, at the suborder level, *M. rosenbergii* is classified as Pleocyemata, whereas *P. monodon* is a Dendrobranchiata (Burkenroad 1963). These two suborders are distinguished by their structure of the gills. The gills of the Dendrobranciata contain two series of branches, each member of a series being subdivided in a way that it appears brushy. All other decapods are assigned to the Pleocyemata which contains gills with either two broad lobes running the length of the central axis or various tiers of filaments (Kozloff 1990). To determine if GnRH or GnRH-like peptides are present in a freshwater prawn, we utilized various GnRH antisera in immunocytochemical studies. In the present study, we show the distribution of GnRH-like peptides in the CNS and ovary of the giant freshwater prawn, *M. rosenbergii.* This finding supports a hypothesis that GnRH or GnRH like peptides occur throughout various species of shrimp and perhaps other crustaceans.

Materials and methods

Animals

Mature female freshwater prawns, weighing between 30 and 40 g, were purchased from a local farm in Chonburi province, Thailand, and kept in a hatchery at Burapha University, Chonburi province for acclimatization for at least 2 weeks. They were maintained in concrete tanks (150×80 cm^2) containing fresh water with continuous aeration, under a natural photoperiod (12L:12D), at a temperature of about 25–30°C, and fed with commercial pellets twice daily.

Antisera and peptides

Five primary antisera used in this study consisted of anti-octopus (oct) GnRH, Lot. 9779 (generously provided by Dr. Pei-San Tsai), anti-salmon (s) GnRH, Lot. 1667 (a kind gift from Dr. Judy King), anti-lamprey (l) GnRH-I, Lot.1467 and anti-lGnRH-III, Lot. 3952, produced in the laboratory of Sower (1993), and anti-mammalian (m) GnRH (Sigma, St Louis, MO). The structures of peptides to which the antisera were raised are described in Table 1 (Gorbman and Sower 2003). Antiserum 9779 was selective for octGnRH, whereas approximately 50% immunoreactivity was abolished after preabsorbing the antisera with lGnRH-III, but not abolished after preabsorption with lGnRH-I (Ngernsoungnern et al. 2008). Antiserum 1667 demonstrated a specificity for sGnRH, but showed no cross-reactivity with lGnRH-III (Robinson et al. 2000). Antiserum 1467 has a specificity with cross-reactivities of 7.3% with lGnRH-III and less than 0.03, 0.02, and 0.01% cross-reactivity for chicken (c) GnRH-II, mGnRH, and cGnRH-I, respectively (Sower et al. 2000). Antiserum 3952 has cross-reactivities of 100% with lGnRH-I and III, less than 0.01% with mGnRH, cGnRH-I, cGnRH-II, and sGnRH (Robinson et al. 2000), and 0.1% with octGnRH (Ngernsoungnern et al. 2008). However, cross-reactivity of anti-mGnRH has not yet been identified in the previous study. To verify the specificities, anti-GnRHs were preabsorbed with lGnRH-I, lGnRH-III (American Peptide Company, Sunnyvale, CA), and octGnRH peptides (from Dr. Pei-San Tsai and Dr. Hiroyuki Minakata).

Immunocytochemistry

The prawn central nervous system (CNS) including eyestalk, supraesophageal, subesophageal, thoracic, and abdominal ganglia, and ovaries at spawn (stage 0), spent (stage 1), previttellogenic (stage 2), vittellogenic (stage 3) and mature stages (stage 4), as described by Meeratana and Sobhon (2007), were obtained from 10 adult female prawns, immediately fixed in Bouin's fixative overnight, and processed routinely for paraffin embedding. Serial sections were cut at 5 μm thick in horizontal plane, and then placed on poly-L-lysine coated slides. Immunoperoxidase technique used in this study was modified from the methods described by Sower et al. (1995). Briefly, the sections were deparaffinized, rehydrated, immersed in 70% ethanol

Table 1 The GnRH peptides to which the antisera were raised

Antiserum Lot.	Raised against	Amino acids of peptides positions										
		1			2	3	4	5	6	7	8	9	10
Unnamed	mGnRH	pGlu-			His-	Trp-	Ser-	Tyr-	Gly-	Leu-	Arg-	Pro-	Gly- NH2
1667	sGnRH	pGlu-			His-	Trp-	Ser-	Tyr-	Gly-	Trp-	Leu-	Pro-	Gly- NH2
1467	lGnRH-I	pGlu-			His-	Tyr-	Ser-	Leu-	Glu-	Trp-	Lys-	Pro-	Gly- NH2
3952	lGnRH-III	pGlu-			His-	Trp-	Ser-	His-	Asp-	Trp-	Lys-	Pro-	Gly- NH2
9779	octGnRH	pGlu-	Asn-	Tyr-	His-	Phe-	Ser-	Asn-	Gly-	Trp-	His-	Pro-	Gly- NH2

Data from Gorbman and Sower (2003)

containing 1% saturated $LiCO_3$ and 1% H_2O_2, and subsequently immersed in 0.1 M glycine and 0.1% Triton X-100 in order to get rid of picric acid, endogenous peroxidase, free aldehyde groups, and for tissue permeabilization, respectively. After blocking non-specific bindings with 4% bovine serum albumin (BSA), the sections were exposed to anti-mGnRH (1:20), anti-sGnRH (1:500), anti-octGnRH (1:500), anti-lGnRH-I (1:1,000), or anti-lGnRH-III (1:4,000) for overnight at 4°C. After extensive washing with phosphate buffer saline (PBS) containing 0.1% Tween-20 (PBST), the sections were incubated with horseradish peroxidase (HRP)-conjugated goat anti-rabbit IgG (1:500) (Zymed Laboratories, San Francisco, CA) for 60 min. Enzymatic reaction was developed by incubating the sections in 0.05% diaminobenzidine (DAB) and 0.03% H_2O_2. The sections were then dehydrated, cleared, mounted with mounting medium, observed under a Nikon ECLIPESE E600 light microscope, and images captured by Nikon ECIPESE 2000 CCD camera. The experiments were repeated at least three times for each tissue.

Immunofluorescence

The CNS and ovaries (as previously described) were immediately fixed in 4% paraformaldehyde in PBS overnight, extensively washed with PBS, followed by immersing in PBS containing 30% sucrose for overnight. The tissues were then embedded in O.C.T. compound (Miles Inc., Elkhart, IN), and serial cryosections were cut at 40 μm thick in horizontal plane and placed on poly-L-lysine coated slides. The cryosections were subsequently immersed in 0.1 M glycine and 0.1% Triton X-100, followed by blocking non-specific bindings with 4% BSA. The sections were then incubated with the same primary antisera at the same condition as previously described, and subsequently incubated with Alexa 488-conjugated goat anti-rabbit IgG (1:500) (Molecular Probes, Eugene, OR) for 60 min. In addition, the nuclei of cells in the CNS sections were stained with TO-PRO-3 (1:4,000) (Molecular Probes). The slides were viewed under an Olympus confocal laser scanning microscope (FV1000).

Specificities of antisera

The specificities of primary antisera were tested by preabsorption technique. Briefly, each of the primary antisera (100 μl at working dilution) was incubated with 100 μg of corresponding GnRH peptides, including octGnRH, sGnRH, lGnRH-I, and lGnRH-III for overnight, at 4°C. These preabsorbed antisera were then used in the immunoperoxidase and immunofluorescence staining instead of the non-absorbed antisera using the same conditions. The specificity of the secondary antiserum was performed by replacing the primary antisera with PBS.

Results

Immunocytochemistry

Five antisera (sGnRH, octGnRH, lGnRH-I, lGnRH-III and mGnRH) were used for detecting the existence of GnRHs in CNS and ovary of the prawn. Two ir-GnRHs (ir-lGnRH-III and ir-octGnRH) were detected in the CNS, whereas one ir-GnRH (ir-lGnRH-I) was observed in the ovary. The ir-lGnRH-III was detected in the soma of neurons located in deutocerebrum (Fig. 1a), within the neuronal cluster number 11 as classified by Sandeman et al. (1992) (Fig. 1c). All of the ir-lGnRH-III positive neuronal cell bodies belonged to medium-sized neurons with the diameter about 15 μm (Fig. 1a, inset). This result was confirmed by immunofluorescence which revealed the presence of the ir-lGnRH-III in the soma of medium-sized neuronal cells within the same cluster (Fig. 1d, e). More ir-lGnRH-III positive neuronal bodies were detected by the immunofluorescence when compared with those detected by the immunoperoxidase technique as a result of using thicker sections for detection of positive cells by confocal microscope, and the use of less denaturing conditions in immunofluorescence method. There was no ir-lGnRH-III observed in the sections incubated with preabsorbed anti-lGnRH-III (Fig. 1b, f). Interestingly, the ir-octGnRH was present only in the thoracic ganglia. Unlike the ir-lGnRH-

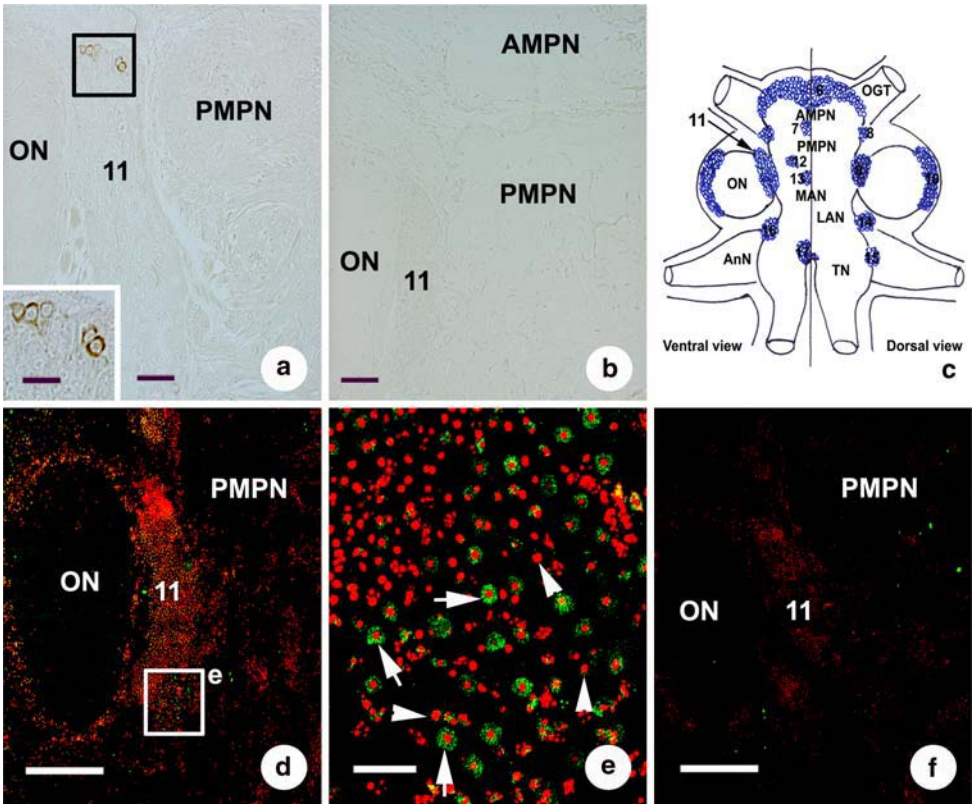


Fig. 1 Immunoperoxidase (**a**–**b**) and immunofluorescence (**d**–**f**), showing the distribution of ir-lGnRH-III in the prawn supraesophageal ganglion. **a** The ir-lGnRH-III is present in neuronal cell bodies within cluster 11 of the deutocerebrum. (**a**, inset) Higher magnification of boxed area in (**a**), showing the ir-lGnRH-III in neuronal cell bodies of medium-sized neurons. **b** Negative control section of immunoperoxidase, using lGnRH-III-preabsorbed antiserum as a probe, showing no ir-lGnRH-III. **c** A diagram showing the locations of neuronal cell clusters as numbered in the supraesophageal ganglion (modified from Sandeman et al. 1992). **d** Immunofluorescence showing the ir-lGnRH-III neuronal cell bodies in cluster 11. **e** Higher magnification of the *boxed area* in (**d**), revealing the ir-lGnRH-III in medium-sized neuronal cell bodies (*arrows*). There was no ir-lGnRH-III in some neuronal cells within the same cluster (*arrowheads*). **f** Negative control section of immunofluorescence using lGnRH-III-preabsorbed antiserum as a probe, showing no immunoreactivity. *AMPN* anterior medial protocerebral neuropil, *AnN* antenna II neuropil, *LAN* lateral antenna I neuropil, *MAN* medial antenna I neuropil, *PMPN* posterior medial protocerebral neuropil, *OGT* olfactory globular tract, *ON* olfactory neuropil, *TN* tegumental neuropil. Scale bars: 100 μm (**a** and **b**); 300 μm (**d** and **f**); 30 μm (**e**); 25 μm (**a**, inset)

III, the ir-octGnRH was not only detected in neuronal cell bodies, but was shown in the nerve fibers distributed in thoracic ganglia (Fig. 2). The ir-octGnRH was present in some medium-sized neurons located at dorsolateral neuronal cell cluster (DLC) (Fig. 2a, b, f), and some large-sized neurons (diameter of >25 μm) at ventromedial neuronal cell cluster (VMC) (data not shown). In addition, the ir-octGnRH fibers innervated some of the medium-sized and large-sized neuronal cells of the thoracic ganglion (Fig. 2c, d). This result was supported by immunofluorescence showing the existence of ir-octGnRH in the large-sized and medium-sized neuronal cells (Fig. 2g, h). In contrast, there were no ir-lGnRH-I, ir-sGnRH, and ir-mGnRH observed in any part of the prawn CNS. In the related control sections where anti-octGnRH was preabsorbed with octGnRH peptide, there was no immunostaining (Fig. 2e, i). The data of the distribution and intensities of ir-GnRHs in the prawn CNS are summarized in Table 2.

In the ovaries, the intense ir-lGnRH-I was detected in the cytoplasm of late previtellogenic oocyte (oocyte stage 2, Oc2) and early vitellogenic oocyte (oocyte stage 3, Oc3) as classified by Meeratana and Sobhon (2007) (Fig. 3a, b). In Oc2, the ir-lGnRH-I was observed at the perinuclear region and observed in the cytoplasm of Oc3 (Fig. 3b). The results obtained from immunofluorescence were consistent with the immunoperoxidase staining, showing the distribution of ir-lGnRH-I at the perinuclear region of the Oc2 and throughout the cytoplasm of the Oc3 (Fig. 3d, e). There was no ir-lGnRH-I observed in other areas of the ovary. In the control sections where anti-lGnRH-I was preabsorbed with lGnRH-I, there was no immunostaining (Fig. 3c, f). The detection of the ir-lGnRH-I in the prawn ovary is summarized in Table 3.

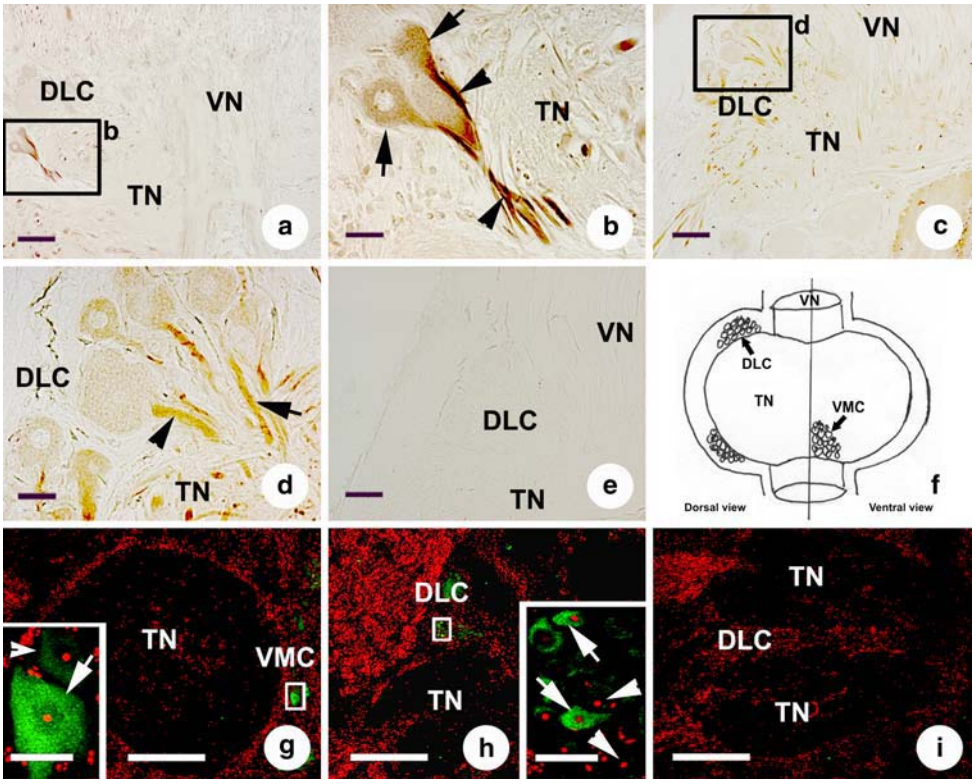


Fig. 2 Immunoperoxidase (**a–e**) and immunofluorescence (**g–i**), showing the distribution of ir-octGnRH in the prawn thoracic ganglia. **a** The ir-octGnRH is present in medium-sized neuronal cells in the dorsolateral neuronal cell cluster (DLC). **b** Higher magnification showing the ir-octGnRH in the soma of neuronal cells (*arrows*) and fibers (*arrowheads*) extending from the soma. **c** and **d** Light micrographs showing the ir-octGnRH positive fibers innervating medium-sized (**d**, *arrow*) and large-sized (**d**, *arrowhead*) neuronal cells. **e** Negative control using octGnRH-preabsorbed antiserum as a probe, revealing only background staining. **f** A diagram showing the locations of neuronal cell clusters in the thoracic ganglion. **g** and **h** Showing the ir-octGnRH in the soma of some large-sized neuronal cells in ventromedial neuronal cell cluster (VMC) (**g** and inset, *arrow*) and in medium-sized neuronal cells in DLC (**h** and inset, *arrows*). However, some neuronal cells within the same cluster show no ir-octGnRH (**g** and **h**, insets, *arrowheads*). **i** Negative control section of immunofluorescence using octGnRH-preabsorbed antiserum as a probe, showing only nuclear staining. *TN* thoracic neuropil, *VN* ventral nerve cord. Scale bars 100 μm (**a**, **c** and **e**); 25 μm (**b** and **d**); 300 μm (**g**, **h** and **i**); 30 μm (**g** and **h**, insets)

Antisera specificity

The immunoreactivities of anti-lGnRH-I, anti-lGnRH-III and anti-octGnRH were completely abolished when pre-absorbed with lGnRH-I, lGnRH-III and octGnRH peptides, respectively (Figs. 1b, f, 2e, i, 3c, f). The specificities of the five antisera are summarized in Table 4.

Discussion

In the present study, we demonstrated the presence of immunoreactive GnRH-like peptides in the CNS and ovary of the giant freshwater prawn. Interestingly, two of the five GnRH isoforms were detected in the neural tissue, whereas another one of the tested five GnRH isoforms was

Table 2 The distribution of ir-GnRHs in the CNS of *M. rosenbergii*

CNS parts	ir-lGnRH-III				ir-octGnRH			
	Neuronal cells[a]			Fibers	Neuronal cells[a]			Fibers
	Small	Medium	Large		Small	Medium	Large	
Eyestalk	–	–	–	–	–	–	–	–
Supraesophageal ganglion (neuronal cluster 11)	–	+ + +	–	–	–	–	–	–
Subesophageal ganglion	–	–	–	–	–	–	–	–
Thoracic ganglia	–	–	–	–	–	+ + +	+ + +	+ + +
Abdominal ganglia	–	–	–	–	–	–	–	–

–, no immunoreactivity; + + +, strong immunoreactivity

[a] Small neuronal cell, <15 μm in diameter; medium neuronal cell, 15–25 μm in diameter; large neuronal cell, >25 μm in diameter

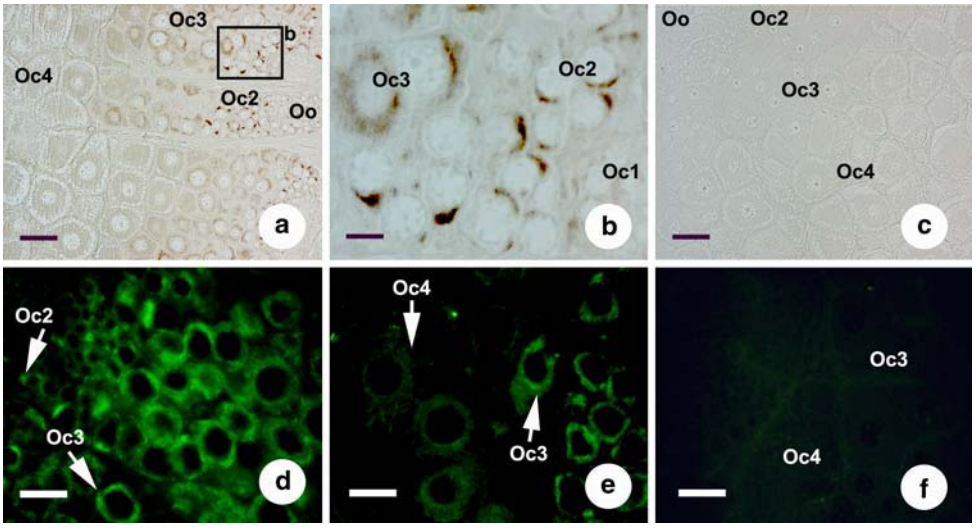


Fig. 3 Immunoperoxidase (**a–c**) and immmunofluorescence (**d–f**) showing the distribution of ir-lGnRH-I in the prawn ovary. The ir-lGnRH-I is present in Oc2 and Oc3 oocytes (**a** and **d**). Higher magnification showing the ir-lGnRH-I localized at the perinuclear region of Oc2 and in the cytoplasm of Oc3 (**b**, **d**, and **e**). Negative control sections of immunoperoxidase (**c**) and immunofluorescence (**f**) using lGnRH-I-preabsorbed antiserum as a probe, showing only background staining. *Oo* oogonia, *Oc2* oocyte stage 2 (late previtellogenic oocyte), *Oc3* oocyte stage 3 (early vitellogenic oocyte), *Oc4* oocyte stage 4 (late vitellogenic oocyte). Scale bars: 100 μm (**a** and **c**); 25 μm (**b**); 50 μm (**d**, **e** and **f**)

present in the ovary. These results suggest that there may be at least three GnRH-like peptides present in this prawn. The first GnRH isoform which was found in neuronal cell cluster 11 of the deutocerebrum was closely related to lGnRH-III. The second isoform which was found in soma and fibers of thoracic ganglia was closely related to octGnRH, and the third isoform observed in the oocytes was closely related to lGnRH-I. These results support previous findings that in one species of animal, either vertebrate or invertebrate, there are at lease two isoforms of GnRH (Fernald and White 1999; Gorbman and Sower 2003; Morgan and Millar 2004). The immunoreactivities of the anti-lGnRH-I and anti-lGnRH-III were observed in the different tissues of the prawn, i.e., ovary and CNS, respectively. In addition, the ir-octGnRH was also observed in the different parts of the prawn CNS compared to the ir-lGnRH-III. As shown in Table 1, these three GnRH isoforms are structurally different and that these differences are sufficient to have distinct epitopes that could generate antiserum-specific responses. The results from the preabsorption study further confirmed the specificity of the three antisera, because the immunoreactivities were completely abolished when the antisera were preabsorbed with corresponding GnRH peptides. These results suggested that there are at least three isoforms of GnRH in the prawn tissues. However, the primary structures of these GnRH-like peptides in the prawn might be similar but not identical to lGnRH-III, octGnRH, and lGnRH-I. Furthermore, these tissue-specific GnRH-like peptides could serve multiple functions including a possible role in reproduction.

In crustaceans, deutocerebrum is a major chemo-sensory organ that regulates various behaviors including feeding, locomotion, and mating (Sandeman et al. 1992). Similarly, in the aplysia, *A. californica*, ir-GnRH was detected in the osphradium, the major chemo-sensory structure of opisthobranch gastropod, and in CNS ganglia including cerebral, buccal, pedal, pleural, and abdominal (Tsai et al. 2003; Zhang et al. 2007) which regulate certain behaviors, including feeding, locomotion, copulation (Kandel 1979). In the present study, the ir-lGnRH-III neurons located in the prawn deutocerebrum may be involved in chemoreception that could be related indirectly to the control of reproductive behavior similar to the aplysia. However, the

Table 3 The distribution of ir-lGnRH-I in the ovary of *M. rosenbergii*

Ovarian follicles						
Oogonia	Early Previtellogenic oocyte	Late Previtellogenic oocyte	Early Vitellogenic oocyte	Late Vitellogenic oocyte	Mature Oocyte	Follicular cell
(Oo)	(Oc1)	(Oc2)	(Oc3)	(Oc4)	(Oc5)	
−	−	+ + +	+ + +	−	−	−

−, no immunoreactivity; + + +, strong immunoreactivity

Table 4 Specificities of the antisera tested with the preabsorption with various GnRH peptides

Antisera against	Immunoreactivity					
	Without preabsorption	Preabsorbed with				
		mGnRH	sGnRH	octGnRH	lGnRH-I	lGnRH-III
mGnRH (unnamed)	−	ND	ND	ND	ND	ND
sGnRH (1667)	−	ND	ND	ND	ND	ND
octGnRH (9779)	+ + +	ND	+ + +	−	+ + +	+ + +
lGnRH-I (1467)	+ + +	ND	+ + +	+ + +	−	+ + +
lGnRH-III (3952)	+ + +	ND	+ + +	+ + +	−	−

−, no immunoreactivity; + + +, strong immunoreactivity; *ND* not determined

exact function of GnRH-like peptide in deutocerebrum needs to be further elucidated. The finding that ir-octGnRH was present in neurons of thoracic ganglia and in the immunoreactive fibers innervating some neurons of the same ganglia suggest that the octGnRH-like peptide could be involved in regulating the release of certain neuroendocrine substance(s), such as gonad-stimulating hormone (GSH) which controls gonad maturation in prawn (Huberman 2000) and vitellogenenin synthesis in hepatopancreas (Van Herp and Payen 1991). Many studies have suggested that GSH is synthesized and excreted by neurosecretory cells in thoracic ganglia (Huberman 2000; Meeratana et al. 2006). Additionally, 5-hydroxytryptamine (5-HT) was also detected in the neurons of the freshwater prawn, *M. rosenbergii* thoracic ganglia (Sosa et al. 2004), and that the release of GSH could be induced by 5-HT (Fingerman 1997; Vaca and Alfaro 2000). Unfortunately, the relationship of GnRH and 5-HT has not yet been investigated in the freshwater prawn or related species. It is possible that the ir-octGnRH neurons observed in the present study may be involved in the prawn reproduction by stimulating the neurosecretory cells in thoracic ganglia to secrete GSH directly, or it could act in concert with 5-HT positive neurons. The co-localization of GnRH and 5-HT in the prawn CNS and the exact relationship between GnRH and 5-HT in stimulating the synthesis and release of GSH need more investigation before a firm conclusion can be reached.

In the present study, we demonstrated for the first time that a lGnRH-I-like peptide occurred in the prawn ovary. In vertebrates, it has been shown that GnRH was expressed in the ovary of human (Choi et al. 2006), a gold fish, *Carassius auratus* (Pati and Habibi 1998), and a rainbow trout, *Oncorhynchus mykiss* (Schalburg et al. 1999). In addition, GnRH receptors were also detected in the ovary of a goldfish, *C. auratus* (Pati and Habibi 1993), a common crap, *Cyprinus carpio* (Pati and Habibi 1992), and a mollusk, *O. vulgaris* (Kanda et al. 2006). These findings confirmed that a GnRH-like peptide exists in the fish ovaries, and that it may have paracrine/autocrine roles in the regulation of ovarian maturation (Pati and Habibi 1998). In a protochrodate, *C. intestinalis*, ir-mGnRH and ir-cGnRH-I were detected in the ovary, and it was further shown that these two isoforms of GnRH were involved in reproduction, including stimulating the synthesis and release of sex steroids from gonads, and the synthesis and release of luteinizing hormone from rat pituitary (Di Fiore et al. 2000). Tunicate (t) GnRH-III and l-GnRH-I were reported to induce gamete release from a chiton, *Mopalia* sp. (Gorbman et al. 2003). Moreover, in *A. californica*, the transcript for aplysia (ap) GnRH was expressed in the ovotestis, but its exact function has not yet been elucidated (Zhang et al. 2007). In the present study, the ir-lGnRH-I was detected at the perinuclear region of Oc2 and in cytoplasm of Oc3. It is possible that the lGnRH-I-like peptide was first synthesized in late previtellogenic oocytes (Oc2), accumulated in the cytoplasm of early vitellogenic oocytes (Oc3), and disappeared before these oocytes reached maturation. These findings suggest that in this prawn, lGnRH-I-like peptide may be directly involved in oocyte development. Similarly, GnRH was suggested to play a significant role in controlling of the oocyte maturation and spawning in a coral (Twan et al. 2006). The relationship between 5-HT and GnRH in the stimulation of oocyte maturation may also be possible as 5-HT was detected in the cytoplasm of the follicular cells and primary oocytes of *P. monodon* ovary. The ir-5-HT gradually increased in the cytoplasm of the oocytes in stage II to stage IV ovaries, and in addition to ovarian maturation, 5-HT was also shown to induce spawning in this shrimp (Wongprasert et al. 2006). Egg-laying hormone (ELH), a peptide, which is known to induce spawning in mollusks (Wayne 2001), was detected in the follicular cells surrounding oocytes of *Haliotis asinina* (Saitongdee et al. 2005) and *P. monodon*, thus it was also suggested that ELH may play a role in the induction of the ovarian maturation and spawning in shrimp (Liu et al. 2006). It is, therefore, possible that lGnRH-I-like peptide in the prawn ovary may act synergistically in some way with 5-HT and ELH in regulating the ovarian maturation and spawning of *P. monodon* as well as in this freshwater prawn. However, the

relationship of GnRH, 5-HT, and ELH should be explored by further research, particularly once the primary structure(s) of GnRH(s) are determined. An experiment determining the structure of the prawn GnRH is being attempted.

In conclusion, the present study demonstrated the presence of three isoforms of GnRH-like peptide in the CNS and ovarian tissues of *M. rosenbergii*. Two of these isoforms were closely related to ancient vertebrate GnRH peptides, namely lGnRH-I and lGnRH-III, whereas the other isoform was closely related to an invertebrate GnRH peptide, octGnRH. The three different isoforms of GnRH-like peptides are tissue specific and each may play different yet synergistic roles in the reproductive processes, i.e., neuromodulation and oocyte maturation, and/or chemosensory functions.

Acknowledgements This study was supported by the Thailand Research Fund (Royal Golden Jubilee Ph.D. Program (Grant No. PHD/0249/2546) to A. Ngernsoungnern and P. Sretarugsa, and Senior Research Scholar Fellowship to P. Sobhon), Commission on Higher Education, Ministry of Education (Research Group Development Grant to P. Sobhon) and NSF0421923 grant to Stacia A. Sower. The authors would like to thank Dr. Pei-San Tsai, Dr. Judy King, and Dr. Hiroyuki Minakata for generously providing GnRH antisera and peptides.

References

Adams BA, Tello JA, Erchegyi J, Warby C, Hong DJ, Akinsanya KO, Mackie GO, Vale W, Rivier JE, Sherwood NM (2003) Six novel gonadotropin-releasing hormones are encoded as triplets on each of two genes in the protochordate, *Ciona intestinalis*. Endocrinology 144:1907–1919

Anctil M (2000) Evidence for gonadotropin-releasing hormone-like peptides in a Cnidarian nervous system. Gen Comp Endocrinol 119:317–328

Anctil M, Tekaya S (2005) Gonadotropin-releasing hormone-like immunoreactivity in the planarian *Bdelloura candida* (Platyhelminthes, Tricladida). Invert Biol 124:11–17

Burkenroad MD (1963) The evolution of the Eucarida (Crustacea, Eumalacostraca), in relation to the fossil record. Tulane Stud Geol 1:1–17

Cameron CB, Mackie GO, Powell JFF, Lescheid DW, Sherwood NM (1999) Gonadotropin-releasing hormone in mulberry cells of *Saccoglossus* and *Ptychodera* (Hemichordata: Enteropneusta). Gen Comp Endocrinol 114:2–10

Choi JH, Gilks CB, Auersperg N, Leung PCK (2006) Immunolocalization of gonadotropin-releasing hormone (GnRH)-I, GnRH-II, and type-I GnRH receptor during follicular development in the human ovary. J Clin Endocrin Metab 91:4562–4570

Di Cosmo A, Di Cristo C (1998) Neuropeptidergic control of the optic gland of *Octopus valgaris*: FMRF-amide and GnRH immunoreactivity. J Comp Neurol 398:1–12

Di Cristo C, Paolucci M, Iglesias J, Sanchez J, Di Cosmo A (2002) Presence of two neuropeptides in the fusiform ganglion and reproductive ducts of *Octopus vulgaris*: FMRFamide and gonadotropin-releasing hormone (GnRH). J Exp Zool 292:267–276

Di Fiore MM, Rastogi RK, Ceciliani F, Messi E, Botte V, Botte L, Pinelli C, D'Aniello B, D'Aniello A (2000) Mammalian and chicken I forms of gonadotropin-releasing hormone in the gonads of a protochordate, *Ciona intestinalis*. PNAS 97:2343–2348

Fernald RD, White RB (1999) Gonadotropin-releasing hormone genes: phylogeny, structure, and functions. Front Neuroendocrin 20:224–240

Fingerman M (1997) Crustacean endocrinology: a retrospective, prospective, and introspective analysis. Physiol Zool 70:257–269

Goldberg JI, Garofalo R, Price CJ, Chang JP (1993) Presence and biological activity of a GnRH-like factor in the nervous system of *Helisoma trivolvis*. J Comp Neurol 336:571–582

Gorbman A, Sower SA (2003) Evolution of the role of GnRH in animal (Metazoan) biology. Gen Comp Endocrinol 134:207–213

Gorbman A, Whiteley A, Kavanaugh S (2003) Pheromonal stimulation of spawning release of gametes by gonadotropin releasing hormone in the chiton, *Mopalia* sp. Gen Comp Endocrinol 131:62–65

Huberman A (2000) Shrimp endocrinology. A review. Aquaculture 191:191–208

Iwakoshi E, Takuwa-Kuroda K, Fujisawa Y, Hisada M, Ukena K, Tsutsui K, Minakata H (2002) Isolation and characterization of a GnRH-like peptide from *Octopus valgaris*. Biochem Biophy Res Com 291:1187–1193

Iwakoshi-Ukena E, Ukena K, Takuwa-Kuroda K, Kanda A, Tsutsui K, Minakata H (2004) Expression and distribution of octopus gonadotropin-releasing hormone in the central nervous system and peripheral organs of the octopus (*Octopus vulgaris*) by in situ hybridization and immunohistochemistry. J Comp Neurol 477:310–323

Kah O, Lethimonier C, Somoza G, Guilgur LG, Vaillant C, Lareyre JJ (2007) GnRH and GnRH receptors in metazoa: a historical, comparative, and evolutive prespective. Gen Comp Endocrinol 153:346–364

Kanda A, Takahashi T, Satake H, Minakata H (2006) Molecular and functional characterization of a novel gonadotropin-releasing-hormone receptor isolated from the common octopus (*Octopus valgaris*). Biochem J 395:125–135

Kandel ER (1979) Behavioral biology of *Aplysia*. W.H. Freeman and Company, San Francisco

Kavanaugh SI, Root AR, Sower SA (2005) Distribution of gonadotropin-releasing hormone (GnRH) by in situ hybridization in the tunicate *Ciona intestinalis*. Gen Comp Endocrinol 141:76–83

Kozloff EN (1990) Invertebrates. Saunders College Publishing, Philadelphia

Liu Z, Sobhon P, Withyachumnarnkul B, Hanna P (2006) Identification of a putative egg-laying hormone in neural and ovarian tissues of the black tiger shrimp, *Penaeus monodon*, using immunocytochemistry. Invert Neurosci 6:41–46

Meeratana P, Withyachumnarnkul B, Damrongphol P, Wongprasert K, Suseangtham A, Sobhon P (2006) Serotonin induces ovarian maturation in giant freshwater prawn broodstock, *Macrobrachium rosenbergii* de Man. Aquaculture 260:315–325

Meeratana P, Sobhon P (2007) Classification of differentiating oocytes during ovarian cycle in the giant fresh water prawn, *Macrobrachium rosenbergii* de Man. Aquaculture 270:249–258

Morgan K, Millar RP (2004) Evolution of GnRH ligand precursors and GnRH receptors in protochordate and vertebrate species. Gen Comp Endocrinol 139:191–197

Ngernsoungnern P, Ngernsoungnern A, Kavanaugh S, Sobhon P, Sower SA, Sretarugsa P (2008) The presence and distribution of gonadotropin-releasing hormone-liked factor in the central nervous system of the black tiger shrimp, *Penaeus monodon*. Gen Comp Endocrinol 155:613–622

Pati D, Habibi HR (1992) Characterization of gonadotropin-releasing hormone (GnRH) receptors in the ovary of common crap (*Cyprinus carpio*). Can J Physiol Pharmacol 70:268–274

Pati D, Habibi HR (1993) Characterization of gonadotropin-releasing hormone receptors in goldfish ovary: variation during follicular development. Am J Physiol 264:R227–R234

Pati D, Habibi HR (1998) Presence of salmon gonadotropin-releasing hormone (GnRH) and compounds with GnRH-like activity in the ovary of goldfish. Endocrinology 139:2015–2024

Pazos AJ, Mathieu M (1999) Effects of five natural gonadotropin-releasing hormones on cell suspensions of marine bivalve gonad: stimulation of gonial DNA synthesis. Gen Comp Endocrinol 113:112–120

Powell JFF, Reska-Skinner SM, Prakash MO, Fischer WH, Park M, Rivier JE, Craig AG, Mackie GO, Sherwood NM (1996) Two new forms of gonadrotropin-releasing hormone in a protochordate and the evolutionary implications. Proc Natl Acad Sci USA 93:10461–10464

Robinson CT, Tobet SA, Chase C, Waldron T, Sower SA (2000) Gonadotropin-releasing hormones in the brain and pituitary of the teleost, the white sucker. Gen Comp Endocrinol 117:381–394

Saitongdee P, Apisawetakan S, Anunruang N, Poomthong T, Hanna P, Sobhon P (2005) Egg-laying-hormone immunoreactivity in the neural ganglia and ovary of *Haliotis asinina* Linnaeus. Invert Neurosci 5:165–172

Sandeman D, Sandeman R, Derby C, Schmidt M (1992) Morphology of the brain of crayfish, crabs, and spiny lobsters: A common nomenclature for homologous structures. Biol Bul 183:304–326

Schalburg KR, Warby CM, Sherwood NM (1999) Evidence for gonadotropin-releasing hormone peptides in the ovary and testis of rainbow trout. Biol Reprod 60:1338–1344

Sosa MA, Spitzer N, Edwards DH, Baro DJ (2004) A crustacean serotonin receptor: cloning and distribution in the thoracic ganglia of crayfish and freshwater prawn. J Comp Neurol 473:526–537

Sower SA, Chiang YC, Lovas S, Conlon JM (1993) Primary structure and biological activity of a third gonadotropin-releasing hormone from lamprey brain. Endocrinology 132:1125–1131

Sower SA, Nozaki M, Knox C, Gorbman A (1995) The occurrence and distribution of GnRH in the brain of Atlantic hagfish, an agnatha, determined by chromatography and immunocytochemistry. Gen Comp Endocrinol 97:300–307

Sower SA, McGregor AJ, Materne OLJ, Chase C, Potter I, Joss J (2000) Evidence for lamprey GnRH-I and -III-like molecules in the brains of the southern hemisphere lampreys *Geotria australis* and *Mordacia mordax*. Gen Comp Endocrinol 120:168–175

Terakado K (2001) Induction of gamete release by gonadotropin-releasing hormone in a protochordate, *Ciona intestinalis*. Gen Comp Endocrinol 124:277–284

Tsai PS, Maldonado TA, Lunden JB (2003) Localization of gonadotropin-releasing hormone in the central nervous system and a peripheral chemosensory organ of *Aplysia californica*. Gen Comp Endocrinol 130:20–28

Tsai PS (2006) Gonadotropin-releasing hormone in invertebrates: structure, function, and evolution. Gen Comp Endocrinol 148:48–53

Twan WH, Hwang JS, Lee YH, Jeng SR, Yueh WS, Tung YH, Wu HF, Dufour S, Chang CF (2006) The presence and ancestral role of gonadotropin-releasing hormone in the reproduction of scleractinian coral, *Euphyllia ancora*. Endocrinology 147:397–406

Vaca AA, Alfaro J (2000) Ovarian maturation and spawning in the white shrimp, *Penaeus vannamei*, by serotonin injection. Aquaculture 182:373–385

Van Herp F, Payen GG (1991) Crustacean neuroendocrinology: perspectives for the control of reproduction in aquacultural system. Bull Inst Zool Acad Sinica Monograph 16:513–539

Wayne NL (2001) Regulation of seasonal reproduction in mollusks. J Biol Rhythms 16:391–402

Wongprasert K, Asuvapongpatana S, Poltana P, Tiensuwan M, Withyachumnarnkul B (2006) Serotonin stimulates ovarian maturation and spawning in the black tiger shrimp *Penaeus monodon*. Aquaculture 261:1447–1454

Young KG, Chang JP, Goldberg JI (1999) Gonadotropin-releasing hormone neuronal system of the fresh water snails *Helisoma trivolvis* and *Lymnaea stagnalis*: possible involvement in reproduction. J Comp Neurol 404:427–437

Zhang L, Wayne NL, Sherwood NM, Postigo HR, Tsai PS (2000) Biological and immunological characterization of multiple GnRH in an opisthobranch mollusk, *Aplysia californica*. Gen Comp Endocrinol 11:77–89

Zhang L, Tello JA, Zhang W, Tsai PS (2007) Molecular cloning, expression pattern, and immunocytochemical localization of a gonadotropin-releasing hormone-like molecule in the gastropod mollusk, *Aplysia californica*. Gen Comp Endocrinol. doi: 10.1016/j.ygcen.2007.11.015

Aquaculture 279 (2008) 197–203

Contents lists available at ScienceDirect

Aquaculture

journal homepage: www.elsevier.com/locate/aqua-online

The existence of gonadotropin-releasing hormone (GnRH) immunoreactivity in the ovary and the effects of GnRHs on the ovarian maturation in the black tiger shrimp *Penaeus monodon*

Apichart Ngernsoungnern [a,b], Piyada Ngernsoungnern [a,b], Wattana Weerachatyanukul [a], Jittipan Chavadej [a], Prasert Sobhon [a], Prapee Sretarugsa [a,*]

[a] Department of Anatomy, Faculty of Science, Mahidol University, Bangkok, 10400, Thailand
[b] Department of Biology, Faculty of Science, Mahasarakham University, Mahasarakham, 44150, Thailand

ARTICLE INFO

Article history:
Received 31 August 2007
Received in revised form 29 March 2008
Accepted 9 April 2008

Keywords:
Penaeus monodon
GnRH
Ovarian maturation
Immunolocalization

ABSTRACT

Immunocytochemical localization using antibodies against five isoforms of gonadotropin-releasing hormone (GnRH), namely, luteinizing hormone-releasing hormone (LHRH), salmon (s)GnRH, octopus (oct)GnRH, lamprey (l)GnRH-I, and lGnRH-III, showed that only lGnRH-I immunoreactivity (ir-lGnRH-I) was localized in follicular cells of proliferative, vitellogenic, and mature ovaries. The effects of exogenous GnRHs on the ovarian maturation cycle of *Penaeus monodon* were compared by treating female broodstocks with LHRH, sGnRH, and lGnRH-I. The cycle of ovarian maturation in both eyestalk-ablated and eyestalk-intact shrimp administered with the three isoforms of GnRH was significantly shorter than that of the control animals. Moreover, administrations of all GnRH isoforms showed similar numbers of spawned eggs and the percentage of successful fertilization as in the control animals. These findings suggest that GnRHs may be highly conserved peptides that play an important role in inducing the ovarian maturation in the shrimp.
© 2008 Elsevier B.V. All rights reserved.

1. Introduction

In penaeid shrimp, the practical technique for the induction of ovarian maturation and spawning, is eyestalk ablation (Panouse, 1943). It is generally believed that reproduction-inhibiting factors, including gonad-inhibiting hormone (GIH) and mandibular organ-inhibiting hormone (MOIH), produced and secreted from the X-organ-sinus gland system in the eyestalk, are eliminated upon eyestalk ablation, thus the gonadal development is no longer inhibited (Huberman, 2000; Okumura, 2004). Although this method provides a reliable way to obtain oocyte maturation and spawning, it causes deterioration in egg quantity and quality over time, as well as limited use of the female broodstock (Vaca and Alfaro, 2000). Consequently, many alternative approaches have been proposed to replace eyestalk ablation, one of which is the endocrine manipulation. Attempts have been made to apply many reproductive-related factors identified in crustaceans, including neurotransmitters, peptide hormones, and steroids, in order to obviate eyestalk ablation. It has been reported that oocyte development of the sand shrimp, *Crangon crangon*, can be stimulated by human chorionic gonadotropin (HCG) (Bomirski and Klek-Kawinska, 1976). Similar effect has been obtained using terpenoid hormones including methyl farnesoate (MF) or juvenile hormone-III (JH-III), which could stimulate ovarian maturation and increase oocyte diameters in *P. vannamei* (Tsukimura and Kamemoto, 1991). Furthermore, one of the well-known neurotransmitter, 5-hydroxytryptamine (5-HT), has been shown to stimulate ovarian maturation in *Procambarus clarkii* (Sarojini et al., 1995), *P. vannamei* (Vaca and Alfaro, 2000), *Macrobrachium rosenbergii* (Meeratana et al., 2006), and also in *P. monodon* (Wongprasert et al., 2006). However, at present the diversity of hormones involved in shrimp reproduction, their individual roles and relatedness, have not yet been fully defined. A better understanding of shrimp endocrinology is essential for hormonal manipulation to be applied in shrimp aquaculture.

GnRH, a well characterized peptide hormone, has long been known to function in regulating gonadal development and reproduction in both vertebrates and invertebrates (Sherwood et al., 1993; Fernald and White, 1999; Gorbman and Sower, 2003; Tsai, 2006). Presently, GnRH is characterized into 25 isoforms: 14 isoforms in vertebrates and 11 isoforms in invertebrates. All these isoforms are classified into 5 major groups: GnRH1, GnRH2, GnRH3, GnRH4, and GnRH5, based on phylogenetic analysis, function, distribution, and developmental origin (Silver et al., 2004; Sower et al., 2004; Zhang et al., 2008). The existence of GnRH immunoreactivity (ir-GnRH) had been demonstrated in

* Corresponding author. Department of Anatomy, Faculty of Science, Mahidol University, Rama 6 Rd., Rajathevi, Bangkok, 10400, Thailand. Tel.: +66 2 201 5410; fax: +66 2 354 7168.
E-mail addresses: scpsr@mahidol.ac.th, pchittanon@yahoo.com (P. Sretarugsa).

0044-8486/$ – see front matter © 2008 Elsevier B.V. All rights reserved.
doi:10.1016/j.aquaculture.2008.04.018

various tissues of invertebrate species, for examples, neural tissue of mollusks (Goldberg et al., 1993; Di Cosmo and Di Cristo, 1998; Pazos and Mathieu, 1999; Young et al., 1999; Zhang et al., 2000; Di Cristo et al., 2002; Iwakoshi et al., 2002; Tsai et al., 2003; Iwakoshi-Ukena et al., 2004; Zhang et al., 2008), and gonadal tissue of mollusks (Young et al., 1999; Zhang et al., 2000), and a tunicate (Tsutsui et al., 1998; Di Fiore et al., 2000). In addition, the reproductive-related function of GnRH had been demonstrated in a number of invertebrate species, including a tunicate, *Ciona intestinalis* (Terakado, 2001; Adams et al., 2003), mollusks, *Octopus vulgaris*, *Mopalia* sp., and *Aplysia californica* (Iwakoshi et al., 2002; Gorbman et al., 2003; Tsai et al., 2003; Iwakoshi-Ukena et al., 2004), and a coral, *Euphyllia ancora* (Twan et al., 2006). The reproductive function of GnRH has also been indirectly demonstrated in *P. monodon* by the ability of its hepatopancreatic extract in inducing LH release from rat anterior pituitary glands *in vitro* (Fann et al., 1990). Our research group has recently demonstrated the existence of GnRH-like factors in *P. monodon* by detecting the presence of immunoreactivities against lGnRH-III and octGnRH in neurons of the supraesophageal ganglion and some nerve tracts of *P. monodon* CNS (Ngernsoungnern et al., 2008b). Nevertheless, the role of GnRH in shrimp reproduction is still not yet understood. We demonstrate, herein, the presence of a GnRH-like factor in the ovary of *P. monodon*, and the effect of three GnRH isoforms on enhancing the ovarian maturation in this species.

2. Materials and methods

2.1. Animals

Male and female *P. monodon* broodstocks weighing about 120–180 g and 200–280 g, respectively, were caught from Andaman Sea, and subsequently acclimatized for at least one week at a commercial farm in Rayong Province, Thailand. The shrimp were maintained in concrete tanks containing filtered seawater with ~30 ppt salinity, at 25–28 °C, and continuous aeration. The male and female shrimp were kept together at the ratio, 1:3 to allow natural mating. The shrimp were fed twice a day with minced squids. Approximately 70% of seawater was replaced daily. Unilateral eyestalk ablation was performed on one group of the female shrimp.

2.2. Antibodies and peptides

For immunocytochemistry, five available antibodies against GnRHs were used. Because the shrimp is considered to be a protostome, the first antibody chosen had been the antibody raised against octGnRH (anti-octGnRH, Lot 9779, generously provided by Dr. Pei-San Tsai). The other three antibodies were generated against GnRH isoforms of one lower vertebrate (lamprey) and one higher vertebrate (salmon). These three antibodies included anti-sGnRH, Lot 1667 (a gift from Dr. Judy King), anti-lGnRH-I, Lot 1467, and anti-lGnRH-III, Lot 3952 (gifts from Dr. Stacia A. Sower). Moreover, anti-LHRH (Sigma, St. Louis, MO) was also used to determine the presence of LHRH, which may be similar to higher vertebrate GnRH, in the shrimp tissue. For preabsorption and bioassay studies, lGnRH-I (generously provided by Dr. Stacia A. Sower), sGnRH and LHRH (Sigma) were used.

2.3. Immunocytochemistry for detecting GnRH-immunoreactivity in the ovary

The ovaries from shrimp at different stages of ovarian maturation (proliferative, vitellogenic, and mature) were carefully removed and fixed in Bouin's fixative overnight. The tissue blocks were then dehydrated with increasing concentrations of ethanol, cleared in dioxane, and further processed for routine paraffin embedding. Five-micron thick sections were deparaffinized, rehydrated, and immersed in 1% H_2O_2 and 1% $LiCO_3$ in 70% ethanol to eliminate endogenous peroxidase and residual picric acid, respectively. Free aldehydes in the tissue were minimized by immersing slides in 0.1 M glycine in phospahate buffered saline (PBS). Tissue was permeabilized with 1% Triton X-100 in PBS, and non-specific binding was blocked with 4% BSA in PBS. The sections were then incubated with anti-LHRH (dilution 1:40), anti-sGnRH (1:500), anti-lGnRH-I (1:1000), anti-lGnRH-III (1:4000), or anti-octGnRH (1:500) antibodies overnight at 4 °C. The negative controls were done by omitting the primary antibodies in the initial incubation step or incubating tissue sections in primary antibodies preabsorbed with the corresponding GnRH peptides (50 μg/0.1 mL antisera at the working dilutions). The sections were washed extensively with PBS containing 0.1% Tween-20, and subsequently exposed to peroxidase-conjugated goat anti-rabbit IgG (Sigma) at a 1:1500 dilution for 1 h at room temperature. The antigen-antibody complexes, indicating the existence of GnRH-liked factor, were visualized by incubating the sections with diaminobenzidine (DAB) enhanced liquid substrate system (Sigma). The sections were then dehydrated, cleared, and mounted with mounting reagent prior to observation under a Nikon Eclipse light microscope equipped with a Nikon DXM 1200 CCD camera.

Since anti-lGnRH-I was the only antibody that showed positive results in immunoperoxidase staining, an immunofluorescence technique was also performed to confirm the result in ovarian sections using anti-lGnRH-I (1:1000) under the same conditions as previously described for immunoperoxidase technique, except the corresponding secondary antibody was Alexa-488 conjugated goat anti-rabbit IgG (Molecular Probes, Eugene, OR) diluted at 1:300. The fluorescent micrographs were captured by the same Nikon microscope.

2.4. GnRH administrations to stimulate ovarian maturation

Three isoforms of GnRH used to stimulate ovarian maturation in this study included LHRH, lGnRH-I and sGnRH. This was based on the reports which showed that LHRH was used to stimulate gonadal maturation and spawning in a shrimp, *P. semisulcatus* (Aktas, 2005), whereas lGnRH-I was reported to have an effect on gamete release in a protochordate, *Ciona intestinalis* (Gorbman et al., 2003). Each isoform of GnRHs was diluted in normal saline (NS) to a desired dosage immediately before administration. The unilateral eyestalk-ablated female shrimp were divided into 6 groups ($n=7$ each), and designated as follows: 1) NS injection which served as the control group; 2) and 3) sGnRH injections at 10 and 50 ng/g body weight (BW), respectively; 4) and 5) LHRH injections at 10 and 50 ng/g BW, respectively; and 6) lGnRH-I injection at 50 ng/g BW. Because the preliminary result showed that the low dose of LHRH and sGnRH (10 ng/g BW) had no effect on shortening the duration of ovarian maturation, and because its availability was limited, the low dose of lGnRH-I was not performed. And because of its limited availability, octGnRH was not used in this experiment. Approximately 0.1 mL of NS or diluted GnRHs was injected into the shrimp dorsal muscles between the 1st and 2nd thoracoabdominal segments. Hormonal injections were carried out on day 1 after spawning. Stages of ovarian development following the hormonal administration were checked daily by flashing the light through thoracoabdominal segments of the shrimp to confirm the ovarian stages as described in the Results.

Another experiment was also conducted on non-ablated female broodstocks. Because of a limited number of these shrimp, the dose of GnRH used in this experiment was greater than that used in a report of Aktas (2005), which showed that GnRH at the 200 ng/g BW did not show marked changes in gonadal development and spawning. We, therefore, decided to increase the dose by 2.5 fold to 500 ng/g BW of GnRHs in this experiment, which was 10 times higher than the highest dose tested with the eyestalk-ablated shrimp. The non-ablated shrimp were divided into 3 groups ($n=7$ each) as follows: 1) NS injection which served as the control group; 2) sGnRH injection at 500 ng/g BW; and 3) lGnRH-I injection at 500 ng/g BW. Thereafter, the shrimp were

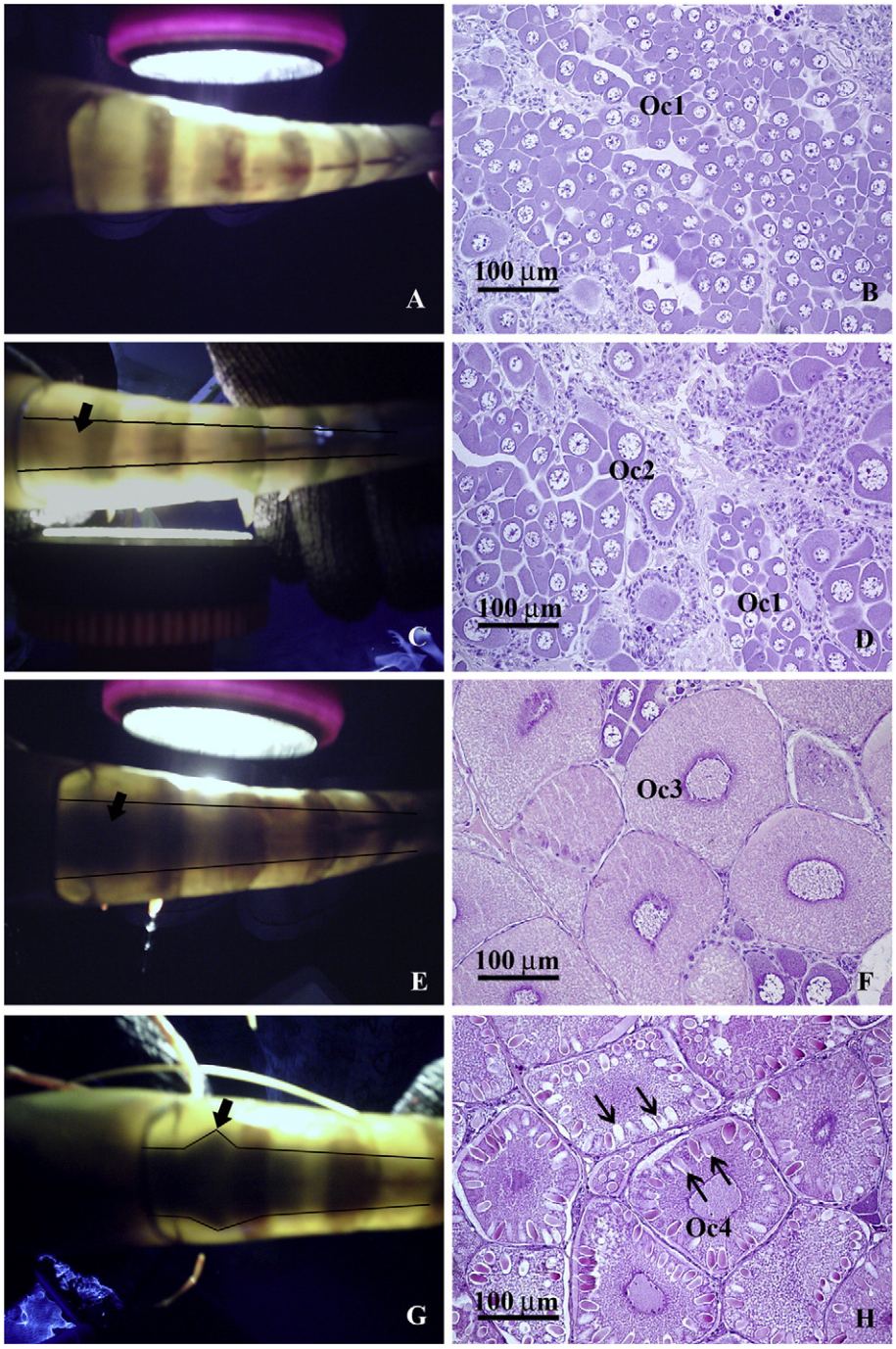


Fig. 1. The external appearances shown by transmitted light and correlative histology of ovaries at various stages of development. (A) The external appearance of stage I ovary, showing clear dorsal surface and (B) the histology, showing predominating step 1 oocytes (Oc1). (C) The external appearance of stage II ovary as a thin dense midline (arrow). This stage of ovary contained mostly step 2 oocytes (D, Oc2). (E) Stage III ovary appeared as a thick band (arrow) and contained mostly step 3 oocytes (F, Oc3). (G) Stage IV ovary appeared as a thick, broad band with wing-like structure representing lateral lobes (arrow), and it contained a large number of step 4 or mature oocytes (H, Oc4), with numerous cortical rods (arrows) in their peripheries.

boosted twice with either NS or GnRH at 10 day-intervals (on days 1, 11, 21). Ovarian maturation and spawning in all groups were carefully observed on the daily basis throughout a 60 day period after the final injection.

2.5. Examination of ovarian maturation

The light transmission method is a simple technique routinely used to verify the stages of ovarian maturation by shining a torch light through the shrimp body. The developmental stages of ovarian cycle were judged according to the criteria shown in Results, Fig. 1. Prior histological study was performed in other groups of shrimp to ascertain correlation between the external appearances of ovarian stages as determined by the light transmission method and the ovarian histology. The stages of ovarian development were determined by a person who had an expertise in using the light transmission method but did not know the treatment conditions of various experimental groups. For histological examination, the ovaries were removed from shrimp at each stage of ovarian development, fixed in Bouin's fixative overnight, and processed conventionally for paraffin embedding. The sections were placed on gelatin-coated slides, processed for staining with hematoxylin and eosin, and viewed under an optical microscope.

In the GnRH-primed animals, the development of ovaries from stage I to stage IV (mature stage) was checked every 24 h post-injection using the light transmission method as previously mentioned. The number of days for the ovaries to reach the final maturation stage were recorded and compared among each treatment and control groups. The ovarian maturation was confirmed by allowing the shrimp to spawn at the following night after full ovarian maturation.

2.6. Assessment of egg quantity and quality after spawning

The quantity and quality of spawned eggs were evaluated and expressed as the number of eggs per spawn and the percentage of fertilized eggs. Each shrimp with a fully mature ovary was allowed to spawn in a tank containing 400 L of sea water. After spawning, the eggs were randomly sampled (from 100 mL of sea water, 3 times) and

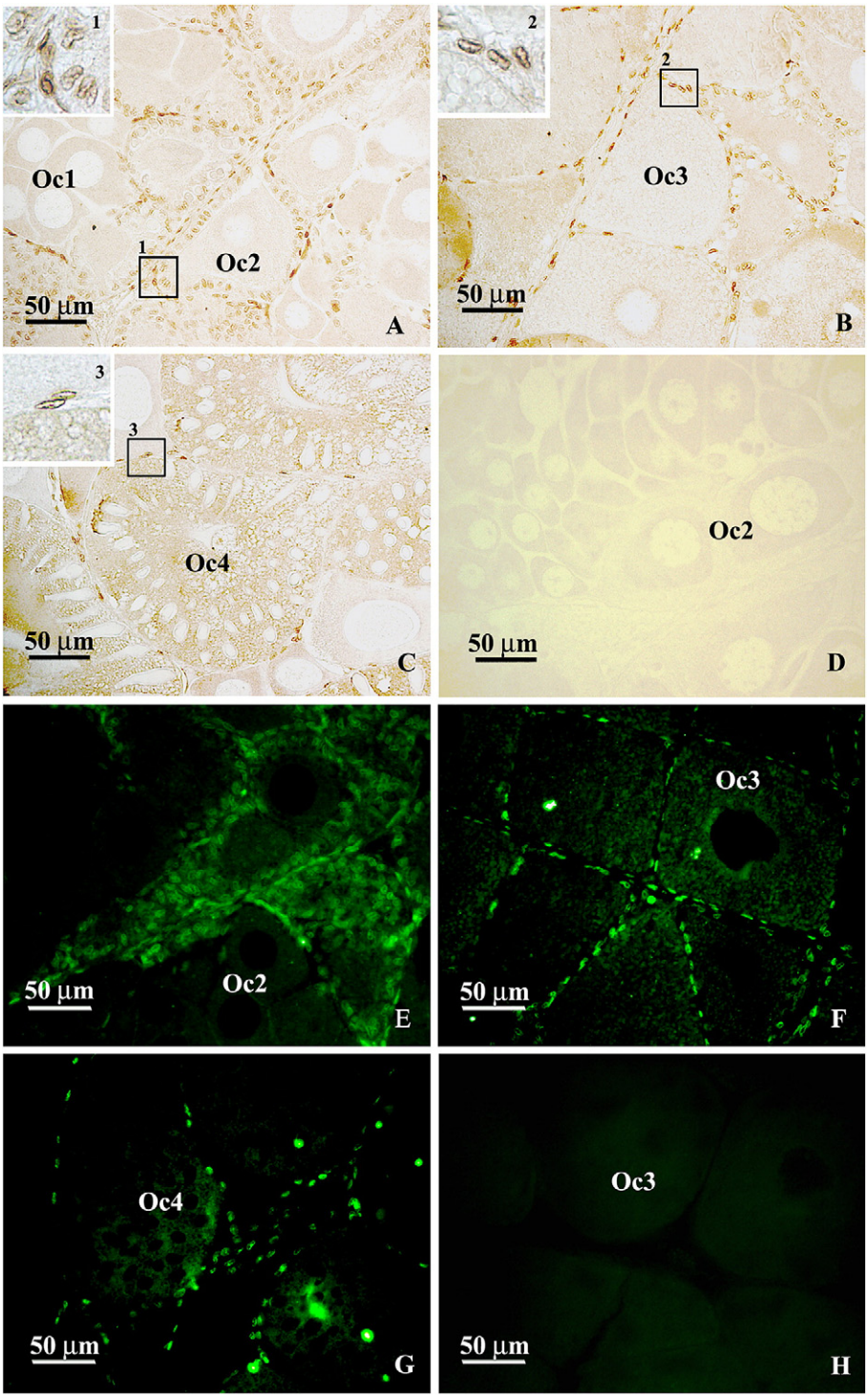


Fig. 2. (A–C) Immunoperoxidase localization of lGnRH-I-like substance in the shrimp ovaries, demonstrating the ir-lGnRH-I in the follicular cells surrounding oocytes in different ovarian stages: proliferative (A), vitellogenic (B), and mature (C). At higher magnification, the ir-lGnRH-I was observed in the cytoplasm of the follicular cells (A–C, insets). (D) The section incubated with anti-lGnRH-I preadsorbed with l\GnRH-I peptide showed no staining. (E–G) Immunofluorescence of lGnRH-I-like substance in the shrimp ovaries. The follicular cells surrounding step 2 (E, Oc2), step 3 (F, Oc3), and step 4 (G, Oc4) oocytes displayed ir-lGnRH-I. (H) Section incubated with PBS instead of the primary antibody showed no fluorescence.

counted to assess the total number of spawned eggs. To determine the percentage of fertilization, at least 200 eggs were observed under an optical microscope and only the normal developing embryos (gauged from the appearance of gastrulation at 6–8 h after spawning) were indicated as successful fertilization. This embryonic stage allowed us to easily distinguish between fertilized and non-fertilized eggs. Data were expressed as mean±S.D from triplicates. The duration for the ovaries to reach maturation, the number of eggs spawned, and the percentage of fertilizations were compared among GnRH-treated and NS-treated groups using one-way analysis of variance (ANOVA), followed by a Tukey Post Hoc multiple comparison. The probability value less than 0.05 ($P<0.05$) indicated a significant difference.

3. Results

3.1. Correlation of ovarian stages by external observations with ovarian histology

According to King (1948) and Yano et al. (1988), the ovarian cycle in the shrimp can be classified into 4 stages: spent, proliferative, vitellogenic, and mature. From observations of the external appearance; in stage I (spent stage) the ovary was transparent with no distinguishable ovarian outline (Fig. 1, A); in stage II (proliferative stage) the ovary appeared as a thin opaque line along the dorsal axis of the body (Fig. 1, C); in stage III (vitellogenic stage) the ovary appeared as a thick band covering approximately the middle half of the dorsal surface (Fig. 1, E); and in stage IV (mature stage) the ovary appeared turgid, broad with wing-like lateral lobes, and was intensely dark and occupied almost the whole dorsal surface of the shrimp (Fig. 1, G). Histologically, stage I ovary was characterized by the predominance of step 1 oocytes (Oc1) surrounded by connective tissue (Fig. 1, B). Stage II ovary was marked by the abundance of step 2 oocytes (Oc2) with basophilic cytoplasm (Fig. 1, D). Stage III ovary contained mostly step 3 or yolky, vitellogenic oocytes (Oc3) (Fig. 1, F). Stage IV ovary was distinguished by the presence of numerous step 4 or mature oocytes (Oc4) which contained rod-like bodies (cortical rods) in their peripheral cytoplasm (Fig. 1, H). These observations confirmed that light transmission method is a reliable technique which could be used to predict the stages of ovarian development, as the ovarian stages gauged from external appearance corresponded well with the histological characteristics.

3.2. The presence of a GnRH-like factor in the ovarian tissue

Using antibodies against five GnRH isoforms to determine the presence of ir-GnRH in the shrimp ovary, only ir-lGnRH-I was found to be localized in the cytoplasm of follicular cells which surrounded developing and mature oocytes in proliferative, vitellogenic and mature stages of ovaries (Fig. 2, A–C). However, positive immunostained follicular cells were more abundant in proliferative and vitellogenic stages (Fig. 2, A–C). There was no ir-lGnRH-I detected in the cytoplasm of oocytes at any stages, as well as in the surrounding connective tissue. Similar findings were observed using immunofluorescence technique in which no false positive could occur as in immunoperoxidase stain where the effect of endogenous peroxidase might not be totally suppressed (Fig. 2, E–G). In contrast, there were no ir-GnRHs in any of the ovarian stages using the other four antibodies, i.e., anti-LHRH, anti-sGnRH, anti-lGnRH-III, and anti-octGnRH (negative data not shown). Both controls of immunoperoxidase and immunofluorescence were unstained (Fig. 2, D and H).

3.3. The shortening of ovarian maturation period by GnRH administration

There are cumulative data indicating that several isoforms of GnRH share a common receptor (Millar et al., 2004). Therefore, we hypothesized that the three GnRH isoforms used in this bioassay experiment may be able to have reproductive effects, although the immunoreactivities of LHRH and sGnRH were not detectable in the ovarian tissue. Intramuscular administration of exogenous LHRH, sGnRH, and lGnRH-I into female shrimp appeared to shorten the ovarian maturation period when compared to the control shrimp injected with NS only (Table 1). After eyestalk-ablation, the ovary of the NS-treated shrimp reached maturation from stage I to IV within 7.43±0.98 days. At a dose of 10 ng/g BW, both sGnRH and LHRH shortened ovarian maturation period to 6.00±0.82 and 6.14±1.21 days, respectively, but were not significantly different from that of the control. Notably, eyestalk-ablated shrimp which were administered 50 ng/g BW of sGnRH, LHRH, and lGnRH-I developed fully mature ovaries within 4.29±1.38, 4.43±0.79, and 4.00±0.82 days, respectively. Statistical analysis revealed a significant shortening of ovarian maturation period by all GnRH isoforms at this dose of 50 ng/g BW. All of the controls, and GnRH-induced shrimp whose ovaries were determined as “mature” by external observation method, underwent spawning on the following night. The results are summarized in Table 1.

Administration of exogenous GnRHs also shortened the duration of ovarian maturation in non-ablated shrimp (Table 1). The ovaries of the eyestalk-intact, NS-treated shrimp developed into fully mature stage within 34.50±5.00 days. Upon treatment with 500 ng/g BW of both sGnRH and lGnRH-I, the shrimp developed fully mature ovaries within 23.20±2.59 and 22.80±2.17 days, respectively. These durations were significantly shortened when compared to that of the control group. However, 71.43% of the eyestalk-intact shrimp spawned after sGnRH and lGnRH-I treatments, but only 57.14% of the control shrimp underwent spawning.

Table 1
Effect of GnRHs on the period of ovarian maturation, quantity of spawned eggs, and fertilization

Groups	Treatments	Number of shrimp	Doses (ng/g BW)	Period of maturation (days)	% of spawners	Number of % eggs/spawn	% Fertilization
Eyestalk-ablated groups							
1	NS	7	–	7.43±0.98	100	$0.98\times10^6\pm4.59\times10^5$	84.53±3.55
2	sGnRH	7	10	6.00±0.82	100	$0.94\times10^6\pm2.26\times10^5$	-
3	sGnRH	7	50	4.29±1.38*	100	$0.95\times10^6\pm2.59\times10^5$	79.91±7.09
4	LHRH	7	10	6.14±1.21	100	$0.86\times10^6\pm1.53\times10^5$	-
5	LHRH	7	50	4.43±0.79*	100	$0.91\times10^6\pm4.24\times10^5$	81.57±4.51
6	lGnRH-I	7	50	4.00±0.82*	100	$0.89\times10^6\pm1.41\times10^5$	82.07±7.17
Eyestalk-intact groups							
7	NS	7	-	34.50±5.00	57.14	$1.15\times10^6\pm1.37\times10^5$	80.13±6.16
8	sGnRH	7	500	23.20±2.59*	71.43	$1.06\times10^6\pm2.81\times10^5$	81.26±4.78
9	lGnRH-I	7	500	22.80±2.17*	71.43	$1.01\times10^6\pm1.37\times10^5$	82.00±3.98

Note: * means statistically difference between control and GnRH-treated groups at $P<0.05$.
NS, normal saline.

3.4. Quantity and quality of the spawned eggs following GnRH treatment

The effect of GnRH on the quantity and quality of spawned eggs were estimated by the number of eggs per spawn and the percent of successfully fertilized eggs as demonstrated in Table 1. The numbers of spawned eggs were not significantly different among LHRH-, sGnRH-, lGnRH-I-injected and NS-injected groups in both eyestalk-ablated and eyestalk-intact shrimp. The numbers of spawned eggs in GnRH-treated groups ranged between $0.86–0.95\times10^6$ and $\sim1.0\times10^6$ in eyestalk-ablated and eyestalk-intact shrimp, respectively. Similarly, the numbers of spawned eggs in NS-treated groups were 0.98×10^6 for eyestalk-ablated and 1.15×10^6 for eyestalk-intact. These results showed no significant difference in the number of eggs per spawn between eyestalk-ablated and eyestalk-intact groups.

The percentages of successful fertilization, as the indicator for determining the quality of spawned eggs, were not significantly different among all groups (Table 1). In NS-treated groups, the percentages of fertilization were 84.53 and 80.13% for eyestalk-ablated and eyestalk-intact, respectively. In the GnRH-treated groups, the percentages of fertilization ranged from 79.91 to 82.07% for eyestalk-ablated and eyestalk-intact, which were not significantly different when compared to the controls. This suggested that the doses of GnRH used in this study had no effect on egg number and their fertilizability.

4. Discussion

In the present study, we have demonstrated the presence of ir-lGnRH-I in the shrimp ovary. Many previous studies have also reported the presence of a GnRH or GnRH-like factor in the gonads of other invertebrates, for examples, a protochrodate, *Ciona intestinalis*, (Tsutsui et al., 1998; Terakado, 2001), mollusks, *Haliotis trivolvis, Lymnea stagnalis* (Young et al., 1999), and *Aplysia californica* (Zhang et al., 2000), and a prawn, *Macrobrachium rosenbergii* (Ngernsoungnern et al., 2008a). Notably, ir-GnRH in the shrimp ovaries was found exclusively in the follicular cells surrounding the developing and mature oocytes, and was similar to GnRH localization in the granulosa cells of *C. intestinalis* ovary. It was shown that the peptides purified from *C. intestinalis* gonadal extract stimulated sex steroid production from this organ (Di Fiore et al., 2000).

Follicular cells in the ovaries of invertebrates have been reported to secrete various substances. In crustaceans, the follicular cells have been shown to secrete vitellogenin-stimulating ovarian hormone (VSOH) which is believed to play a central role in ovarian maturation (Van, 1992). Serotonin or 5-HT was detected in ovarian follicular cells of *P. monodon*, and was shown to stimulate ovarian maturation (Wongprasert et al., 2006). Moreover, 5-HT receptor was expressed in cytoplasm of Oc3 and Oc4 of *P. monodon* (Ongvarrasopone et al., 2006). Egg-laying hormone (ELH), has also been observed in the ovarian follicular cells of abalones (Chanpoo et al., 2001; Saitongdee et al., 2005), as well as in *P. monodon* (Liu et al., 2006). The latter study also suggested a role of ELH in the induction of shrimp spawning. Therefore, it is possible that the follicular cells produce GnRH locally and this local GnRH may play an autocrine and/or paracrine role in the induction of ovarian maturation and spawning. It is also possible that the ovarian GnRH may act in concert with 5-HT, ELH or VSOH in controlling ovarian maturation. However, further studies are needed before a conclusion can be made.

It has been reported that most vertebrates GnRHs exert similarly high activities with all receptors of non-mammalian vertebrates (Sealfon et al., 1997). In chiton, lGnRH-I and tunicate (t)GnRH-II were found to be both capable of stimulating the release of ripe gametes (Gorbman et al., 2003). Likewise, different GnRH isoforms including mammalian (m)GnRH, sGnRH, chicken (c)GnRH-II, and tGnRH-I, injected into *C. intestinalis* have been shown to induce gamete release (Terakado, 2001). In the present study, we have demonstrated that LHRH, sGnRH, and lGnRH-I also exerted shortening of the ovarian maturation period, which may be due to the ability of different GnRH isoforms in binding to the same receptor, or that they could stimulate a common signal transduction pathway. However, the presence of GnRH receptor in the shrimp and its binding to different isoforms of GnRHs should be studied before a firm conclusion can be made. It is interesting to note that the amino acids which determine the conformation of the GnRH peptides and responsible for binding with the receptors are all located at the distal ends of both N and C termini, and that they are highly conserved among GnRH peptides (Sower et al., 2004). Thus, this might explain the similar effect of LHRH, sGnRH, and lGnRH-I on enhancing the shrimp ovarian maturation observed in the present study. Although octGnRH and lGnRH-III were not used in our study because of its limited availability, our previous research has demonstrated that ir-octGnRH and ir-lGnRH-III were present in the CNS of *P. monodon* (Ngernsoungnern et al., 2008b). We believe that octGnRH and lGnRH-III could also exert effects similar to the three GnRH isoforms used in the current study. We plan to test the effects of these GnRHs on the shrimp ovarian maturation in a further study.

The three GnRH isoforms exerted a strong effect on ovarian maturation in the eyestalk-ablated (treated at 50 ng/g BW) as well as in eyestalk-intact (treated at 500 ng/g BW) shrimp. The shorter ovarian maturation cycle in the eyestalk-ablated animals may be due in part to the elimination of inhibition by GIH and MOIH which are synthesized and released from the eyestalk X-organ-sinus gland system (Okumura and Aida, 2001). The exogenous administration of GnRHs in eyestalk-intact groups also significantly shortened the ovarian maturation period, but appeared to be less effective when compared to eyestalk-ablated group. This may be due to gonad-inhibiting hormone still being intact in the eyestalks, thus a much higher level of exogenous GnRH was needed to override the effects. Because a high dose of GnRH was required for exerting its effect on the eyestalk-intact animals, one question that could be raised and need to be addressed is whether the high concentration used herein could be due to the non-specific action of the administered hormone. Further research is being performed by using of combined doses of known reproductive stimulating hormones, such as ELH, in single or in combination with GnRH to test their effects at the lowest effective doses. In addition, The relationship between exogenous (circulating) and local (ovarian) GnRH, 5-HT, and ELH in induction of ovarian maturation in penaeid shrimp needs to be investigated further, as the research could provide basic knowledge as well as practical use of the hormonal control of ovarian maturation and spawning. With further studies to refine the effective doses of GnRH to elicit positive results, there is a high possibility that hormone-priming could be used instead of the eyestalk ablation technique. If possible, a stimulatory method will be more humane and acceptable in shrimp aquaculture.

Acknowledgements

This study was supported by the Thailand Research Fund (Royal Golden Jubilee Ph.D. Program (Grant No. PHD/0249/2546) to A. Ngernsoungnern and P. Sretarugsa, and Senior Research Scholar Fellowship to P. Sobhon), and Commission on Higher Education (Research Team Development Grant to P. Sobhon). The authors would like to thank Dr. Stacia A. Sower, Dr. Pei-San Tsai, and Dr. Judy King for generously providing GnRH antibodies and peptides, and Dr. Peter Hanna for proof-reading of this manuscript.

References

Adams, B.A., Tello, J.A., Erchegyi, J., Warby, C., Hong, D.J., Akinsanya, K.O., Mackie, G.O., Vale, W., Rivier, J.E., Sherwood, N.M., 2003. Six novel gonadotropin-releasing hormones are encoded as triplets on each of two genes in the protochordate, *Ciona intestinalis*. Endocrinology 144, 1907–1919.

Aktas, M., 2005. Gonadal maturation and spawning in *Penaeus semisulcatus* de Hann, 1844 by hormone injection. Turk. J. Zoolog. 29, 193–199.

Bomirski, A., Klek-Kawinska, E., 1976. Stimulation of oogenesis in the sand shrimp, *Crangon crangon*, by a human gonadotropin. Gen. Comp. Endocrinol. 30, 239–242.
Chanpoo, M., Apisawetakan, S., Thongkukiatkul, A., Wanichanon, C., Linthong, V., Kruatrachue, M., Upatham, E.S., Pumthong, T., Hanna, P.J., Sobhon, P., 2001. Localization of egg-laying hormone in the gonads of tropical abalone, *Haliotis asinina* Linnaeus. J. Shellfish. Res. 20, 725–731.
Di Cosmo, A., Di Cristo, C., 1998. Neuropeptidergic control of the optic gland of *Octopus vulgaris*: FMRF-Amide and GnRH immunoreactivity. J. Comp. Neurol. 398, 1–12.
Di Cristo, C., Paolucci, M., Iglesias, J., Sanchez, J., Di Cosmo, A., 2002. Presence of two neuropeptides in the fusiform ganglion and reproductive ducts of *Octopus vulgaris*: FMRFamide and gonadotropin-releasing hormone (GnRH). J. Exp. Zool. 292, 267–276.
Di Fiore, M.M., Rastogi, R.K., Ceciliani, F., Messi, E., Botte, V., Botte, L., Pinelli, C., D'Aniello, B., D'Aniello, A., 2000. Mammalian and chicken I forms of gonadotropin-releasing hormone in the gonads of a protochordate, *Ciona intestinalis*. PNAS. 97, 2343–2348.
Fann, M.C., Wan, W.C., Wang, P.S., 1990. Existence of a gonadotropin-releasing hormone-like factor in the grass shrimp (black tiger prawn, *Penaeus monodon*). Chin. J. Physiol. 33, 169–178.
Fernald, R.D., White, R.B., 1999. Gonadotropin-releasing hormone genes: phylogeny, structure, and functions. Front. Neuroendocrin. 20, 224–240.
Goldberg, J.I., Garofalo, R., Price, C.J., Chang, J.P., 1993. Presence and biological activity of a GnRH-like factor in the nervous system of *Helisoma trivolvis*. J. Comp. Neurol. 336, 571–582.
Gorbman, A., Sower, S.A., 2003. Evolution of the role of GnRH in animal (Metazoan) biology. Gen. Comp. Endocrinol. 134, 207–213.
Gorbman, A., Whiteley, A., Kavanaugh, S., 2003. Pheromonal stimulation of spawning release of gametes by gonadotropin releasing hormone in the chiton, *Mopalia* sp. Gen. Comp. Endocrinol. 131, 62–65.
Huberman, A., 2000. Shrimp endocrinology a review. Aquaculture 191, 191–208.
Iwakoshi, E., Takuwa-Kuroda, K., Fujisawa, Y., Hisada, M., Ukena, K., Tsutsui, K., Minakata, H., 2002. Isolation and characterization of a GnRH-like peptide from *Octopus vulgaris*. Biochem. Biophy. Res. Commun. 291, 1187–1193.
Iwakoshi-Ukena, E., Ukena, K., Takuwa-Kuroda, K., Kanda, A., Tsutsui, K., Minakata, H., 2004. Expression and distribution of octopus gonadotropin-releasing hormone in the central nervous system and peripheral organs of the octopus (*Octopus vulgaris*) by in situ hybridization and immunohistochemistry. J. Comp. Neurol. 477, 310–323.
King, J.E., 1948. A study of the reproductive organs of the common marine shrimp, *Penaeus setiferus (Linnaeus)*. Biol. Bull. 94, 244–262.
Liu, Z., Sobhon, P., Withyachumnarnkul, B., Hanna, P., 2006. Identification of a putative egg-laying hormone in neural and ovarian tissues of the black tiger shrimp, *Penaeus monodon*, using immunocytochemistry. Invertebr. Neurosci. 6, 41–46.
Meeratana, P., Withyachumnarnkul, B., Damrongphol, P., Wongprasert, K., Suseangtham, A., Sobhon, P., 2006. Serotonin induces ovarian maturation in giant freshwater prawn broodstock, *Macrobrachium rosenbergii* de Man. Aquaculture 260, 315–325.
Millar, R.P., Lu, Z.L., Pawson, A.J., Flanagan, C.A., Morgan, K., Maudsley, S.R., 2004. Gonadotropin-releasing hormone receptors. Endocr. Rev. 25, 235–275.
Ngernsoungnern, A., Ngernsoungnern, P., Kavanaugh, S., Sower, S.A., Sobhon, P., Sretarugsa, P., 2008a. The identification and distribution of gonadotropin-releasing hormone-like peptides in the central nervous system and ovary of the giant freshwater prawn, *Macrobrachium rosenbergii*. Invertebr. Neurosci. 8, 49–57.
Ngernsoungnern, P., Ngernsoungnern, A., Kavanaugh, S., Sobhon, P., Sower, S.A., Sretarugsa, P., 2008b. The presence and distribution of gonadotropin-releasing hormone-liked factor in the central nervous system of the black tiger shrimp, *Penaeus monodon*. Gen. Comp. Endocrinol. 155, 613–622.
Okumura, T., 2004. Perspectives on hormonal manipulation of shrimp reproduction. JARQ. 38, 49–54.
Okumura, T., Aida, K., 2001. Effects of bilateral eyestalk ablation on molting and ovarian development in the giant freshwater prawn, *Macrobrachium rosenbergii*. Fish. Sci. 67, 1125–1135.
Ongvarrasopone, C., Roshorm, Y., Somyong, S., Pothiratana, C., Petchdee, S., Tangkhabuanbutra, J., Sophasan, S., Panyim, S., 2006. Molecular cloning and functional expression of the *Penaeus monodon* 5-HT receptor. Biochim. Biophys. Acta. 1759, 328–339.
Panouse, J.B., 1943. Influence de l'ablation du pedoncule oculaire sur la croissance de l'ovaire chez la crevette Leander serratus. C.R. Acad. Sci. Paris. 217, 553–555.
Pazos, A.J., Mathieu, M., 1999. Effects of five natural gonadotropin-releasing hormones on cell suspensions of marine bivalve gonad: stimulation of gonial DNA synthesis. Gen. Comp. Endocrinol. 113, 112–120.
Saitongdee, P., Apisawetakan, S., Anunruang, N., Poomthong, T., Hanna, P., Sobhon, P., 2005. Egg-laying-hormone immunoreactivity in the neural ganglia and ovary of *Haliotis asinina* Linnaeus. Invertebr. Neurosci. 5, 165–172.
Sarojini, R., Nagabhushanam, R., Fingerman, M., 1995. Mode of action of the neurotransmitter 5-hydroxytryptamine in stimulating ovarian maturation in the red swamp crayfish, *Procambarus clarkii*: an in vivo and in vitro study. J. Exp. Zool. 271, 395–400.
Sealfon, S.C., Weinstein, H., Millar, R.P., 1997. Molecular mechanisms of ligand interaction with the gonadotropin-releasing hormone receptor. Endocr. Rev. 18, 180–205.
Sherwood, N.M., Lovejoy, D.A., Coe, I.R., 1993. Origin of mammalian gonadotropin-releasing hormones. Endocrin. Rev. 14, 241–254.
Silver, M.R., Kawauchi, H., Nozaki, M., Sower, S.A., 2004. Cloning and analysis of the lamprey GnRH-III cDNA from eight species of lamprey representing the three families of Petromyzoniformes. Gen. Comp. Endocrinol. 139, 85–94.
Sower, S.A., Nucci, N.V., Silver, M.R., 2004. Family of Gonadotropin-releasing hormone. Encyclopedia of Endocrine Diseases 2, 306-317.
Terakado, K., 2001. Induction of gamete release by gonadotropin-releasing hormone in a protochordate, *Ciona intestinalis*. Gen. Comp. Endocrinol. 124, 277–284.
Tsai, P.S., Maldonado, T.A., Lunden, J.B., 2003. Localization of gonadotropin-releasing hormone in the central nervous system and a peripheral chemosensory organ of *Aplysia californica*. Gen. Comp. Endocrinol. 130, 20–28.
Tsai, P.S., 2006. Gonadotropin-releasing hormone in invertebrates: structure, function, and evolution. Gen. Comp. Endocrinol. 148, 48–53.
Tsukimura, B., Kamemoto, F.I., 1991. In vitro stimulation of oocytes by presumptive mandibular organ secretions in the shrimp, *Penaeus vannamei*. Aquaculture 92, 59–66.
Tsutsui, H., Yamamoto, N., Ito, H., Oka, Y., 1998. GnRH-immunoreactive neuronal system in the presumptive ancestral Chordate *Ciona intestinalis* (Ascidian). Gen. Comp. Endocrinol. 112, 426–432.
Twan, W.H., Hwang, J.S., Lee, Y.H., Jeng, S.R., Yueh, W.S., Tung, Y.H., Wu, H.F., Dufour, S., Chang, C.F., 2006. The presence and ancestral role of gonadotropin-releasing hormone in the reproduction of scleractinian coral, *Euphyllia ancora*. Endocrinology 147, 397–406.
Vaca, A.A., Alfaro, J., 2000. Ovarian maturation and spawning in the white shrimp, *Penaeus vannamei*, by serotonin injection. Aquaculture 182, 373–385.
Van, H.F., 1992. Inhibiting and stimulating neuropeptides controlling reproduction in Crustacea. Invertebr. Reprod. Dev. 22, 21–30.
Wongprasert, K., Asuvapongpatana, S., Poltana, P., Tiensuwan, M., Withyachumnarnkul, B., 2006. Serotonin stimulates ovarian maturation and spawning in the black tiger shrimp *Penaeus monodon*. Aquaculture 261, 1447–1454.
Yano, I., Tsukimura, B.T., Sweeny, J.N., Wyban, J.A., 1988. Induced ovarian maturation by implantation of lobster ganglion. J. World Aquac. Soc. 19, 204–209.
Young, K.G., Chang, J.P., Goldberg, J.I., 1999. Gonadotropin-releasing hormone neuronal system of the fresh water snails *Helisoma trivolvis* and *Lymnaea stagnalis*: possible involvement in reproduction. J. Comp. Neurol. 404, 427–437.
Zhang, L., Wayne, N.L., Sherwood, N.M., Postigo, H.R., Tsai, P.S., 2000. Biological and immunological characterization of multiple GnRH in an opisthobranch mollusk, *Aplysia californica*. Gen. Comp. Endocrinol. 118, 77–89.
Zhang, L., Tello, J.A., Zhang, W., Tsai, P.S., 2008. Molecular cloning, expression pattern, and immunocytochemical localization of a gonadotropin-releasing hormone-like molecule in the gastropod mollusk, *Aplysia californica*. Gen. Comp. Endocrinol. 156, 201–209.

ELSEVIER

Journal of Experimental Marine Biology and Ecology 354 (2008) 182–191

Journal of EXPERIMENTAL MARINE BIOLOGY AND ECOLOGY

www.elsevier.com/locate/jembe

The presence of GABA in gastropod mucus and its role in inducing larval settlement

Praphaporn Laimek [a], Shona Clark [b], Michael Stewart [c], Fred Pfeffer [b], Chaitip Wanichanon [a], Peter Hanna [b], Prasert Sobhon [a,*]

[a] *Department of Anatomy, Faculty of Science, Mahidol University, Rama 6 Road, Bangkok 10400, Thailand*
[b] *School of Life & Environmental Sciences, Deakin University, Geelong, VIC 3217, Australia*
[c] *BioDeakin and School of Medicine, Deakin University, Geelong, VIC 3217, Australia*

Received 17 August 2007; received in revised form 31 October 2007; accepted 5 November 2007

Abstract

Chemical substances that induce larval settlement have been the focus of many gastropod studies due to the importance of wild stock recruitment and production within aquaculture facilities. Gamma-aminobutyric acid (GABA), GABA analogs, and GABA-mimetics associated with certain crustose coralline algae (CCA), are known to induce larval settlement in commercial abalone (*Haliotis*) species, and other gastropods. Furthermore, mucus secreted from these gastropods has been shown to induce larval settlement, but the stimulatory components of mucus have not been thoroughly investigated. We now present data confirming that GABA is the settlement-inducing effector molecule contained within abalone mucus. To do this, we initially generated anti-GABA for use in immunoenzyme and immunofluorescent microscopy. Using these techniques GABA was identified in the nerves and epithelial cells of the foot, including mucus. Dried mucus samples subject to HPLC analysis revealed a mean concentration of 0.68 mM GABA after sample rehydration. The presence of GABA in these samples was confirmed by time-of-flight mass spectroscopy (TOF-MS). In addition, GABA was detected in the mucus of several abalone species and other gastropods by immunocytochemistry. Subsequent bioassays using both dry and fresh mucus strongly promoted induction of larval settlement.
© 2007 Elsevier B.V. All rights reserved.

Keywords: Abalone; GABA; Gastropod; *Haliotis*; HPLC; Immunohistochemistry; Larval settlement; Mucus; TOF-MS

1. Introduction

The amino acid, γ-aminobutyric acid (GABA), was the first molecule shown to induce synchronous larval settlement and metamorphosis of *Haliotis rufescens* into juveniles (Morse et al., 1979a). Later investigations revealed many isoforms of GABA (e.g. γ-hydroxybutyric acid, δ-aminovaleric acid and ε-aminocaproic acid), together with the accessory photosynthetic pigments in coralline algae and cyanobacteria, such as phycoerythrobilin, possess GABA-like settlement-inducing properties (Morse et al., 1979a, 1980, 1984; Morse and Morse, 1984a,b). The mechanism of action involved inhibition of cilia movement of swimming mollusc larvae (Akashige et al., 1981; Barlow, 1990).

It is now known that GABA can induce larval settlement in a number of molluscan species, including the mussel *Mytilus galloprovincialis*, the clam *Venerupis pullastra*, the oyster *Ostera edulis* (Garcia-Lavandeira et al., 2005), the black chiton, *Katharina tunicate* (Rumrill and Cameron, 1983), and in other various abalone species. The effective doses for the settlement of abalone species, viz, *H. rufescens*, *H. iris*, *H. discus hannai*, *H. virginea*, *H. australis*, *H. asinina* and *H. diversicolor* has been found to vary from 0.5 to 10 μM (Morse et al., 1979a,b; Moss and Tong, 1992; Yang and Wu, 1995; Roberts and Nicholson, 1997; Bryan and Qian, 1998; Moss, 1999; Roberts, 2001; Gapasin and Polohan, 2004), but it is apparent from these studies, that no single concentration of GABA has been optimal for settlement of all abalone species.

* Corresponding author. Tel.: +66 2 2015406; fax: +66 2 3547168.
E-mail address: scpso@mahidol.ac.th (P. Sobhon).

0022-0981/$ - see front matter © 2007 Elsevier B.V. All rights reserved.
doi:10.1016/j.jembe.2007.11.003

Apart from GABA, the presence of crustose coralline algae (CCA) has been confirmed as a contributing factor to settlement (Morse et al., 1979a,b, 1984; Morse and Morse, 1984a,b; Suenaga et al., 2004). In earlier analyses of CCA, precursors and metabolites of phycoerythrobilin were isolated. Later, algal photosynthetic accessory pigments were found that were structurally related to GABA (Morse et al., 1979a, 1984), and subsequently identified as inducers of settlement and metamorphosis of *Haliotis* larvae (Morse et al., 1979a,b, 1984; Morse and Morse, 1984a,b). Another study of larval settlement using the red crustose alga *Hydrolithon samoense* (Suenaga et al., 2004), showed GABA was not responsible, however, a GABA analog (δ-aminovaleric acid) was effective in settling *H. discus discus* and *H. discus hannai* larvae. CCA species can induce *H. rubra*, *H. laevigata*, *H. iris* and *H. virginea* larval settlement, but with a selective preference to CCA with thin crusts (Roberts and Nicholson, 1997; Daume et al., 1999a,b; Roberts et al., 2004). Several investigations have compared the roles of settlement-inducing agents (GABA, GABA derivatives, and CCA), using mixtures of diatoms and "mucus", as well as excluding them (Roberts, 2001; Gallardo and Buen, 2003).

Gastropod mucus has been shown to have many functions, such as aiding locomotion, feeding, protection, and settlement (Denny, 1983; Seki and Taniguchi, 1996; Davies and Hawkins, 1998). In an investigation of *H. discus hannai* larval settlement on the green alga, *Ulvella lens*, significant settlement occurred if mucus was present from previously grazing juveniles (Takahashi and Koganezawa, 1988). More recently, Slattery (1992) found that mucus alone was better than mucus plus diatoms, or diatoms plus 1 μM GABA, as an inductive cue for settlement of *H. rufescens* larvae. In a study of *H. asinina*, mucus together with benthic diatoms, *Navicula sp.*, or mucus mixed with diatoms, showed considerably higher larval settlement and metamorphosis than algae alone (Gallardo and Buen, 2003). In a comparative study using mucus, KCl or GABA, to induce larval settlement of *H. discus hannai*, mucus was most successful (Yang and Wu, 1995). This study also concluded that the amount of K^+ required was larval stage-dependent, and only the mucus was dose-independent. Overall, these studies support the earlier findings of Seki and Kan-no (1981) that larvae of *Haliotis* species preferentially settle on conspecific mucus trails.

In a recent immunocytological study of *H. asinina,* GABA was localized within neuron bundles, as well as in the epithelial cells of the cephalic and epipodial tentacles (Wanichanon et al., 2004). In the current study we have used immunocytochemistry to examine the presence of GABA in epithelial cells of the foot muscle, mantle mucus secreting cells, as well as mucus of the Australian blacklip abalone, *H. rubra*. We also established the presence of GABA in mucus using high performance liquid chromatography (HPLC) and time-of-flight mass spectroscopy (TOF-MS). In addition, we investigated the mucus of other haliotids and gastropods for the presence of GABA, and conducted a series of bioassays showing that mucus contains the settlement inducer.

2. Materials and methods

2.1. Animals

H. rubra were obtained from Port Phillip Bay and Bay City Sea Farm, Victoria, Australia. *H. asinina*, *H. diversicolor*, *Babylonia areolata*, *Chicoreus ramosus*, and *Strombus canarium*, were obtained from the Coastal Aquaculture Research and Development Center, Prachaubkirikun Province, Thailand.

2.2. Preparation of samples and immunolocalization

2.2.1. Specimen preparations

For section preparations, animals were anesthetized in seawater containing 5% $MgCl_2$, their shells removed and the foot muscle dissected. For light microscopy, dissected tissue was fixed in 4% paraformaldehyde overnight at 4 °C and subsequently dehydrated in ascending concentrations of ethyl alcohol for 30 min each. This was cleared with two changes of dioxane and a final dioxane-paraplast mixture for 30 min. Following paraffin wax embedding, 5 μm serial sections were prepared with a rotary microtome.

Mucus for immunocytological tests was obtained by wiping the foot muscle of individual gastropods using glass slides pre-coated with (3-aminopropyl) triethoxy-silane, then dried. Mucus for dot blot analysis, HPLC and TOF-MS analyses was prepared according to the method of Donovan and Carefoot (1997). Briefly, individual males and females (100±10 mm) were left for 15 min to attach to large glass petri dishes. The animals were then removed so that remaining mucus samples could be collected and dried at 60 °C for 1 h. A new razor blade was used to scrape and collect each mucus sample, which was then separated into 0.02 g aliquots and stored at 4 °C. When required for dot blot analyses, HPLC, and TOF-MS, samples were rehydrated with 100 μL of sterile deionised water (Millipore, Milli Q water System, Bendford MA), then centrifuged at 10,000 rpm (Model 13 Biofuge, Heraeus Instruments ™) for 5 min and the supernatant collected.

2.2.2. Polyclonal antibody production against GABA

Six-week-old imprinting control region male mice were obtained from the Animal Care Unit, Mahidol University and used with the approval of the Animal Ethics Committee to produce antiserum. GABA was linked to bovine serum albumin (BSA) by mixing 100 μM of GABA and 12 mg BSA (fraction V, Sigma), as well as 100 μM of glutaraldehyde in 0.1 M sodium phosphate buffer, pH 7.4. Animal immunizations were conducted following adapted procedures of Matute and Streit (1986). Sera was collected every alternate week and kept at −20 °C. Antibody titer against GABA was tested using ELISA (Polak and Noorden, 1997) and the optical density (OD) of each well read at 492 nm using a spectrophotometer (Titertex Multiscan Flow Laboratories, Australia Pty. Ltd,) followed by BSA pre-absorption. Negative control samples included mouse pre-immune serum in place of the primary antibody (mouse anti-GABA).

2.2.3. Immunohistochemical detection of GABA in abalone tissues and gastropod mucus

Endogenous peroxidase activity detected in dewaxed tissue sections, as well as dried mucus, was inactivated by treatment with 0.3% H_2O_2 in 30% methanol for 30 min. Sections were washed in PBS containing 0.4% Triton X-100 (PBST), and non-specific antibody binding blocked by incubating sections in blocking buffer (2% normal goat serum, 4% bovine serum albumin in PBST) for 2 h. Preparations were then incubated with primary antibody, overnight in a moist chamber (at 4 °C), washed 3 times for 10 min each in PBS, and incubated with secondary antibody (1:200; goat anti-mouse-Biotin Ig, Sigma) in blocking solution for 45 min at room temperature (RT). After rinsing in PBS, tissue sections and mucus preparations were incubated in streptavidin-HRP (1:200 in PBST) for 45 min. Samples were then exposed to NovaRED substrate solution (Vector laboratory) containing H_2O_2 for 2-5 min (i.e. until color development). Samples were washed with tap water, counter-stained with hematoxylin, dehydrated and mounted in Permount solution. For controls, preparations were processed in the same manner but with primary antibody excluded. Additionally, consecutive slides were stained with Periodic acid-Schiff solution (PAS) to identify the presence of carbohydrate.

Immunofluorescent detections of GABA were performed on tissue sections and mucus collected on slides. Preparations were initially blocked in 4% BSA for 30 min, then washed 3 times for 5 min each in PBS (pH 7.4), and incubated in buffer containing 0.1% glycine for 15 min. Preparations were then incubated overnight with mouse anti-GABA in PBS (1:100), washed with buffer, then incubated with FITC-conjugated goat anti-mouse IgG (1:200; Zymed Laboratories), for 1 h. They were then washed three times with PBS and mounted in buffered glycerol. Slides not incubated with anti-GABA were used as negative controls.

All preparations were photographed under a Nikon Eclipse E600 microscope with Nikon digital camera DXM1200F.

2.2.4. Dot blots of mucus extracts

Supernatant obtained from mucus extractions were spotted (20 μL) onto nitrocellulose membranes and dried at RT. Membranes were washed in PBS (pH 7.4) then incubated in blocking buffer (5% skim milk in PBS) for 15 min. Following a 15 min wash in PBS, membranes were incubated with mouse anti-GABA (1:200) in 5% skim milk for 1 h at RT. The membranes were washed with PBS and then incubated for 30 min at RT with HRP-conjugated goat anti-mouse IgG (Zymed Laboratories) at a dilution of 1:500 containing 5% skim milk. Finally, membranes were incubated with tetraethylbenzidine (TMB) membrane peroxidase substrate 1-C (KPL, Gaithersburg, ML) until color development, then washed in water and dried.

2.3. Chemical analysis of mucus

Determination of GABA within aqueous mucus extracts was performed with an Agilent Hewlett-Packard 1100 series HPLC system with solvent degasser system, quaternary pump, and autosampler fitted with a UV and fluorescence detector. The system was controlled by a Hewlett-Packard Vectra X_m series 4 data analysis work station. The column used was a Lichropher 100 Rp-18 column 150×4.6 mm I.D., 5 μm (Agilent). The separation conditions were performed as described by Henderson et al. (2006). Derivatisation reagents included 10 mg OPA reagent [*o*-pthaldialdehyde (Sigma-Aldrich) dissolved in 100 μL of methanol (Univar)], 900 μL 0.4 M sodium borate (pH 10.4) (BDH AnalaR), and 20 μL 3-mercaptopropionic acid, which was added to FMOC reagent [2.5 mg 9-fluorenylmethyl chloroformate (Sigma-Aldrich) dissolved in 1 mL of dry acetone (Univar)]. Calibration standards of GABA (Sigma-Aldrich) at concentrations of 1×10^{-2}, 5×10^{-3}, 1×10^{-3}, 5×10^{-4}, 1×10^{-4}, 5×10^{-5}, and 1×10^{-5} M were prepared as standard references. Valine (Sigma-Aldrich), was used at a concentration of 1×10^{-3} M as an internal standard.

Time-of-flight mass spectrometry was performed on an Agilent 6210 MSDTOF instrument using acetonitrile as the mobile phase. The following ESI conditions were selected: drying gas, nitrogen (7 mL/min, 350 °C), nebulizer gas, nitrogen (16psi), capillary voltage 4.0 kV, vaporizer temperature 350 °C and cone voltage 60 V.

2.4. Mucus settlement induction assays with statistical analysis

Mucus samples from *H. rubra*, *H. asinina* and *H. diversicolor* were collected on plastic sheets following a 15 min attachment and removal of adults. The animals were either immobilized "fixed" at the same area or allowed to walk "trail" on the sheet to test settlement of larvae on the mucus from fixed or trailed abalone. The mucus collected on sheets was used immediately as fresh mucus, or used following rehydration of stored dried samples. Bioassays were performed by placing three sheets in plastic cylindrical containers containing 1.2 L UV filter-treated sea water supplemented with streptomycin and neomycin (Sigma) at 7.5 mg/L. Larvae which were competent to settle at 24 h post fertilization ($n=1300$), were each placed into nine containers (3 replicates of 3) to assess settlement after 6, 24 and 72 h. Counts were then made of the larvae settling on mucus covered areas, compared with the equivalent mucus-free areas.

2.4.1. Statistics

The settlement data was analyzed using SPSS11.5 software (SigmaStat; SPSS), for testing normality, and homogeneity of variance, of each data set (mucus types). Group comparisons were then made using multiple group analyses with one-way ANOVA, and post hoc Tukey's HSD test. Interspecies differences, as well as settlement with time were also analyzed.

3. Results

3.1. Immunolocalization of GABA in foot muscle and mucus of gastropods

Histologically, the foot of most gastropods is comprised of muscle cells, mixed fibers, and is covered by an epithelium which has numerous ciliated columnar cells (see control

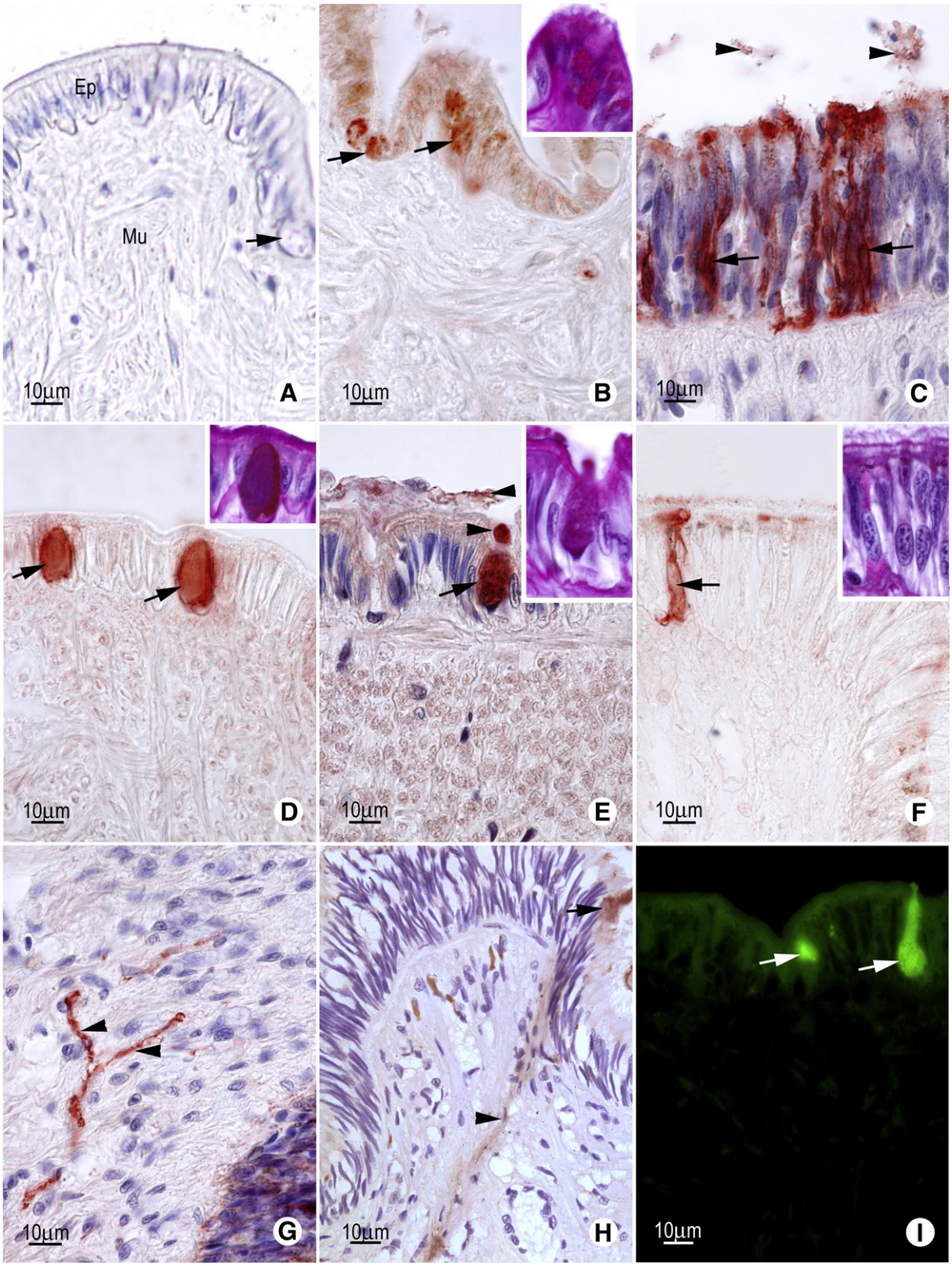


Fig. 1. Paraffin sections showing GABA-immunostaining in the foot region of gastropods. A, control (no anti-GABA) cross section of the foot of *H. asinina*, Ep-epithelium, Mu-muscle. B is an adjacent section to A, exhibiting GABA immunoreactivity in some mucosal cells (arrows) which was PAS positive (inset). C-I, GABA immunoreactivity in foot and mucus C, in mucosal cells of the foot epithelium of *H. diversicolor* (arrows), and mucus (arrow heads); D-F, in mucosal cells (arrows), as well as released mucus (arrow heads), in *Babylonia areolata*, *Strombus canarium*, and *Chicoreus ramosus*, respectively. Inset: cells were positive with PAS staining; G, within the foot of *H. diversicolor* (arrow heads); H and I, in mucosal cells (arrows), as well as nerve fibers in the foot (arrow head) of *H. rubra,* using immunoenzyme and immunofluorescence techniques, respectively.

Fig. 1A). The mucus secreting cells showed no staining in control sections, probed with pre-immune serum (Fig. 1A). When tissue sections were probed with anti-GABA, GABA was identified inside mucus secreting cells of the foot epithelia in *H. asinina*, *H. diversicolor*, *H. rubra, B. areolata*, *S. canarium*, and *C. ramosus* (Fig. 1B–F). These positive cells were typically goblet-shaped with distinctive oval nuclei. Moreover, their cytoplasm contained numerous GABA immunoreactive granules, which when stained with PAS contained high proportions of carbohydrate (glycogen, glycoprotein, proteoglycans), typically observed in mucus (Smith and Morin, 2002) secreting cells (Fig. 1B, D–F insets). Nerve fibers beneath the epithelium, and others located throughout the muscle tissue, displayed GABA reactivity (Fig. 1G, H), as did secreted mucus, which also contained GABA (Fig. 1C, E). Immunofluorescence also confirmed GABA immunoreactivity in the goblet cells, distributed throughout the epithelium of *H. rubra* (Fig. 1I).

GABA immunoreactivity was not observed in negative controls in which there was no anti-GABA applied (Fig. 2A). GABA immunoreactivity was observed in mucus wiped from the foot muscle of *H. rubra* (Fig. 2B), and in the mucus of the other gastropods investigated (data not shown). In particular, GABA was highly concentrated in some cells shed into the mucus (Fig. 2B), which are likely to be remnant goblet cells, based on appearance.

3.2. Chemical determination of GABA in mucus

Aqueous extracts of rehydrated mucus taken from *H. rubra* were tested for the presence of GABA by dot blots. GABA was detected at all dilutions between 1 µg and 0.01 µg (Fig. 3A). Controls were negative.

GABA was clearly present in *H. rubra* mucus as illustrated by HPLC chromatographs (Fig. 3B). The GABA standard (1.0×10^{-5} M) showed a peak with a retention time of 9.3 min, and a peak at 11.6 min corresponding to valine (internal standard). When the GABA standard was spiked with abalone mucus extract a significant additive increase in the height of the peak assigned to GABA was observed, whereas the peak height for the internal standard remained constant. Using time-of-flight mass spectrometry (TOF-MS), GABA was shown to be present in rehydrated mucus. This was achieved by identifying several characteristic ions that were present in both the rehydrated mucus and a standard GABA sample. The most significant of these peaks were m/z 104.1 which corresponds to the $[M+H]^+$ of GABA ($C_4H_9NO_2$) (Fig. 3C).

Although GABA was detected by HPLC in all abalone mucus extracts, the concentration varied. To investigate whether this variation was dependent on gender, the mucus of males and females ($n=20$; 100±10 mm) were separately analyzed. No significant difference could be detected (Fig. 4). The concentration of GABA in the sample group ranged from 2.8 to 0.13 mM, with a mean of 0.68 mM.

3.3. Settlement induction of larvae by mucus

H. asinina larval settlement was tested on the mucus of three abalone species, *H. asinina*, *H. rubra*, and *H. diversicolor* (Table 1). Six hours after exposure of competent larvae to *Haliotis* mucus, the total settlement was 11.7±1.2%. This value was significantly greater than that on control areas devoid of mucus, 1.4±0.4% ($p<0.05$). Settlement of larvae was 9.7±1.3% on *H. asinina* mucus, 12.1±0.9% on *H. rubra* mucus, and 13.7±1.7% on *H. diversicolor* mucus ($p<0.05$).

After 24 h, total larvae settlement on mucus increased to 41.4±3.6%, nearly four-fold of that at 6 h (11.7±1.2%, $p<0.05$). Moreover, this value was still greater than 2.5±0.9%; being the total settlement on controls ($p<0.05$). Larvae settlement at 24 h was 36.1±3% on *H. asinina* mucus, 33.1±3.1% on *H. rubra* mucus, and 48.9±4.4% on *H. diversicolor* mucus. The value of settled larvae to *H. diversicolor* mucus was significantly higher in proportion to the other two values ($p<0.001$).

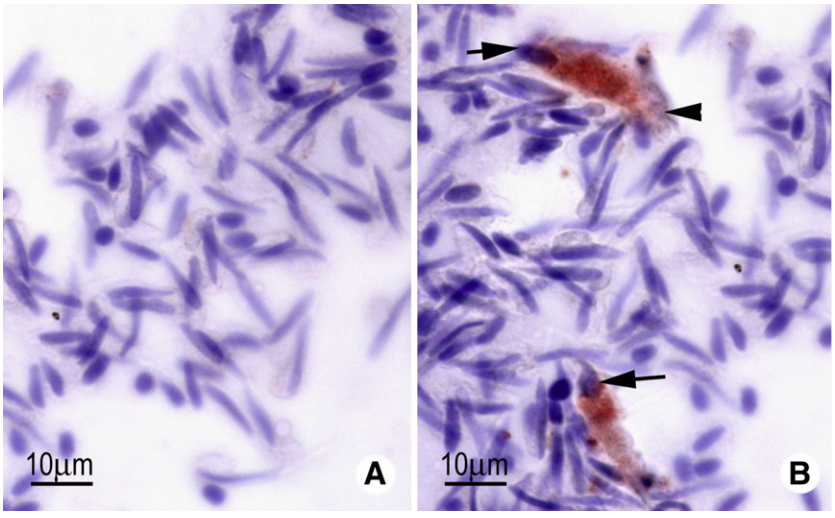


Fig. 2. Immunolocalization of GABA in mucus taken from the foot of *H. asinina*. A, micrograph of mucus used as a negative control (immunostaining without anti-GABA). B, mucus showing GABA immunoreactivity located in "shed cells" (arrows), as well as some reactivity in the mucus (arrowhead).

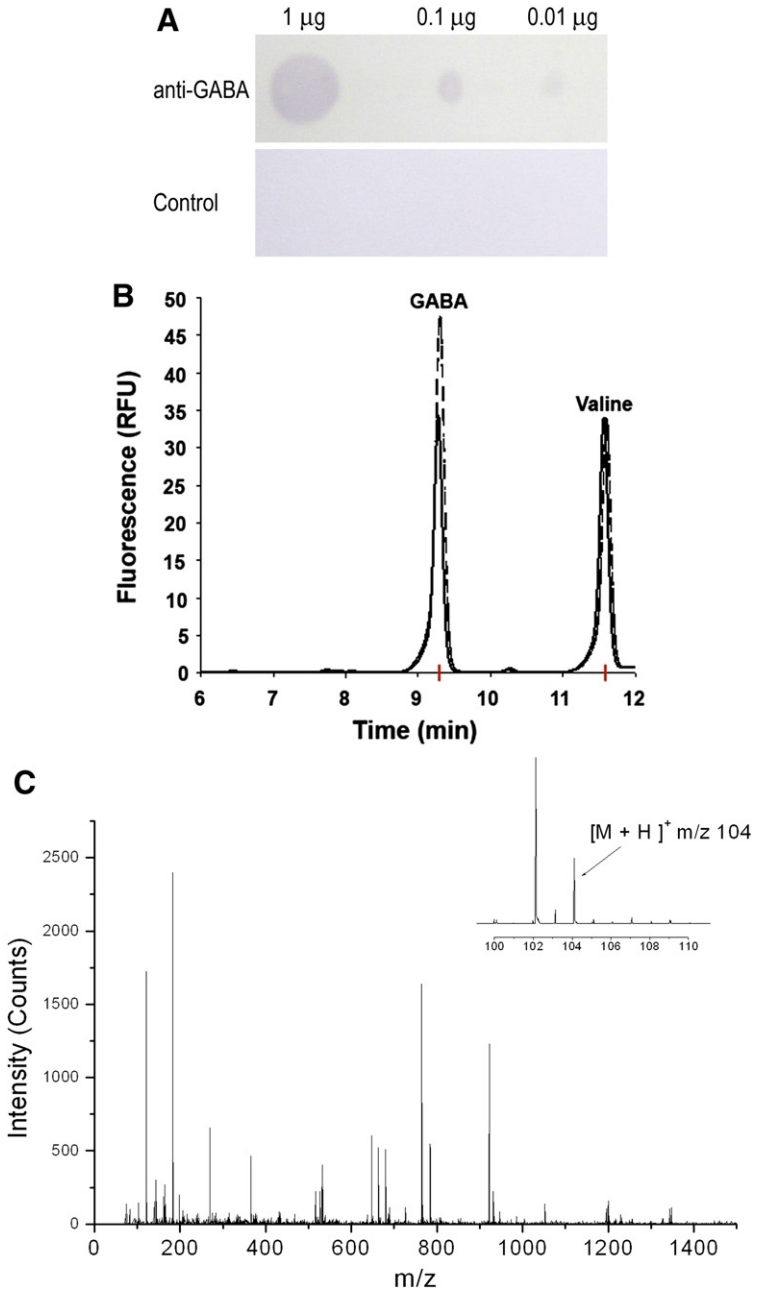


Fig. 3. Chemical determination of GABA in mucus. A, Dot blot analysis of an aqueous extract of rehydrated mucus from *H. rubra* stained with anti-GABA, and without anti-GABA as a control. B, HPLC chromatograph of a GABA standard (_____), plus a GABA standard spiked with abalone mucus (— — —), GABA retention time of 9.3 min. Valine was used as an internal standard with retention time of approximately 11.6 min. C, TOF-MS chromatograph of rehydrated mucus showing the peak of m/z 104.1 which corresponds to the $[M+H]^+$of GABA.

After 72 h, total larval settlement on mucus was 29.7±2.1%, compared to control (3.8±0.6%), $p<0.05$. Settlement numbers were still higher than that observed at 6 h, but reduced when compared with that at 24 h. Larval settlement on mucus at 72 h was significantly different on *H. asinina* mucus 29.7±2%, compared to *H. rubra* mucus 8.3±1.3%, and *H. diversicolor* mucus 35±2.4% ($p<0.05$).

Mucus obtained from abalone trails induced significantly greater larval settlement when compared to mucus collected from stationary (fixed) abalone (Fig. 5). As well, it was noted that fresh mucus resulted in better settlement than dried mucus. After 6 h (Fig. 5A), settlement on trail mucus was 14.4±1.3%; compared to that on fixed mucus, at 9.6±1.1% ($p<0.05$). Moreover, at 24 h (Fig. 5B) and 72 h (Fig. 5C), settlement increased on trail mucus to 44.6±3.8% and 35.5±1.9% respectively, and at values significantly higher than that on fixed mucus, viz, 38.9±3.5% and 25±2.2%, respectively ($p<0.05$).

In comparing fresh and dried mucus for induction of larvae, it was found that larval settlement on fresh mucus was 12.1±1.6%, and on dried mucus 11.4±0.9%. These were not significantly different at 6 h, but at 24 h and 72 h, fresh

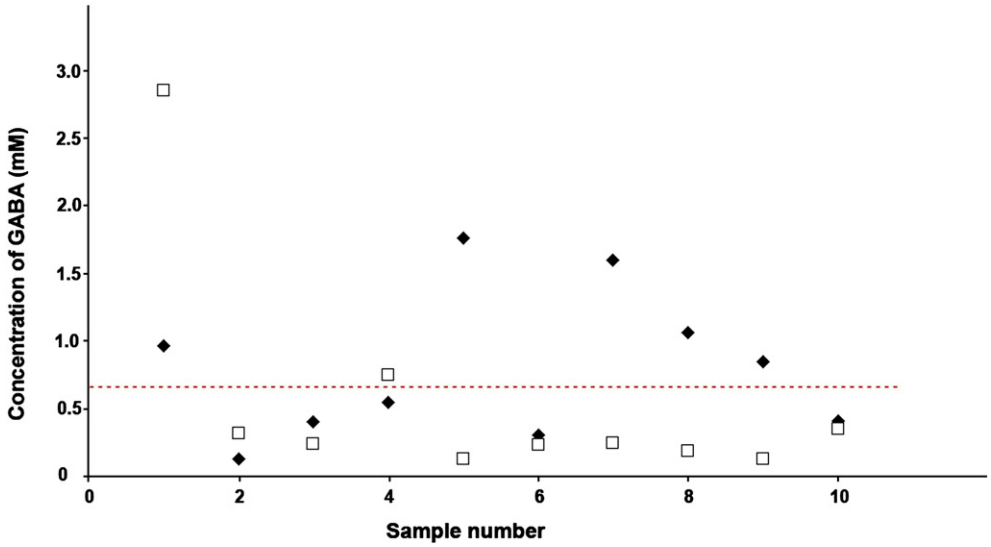


Fig. 4. Concentrations of GABA in aqueous extracts of mucus samples of *H. rubra* (◆, males; □, females). Mean (- - -) of all samples (n=20) was 0.68 mM.

mucus had significantly higher settlement values, i.e. 49.6± 3.5% and 34.9±3.7% respectively, than dried mucus i.e. 40.9± 2.8% and 20.7±1.6%, respectively (p<0.05).

4. Discussion

There have been numerous reports of GABAergic neurons in the CNS of different gastropod species (Cooke and Gelperin, 1988; Vehovszky et al., 1989; Richmond et al., 1991; Arshavky et al., 1993; Hernadi, 1994). However, similar studies in abalone species have been limited to a recent investigation in which evidence for GABA reactivity in the nerve bundles and radiating nerve fibers of *H. asinina* was shown (Wanichanon et al., 2004). They found that GABA was highly concentrated in neuroepithelial cells, which were distributed widely among the epithelial columnar cells and goblet-like cells of the tentacles. This current study has now shown that in *H. rubra*, GABAergic nerve fibers are distributed throughout the foot muscle and beneath the epithelium.

Our most important finding has been that haliotids and other gastropods possess GABA producing goblet-like cells in foot epithelia. When these cells are shed with mucus, they provide high concentrations of GABA which appeared to be slowly released into the surrounding seawater. We infer that the function of these cells is to secrete GABA in complex with mucus, thereby creating an inducer for gastropod larval settlement. It is possible that GABA is a general inducer whereas another component of mucus may provide species or genus specificity.

The supernatant obtained from rehydrated dried mucus samples were assayed for the presence of GABA by preliminary dot blot assays, followed by more detailed HPLC and TOF-MS analysis. The concentration of GABA (mean 0.68 mM), as determined by HPLC, was considerably higher than the 0.4–10 μM GABA concentrations that have been used in aquaculture trials (Roberts, 2001; Gapasin and Polohan, 2004). It should be noted that the concentrations determined in these experiments were entirely dependent on the volume of water used for rehydration, and the concentration of GABA in any secreted mucus sample might be higher than the current values. Variables that could attribute to, or minimize calculated GABA concentrations include (1) solubility of GABA from dried mucus into solution upon rehydration, (2) numbers of GABAergic cells shed-shed cells containing high levels of GABA were, however, identified by immunocytochemistry, (3) unknown dynamics of GABA degradation and or leaching from mucus, and (4) bacterial degradation or production of GABA. The latter notion is unlikely considering mucus samples were immediately incubated for 1 h at 60 °C, thereby minimizing any subsequent contribution by endogenous marine bacteria during extractions.

Abalone larvae have been shown to have highly specific cues (GABA and analogs) for initiating settlement and metamorphosis. Morse et al. (1979a) demonstrated that GABA induced planktonic larvae of the red abalone, *H. rufescens*, to settle and commence behavioral and developmental metamorphosis. Additional findings generally have shown that to stimulate settlement and metamorphosis of competent larvae, it is better to have a substratum covered with encrusting diatoms, and mucus secretions from grazing juveniles (Seki and Kan-no, 1981; Searcy-Bernal et al., 1992). In the present study, abalone larvae settled in greater numbers when exposed to either freshly

Table 1
Settlement of *H. asinina* larvae at 6, 24 and 72 h, when given a choice of mucus from three species of *Haliotis* (pooled data, n=9 replicates, means of percentages±s.e.m.)

Species	Percent settlement at 6 h	Percent settlement at 24 h	Percent settlement at 72 h
H. asinina	9.7±1.3 [a]	36.1±3.0	29.7±2.0 [a]
H. rubra	12.0±0.9	33.0±3.1	8.3±1.3 [a]
H. diversicolor	13.7±1.7	48.9±4.4 [b]	35.0±2.4 [a]
Mean (total)	11.7±1.2	41.4±3.6	29.7±2.1
Control	1.4±0.4 [a]	2.5±0.9 [b]	3.8±0.6 [a]

[a] Significant differences between species (Tukey's post hoc test), p<0.05.
[b] p<0.001.

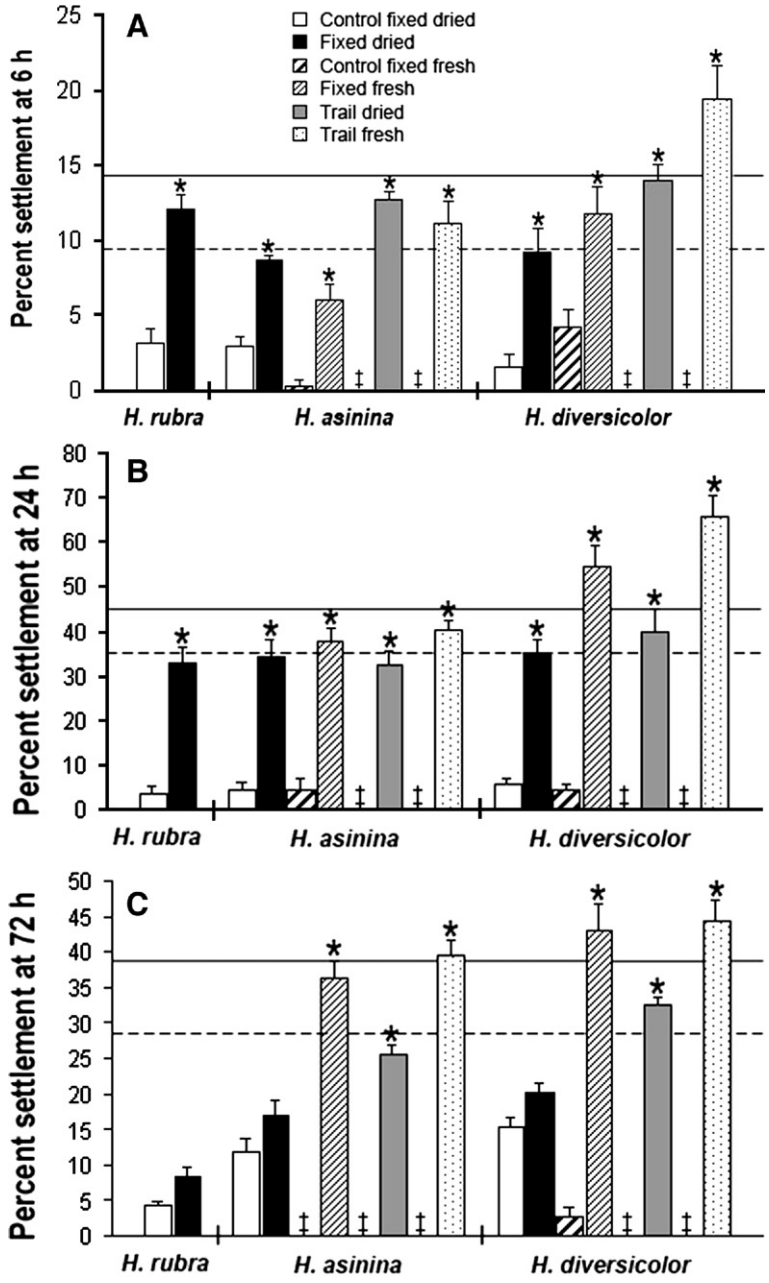


Fig. 5. Settlement of competent *H. asinina* larvae on mucus obtained from *H. asinina*, *H. rubra* and *H. diversicolor*, at 6 h (A), 24 h (B), and 72 h (C), following the addition of larvae. Columns indicate settlement on mucus (mean ± s.e.m.; $n = 9$ replicates) collected from abalone immobilized (fixed), or allowed to crawl freely (trail), on plastic sheets for 15 min. Treatments included: control for fixed dried (no mucus), fixed dried mucus, control for fixed fresh mucus (no mucus), fixed fresh mucus, trail dried mucus, and trail fresh mucus. Settlement in controls for treatments which have zero values, have no columns and are shown as fixed fresh, trail dried and trail fresh (‡).

obtained mucus, or rehydrated dried mucus samples. However, when mucus was absent, settlement was much lower. We observed no differences between the numbers of larvae settling on the mucus of three *Haliotis* species. However, when trail and fixed mucus preparations were compared, variations became apparent. Differences also emerged when settlement over time was compared. In particular, the reduction at 72 h was possibly attributed to natural mortality and/or waste build-up. These data support the findings of Seki and Kan-no (1981), who found that larvae of *H. discus hannai* settled on conspecific mucus trails, as well as the mucus trails of three other haliotids. Furthermore, they found that larvae did not settle as well on mucus trails of non-haliotid gastropods. Bryan and Qian (1998) found that the addition of mucus from animals with free movement increased larval settlement. Likewise, our tests showed that significantly more larvae settled on conspecific mucus trails from free moving animals, rather than on mucus from stationary individuals.

We have found that gastropod mucus contains GABA in sufficient quantities to induce larval settlement. It was already known that GABA-like molecules on the substrate surface of CCA also stimulate efficient settlement of gastropods (Morse

et al., 1979a, 1984), however, there appear to be unknown cues that distinguish one mucus form from another, particularly in attracting larvae. We believe the unknown cues could either be the mucus itself or released into the seawater as pheromones. Water-borne pheromones, as well as contact pheromones have recently been characterized in a number of marine invertebrates, including *Aplysia vaccaria, A. californica*, *Loligo pealeii*, and *Telmessus cheiragonus* (Buresch et al., 2003; Susswein and Nagle, 2004; Kamio et al., 2005). In *A. californica*, egg capsule secreting glands are responsible for the release of pheromones for sexual attraction (Cummins et al., 2004; Painter et al., 2004). In marine arthropods, copulatory behavior occurs in response to chemical cues released in urine (Kamio et al., 2005). We are now investigating the possible presence of pheromones in gastropod mucus, and such findings would strengthen our understanding of gastropod recruitment in the wild, which could be applied in aquaculture.

Acknowledgements

We thank Tony Smith at Bay City Seafarm, Geelong, Australia, and Tanes Poomtong at the Coastal Aquaculture Research and Development Center Prachuabkirikun, Thailand, for the use of animals. Critical comments about the statistical outcomes by Assoc. Prof. Montip Tiensuwan were appreciated. Assistance by Dr Xavier Conlon, from the Institute of Biotechnology (BioDeakin) Deakin University, in the TOF-MS instrument set up, and subsequent analysis of results was also greatly appreciated. This project was supported by grants from the Thailand Research Fund (Senior Research Scholar Fellowship to Prof. Prasert Sobhon), the Commission on Higher Education Thailand (Ph.D. scholarship to Praphaporn Laimek), and Mahidol University. **[RH]**

References

Akashige, S., Seki, T., Kan-no, H., Nomura, T., 1981. Effects of gamma-aminobutyric acid and certain neuro-transmitters on the settlement and metamorphosis of the larvae of *Haliotis discus hannai* Ino (Gastropoda). Bull. Tohoku Reg. Fish. Res. Lab. 43, 37–45.

Arshavky, Y.I., Deliagina, T.G., Gamkreldze, G.N., Orlovky, G.N., Panchin, Y.V., Popova, L.B., 1993. Phamacologically induced elements of the hunting and feeding behavior in the pteropod mollusk *Clione limacina* I. Effects of GABA. J. Neurophysiol. 69, 512–521.

Barlow, L.A., 1990. Electrophysiological and behavioral responses of the larvae of the red abalone (*Haliotis rufescens*) to settlement-inducing substance. Bull. Mar. Sci. 46, 537–554.

Bryan, P.J., Qian, P., 1998. Induction of larval attachment and metamorphosis in the abalone *Haliotis diversicolor* (Reeve). J. Exp. Mar. Biol. Ecol. 223, 39–51.

Buresch, K.C., Boal, J.G., Knowles, J., Debose, J., Nichols, A., Win, A., Painter, S.D., Nagle, G.T., Hanlon, R.T., 2003. Contact chemosensory cues in egg bundles elicit male-male agonistic conflicts in the squid *Loligo pealeii*. J. Chem. Ecol. 29, 547–560.

Cooke, I.R.C., Gelperin, A., 1988. Distribution of GABA-like immunoreactive neurons in the slug *Limax maximus*. Cell Tissue Res. 253, 77–81.

Cummins, S.F., Nichols, A.E., Amare, A., Hummon, A.B., Sweedler, J.V., Nagle, G.T., 2004. Characterization of *Aplysia* enticin and temptin, two novel water-borne protein pheromones that act in concert with attractin to stimulate mate attraction. J. Biol. Chem. 279, 25614–25622.

Daume, S., Brand-Gardner, S., Woerkling, W.J., 1999a. Preferential settlement of abalone larvae: diatom films vs non-geniculate coralline red algae. Aquaculture 174, 243–254.

Daume, S., Brand-Gardner, S., Woerkling, W.J., 1999b. Settlement of abalone larvae (Donovan) in response to non-geniculate coralline red algae (Corallines, Rhodophyta). J. Exp. Mar. Biol. Ecol. 234, 125–143.

Davies, M.S., Hawkins, S.J., 1998. Mucus from marine molluscs. In: Blaxter, J.H.S., Southward, A.J., Tyler, P.A. (Eds.), Advances in Marine Biology. Academic press, London, UK, pp. 4–34.

Denny, M.W., 1983. Molecular biomechanics of molluscan mucous secretions. In: Wilbur, K.M. (Ed.), The Mollusca, Volume 1: Metabolic biochemistry and molecular biomechanics. Academic press, London, UK, pp. 431–465.

Donovan, D.A., Carefoot, T.H., 1997. Locomotion in the abalone *Haliotis kamschatkana*: pedal morphology and cost of transport. J. Exp. Biol. 200, 1145–1153.

Gallardo, W.G., Buen, S.A., 2003. Evaluation of mucus, *Navicula*, and mixed diatoms as larval settlement inducers for the tropical abalone *Haliotis asinina*. Aquaculture 221, 357–364.

Gapasin, R.S.J., Polohan, B.B., 2004. Induction of larval settlement in the donkey-ear abalone, *Haliotis asinina* Linnaeus, by chemical cues. Hydrobiologia 519, 9–17.

Garcia-Lavandeira, M., Silva, A., Abad, M., Pazos, A.J., Sánchez, J.L., Parallé, L., 2005. Effects of GABA and epinephrine on the settlement and metamorphosis of the larvae of four species of bivalve molluscs. J. Exp. Mar. Biol. Ecol. 316, 149–156.

Henderson, J.W., Richer, R.D., Bidlingmeyer, B.A., Woodward, C., 2006. Rapid, accurate, sensitive, and reproducible HPLC analysis of amino acids. Agilent Technologies, Publication Number 5980-1193EN, p. 10.

Hernadi, L., 1994. Distribution and anatomy of GABA-like immunoreactive neurons in the central and peripheral nervous system of the snail *Helix pomatia* L. Cell Tissue Res. 277, 189–198.

Kamio, M., Araki, M., Nagayama, T., Matsunaga, S., Fusetani, N., 2005. Behavioral and electrophysiological experiments suggest that the antennular outer flagellum is the site of pheromone reception in the male helmet crab *Telmessus cheiragonus*. Biol. Bull. 208, 12–19.

Matute, C., Streit, P., 1986. Monoclonal antibodies demonstrating GABA-like immunoreactivity. Histochemistry 86, 147–157.

Morse, A.N.C., Morse, D.E., 1984a. Recruitment and metamorphosis of *Haliotis* larvae induced by molecules uniquely available at the surfaces of crustose red algae. J. Exp. Mar. Biol. Ecol. 75, 191–215.

Morse, A.N.C., Morse, D.E., 1984b. GABA mimetic molecules from *Porphyra* (Rhodophyta) induce metamorphosis of *Haliotis* (Gastropoda) larvae. Hydrobiologia 116, 155–158.

Morse, D.E., Hooker, N., Duncan, H., Jensen, L., 1979a. γ-Aminobutyric acid, a neurotransmitter, induces planktonic abalone larvae to settle and begin metamorphosis. Science 204, 407–410.

Morse, D.E., Morse, A.N.C., Jensen, L., Duncan, H., 1979b. Induction of larval abalone settlement and metamorphosis by γ-aminobutyric acid and its congeners from crustose red algae: II. applications to cultivation, seed-production, and bioassays; principle cues of mortality and interference. Proc. World. Maricult. Soc. 10, 81–91.

Morse, D.E., Hooker, N., Duncan, H., 1980. GABA induces metamorphosis in *Haliotis*, V: stereochemical specificity. Brain Res. Bull. 5, 381–387.

Morse, A.N.C., Froyd, C., Morse, D.E., 1984. Molecules from cyanobacteria and red algae that induce larvae settlement and metamorphosis in the mollusc *Haliotis rufescens*. Mar. Biol. 81, 293–298.

Moss, G.A., 1999. Factors affecting settlement and early post-settlement survival of the New Zealand abalone *Haliotis australis*. NZ. J. Mar. Freshwater Res. 33, 271–278.

Moss, G.A., Tong, L.J., 1992. Techniques for enhancing larval settlement of the abalone, *Haliotis iris*, on artificial surfaces. NZ. J. Mar. Freshwater Res. 26, 75–79.

Painter, S.D., Cummins, S.F., Nichols, A.E., Akalal, D.G., Schien, C.H., Braun, W., Smith, J.S., Susswein, A.J., Levy, M., de Boer, P.A.C.M., Maat, A., Miller, M.W., Scanlan, C., Milberg, R.M., Sweedler, J.V., Nagle, G.T., 2004. Structural and functional analysis of Aplysia attractins, a family of water-borne protein pheromones with interspecific attractiveness. PNAS 101, 6929–6933.

Polak, J.M., Noorden, S.V., 1997. In: Polak, J.M., Noorden, S.V. (Eds.), Introduction to immunocytochemistry. Bios Scientific Publishers, London, UK.

Richmond, J.E., Bulloch, A.G.M., Bauce, L., Lukowiak, K., 1991. Evidence for presence, synthesis, immunoreactivity, and uptake of GABA in the nervous system of the snail *Helisoma trivolvis*. J. Comp. Neurol. 307, 131–143.

Roberts, R., 2001. A review of settlement cues for larval abalone (*Haliotis* spp.). J. Shellfish Res. 20, 571–586.

Roberts, R., Nicholson, C., 1997. Variable response from abalone larvae (*Haliotis iris, H.* virginea) to a range of settlement cues. Mol. Res. Abs. 18, 131–141.

Roberts, R.D., Kaspar, H.F., Barker, R.J., 2004. Settlement of abalone (*Haliotis iris*) larvae in response to five species of coralline algae. J. Shellfish Res. 23, 975–987.

Rumrill, S.S., Cameron, R.A., 1983. Effects of gamma-aminobutyric acid on the settlement of larvae of the black chiton *Katharina tunicate*. Mar. Biol. 72, 243–247.

Searcy-Bernal, R., Salas-Garza, A.E., Flores-Aguilar, R.A., Hinojosa-Rivera, P.R., 1992. Aquaculture 108, 241–250.

Seki, T., Kan-no, H., 1981. Induced settlement of the Japanese abalone, *Haliotis discus hannai*, veliger by the mucous of the juvenile and adult abalones. Bull. Tohoku Reg. Fish. Res. Lab. 43, 29–36.

Seki, T., Taniguchi, K., 1996. Factors critical to the survival of herbivorous animals during settlement and metamorphosis. In: Watanabe, Y., Yamashita, Y., Oozeki, Y. (Eds.), Survival strategies in early life stages of marine resources. Brookfield Balkema, Rotterdam, Netherlands, pp. 341–354.

Slattery, M., 1992. Larval settlement and juvenile survival in the red abalone (*Haliotis rufescens*): an examination of inductive cues and substrate selection. Aquaculture 102, 143–153.

Smith, A.M., Morin, M.C., 2002. Biochemical differences between trail mucus and adhesive mucus from marsh periwinkle snails. Biol. Bull. 203, 338–346.

Suenaga, K., Hori, H., Ishida, H., Nukaya, H., Roberts, R.D., Tsuji, K., 2004. Inducing substance for abalone larval metamorphosis from the crustose coralline alga *Hydrolithon samoense*. Fish. Sci. 70, 342–344.

Susswein, A.J., Nagle, G.T., 2004. Peptide and protein pheromones in molluscs. Peptides 25, 1523–1530.

Takahashi, K., Koganezawa, A., 1988. Mass culture of *Ulvella lens* as a feed for abalone *Haliotis discus hannai*. NOAA Tech. Rep. NMFS 70, 25–36.

Vehovszky, A., Bokisch, A.J., Krogsgaard-Larsen, P., Walker, R.J., 1989. Pharmacological profile of γ-aminobutyric acid (GABA) receptors of identified central neurons from *Helix aspera*. Comp. Biochem. Physiol. 92, 391–399.

Wanichanon, C., Laimek, P., Chitchulanon, N., Suphamungmee, W., Apisawetakan, S., Linthong, V., Sretarugsa, P., Kruatrachue, M., Upatham, E.S., Poomtong, T., Sobhon, P., 2004. Sensory receptors on cephalic and epipodial tentacles of *Haliotis asinina* Linnaeus. J. Shellfish Res. 4, 1097–1106.

Yang, Y., Wu, B.L., 1995. Induction of larval settlement and metamorphosis of *Haliotis discus hannai* Ino (Gastropoda, Mollusca). Chin. J. Oceanol. Limnol. 13, 71–77.

Aquaculture 279 (2008) 142–149

Contents lists available at ScienceDirect

Aquaculture

journal homepage: www.elsevier.com/locate/aqua-online

Existence of APGWamide in the testis and its induction of spermiation in *Haliotis asinina* Linnaeus

Piyachat Chansela [a], Porncharn Saitongdee [a], Praphaporn Stewart [b], Nantawan Soonklang [b], Michael Stewart [c], Worawit Suphamungmee [a], Tanes Poomtong [c], Prasert Sobhon [a,*]

[a] Department of Anatomy, Faculty of Science, Mahidol University, Bangkok 10400, Thailand
[b] Department of Preclinical Science, Faculty of Medicine, Thammasat University, Pathumthani 12121, Thailand
[c] School of Medicine, Deakin University, Geelong, Victoria 3217, Australia
[d] The Coastal Aquaculture Research and Development Center, Department of Fisheries, Klongwan, Prachaubkirikhun 77000, Thailand

ARTICLE INFO

Article history:
Received 7 September 2007
Received in revised form 10 March 2008
Accepted 21 March 2008

Keywords:
Haliotis asinina
Spawning
APGWamide
Immunolocalization

ABSTRACT

Immunolocalization by using rabbit polyclonal antibody against APGWamide demonstrated that there was APGWamide immunoreactivity (APGW-ir) in the varicosed nerve fibers in the capsule, connective tissue and trabeculae of the testis whereas there was no APGW-ir in the ovary of sexually mature broodstocks of *Haliotis asinina*. *In vivo* bioassay, by injecting APGWamide into foot muscle of mature males and females (age over 24 months), showed that most males (87.50%) injected with 200 μl of 10^{-3} M APGWamide (170 μg APGWamide/animal) could be induced to spermiate whereas fewer males (43.75%) injected with 200 μl of 10^{-6} M APGWamide (0.17 μg APGWamide/animal) could spermiate. Following injection with 10^{-3} M, 53% of males spawned within 3 to 4 h, while the remaining males spawned within 2 to 3 h. The former tended to release more sperm at the range of 1.04 to 2×10^9, and the latter at the range 3.62×10^7 to 2.07×10^8 cells, respectively, and that the sperm of the former group appeared to be more motile. Following the injection of 10^{-6} M, all inducible males spawned within 2–3 h, and 43% of spawned males have sperm around 2×10^9, while 57% have fewer sperm number ranging from 2.75×10^7 to 9.94×10^8 cells. In contrast to males, none of the mature females with ripen ovary could be induced to ovulate. These data suggest that APGWamide is an important signaling molecule that plays a role in the male reproductive process that could be used to induce spermiation.

© 2008 Elsevier B.V. All rights reserved.

1. Introduction

APGWamide, an amidated tetrapeptide Ala–Pro–Gly–Trp–NH_2, was first isolated from neural ganglia of a prosobranch, *Fusinus ferrugineus* (Kuroki et al., 1990), and African giant snail *Achatina fulica* (Liu et al., 1991). It acts as a neurotransmitter and neuromodulator in many invertebrate species, such as *Lymnaea* (Croll and Van Minnen, 1992; De Boer et al., 1997; McCrohan and Croll, 1997), *Aplysia* (Fan et al., 1997), bivalve mollusks (Henry et al., 2000), sea mussel (Ohtania et al., 2000), and cuttlefish (Henry and Zatylny, 2002). APGWamide is thought to play a key role in the regulation of reproduction (Croll and Van Minnen, 1992; De Boer et al., 1997) and feeding behaviors in these animals (De Boer et al., 1997). Evidence for these functions comes from injection of APGWamide and *in vivo* electrical stimulation of the neurons in the right anterior lobe of cerebral ganglia, both of which cause eversion of the penial complex in the snail *Lymnaea stagnalis* (De Boer et al., 1997). Studies in *Helix aspersa* using anterograde and retrograde tracing methods infer the axon projection from the mesocerebral neurons to the penis, via penile nerves containing APGWamide (Li and Chase, 1995). In *Aplysia*, the movement of radula during feeding is controlled by APGWamide-containing neurons (Jing and Weiss, 2001; Morgan et al., 2002). Moreover, immunohistochemical analysis demonstrated APGWamide-containing axonal projections in the central nervous system as well as in peripheral tissues including the adductor muscle, foot, gill, labial pulps, lips, tentacles of a wide range of gastropods and bivalves (Croll and Van Minnen, 1992; De Lange and Van Minnen, 1998). Additionally, the gonads of juvenile and adult sea scallop of both sexes also contain this neuropeptide (Smith et al., 1997). In the oyster *Crassostrea gigas*, APGWamide is directly involved in the oocyte transport by modulating the contraction of adductor muscle that causes repetitive shell closure (Bernay et al., 2006).

Like other snails *Haliotis asinina*, a tropical abalone, is expected to use this amide as a neuromodulator for ovulation and spermiation. In this study we reported on the existence of APGWamide in the gonad and its function in the induction of ovulation and spermiation. Sexually mature male and female abalones raised in aquaculture

* Corresponding author. Department of Anatomy, Faculty of Science, Mahidol University, Rama 6 Road, Bangkok 10400, Thailand. Tel.: +66 2 2015406; fax: +66 2 3547168.
E-mail address: scpso@mahidol.ac.th (P. Sobhon).

0044-8486/$ – see front matter © 2008 Elsevier B.V. All rights reserved.
doi:10.1016/j.aquaculture.2008.03.058

system usually have asynchronous spawning, so there may not be sufficient numbers of eggs and sperm available for fertilization at the same time. The priming of either fully ripe males or females, or both, by this amide could help inducing simultaneous spawning of eggs and sperm, and thus increase fertilization success.

2. Materials and methods

2.1. Preparation of antibody

To produce polyclonal antibody against APGWamide, two 6-week-old female New Zealand white rabbits, obtained from the Animal Care Unit, Mahidol University, with the approval of the Animal Ethics Committee, were used. Before immunization the preimmune sera were collected from both rabbits. Then the immunogen was prepared by coupling 2 mg of APGWamide to 10 mg of bovine serum albumin (BSA) (Sigma-Aldrich, St. Louise, MO, USA) as carrier protein by using 20 mg of linking reagent, 1-ethyl-3-dimethylaminopropyl carbodiimide (EDC) (Sigma-Aldrich), in a 0.5 ml of 50 mM NaH_2PO_4, at pH 7.2. The mixture was incubated overnight at 4 °C, and then concentrated using Centricon-10 microconcentrator (Millipore, Bedford, MA, USA). After centrifugation at 10,000 rpm, 10 min, 4 °C, the precipitated component was washed four times with 2 ml of 50 mM NaH_2PO_4 (pH 7.2), then resuspended in 0.5 ml of the same buffer and transferred to a new tube. The antigen (~200 μg) in 0.25 ml phosphate-buffered saline (PBS) was mixed into emulsion with 0.25 ml of Freund's complete adjuvant, and then this antigen mixture was used to immunize the rabbits by subcutaneous injections. At 14, 28 and 42 days following the first injections, the rabbits were further boosted by subcutaneous injection with the same amount of protein mixed with Freund's incomplete adjuvant. The animals were killed at 56 days after the first injection, and the antisera were collected and kept at −20 °C until use.

2.2. Specificity of polyclonal antibody against APGWamide

BSA and BSA-linked to APGWamide were separated on 10% sodium dodecyl sulfate-polyacrylamide gel electrophoresis (SDS-PAGE). A five microliter aliquot containing 5 μg of protein of the respective sample (BSA and BSA-linked to APGWamide) was applied to the gel, and the broad range molecular weight standards (Bio-Rad Laboratories, Hercules, CA, USA) were run in parallel as the molecular weight markers. The separated proteins were blotted onto nitrocellulose membranes, and non-specific bindings were blocked with 5% skim milk in 10 mM Tris buffer saline, 0.1% Tween-20, pH 7.4. Rabbit antiserum against BSA-APGWamide was preabsorbed with BSA in 0.1 M PBS (250 mg/ml) at the ratios 1:20, 1:40, and 1:80 of antiserum: BSA (v/v). The nitrocellulose strips were incubated in the non-absorbed as well as the BSA-preabsorbed antisera, and bound antigen–antibody complexes were detected by using goat anti-rabbit IgG labeled with HRP (Zymed Laboratory Inc. San Francisco, CA, USA). Reactions were detected using the ECL detection kit (Amersham Biosciences, Buckinghamshire, England), according to the manufacturer's instructions. For negative control, the membrane was incubated with rabbit preimmune serum instead of non-absorbed and preabsorbed antisera. In addition BSA-preabsorbed antiserum was also preabsorbed again by APGWamide in 0.1 M PBS (250 mg/ml) at the ratio of 1:80 of antiserum:APGWamide (v/v). This BSA-APGWamide preabsorbed antiserum was then used to detect the bands on the nitrocellulose membrane as another negative control.

2.3. Screening of APGWamide in various organs by dot blot assay

To demonstrate the presence of APGWamide in different organs, dot blot assay was carried out using specific anti-APGWamide antiserum that has been preabsorbed with BSA as mentioned in Section 2.2. Various organs including male and female gonads, hepatopancreas, cerebral ganglia and pleuropedal ganglia were dissected. The organs were homogenized in a buffer containing 10 mM Tris–HCl, 150 mM NaCl, 0.5% TritonX-100, 1 mM EDTA, and 1 mM phenylmethylsulfonyl fluoride was added during the procedure. Protein-containing supernatants were collected following centrifugation at 10,000 rpm, 20 min 4 °C. After measuring the protein concentrations by Lowry method (Lowry et al., 1951) the proteins were diluted to obtain the concentrations of 1 μg, 100 ng, 10 ng, to 1 ng per 1 μl. One microliter of each sample was applied onto a nitrocellulose membrane pre-soaked in PBS and air-dried for 15 min. The membrane was blocked with 3% skim milk and 1% BSA in PBS and then incubated in the BSA-preabsorbed rabbit anti-APGWamide serum. For a negative control, the membrane was incubated with rabbit preimmune serum and BSA-APGWamide-preabsorbed antiserum instead of BSA-preabsorbed antiserum. After washing, the membrane was then incubated with goat anti-rabbit IgG labeled with HRP and treated with ECL detection kit. Stained dots on a white background indicated positive results. APGWamide at the same serial concentrations as those in the homogenates of organs were also dot-blotted on the nitrocellulose strip, and probed with the same set of antibodies for detection as a positive control.

2.4. Immunolocalization of APGWamide

2.4.1. Specimen preparation

Adult male and female *H. asinina*, with age over 24 months and body weight ranging between 70 and 80 g were obtained from a land-based aquaculture system at the Coastal Aquaculture Research and Development Center, Department of Fisheries, Prachaubkirikun Province, Thailand. They were anesthetized by immersing in 5% $MgCl_2$ in sea water, and then their shells were removed. The gonads were quickly dissected and fixed in Bouin's solution in 0.14 M NaCl for 24 h. After washing with 70% ethanol, the specimens were dehydrated in ascending concentrations of ethanol, cleared in dioxane three times, infiltrated, and embedded in paraffin. Serial transverse sections of the gonads were cut at 5 μm thickness using a rotary microtome, and mounted on glass slides coated with 3-aminopropyl triethoxy silane solution for strong adhesion. For a positive control the cerebral ganglion of *Aplysia californica* embedded in a paraffin block (courtesy of Dr. Scott Cummins University of Queensland, Australia) was also cut at the same thickness and treated similarly.

2.4.2. Immunoperoxidase staining

The gonad sections, as well as sections of *Aplysia* cerebral ganglion, were deparaffinized in xylene and rehydrated in descending concentration of ethanol (in 100% three times, 95%, 90%, 80%, and 70% once each). The residual picric acid from Bouin's solution was neutralized in 70% ethanol containing 1% Li_2CO_3 for 15 min (Wener et al., 1997). Subsequently, the endogenous peroxidase and free aldehyde groups from the fixative were blocked by immersing the sections in 0.3% H_2O_2 in 30% methanol for 30 min, and 0.1% glycine in PBS for 5 min, and washed three times with 0.05 M PBS containing 0.4% Triton X-100 (PBST). Non-specific binding was blocked by incubating the sections in 2% normal goat serum and with 4% BSA in PBST for 2 h. The sections were incubated overnight in the primary antibody (BSA-preabsorbed anti-APGWamide at the absorption ratio of 1:80 v/v) at a dilution of 1:200 in blocking solution, at room temperature overnight. Afterwards the sections were washed three times in PBST, and incubated in the secondary antibody (biotinylated goat anti-rabbit IgG, Sigma-Aldrich) diluted 1:200 in blocking solution for 45 min. After four washes, the slides were incubated with HRP-conjugated streptavidin (diluted 1:200 in PBST), for 45 min before exposure to substrate solution, Nova Red (Vector, Burlingame CA, USA.) containing H_2O_2 for 2–5 min, to develop color reaction. Finally, sections were rinsed with tap water for 10 min, dehydrated, and then

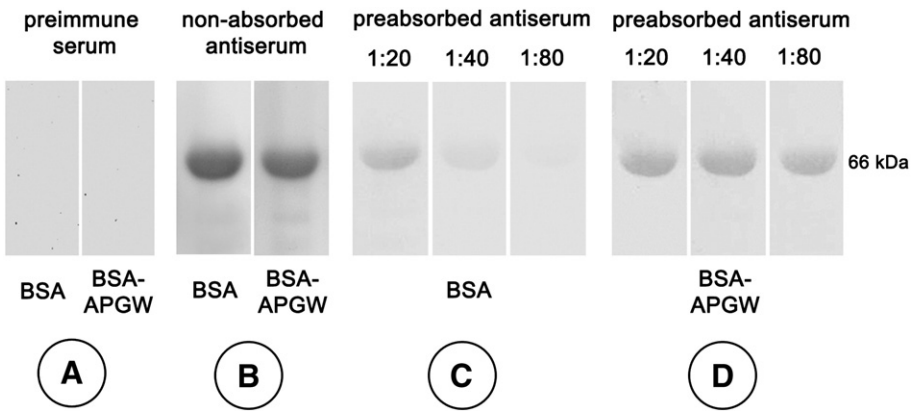


Fig. 1. Immunoblotting of BSA and BSA-APGWamide by non-absorbed and BSA-preabsorbed antiserum. (A) In controls, neither BSA nor BSA-APGW lanes show positive band with preimmune serum. (B) When using non-absorbed antiserum on BSA and BSA-APGW, both lanes show a similar pattern of positive banding. (C) Immunoblotting of BSA and BSA-APGW separated by SDS-PAGE and blotted onto nitrocellulose strips using rabbit antiserum preabsorbed with BSA in 0.1 M PBS (250 mg/ml) at the ratios of 1:20; 1:40; 1:80 (v/v) shows positive bands at 66 kDa in BSA lanes at the absorption ratios of 1: 20 and 1:40 but not at 1:80. (D) In BSA-APGW lanes, the positive bands appear equally intense, at all absorption ratios, i.e., 1:20; 1:40; and 1:80, respectively. Thus, BSA-preabsorbed antiserum at the ratio 1:80 is considered highly specific to APGWamide and was used for dot blot assays (Fig. 2) and immunolocalization (Figs. 3–5).

mounted with Permount medium (Sigma-Aldrich). However, to reveal histological details, some treated sections were counter-stained with Mayer's hematoxylin, washed in water, and processed similarly. For negative controls, the sections were processed in the same manner using preimmune rabbit serum or BSA-APGWamide-preabsorbed antiserum instead of the BSA-preabsorbed antiserum. All sections were examined and photographed using Nikon Eclipse E600 microscope fitted with Nikon digital camera DXM1200.

2.5. Spawning induction

Twenty-four mature males with fully ripen creamy yellow testis and twenty-four mature females with fully ripen dark-green ovary with and the body weight ranging between 70 and 80 g were each divided into 3 groups. The animals were each kept in separate 5-l tanks placed in a reversed day–night room for at least 3 days to allow the animals to acclimatize before beginning the experiment, which was carried out in the day time at 7 days prior to the full moon, which is the natural time that the animals usually spawn. In the two experimental groups, the animals were intramuscularly injected with APGWamide into the sole of foot muscle at two different doses, i.e., 200 µl of 10^{-3} M (170 µg APGWamide/animal) and 200 µl of 10^{-6} M (0.17 µg APGWamide/animal) respectively. Afterwards each animal was placed in a clear plastic tank filled with 2 l of filtered sea water and observed for their spawning behavior at half an hour intervals. Immediately following spawning a 20 µl of sea water containing spawned sperm was taken from the tank and placed in a glass slide with concave well and the sperm motility was assessed by observing under the light microscope, and another 10 µl aliquot was taken, fixed in equal volume of 4% paraformaldehyde in 0.1 M PBS and the sperm number counted under a light microscope using hemocytometer. The total number of sperm per spawn (i.e., in total volume of each tank) was then calculated. In the control groups the injections of mollusc physiological saline (Hepes 13 g, NaCl 25.66 g, KCl 0.82 g, $CaCl_2$ 1.69 g, $MgCl_2$ 10.17 g, Na_2SO_4 2.56 g, dH_2O 1 l, at pH 7.2) at the sxame volume per animal was performed instead of APGWamide. Each experiment was duplicated.

3. Results

3.1. Specificity of anti-APGWamide

The specificity of preabsorbed APGWamide antiserum was tested by western blot analysis (Fig. 1). No positive bands were detected in

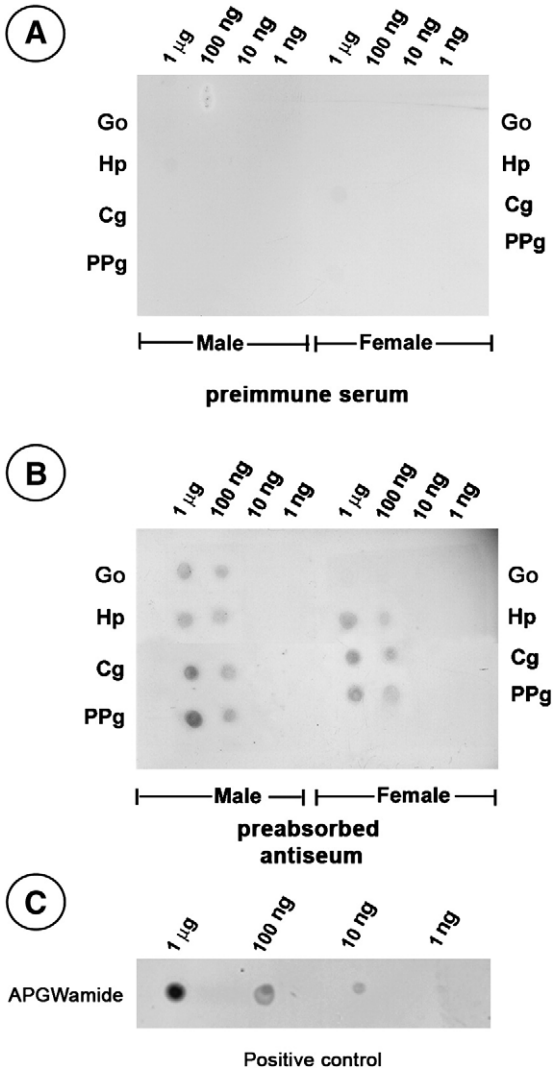


Fig. 2. (A, B) Dot blot assays to detect APGW-ir in homogenates of various organs of the male and female abalone. The amount of proteins of homogenates was serially diluted at 1 µg, 100, 10, and 1 ng/µl, and one microliter was the final aliquot dotted on nitrocellulose paper. APGW-ir could be observed in all organ samples except in the female gonad. (C) Positive control with similar concentrations of APGWamide at 1 µg, 100, 10, and 1 ng/µl showing detection levels of APGWamide in dot blot assays. Cg–cerebral ganglia, Hp–Hepatopancreas, Go–Gonads, PPg–pleuropedal ganglia.

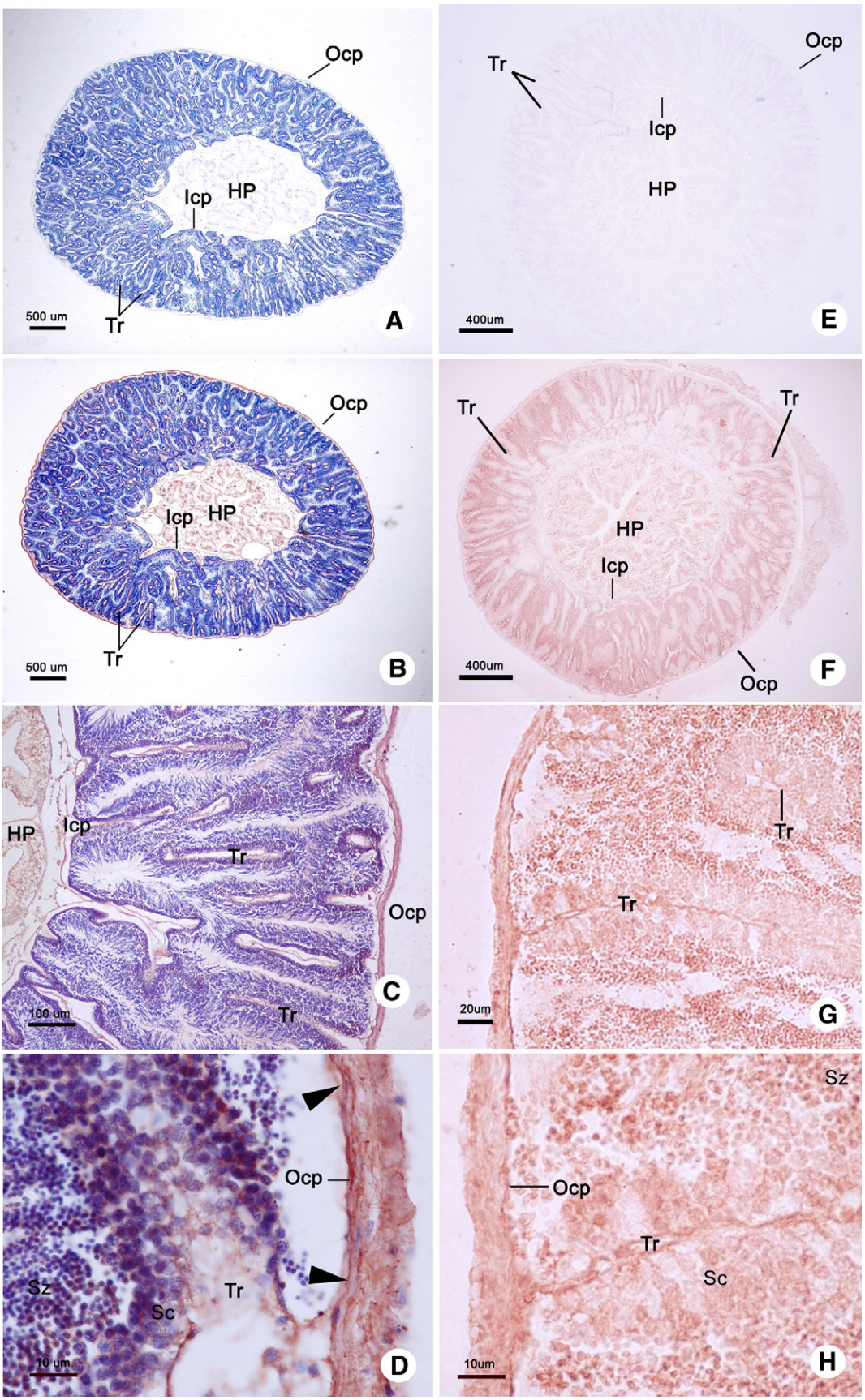


Fig. 3. Sections of fully mature testis stained with anti-APGWamide. (A) Low power micrographs of control sections of fully mature testis stained with preimmune serum and counter-stained with hematoxylin, and without counter stain (E). Low power micrographs of testicular sections showing APGW-ir in the capsule and trabeculae in counter-stained (B) and noncounter-stained sections (F). Medium power micrographs showing APGW-ir in the outer capsule (Ocp), hepatopancreas (HP) and trabeculae (Tr) of counter-stained(C) and noncounter-stained (G) sections. High powered micrographs showing APGW-ir in the nerve fibers (arrow head) in the outer capsule and trabeculae in counter-stained (D) and noncounter-stained(H) sections. Ocp–outer capsule, HP–hepatopancreas, Icp–inner capsule, Tr–trabeculae, Sz–spermatozoa, Sc–spermatocytes.

either lane of the negative controls, which were probed by rabbit preimmune serum (Fig. 1A), whereas lanes containing either BSA or BSA-APGW showed positive bands with non-absorbed antiserum (Fig. 1B). In BSA lanes, a less intense but still positive band was detected by the antiserum preabsorbed with BSA at the ratios 1:20 and 1:40 while no positive band was detected at the ratio 1:80 (Fig. 1C). However positively stained protein bands at a molecular weight 66 kDa was observed in all BSA-APGWamide lanes probed with antiserum preabsorbed with BSA at the ratio 1:20, 1:40 and 1:80 (v/v) (Fig. 1D). On the other hand no band was detected using antiserum preabsorbed with both BSA and APGWamide at the ratio 1:80 (v/v) (data not shown). Hence antiserum after preabsorption with BSA at the ratio 1:80 was quite specific to APGWamide, and this was used for the detection of APGW-ir in dot blot assay and in gonadal tissue sections.

3.2. Dot blot assay for APGWamide

The homogenates from different organs were tested by dot blot assay for the presence of APGW-ir (Fig. 2). No staining was detected in the dot blots of male or female organs probe with preimmune serum (Fig. 2A). In males, APGW-ir was detected in the homogenates of testis, hepatopancreas, cerebral ganglia, and pleuropedal ganglia, with the least intensity in hepatopancreas at the lowest concentration of 100 ng/1 µl. In females APGW-ir was found in the homogenates of cerebral ganglia, pleuropedal ganglia and hepatopancreas, but was absent in ovary (Fig. 2B). The dot blot of APGWamide at comparable concentrations by the same antibody showed positive staining at the lowest concentration of 10 ng/1 µl (Fig. 2C). This suggests that the amount of APGWamide detectable in homogenates could be approximately ten times lower than when using pure APGWamide in comparable dot blot assays.

3.3. Distribution of APGWamide in gonadal tissue using immunoperoxidase staining

There was no APGW-ir in the control gonadal sections both counter-stained and noncounter-stained (Figs. 3A, E, 4A). Intense APGW-ir was observed in the outer capsule of the testis which contained muscle, nerve fibers, and epithelial cells in both counter-stained (Fig. 3B, C, D) and noncounter-stained sections (Fig. 3F, G, H). Similar level of intense staining was found in the trabeculae which were the extending parts of the capsule separating the testis into many compartments (Fig. 3B–D, F–H). In both the capsule and trabeculae, APGW-ir was confined to connective tissue and possibly nerve fibers shown as wavy and varicosed lines (Fig. 3D, H). Hepatopancreas in males exhibited very light staining (Fig. 3B, C, F). In contrast both the control (Fig. 4A,B) and experimental sections (Fig. 4C,D) of the ovary displayed no APGW-ir although the hepatopancreas in females also exhibited very light staining (Fig. 4C). For positive control APGW-ir in the cerebral ganglion of *Aplysia* was distinct (Fig. 5), with fairly intense immunoreactivity present in the giant neurons located at the right and left sides of the ganglion, with slightly fewer positive cells in the latter (Fig. 5A). The strong immunostaining was noted in the neurons of both noncounter-stained (Fig. 5B) and counter-stained sections

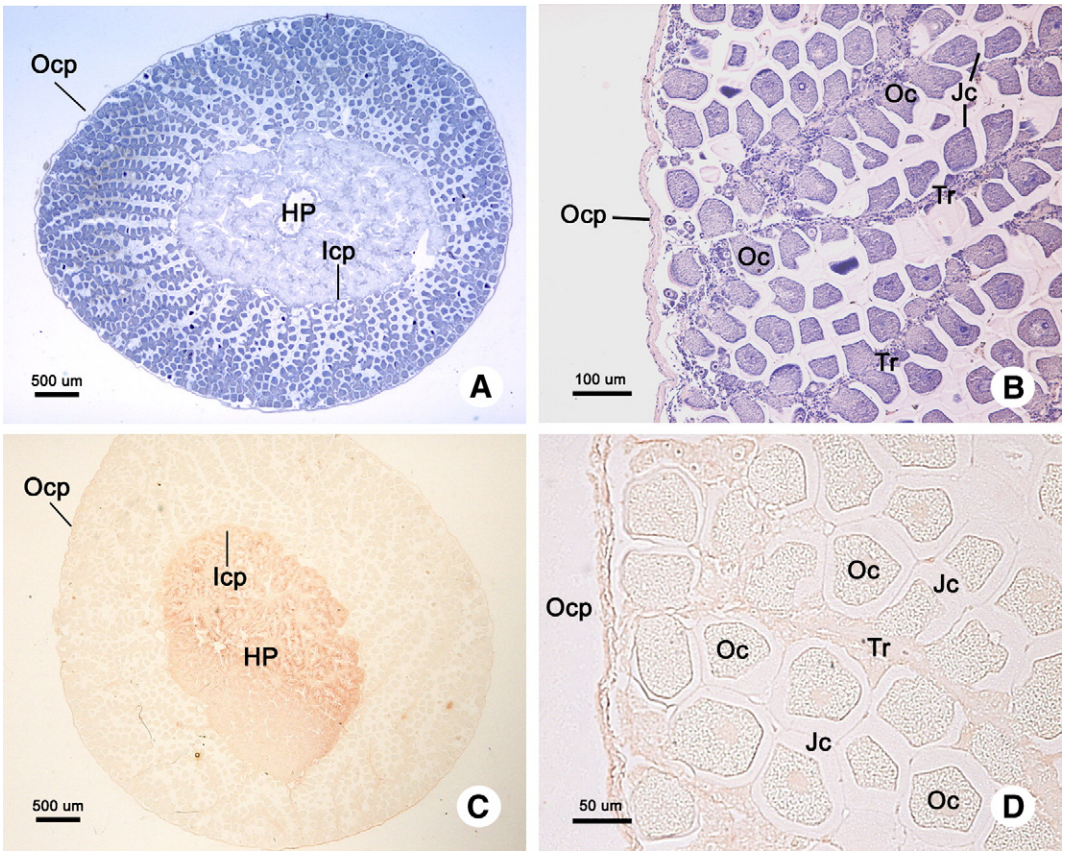


Fig. 4. Sections of fully mature ovary stained with anti-APGWamide. (A) A low power micrograph of a control ovarian section, counter-stained with hematoxylin showing no positive staining. (B) A medium power micrograph of counter-stained control ovarian section showing no positive staining for APGW-ir. (C) A low power micrograph of an ovarian section which is probed with anti-APGWamide and not counter-stained with hematoxylin, showing no positive signal for APGW-ir. Only hepatopancreas (HP) showed light staining. (D) A high power micrograph of C showing no staining for APGW-ir in the capsule or trabeculae of the mature ovary that contains fully developed oocytes. Oc–oocyte, Jc–jelly coated, Ocp–outer capsule, HP–hepatopancreas, Icp–inner capsule.

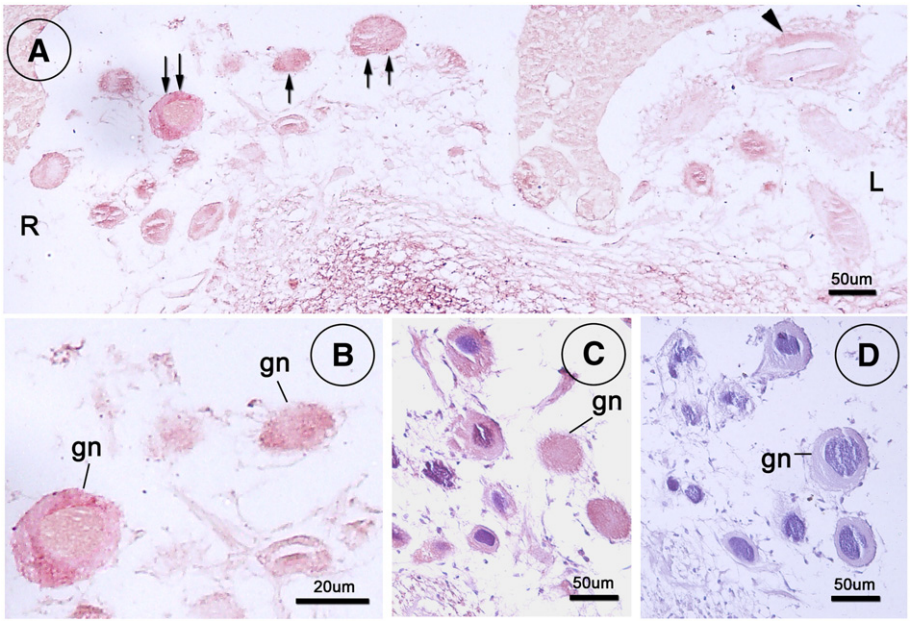


Fig. 5. Cerebral ganglia of *Aplysia californica* stained with anti-APGWamide. (A) A low power micrograph of the *Aplysia* cerebral ganglion showing APGW-ir in neurons,with more numbers and more staining intensity on the right side (arrow) than on the left side (arrow head). (B) A high power micrograph of (A) show intensely stained giant neurons (gn) in noncouter-stained (B) as well as in counter-stained (C) sections. (D) The control section using preimmune serum showing no positive immunoreactivity in the giant neurons (gn) where nuclei are counter-stained with hematoxylin. R–right side, L–left side.

(Fig. 5C). Immunoreactivity was not observed in control sections using preimmune serum (Fig. 5D) nor in sections that were stained with antiserum preabsorbed with BSA-APGW (data not shown).

3.4. Induction of spawning by APGWamide

The injection of APGWamide induced spawning (spermiation) only in the male abalones. Immediately after APGWamide injection, the foot muscle became spasmodic and all tentacles rose up for about 5 min, subsequently the treated males released their gametes within 2 to 4 h. After the injection of APGWamide at dosage of 200 μl of 10^{-3} M (170 μg/animal) most males (87.5%) could be induced to spawn (Fig. 6), whereas only 43.75% of males could be induced to spawn with the injection of 200 μl of 10^{-6} M (0.17 μg/animal) of APGWamide (Fig. 6). The sperm was immediately checked for motility by examination of the movement of their tails for half an hour in the light microscope. The motility was rated from + to +++. At +++ all sperm exhibited fast movement over the period of observation time, at ++ some sperm exhibited fast while the rest exhibited slow movement, and at + all sperm exhibited very slow movement to no movement (Table 1). It was noted that, following injection of 10^{-3} M APGWamide 53% of male abalones spawned within 3–4 h, with the lowest to highest sperm number ranging from 1.04 to 2×10^9 cells, and 47% of male abalones spawned within 2–3 h with the range of sperm number from 3.62×10^7 to 2.07×10^8 cells following injections. Hence, the males that spawned later (3–4 h) tended to release more sperm that were also more active than those that spawned earlier (2–3 h). In comparison, following the injection of 10^{-6} M APGWamide the spawned males released their sperm at 2–3 h and 43% of these spawning male exhibited around 2×10^9 sperm per spawn, whereas 57% exhibited sperm number that ranged from 2.75×10^7 to 9.94×10^8 cells. The numbers of sperm per spawn are within the range observed in natural spawning occurring at full moon, which is about 1.15–6.2×10^9 cells per spawn. In contrast, mature females could not be induced to spawn at either dose, nor control males that received mollusc physiological saline.

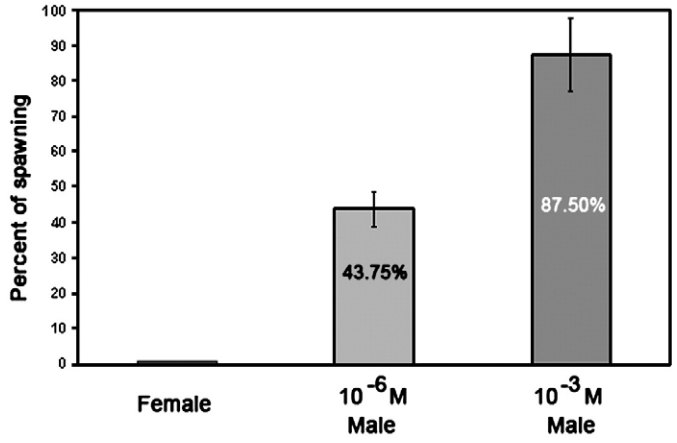


Fig. 6. Effect of APGWamide on spawning induction in male and female abalones. APGWamide injected at the dose of 200 μl of 10^{-3} M could induce sperm release in 87.50% of the treated male animals, whereas APGWamide injected at the dose of 200 μl of 10^{-6} M could induce spermiation in only about 43.75% of treated male, whereas female could not be induced to spawn at either dose. Bars represent standard deviation.

Table 1
The motility and quantity of the released sperm after injecting male abalones with APGWamide at 200 μl per animal of 10^{-3} and 10^{-6} M

APGW Conc.	Ratio% of male that spermiate	Time of spawning (h)	Motility	Range of sperm number per spawn
10^{-3}	53	3–4	+++	$1.04–2\times10^9$
	47	2–3	++	$3.62\times10^7–2.07\times10^8$
10^{-6}	43	2–3	+++	2×10^9
	57	2–3	++	$2.75\times10^7–9.94\times10^8$
Natural spawning	N/A	N/A	+++	$1.15–6.2\times10^9$

The sperm motility is qualitatively estimated as follows: +++, all sperm exhibit fast movement over the period of observation time; ++, some sperm exhibited fast while the rest exhibited slow movement; + all sperm exhibited very slow movement to no movement. Time of spawning is the hours that spawning occurs post injection.

4. Discussion

APGWamide is a well known regulatory neuropeptide that controls the reproductive and feeding behaviors in many mollusks (Li and Chase, 1995; De Boer et al., 1996; De Lange and Van Minnen, 1998). Immunohistochemical localization of APGWamide in several species of gastropod mollusks suggests that APGWamide is a major neuromodulator present in the neural tissue. In a comparative study by De Lange and Van Minnen (1998), it was found that APGW-ir was present in clusters of neurons of cerebral ganglia in the basommatophoran gastropod, *Bulinus truncates*, the stylommatophoran gastropods, *Arion ater* and *Limax maximus*, and in a prosobranch, *Littorina littorea*. Additionally, there are cluster of APGWamide-containing neurons located in the neural ganglia of *A. californica* (Fan et al., 1997), right pedal ganglion of *H. aspersa* (Li and Chase, 1995), and neural ganglia of *L. stagnalis* (Croll and Van Minnen, 1992; De Boer et al., 1997). Most of these cells have projections into the penial nerve which control muscles of the penile complex, or into a pedal nerve which has a pathway into the penial complex (Koene et al., 2000). In this study we chiefly aimed to investigate the distribution of APGWamide in both gonad and neural tissues of male and female *H. asinina*. In dot blot assays, it was observed that the male gonad exhibited more APGW-ir than the female gonad, and APGW-ir was also detected substantially in the neural ganglia including cerebral and pleuropedal ganglia of *H. asinina*, however grading from the intensity the level of APGWamide in the neural ganglia of both sexes, indicates no gender specific differences. Our initial immunohistochemical staining of these neural ganglia also showed APGW-ir in neurons lying in clusters in cerebral and pleuropedal ganglia of both male and female (data not shown), which also supports the dot blot assays. It has been suggested that APGWamide in the neural ganglia may play other neuromodulatory roles, like those observed in *L. stagnalis*, where the isolated light green cells in the cerebral ganglia may be induced to release insulin-like hormone by the action of APGWamide (Geraerts, 1976; Tol-Steye et al., 1999). However, the different levels of gonadal APGWamide in males and females of *H. asinina* may have a more direct bearing on the different pattern of gamete release in both sexes. Our immunohistochemical staining supports this latter notion as APGW-ir is more intense in the connective tissue scaffold, viz., the capsule and trabeculae of the testis. Earlier our group investigated the detailed organization of these two structures and found that they are composed of varicosed nerve fibers and muscle cells arranged as layers in the connective tissue scaffold (Apisawetakan et al., 2001). The pattern of APGW-ir distribution in this structure matches the pattern of varicosed nerve fibers observed in our earlier study. Furthermore the anti-APGWamide that was used as a probe and the existence of APGWamide in these locations are quite specific as it has been proven that anti-APGWamide also specifically stained the APGW-ir containing-giant neurons of *Aplysia* cerebral ganglion as reported earlier (Fan et al., 1997; De Lange and Van Minnen, 1998). Hence, we believe that APGWamide stored in the nerve fibers may be released to stimulate the contraction of muscle cells in the capsule and trabeculae, so that this contraction initiates the release of sperm from the testis.

In functional studies, electrical stimulation of clusters of the APGWamide neurons in the right cerebral ganglion of *A. califonica* and *H. aspersa* causes contraction of the penial complex (Koene et al., 2000), whereas injection of APGWamide can evoke penial eversion (Yu and Blankenship, 1997). In this study, the injection of two concentrations of APGWamide 10^{-3} M and 10^{-6} M could induce sperm release in males *H. asinina*, with 87.50% positive response in the group treated with the higher concentration. In contrast, ovulation could not be induced in females by APGWamide given at the same concentrations and doses. Altogether, it is suggestive that in *H. asinina* this peptide plays a major role in spermiation. This observation does however appear to be different from an earlier report, which demonstrated that SepOvatropin, APGWamide-liked peptide is involved in the oocyte transport in cuttlefish, *Sepia officinalis* (Zatylny et al., 2000). Furthermore, in a more recent investigation in the oyster, *C. gigas*, APGWamide in association with the hexapeptide PIESVD, triggers a contraction of the adductor muscle to cause the release of oocytes to the external medium (Bernay et al., 2006). These two findings suggest that APGWamide can induce germ cell release in both males and females of these species. In contrast, in our study it was demonstrated that APGWamide has a predominantly more male-associated function, perhaps, due to the presence of different amounts of APGWamide in the gonads of the two sexes. It is also possible that the difference in observations from those of Zatylny et al. (2000) is due to the varied peptides structures of both APGWamide and SepOvatropin, as well as species specifications, leading to tangibly different outcomes (Cummins and Hanna, 2004). In the latter investigation it appears that APGWamide might operate in conjunction with PIESVD in females. Therefore stimulation by both peptides may be needed to induce female spawning, whereas one peptide is insufficient. This assumption is possible, as it was recently suggested that mollusc APGWamide family members act through the gonadotrophin releasing hormone (GnRH) along with it's receptor (GnRH-R) (Filipe et al., 2007) to induce imposex, namely, development of the male accessory sex organs in females (Oberdörster and McClellan-Green, 2002). Therefore it is possible that APGWamide directly triggers the onset of spawning in male abalone, whereas in females, it may require other cofactors to have any significant physiological effects on gamete release.

The numbers of sperm received per spawn from animals after treatment with different doses of APGWamide were not significantly different from one another, and fell within the range of numbers of sperm per spawn released during natural spermiation during the full moon period. Furthermore, the sperm released by APGWamide induction exhibited similar level of motility as those released under natural conditions. This implies that the APGWamide-induced released sperm should comprise mostly of mature sperm, although their ability to fertilize eggs needs to be tested further. Additionally, we have lower percentages of spermiation when using FMRFamide (unpublished observation), suggesting that the APGWamide effect is specific, although given the high dose used we cannot yet totally exclude an effect though an unspecific pathway.

Acknowledgements

This research was supported by the Thailand Research Fund (Senior Research Scholar Fellowship to Prasert Sobhon) and the Mahidol University. We would also like to thank the Coastal Aquaculture Research and Development Center, Department of Fisheries, Prachaubkirikun Province, Thailand, for providing abalone specimens, and Dr. Scott Cummins from the University of Queensland, Australia for providing the block of cerebral ganglion of *A. californica*.

References

Apisawetakan, S., Chanpoo, M., Wanichanon, C., Linthong, V., Kruatrachue, M., Upatham, E.S., Pumthong, T., Sobhon, P., 2001. Characterization of trabecular cells in the gonad of *Haliotis asinina* Linnaeus. J. Shellfish Res. 20, 717–724.

Bernay, B., Baudy-Floc, H.M., Zanuttini, B., Zatylny, C., Pouvreau, S., Henry, J., 2006. Ovarian and sperm regulation peptides regulate ovulation in the oyster *Crassostrea gigas*. Mol. Reprod. Dev. 73, 607–616.

Croll, R., Van Minnen, J., 1992. Distribution of the peptide Ala–Pro–Gly–Trp–NH_2 (APGWamide) in the nervous system and periphery of the snail *Lymnaea stagnalis* as revealed by immunocytochemistry and *in situ* hybridization. J. Comp. Neurol. 324, 567–574.

Cummins, S., Hanna, P., 2004. Identification of an α-peptide in *Haliotis asinina*. J. Shellfish Res. 23 (4), 1129–1134.

De Boer, P.A.C.M., Jansen, R.F., Maat, A.T., 1996. Copulation in the hermaphroditic snail *Lymnaea stagnalis*. Inv. Reprod. Dev. 30, 167–176.

De Boer, P.A.C.M., Ter Maat, A., Pieneman, A.W., Croll, R.P., Kurokawa, M., Jansen, R.F., 1997. Functional role of peptidergic anterior lobe neurons in male sexual behavior of the snail *Lymnaea stagnalis*. J. Neurophysiol. 78, 2823–2833.

De Lange, R.P.J., Van Minnen, J., 1998. Localization of the neuropeptide APGWamide in gastropod molluscs by *in situ* hybridization and immunocytochemistry. Gen. Comp. Endocrinol. 109, 166–174.

Fan, X., Croll, R.P., Wu, B., Fang, L., Shen, Q., Painter, S.D., Nagle, G.T., 1997. Molecular cloning of a cDNA encoding the neuropeptides APGWamide and cerebral peptide 1: localization of APGWamide-like immunoreactivity in the central nervous system and male reproductive organs of *Aplysia*. J. Comp. Neurol. 387, 53–62.

Filipe, L., Castro, C., Lima, D., Machadoa, A., Meloa, C., Hiromori, Y., Nishikawa, J., Nakanishi, T., Reis-Henriques, M.A., Santos, M.M., 2007. Imposex induction is mediated through the Retinoid X Receptor signalling pathway in the neogastropod *Nucella lapillus*. Aquat. Toxicol. 85, 57–66.

Geraerts, W.P., 1976. Control of growth by the neurosecretory hormone of the light green cells in the freshwater snail *Lymnaea stagnalis*. Gen. Comp. Endocrinol. 29, 61–71.

Henry, J., Zatylny, C., 2002. Identification and tissue mapping of APGWamide-related peptides in *Sepia officinalis* using LC-ESI-MS/MS. Peptides 6, 1031–1037.

Henry, J., Zatylny, C., Favrel, P., 2000. HPLC and electrospray ionization mass spectrometry as tools for the identification of APGWamide-related peptides in gastropod and bivalve mollusks. Brain Res. 862, 162–170.

Jing, J., Weiss, K.R., 2001. Neural mechanisms of motor program switching in *Aplysia*. J. Neurosci. 21, 7349–7362.

Koene, J.M., Jansen, R.F., Maat, A.T., Chase, R., 2000. A conserved location for the central nervous system control of mating behaviour in gastropod molluscs: evidence from a terrestrial snail. J. Exp. Biol. 203, 1071–1080.

Kuroki, Y., Kanda, T., Kubota, I., Fujisawa, Y., Ikeda, T., Miura, A., Minamitake, Y., Muneoka, Y., 1990. A molluscan neuropeptide related to the crustacean hormone RPCH. Biochem. Biophys. Res. Commun. 167, 273–279.

Li, G., Chase, R., 1995. Correlation of axon projections and peptide immunoreactivity in mesocerebral neurons of the snail *Helix aspersa*. J. Comp. Neurol. 353, 9–17.

Liu, G.J., Santos, D.E., Takeuchi, H., Kamatani, Y., Minakata, H., Nomoto, K., Kubota, I., Ikeda, T., Muneoka, Y., 1991. APGW-amide as an inhibitory neurotransmitter of *Achatina fulica* Ferussac. Biochem. Biophys. Res. Commun. 177, 27–33.

Lowry, O.I., Rosebrough, N.J., Farr, A.G., Rancealer, R.J., 1951. Protein measurement with the Folin phenol reagent. J. Biol. Chem. 193, 265.

McCrohan, C., Croll, R.P., 1997. Characterization of an identified cerebrobuccal neuron containing the neuropeptide APGWamide (Ala–Pro–Gly–Try–NH_2) in the snail *Lymnaea stagnalis*. Inv. Neurosci. 2, 273–282.

Morgan, P.T., Jing, J., Vilim, F.S., Weiss, K.R., 2002. Interneuronal and peptidergic control of motor pattern switching in *Aplysia*. J. Neurophysiol. 87, 49–61.

Oberdörster, E., McClellan-Green, P., 2002. Mechanisms of imposex induction in the mud snail, *Ilyanassa obsoleta*: TBT as a neurotoxin and aromatase inhibitor. Mar. Environ Res. 54 (3–5), 715–718.

Ohtania, M., Aimotoa, S., Muneokab, Y., 2000. Development of an antagonist of molluscan neuropeptide APGWamide with a peptide library. Peptides 21, 1193–1201.

Smith, S., Nason, J., Croll, R.P., 1997. Detection of APGWamide-like immunoreactivity in the sea scallop, *Placopecten magellanicus*. Neuropeptides 31, 155–165.

Tol-Steye, H., Lodder, J.C., Mansvelder, H.D., Planta, R.J., van Heerikhuizen, H., Kit, K., 1999. Role of G-protein $\beta\gamma$, arachidonic acid, and phosphorylation in convergent activation of an S-like potassium conductance by dopamine, Ala–Pro–Glu–Trp–NH_2 and Phe–Met–Arg–Phe–NH_2. J. Neurosci. 19, 3739–3751.

Wener, M.K., Morales, R.C., Brawer, R.J., 1997. The effect of estradiol-induced hypothalamic pathology on sulfated glycoprotein-2 (clusterin) expression in the hypothalamus. Brain Res. 745, 37–45.

Yu, B., Blankenship, J.E., 1997. Functional roles of neuropeptide APGWamide in penial complex and bag cells of *Aplysia*. Soc. Neurosci. Abstr. 23, 1238.

Zatylny, C., Gagnon, J., Boucaud-Camou, E., Henry, J., 2000. SepOvotropin: a new ovarian peptide regulating oocyte transport in *Sepia officinalis*. Biochem. Biophys. Res. Commun. 276 (3), 1013–1018.

Aquaculture Research

Aquaculture Research, 2008, 1–9 doi: 10.1111/j.1365-2109.2008.01982.x

Larval settlement of the tropical abalone, *Haliotis asinina* Linnaeus, using natural and artificial chemical inducers

Praphaporn Stewart[1], Nantawan Soonklang[2], Michael J Stewart[3], Chaitip Wanichanon[1], Peter J Hanna[4], Tanes Poomtong[5] & Prasert Sobhon[1]

[1]Department of Anatomy, Faculty of Science, Mahidol University, Bangkok, Thailand

[2]Department of Preclinical Science, Faculty of Medicine, Thammasat University, Pathumthani, Thailand

[3]School of Medicine, Deakin University, Geelong, Australia

[4]School of Life and Environmental Sciences, Deakin University, Geelong, Australia

[5]Department of Fisheries, Coastal Aquaculture Research and Development Center, Prachuabkirikun, Thailand

Correspondence: Prof. P Sobhon, Department of Anatomy, Faculty of Science, Mahidol University, Rama 6 Road, Bangkok 10400, Thailand. E-mail: scpso@mahidol.ac.th

Abstract

Many kinds of chemical and biological materials have been used as inducers of settlement of abalone larvae, as well as other species of marine gastropods, with responses being highly variable, even to the same chemical cue. The present study tested chemical inducers, γ-aminobutyric acid (GABA), δ-aminovaleric acid (5-AVA) and L-glutamic acid (GA) and the effects they have on larval settlement of *Haliotis asinina*. Additionally, a relatively inexpensive commercial substance, monosodium glutamate (MSG), was trialed. The datum provided shows all chemicals to be active inducers of settlement in this study, in order of effectiveness of 5-AVA, GABA, MSG to GA. Induction as adjudged from larval numbers settled was best at 6 h 62%, with 10^{-1} mM 5-AVA. At 24 h, induction was the highest at 78% when exposed to 10^{-2} mM 5-AVA. Larvae that were allowed to settle up to 72 h showed the highest numbers of settled larvae, and declined back to 60% when exposed to 10^{-2} 5-AVA and 10^{-1} mM GABA respectively. Monosodium glutamate, although third in settlement standings would bypass the other chemicals, with regard to cost versus yield. The assessment of settlement surface, rough or smooth proved to be irrelevant, which had no significant impact on larval settlement.

Keywords: *Haliotis asinina*, larval settlement, 5-AVA, GABA, L-glutamic acid, MSG

Introduction

Abalone cultivation in both wild and commercial aquaculture requires reliable production of large quantities of seeds. Although production is often compounded by disease, the numbers of larvae that complete settlement and metamorphose are important (Anguiano, Seary, Lizarraga & Marcial 1998; Huang, Liu & Lee 2001; Nicolas, Basuyaux, Mazurie & Thebault 2002). As such, attempts to improve settlement by researchers have yielded variable results, and the numbers of artificial cues known to influence the settlement of larvae are broad (Morse 1990; Roberts & Nicholson 1997; Roberts 2001).

Morse, Hooker, Duncan and Jensen (1979) first reported that 10^{-3} mM γ-aminobutyric acid (GABA) could significantly promote settlement and metamorphosis of larvae of *Haliotis rufescens*. Using larvae of *Haliotis iris*, Roberts and Nicholson (1997) showed that 10^{-3} mM GABA could induce 90–100% attachment and 20–60% metamorphosis within 2 days, and with *H. virginea* larvae, 65–100% settlement over the same time period. γ-aminobutyric acid in seawater stimulated attachment, and to a minor extent metamorphosis in *Haliotis diversicolor*, at 10^{-6}–10^{-7} mM (Bryan & Qian 1998). Larvae of *Haliotis asinina* exposed to GABA over 72 h showed settlement and metamorphosis, but the results varied according to the dose, with the optimal concentration being 0.45 μM (Gapasin & Polohan 2005). Overall, GABA

© 2008 The Authors
Journal Compilation © 2008 Blackwell Publishing Ltd

treatment has been found to induce successfully settlement of competent *Haliotis* larvae (Searcy-Bernal, Salas-Garza, Flores-Aguilar & Hinojosa-Rivera 1992; Moss 1999; Roberts 2001; Gapasin & Polohan 2005).

The settlement-inducing action of GABA has been shown to occur through the inhibition of veliger cilia movement (Morse Hooker, Duncan *et al.* 1979). γ-aminobutyric acid analogues, in particular, the isoforms of GABA, viz. γ-hydroxybutyric acid, γ-aminovaleric acid (5-AVA) and ε-aminocaproic acids, could stimulate synchronous settlement induction of planktonic larvae and metamorphosis into juveniles of several *Haliotis* spp. (Morse Hooker, Duncan *et al.* 1979; Morse, Hooker & Duncan 1980; Morse, Froyd & Morse 1984; Morse & Morse 1984a, b).

Recently, 5-AVA was isolated from the coralline alga *Hydrolithon samoense* (Suenaga, Hori, Ishida, Nukaya, Roberts & Tsuji 2004). In the examination of algal crusts, 5-AVA was found to be a naturally occurring compound in dry weight extracts (0.72 mg g^{-1}), whereas the presence for GABA could not be established. Using *H. rufescens* larvae, commercially available 5-AVA at 1 mM has produced a settlement efficacy similar to GABA, and attachment without metamorphosis, in *H. virginea* at the same concentration (Suenaga *et al.* 2004).

Other compounds have also been used to induce settlement of Haliotid larvae. For example, KCl at 10, 20 and 30 mM has also stimulated attachment behaviour in *H. diversicolor* (Bryan & Qian 1998). However, GABA has generally promoted better attachment, metamorphic responses and survival than KCl (Gapasin & Polohan 2004).

L-glutamic acid and L-aspartic acid have induced *Haliotis discus hannai* larvae to settle on substrates with benthic diatoms present at 82 ± 6.9% and 78.7 ± 5.1%, respectively, after 24 h (Kang, Kim, Kim & Kim 2003). However, without benthic diatoms present, settlement induction was significantly reduced with 33.3 ± 8.8% for GA and 16.7 ± 3.3 for L-aspartic acid (Kang *et al.* 2003).

Another cue also known to be effective in settlement induction of *Haliotis* spp. is mucus (Seki & Kan-no 1981; Takahashi & Koganezawa 1988; Yang & Wu 1995; Gallardo & Buen 2003). The role of mucus in the induction of settlement has been investigated recently in *H. asinina* (Laimek, Clark, Stewart, Pfeffer, Wanichanon, Hanna & Sobhon 2008), where the presence of GABA in mucus was determined and effective in inducing larval settlement, provided GABA was present in sufficient quantities.

In Thailand, the main cultivated species for commercial purpose is the tropical abalone *H. asinina*, commonly called donkey's ear abalone. It is considered to be suitable for artificial propagation in view of its relatively large size and high proportion of edible foot muscle (Singhagraiwan & Sasaki 1991). In order to increase *H. asinina* stocks and yields, research output in this species has grown extensively. One limiting factor, however, has been lack of knowledge on the settlement of this species. In this paper, we have focused on the effects of chemical inducers GABA, 5-AVA and GA, and have also explored the potential usefulness of monosodium glutamate (MSG) as a cheap alternative for settlement induction of this species. Monosodium glutamate has not been used in any previous settlement assay, but because its chemical properties are analogous to GA, its potential for settlement induction was investigated. Positive outcomes of the tests could provide better strategies to be implemented in settlement, and thereby aid in developing a sustainable aquaculture for *H. asinina* and other abalone species.

Materials and methods

Larval culture

Larvae of *H. asinina* were obtained from the Coastal Aquaculture Research and Development Center, Department of Fisheries, Klongwan, Prachaubkirikhun Province, Thailand. Sperm and eggs were obtained from a mixed mass spawning for a period of 20 min, and the eggs were washed to remove excess sperm. The fertilized eggs were transferred and allowed to develop to the late veliger stage in round plastic tanks housed in the shade, with circulated sand-filtered seawater and continuous aeration. The level of salinity used was 2.5–3.2 × 10^{-4} g L^{-1}, and the temperature was maintained between 25 and 26 °C (Singhagraiwan & Doi 1993). When competent to settle, late veligers that were suspended at the top of the water surface began displaying creeping and alternative suspending behaviour at 26 h. The proportion of these veliger that made the transition to creeping stage larvae were approximately 80%, as observed by the naked eye, and were used in bioassays.

Preparation of test chemicals

Before the assay, solutions of δ-aminovaleric acid (5-AVA), GABA, GA (Sigma, St Louise, MO, USA) and

© 2008 The Authors

MSG (Ayinomoto, Bangkok, Thailand) were freshly prepared as stock solutions and then 5-AVA, GABA and GA were assayed at concentrations of 10^{-1}, 10^{-2} and 10^{-3} mM. Monosodium glutamate was used at 5, 10, 15, 20 and 25 mM. Each solution was prepared using 0.45 μm filtered ultraviolet irradiated (500 mW h^{-1}) natural seawater, with salinity between 2.5 and 3.2 × 10^{-4} g L^{-1}.

Settlement bioassays

Assays were conducted in plastic containers with 1200 mL of filtered, ultraviolet-treated seawater, containing streptomycin and neomycin (Sigma) at concentrations of 0.0075 g L^{-1}. All cultures were maintained at 25–26 °C (approximate ambient water temperature), and under diffuse light. Competent veligers were used at a designated density of 600 $tank^{-1}$.

Assays were designed to test two kinds of conditioned plastic sheets (i.e. rough by crumpling the sheet or smooth) and three types of methods for treatment. Three separate assays were performed: (1) transparent plastic sheets, made of the same material, 10 × 15 cm in size, pre-coated with *Nitzschia* spp. for 5 days ($n = 3$ replicates $condition^{-1}$ $tank^{-1}$), were immersed in chemical solutions (5-AVA, GABA, GA) at concentrations of 10^{-1}, 10^{-2} and 10^{-3} mM, and MSG at 5, 10, 15, 20 and 25 mM, for 1 h, before being placed in tanks with filtered seawater, followed by 600 competent veligers; (2) 600 veligers were pre-immersed for 1 h in filtered seawater containing the chemical solutions at the same concentrations, after which the veligers were transferred, using an 80 μm sieve, into tanks that contained plastic sheets and filtered seawater; and (3) both the 600 veligers and the plastic sheets were exposed continuously in tanks with filtered seawater containing the chemical solutions at the concentrations as described in assay 1.

Data analysis

The numbers of larval settled on each plastic sheet were counted at 6, 24 and 72 h after the commencement of the experiment. Three replicates were performed. Data were expressed as a percentage of larval settlement. Statistical analyses were performed using statistical software SPSS 11.5 (SIGMASTAT, SPSS). One-way ANOVA with *post-hoc* Tukey's HSD tests were used to compare variance among the solutions, types of plastic sheets and experimental treatments. The results were considered to be significantly different at $P < 0.05$.

Results

The types of substrates (smooth or rough plastic sheets) had no influence on larval settlement numbers at each sampling time ($P > 0.05$). However, larvae preferred to settle on smooth sheets rather than on rough sheets, with an approximately 5–10% difference in assays with GA solution ($P < 0.05$). The exposure times of both larvae and plastic sheet were not related to the settlement of larvae.

In order of effectiveness, 5-AVA (greatest), GABA, MSG and GA (least) were identified as active inducers of settlement ($P < 0.05$). Details of the chemical assays are described below.

Effects of GABA concentration, type of plastic sheet and different modes of exposure to GABA on larval settlement

The values of the percentage settlement of *H. asinina* obtained under the different chemical treatments after 6, 24 and 72 h are shown in Figs 1–3 respectively.

Overall, GABA induced larval settlement with over 35% on plastic sheets at 6 h after commencement (Fig. 1) and around 45% after 24 h (Fig. 2). However, the numbers decreased to 43% at 72 h (Fig. 3). At a concentration of 10^{-1} mM, GABA induced 40–45% of larvae to settle at 6 h in experiments 1 and 2 (Fig. 1a–d). But the highest induction at 59% was observed with 10^{-3} mM GABA ($P < 0.05$) on the rough sheet on continuously exposing both larvae and the plastic sheet to GABA solution (Fig. 1e). Settlement increased at 24 h, and reached 65% when larvae were pre-exposed to 10^{-1} mM GABA for 1 h ($P < 0.05$; Fig. 2b) and 63% with continuous exposure of both the animal and the substrate in 10^{-3} mM GABA (Fig. 2e). However, these concentrations appeared to be possibly toxic as the numbers decreased when exposed to GABA for 72 h (Fig. 3).

Effects of 5-AVA concentration, type of plastic sheet and different modes of exposure to 5-AVA on larval settlement

Overall exposure of larvae to 5-AVA at 6 h after the commencement of the experiment demonstrated

© 2008 The Authors
Journal Compilation © 2008 Blackwell Publishing Ltd,

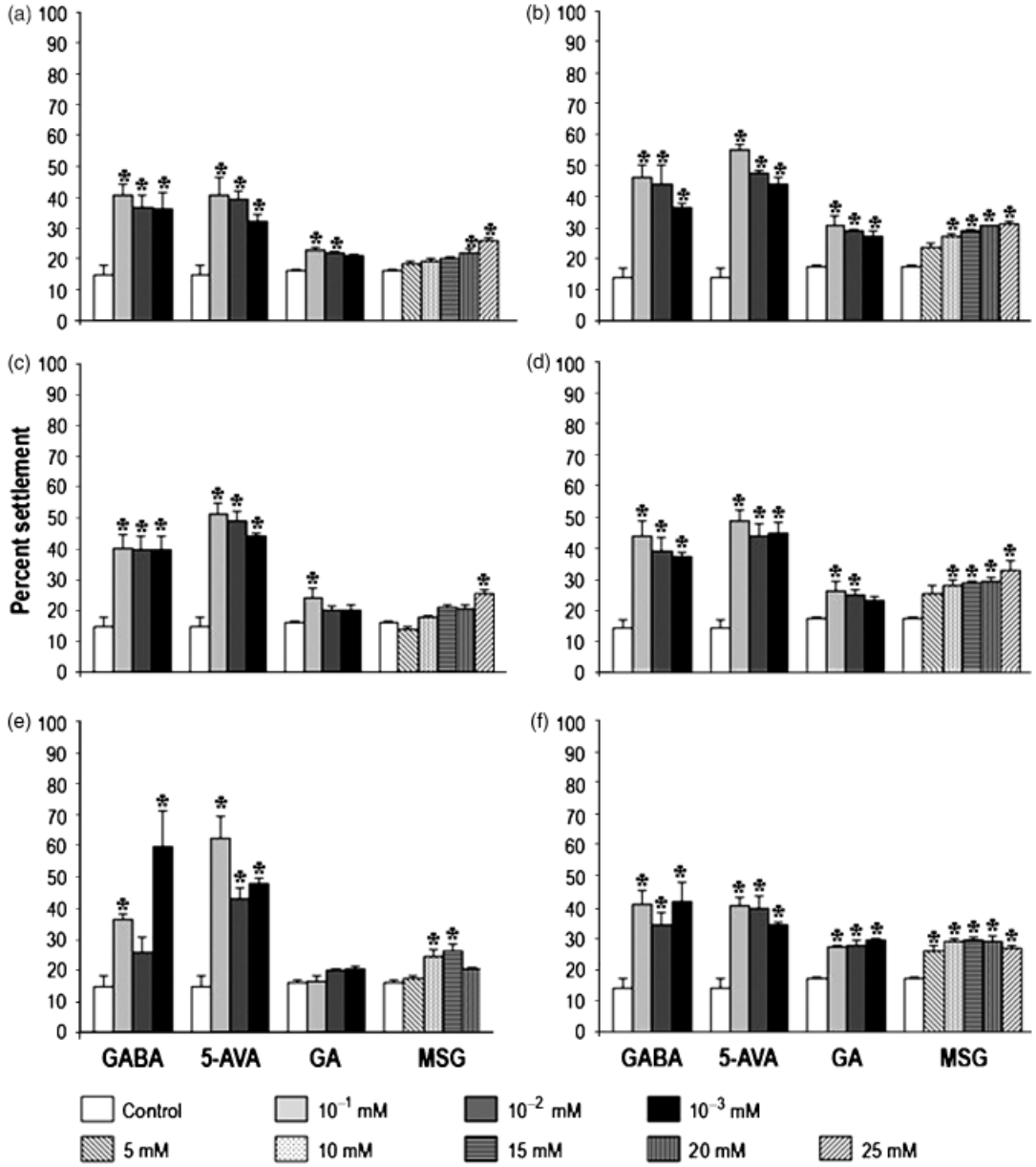


Figure 1 Effect of different chemicals, GABA, 5-AVA, GA and MSG, when compared with seawater (Control) on the settlement of *H. asinina* larvae at 6 h, using two types of substrates, i.e. rough plastic sheets (a, c, e) and smooth plastic sheets (b, d, f). Three experiments of chemical exposure were compared: either plastic sheets (a, b) or larvae (c, d) were pre-exposed for 1 h in a chemical solution or both were continuously exposed (e, f). All points represent the mean ± SEM. of triplicate determinations for each concentration. Asterisks indicate significant differences (*$P < 0.05$) from controls. GABA, γ-aminobutyric acid; 5-AVA, δ-aminovaleric acid; GA, L-glutamic acid; MSG, monosodium glutamate.

settlement of over 30% (Fig. 1). Settlement at 24 h increased to 55% (Fig. 2), but then decreased to 40% after 72 h (Fig. 3). Maximum numbers of larvae were induced to settle on rough sheets after continuous exposure for 6 h in 10^{-1} mM 5-AVA ($P < 0.05$; Fig. 1e). After 24 h, 10^{-2} mM 5-AVA induced the highest larval settlement, at 78%, on smooth sheets when the larvae were pre-exposed in 5-AVA solution for 1 h ($P < 0.05$; Fig. 2d). However, approximately 60% of larvae were settled on the smooth sheet, using the same exposure method with 10^{-2} mM 5-AVA at 72 h ($P < 0.05$; Fig. 3d).

© 2008 The Authors

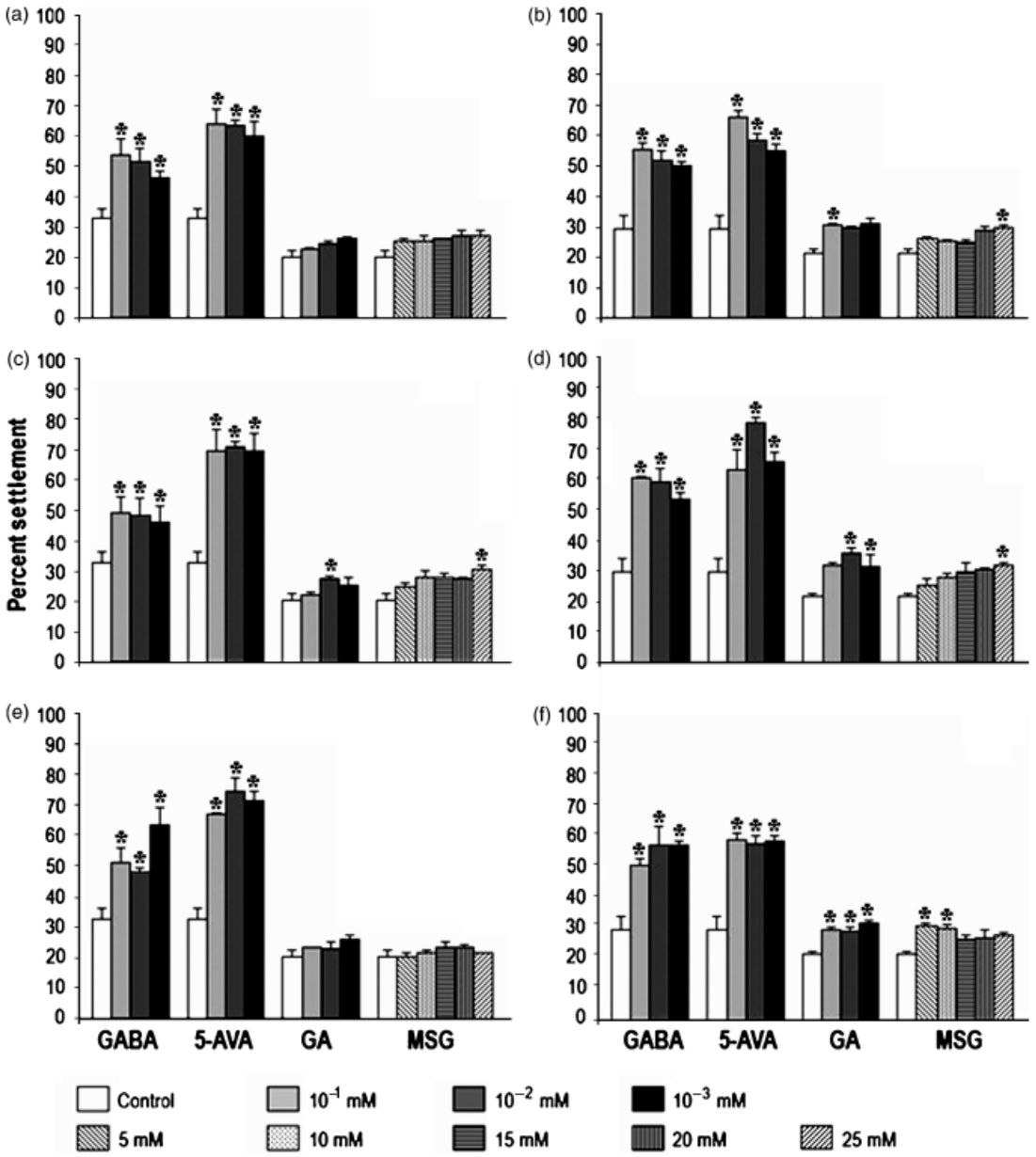


Figure 2 Effect of different chemical solutions, GABA, 5-AVA, GA and MSG, when compared with seawater (Control) on the settlement of *H. asinina* larvae at 24 h, using two types of substrates, i.e. rough plastic sheets (a, c, e) and smooth plastic sheets (b, d, f). Three experiments of chemical exposure were compared: either plastic sheets (a, b) or larvae (c, d) were pre-exposed for 1 h in a chemical solution or both were continuously exposed (e, f). All points represent the mean ± SEM of triplicate determinations for each concentration. Asterisks indicate significant differences ($^{*}P < 0.05$) from controls. GABA, γ-aminobutyric acid; 5-AVA, δ-aminovaleric acid; GA, L-glutamic acid; MSG, monosodium glutamate.

Similar percentages were obtained when both the plastic sheet and the larvae were continuously exposed to 10^{-2} mM 5-AVA (Fig. 3e). Therefore, doses of 10^{-1} and 10^{-2} mM 5-AVA induced higher percentages of settlement ($P < 0.05$) than the other doses.

Effects of GA concentration, type of plastic sheet and different modes of exposure to GA on larval settlement

Settlement of larvae was over 15% on plastic sheets at 6 h (Fig. 1), over 20% after 24 h (Fig. 2) and had

© 2008 The Authors
Journal Compilation © 2008 Blackwell Publishing Ltd,

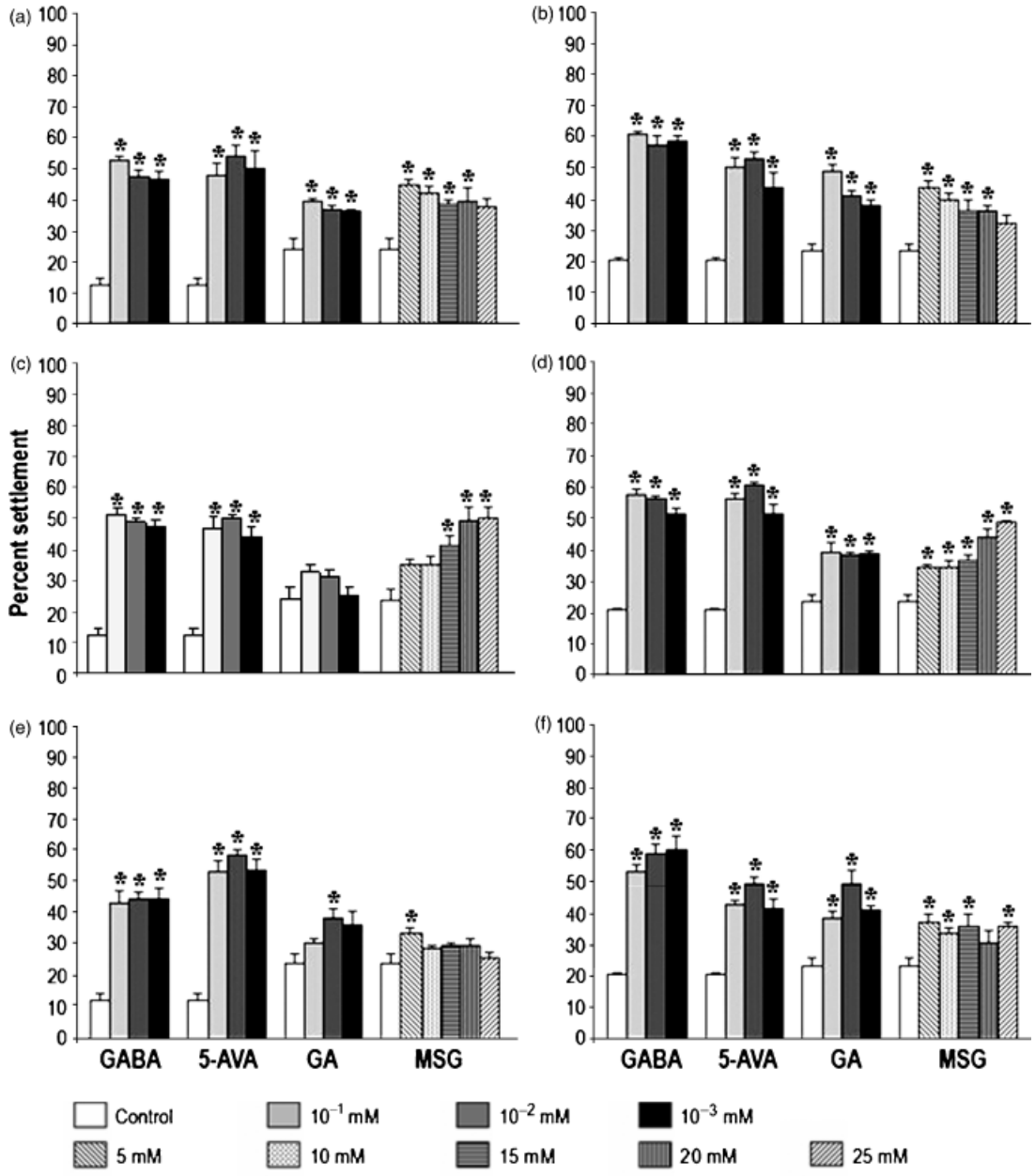


Figure 3 Effect of different chemical solutions, GABA, 5-AVA, GA and MSG, when compared with seawater (Control) on the settlement of *H. asinina* larvae at 72 h, using two types of substrates, i.e. rough plastic sheets (a, c, e) and smooth plastic sheets (b, d, f). Three experiments of chemical exposure were compared: either plastic sheets (a, b) or larvae (c, d) were pre-exposed for 1 h in a chemical solution or both were continuously exposed (e, f). All points represent the mean ± SEM of triplicate determinations for each concentration. Asterisks indicate significant differences ($^*P < 0.05$) from controls. GABA, γ-aminobutyric acid; 5-AVA, δ-aminovaleric acid; GA, L-glutamic acid; MSG, monosodium glutamate.

increased to 25% at 72 h (Fig. 3). At a concentration of 10^{-1} mM, GA induced significantly higher settlement behaviour at 6 h than at the other concentrations tested ($P < 0.05$) on both rough and smooth sheets. This was different when compared with exposure of larvae and plastic sheets in GA solution for 1 h (Fig. 1a–d), where higher responses occurred at a concentration of 10^{-3} mM ($P < 0.05$). At 24 h, more larvae settled on plastic sheets than at 6 h. An increase in the settlement percentage was also observed using

© 2008 The Authors

10^{-1} mM GA at 72 h ($P < 0.05$). Approximately 38–48% of the larvae were induced to settle on rough and smooth sheets when both larvae and plastic sheets were continuously exposed to 10^{-3} mM GA ($P < 0.05$).

Effects of MSG concentration with type of plastic sheet and different modes of exposure to MSG on larval settlement

Exposure to MSG resulted in settlements of over 12% for all treatment methods at 6 h. However, the settlement percentage at 24 h had increased to 20% (Fig. 2) and increased to 30% after 72 h (Fig. 3). Concentrations of 15 and 25 mM MSG significantly induced larvae to settle (30%) on both types of plastic sheets by 6 h with continuous exposure, and 33% at 6 h when exposing either larvae or the plastic sheet only for 1 h in MSG solution ($P < 0.05$; Fig. 1). The numbers settled remained about 30% for the same treatment at 24 h ($P < 0.05$; Fig. 2) and increased to 37–44% with continuous exposure to MSG for 1 h at a 5 mM concentration after 72 h ($P < 0.05$; Fig. 3a, b, e and f). Settlement increased up to 50% after larvae were immersed in 25 mM for 1 h, and then allowed to settle in seawater for 72 h (Fig. 3c and d).

Discussion

Most pelagic marine invertebrate larvae must pass through a period of settlement, thereby becoming benthic and then growing into adults. During the lifespan, this settlement stage is the bottle neck to reproductive capacity due to high mortality (Roberts 2001). In abalone aquaculture, this can be an obstacle in obtaining high production.

Settlement behaviour in larvae of *H. asinina* has been recorded previously (Singhagraiwan & Doi 1993). They found that at 26 h post fertilization competent larvae of *H. asinina* begin to swim downward and towards the substratum, periodically attaching their foot to the substratum, before settling and crawling.

In the present study, we have shown that competent larvae (26 h post fertilization) of *H. asinina* could be induced to settle, when exposed to 5-AVA, GABA, MSG or GA. Our data confirm earlier reports of the ability of the classic settlement inducer, GABA, to be effective in *H. asinina* larval settlement. γ-aminobutyric acid has previously been found to be effective in settlement in other abalone species, viz. *H. rufescens* (Morse Hooker, Duncan *et al.* 1979; Searcy-Bernal *et al.* 1992), *H. discus hannai* (Yang & Wu 1995), *H. iris* and *H. virginea* (Roberts & Nicholson 1997), *H. diversicolor* (Bryan & Qian 1998), *H. asinina* (Gapasin & Polohan 2004), as well as other marine species such as the mussel *Mytilus edulis* (Dobretsov & Qian 2003), *M. galloprovincialis*, the clam, *Venerupis pullastra*, the oyster, *Ostrea edulis* (Gacía-Lavandeira, Silva, Abad, Pazos, Sánchez & Parallé 2005), and the black chiton, *Katharina tunicata* (Rumrill & Cameron 1983). In our study, we found that GABA induced the best settlement of larvae at a concentration of 10^{-3} mM, which agrees with the report on *H. rufescens* (Morse 1992). It has also been shown that GABA can be ineffective at very low concentrations, while high doses can cause abnormal development (Searcy-Bernal & Anguiano-Beltran 1998), toxicity (as our results have indicated) or death of postlarvae (Morse, Hooker, Jensen & Duncan 1979). Akashige, Seki, Kan-no and Nomura (1981) reported that when *H. discus hannai* larvae were overexposed to GABA, velum ciliation movement was suspended, and after a temporary falling off, rotation occurred and they proceeded to die. We found that GABA at a temporary high concentration, such as 10^{-1} mM, was effective for inducing settlement, but not so if the larvae were exposed constantly to GABA. In contrast, when larvae were immersed in 10^{-3} mM (a lower dose) GABA or continuously exposed over 72 h, settlement numbers were good.

Previously reported differences in the efficacy of different chemicals in inducing settlement indicated that settlement may be due to a number of factors, including species differences, age and the differences in the methodologies used (Searcy-Bernal *et al.* 1992; Gapasin & Polohan 2004). This also extends to qualitative genetic differences as well, among batches of cultures of the same species, resulting in varying degrees of larval competence and responsiveness to chemical inducers. For example, in a previous study, 0.45–0.50 μM GABA elicited the best settlement (38–52%) and metamorphosis (42–55%) response in *H. asinina* after 72 h post commencement (Gapasin & Polohan 2004). However, we found that at 72 h, 10^{-3} mM GABA induced larvae to settle at 58%, and up to 60% at 10^{-1} mM in all the experimental methods used.

Neurotransmitter-related amino acid-derived compounds have proved effective for the reliable induction of settlement in a number of other economically valuable molluscan species. However, levels of settlement induction by GABA were significantly

© 2008 The Authors
Journal Compilation © 2008 Blackwell Publishing Ltd,

lower than those for 5-AVA, at a concentration of 10^{-3} mM. Previously, 5-AVA was shown to stimulate larval attachment in *H. rufescens* at 1 mM (Morse Hooker, Duncan *et al.* 1979), and attachment without metamorphosis in *H. virginea* at 1 mM. Commercially available 5-AVA at 10^{-3} mM has been shown to induce 43% of *H. discus discus* and *H. discus hannai* larvae to metamorphosis at 43%. Subsequently, 5-AVA has been isolated from the alga *H. samoense* (Suenaga *et al.* 2004), but not tested for settlement potential. We have found 5-AVA to be better than GABA. Previously, Kaspar and Mountfort (1995) demonstrated that GABA receptors have an absolute need for the primary carboxyl group, with minor substitutions at the γ position, but with no major deviation in chain length. Hence, compounds with GABA-like settlement-inducing properties are dependent on receptor requirements. Therefore, we hypothesize that GABA and 5-AVA may have induced more settlement numbers due to a structural feature of a selective external receptor or a receptor within ciliated larvae, as GABA seems to be a true inducer and 5-AVA as well, as it is structurally analogous (Morse Hooker, Duncan *et al.* 1979).

L-glutamic acid, the precursor of GABA, was also used in our study and was effective in inducing larval settlement. Although Morse *et al.* (1979) reported that GA induced *H. rufescens* to settle in low numbers (12%), later investigations showed that this chemical was a potent larval settlement inducer and induced 33% larvae of *H. discus hannai* to settle after 24 h (Kang *et al.* 2003). When GA was used in conjunction with benthic diatoms, the numbers of settled larvae increased to 82% (Kang *et al.* 2003). Our data are consistent with their results regarding GA ability to induce settlement in *H. asinina*. We also tested another form of glutamate, MSG, which is inexpensive when compared with the other three chemicals. MSG showed settlement-inducing responses similar to L-glutamate, but a much higher dose is required, where MSG at 25 mM was effective (50%) in settling larva. Moreover, MSG appeared to be the least toxic. Due to its easy availability in local markets, including efficiency, when compared with expenditure (\$US 2.6 kg^{-1}) for the other chemicals, GABA (\$US 654), 5-AVA (\$US 9880) and GA (\$US 158) (prices sourced from Sigma-Aldrich and local markets 2006), therefore, it may be of more practical use for lower-funded facilities and farmers. Publication of the results of this study provides much-needed information for aquaculture of abalone, which are important economically. The yield of larvae in abalone farms could be increased by using any one of these inducers, especially MSG, which is a cheap alternative to the other expensive chemical inducers.

Acknowledgments

We thank the Thailand Research Fund (Senior Research Scholar Fellowship to Prof. Prasert Sobhon) and the Commission on Higher Education Thailand (PhD scholarship to Praphaporn Stewart) and Mahidol University for research support.

References

Akashige S., Seki T., Kan-no H. & Nomura T. (1981) Effects of γ-aminobutyric acid and certain neurotransmitters on the settlement and the metamorphosis of the larvae of *Haliotis discus hannai* Ino (Gastropoda). *Bulletin Tohoku Regional Fisheries Research Laboratory* **43**, 37–45.

Anguiano B.C., Seary B.R., Lizarraga P. & Marcial L. (1998) Pathogenic effects of *Vibrio alginolyctus* on larvae and postlarvae of the red abalone *Haliotis rufescens*. *Diseases of Aquatic Organism* **33**, 119–122.

Bryan P.J. & Qian P. (1998) Induction of larval attachment and metamorphosis in the abalone *Haliotis diversicolor* (Reeve). *Journal of Experimental Marine Biology and Ecology* **223**, 39–51.

Dobretsov S.V. & Qian P. (2003) Pharmacological induction of larval settlement and metamorphosis in the blue mussel *Mytilus edulis* L. *Biofouling* **19**, 57–63.

Gacía-Lavandeira M., Silva A., Abad M., Pazos A.J., Sánchez J.L. & Parallé L. (2005) Effects of GABA and epinephrine on the settlement and metamorphosis of the larvae of four species of bivalve molluscs. *Journal of Experimental Marine Biology and Ecology* **316**, 149–156.

Gallardo W.G. & Buen S.M.A. (2003) Evaluation of mucus, *Navicula,* and mixed diatoms as larval settlement inducers for the tropical abalone *Haliotis asinina*. *Aquaculture* **221**, 357–364.

Gapasin R.S.J. & Polohan B.B. (2004) Induction of larval settlement and metamorphosis in the donkey-ear abalone, *Haliotis asinina* Linnaeus, by chemical cues. *Hydrobiologia* **519**, 9–17.

Gapasin R.S.J. & Polohan B.B. (2005) Response of the tropical abalone, *Haliotis asinina*, larvae on combinations of attachment cues. *Hydrobiologia* **548**, 301–306.

Huang C., Liu P. & Lee K. (2001) Withering syndrome of the small abalone, *Haliotis diversicolor supertexta*, is caused by *Vibrio parahaemolyticus* and associated with thermal induction. *Zeitschrift Fur Naturforschuny C – A Journal of Bioscience* **56**, 898–901.

Kang K.H., Kim B., Kim J.M. & Kim Y.H. (2003) Effects of amino acids on larval settlement and metamorphosis in

© 2008 The Authors

Haliotis discus hannai. *Korean Journal of Malacology* **19**, 95–106.

Kaspar H.F. & Mountfort D.O. (1995) Microbial production and degradation of γ-aminobutyric acid (GABA) in the abalone larval settlement habitat. *FEMS Microbiology Ecology* **17**, 205–212.

Laimek P., Clark S., Stewart M., Pfeffer F., Wanichanon C., Hanna P. & Sobhon P. (2008) The presence of GABA in gastropod mucus and its role in inducing larval settlement. *Journal of Experimental Marine Biology and Ecology* **354**, 182–191.

Morse D.E., Hooker N., Duncan H. & Jensen L. (1979) γ-aminobutyric acid, a neurotransmitter, induces planktonic abalone larvae to settle and begin metamorphosis. *Science* **204**, 407–410.

Morse D.E., Hooker N., Jensen L. & Duncan H. (1979) Induction of larval settling and metamorphosis by γ-aminobutyric acid and its congeners from crustose red algae. II. Applications to cultivation, seed-production and bioassays; principle causes of mortality and interference. *Proceedings World Marine Society* **10**, 81–91.

Morse D.E., Hooker N. & Duncan H. (1980) GABA induces metamorphosis in *Haliotis*, V: stereochemical specificity. *Brain Research Bulletin* **5**, 381–387.

Morse A.N.C. & Morse D.E. (1984a) GABA-mimetic molecules from *Porphyra* (Rhodophyte) induce metamorphosis of *Haliotis* (Gastropoda) larvae. *Hydrobiologia* **116**, 155–158.

Morse A.N.C. & Morse D.E. (1984b) Recruitment and metamorphosis of *Haliotis* larvae induced by molecules uniquely available at the surfaces of crustose red algae. *Journal of Experimental Marine Biology and Ecology* **75**, 191–215.

Morse A.N.C., Froyd C.A. & Morse D.E. (1984) Molecules from cyanobacteria and red algae that induce larval settlement and metamorphosis in the mollusc *Haliotis rufescens*. *Marine Biology* **81**, 293–298.

Morse D.E. (1990) Recent progress in larval settlement and metamorphosis: closing the gap between molecular biology and ecology. *Bulletin Marine Science* **46**, 465–483.

Morse D.E. (1992) Molecular mechanisms controlling metamorphosis and recruitment in abalone larvae. In: *Abalone of the World. Biology, Fisheries and Culture, Fishing* (ed. by S.A. Shepherd, M. Tegner & S.A. Guzman), pp. 107–119. News Books, Oxford, USA.

Moss G.A. (1999) Factors affecting settlement and early post-settlement survival of the New Zealand abalone *Haliotis australis*. *New Zealand Journal of Marine and Freshwater Research* **33**, 271–278.

Nicolas J.L., Basuyaux O., Mazurie J. & Thebault A. (2002) *Vibrio carchariae*, a pathogen of the abalone *Haliotis tuberculata*. *Diseases of Aquatic organisms* **50**, 35–43.

Roberts R. (2001) A review of settlement cues for larval abalone (*Haliotis* spp.). *Journal of Shellfish Research* **20**, 571–586.

Roberts R.D. & Nicholson C.M. (1997) Variable response from abalone larvae (*Haliotis iris*, *H. virginea*) to a range of settlement cues. *Molluscan Research* **18**, 131–141.

Rumrill S.S. & Cameron R.A. (1983) Effects of gamma-aminobutyric acid on the settlement of larvae of the black chiton *Katharina tunicata*. *Marine Biology* **72**, 243–247.

Searcy-Bernal R. & Anguiano-Beltran C. (1998) Optimizing the concentration of gamma-aminobutyric acid (GABA) for inducing larval metamorphosis in red abalone, *Haliotis rufescens* (Mollusca: Gastropod). *Journal of World Aquaculture Society* **29**, 463–470.

Searcy-Bernal R., Salas-Garza A.E., Flores-Aguilar R.A. & Hinojosa-Rivera P.R (1992) Simultaneous comparison of methods for settlement and metamorphosis induction in the red abalone (*Haliotis rufescens*). *Aquaculture* **105**, 241–250.

Seki T. & Kan-no H. (1981) Induced settlement of the Japanese abalone *Haliotis discus hannai*, veliger by the mucous trails of the juvenile and adult abalones. *Bulletin Tohoku. Regional Fishery Research Laboratory* **43**, 29–36.

Singhagraiwan T. & Sasaki M. (1991) Breeding and early development of the donkey's ear abalone, *Haliotis asinina* Linne. *Thailand Marine Fisheries Research Bulletin* **2**, 83–94.

Singhagraiwan T. & Doi M. (1993) *Seed Production and Culture of a Tropical Abalone, Haliotis asinine Linné*, 1st edn. EMDEC, Rayong, Thailand.

Suenaga K., Hori H., Ishida H., Nukaya H., Roberts R.D. & Tsuji K. (2004) Inducing substance for abalone larval metamorphosis from the crustose coralline alga *Hydrolithon samoense*. *Fisheries Science* **70**, 342–344.

Takahashi K. & Koganezawa A. (1988) Mass culture of *Ulvella lens* as a feed for abalone *Haliotis discus hannai*. *NOAA Technical Report NMFS* **70**, 29–36.

Yang Y. & Wu B. (1995) Induction of larval settlement and metamorphosis of *Haliotis discus hannai* Ino (Gastropoda, Mollusca). *Chinese Journal of Oceanology and Limnology* **13**, 71–77.

© 2008 The Authors
Journal Compilation © 2008 Blackwell Publishing Ltd,

Mar Biotechnol (2008) 10:593–601
DOI 10.1007/s10126-008-9097-6

ORIGINAL ARTICLE

Morphological and Biochemical Alterations of Abalone Testicular Germ Cells and Spawned Sperm and their Fertilizing Ability

Worawit Suphamungmee · Wattana Weerachatyanukul · Tanes Poomtong · Peter Hanna · Prasert Sobhon

Received: 17 July 2007 / Accepted: 15 March 2008 / Published online: 1 May 2008
© Springer Science + Business Media, LLC 2008

Abstract In this study, we aimed to detect morphological and biochemical changes in developing germ cells (Gc), testicular sperm (Tsp), and spawned sperm (Ssp) using capacitation-associated characteristics. Gradual changes in the profiles of two membrane proteins, namely NaCl- and detergent-extractable proteins, were observed as compared Gc with Tsp and Tsp with Ssp. These membrane modifications were accomplished mostly through the introduction of new protein sets, both peripheral and integral, into Tsp and Ssp membranes. Activation of serine proteases, particularly in Ssp detergent-extracted proteins with the molecular masses of 38–130 kDa was evident and marked a major difference between Ssp and Tsp. An increase in the level of tyrosine phosphorylation of the proteins ranging from 15 to 20 kDa was noted in Tsp and remained constant in Ssp. Specifically, these three capacitation-associated characteristics could be detected in Ssp, possessing full fertilizing capacity. The lack of an activated proteolytic activity in Tsp resulted in a delayed fertilization, but not affected fertilizing ability. We believe that these characteristics should be advantageous in predicting abalone sperm fertilizing capability, particularly in cases when isolated germ cells or purified Tsp are used in place of spawned sperm in abalone aquaculture.

W. Suphamungmee · W. Weerachatyanukul (✉) · P. Hanna · P. Sobhon
Department of Anatomy, Faculty of Science, Mahidol University, Rama 6 Road,
Bangkok 10400, Thailand
e-mail: scwwy@mahidol.ac.th

T. Poomtong
The Coastal Aquaculture Research and Development Center, Department of Fisheries, Klongwan,
Prachuabkirikhun 77000, Thailand

Keywords Abalone · Sperm · Capacitation · Phosphorylation · Acrosomal enzymes

Introduction

In marine invertebrates, sperm readily possess fertilizing capability upon their release into seawater to fertilize eggs externally in natural habitats. Success of gamete interaction appears to be limited by a rapid dispersion of the released gametes upon spawning (Giese and Kanatani 1987; Levitan et al. 1991). Therefore, synchronization or "broadcast" release of the gametes significantly enhances a chance of contact between sperm and eggs (Dusenbury 2000). In addition, factors such as period of time over which the gametes are released, the number of gamete released, and the proper ratio between sperm and eggs determine the success of fertilization (Yund 2000; Meidel and Yund 2001). In abalones, the low yield of fertilization rate encountered in their aquaculture is frequently due to the non-simultaneous spawning of male and female animals (Encena II et al. 1998; Grubert et al. 2005). Therefore in practice, testicular cell isolates are sometimes used in place of spawned sperm to fertilize the freshly spawned eggs, which results in some degree of success but also with highly variable outcomes. This inconsistency may be partly due to the variable amount of mature testicular sperm and contamination from testicular extracts.

Many molecular events required for enhancing sperm fertilizing capability are associated with the process known as "sperm capacitation" (Bedford 1983; Yanagimachi 1994). Although extensive accounts on sperm capacitation have been mostly reported in mammals, the evidence of capacitation-like process in some crustaceans, such as

shrimp (*Sicyonia ingentis* and *Penaeus monodon*) and crabs (*Pseudocarcinus gigas*), has also been reported (Lindsay and Clark 1992; Gardner and Williams 2002; Alfaro et al. 2003; Vanichviriyakit et al. 2004). Most biochemical alterations during capacitation take place at sperm plasma membranes which involve extensive modifications of sperm membranes through the adsorption of proteins from the fluid environment where sperm reside or the removal of preexisting membrane proteins (Yanagimachi 1994; Vanichviriyakit et al. 2004). In addition, a pronounced increase in the level of protein tyrosine phosphorylation closely associated with sperm capacitation has been extensively evident in mammals (Visconti and Kopf 1998; Naz and Rajesh 2004) and to some extent in invertebrates (Vanichviriyakit et al. 2004). Additionally, it has also been reported in penaeoid shrimp that sperm serine proteases, in particular trypsin-like enzymes, known to be crucial for acrosome reaction (Rios and Barros 1997; Griffin and Clark 1990), are activated upon transfer of spermatophoric sperm into female storing sac (thelycum), the site where sperm of the closed-thelycal shrimp acquire their fertilizing ability (Lindsay and Clark 1992; our unpublished results). In this study, we monitored the distinctive morphological and biochemical changes that occurred in developing germ cells, testicular sperm, and spawned sperm using capacitation-associated characteristics which may be used to predict sperm fertilizing ability, thus enhancing the successful fertilization rates in abalone aquaculture.

Materials and Methods

Preparations of Germ Cells and Sperm

Sexually mature males (>24 months old with 250–280 g in body weight) were maintained in concrete tanks at the Coastal Aquaculture Research and Development Center, Prachuabkirikhun province, Thailand. To collect testicular germ cells, fully mature testes with a creamy yellowish appearance were carefully dissected free from hepatopancreas in filtered seawater (FSW). The tissues were washed extensively with FSW, minced into small pieces, and subjected to gentle agitation (room temperature, 30 min) to release testicular germ cells. The cell suspension was centrifuged (600×*g*, 4°C, 10 min), and the pellet was resuspended in FSW. Separation of testicular sperm from other germ cells was performed by a discontinuous Percoll gradient centrifugation. Briefly, 2 ml of testicular cell suspension was layered on top of an 8-ml Percoll gradient (20–80%) in FSW and centrifuged (1,000×*g*, 4°C, 30 min). Two population of cells, one sedimented at the interphase between 40% and 60% Percoll (composed mainly developing germ cells—Gc) and the other pelleted at the bottom of the tubes (enriched in testicular sperm—Tsp, see "Results"), were carefully collected and processed for a Hoechst 33258 nuclear staining according to the manufacturer's protocol (Molecular Probes, Eugene, OR, USA). Cell identification and counting were performed under light and fluorescence microscopes. For physiological tests, the isolated cells were washed (600×*g*, 4°C, 5 min) with FSW, and the pellet was resuspended with FSW to a final concentration of 10^7 sperm/ml. Spawned sperm were freshly collected from seawater surrounding the male broodstocks during spawning (referred to as "Ssp"). They were washed and resuspended as mentioned above and immediately used in the following experiments.

Scanning and Transmission Electron Microscopy

Samples of Tsp and Ssp were immediately fixed with 2.5% glutaraldehyde in 0.1 M cacodylate buffer, pH 7.8 (4°C, 4 h). After washing, samples were post-fixed with 1% osmium tetroxide in the same buffer (4°C, 1 h). Subsequently, samples were washed twice and dehydrated with a series of increasing concentrations of ethanol. For scanning electron microscopy (SEM), samples were further subjected to critical point drying in liquid CO_2 and sputter-coated with palladium. Finally, they were observed under a Hitachi S-2000 SEM at 20 kV. For transmission electron microscopy (TEM), the dehydrated samples were transferred to acetone, infiltrated in the mixture of acetone/resin, and embedded in Araldite 502 resin (Electron Microscopy Sciences, Fort Washington, PA, USA). Thin sections (70 nm thick) were cut and placed on 300-mesh copper grids, stained sequentially with uranyl acetate and lead citrate, and then observed under a Tecnai T20 TEM at 80 kV. The dimension (width × length) of the sperm head were measured from at least 25 sperm to obtain mean±SD, and the data were analyzed statistically by a Student's *t* test.

Extraction of Cell Surface Proteins

Isolated Gc, Tsp, and Ssp were washed twice with prechilled phosphate-buffered saline (PBS) and centrifuged (600×*g*, 4°C, 5 min) to eliminate loosely bound molecules from the cell surface. The pellet was then resuspended and incubated (4°C, 30 min) with 1 M NaCl in PBS with gentle shaking. After centrifugation, the supernatant (referred to as "NaCl extract") was collected and re-centrifuged (12,000×*g*, 4°C, 10 min) to eliminate any small particulates. Protein concentration was measured by Bradford's protein assay (Bradford 1976) using a Sigma Bradford's protein assay reagent (Sigma, Saint Louis, MO, USA).

To isolate integral membrane proteins, a detergent partitioning protocol was followed (Bordier 1981). Briefly, Triton X-114 in PBS at a final concentration of 1% was

added to the pellets remaining from NaCl treatment. This cell suspension was briefly sonicated (100-W output, 15-s intervals, three times) and allowed to stand on ice (15 min) with occasional agitations. The cellular fragments were then pelleted (12,000×*g*, 4°C, 10 min), and the resulting supernatants were left at room temperature until cloudiness in the suspension was observed. Thereafter, this suspension was then laid on a sucrose cushion containing 6% sucrose and 0.06% Triton X-114, and the phase separation was facilitated by centrifugation (500×*g*, room temperature, 3 min). The bottom detergent phase was collected, and the phase separation on sucrose cushion was repeated to clean the detergent soluble materials (assigned as "detergent extract"). To remove detergent from the extracted membrane proteins, an ice-cold delipidation mixture consisting of tri-*n*-butylphosphate:acetone:methanol (1:12:1, *v*/*v*/*v*) was used in an incubation (4°C, 4–5 h) with the detergent extracts at a final proportion of 14:1 (Mastro and Hall 1999). The precipitated proteins were pelleted (2,000×*g*, 4°C, 10 min), washed twice with cold acidified acetone (100:1, acetone/1 N HCl, *v*/*v*), and finally resuspended in 10 mM Tris-buffered saline (TBS). Protein concentration was determined by a detergent compatible Lowry's protein assay using bovine serum albumin (BSA) as the standard (Lowry et al. 1951).

SDS–PAGE and Immunoblotting

Sperm proteins (~10 μg) including whole cell lysates, NaCl- and detergent-extracted fractions obtained from Gc, Tsp, and Ssp were denatured in sample buffer and electrophoretically resolved in 12.5% sodium dodecyl sulfate–polyacrylamide gel electrophoresis (SDS–PAGE) under a reducing condition (Laemmli 1970). Molecular weight standards were co-electrophoresed as protein markers. The protein profile in one set of gel was visualized by silver staining. Resolved proteins in the duplicated gel were electro-transferred onto a 0.45-μm nitrocellulose membrane (Amersham Biosciences, Buckinghamshire, UK). These transferred protein were treated with 5% skimmed milk in TBS containing 0.1% Tween-20 (TBS-T) to block non-specific binding and further exposed (1 h, room temperature) to an anti-tyrosine phosphate monoclonal antibody (clone P-Tyr 102, Cell Signaling, Beverly, MA, USA) at a dilution of 1:20,000 followed by a horse radish peroxidase (HRP) conjugated rabbit anti-mouse IgG (Zymed Laboratory, San Francisco, CA, USA) at a dilution of 1:3,000. The immunoreactivity was visualized with an enhanced chemiluminescence detection kit (ECL, Amersham Biosciences). Specificity of the anti-tyrosine phosphate antibody was determined by an inclusion of an excess amount (20-fold) of tyrosine phosphate conjugated with BSA (Sigma) into the antibody suspension before proceeding for antibody staining as described above.

Zymography

The isolated protein samples from Gc, Tsp, and Ssp were separated by 10% SDS–PAGE containing 0.3% gelatin under a non-reducing condition. Purified porcine pancreatic trypsin (500 ng) was also co-electrophoresed as a positive control. After protein separation, the sample was treated with 3% Triton X-100 and further incubated in the reaction buffer containing 100 mM NaCl and 10 mM Tris–HCl, pH 7.4 (37°C, overnight). Visualization of the proteolytically active band (as a clear band against dark background) was performed by staining the gel with 0.125% Coomassie brilliant blue R-250 and then de-staining with 70% ethanol containing 10% acetic acid. Alternatively, the resolved proteins in the duplicate gel were pretreated with 1 mM phenylmethylsulphonyl fluoride (PMSF) or 0.5 mM soybean trypsin inhibitor before developing enzymatic reaction in the reaction buffer.

Sperm Fertilization Assays

Spawned eggs released naturally from fully mature females (aged >24 months) were freshly collected in FSW. Aliquots of 3 ml FSW containing 10^3 spawned eggs were added to the wells of a 16-well plate and kept at 27°C in a water bath. Upon isolation, 10^5 Tsp as well as the freshly released Ssp, resuspended in 200 μl FSW, were gently added to the egg suspensions. Sequential changes of fertilized eggs including extrusions of polar bodies and occurrence of two-cell embryos were used as indicators of successful fertilization which has been reported in many abalone species (Septo and Cook 1998; Yi et al. 2002; Liu et al. 2004). These parameters were monitored at 8, 15, and 20 min post-sperm addition. The data were expressed as mean±S.D. calculated from six replicates and analyzed statistically using a one-way analysis of variance.

Results

Morphological Comparison Between Tsp and Ssp

Initially, we performed discontinuous Percoll gradient centrifugation to select testicular sperm from the mixed population of other germ cells. It was found that testicular sperm constituted 20–25% of the total population of the isolated germ cells (Fig. 1b, left bar). Upon subjecting the isolated cells to Percoll gradient centrifugation, the proportion of testicular sperm (pelleted fraction) increased to >90% (Fig. 1b, right bar), and the vast majority of these sperm were motile. The major contaminants in this sperm preparation were spermatocytes and early spermatids (~5–7%).

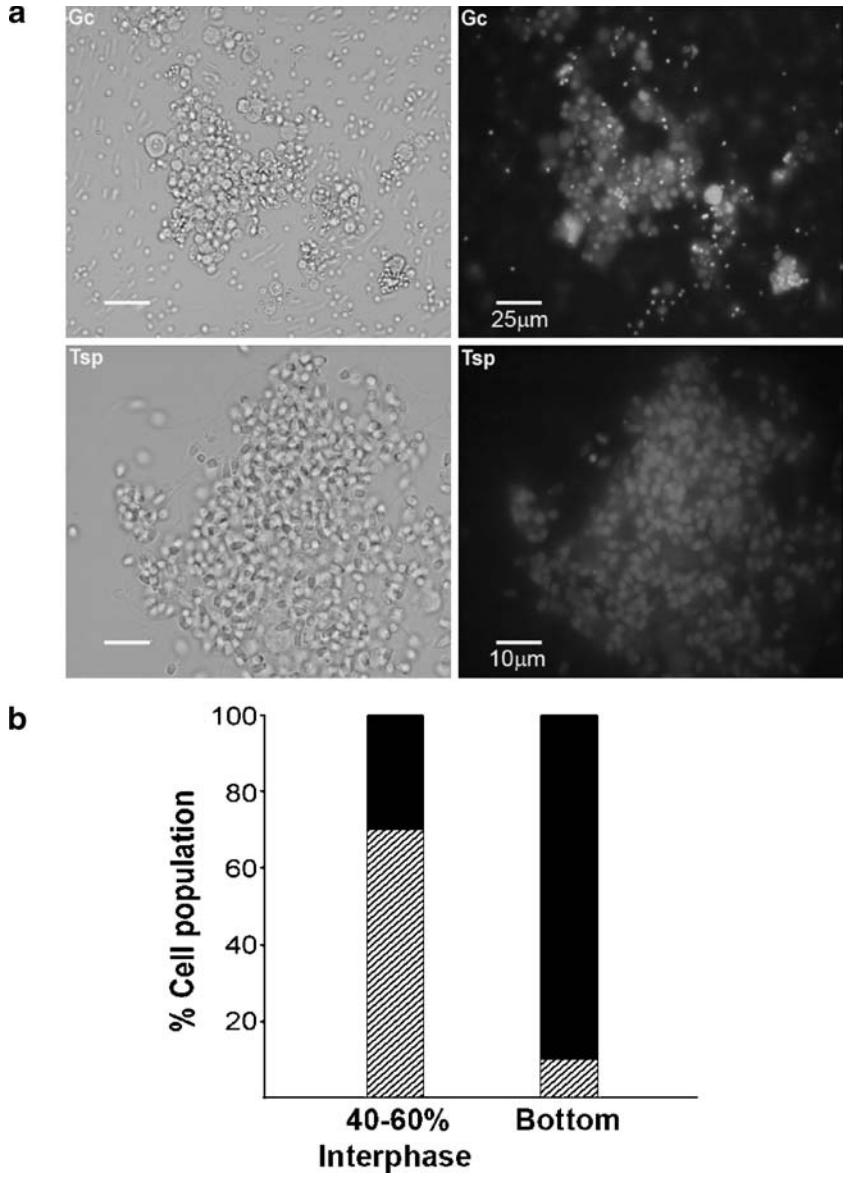


Fig. 1 Separation of *H. asinina* testicular germ cells using a discontinuous Percoll gradient (20%–80%) centrifugation. **a** Cells sedimented at the interphase between 40% and 60% and at the bottom of the gradient were subjected to Hoechst 33258 DNA staining and examined under a light microscope. *Left*, phase contrast micrographs; *right*, corresponding fluorescent micrographs. **b** The proportion of Gc (*hatched bars*) and Tsp (*solid bars*) collected as in **a**

The ultrastructural comparison between Tsp and Ssp was demonstrated in Fig. 2. As observed under SEM, the surface architecture and the cornical contour of the sperm head for both sperm samples were quite similar. However, the width of the posterior part of Tsp sperm head (1.24± 0.03 μm×2.78±0.02 μm) was notably narrower (but not significantly different, P=5.12) than that of Ssp (1.41± 0.03 μm×2.80±0.03 μm), making Tsp appear slightly slender than Ssp (panels a, d). At the TEM level, the plasma membranes (Pm) of both sperm samples were readily distinguishable from the underlying outer acrosomal membrane (Am, panels b, e). There was no apparent difference in the thickness of the outer Pm leaflet in Ssp, which may suggest the adsorption of glycosylated proteins onto the sperm surface. The electron dense acrosomal matrix appeared to be uniformly distributed throughout the large, U-shaped acrosome in both sperm samples (panels b, e). Despite having large acrosome, there was no evidence to suggest any compartmentalization of the acrosomal matrices in the manner that have been reported for mammalian sperm possessing the large acrosomes (Foster et al. 1997; Kim and Gerton 2003). The acrosome and nuclear membrane of both Tsp and Ssp were separated by subacrosomal space, filled with crystalline-like structures surrounded with electron lucent materials (panels b, e). The nuclei of both sperm samples were occupied by highly condensed chromatin, leaving few vacuolar spaces in between (panels c, f). In the sperm tail, mitochondria were organized into annular structures around the proximal part of the tail. The axonemal complexes were surrounded only by a thin layer of plasma membrane (panels c, f).

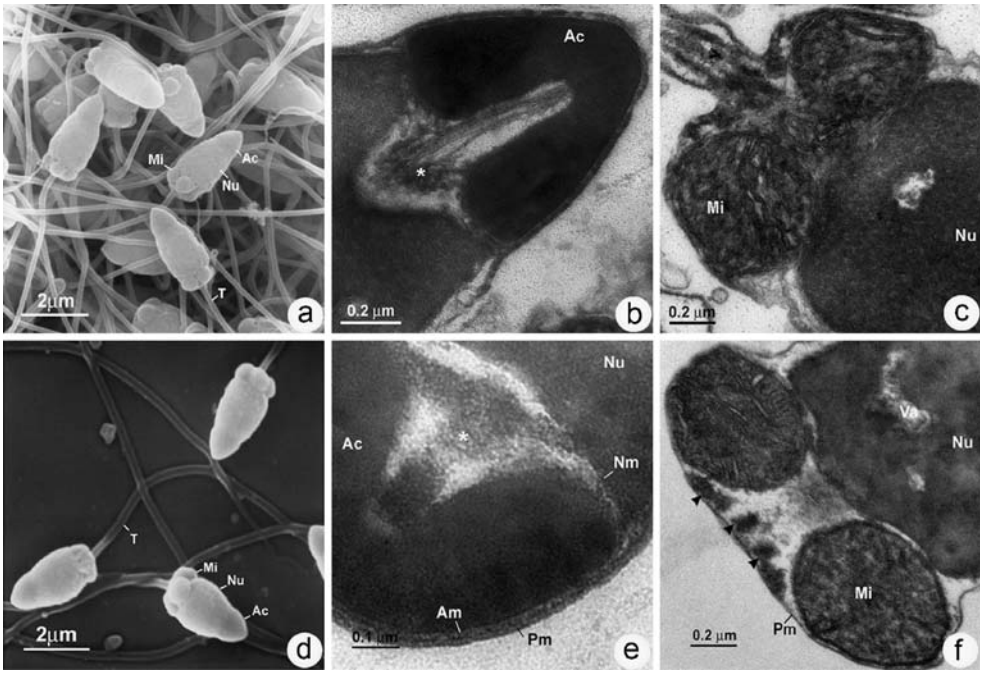


Fig. 2 Scanning and transmission electron micrographs of Tsp (*upper panels*) and Ssp (*lower panels*). SEM (**a** and **d**) showing similar conical sperm heads and three to four spherical mitochondria around the neck and long flagella in both Tsp and Ssp. TEM (**b**, **c**, **e**, and **f**) showing large U-shaped acrosomal vesicle (*Ac*) with a uniform electron dense materials (**b** and **e**), a crystalline-like structure in the subacrosomal region (*asterisk*), a highly condensed chromatin with some vacular-like structures (*Va*) in the sperm nuclei (*Nu*), and large globular mitochondria (*Mi*, **c** and **f**) in both sperm samples. *T* sperm tail, *Pm* plasma membrane, *Am* acrosomal membrane, *Nm* nuclear membrane

Profiles of the Membrane Proteins among Different Sperm Samples

Modification of sperm plasma membrane has been known to be one of the major events associated with post-testicular sperm maturation/capacitation process (Yanagimachi 1994; Vanichviriyakit et al. 2004). Two types of membrane proteins (based on their extractability) were analyzed, peripheral (NaCl-extractable) proteins and integral (Triton X-114-partitioning) proteins. NaCl-extractable proteins observed in Gc were mostly intermediate- and slow-migrating proteins ranging from 38 to 200 kDa. In addition, the fast migrating proteins of 15–33 kDa were mainly present in the peripheral proteins of Tsp, but were rarely detected in Gc proteins (Fig. 3, left panel, arrowheads). Compared with Tsp, the peripheral proteins of Ssp possessed at least three additional bands with the molecular masses of 26, 42, and 48 kDa (Fig. 3, left panel, arrows). Notably, the 23 kDa protein was present specifically in the Tsp peripheral proteins, but not in Ssp. For detergent-extractable proteins, two major protein bands of 33 and 130 kDa were apparent in the Gc extracts. Two additional detergent-miscible proteins with the molecular masses of 27 and 52 kDa and a set of 45–50 kDa proteins were visualized in the Tsp extracts, but not in that of Gc (Fig. 3, right panel, arrowheads). In Ssp, at least six additional integral proteins with the molecular masses of 24, 51, 78, 80, 97, and 100 kDa were observed additionally to those found in Tsp (Fig. 3, right panel, arrows).

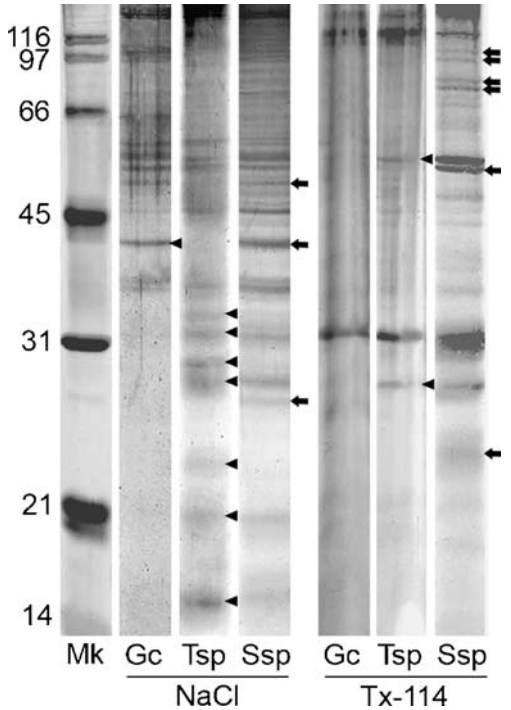


Fig. 3 Comparative profiles of the sperm surface proteins extracted from Gc, Tsp, and Ssp. High salt (NaCl) and detergent (Triton X-114) extracted proteins were resolved by 12.5% SDS–PAGE and visualized by silver staining. *Arrowheads* and *arrows* indicate the major differences in the protein patterns between Gc and Tsp and Tsp and Ssp, respectively. *Mk* molecular weight marker

Activation of Sperm Serine Proteases in Ssp Detergent Extracts

Sperm serine proteases, significant for the acrosome reaction, have been shown to be activated upon sperm transit into female reproductive organs (Lindsay and Clark 1992). This led us to hypothesize that activation of these serine proteases may also be a crucial step for abalone sperm to gain their full fertilizing ability. As shown in Fig. 4A, at least five proteolytically active proteins having the molecular masses of 38, 40, 46, 68, and 130 kDa were present in the detergent extracts of Ssp. It should be noted that these proteolytically active proteins had the different mobility pattern from those proteins that were additionally found in the integral proteins of Ssp compared with Tsp (Fig. 3, right panel, rightmost lane). Conversely, the enzymatic activity was minimal or absent in the detergent fractions of either Gc or Tsp. Notably, the only active protein band that was detectable in the NaCl extracts of all samples was an 18-kDa protein (Fig. 4A, arrow). This protein was also found to be active in the detergent extract of Ssp, but not in Gc or Tsp. Most of the enzyme activities in the aforementioned proteins including trypsin (as a positive control) were abolished upon pretreatment of sperm membrane proteins with either 2 mM PMSF (Fig. 4B) or SBTI (data not shown). However, some residual activity was still visible at the 68- and 130-kDa protein bands (Fig. 4B, empty arrowheads). Taken together, these results suggested that sperm proteases, mainly serine ones, were activated upon the sperm release into seawater during spawning.

Changes in Protein Tyrosine Phosphorylation in the Sperm Extracts

Enhanced level of protein tyrosine phosphorylation is generally anticipated to be a key characteristic that is tightly related to sperm capacitation in both invertebrates and vertebrates (Vanichviriyakit et al. 2004; Visconti and Kopf 1998). Therefore, we also used this characteristic to detect biochemical changes within the three samples studied. Notably, immunoreactivity of anti-tyrosine phosphate was found to be limited to the small proteins with the molecular masses ranging from 15 to 20 kDa (Fig. 5A). The level of immunoreactive intensity of the phosphorylated proteins was relatively low in Gc, with only a trace amount of the 16-, 17-, and 19-kDa proteins detected. However, the intensity level of these three tyrosine phosphorylated protein bands and the additional 15 and 20 kDa ones were greatly enhanced in the Tsp sample. This high phosphorylation level remained constant in the Ssp sample (Fig. 5A). When an excess amount of phosphotyrosine–BSA was included to demonstrate a specific binding of the anti-tyrosine phosphate antibody, only a background level of the antibody staining was observed (Fig. 5B).

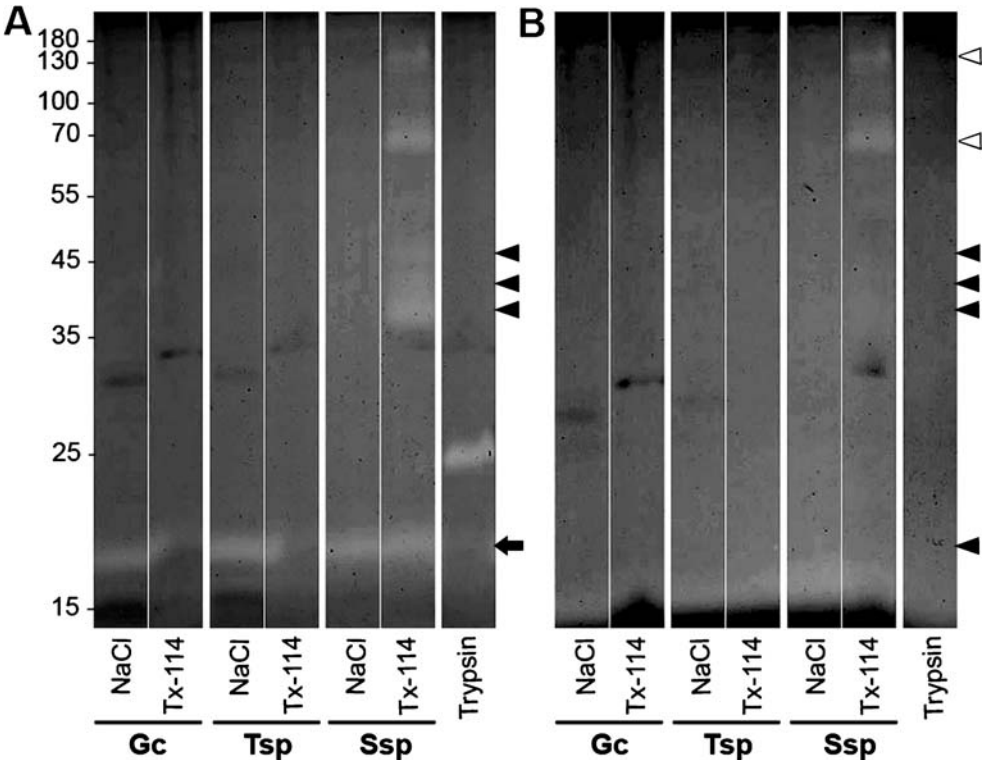


Fig. 4 Proteolytic activity of the extracted membrane proteins in Gc, Tsp, and Ssp. NaCl- and detergent-extracted proteins of the three samples were resolved in 10% SDS–PAGE containing 0.3% gelatin under non-reducing condition. The resolved proteins were either untreated (**A**) or treated with 2 mM PMSF (**B**) before developing enzymatic reactions in the reaction buffer. Trypsin (*rightmost lane* in each panel) was also co-electrophoresed as a positive control. *Clear bands* against *dark background* represent enzymatically active protein bands. *Solid* and *empty arrowheads* indicate the diminished and remaining enzyme activities, respectively, upon treatment of the resolved proteins with inhibitors. Note the presence an 18-kDa active protein within the NaCl extracts of all three samples and in the detergent extract of Ssp (*arrow*)

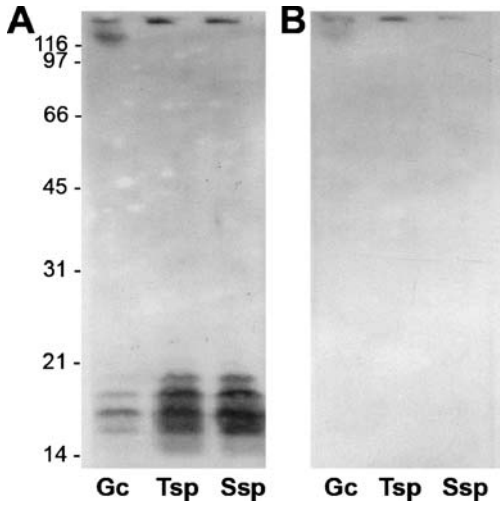


Fig. 5 Detection of protein tyrosine phosphorylation in the different germ cells. **A** Western blotted proteins of the whole cell lysates extracted from Gc, Tsp, and Ssp probed with monoclonal anti-tyrosine phosphate (1:20,000) and a corresponding HRP-conjugated secondary antibody (1: 3,000). **B** Negative control in which the primary antibody was pre-absorbed with a tyrosine phosphate–BSA conjugate

Comparative Fertilizing Abilities of Tsp and Ssp

Figure 6 demonstrated fertilizing abilities of both purified Tsp and Ssp as successful fertilization rates based on protrusion of polar bodies at 8- and 15-min post-insemination and occurrence of two-cell embryos at 20-min post-insemination. Fertilization rates of Tsp at 8 min were ~25% compared to ~34% in Ssp. Notably, fertilization rates at 15 min were ~27% and 77% for Tsp and Ssp, respectively, which were significantly different ($P<0.05$). However, the percent fertilization rates at 20 min of the Tsp samples greatly increased to ~66%, closely approaching to that observed in the Ssp samples (~76%). The implication drawn from these results was that the isolated Tsp sperm possessed a fertilizing ability not dissimilar to Ssp; however, the activation to full fertilizing capacity might be delayed.

Discussion

Based on their ultrastructural features studied herein, *H. asinina* sperm could be classified as a primitive type because of the following criteria: a very large acrosome covering the anterior part of the nucleus, large-sized mitochondria around the neck region, and a simple structure of the tail consisting of 9 + 2 microtubule doublets surrounded by plasma membrane (Franzen 1983). In general, ultrastructures of Ssp were quite similar to those of the isolated Tsp and also to those sperm residing in the germinal epithelial cords of the testis (Apisawetakan et al. 2000). The only difference that could be detected was that sperm head contour of Ssp was slightly wider than that of isolated Tsp, especially at the posterior region. A possible explanation of this could be due to the mechanical compression applied to the Tsp sperm head while they were embedded in cytoplasm of supporting epithelium or the swelling of Ssp upon their contact with seawater. It has been reported that a higher level of intermolecular cross-linking of protamines rendering higher compaction of chromosome and sperm head is associated with post-testicular sperm modification (Yanagimachi 1994). In *H. asinina*, chromatin condensation is also modulated by protamine-like basic nuclear proteins (Suphamungmee et al. 2005), consistent with other mollusks and even mammals (Ausio 1999; Balhorn et al. 1999). However, our results revealing the larger Ssp heads than those of Tsp (Fig. 2) would suggest that a post-testicular cross-linking of protamines resulting in the highly compacted sperm head may not occur in this abalone species.

In this study, we also compared the biochemical and physiological properties of the isolated germ cells (Gc, routinely used for fertilizing the spawned eggs in abalone aquaculture with a variable proportion of developing germ cells), purified testicular sperm (Tsp, having purity >90%), and the naturally spawned sperm (Ssp, having full fertilizing ability). Three lines of experimental evidence shown herein allowed us to imply that capacitation-related mechanisms took place during differentiation of testicular germ cells, which may associate with fertilizing capacity of these cells, particularly Tsp. Firstly, gradual modifications of membrane-associated proteins, both peripheral and integral proteins, could be detected from Gc to Tsp and Ssp (Fig. 3). These sperm membrane alterations noticed

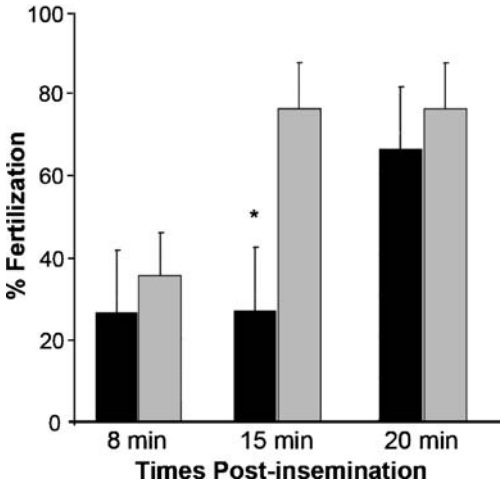


Fig. 6 Comparative fertilization rates of Tsp and Ssp. The rates were determined by the occurrence of polar bodies at 8 and 15 min as well as the presence of two-cell embryos at 20 min under a phase contrast microscope. One thousand eggs were loaded into each well of a 16-well plate, followed by the addition of 10^5 Tsp (*black bars*) and Ssp (*gray bars*). The data were expressed as mean±SD from six replicates. *Asterisk* denotes significant difference ($P<0.05$)

along with the enhanced fertilizing ability are known to be coupled with both sperm maturation and capacitation processes in invertebrates and mammals (Yanagimachi 1994, Vanichviriyakit et al. 2004). Secondly, an enhanced level of protein tyrosine phosphorylation was detectable as early as in Tsp (Fig. 5). Increased phosphorylation in a broad spectrum of sperm proteins has been thought to be a characteristic of downstream-signaling event closely associated with sperm capacitation in many mammals as well as in some invertebrates (Asquith et al. 2004; Naz and Rajesh 2004; Vanichviriyakit et al. 2004; Krapf et al. 2007). Our results reveal for the first time the enhancement of this signal transduction pathway in the isolated Tsp at a level comparable with Ssp. These results suggest that the molecular machineries that mark full fertilizing capability of the sperm are readily present in Tsp (Fig. 5). Thirdly, the activation of sperm serine proteases was observed in the sperm upon spawning into seawater (Fig. 4). This finding was consistent with the activation of serine proteases, particularly trypsin-like enzymes, during sperm transit into the closed-thelycum of female reproductive tracts as part of capacitation process in penaeoid shrimp (Lindsay and Clark 1992; our unpublished results). These shrimp enzymes belong to the acrosomal contents that serve their crucial function in the acrosomal reaction. This function corresponds with the function of the well-studied mammalian acrosomal serine proteases, proacrosin/acrosin (Arboleda and Gerton 1988; Barros et al. 1992; Pasten et al. 2005). Knocking out of this proacrosin/acrosin system has led to a prolonged delay in fertilization process (Baba et al. 1994; Adham et al. 1997; Nayernia et al. 2002). It should be noted that other proteases aside from serine ones (resistant to PMSF with the molecular masses of 68 and 180 kDa; Fig. 4b) were also present in the detergent extracts of Ssp. Identification and physiological function related to fertilization of these proteases still require further investigation.

The high levels of fertilization rate observed for the isolated Tsp, comparable with Ssp (Fig. 6), correlated with the onset of at least two capacitation associated characteristics detected in Tsp, namely, the membrane protein alterations and the enhanced protein tyrosine phosphorylation. The lack of proteolytic activation in the isolated Tsp made them biochemically different from Ssp (Fig. 4). This absence of proteolytic activity in Tsp may account for the delay of fertilization (as gauged from a significant difference in polar body extrusion at 15 min; Fig. 6). However, it appeared not to affect the final fertilizing capacity of Tsp (as deduced from the comparable fertilization rate at 20 min of Tsp and Ssp). In fact, this finding was in agreement with the aforementioned knockout studies of the proacrosin/acrosin system which results in a delayed fertilization time but not fertilizing ability (Baba et al. 1994; Adham et al. 1997; Nayernia et al. 2002). It remains to be proven whether trypsin-like enzymes in the abalone Tsp are activated upon the contact of these sperm with the egg surface. From these results, we believe that the fertilizing ability of abalone sperm is acquired during testicular residence via capacitation-like molecular machineries. These capacitation-related characteristics could be used as biomarkers for predicting sperm fertilizing capability especially in cases when isolated germ cells are used in place of naturally spawned sperm. Moreover, the use of purified Tsp to replace spawned sperm may improve both fertilization rates and consistency in the abalone aquaculture.

Acknowledgments This research was supported by Thailand Research Fund (to PS and WW and Royal Golden Jubilee Ph.D. Scholarship Program to WS) and Mahidol University.

References

Adham IM, Nayernia K, Engel W (1997) Spermatozoa lacking acrosin protein show delayed fertilization. Mol Reprod Dev 46:370–376

Alfaro J, Munoz N, Vargas M, Komen J (2003) Induction of sperm activation in open and closed thelycum penaeoid shrimps. Aquaculture 216:371–381

Apisawetakan S, Sobhon P, Wanichanon C, Linthong V, Kruatrachue M, Upatham ES, Jarayabhand P, Pumthong T, Nugranad J (2000) Ultrastructure of spermatozoa in the testis of *Haliotis asinina* Linnaeus. J Med Appl Malacol 10:101–109

Arboleda CE, Gerton GL (1988) Proacrosin/acrosin during guinea pig spermatogenesis. Dev Biol 125:217–225

Asquith KL, Baleato RM, McLaughlin EA, Nixon B, Aitken RJ (2004) Tyrosine phosphorylation activates surface chaperones facilitating sperm-zona recognition. J Cell Sci 117:3645–3657

Ausio J (1999) Histone H1 and evolution of sperm nuclear basic proteins. J Biol Chem 274:31115–31118

Baba T, Azuma S, Kashiwabara S, Toyada Y (1994) Sperm from mice carrying a targeted mutation of the acrosin gene can penetrate the oocyte zona pellucida and effect fertilization. J Biol Chem 269 (50):31845–31849

Balhorn R, Cosman M, Thornton K, Krishnan VV, Corzett M, Bench G, Kramer C, Lee JD IV, Hud NV, Allen MJ, Prieto M, Meyer-Iese W, Brown JT, Kirz J, Zhang X, Bradbury EM, Maki G, Braun RE, Breed W (1999) Protamine mediated condensation of DNA in mammalian sperm. In: Gagnon C (ed) The male gamete: from basic science to clinical applications. Cache River Press, Vienna IL, pp 55–70

Barros C, Capote C, Perez C, Crosby JA, Becker MI, De Ioannes A (1992) Immunodetection of acrosin during the acrosome reaction of hamster, guinea-pig and human spermatozoa. Biol Res 25:31–40

Bedford JM (1983) Significance of the need for sperm capacitation before fertilization in eutherian mammal. Biol Reprod 28:108–120

Bordier C (1981) Phase separation of integral membrane proteins in Triton X-114 solution. J Biol Chem 256:1604–1607

Bradford MM (1976) A rapid and sensitive method for the quantitation of microgram quantities of protein utilizing the principle of protein-dye binding. Anal Biochem 72:248–254

Dusenbury DB (2000) Selection for high gamete encounter rates explains the success of male and female mating types. J Theor Biol 202:1–10

Encena VC II, Capinpin EC Jr, Bayona NC (1998) Optimal sperm concentration and time for fertilization of the tropical abalone, *Haliotis asinina* Linné 1758. Aquaculture 165:347–352

Foster JA, Friday BB, Maulit MT, Blobel C, Winfrey VP, Olson GE, Kim KS, Gerton GL (1997) AM67, a secretory component of the guinea pig sperm acrosomal matrix, is related to mouse sperm protein sp56 and the complement component 4-binding proteins. J Biol Chem 272:12714–12722

Franzen A (1983) Ultrastructural studies of spermatozoa in three bivalve species with notes on evolution of elongated sperm nucleus in primitive spermatozoa. Gamete Res 7:199–214

Gardner C, Williams H (2002) Maturation in the male giant crab, *Pseudocarcinus gigas*, and the potential for sperm limitation in the Tasmanian fishery. Mar Freshwater Res 53:661–667

Giese AC, Kanatani H (1987) Maturation and spawning. In: Giese AC, Pearse JS, Pearse VB (eds) Reproductive Biology of Invertebrates. Boxwood Press, Pacific Grove, CA, pp 251–329

Griffin FJ, Clark WH Jr (1990) Induction of acrosomal filament formation in the sperm of *Sicyonia ingentis*. J Exp Zool 254:296–304

Grubert MA, Mundy CN, Ritar AJ (2005) The effects of sperm density and gamete contact time on the fertilization success of blacklip (*Haliotis rubra*; Leach, 1814) and greenlip (*H. laevigata*; Donovan, 1808) abalone. J Shellfish Res 24:407–413

Kim KS, Gerton GL (2003) Differential release of soluble and matrix components: evidence for intermediate states of secretion during spontaneous acrosomal exocytosis in mouse sperm. Dev Biol 264 (1):141–152

Krapf D, Visconti PE, Arranz SE, Cabada MO (2007) Egg water from the amphibian Bufo arenarum induces capacitation-like changes in homologous spermatozoa. Dev Biol 306:516–524

Laemmli UK (1970) Cleavage of structural proteins during the assembly of the head of bacteriophage T4. Nature 227:680–685

Levitan DR, Sewell MA, Chia FS (1991) Kinetics of fertilization in the sea urchin *Strongylocentrotus franciscanus*: interaction of gamete dilution, age, and contact time. Biol Bull 181:371–378

Lindsay LL, Clark WH Jr (1992) Preloading of micromolar intracellular Ca^{2+} during capacitation of *Sicyonia ingentis* sperm, and the role of the pHi decrease during the acrosome reaction. J Exp Zool 262:219–229

Liu W, Heasman M, Simpson R (2004) Evaluation of cytochalasin B (CB) treatments for triploidy induction in the blacklip abalone, *Haliotis rubra*. Aquaculture Res 35:1062–1075

Lowry OH, Rosenbrough NJ, Farr AL, Randall RJ (1951) Protein measurement with the Folin phenol reagent. J Biol Chem 193:265–275

Mastro R, Hall M (1999) Protein delipidation and precipitation by tri-*n*-butylphosphate, acetone, and methanol treatment for isoelectric focusing and two-dimensional gel electrophoresis. Anal Biochem 273:313–315

Meidel SK, Yund PO (2001) Egg longevity and time-integrated fertilization in a temperate sea urchin (*Strongylocentrotus droebachiensis*). Biol Bull 201(1):84–94

Nayernia K, Adham IM, Shamsadin R, Müller C, Sancken U, Engel W (2002) Proacrosin-deficient mice and zona pellucida modifications in an experimental model of multifactorial infertility. Mol Hum Reprod 8:434–440

Naz RK, Rajesh PB (2004) Role of tyrosine phosphorylation in sperm capacitatation/acrosome reaction. Reprod Biol Endocinol 2:75

Pasten C, Morales P, Kong M (2005) Role of the sperm proteasome during fertilization and gamete interaction in the mouse. Mol Reprod Dev 71:209–219

Rios M, Barros C (1997) Trypsin-like enzymes during fertilization in the shrimp *Rhynchocinetes typus*. Mol Reprod Dev 46:581–586

Septo NK, Cook PA (1998) Induction of triploidy in the South African abalone using cytochalasin B. Aquaculture Int 6:161–169

Suphamungmee W, Apisawetakan S, Weerachatyanukul W, Wanichanon C, Sretarugsa P, Poomtong T, Sobhon P (2005) Basic nuclear protein pattern and chromatin condensation in the male germ cells of a tropical abalone, *Haliotis asinina*. Mol Reprod Dev 70:211–221

Vanichviriyakit R, Kruevaisayawan H, Weerachatyanukul W, Tawipreeda P, Withyachumnarnkul B, Pratoomchat B, Chavadej J, Sobhon P (2004) Molecular modification of *Penaeus monodon* sperm in female thelycum and its consequent responses. Mol Reprod Dev 69:356–363

Visconti PE, Kopf GS (1998) Regulation of protein phosphorylation during sperm capacitation. Biol Reprod 59:1–6

Yanagimachi R (1994) Mammalian fertilization. In: Knobil E, Neill JD (eds) Physiology of reproduction. 2nd edn. Raven, NY, pp 189–317

Yi JH, Lefievre L, Gagnon C, Anctil M, Dube F (2002) Increase of cAMP upon release from prophase arrest in surf clam oocytes. J Cell Sci 115:311–320

Yund PO (2000) How severe is sperm limitation in natural populations of marine free-spawners? Trends Ecol Evol 15(1):10–13

BIOLOGY OF REPRODUCTION **79,** 134–141 (2008)
Published online before print 16 April 2008.
DOI 10.1095/biolreprod.107.066316

Induction of the Acrosome Reaction in Black Tiger Shrimp (*Penaeus monodon*) Requires Sperm Trypsin-Like Enzyme Activity[1]

Hathairat Kruevaisayawan,[3,4] Rapeepun Vanichviriyakit,[3,4] Wattana Weerachatyanukul,[2,4] Sitthichai Iamsaard,[4,5] Boonsirm Withyachumnarnkul,[4,5] Ajoy Basak,[6,7,8] Nongnuj Tanphaichitr,[3,6,7,9] and Prasert Sobhon[3,4]

Department of Anatomy[4] and Center of Excellence for Shrimp Molecular Biology and Biotechnology (Centex Shrimp),[5] Faculty of Science, Mahidol University, Bangkok 10400, Thailand
Chronic Disease,[6] Ottawa Health Research Institute, Ottawa, Ontario K1Y 4E9, Canada
Departments of Biochemistry/Microbiology/Immunology,[7] Medicine,[8] and Obstetrics and Gynecology,[9] University of Ottawa, Ottawa, Ontario K1H 8M5, Canada

ABSTRACT

Trypsin-like enzymes in egg water (EW), a natural acrosome reaction (AR) inducer, are known for their importance in shrimp AR. In this report, we describe a unique phenomenon of the AR of black tiger shrimp (*Penaeus monodon*) sperm. It was completed within 45–60 sec and comprised only the acrosomal exocytosis and depolymerization of the sperm head anterior spike. We used peptidyl fluorogenic substrates to show the presence of trypsin-like enzymes in *P. monodon* EW and sperm, but minimal activities of chymotrypsin-like enzymes. In sperm, these trypsin-like enzymes existed both on the sperm surface and in the acrosome. The acrosomal enzyme was revealed as a 45-kDa band by fluorogenic substrate in-gel zymography. Although EW possessed high trypsin-like enzyme activities, they were not essential for the AR induction; EW pretreated with an irreversible trypsin inhibitor, or heat-inactivated EW (HI-EW), to abolish the trypsin-like activities could still induce the AR. The HI-EW-induced AR was inhibited by the presence of a membrane impermeant soybean trypsin inhibitor (SBTI) in the sperm suspension, indicating the significance of sperm-borne trypsin-like enzymes (on the surface and/or in the acrosome) in this AR process. However, pretreatment of sperm with SBTI followed by its removal from the suspension still allowed the AR to occur within 5 min of sperm exposure to HI-EW. Since trypsin-like activity of the SBTI-pretreated sperm surface at 5 min after SBTI removal was at the minimal level, our results suggest the importance of the acrosomal trypsin-like enzyme in the AR process.

acrosome reaction, egg water, fertilization, gamete biology, P. monodon, sperm, trypsin

INTRODUCTION

In penaeoid shrimp, spermatophores have to be inserted into the female seminal receptacle (called thelycum) before the release of sperm together with eggs during spawning [1]. It has been shown previously that sperm gain fertilizing ability during their storage in the thelycum [2, 3]. Unlike sperm of other marine invertebrates, penaeoid sperm are nonflagellated and immotile [4, 5]. The success of fertilization in these shrimp thus relies on two key steps: contact of the sperm anterior spike with the egg outer vestment and the subsequent acrosome reaction (AR). The AR process involves a triggered fusion of the sperm plasma membrane with the outer acrosomal membrane, leading to the release of the acrosomal vesicles and soluble content. Thereafter, the AR spermatozoon interacts, fuses, and incorporates into the egg proper. In *Sicyonia ingentis*, the AR has been shown to be a biphasic process. During the first phase, the anterior spike of the sperm becomes depolymerized upon contacting the vitelline envelope (VE), leading to an acrosomal exocytosis. The second phase involves the formation of the acrosomal filament, which binds to the egg plasma membrane, followed by gamete plasma membrane fusion [5–7]. These two distinct events are temporally separated, and can be induced by two different inducers [7]. While the event in the first AR phase is common in all penaeoid sperm, formation of the acrosomal filament during the second AR phase cannot be detected in some penaeoid shrimp, including *Penaeus aztecus*, *Penaeus setiferus*, and *Penaeus stylirostris* [8].

In *Penaeus monodon*, detailed information of the AR has not yet been described. Our preliminary work indicates that the AR in *P. monodon* differs drastically from that of *S. ingentis* in both timing and morphological alterations [9]. The AR occurring as part of the fertilization process of *P. monodon* takes only a few minutes compared with ~45–60 min in *S. ingentis* [10]. This rapid process makes it difficult to detect the various steps of morphological changes during the AR in this species. Overall structural alterations during the AR in *P. monodon*, as detected at the light microscopic level, include depolymerization of the anterior spike, in conjunction with the swelling and rupturing of the acrosomal vesicle. However, the formation of the acrosomal filament during the AR is not notable in *P. monodon* sperm. Therefore, spike depolymerization and rupture of the acrosomal vesicle are used to mark completion of AR in this species.

Egg water (EW), a flocculent material in seawater that is generated during egg spawning, has been commonly used for in vitro induction of sperm AR in several aquatic species,

[1]Supported by funding from the National Science and Technology Development Agency of Thailand to B.W., the Thailand Research Fund to W.W. and P.S., Thailand Research Fund-Royal Golden Jubilee Ph.D. Program grant PHD/0275/2545 to R.V., and from the Commission on Higher Education to H.K. and S.I.
[2]Correspondence: Wattana Weerachatyanukul, Department of Anatomy, Faculty of Science, Mahidol University, Rama 6 Rd., Payathai, Bangkok 10400, Thailand. FAX: 66 2 354 7168;
e-mail: scwwy@mahidol.ac.th
[3]These authors contributed equally to this work.

Received: 25 October 2007.
First decision: 21 November 2007.
Accepted: 27 March 2008.
© 2008 by the Society for the Study of Reproduction, Inc.
ISSN: 0006-3363. http://www.biolreprod.org

including sea urchins [11, 12], sturgeons [13], and shrimp [10]. EW of penaeoid shrimp is made up of components released from the female during spawning, including the outermost layer of the eggs, VE, cortical rods (CRs), which are the egg jelly components embedded in the egg surface crypts, and some thelycal (T) substances. In *S. ingentis,* the trypsin-like proteolytic activity in EW is important for acrosomal filament formation during the second AR phase [7, 14]. The given explanation is that trypsin may hydrolyze enzymes or channel proteins in the inner acrosomal membrane, thus activating filament formation [14]. Whether or not these EW enzymes are involved in any steps of the AR induction in *P. monodon* remains to be addressed. In this study, we determined whether EW trypsin-like enzymes were involved in any steps of the AR induction in *P. monodon*. Alternatively, EW may be involved in the initial part of AR induction, simply through its binding to the sperm surface. Furthermore, since sperm of many invertebrate species have been known to contain trypsin-like enzymes [14–16], we investigated their existence and possible involvement in *P. monodon* sperm AR induction.

MATERIALS AND METHODS

Sample Collection

Collection of EW was carried out at the Bangkok Aquaculture Farm Company, Nakhon Sri Thammarat Province, Thailand. Female shrimp possessing mature ovaries (stage IV) were individually placed in a 500-L plastic tank. In order to exclude sperm factors in the EW, only shrimp that had not been inseminated were used in this study. The shrimp were held firmly over a 500-ml container and allowed to spawn their eggs into filtered seawater. After swirling gently to settle the eggs to the bottom, seawater without spawned eggs was collected and designated as EW. This EW was centrifuged (10 000 × *g*, 15 min, 4°C) to remove particulates, and kept at −80°C until use. Proteins in the EW were quantified with a Bradford's reagent (Sigma, St. Louis, MO) [17].

To collect T sperm , inseminated females were anesthetized under ice, and the thelyca located at the fifth pair of walking legs were carefully removed and placed in calcium-free artificial seawater (CFASW; 423 mM NaCl, 9 mM KCl, 23 mM $MgCl_2$, 9.3 mM $MgSO_4$, 2.1 mM $NaHCO_3$, pH 7.8). Subsequently, they were teased with dissecting forceps to release sperm masses and fluid. The T-sperm suspension was filtered through a 212-μm metal sieve (Endecotts, London, UK) to remove aggregates, washed (500 × *g*, 5 min), and resuspended in CFASW at the final concentration of 1×10^7 sperm/ml before use. T fluid (TF) was also collected from the female shrimp, which had not been inseminated, following the dissecting method described above. This fluid was centrifuged (12 000 × *g*, 10 min, 4°C) to remove any small particulates, assayed for the protein concentration as mentioned above and kept frozen at −80°C until use.

CRs were isolated from mature ovaries according to the method described by Lynn and Clark [18]. Briefly, pieces of ovaries were homogenized in an isolation medium (IM; 500 mM NaCl, 9 mM $CaCl_2$, 14 mM KCl, 15 mM $MgCl_2$, and 10 mM Tris-HCl, pH 7.6) containing 30% sucrose. The homogenate was centrifuged (1000 × *g*, 5 min, 4°C). The pellet containing CRs was resuspended in IM, and the suspension was overlaid onto 60% sucrose in IM and centrifuged (8000 × *g*, 60 min, 4°C). The white pellet containing mainly CRs was washed four times with IM. As in physiological conditions, isolated CRs were left overnight (4°C) in artificial seawater (ASW; same compositions as CFASW, but with 9.3 mM $CaCl_2$, pH 7.8) to obtain soluble materials. Solubilization of CRs was also facilitated by brief sonications (100 W, 15 sec, 4°C, three times) before the overnight incubation. Protein concentration of the solubilized CRs was measured as described above.

Induction of the Sperm AR with EW

Isolated T-sperm in CFASW were pelleted and resuspended in ASW. The sperm were then treated with various concentrations of EW (1–64 μg/ml) for 5 min or with 16 μg/ml EW for various time periods (0–600 sec) at room temperature to induce the AR. Alternatively, EW treated with amidino-PMSF (APMSF; a trypsin inhibitor) (APMSF-EW) or heat-inactivated EW (HI-EW) (see below) was used in place of native EW in the AR induction. Treated sperm were fixed with 4% paraformaldehyde in ASW and the percentages of unreacted (with an intact long anterior spike) and reacted (without the anterior spike) sperm were scored under a phase contrast microscope. The percentage of spontaneous AR was assessed from sperm treated with ASW. Approximately 200 sperm were counted for each data point. Each experiment was repeated at least three times with different sperm samples.

Electron Microscopy of Acrosome Intact and Reacted Sperm

Sperm were fixed with 2% glutaraldehyde and 4% paraformaledehyde in ASW (pH 7.8, 2 h, 4°C). They were then postfixed in 1% OsO_4 in ASW, dehydrated in increasing percentages of cold ethanol, and finally embedded in Spurr's resin (EMS, Fort Washington, PA). Thin sections (~70 nm) were cut and mounted on formvar-coated copper grids and counterstained with lead citrate and uranyl acetate before being viewed under an FEI Tecni-20 transmission electron microscope (FEI-USA, Hillboro, OR) at 80 kV.

Binding of Fluorescently Labeled EW to the Sperm Surface

EW was conjugated to an Alexa-488 fluorescent reactive dye (Molecular Probes, Eugene, OR) according to the manufacturer's procedures. Since EW initiated AR very rapidly (see Fig. 1C), we used aldehyde-fixed AI sperm for the EW-sperm binding experiments. T-sperm collected in CFASW were fixed with 4% paraformaldehyde in ASW (1 h, room temperature). Fixed sperm were washed twice with ASW and blocked with 4% BSA containing 0.1 M glycine in ASW (30 min, room temperature). The sperm were incubated (15 min, room temperature) with 16 μg/ml fluorescently labeled EW, washed twice (500 × *g*, 10 min) to eliminate unbound EW, plated on a slide, and topped with a coverslip before being observed under a Nikon Eclipse epifluorescent microscope equipped with a Nikon DXM 1200 CCD camera (Nikon Corp., Kanagawa, Japan). T-sperm were also incubated with Alexa-488 EW in the presence of a 50-fold unlabeled EW.

Effects of Protease Inhibitors on the EW-Induced AR

To test whether AR induction was dependent on protease activities, various concentrations of protease inhibitors (all from Sigma) were preadded to EW prior to coincubation with T-sperm resuspended in ASW. These inhibitors included the following: 1) serine protease inhibitors, PMSF (0.1–1 mM), APMSF (0.2–1 mM), soybean trypsin inhibitor (SBTI; 0.1–0.4 mM); 2) cysteine protease inhibitor, E-64 (1–100 μM); 3) aspartic protease inhibitor, pepstatin A (1–10 μM); and 4) metalloprotease inhibitor, EGTA (0.25–1 mM). The percentage of the AR response was analyzed according to the aforementioned protocol.

To determine whether EW-derived proteases, especially trypsin-like ones, were mediators of AR, HI-EW or APMSF-EW was used in place of native EW to treat sperm. HI-EW was prepared by heating EW to 100°C for 2 h, followed by freezing at −20°C overnight. The activity of this HI-EW was examined with a trypsin-specific fluorogenic substrate (as described below) in parallel with native EW. The remaining activity of HI-EW was compared with that of native EW. APMSF-EW was prepared by preincubating EW with 0.5 mM APMSF at 4°C for 2 h. The mixture was washed and concentrated (10 000 × *g*, 15–30 min, 4°C) three times with ASW through a Microcon YM-10 centrifugal device (Millipore, Bedford, MA) to remove unbound APMSF, which came down in the flow-through fraction. Native EW that washed and concentrated in a similar fashion as APMSF-EW served as an experimental sham control. The remaining activity of APMSF-EW was then determined and compared with that of the EW sham control. HI-EW, APMSF-EW, and sham-EW were used to treat the sperm in place of native EW and the number of AR sperm was scored as described above.

In an alternative experiment, sperm-borne trypsin-like enzymes of acrosome-intact (AI) sperm were inhibited with 0.4 mM membrane impermeant SBTI (15 min, room temperature). The excess amount of the inhibitor was washed from sperm by centrifugation (500 × *g*, 5 min, twice). Aliquots of this sperm suspension were then induced to undergo AR with 16 μg/ml HI-EW (5 min, room temperature), and assayed for the AR responses following the protocol described above. Another aliquot of sperm was used for trypsin-like enzyme assays at various time points after the removal of SBTI.

Enzyme Assays

Serine protease assay was performed according to the previously described method [19] with some modifications. Fluorogenic-4-methylcoumarin-7-amide (MCA) substrates were used in these assays. These included a final concentration of 20 μM of Boc-Gln-Ala-Arg-MCA (Boc = *t*-butyloxycarbonyl; Peptide Institute, Louisville, KY) for trypsin-like enzymes, and Suc-Ala-Ala-Pro-Phe-MCA (Suc = succinyl; Bachem, Torrance, CA) for chymotrypsin-like enzymes. All assays were performed at room temperature in a final volume of

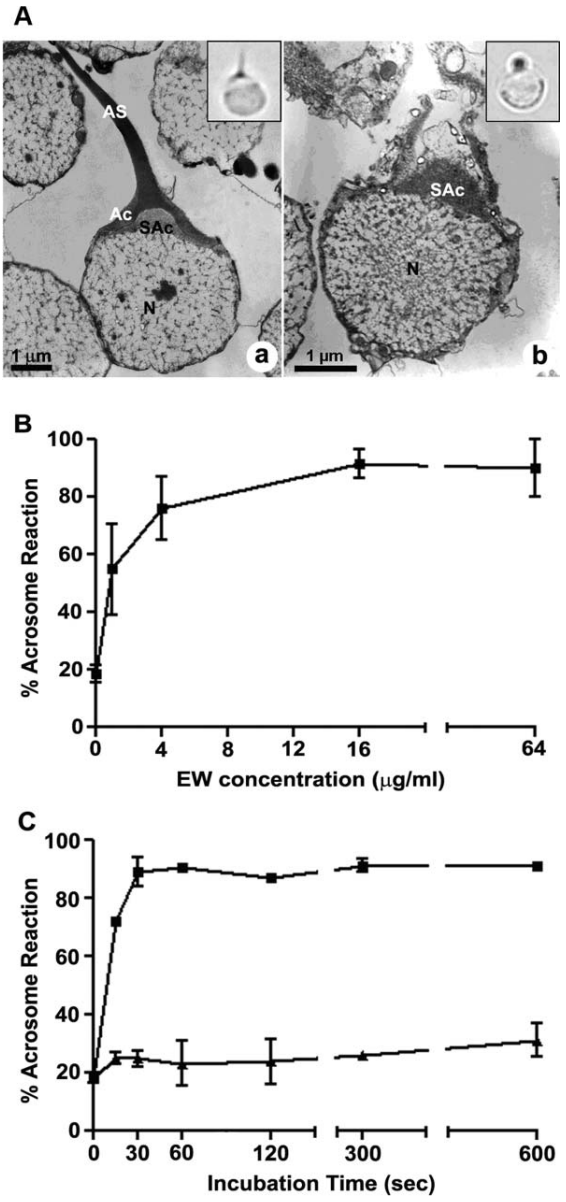


FIG. 1. **A**) Transmission electron micrographs of the AI (**a**) and AR (**b**) sperm after 5-min induction with EW. Inset in each figure represents the corresponding phase contrast micrograph. Increases in the AR responses were dependent on the concentration (**B**) of and incubation time with EW (**C**, square symbol). Triangles in **C** represent spontaneous AR when ASW was used in place of EW for sperm incubation. Data in this figure and the remainder are expressed as mean ± SD from three replicates performed on different sperm samples. Ac, Acrosome; AS, anterior spike; N, nucleus; Sac, subacrosomal region.

100 μl in a 96-well, flat-bottom black plate (Corning Inc., Corning, NY). The samples included EW-related samples (native EW, HI-EW, and APMSF-EW) and T-sperm-related samples (untreated live sperm and SBTI-treated live sperm, AR sperm, and acrosomal vesicles and content). The reaction mixture was comprised of 10 μl of each sample, 10 μl of 0.2 mM substrate solution in 10% dimethyl sulfoxide, and 80 μl of buffer A (10 mM $CaCl_2$, 0.001% Triton X-100 in 50 mM Tris-HCl, pH 7.5) for trypsin-like enzyme assay, or buffer B (10 mM $CaCl_2$ in 50 mM Tris-HCl, pH 8.0) for chymotrypsin-like enzyme assay. Fluorescent 7-amino-4-methylcoumarin (AMC), the released product from substrate hydrolysis, was monitored spectrofluorometrically at various time points with a Spectra Max Gemini XS (Molecular Dynamics, Sunnydale, CA), with excitation and emission wavelengths of 360 and 470 nm, respectively. The measured raw fluorescence units were converted to the amount of free AMC released by using an AMC standard curve. One unit of the enzyme activity was defined as a picomole of AMC released per hour at 25°C from Boc-Gln-Ala-Arg-MCA for trypsin-like activity or from Suc-Ala-Ala-Pro-Phe-MCA for chymotrypsin-like activity. Specific activity of the enzyme was defined as unit activity per microgram protein.

Characterization of a Trypsin-Like Acrosomal Enzyme by Fluorogenic Substrate in-Gel Zymography

The released acrosomal vesicles and content of *P. monodon* sperm were collected as a supernatant of T-sperm that were induced to undergo the AR by HI-EW, as described above. This AR supernatant collected from 5×10^6 sperm possessed 1500 U of trypsin like activity, when Boc-Gln-Ala-Arg-MCA was used as the substrate (see the enzyme assay method above). The supernatant of AI sperm (sham-treated with ASW) was also collected from the same number of sperm and used as a negative control; it contained only 100 U of trypsin-like activity. The zymography method described by Yasothornsrikul and Hook [20] was used to characterize the trypsin-like enzyme in the supernatant of AR sperm. An SDS-10% polyacrylamide gel was copolymerized with 200 μM Boc-Gln-Ala-Arg-MCA in 0.375 Tris-HCl, pH 8.8, and 0.4% SDS. The separation gel was allowed to polymerize in the dark at room temperature. When polymerization of the separation gel was complete, the stacking gel, consisting of 4% polyacrylamide, 0.330 mM Tris-HCl, pH 6.8, and 0.1% SDS, was cast and polymerized. Subsequently, 10 μl of the supernatant from AR or AI sperm, or purified trypsin (0.5 ng of 8000 U; Roche Applied Science, Indianapolis, IN) was mixed with 10 μl of 2× Laemmli sample loading buffer [21] without heating, and then loaded into the gel well. Electrophoresis was performed in the dark at 4°C at a constant current of 10 mA until completed. The gel was then washed in 2.5% Triton X-100 solution to remove SDS for 15 min at room temperature, followed by washing seven times in cold distilled water (5 min for each wash). The gel was subsequently incubated in trypsin zymography developing buffer (200 mM NaCl, pH 7.5, 20 mM Hepes, 10 mM $CaCl_2$ and 0.005% Triton X-100) at 37°C for 30 min. Fluorescent bands indicating trypsin activity were immediately observed and recorded with an Ultraviolet Transilluminator (Alpha Innotech Inc, San Leandro, CA).

RESULTS

Induction of the AR with EW

The morphology of the AI and AR *P. monodon* sperm are shown in Figure 1A. Transmission electron microscopy revealed the presence of electron-dense materials in the anterior spike, and moderately electron-dense materials in the acrosome and subacrosomal region of the AI sperm (Fig. 1A, a). Within 5 min of EW addition, the anterior spike completely disappeared along with the rupture of the acrosome (Fig. 1A, b). The subacrosomal region of the AR sperm became somewhat larger and more electron dense compared with that of the AI sperm (Fig. 1A, b versus Fig. 1A, a). There was no evidence for the acrosomal filament formation (as seen in *S. ingentis*) [22], even at the longer incubation time period (>10 min) (data not shown). At the light microscopic level, the disappearance of the anterior spike and the presence of dark subacrosomal materials in the AR sperm were evident. These features were thus used to differentiate between AI and reacted sperm in all experiments described below.

The ability of a natural inducer, EW, to induce the AR in *P. monodon* sperm was concentration dependent (Fig. 1B). Within 5 min of sperm treatment with 1 and 4 μg/ml EW, the AR levels were 54.9 ± 15.7% and 76.1 ± 11.0%, respectively. At 16 μg/ml of EW, the maximal AR response was reached (90.1 ± 9.9%). This EW concentration was therefore selected for all subsequent experiments. When ASW was used in place of EW, ~20% of sperm underwent spontaneous AR.

Time-dependent AR induction of *P. monodon* sperm by EW is demonstrated in Figure 1C. Within 15 sec of the EW treatment, 71.9 ± 0.9% of sperm underwent AR, whereas only 25.0 ± 2.0% of sperm treated with ASW became AR. The percentage of AR sperm increased to the maximal value of 89.3 ± 4.9% within 30 sec of EW incubation time, and remained

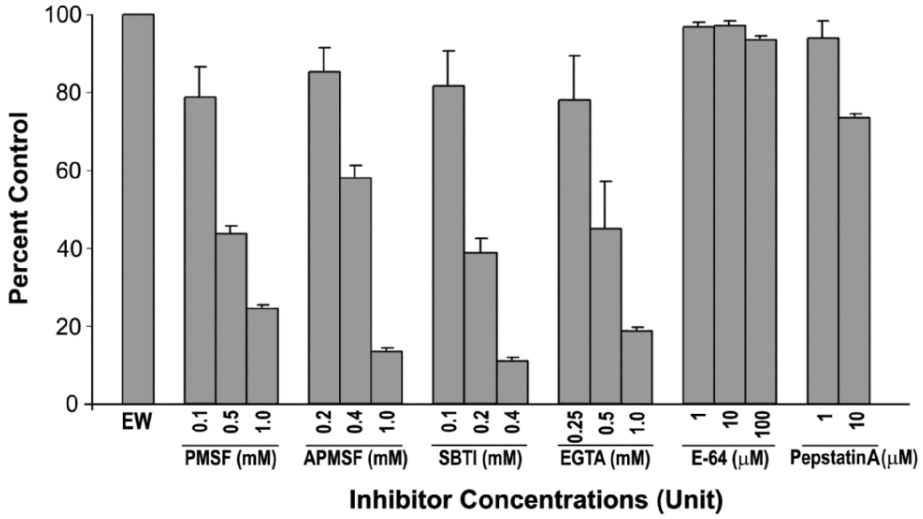


FIG. 2. Effects of various protease inhibitors on the EW-induced AR. T-sperm ($\sim 5 \times 10^5$) were incubated at room temperature with EW (16 μg/ml) in 50 μl ASW in the presence of various concentrations of different protease inhibitors (PMSF, APMSF, SBTI, EGTA, E-64, and pepstatin A). The AR levels obtained from control sperm (incubated with EW without any inhibitors) were assigned as 100%, and the AR extent of sperm incubated with EW in the presence of the protease inhibitor was expressed as percent of control. Data are expressed as mean ± SD of results of three or more replicate experiments.

constant afterwards. In contrast, the spontaneous AR rate of sperm incubated with ASW remained at ~25%–30% within 5 min of the ASW incubation. We therefore chose the 5-min incubation period for subsequent experiments.

Trypsin-Like Proteases Mediated AR Induction in Shrimp Sperm

We investigated the possible involvement of proteases in sperm AR induction. Results shown in Figure 2 indicate that inhibitors of trypsin (PMSF, APMSF, and SBTI) inhibited EW-induced AR in a dose-dependent manner. Notably, SBTI at 0.4 mM decreased EW-induced AR to only 12% of the control values. PMSF and APMSF at 1 mM also exerted marked inhibition (75%–85%) of the EW-induced AR. Inclusion of EGTA, a specific Ca^{2+} chelator and metalloprotease inhibitor, also showed a dose-dependent inhibitory effect, and, at 1.0 mM EGTA, the inhibition of the EW-induced AR was ~80%. E-64 and pepstatin A, inhibitors of cysteine and aspartic proteases, respectively, exerted no or very low inhibitory effects on sperm AR induction at all concentrations tested.

Existence of Trypsin-Like Enzymes in EW

Among serine proteases, trypsin and chymotrypsin have been shown to be significant for sperm AR induction [15, 23]. We thus investigated the existence and physiological functions of these two proteases in EW. Results in Table 1 show that EW demonstrated trypsin-like activity. It selectively hydrolyzed the trypsin-specific substrate (Boc-Gln-Ala-Arg-MCA), with a specific activity of 30.7 U/μg protein. In contrast, EW possessed minimal chymotrypsin-like activity when testing with suc-Ala-Ala-Pro-Phe-MCA as the substrate (i.e., 0.2 U/μg protein).

Further attempts were made to determine the source of trypsin-like activity in the two major components of EW, CRs, and TF. Comparatively, high trypsin-like activity (171.0 U/μg protein) was detected in TF, whereas minimal trypsin-like activity (2.4 U/μg protein) was present in isolated CRs (Table 1). These results suggest that the enzymatic activity detected in EW was mainly derived from TF.

Trypsin-Like Enzymes in EW Were Not Involved in the AR Induction

Previous evidence has indicated that EW trypsin-like enzymes mediate the AR induction in *S. ingentis* [7]. This prompted us to determine whether this mechanism also held true in *P. monodon* sperm. Activity of trypsin-like enzymes in EW was abolished by either HI-EW or APMSF-EW. The remaining trypsin-like activities of HI-EW and APMSF-EW were 1.5 and 1.9 U/μg protein, respectively, compared with that of native EW (Table 1). Surprisingly, treatment of sperm with HI-EW or APMSF-EW produced AR responses of 84% and 82%, respectively, a result that was similar to that observed in sperm treated with native EW (~90%) (Fig. 3). The percentage of spontaneous AR in these experiments was ~16%. This result indicated that trypsin-like activity involved in AR induction was not derived from EW.

Binding of EW to the Sperm Surface

Binding of the EW to the sperm surface may initiate sperm signaling events leading to the AR. Our results showed that fluorescently labeled EW bound to the entire sperm surface as well as the anterior spike (Fig. 4, a and b) in the overall sperm population. A slight difference in fluorescence intensity was noted among individual sperm. A background level of fluorescent staining was observed when an excess amount of unlabeled EW was included in the sperm-EW coincubates to compete with fluorescently labeled EW in sperm binding (Fig. 4, c and d); this indicated specific interaction of EW to the sperm surface.

Presence of Sperm Trypsin-Like Enzymes and Their Putative Roles in AR Induction

Inhibitor studies indicated the significance of trypsin-like enzymes in sperm AR induction (Fig. 2). However, since

TABLE 1. Trypsin- and chymotrypsin-like activities in egg water (EW)-related samples.

	Specific activity (units/μg protein)	
Sample	Trypsin (Boc-Gln-Ala-Arg-MCA)	Chymotrypsin (Suc-Ala-Ala-Pro-Phe-MCA)[a]
Native EW	30.7 ± 0.5	0.2 ± 0.1
Heat-inactivated EW	1.5 ± 1.9	NA
APMSF-treated EW	1.9 ± 0.1	NA
Thelycal fluid	171.0 ± 4.1	NA
Cortical rods	2.4 ± 0.1	NA

[a]NA = Data not available

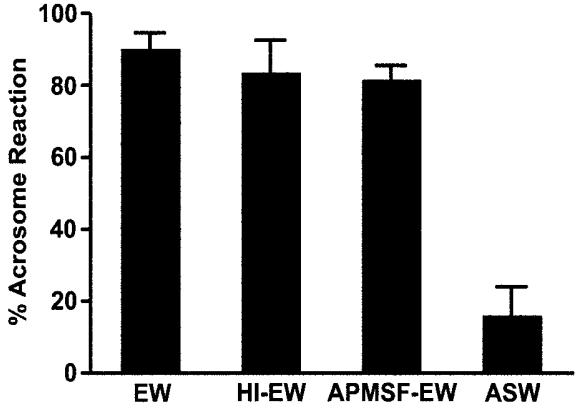


FIG. 3. EW with very low trypsin-like activity could still induce sperm AR. Native EW, HI-EW, or AMPSF-EW (see *Materials and Methods* for their preparation) was added to 50 µl T-sperm suspension (~5 × 10^5 sperm). Note that HI-EW and APMSF-EW, having very low trypsin activity (Table 1), were able to induce the AR to the same extent as native EW. Spontaneous AR was assessed in sperm exposed to ASW.

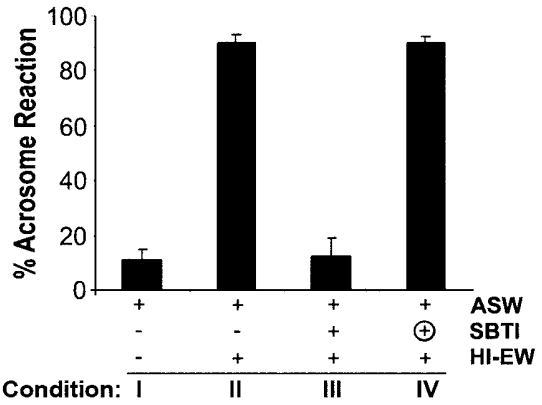


FIG. 5. Decreases in sperm surface trypsin-like activity did not affect the ability of HI-EW to induce the AR. Approximately 5 × 10^5 T-sperm in 50 µl were induced to undergo the AR by 16 µg/ml HI-EW (condition II) or ASW (condition I, control). SBTI (0.4 mM) present in the coincubate (condition III) inhibited the HI-EW-induced AR. Under condition IV, T-sperm were pretreated with cell-impermeant SBTI (denoted by the encircled "plus" symbol) to inhibit surface trypsin-like enzymes (see *Materials and Methods*) prior to incubation with HI-EW. Note that the same extent of the AR was still observed in these SBTI-pretreated sperm as that occurring in untreated sperm (condition II).

APMSF-EW and HI-EW could still induce the AR, the trypsin-like enzymes participating in the AR induction would have belonged to sperm, and they could be localized, either on the sperm surface or in the acrosome. Results show that live AI sperm did possess trypsin-like activity (77.1 ± 11.4 U/10^6 sperm), which would reflect the presence of trypsin-like enzymes on the AI sperm surface. The supernatant of AI sperm contained trypsin-like activity of only 11.8 ± 9.9 U/10^6 sperm, and this may reflect a low degree of trypsin-like enzyme release from sperm. When these live AI sperm were treated with a membrane-impermeable SBTI, the trypsin-like activity measured at 30 sec after SBTI removal was 2.2 ± 0.6 U/10^6 (Table 2), indicating the marked inhibition of SBTI on sperm surface trypsin. At 5 and 10 min after the removal of the excess amount of SBTI from sperm, the sperm surface trypsin-like activity was still relatively low (i.e., 6.8 ± 3.4 and 12.9 ± 6.0 U/10^6 sperm, respectively [<16% of the activity of untreated control sperm]). However, this enzyme activity was restored to 46.4 ± 13.8 and 71.7 ± 8.5 U/10^6 sperm 30 and 60 min post-SBTI removal, respectively (Table 2). AR sperm induced by HI-EW also possessed trypsin-like enzyme activity, but to a lesser extent than AI sperm (53.2 ± 8.5 U/10^6 sperm).

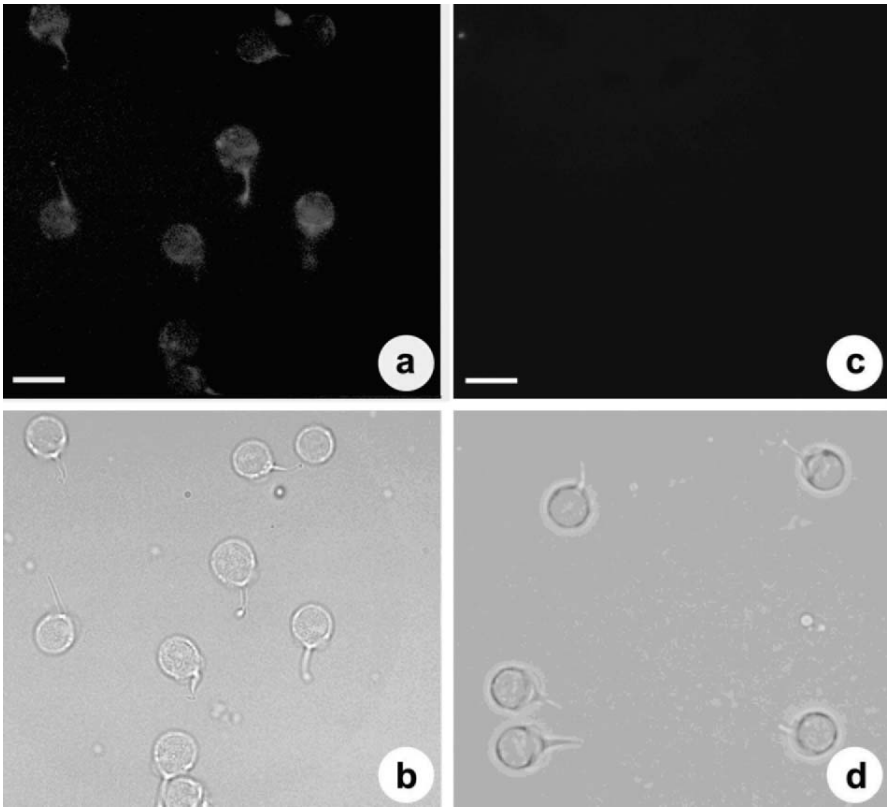


FIG. 4. Binding of Alexa-488-labeled EW to aldehyde-fixed sperm. Approximately 5 × 10^5 T-sperm in 50 µl were incubated (room temperature) with 16 µg/ml Alexa-488-labeled EW in the presence (**c** and **d**) and the absence (**a** and **b**) of 50-fold excess of unlabeled EW. **a** and **c**) Fluorescent micrographs. **b** and **d**) Corresponding phase contrast micrographs. Bars = 10 µm.

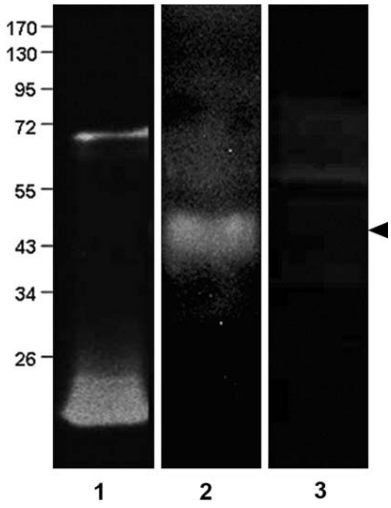


FIG. 6. Characterization of sperm acrosomal trypsin-like protease. The supernatant of 5×10^6 AR sperm containing acrosomal vesicles and content (lane 2) and the supernatant of the same number of AI sperm (lane 3), as well as 0.5 ng purified trypsin (lane 1), were subjected to fluorogenic substrate in-gel zymography with Boc-Gln-Ala-Arg-MCA as the substrate. The fluorescent bands (arrowhead) were indicative of trypsin-like activities.

However, the supernatant of these HI-EW-treated sperm (containing acrosomal vesicles and soluble content) showed a significant level of trypsin-like activity (84.0 ± 27.9 U/10^6 sperm).

To determine which trypsin-like enzymes (i.e., those at the sperm surface versus those in the acrosome) were significant for AR induction, the sperm surface enzymes were inhibited by pretreating AI live sperm with 0.4 mM of cell-impermeant SBTI. These SBTI-treated sperm still contained low surface trypsin activity within 5–10 min after SBTI removal by centrifugation (Table 2). Significantly, the SBTI-pretreated sperm were still responsive to HI-EW following 5-min exposure to this inducer; 88.3% of these sperm underwent AR (Fig. 5, fourth bar), a rate that was comparable to that observed with untreated sperm incubated with either HI-EW or native EW (Fig. 5, second bar; Fig. 3, first bar). However, when SBTI was present throughout the HI-EW-sperm coincubation, the AR rate was only ~12%, similar to the spontaneous AR rate (Fig. 5, first and third bars). All of these results suggest that the sperm surface trypsin-like enzymes may not be essential for the AR induction. Instead, the trypsin-like enzyme(s) in the acrosome would play a more pertinent role in inducing AR in *P. monodon* sperm.

TABLE 2. Recovery of trypsin-like activities of SBTI-pretreated acrosome intact sperm.

Time after SBTI removal (min)	Activities (units/10^6 sperm)
0.5	2.2 ± 0.6
5	6.8 ± 3.4
10	12.9 ± 6.0
30	46.4 ± 13.8
60	71.7 ± 8.5

To further characterize the trypsin-like enzyme(s) in the acrosome, the supernatant of the HI-EW-treated sperm, containing the acrosomal vesicles and soluble content, was subjected to fluorogenic substrate in-gel zymography. Figure 6 indicates that this supernatant generated a major fluorescent band (indicating the presence of a trypsin-like activity) of a 45-kDa molecular mass. As expected, purified trypsin generated a major fluorescent band at 21 kDa and a minor fluorescent band at 69 kDa (possibly due to the polymerization of the enzyme). In contrast, the supernatant of the AI sperm treated with ASW showed no fluorescent bands in the zymogram (Fig. 6).

DISCUSSION

We report here that the AR induction in *P. monodon* sperm involved EW binding and enzymatic action of sperm trypsin-like enzymes. In spite of an extremely short period of AR in this species, two morphological changes—spike depolymerization and the rupture of the acrosome (Fig. 1A)—were recognized and, therefore, used as criteria for determining a complete AR in *P. monodon*. Serine proteases, particularly trypsin- and chymotrypsin-like enzymes, have been shown to play significant roles in sperm AR induction [15, 23]. In this study, we also demonstrated the physiological relevance of trypsin-like proteases in this process in *P. monodon* sperm (Fig. 2). This was deduced from our results showing that the EW-induced AR was inhibited by trypsin inhibitors (APMSF, PMSF, and SBTI). We used fluorogenic substrates specific for trypsin and chymotrypsin to show that *P. monodon* sperm and their acrosomal vesicles and content contained substantial levels of trypsin-like activity, but minimal amounts of chymotrypsin-like activity. The results of inhibitor studies suggest that metalloproteases (an inhibitor of which is EGTA) may also be important for sperm AR induction. However, this

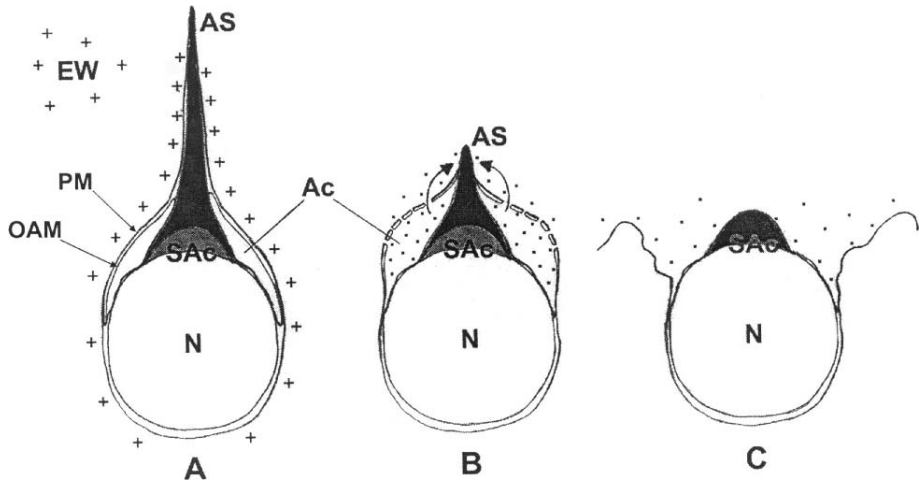


FIG. 7. Pictorial diagram postulating the temporal events of the EW-induced AR in *P. monodon*. **A**) Components in EW (+) initially bind to the sperm surface. This binding may trigger the fusion of the sperm plasma membrane (PM) and the outer acrosomal membrane (OAM), creating pores on the membrane overlying the acrosome (Ac). This would lead to a leakage of trypsin-like enzymes (dots) from the sperm acrosome. Depolymerization of the anterior spike (AS) may then occur due to the hydrolytic activity of the released trypsin-like enzymes (**B**). Shortly afterwards, the anterior spike was completely depolymerized along with the rupturing of the entire acrosome (**C**). N, Nucleus; Sac, subacromal region.

inhibition can also be due to the effect of EGTA on chelating extracellular calcium, the role of which during the AR process has been extensively documented [22, 24].

The significance of trypsin-like proteases in AR induction has long been reported in many invertebrates, including sea urchins [15] and the penaeoid shrimp, *S. ingentis* [7, 14]. However, the mechanisms of these enzymes in the AR response in the two shrimp species, *S. ingentis* and *P. monodon*, are dissimilar. The proteolytic activity in *S. ingentis* specifically mediates the acrosomal filament formation [7, 14]. This mechanism does not apply to *P. monodon* sperm, since such a morphological change does not occur in sperm undergoing the AR in this species. EW trypsin-like proteases of *S. ingentis* is involved in the AR induction, whereas EW trypsin-like enzymes of *P. monodon* appear to be unimportant for this event. This observation stems from the fact that denatured EW (HI-EW) or APMSF-EW was still capable of inducing AR responses to a similar extent to that of native EW (Fig. 3). Therefore, trypsin-like proteases essential for the AR induction in *P. monodon* likely belonged to sperm. We provide the results here indicating that trypsin-like enzymes existed both on the sperm surface and in the acrosome, the latter of which was revealed as a 45-kDa band in the zymogram (Fig. 6).

Our results also revealed that sperm AR was inhibited when SBTI was present throughout sperm-EW coincubates (Figs. 2 and 5), while the AR was still inducible with 5-min exposure of SBTI-treated sperm with HI-EW (Fig. 5). Since the surface of SBTI-pretreated sperm contained only minimal levels of trypsin-like activity within 5–10 min after SBTI removal (Table 2), our AR results shown in Figure 5 (condition IV) suggest that the sperm surface trypsin activity might not be essential for AR induction (Fig. 5). Rather, the trypsin-like activity in the acrosomal vesicles/content may be more pertinent for sperm AR in *P. monodon* shrimp. In fact, the presence of a 45-kDa trypsin-like enzyme was observed in this study (Fig. 6). In the cases in which PMSF and APMSF were used for incubation with sperm, these cell-permeant inhibitors could readily reach the acrosome and inhibit the trypsin-like activity in this organelle. However, for the sperm incubation with SBTI, it would reach the trypsin-like enzyme(s) in the acrosome once pores on the sperm surface membranes were formed via fusion between the sperm plasma membrane and the outer acrosomal membrane at the onset of AR. Our results also suggest that the participation of these acrosomal trypsin enzymes in AR events was downstream of the initial interaction between the EW and the sperm head plasma membrane, which may lead to the fusion between the sperm plasma membrane and outer acrosomal membrane. This would allow the release of the acrosomal trypsin-like enzyme, which might be responsible for the digestion of the sperm anterior spike. Our ongoing work involves the purification and proteomic analyses of this acrosomal 45-kDa trypsin-like protease. We intend to discern its peptide sequence which will then be comapred with that of acrosomal trypsin-like enzymes of invertebrate animals (ascidians [16] and abalones [25]), known to be involved in enzymatic and nonenzymatic egg coat digestion, respectively. In addition, comparison will be made with acrosin and testis serine protease 5, two well-characterized serine proteases in the mammalian sperm acrosome that are believed to engage in sperm acrosomal matrix dispersion and zona pellucida digestion, respectively [26, 27].

Recently, sperm proteasomes have been shown to be involved in egg jelly-induced AR [28, 29] and vitelline layer hydrolysis [29] in sea urchins. Proteasomes have also been found in mammalian sperm, and play similar roles in AR induction, as observed in sea urchin gametes and in sperm-zona pellucida interaction [30, 31]. The 26S proteasome is a large protein complex, consisting of a 19S regulatory particle and a 20S core particle. Based on their substrate specificity, three threonine proteases, present in the latter particle, are categorized to be trypsin-like, chymotrypsin-like, and peptidyl-glutamyl peptide hydrolyzing enzymes. The confinement of these three different enzymes within the 20S particle may accelerate the hydrolysis of their common substrates, which are usually ubiquitinated [32]. While it is tempting to speculate that the trypsin-like enzyme found in the acrosome of *P. monodon* sperm may be a component of proteosomes, evidence available so far argues against this possibility. First, the molecular masses of proteases in the 20S proteasome particle are usually in the range of 20–30 kDa [33]. Second, our unpublished results also revealed relatively low chymotrypsin-like activity, both in the acrosome and on the sperm surface of this shrimp species. Experiments are ongoing in our laboratory to determine whether the 20S α subunits of the proteasome exist in the sperm lysate of *P. monodon*.

Despite the deficit in proteolytic activity, HI-EW still possessed high competency in inducing AR (Fig. 3). The initial step of the AR induction was likely dependent on the direct interaction of EW components with sperm (Fig. 4). These EW constituents were derived from TF and egg components, including the egg jelly (originated from the CR precursor upon spawning [34, 35]) and the egg VE. Both the egg jelly in echinoderms [36–38] and VE in shrimp [39, 40] have been known to engage in AR induction, presumably through their binding to the sperm surface. Since *P. monodon* sperm that were stored in the thelycum and continuously exposed to TF (T-sperm) only had a minimal level of spontaneous AR (as described previously here), EW components from the CR and VE may be of greater importance in the sperm binding that leads to AR induction.

The significance of EW components and sperm acrosomal trypsin-like proteases in the acrosomal exocytosis in *P. monodon* is summarized pictorially in Figure 7. Initially, EW components bind specifically to the sperm membrane receptors (Fig. 7A). This ligand-receptor binding would likely induce the downstream signaling events that lead to the fusion of the sperm plasma membrane and the acrosomal membrane. The acrosomal trypsin-like enzymes that are then released through the membrane pores may be responsible for dissociating the sperm anterior spike (Fig. 7B). Subsequently, the acrosome is completely ruptured, leaving a dense spherical mass lying in place of the anterior spike against the nuclear pole of the AR sperm (Fig. 7C). Whether the dense spherical material is analogous to the acrosomal filament of *S. ingentis*, or a protease-resistant remnant of the depolymerized spike, is currently under investigation.

ACKNOWLEDGMENTS

The authors would like to thank Dr. Athula Wikramanayake for his valuable comments and proof reading of this manuscript, and Dr. Boonyarath Pratoomchat, Department of Aquatic Science, Faculty of Science, Buraphar University, for kindly providing shrimp samples.

REFERENCES

1. Clark WH Jr, Yudin AI, Griffin FJ, Shigekawa K. The control of gamete activation and fertilization in the marine penaeidae, *Sicyonia ingentis*. In: Engels W (ed.), Advances in Invertebrate Reproduction, 3rd ed. Amsterdam: Elsevier Science Publishers; 1984:459–472.
2. Alfaro J, Munoz N, Vargas M, Komen J. Induction of sperm activation in open and closed thelycum penaeoid shrimps. Aquaculture 2003; 216:371–381.

3. Vanichviriyakit R, Kruevaisayawan H, Weerachatyanukul W, Tawipreeda P, Withyachumnarnkul B, Pratoomchat B, Chavadej J, Sobhon P. Molecular modification of *Penaeus monodon* sperm in female thelycum and its consequent responses. Mol Reprod Dev 2004; 69:356–363.
4. Kleve MG, Yudin AI, Clark WH Jr. Fine structure of the unistellate sperm of the shrimp, *Sicyonia ingentis* (Natantia). Tissue Cell 1980; 12:29–45.
5. Clark WH Jr, Kleve MG, Yudin AI. An acrosome reaction in natantian sperm. J Exp Zool 1981; 218:279–291.
6. Griffin FJ, Shigekawa K, Clark WH Jr. Formation and structure of the acrosomal filament in the sperm of *Sicyonia ingentis*. J Exp Zool 1988; 246:94–102.
7. Griffin FJ, Clark WH Jr. Induction of acrosomal filament formation in the sperm of *Sicyonia ingentis*. J Exp Zool 1990; 254:296–304.
8. Clark WH Jr, Griffin FJ. Acquisition and manipulation of penaeoidean gametes. In: McVew J (ed.), Handbook of Techniques for Crustacean Aquaculture, vol. 1, 2nd ed. Boca Raton: CRC Press; 1993:133–152.
9. Pongtippatee-Taweepreda P, Chavadaj J, Plodpai P, Pratoomchart B, Sobhon P, Weerachatyanukul W, Withyachumnarnkul B. Egg activation in the black tiger shrimp *Penaeus monodon*. Aquaculture 2004; 234:183–198.
10. Griffin FJ, Clark WH Jr, Crowe JH, Crowe LM. Intracellular pH decreases during the in vitro induction of the acrosome reaction in the sperm of *Sicyonia ingentis*. Biol Bull 1987; 173:311–323.
11. Dan JC. Studies on the acrosome. I. Reaction to egg-water and other stimuli. Biol Bull 1952; 103:54–66.
12. Afzelius BA, Murray A. The acrosomal reaction of spermatozoa during fertilization or treatment with egg water. Exp Cell Res 1957; 12:325–337.
13. Cherr GN, Clark WH Jr. An egg envelope component induces the acrosome reaction in sturgeon sperm. J Exp Zool 1985; 234:75–85.
14. Lindsay LL, Clark WH Jr. Protease-induced formation of the sperm acrosomal filament. Develop Growth Differ 1992; 34:189–197.
15. Levine AE, Walsh KA. Involvement of an acrosin-like enzyme in the acrosome reaction of sea urchin sperm. Dev Biol 1979; 72:126–137.
16. Sawada H. Ascidian sperm lysin system. Zoolog Sci 2002; 19:139–151.
17. Bradford MM. A rapid and sensitive method for the quantitation of microgram quantities of protein utilizing the principle of protein-dye binding. Anal Biochem 1976; 72:248–254.
18. Lynn JW, Clark WH Jr. Physiological and biochemical investigations of the egg jelly release in *Penaeus aztecus*. Biol Bull 1987; 173:451–460.
19. Zimmerman M, Ashe B, Yurewicz EC, Patel G. Sensitive assays for trypsin, elastase, and chymotrypsin using new fluorogenic substrates. Anal Biochem 1977; 78:47–51.
20. Yasothornsrikul S, Hook VY. Detection of proteolytic activity by fluorescent zymogram in-gel assays. Biotechniques 2000; 28:1166–1168,1170,1172–1163.
21. Laemmli UK. Cleavage of structural proteins during the assembly of the head of bacteriophage T4. Nature 1970; 227:680–685.
22. Clark WH Jr, Griffin FJ. The morphology and physiology of the acrosome reaction in the sperm of the decapod, *Sicyonia ingentis*. Develop Growth Differ 1988; 30:451–462.
23. Morales P, Socias T, Cortez J, Llanos MN. Evidences for the presence of chymotrypsin-like activity in human spermatozoa with a role in the acrosome reaction. Mol Reprod Dev 1994; 38:222–230.
24. Collins F, Epel D. The role of calcium ions in the acrosome reaction of sea urchin sperm: regulation of exocytosis. Exp Cell Res 1977; 106:211–222.
25. Lewis CA, Talbot CF, Vacquier VD. A protein from abalone sperm dissolves the egg vitelline layer by a nonenzymatic mechanism. Dev Biol 1982; 92:227–239.
26. Yamagata K, Murayama K, Okabe M, Toshimori K, Nakanishi T, Kashiwabara S, Baba T. Acrosin accelerates the dispersal of sperm acrosomal proteins during acrosome reaction. J Biol Chem 1998; 273: 10470–10474.
27. Honda A, Yamagata K, Sugiura S, Watanabe K, Baba T. A mouse serine protease TESP5 is selectively included into lipid rafts of sperm membrane presumably as a glycosylphosphatidylinositol-anchored protein. J Biol Chem 2002; 277:16976–16984.
28. Matsumura K, Aketa K. Proteasome (multicatalytic proteinase) of sea urchin sperm and its possible participation in the acrosome reaction. Mol Reprod Dev 1991; 29:189–199.
29. Yokota Y, Sawada H. Sperm proteasomes are responsible for the acrosome reaction and sperm penetration of the vitelline envelope during fertilization of the sea urchin *Pseudocentrotus depressus*. Dev Biol 2007; 308:222–231.
30. Pasten C, Morale P, Kong M. Role of sperm proteasome during fertilization and gamete interaction in the mouse. Mol Reprod Dev 2005; 71:209–219.
31. Sutovsky P, Manandhar G, McCauley TC, Caamaño JN, Sutovsky M, Thompson WE, Day BN. Proteasomal interference prevents zona pellucida penetration and fertilization in mammals. Biol Reprod 2004; 71:1625–1637.
32. Carrard G, Bulteau AL, Petropoulos I, Friguet B. Impairment of proteasome structure and function in aging. Int J Biochem Cell Biol 2002; 34:1461–1474.
33. Heinemeyer W, Fischer M, Krimmer T, Stachon U, Wolf DH. The active sites of the eukaryotic 20S proteasome and their involvement in subunit precursor processing. J Biol Chem 1997; 272:25200–25209.
34. Bradfield JY, Berlin RL, Rankin SM, Keeley LL. Cloned cDNA and antibody for an ovarian cortical granule polypeptide of the shrimp *Penaeus vannamei*. Biol Bull 1989; 177:344–349.
35. Clark WH Jr, Yudin AI, Lynn JW, Griffin FJ, Pillai MC. Jelly layer formation in Penaeoidean shrimp eggs. Biol Bull 1990; 178:295–299.
36. Alves AP, Mulloy B, Diniz JA, Mourao PA. Sulfated polysaccharides from the egg jelly layer are species-specific inducers of acrosomal reaction in sperm of sea urchins. J Biol Chem 1997; 272:6965–6971.
37. Alves AP, Mulloy B, Moy GW, Vacquier VD, Mourao PA. Females of the sea urchin *Strongylocentrotus purpuratus* differ in the structures of their egg jelly sulfated fucans. Glycobiology 1998; 8:939–946.
38. Vilela-Silva AC, Castro MO, Valente AP, Biermann CH, Mourao PA. Sulfated fucans from the egg jellies of the closely related sea urchins *Strongylocentrotus droebachiensis* and *Strongylocentrotus pallidus* ensure species-specific fertilization. J Biol Chem 2002; 277:379–387.
39. Clark WH Jr, Griffin FJ, Wikramanayake AH. Prefusion events of sperm-oocyte interaction in the marine shrimp, *Sicyonia ingentis*. Semin Dev Biol 1994; 5:225–231.
40. Wikramanayake AH, Clark WH Jr. Two extracellular matrices from oocytes of the marine shrimp *Sicyonia ingentis* that independently mediate only primary or secondary sperm binding. Dev Growth Differ 1994; 36:89–101.

General and Comparative Endocrinology 158 (2008) 250–258

Contents lists available at ScienceDirect

General and Comparative Endocrinology

journal homepage: www.elsevier.com/locate/ygcen

Changes in the levels of serotonin and dopamine in the central nervous system and ovary, and their possible roles in the ovarian development in the giant freshwater prawn, *Macrobrachium rosenbergii*

Yotsawan Tinikul [a], A. Joffre Mercier [b], Nantawan Soonklang [a], Prasert Sobhon [a,*]

[a] Department of Anatomy, Faculty of Science, Mahidol University, Rama VI Road, Ratchathewi, Bangkok 10400, Thailand
[b] Department of Biological Sciences, Brock University, St. Catharines, Ont., Canada L2S 3A1

ARTICLE INFO

Article history:
Received 8 May 2008
Revised 14 July 2008
Accepted 22 July 2008
Available online 5 August 2008

Keywords:
Macrobrachium rosenbergii
Serotonin
Dopamine
HPLC
CNS
Ovary
Vitellin

ABSTRACT

Serotonin or 5-hydroxytryptamine (5-HT) and dopamine (DA) are the two key neurotransmitters that control gonadal development in decapod crustaceans. This study investigated changes in the levels of 5-HT and DA in the CNS and ovary during different phases of the ovarian cycle of the freshwater prawn, *Macrobrachium rosenbergii*. The levels of 5-HT and DA were quantified by using High Performance Liquid Chromatography with electrochemical detection (HPLC-ECD). Moreover, changes of vitellogenin (Vg) concentrations in the hemolymph after treatment with 5-HT and DA (at doses of 2.5×10^{-6} and 2.5×10^{-7} mol per prawn) were also examined. 5-HT exhibited a gradual increase in concentration in the brain and thoracic ganglia from ovarian stage I (0.12 ± 0.01 nmol/mg, 0.22 ± 0.01 nmol/mg, respectively) to reach a maximum (0.66 ± 0.03 nmol/mg, 1.48 ± 0.03 nmol/mg, respectively) at ovarian stage IV. In contrast, DA in the brain and thoracic ganglia showed the highest concentrations at ovarian stage II (0.20 ± 0.01 nmol/mg, 1.27 ± 0.06 nmol/mg, respectively) and then decreased to the lowest concentrations (0.06 ± 0.01 nmol/mg, 0.28 ± 0.04 nmol/mg, respectively) at ovarian stage IV. The ovarian concentration of 5-HT was 0.53 ± 0.11 nmol/mg at ovarian stage I and gradually increased to 1.63 ± 0.16 nmol/mg at ovarian stage IV. In contrast, the concentration of DA was highest at ovarian stage I (29.05 ± 1.31 nmol/mg), and lowest at the ovarian stage IV (11.43 ± 0.74 nmol/mg). Injecting 5-HT into prawns significantly increased Vg concentration in the hemolymph at ovarian stage IV compared to control groups, and injecting DA into prawns had the opposite effect. The inverse relationship between 5-HT and DA levels in neural ganglia and ovaries, and their opposing effects on hemolymph Vg levels suggest that these two transmitters play opposite regulatory roles in controlling ovarian maturation and oocyte development in this species.

© 2008 Elsevier Inc. All rights reserved.

1. Introduction

The giant freshwater prawn, *Macrobrachium rosenbergii*, is an important food source that is cultured in Thailand and other Asian countries (Sandifer and Smith, 1985). Reproduction of this as well as other decapod crustaceans is regulated by various neurohormones that are synthesized and released from the X-organ–sinus gland complex located in the eyestalks (Chen et al., 2003). The synthesis and release of these neurohormones are believed to be regulated by biogenic amines (Ridchardson et al., 1991), particularly 5-HT and DA that are present in the CNS of these crustaceans (Kerkut et al., 1966; Butler and Fingerman, 1983; Laxmyr, 1984; Fingerman et al., 1994). Several previous studies have reported a stimulatory effect of 5-HT on gonadal maturation in some decapods, including *Procambarus clarkii* (Kulkarni et al., 1992), *Penaeus monodon* (Wongprasert et al., 2006), and *M. rosenbergii* (Meeratana et al., 2006). It was suggested that 5-HT stimulates gonadal maturation by inhibiting the release of gonad-inhibiting hormone (GIH) and/or by enhancing the release of gonad-stimulating hormone (GSH), whereas DA plays the opposite role (Sarojini et al., 1995; Fingerman, 1997). 5-HT and the rate limiting enzymes (tryptophan hydroxylase and 5-hydroxy-L-tryptophan decarboxylase) involved in its synthesis were found at measurable levels in several regions of the CNS of a crustacean, *Panulirus homarus* (Kirubagaran et al., 2005). Moreover, 5-HT and DA have been detected by HPLC in various regions of the CNS of *Pacifastacus leniusculus* (Elofsson et al., 1982; Laxmyr, 1984), the eyestalks of *P. clarkii* (Alvarez et al., 2005), and the intestinal nerve of *P. clarkii* (Mercier et al., 1991). Major tissues that exhibited a high level of 5-HT are the optic ganglion, cerebral ganglion, circumoesophageal connectives, stomatogastric ganglion, and thoracic ganglia (Aramant and Elofsson, 1976; Beltz et al., 1984). However, quantification of the levels of these two neurotransmitters in correlation with different phases of the

* Corresponding author. Fax: +66 2 354 7168.
E-mail addresses: scpso@mahidol.ac.th, anatch2002@yahoo.com (P. Sobhon).

0016-6480/$ - see front matter © 2008 Elsevier Inc. All rights reserved.
doi:10.1016/j.ygcen.2008.07.009

decapod crustacean ovarian cycle has not yet been performed. In this study, we have investigated changes in 5-HT and DA concentrations in various parts of the CNS and the ovary during various phases of the ovarian maturation in *M. rosenbergii*. Moreover, hemolymph vitellogenin (Vg) concentrations were also determined during various phases of ovarian cycle following the treatments with 5-HT and DA in order to assess possible effects of these two neurotransmitters on ovarian maturation more directly.

2. Materials and methods

2.1. Experimental animals

Mature female freshwater prawns (each weighing on average about 30.88 ± 3.6 g) were obtained from commercial farms in Chonburi Province, Thailand. The animals were kept in outdoor circular concrete tanks, each with 1.50 m diameter with the water depth at 0.80 m, and about 30% of water changed every 2 days. The prawns were fed commercial food pellets twice per day. Aeration was given all day. Small plastic cages were added in every tank (30 per tank) for molting animals to hide in and avoid being killed from the cannibalistic behavior of this species. The prawns were acclimatized under a photoperiod of 12:12 h light–dark for two weeks before beginning the experiments.

2.2. Determination of ovarian stages

The changing phases of the ovarian cycle in female broodstock could be observed directly and classified into five stages based on the size, color, and histology of the ovary as reported by Chang and Shih (1995) and Meeratana and Sobhon (2007). Stages 0 and I were spawn and spent phases, respectively, when the ovaries appeared white and indistinct when observed through the carapace (Fig. 1A).[1] In stage II (proliferative) a small yellow mass of ovary could be observed dorsally under the carapace (Fig. 1B). In stage III (premature), the ovary became orange (Fig. 1C). In stage IV (mature), the reddish-orange ovary extended from behind the eye posteriorly to the first abdominal segment (Fig. 1D). These ovarian stages were confirmed by histological study (Fig. 1E–H) based on the criteria described by Meeratana and Sobhon (2007).

2.3. Chemicals and standard solutions

5-HT, DA, and all other chemicals used in the experiments were obtained from Sigma Chemical Co. (St. Louis, MO, USA). Standard solutions were freshly prepared by dissolving 5-HT and DA in ice-cold 0.1 M perchloric acid on the day of analysis and were stored in ice between injections onto the HPLC system.

2.4. Sample preparations

The brain (supraesophageal ganglion), the five thoracic ganglia (combined), the six abdominal ganglia (combined), and the ovaries were collected at mid-day from ten animals at each ovarian stage (as defined by Meeratana and Sobhon, 2007). Each organ was carefully dissected, and its wet mass was weighed. Samples were placed in 50 μl 0.1 M perchloric acid. The mixture was then sonicated and centrifuged at 14,000*g* at 4 °C. The supernatants were then collected and filtered through a 0.22 μm Spin-x centrifugal filter tube before injection onto the HPLC column. Detection and quantification of 5-HT and DA in the CNS and ovaries were performed by using High Performance Liquid Chromatography with electrochemical detection (HPLC-ECD). The average concentrations of 5-HT and DA were estimated in four replicates.

2.5. Quantification of 5-HT and DA by HPLC

HPLC method used in this study was adapted from Mercier et al. (1991) and Molaei and Lange (2003). Each tissue sample was dissected, weighed and placed in 50 μl of 0.1 M perchloric acid and was prepared as described above (Section 2.4). Supernatants from the extracts were injected onto a Brownlee C_{18}-Aquapore OD-300 HPLC column (250 × 4.6 mm i.d.). 5-HT and DA were detected electrochemically using a completely isocratic mode for the determination of the neurotransmitters. A glassy carbon electrode served as the working electrode and was used with an Ag/AgCl reference electrode. The detector potential was set at +0.8 V versus an Ag/AgCl reference electrode. The sensitivity of the detector was maintained at 100 nA with full scale deflection. The mobile phase consisted of 75 mM NaH_2PO_4, 0.3 mM sodium octylsulphate, 50 μM EDTA, 2.5% acetonitrile, and 4% methanol. The pH was adjusted to 2.75 with orthophosphoric acid. The flow rate was kept constant at 0.7 ml/min. The mixture was sonicated, centrifuged at 14,000*g* at 4 °C. The supernatants were collected and then filtered through a 0.22 μm Spin-x centrifugal filter tube before injection. Samples were injected into a 20 μl injection loop. The signals from the electrochemical detector were recorded and integrated using data analysis software (Millennium, Waters). 5-HT and DA levels were quantified using the external standard method. Peaks corresponding to 5-HT and DA were detected in the extracts at the same elution times as their corresponding standards. The identities of the peaks in each sample were further verified by spiking the tissue extracts with known amounts of 5-HT and DA standards. All samples were freshly prepared and analyzed within the same day. The Bio-Rad (Mississauga, Canada) Protein Assay System was employed for protein determination in the extracts according to Bradford (1976).

2.6. Effects of 5-HT and DA on Vg levels

Female prawns at ovarian stage I were divided into six groups (four experimental groups and two control groups) of 28 animals each. Prawns in the experimental groups were injected with 5-HT at doses of 2.5×10^{-6}, 2.5×10^{-7} mol of 5-HT/prawn or DA at doses of 2.5×10^{-6}, 2.5×10^{-7} mol of DA/prawn. 5-HT and DA were dissolved in crustacean physiological saline (CPS) containing the following: NaCl 29 g, KCl 0.71 g, $CaCl_2 \cdot 2H_2O$ 2.38 g, $MgSO_4 \cdot 7H_2O$ 3.16 g, $NaHCO_3$ 0.5 g, $MgCl_2 \cdot 6H_2O$ 0.17 g, HEPES 4.76 g in 1 l of distilled water. The injected volumes of 5-HT and DA were 0.10 ml. All prawns tolerated the injected doses of neurotransmitters without showing any abnormal behavior. All injections were performed at 4-day intervals, covering a period of 49 days. The effects of the neurotransmitter-treated groups were compared with two control groups of 28 animals each. In the first control group, the animals were untreated and served as a negative control (NC). The second control group was a vehicle-injected control (VIC) in which each animal was injected with 0.1 ml of CPS. Animals in each group were identified by tying plastic loops of different colors around the eyestalk. The injections were performed by intramuscular route at the lateral aspect of the second abdominal segment by using a 1 ml syringe (NIPRO) fitted with 26G $\times\frac{1}{2}$" (0.45 × 12 mm) thin-wall needles (NIPRO). The weight and total length of the prawns were measured on every treatment day, before injection. The total length was evaluated from the base of eyestalk to the telson (Eyestalk base-telson length, EBTL).

The hemolymph of treated and control prawns was collected from the substernal hemolymph sinus at 4-day intervals. Each

[1] For interpretation of color mentioned in this figure the reader is referred to the web version of the article.

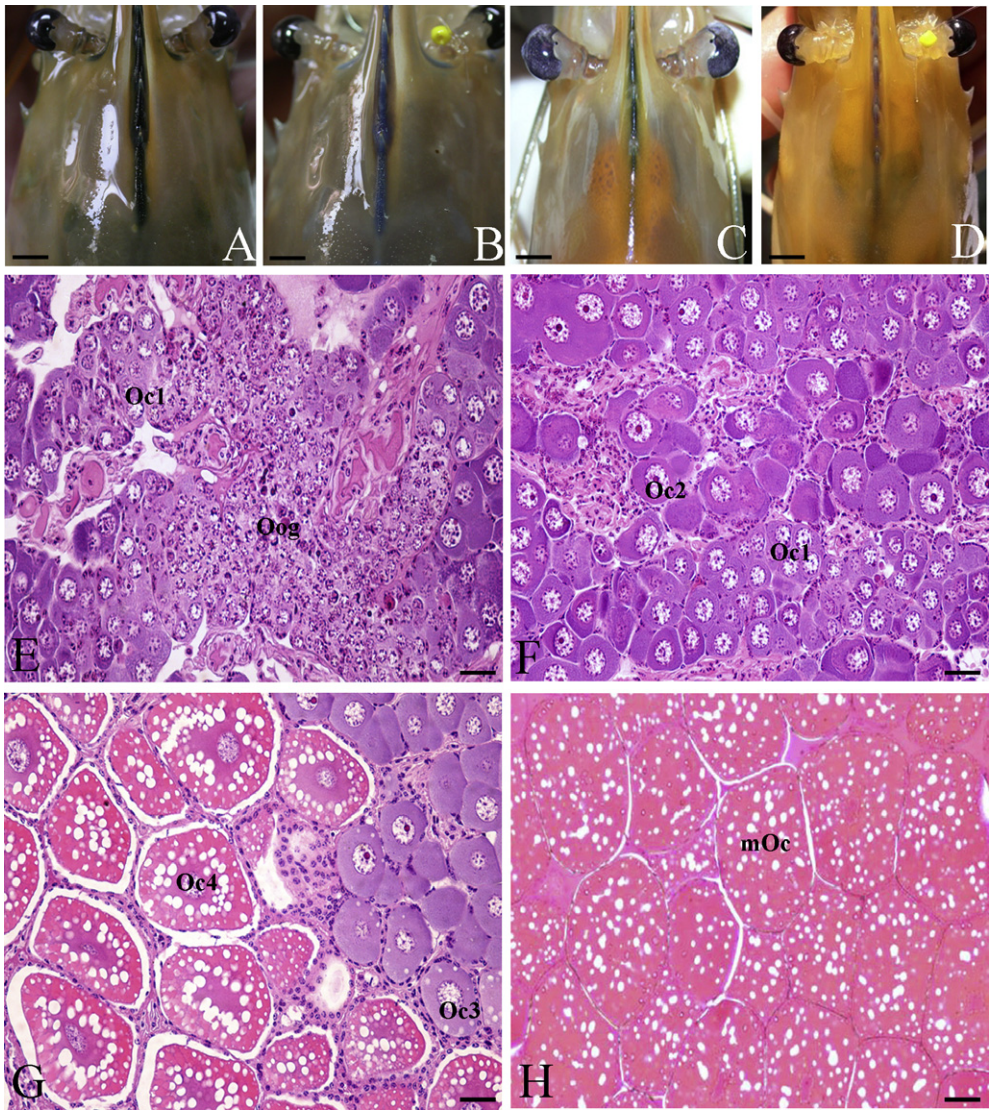


Fig. 1. Top views of female giant freshwater prawn, *M. rosenbergii*, showing ovary at various stages: (A) stage I, (B) stage II, (C) stage III, (D) stage IV. (E–H) Light micrographs of H&E-stained ovarian sections showing histology of various stages of ovarian cycle (I–IV) and steps of oocyte development. Oog, oogonia; Oc1, early previtellogenic oocyte; Oc2, late previtellogenic oocytes; Oc3, early vitellogenic oocytes; Oc4, late vitellogenic oocytes; mOc, mature oocytes (classified according to Meeratana and Sobhon 2007). Scale bars = 1 cm (A–D). Scale bars = 50 μm (E–H).

100 μl sample of hemolymph was mixed together with 100 μl of anticoagulant (containing 0.45 M NaCl, 0.1 M glucose, 30 mM sodium citrate, 26 mM citric acid, 20 mM EDTA in distilled water, pH 4.5; Kwok and Tobe, 2006). The sample was then centrifuged at 2000 rpm at 4 °C, for 10 min. The supernatants were collected and then stored at −80 °C until Vg assays.

2.6.1. Production of anti-vitellin antibody and Enzyme-Linked Immunosorbent Assay (ELISA) to determine the hemolymph vitellogenin (Vg) levels

The anti-vitellin antibody was prepared according to Chen and Kuo (1998). Briefly, frozen ovarian samples were homogenized and centrifuged. The supernatant was concentrated by concentrator (Centreprep-30, Amicon Inc., USA), and then vitellin protein was fractionated by HPLC using UV-detector, and further concentrated by ultrafiltration. The purity of vitellin was then determined using polyacrylamide gel electrophoresis. A 250 μg of purified vitellin was further dissolved in 300 μl of 0.1 M PBS, emulsified with an equal volume of Freund's adjuvant and injected into each of the two New Zealand white rabbits (purchased from the Animal Care Unit, Mahidol University with the approval of the Animal Ethics Committee). The titers of the rabbit immune sera were determined by ELISA following the standard protocol. Serum providing high titer was used in ELISA (anti-vitellin was shown to cross-react with hemolymph vitellogenin (Vg), Chen and Kuo, 1998).

An indirect ELISA technique was used to determine hemolymph Vg levels. In the assay, polystyrene microtiter plates were coated with 100 μl of 1.25 μg/ml hemolymph diluted in coating buffer (15 mM Na_2CO_3, 35 mM $NaHCO_3$ pH 9.6) for 2 h at 37 °C. After incubation, the excess antigen was washed using analytical grade dH_2O three times, 1 min each. Non-specific bindings were blocked with 100 μl of blocking buffer containing 0.25% bovine serum albumin (BSA) in 0.01 M PBS, pH 7.2 and 0.05% Tween 20, at 37 °C for 2 h. After washing three times, the plate was incubated in the primary antibody (anti-vitellin) diluted at 1:2000 in the diluent containing 0.25% BSA in 0.01 M PBS, pH 7.2 and 0.05% Tween 20. One hundred μl of primary antibody was added to each well and incubated at 37 °C for 2 h. The plate was washed as described above, and then 100 μl of HRP-conjugated goat anti-rabbit IgG (Zymed Co., San Francisco, CA, USA) diluted to 1:4000 in blocking solution was added

to each well, and incubated at 37 °C for 1 h. After washing three times, the color reaction was developed by adding 100 μl of *O*-phenylenediamine dihydrochloride (OPD, Sigma, St. Louis, MO, USA) substrate solution (3 mg OPD in 7.5 ml substrate buffer and 3 μl H_2O_2) to each well, and incubating at 37 °C for 30 min in a dimly lit room. Finally, 100 μl of 6 N H_2SO_4 was added to stop the enzymatic reaction, and the optical density (OD) was measured at 492 nm in an automatic spectrophotometer (Titertex Multiscan Flow Laboratories, Pty. Ltd., Australia). A negative control sample was prepared in parallel by using rabbit pre-immune serum in place of primary antibody. The Vg concentrations were calculated from a standard curve established from known concentrations of Vg.

2.7. Statistical analysis

Experimental data were analyzed with the SPSS program using one-way analysis of variance (ANOVA) and Tukey's post hoc test. A probability value less than 0.05 ($P < 0.05$) indicated the statistical significance. Data were presented as means ± SEM.

3. Results

The 5-HT and DA peaks in the extracts of the brain (supraesophageal ganglion), thoracic ganglia, abdominal ganglia, and ovary showed the same elution times as their corresponding standards. Additionally, the spiked peaks and the peaks of corresponding standards appeared at the same position when 5-HT and DA were added to each sample (Fig. 2).

3.1. Changes in the 5-HT concentration in the CNS and ovary

From HPLC-ECD analyses, the concentrations of 5-HT and DA in the organ extracts were expressed as nmol per mg protein (Fig. 3 and 4). The concentration of 5-HT in the brain and thoracic ganglia exhibited a gradual increase from ovarian stage I to stage IV. At stage I, the concentration of 5-HT in the brain was 0.12 ± 0.01 nmol/mg, and it gradually increased through the ovarian stage II (0.18 ± 0.01 nmol/mg), ovarian stage III (0.44 ± 0.05 nmol/mg), and finally reached the highest level (0.66 ± 0.03 nmol/mg) in stage IV, which was approximately a 5.7-fold increase over stage I. A similar pattern was observed in the thoracic ganglia, where the 5-HT concentration was 0.22 ± 0.01 nmol/mg at ovarian stage I, 0.69 ± 0.02 nmol/mg at stage II, 1.06 ± 0.01 nmol/mg at stage III, and finally 1.48 ± 0.03 nmol/mg at stage IV, showing approximately a 6.7-fold increase. In the abdominal ganglia, 5-HT concentration increased from ovarian stage I to stage II (0.08 ± 0.01, 0.21 ± 0.01 nmol/mg, respectively), and then declined at ovarian stage III (0.06 ± 0.01 nmol/mg). When compared within a tissue, the concentration of 5-HT was about 4 and 5 times higher in the brain at ovarian stage III and IV ($P < 0.05$) than in the brain at ovarian stage I, respectively. The concentration of 5-HT was about 3, 5, 7 times higher in the thoracic ganglia at ovarian stage II, III, and IV ($P < 0.05$) than in the thoracic ganglia at ovarian stage I, respec-

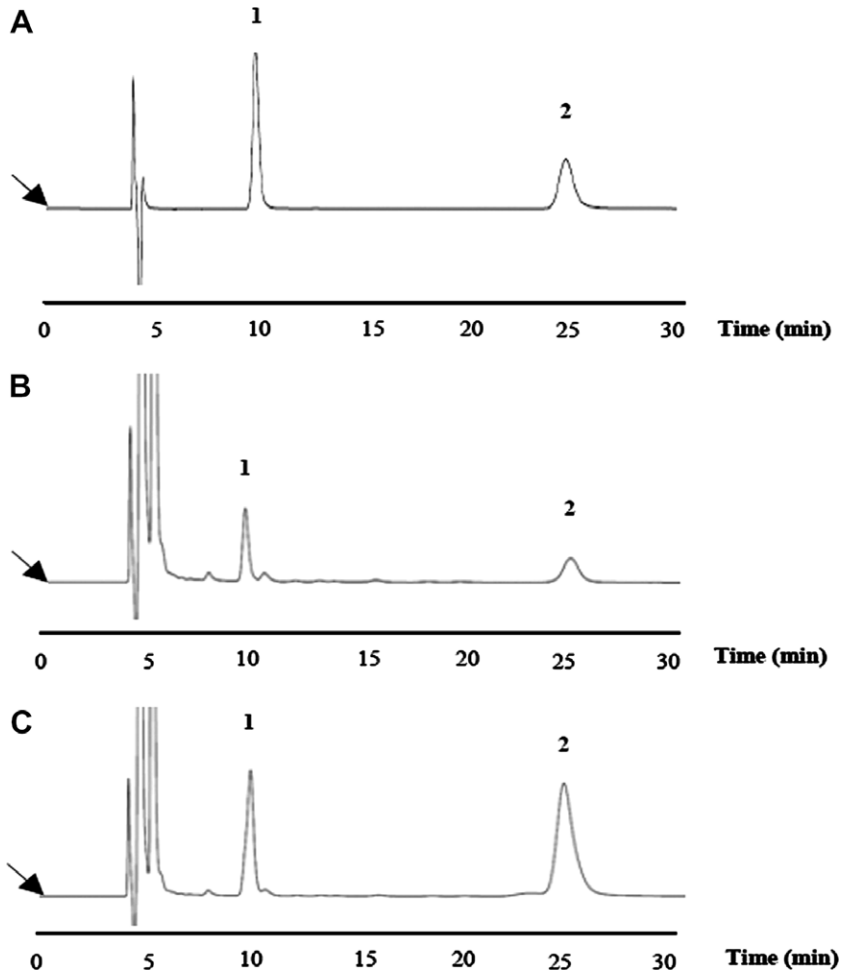


Fig. 2. (A) HPLC chromatogram of standards at 0.7 ml/min flow rate. Solutes: (1) DA; (2) 5-HT. (B) HPLC chromatogram of the brain extract. (C) The brain extract was spiked with DA and 5-HT standards. Samples were injected at the start of each recording trace (arrows).

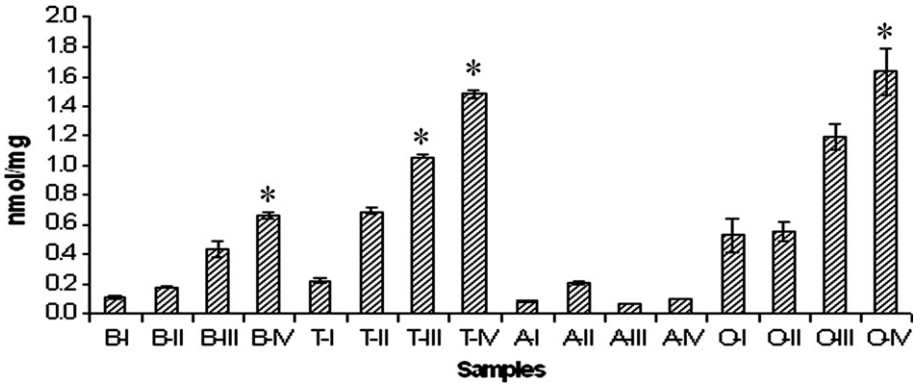


Fig. 3. A graph illustrating the changing concentrations of 5-HT in the brain, thoracic ganglia, abdominal ganglia, and ovary during various stages of the ovarian cycle (stage I–IV). The concentration is expressed as nmol/mg of protein in the organ extract. Numbers are means ± SEM. Asterisks indicate significant differences at $P < 0.05$ in an analysis of variance. B-I to IV are the concentration of 5-HT in brain at ovarian stages I–IV. T-I to IV are the concentration of 5-HT in thoracic ganglia at ovarian stages I–IV. A-I to IV are the concentration of 5-HT in abdominal ganglia at ovarian stages I–IV. O-I to IV are the concentration of 5-HT in ovarian stages I–IV.

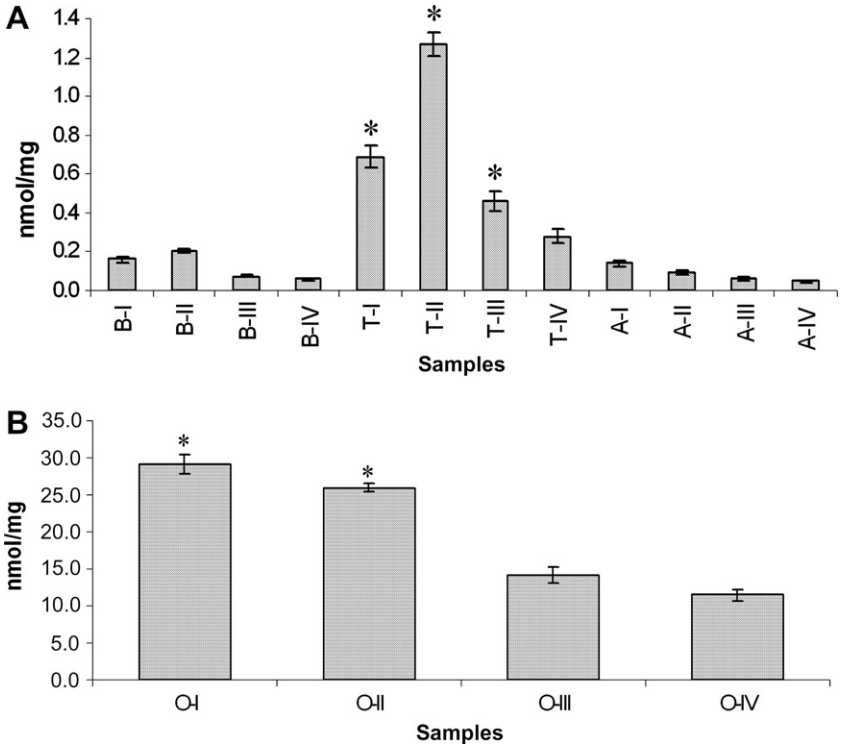


Fig. 4. Graphs illustrating: (A) the changing concentrations of DA in the brain, thoracic ganglia, and abdominal ganglia; (B) the changing concentrations of DA in the ovaries. The concentration is expressed as nmol/mg of protein in the organ extract. Numbers are means ± SEM. Asterisks indicate significant differences at $P < 0.05$ in an analysis of variance. B-I to IV are the concentration of DA in brain at ovarian stages I–IV. T-I to IV are the concentration of DA in thoracic ganglia at ovarian stages I–IV. A-I to IV are the concentration of DA in abdominal ganglia at ovarian stages I–IV. O-I to IV are the concentration of DA in ovarian stages I–IV.

tively. The level of 5-HT in the thoracic ganglia at any one ovarian stage was about two times higher than in the brain, and about 15 times higher than in abdominal ganglia when compared at ovarian stage IV. These results were statistically significant ($P < 0.05$). In the ovaries, the 5-HT concentration showed a gradual increase from a low level at ovarian stage I (0.53 ± 0.11 nmol/mg) to the highest level (1.63 ± 0.16 nmol/mg) at ovarian stage IV (Fig. 3).

3.2. Changes in DA concentration in the CNS and ovary

In the brain, the concentration of DA (Fig. 4A) increased slightly from ovarian stage I to stage II (0.16 ± 0.01, and 0.20 ± 0.01 nmol/mg, respectively) and then declined at ovarian stages III and IV (at 0.08 ± 0.01, and 0.06 ± 0.01 nmol/mg, respectively). The concentration of DA in the thoracic ganglia also increased from ovarian stage I (0.69 ± 0.06 nmol/mg), became highest in stage II (1.27 ± 0.06 nmol/mg), and then decreased in ovarian stages III and IV, (0.46 ± 0.05, and 0.28 ± 0.04 nmol/mg, respectively). In the abdominal ganglia, DA concentration was highest (0.14 ± 0.02 nmol/mg) in ovarian stage I and then decreased from ovarian stages II to IV (0.09 ± 0.01, 0.06 ± 0.01, 0.05 ± 0.01 nmol/mg, respectively). At ovarian stages I to III, the concentration of DA in the thoracic ganglia was 6-fold higher ($P < 0.05$) than in the brain. When compared to the abdominal ganglia, the DA concentration in the thoracic ganglia was higher by 14-fold, 7-fold, and 6-fold at stage I, II, and III, respectively ($P < 0.05$). When compared within a tissue, the concentration

of DA was about 2.5 and 3 times higher in the brain at ovarian stage II than in the brain at ovarian stage III and IV. The concentration of DA was about 2.7 and 4.5 times higher in the thoracic ganglia at ovarian stage II ($P < 0.05$) than in the thoracic ganglia at ovarian stage III and IV, respectively. The highest and the lowest concentrations of DA in each part of CNS were comparable to those of 5-HT, but the stages at which these occurred were in reverse. In the ovaries, the highest concentration of DA was detected at the ovarian stage I (29.05 ± 1.31 nmol/mg), and it declined to the lowest level (11.43 ± 0.74 nmol/mg) at ovarian stage IV (Fig 4B). Additionally, the concentration of DA was about 2 to 3 times higher in ovarian stage I and II ($P < 0.05$) than in the ovarian stage IV (Fig. 4B).

3.3. Changes in Vg concentrations after treatment with 5-HT and DA

The Vg concentrations in the hemolymph of female prawns after injection with various doses of 5-HT and DA during various stages of ovarian cycle were expressed in mg/ml of hemolymph as means ± SEM. The Vg concentration in the NC group exhibited gradual increases from ovarian stage I to reach maximum at stage IV, which were 1.76 ± 0.25, 3.19 ± 0.49, 5.88 ± 0.94, 9.90 ± 1.02 mg/ml, respectively. A similar pattern was also observed in the VIC group, whose Vg concentrations were 1.54 ± 0.13, 3.04 ± 0.24, 6.02 ± 0.68, 9.37 ± 0.93 mg/ml, respectively, from ovarian stage I to stage IV (Fig. 5A and B).

The Vg concentrations after treatment with 2.5×10^{-6} or 2.5×10^{-7} mol of 5-HT/prawn exhibited a gradual increase from ovarian stage I to stage IV (Fig. 5A). At stage I, the Vg concentrations were 2.50 ± 0.15 and 2.33 ± 0.12 mg/ml, respectively, for the two 5-HT doses. Vg concentration gradually increased through ovarian stage II (8.89 ± 1.10 and 7.99 ± 0.82 mg/ml, respectively) and ovarian stage III (16.96 ± 2.01 and 14.37 ± 1.59 mg/ml, respectively), and finally reached the highest level (24.95 ± 1.88 and 20.33 ± 1.60 mg/ml, respectively) in stage IV, which was approximately at 10-fold increase over stage I. The Vg concentrations of prawns treated with 2.5×10^{-6} mol 5-HT/prawn were about 3, 3, and 2–3 times higher than those of control groups at ovarian stage II–IV. These results were statistically significant ($P < 0.05$). The Vg concentrations of prawns treated with 2.5×10^{-7} mol 5-HT/prawn were about 2–3, 2–3, and 2 times higher than those of control groups at ovarian stage II–IV ($P < 0.05$). The Vg concentration of prawns treated with either dose of 5-HT at ovarian stage IV was approximately a 14-fold higher that of control groups at ovarian stage I ($P < 0.05$). Furthermore, injection of 5-HT shortened the ovarian maturation periods (OMP) by about 10 days compared to control groups (OMP, ~29 days for 5-HT vs. ~39 days for NC). The gonado-somatic (GSI) index (i.e., ovarian size) was also significantly increased by about 2.5 fold, when compared to those of the control groups (Tinikul et al., in press).

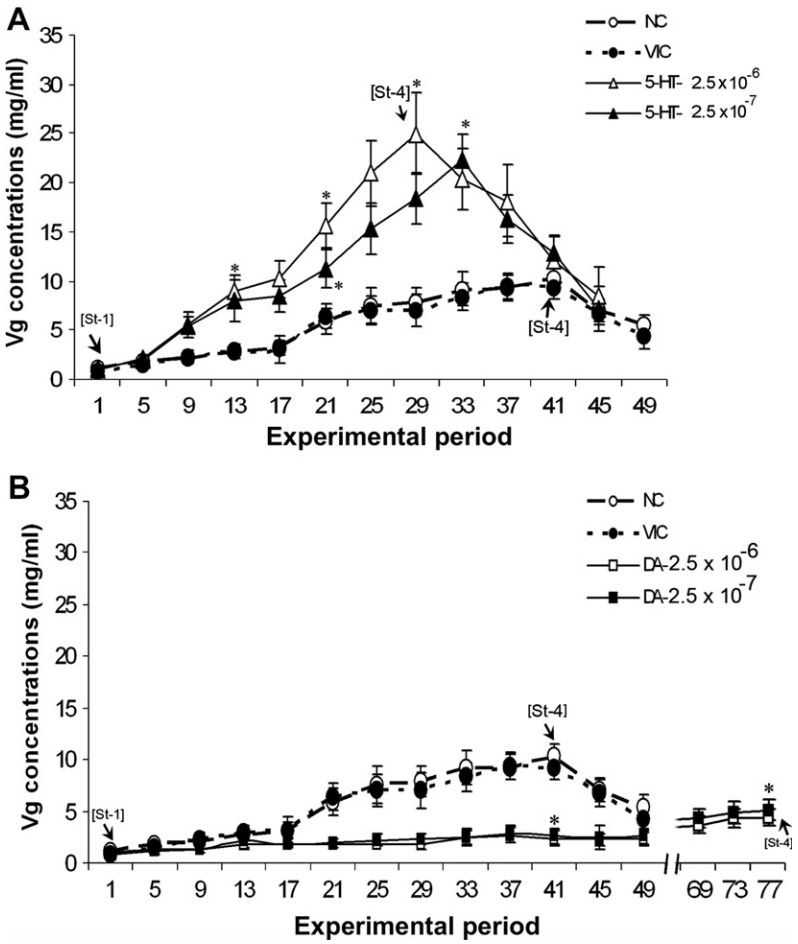


Fig. 5. A graph illustrating the concentrations of hemolymph vitellogenin (Vg) during various phases of the ovarian cycle following administrations of 5-HT (A) and DA (B). The doses of 5-HT and DA were given at 2.5×10^{-6} and 2.5×10^{-7} moles per prawn. The concentration is expressed as mg/ml of hemolymph. Numbers are expressed as means ± SEM. Asterisks indicate significant differences $P < 0.05$, when compared between the experimental groups (5-HT and DA) and the control groups. St-1, at ovarian stage I; St-4, at ovarian stage IV.

In contrast, Vg concentrations after treatment with DA at 2.5×10^{-6} or 2.5×10^{-7} mol of DA/prawn increased slightly from ovarian stage I (1.84 ± 0.36 and 2.06 ± 0.21 mg/ml, respectively) to stage II (2.66 ± 0.18 and 2.77 ± 0.16 mg/ml, respectively), and then slightly increased at ovarian stages III (3.01 ± 0.71 and 3.58 ± 0.83 mg/ml, respectively), and stage IV (3.88 ± 0.65 and 4.49 ± 0.9 mg/ml, respectively). The Vg concentrations of prawns treated with DA (2.5×10^{-6} mol/prawn) were about 2 and 2.5 times lower than those of control groups at ovarian stage III and IV. These results were statistically significant ($P < 0.05$). The Vg concentrations of prawns treated with DA (2.5×10^{-7} mol/prawn) were about 1 and 2 times lower than those of control groups at ovarian stage III and IV ($P < 0.05$) (Fig. 5B). However, prawns treated with DA showed longer ovarian maturation period (OMP ~64–67 days) as well as decreased ovarian size (Tinikul et al., in press).

4. Discussion

The present investigation documents how endogenous levels of 5-HT and DA change in the ovaries and nervous system in *M. rosenbergii* during the ovarian cycle. Variations in the concentration of 5-HT in the ovaries appear to be correlated with changes in brain and thoracic ganglia throughout the four stages of the cycle. Specifically, 5-HT levels rose steadily in all three structures from ovarian stage I to ovarian stage IV. In contrast, levels of DA in the brain, thoracic ganglia, and ovaries were high in ovarian stages I and II, and declined in ovarian stages III and IV. Thus, changes in DA concentration in the brain, thoracic ganglia, and ovaries were essentially opposite to those of 5-HT. This suggests that the two transmitters may play opposite roles in regulating ovarian maturation. Maximal DA levels occurred in stage I in the ovaries and in stage II in the brain and thoracic ganglia. Thus, the relationship between DA levels in the ovaries, brain and thoracic ganglia does not appear to be as tightly correlated as for 5-HT. Changes in DA and 5-HT levels in the abdominal ganglia during various stages of the ovarian cycle were not statistically significant.

The distribution of 5-HT has been extensively mapped using immunohistochemistry on the CNS of various crustaceans, including the crayfish, *Cherax destructor* (Sandeman et al., 1988), *P. leniusculus* (Elofsson, 1983), *P. clarkii* (Real and Czternasty, 1990), the lobster, *Homarus americanus* (Beltz and Kravitz, 1983), and squat lobster, *Munida quadrispina* (Antonsen and Paul, 2001). As well, DA was reported to be present in various regions of the CNS, including the lobster, *Homarus gammarus* (Cournil et al., 1994), the spiny lobster, *Panulirus argus* (Schmidt and Ache, 1997), the blue crab, *Callinectes sapidus* (Wood and Derby, 1996), and several crayfish species (Tierney et al., 2003).

Although immunohistochemistry is a useful method for visualizing and mapping neuronal populations containing biogenic amines, it is not an effective method for estimating and comparing the quantities of these neurotransmitters in various regions of the CNS. HPLC is a better method for this purpose, as pointed out by Hardie and Hirsh (2006). In the crayfish, *P. clarkii*, levels of biogenic amines were quantified in various regions of the CNS, eyestalk, and intestinal nerve using HPLC (Mercier et al., 1991; Kulkarni et al., 1992; Alvarez et al., 2005). In this species, the total concentration of 5-HT in the brain (0.581 ± 0.36 μg/g) was higher than in the eyestalks (0.299 ± 0.15 μg/g) (Cervantes et al., 1999). In the spiny lobster, *P. homarus*, the level of 5-HT was higher in thoracic ganglia than in the brain at ovarian stage IV, and as a result it was suggested that 5-HT could be involved in controlling the ovarian development (Kirubagaran et al., 2005). In the lobsters, *Palinurus interruptus*, *H. americanus*, and the crab, *Cancer irroratus*, major tissues that exhibited high levels of 5-HT were the optic ganglion, cerebral ganglion, circumoesophageal connectives, stomatogastric ganglion, and thoracic ganglia (Aramant and Elofsson, 1976; Beltz et al., 1984). However, fluctuations in the levels of both 5-HT and DA in correlation with different phases of the ovarian cycle have not been previously reported. The present study demonstrates that in the freshwater prawn, *M. rosenbergii*, the levels of 5-HT and DA in the brain, thoracic ganglia and ovaries fluctuate in opposite directions during the ovarian cycle. Specifically, 5-HT levels rose with ovarian maturation, and DA levels fell. Our results agree with those reported earlier in *P. clarkii* and in *P. homarus* by Cervantes et al. (1999) and Kirubagaran et al. (2005), but these authors reported only 5-HT levels. Chen et al. (2003) was the first to report the possible involvement of DA in ovarian development in *M. rosenbergii*, but they did not show the variation pattern of DA in various regions of CNS and ovary as reported here.

The effects of 5-HT and DA on regulation of ovarian maturation in crustaceans have been extensively reported (Martinez and Rivera, 1994; Sarojini et al., 1995; Meeratana et al., 2006). 5-HT induces ovarian maturation in several species, including the crayfish, *P. clarkii*, the lobster, *H. americanus* (Kulkarni et al., 1992; Fingerman, 1997), the giant freshwater prawn, *M. rosenbergii* (Meeratana et al., 2006), the black tiger shrimp, *P. monodon* (Wongprasert et al., 2006), *P. vannamei* (Vaca and Alfaro, 2000), and *Litopenaeus vannamei* and *Litopenaeus stylirostris* (Alfaro et al., 2004). Treatment of the crayfish, *P. clarkii*, with 5-HT causes significant increases in ovarian index and oocyte diameter (Kulkarni et al., 1992). Kulkarni et al. (1991) reported that brain and thoracic ganglia of *P. clarkii* stimulated incorporation of leucine into ovarian protein. In the freshwater prawn, *M. rosenbergii*, treatment with 5-HT also showed a significant increase in the gonadosomatic (GSI) index (Meeratana et al., 2006). In *L. stylirostris*, the combined injection of 5-HT and spiperone elicited higher rates of ovarian maturation compared to application of 5-HT alone (Alfaro et al., 2004). Furthermore, the ovaries of prawns injected with the culture medium of 5-HT-primed thoracic ganglia exhibited an increase in the number of oocytes developing to vitellogenic and mature stages. These findings suggest that 5-HT and/or other hormonal factors from the thoracic ganglia could be major factors that stimulate the ovarian maturation (Meeratana et al., 2006). 5-HT might act indirectly by stimulating the release of some other putative gonadotrophic factor, such as gonad-stimulating hormone (GSH) from the thoracic ganglion, and/or by inhibiting the release of gonad-inhibiting hormone (GIH) from the optic lobe, whereas DA plays the opposite role (Kulkarni et al., 1992; Sarojini et al., 1995; Fingerman, 1997). In the freshwater prawn, *M. rosenbergii*, it was suggested that the inhibitory action of DA could be on the thoracic ganglia through inhibition of vitellogenesis-stimulating hormone (VSH) release, but not at the eyestalk level through stimulation of VIH release from the X-organ–sinus gland complex (Chen et al., 2003). Our finding that the thoracic ganglia contained high levels of 5-HT and DA implies that this part of CNS may play a leading role in controlling the prawn's ovarian maturation, and that the brain may play a secondary role. In contrast, the abdominal ganglia, which had the lowest levels and least fluctuation of both 5-HT and DA levels, may not be involved in this controlling process.

In crustaceans, vitellogenesis is an important process in the female reproductive cycle (Okumura, 2004), which is characterized by the appearance in the hemolymph of vitellogenin (Vg), the precursor of the major yolk protein, vitellin (Vn) (Tsukimura, 2001). Thus, hemolymph Vg level is an important indicator of ovarian maturation. Extracts of the brain and thoracic ganglia stimulate ovarian vitellogenin synthesis and the development of secondary oocytes in the crayfish, *P. leniusculus* and *P. clarkii* (Elofsson et al., 1982; Sarojini et al., 1995), the crab, *Uca pugilator* (Chang, 1985), and the shrimp, *Paratya compressa* (Takayanagi et al., 1986). In the present study, injection of 5-HT and DA, respectively, increased

or decreased levels of hemolymph Vg in *M. rosenbergii*. Vg concentrations of prawns treated with 5-HT were higher at all ovarian stages, especially stage IV, compared to control groups, whereas prawns treated with DA exhibited lower Vg concentrations when compared to those of 5-HT and control groups. These results indicate causal relationships, with 5-HT stimulating Vg synthesis and DA inhibiting Vg synthesis. Taken together with fluctuations in 5-HT and DA levels, the present data suggest that ovarian maturation involves increases in levels of 5-HT and decreases in levels of DA in the CNS and ovary.

In this study, the concentration of 5-HT in the ovary was lowest at ovarian stage I and gradually increased to ovarian stage IV. In contrast, the concentration of DA was highest at ovarian stage I and lowest at the ovarian stage IV. Fluctuations in the level of these two neurotransmitters were also in opposite directions as in the brain and thoracic ganglia. However, the levels of DA in the ovaries were much higher than those of 5-HT at each phase of the ovarian cycle. There have been previous reports on the roles of 5-HT and DA in the oocyte maturation. In mouse, the existence and expression of a 5-HT receptor (5-HT1D) in oocytes implies that 5-HT may be involved in the regulation of oocyte maturation (Vasela et al., 2003). Moreover, increasing levels of 5-HT have been detected in human ovarian follicular fluid in association with the ovulatory cycle (Bodis et al., 1992). In marine memertean worms, 5-HT causes increases in cAMP in immature oocytes, which stimulates meiotic division and maturation of oocytes (Stricker and Smythe, 2001). In bivalves, *Spisula* sp., 5-HT stimulates the completion of meiotic division of isolated cultured oocytes (Hirai et al., 1988). The mechanism by which 5-HT releases oocytes from prophase I arrest appears to involve a G-protein coupled receptor that results in the increase of IP-3 and intracellular Ca^{2+} levels (Gobet et al., 1994). In *P. monodon*, 5-HT1 receptors were expressed in the membrane of mature oocytes in stages III and IV of the ovarian cycle (Ongvarrasopone et al., 2006), which suggest that 5-HT may play a critical role in regulating oocyte maturation in this penaeoid shrimp as well. As a significantly high level of 5-HT appeared in the ovary from stage I to IV in *M. rosenbergii*, and 5-HT was also detected in late and mature oocytes (unpublished observation), we propose that 5-HT may play similar role in the oocyte maturation in this species.

The expression of DA in the ovary appears to be phylogenetically conserved feature (Buznikov, 1991). In sea urchins, the ability of both unfertilized and fertilized eggs to take up DA was demonstrated, and it was shown that the uptake of DA was more prominent before fertilization (Carginale et al., 1995). In the grey mullet, *Mugil cephalus*, DA was found to inhibit the proliferation of early stages of vitellogenic oocytes and the final stage of oocyte maturation and ovulation (Aizen et al., 2005). In the European eel, *Anguilla anguilla*, and in teleost fish, it was demonstrated that DA could inhibit the release of luteinizing hormone (LH) (Peter et al., 1986; Vidal et al., 2004). Consequently, the oocytes fail to mature and ovulate (Yaron, 1995). Even though the role of DA is not as well defined as that of 5-HT, it is possible that in *M. rosenbergii* DA might also delay oocyte maturation by promoting the meiotic arrest at the end of prophase stage. This, however, needs to be further studied.

Acknowledgments

This research was supported by the Thailand Research Fund (Royal Golden Jubilee Ph.D. Program (Grant No. PHD/0171/2547) to Yotsawan Tinikul and Prasert Sobhon, Senior Research Scholar Fellowship to Prasert Sobhon), and the Commission on Higher Education (Research Group Development Grant to Prasert Sobhon). We would like to express our special thanks to Dr. Angela Lange (University of Toronto, Canada), Dr. Jeffrey Atkinson (Brock University, Canada), Dr. Wattana Weerachatyanukul, Ms. Ruchanok Cheotacha, Ms. Rapeepun Kongtoom, Ms. Jaruwan Poljaroen, Mrs. Pornsawan Duangsuwan, and Mr. Ittipon Phoungpetchara for useful suggestions and assistance in the HPLC work.

References

Aizen, J., Meiri, I., Tzchori, I., Levavi-Sivan, B., Rosenfeld, H., 2005. Enhancing spawning in the grey mullet (*Mugil cephalus*) by removal of dopaminergic inhibition. Gen. Comp. Endocr. 142, 212–221.

Alfaro, J., Zuniga, G., Komen, J., 2004. Induction of ovarian maturation and spawning by combined treatment of serotonin and a dopamine antagonist, spiperone in *Litopenaeus stylirostris* and *Litopenaeus vannamei*. Aquaculture 236, 511–522.

Alvarez, R.A., Villalobos, M.G.P., Rosete, G.C., Sosa, L.R., Arechiga, H., 2005. Dopaminergic modulation of neurosecretory cells in the crayfish. Cell. Mol. Neurobiol. 25, 345–370.

Antonsen, B.L., Paul, D.H., 2001. Serotonergic and octopaminergic systems in the squat lobster *Munida quadrispina* (Anomura, Galatheidae). J. Comp. Neurol. 439, 450–468.

Aramant, R., Elofsson, R., 1976. Monoaminergic neurons in the nervous system of crustaceans. Cell Tissue. Res. 170, 231–251.

Beltz, B.S., Kravitz, E.A., 1983. Mapping of serotonin-like immunoreactivity in the lobster nervous system. J. Neurosci. 3, 585–602.

Beltz, B.S., Eisen, J.S., Flamm, R., Harris, R.M., Hooper, S.L., Marder, E., 1984. Serotonergic innervation and modulation of the stomatogastric ganglion of three decapod crustaceans (*Palinurus interruptus*, *Homarus americanus*, and *Cancer irroratus*). J. Exp. Biol. 87, 285–313.

Bodis, J., Torok, A., Tinnberg, H.R., Volker, H., Hamori, M., Cledon, P., 1992. Influence of serotonin on progesterone and estradiol secretion by cultured human granulosa cells. Fertil. Steril. 57, 1008–1011.

Bradford, M.M., 1976. A rapid and sensitive method for the quantitation of microgram quantities of protein utilizing the principle of protein-dye binding. Anal. Biochem. 72, 248–254.

Butler, T.A., Fingerman, M., 1983. Concentration of neurotransmitters in the central nervous system of *Uca panacea* and *Callinectes sapidus*. Am. Zool. 23, 954–958.

Buznikov, G.A., 1991. The biogenic amines as regulators of early (pre-nervous) embryogenesis. Adv. Exp. Med. Biol. 296, 33–48.

Carginale, V., Borrelli, L., Capasso, A., Parisi, E., 1995. Changes in dopamine uptake and developmental effects of dopamine receptor inactivation in the sea urchin. Mol. Reprod. Dev. 40, 379–385.

Cervantes, O.C., Battelle, B.A., Moles, M.L.F., 1999. Rhythmic changes in the serotonin content of the brain and eyestalk of crayfish during development. J. Exp. Biol. 202, 2823–2830.

Chang, E.S., 1985. Hormonal control of molting in decapod crustacean. Am. Zool. 25, 179–185.

Chang, C.F., Shih, T.W., 1995. Reproductive cycle of ovarian development and Vitellin profiles in the freshwater prawns, *Macrobrachium rosenbergii*. Invertebr. Reprod. Dev. 27, 11–20.

Chen, Y.N., Kuo, C.M., 1998. Purification and characterization of vitellin from the freshwater giant prawn, *Macrobrachium rosenbergii*. Zool. Stud. 37, 126–136.

Chen, Y.N., Fan, H.F., Hsieh, S.L., Kuo, C.M., 2003. Physiological involvement of DA in ovarian development of the freshwater giant prawn, *Macrobrachium rosenbergii*. Aquaculture 228, 383–395.

Cournil, I., Helluy, S.M., Beltz, B.S., 1994. Dopamine in the lobster *Homarus gammarus*:I Comparative analysis of dopamine and tyrosine hydroxylase immunoreactivities in the nervous system of the juvenile. J. Comp. Neurol. 344, 455–469.

Elofsson, R., Laxmyr, L., Rosengren, E., Hansson, C., 1982. Identification and quantitative measurement of biogenic amines and DOPA in the central nervous system and hemolymph of the crayfish *Pacifastacus leniusculus* (Crustacea). Comp. Biochem. Physiol. C71, 195–201.

Elofsson, R., 1983. 5-HT-like immunoreactivity in the central nervous system of the crayfish, *Pacifastacus leniusculus*. Cell Tissue. Res. 232, 231–236.

Fingerman, M., Nagabhushanam, R., Sarojini, R., Reddy, P.S., 1994. Biogenic amines in crustaceans: identification, localization, and roles. J. Crustacean. Biol. 14 (3), 413–437.

Fingerman, M., 1997. Roles of neurotransmitters in regulating the reproductive hormone release and gonadal maturation in decapod crustaceans. Invertebr. Reprod. Dev. 31, 47–54.

Gobet, I., Durocher, Y., Lecler, C., Moreau, M., Guerrier, P., 1994. Reception and transduction of the serotonin signal responsible for meiosis reinitiation in oocytes of the Japanese clam *Ruditapes philippinarum*. Dev. Biol. 164, 540–549.

Hardie, S.L., Hirsh, J., 2006. An improved method for the separation and detection of biogenic amines in adult *Drosophila* brain extracts by high performance liquid chromatography. J. Neurosci. Meth. 153, 243–249.

Hirai, S., Kishimoto, T., Kadam, A.L., Kanatani, H., Koide, S.S., 1988. Induction of spawning and oocyte maturation by 5-hydroxytryptamine in the surf clam. J. Exp. Zool. 245, 318–321.

Kerkut, G.A., Sedden, C.B., Walker, R.J., 1966. The effect of DOPA, a-methyl DOPA and reserpine on the DA content of the brain of the snail, *Helix aspersa*. Comp. Biochem. Physiol. 18, 921–930.

Kirubagaran, R., Peter, D.M., Dharani, G., Vinithkumar, N.V., Sreeraj, G., Ravindran, M., 2005. Changes in vertebrate-type steroids and 5-hydroxytryptamine during ovarian recrudescence in the Indian spiny lobster, *Panulirus homarus*. New Zeal. J. Mar. Fresh. 39, 527–537.

Kulkarni, G.K., Glade, L., Fingerman, M., 1991. Oogenesis and effects of neuroendocrine tissues on in vitro synthesis of protein by the ovary of the red swamp crayfish *Procambarus clarkii* (Girard). J. Crustac. Biol. 11, 513–522.

Kulkarni, G.K., Nagabhushanam, R., Amaldoss, G., Jaiswal, R.G., Fingerman, M., 1992. In vitro stimulation of ovarian development in the red swamp crayfish, *Procambarus clarkii* (Girard), by 5-hydroxytryptamine. Invertebr. Reprod. Dev. 21, 231–240.

Kwok, R., Tobe, S.S., 2006. Hemolymph clotting in crustaceans: implications for neuropeptide extraction from invertebrate hemolymph. Peptides 27, 590–596.

Laxmyr, L., 1984. Biogenic amines and DOPA in the central nervous system of decapod crustacean. Comp. Biochem. Physiol. C77, 139–143.

Martinez, G., Rivera, A., 1994. Role of monoamines in the reproductive process of *Argopecten purpurarus*. Invertebr. Reprod. Dev. 25, 167–174.

Meeratana, P., Withyachumnarnkul, B., Damrongphol, P., Wongprasert, K., Suseangtham, A., Sobhon, P., 2006. Serotonin induces ovarian maturation in giant freshwater prawn broodstock, *Macrobrachium rosenbergii* de Man. Aquaculture 260, 315–325.

Meeratana, P., Sobhon, P., 2007. Classification of differentiating oocytes during ovarian cycle in the giant freshwater prawn, *Macrobrachium rosenbergii* de man. Aquaculture 270, 249–258.

Mercier, A.J., Orchard, I., Schmoeckel, A., 1991. Catecholaminergic neurons supplying the hindgut of the crayfish *Procambarus clarkii*. Can. J. Zool. 69, 2778–2785.

Molaei, G., Lange, A.B., 2003. The association of serotonin with the alimentary canal of the African migratory locust, *Locusta migratoria*: distribution, physiology and pharmacological profile. J. Insect. Physiol. 49, 1073–1082.

Okumura, T., 2004. Perspectives on hormonal manipulation of shrimp reproduction review. JARQ 38, 49–54.

Ongvarrasopone, C., Roshorm, Y., Somyong, S., Pothiratana, C., Petchdee, S., Tangkhabuanbutra, J., Sophasan, S., Payim, S., 2006. Molecular cloning and functional expression of the *Penaeus monodon* 5-HT receptor. Biochim. Biophys. Acta 1759, 328–339.

Peter, R.E., Chang, J.P., Nahorniak, C.S., Omeljaniuk, R.J., Sokolowska, M., Shih, S.H., Billard, R., 1986. Interactions of catecholamines and GnRH in regulation of gonadotropin secretion in teleost fish. Recent. Prog. Horm. Res. 42, 513–548.

Real, D., Czternasty, G., 1990. Mapping of serotonin-like immunoreactivity in the ventral nerve cord of crayfish. Brain Res. 521, 203–212.

Ridchardson, H.G.D., Decaraman, M., Fingerman, M., 1991. The effect of biogenic amines on ovarian development in fiddler crab, *Uca pugilator*. Comp. Biochem. Physiol. C99, 53–56.

Sandifer, P.A., Smith, T.J., 1985. Freshwater prawn: crustacean and mollusk aquaculture in the United States. A publishing company, Inc., West port, USA. pp. 1–15.

Sandeman, D.C., Sandeman, R.E., Aitken, A.R., 1988. Atlas of serotonin containing neurons in the optic lobes and brain of the crayfish, *Cherax destructor*. J. Comp. Neurol. 269, 465–478.

Sarojini, R., Nagabhushanam, R., Fingerman, M., 1995. Mode of action of the neurotransmitter 5-hydroxytryptamine in stimulating ovarian maturation in the red swamp crayfish, *Procambarus clarkii*: an in vivo and in vitro study. J. Exp. Zool. 271, 395–400.

Schmidt, M., Ache, B.W., 1997. Immunocytochemical analysis of glomerular regionalization and neuronal diversity in the olfactory deutocerebrum of the spiny lobster. Cell Tissue. Res. 287, 541–563.

Stricker, S.A., Smythe, T.L., 2001. 5-HT causes increase in cAMP that stimulates, rather inhibits, oocyte maturation in marine memertean worms. Development 128, 1415–1427.

Takayanagi, H., Yamamoto, Y., Takeda, N., 1986. An ovary stimulating pheromone in the freshwater shrimp, *Paratya compressa*. J. Exp. Zool. 240, 397–400.

Tierney, A.J., Kim, T., Abrams, R., 2003. Dopamine in crayfish and other crustaceans: distribution in the central nervous system and physiological functions. Microsc. Res. Techniq. 60, 325–335.

Tinikul, Y., Soonthornsumrith, B., Phoungpetchara, I., Meeratana, P., Poljaroen, J., Duangsuwan, P., Soonklang, N., Mercier, A.J., Sobhon, P. in press . Effects of serotonin, dopamine, octopamine, and spiperone on ovarian maturation and embryonic development in the giant freshwater prawn, *Macrobrachium rosenbergii* (De Man), Crustaceana.

Tsukimura, B., 2001. Crustacean vitellogenesis: its role in oocyte development. Amer. Zool. 41, 465–476.

Vaca, A.A., Alfaro, J., 2000. Ovarian maturation and spawning in the white shrimp, *Penaeus vannamei*, by serotonin injection. Aquaculture 182, 373–385.

Vasela, J., Rehak, P., Mihalik, J., Czikkova, S., Pokorny, J., Koppel, J., 2003. Expression of serotonin receptors in mouse oocytes and preimplatation embryos. Physiol. Rev. 52, 223–228.

Vidal, B., Pasqualini, C., Belle, N.L., Holland, M.C.H., Sbaihi, M., Vernier, P., Zohar, Y., Dufour, S., 2004. Dopamine inhibits luteinizing hormone synthesis and release in the juvenile European Eel: a neuroendocrine lock for the onset of puberty1. Biol. Reprod. 71, 1491–1500.

Wongprasert, K., Asuvapongpatana, S., Poltana, P., Tiensuwan, M., Withyachumnarnkul, B., 2006. Serotonin stimulates ovarian maturation and spawning in the black tiger shrimp *Penaeus monodon*. Aquaculture 261, 1447–1454.

Wood, D.E., Derby, C.D., 1996. Distribution of dopamine-like immunoreactivity suggests a role for dopamine in the courtship display behavior of the blue crab *Callinectes sapidus*. Cell Tissue. Res. 285, 321–330.

Yaron, Z., 1995. Endocrine control of gametogenesis and spawning induction in the carp. Aquaculture 129, 49–73.

Cell Tissue Res (2008) 334:135–144
DOI 10.1007/s00441-008-0668-7

REGULAR ARTICLE

Changes in distribution of basic nuclear proteins and chromatin organization during spermiogenesis in the greater bandicoot rat, *Bandicota indica*

Pakawadee Worawittayawong · Chris Leigh · Wattana Weerachatyanukul · Sirikul Manochantr · Prasert Sobhon · William G. Breed · Prapee Sretarugsa

Received: 20 December 2007 / Accepted: 30 June 2008 / Published online: 23 August 2008
© Springer-Verlag 2008

Abstract Male germ cells of the greater bandicoot rat, *Bandicota indica*, have recently been categorized into 12 spermiogenic steps based upon the morphological appearance of the acrosome and nucleus and the cell shape. In the present study, we have found that, in the Golgi and cap phases, round spermatid nuclei contain 10-nm to 30-nm chromatin fibers, and that the acrosomal granule forms a huge cap over the anterior pole of nucleus. In the acrosomal phase, many chromatin fibers are ~50 nm thick; these then thickened to 70-nm fibers and eventually became 90-nm chromatin cords that are tightly packed together into highly condensed chromatin, except where nuclear vacuoles occur. Immunocytochemistry and immunogold localization with anti-histones, anti-transition protein2, and anti-protamine antibodies suggest that histones remain throughout spermiogenesis, that transition proteins are present from step 7 spermatids and remain until the end of spermiogenesis, and that protamines appear at step 8. Spermatozoa from the cauda epididymidis have been analyzed by acid urea Triton X-100 polyacrylamide gel electrophoresis for basic nuclear proteins. The histones, H2A, H3, H2B, and H4, transitional protein2, and protamine are all present in sperm extracts. These findings suggest that, in these sperm of unusual morphology, both transition proteins and some histones are retained, a finding possibly related to the unusual nuclear form of sperm in this species.

Keywords Chromatin organization · Sperm basic nuclear proteins · Immunocytochemistry · Spermiogenesis · *Bandicota indica* (Rodentia)

This work was supported by grants from the Thailand Research Fund (RGJ/PHD/00196/2541 and BGJ/37/2543) to Prapee Sretarugsa and Pakawadee Worawittayawong and by a University of Adelaide grant to William G. Breed.

P. Worawittayawong · W. Weerachatyanukul · P. Sobhon · P. Sretarugsa (✉)
Department of Anatomy, Faculty of Science, Mahidol University,
Rama 6 Road, Rajdhevee,
Bangkok 10400, Thailand
e-mail: scpsr@mahidol.ac.th

P. Worawittayawong · C. Leigh · W. G. Breed (✉)
Discipline of Anatomical Sciences, School of Medical Sciences,
The University of Adelaide,
Adelaide 5005, South Australia
e-mail: bill.breed@adelaide.edu.au

S. Manochantr
Department of Anatomy, Faculty of Medicine,
Thammasart University,
Rangsit Campus,
Pathumthani 12120, Thailand

Introduction

Mammalian spermiogenesis involves the differentiation of spermatids into highly polarized spermatozoa during which time the remodeling and repackaging of the sperm nuclear proteins occurs (Balhorn et al. 1984; Courtens and Loir 1981; Oko et al. 1996). In common laboratory rodents, the chromatin organization, as seen by transmission electron microscopy (TEM), appears early in spermiogenesis as 50-nm fibers, which later aggregate into 100-nm cords that then become highly compacted in the mature sperm nuclei (Ploen and Courtens 1986; Biggiogera et al. 1992; Balhorn et al. 1999; Wanichanon et al. 2001). During chromatin condensation, transition proteins (TPs) initially replace most of the histones. They are then largely, or completely, replaced by protamines (Grimes et al. 1977; Oliva and Dixon 1991; Meistrich 1989; Biggiogera et al. 1992; Wouters-Tyrou et al. 1998; Oko et al. 1996; Corzett et al.

2002) with the TPs probably preparing the chromatin for association with protamines and playing a role in bringing about DNA condensation (Oko et al. 1996; Yu et al. 2000; Brewer et al. 2002; for reviews, see Meistrich et al. 2003; Kimmins and Sassone-Corsi 2005; Pradeepa and Rao 2007). In the spermatid nuclei of laboratory rodents, TPs appear before histone removal is complete (Zhao et al. 2004), and in the rat, TPs appear concurrently with the condensation of chromatin (Oko et al. 1996). In the mouse, histones are replaced by TPs in step 11 to 13 spermatids, the TPs then being replaced by protamines (Yu et al. 2000; Meistrich et al. 2003; Zhao et al. 2004) so that mature sperm lack TPs (Oko et al. 1996; Pradeepa and Rao 2007). Protamines, which are small, highly positively charged, arginine-rich proteins, bind to the phosphate backbone of DNA and initiate DNA coiling (Balhorn 1982; Allen et al. 1993; Balhorn et al. 1999). In some mammal species, two groups of protamines occur. Protamine 1, which is relatively highly conserved, is invariably present, whereas protamine 2 is found only in a few species. The reason for this difference in abundance of protamine 2 is not clear, but to date, no obvious relationship appears to exist between the ratio of protamine 1 and protamine 2 and that of nuclear shape (Balhorn 1989; Queralt et al. 1995; Corzett et al. 2002).

Unlike most murine rodents in which sperm heads have falciform-shaped nuclei (Retzius 1909; Friend 1936; Bishop and Austin 1960; Lalli and Clermont 1981; Breed 2004), those of the greater bandicoot rat, *Bandicota indica*, have a globular-shaped nucleus that is capped by an extremely large acrosome (Breed 1993, 1998, 2004; Worawittayawong et al. 2005). The reason for this dramatic difference in sperm nuclear shape is not clear but may be related to differences in sperm chromatin organization and its nuclear protein profile. In the present study, we show that, in the greater bandicoot rat, both filamentous and globular patterns of chromatin packaging occur during spermiogenesis, and that the mature sperm nucleus appears to contain, in addition to protamine, a TP and some histones.

Materials and methods

Antibodies and chemicals

Rabbit polyclonal anti-H2A, anti-H2B, and anti-H4 antibodies were donated by Dr. Sylviane Muller (IBMC, France), and anti-H3 IgG was purchased from Santa Cruz Biotechnology (Santa Cruz, Calif., USA). Rabbit polyclonal anti-TP2 antibody, originally from Alfonso and Kistler (1993), was kindly provided by Dr. Richard Oko (Department of Anatomy and Cell Biology, Ontario, Canada), and monoclonal antibody against human protamine was from Dr. Rod Balhorn (Lawrence Livermore National Laboratory, Livermore, Calif., USA). Chemicals used in these experiments were purchased from Sigma-Aldrich (St. Louis, Mo., USA) unless mentioned otherwise.

TEM and measurement of chromatin fibers of spermatids

Greater bandicoot rats were caught in rice fields in the northern parts of Thailand and acclimatized for a few days before use. After anesthesia, the testes were removed from the animals, and small pieces of tissue were immediately fixed in 3% glutaraldehyde and 3% paraformaldehyde in 0.1 M phosphate buffer, pH 7.4, at 4°C, overnight. Some of the tissue was then post-fixed in 1% osmium tetroxide (1 h, 4°C), washed in phosphate buffer, dehydrated by being passed through a graded series of ethanols, and embedded in TAAB epoxy resin. Ultrathin sections were cut, mounted on copper grids, stained with uranyl acetate and lead citrate, and observed with a Philips CM100 transmission electron microscope at 80 kV.

Sizes of chromatin fibers at each spermatid step were measured in ten randomly selected areas of each nucleus. At least ten nuclei at each step of spermiogenesis were measured by Adobe Photoshop software at high resolution by using a modified method as described in Manochantr et al. (2005) with a catalase crystal (lattice spacing: 87.5 Å) as a standard.

Immunohistochemistry of spermatids

For immunohistochemistry, testes were removed, fixed in Bouin's fixative overnight, and processed for paraffin embedding. Sections (5 μm thick) were cut, deparaffinized by being passed through a decreasing series of ethanols, and immersed in 1% saturated lithium carbonate in 70% ethanol to eliminate residual picric acid. Endogenous peroxidase activity was minimized by immersion in 1% H_2O_2 in 70% ethanol. The sections were then pre-blocked with 0.1 M glycine and 4% bovine serum albumin (BSA) in 0.1 M phosphate-buffered saline (PBS), and permeabilized with 1% Triton X-100 in PBS for 15 min. Sections were incubated in either anti-histones, anti-TP2, or anti-protamine antibodies at a dilution of 1:100 (1 h, in a humidified chamber). For controls, the primary antibodies were omitted, or the sections were treated with pre-immune sera. Sections were washed twice in 0.1 M TRIS-buffered saline (TBS) containing 0.05% Tween 20 (TBST) and subsequently exposed to the corresponding horseradish peroxidase (HRP)-conjugated secondary antibodies at a dilution of 1:400 (1 h, room temperature). The peroxidase reaction products were obtained by incubating tissue sections in 0.03% H_2O_2, 0.3% $NiCl_2$, and 0.05% diaminobenzidine tetrahydrochloride (DAB) in TBS and washed in distilled water. Sections were dehydrated by being passed through ethanols, cleared in xylene, and a coverslip placed on top. All images were acquired with a Nikon Eclipse E600 microscope equipped with a Nikon DXM 1200 charge-coupled device camera.

Immunoelectron microscopy of spermatids

Small pieces of testes were fixed in 4% paraformaldehyde and 1% glutaraldehyde in 0.1 M phosphate buffer, pH 7.4. They were then dehydrated and processed for embedding in LR White resin (London Resin, Berkshire, UK). Thin sections were cut with a diamond knife, mounted on Formvar-coated nickel grids, placed on drops of 0.1 M glycine solution in PBS, and blocked with 5% normal goat serum (NGS) in TBST (20 min, in a humidified chamber). They were then incubated (4°C, overnight) with one of the primary antibodies (goat anti-rabbit antibody for H2A, H2B, H3, and TP, and goat anti-mouse antibody for protamine) at a dilution of 1:10 in 1% NGS-TBST, washed with NGS-TBST, incubated in the corresponding secondary antibodies coupled with 10-nm gold particles at a dilution of 1:20 (2 h, in a humidified chamber), and washed repeatedly in NGS-TBS and distilled water. For negative controls, the primary antibody was omitted. The sections were then stained with uranyl acetate and observed with a Phillips CM100 transmission electron microscope at 80 kV.

Extraction of basic nuclear proteins from spermatozoa from the cauda epididymidis

Extraction was performed according to the protocol described by Platz et al. (1975) and Manochantr et al. (2005). Briefly, sperm were gently squeezed from the cauda epididymidis, washed in cold PBS, and then centrifuged at 600*g* for 10 min before being resuspended in sodium-magnesium TRIS (SMT) solution (250 mM sucrose, 2 mM $MgCl_2$, and 10 mM TRIS-HCl, pH 7.4). The sperm were then pelleted (600*g*, 10 min), demembranated with 0.5% Triton X-100 in SMT solution, and centrifuged (1500*g*, 10 min) to obtain the sperm nuclear fraction. Nuclei from chick erythrocytes were prepared similarly.

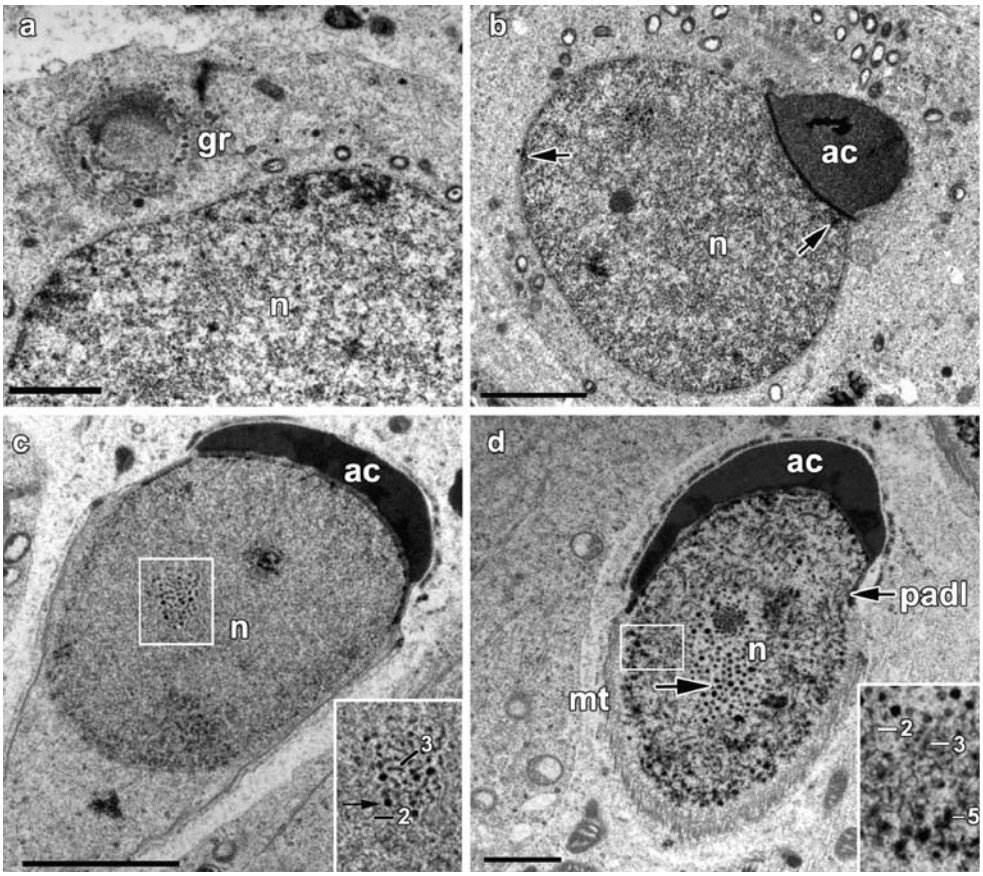
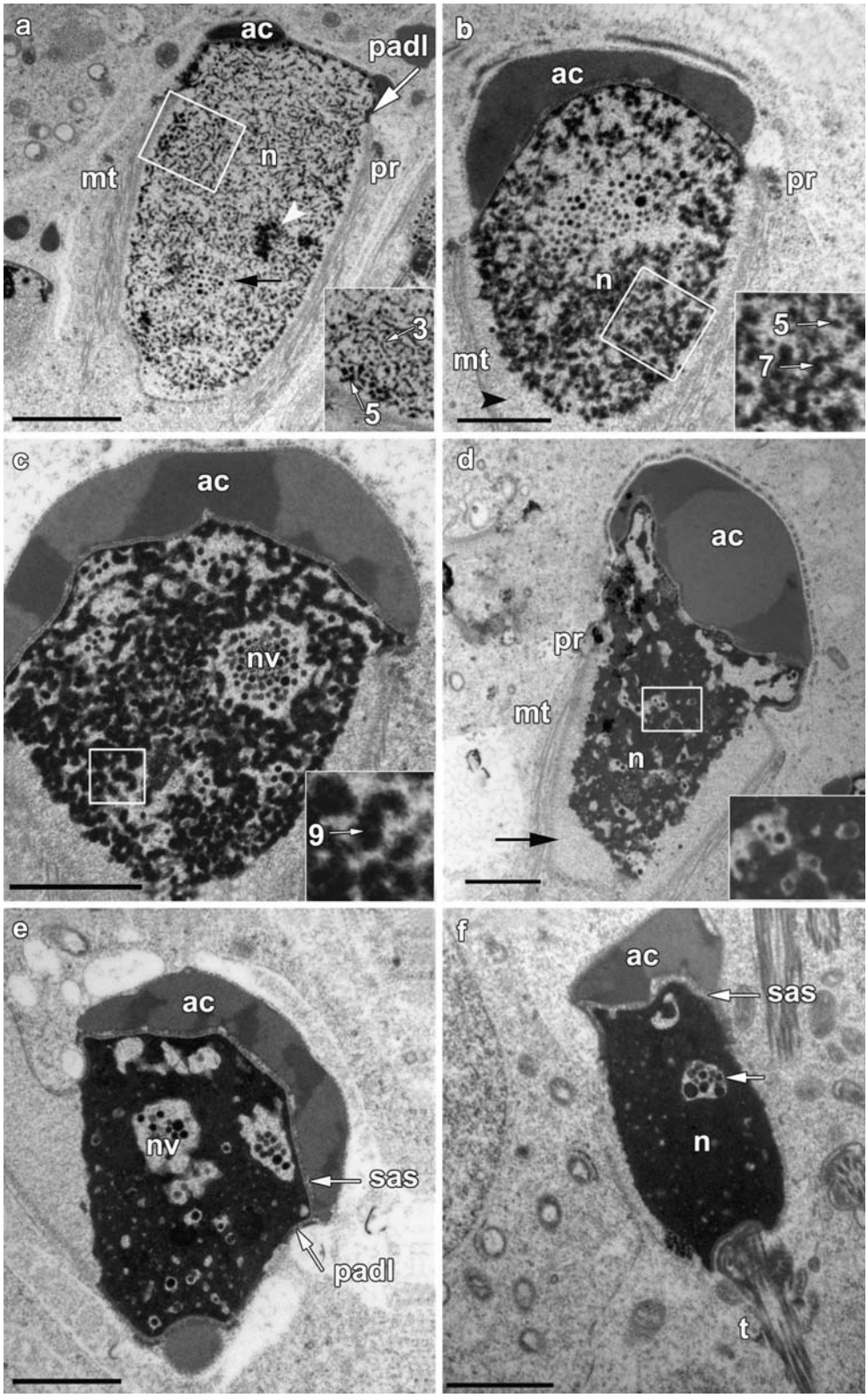


Fig. 1 Transmission electron micrographs of early developing spermatids of *Bandicota indica* testis. **a** A Golgi phase spermatid showing numerous small electron-dense proacrosomal granules (*gr*); the nucleus (*n*) contains 10-nm and 20-nm chromatin threads. **b** An early cap phase spermatid showing a large acrosomal granule (*ac*) attached to the nuclear envelope in the anterior region of nucleus (*n*); condensed chromatin is located just beneath the acrosome and close to other regions of the nuclear envelope (*arrows*). **c** Early acrosome phase spermatid showing cap-shaped acrosome (*ac*) and homogeneous electron-dense chromatin; 30-nm chromatin fibers (*3*) have started to appear in the middle (*inset*) and posterior (*arrow*) regions (*2* 20-nm fibers). **d** An early acrosome phase spermatid showing abundant 30-nm chromatin fibers throughout much of the nucleus (*n*) and thicker chromatin (50-nm fibers) located peripherally. Spherical electron-dense particles lie in the vacuole situated centrally (*arrow*). *Inset*: Three different types of chromatin fibers of 20 (*2*), 30 (*3*), and 50 (*5*) nm (*padl* postacrosomal dense lamina, *mt* microtubule). Bars 1 μm (**a**, **b**, **d**), 2 μm (**c**)



The nuclear fractions of sperm and chick erythrocytes were treated with reducing agent (5 M guanidine HCl, 0.3 M β-mercaptoethanol, and 10 mM dithiothreitol, 0.5 M TRIS-HCl, pH 8.5). To obtain a nuclear suspension, a final concentration of 0.25 N HCl was added, and incubation was carried out for 1 h to extract the basic nuclear proteins (BNPs). Nuclear remnants were then eliminated by centrifugation (12,000*g*, 15 min), and the nuclear proteins in

◀ **Fig. 2** Transmission electron micrographs of late spermatids in the *B. indica* testis. **a** Early acrosome phase showing chromatin fibers of 30 nm (*3*) throughout the nucleus (*n*) with 50-nm fibers (*5*) at the periphery and a localized central region (*arrowhead*, see also *inset*). **b** Mid-acrosome phase spermatid showing 50-nm fibers (*5*, *inset*) throughout the nucleus (*n*) with some 70-nm peripheral chromatin cords (*7*, *inset*); a small region of electron-lucent material occurs posteriorly (*arrowhead*). **c** Mid-acrosome phase spermatid showing large chromatin cords of 90 nm in thickness (*9*, *inset*) with spherical electron-dense particles in the nuclear vacuole (*nv*); the acrosome (*ac*) has two regions of different electron density. **d** Late acrosome phase spermatid showing 90-nm chromatin cords with small region of electron-lucent material posteriorly (*arrow*). **e**, **f** Maturation phase spermatids showing extensive homogeneous electron-dense chromatin, except where nuclear vacuoles (*nv*) are present (*mt* microtubules, *padl* postacrosomal dense lamina, *pr* perinuclear ring, *sas* subacrosomal space, *t* tail). *Bars* 2 μm (**a**), 1 μm (**b-f**)

supernatant were precipitated with 80% trichloro-acetic acid (60 min). The precipitate was recovered by centrifugation (12,000*g*, 10 min), washed twice with cold acidified acetone (−70°C; 2,000:1, v/v: acetone/12 N HCl) and subsequently with cold acetone, and then air-dried.

Acid urea Triton X-100 polyacrylamide gel electrophoresis and immunoblotting of spermatozoa from the cauda epididymidis

BNPs of cauda sperm were separated by 17% acid urea Triton X-100 polyacrylamide gel electrophoresis (AUT-PAGE; 2.5 M urea, 6 mM Triton X-100, and 5% acetic acid; Zweidler 1978). Protein samples were isolated from cauda epididymal sperm and chick erythrocytes, and standard protein markers were dissolved in sample buffer (9 M urea, 0.9 N acetic acid, 5% mercaptoethanol, and 0.2% pyronine-G). Electrophoresis was carried out at a constant current, and some of the gels were stained with Coomassie brilliant blue R-250. Proteins on the other duplicated gels were transferred onto nitrocellulose membrane by using 0.9 N acetic acid, pH 2.3, as the transfer buffer. Non-specific binding of antibodies was blocked with skimmed milk in TBST. The membranes were then flooded with either anti-TP2 or anti-protamine antibodies at a dilution of 1:10,000 (1 h, room temperature), and washed in TBST. Subsequently, the proteins were exposed to the corresponding HRP-conjugated secondary antibodies at a dilution of 1:20,000 (1 h, room temperature) and visualized by enhanced chemiluminescence (ECL) using an ECL Kit (Amersham Pharmacia, Buckinghamshire, UK).

Results

Ultrastructure of spermatids and chromatin organization

We have previously categorized *B. indica* spermatids into 12 steps by light microscopy based on their appearance and the patterns of the germ cell associations (Worawittayawong et al. 2005). In the present study, we extend these

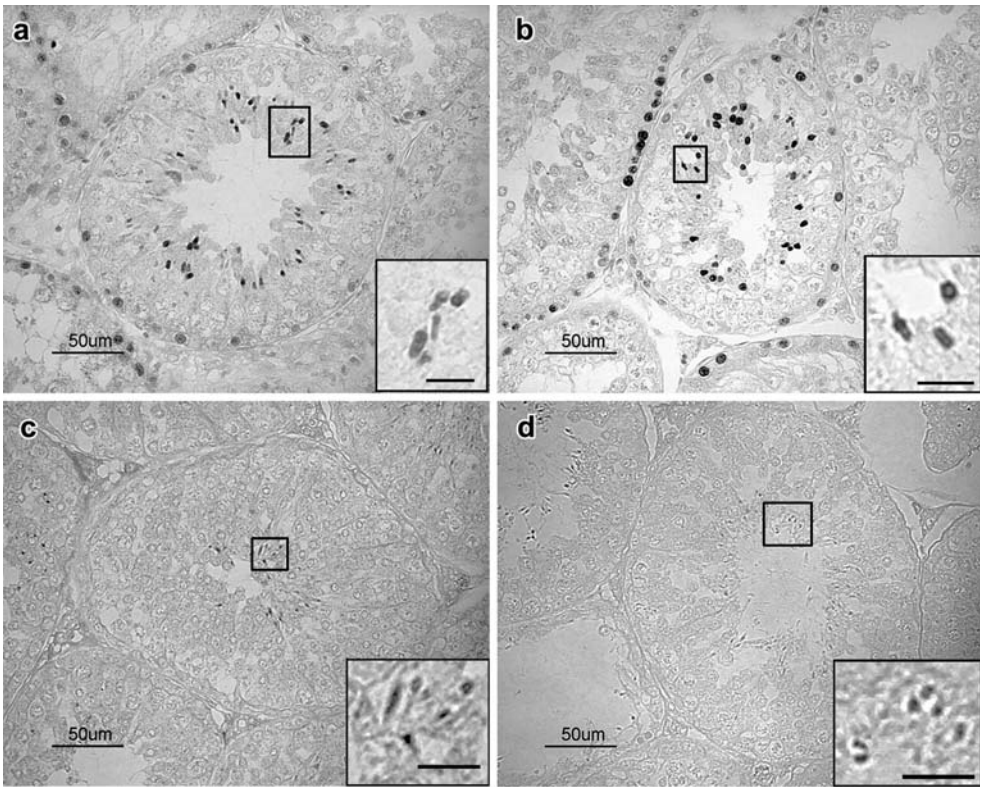


Fig. 3 Immunocytochemistry of BNPs in seminiferous tubules of *B. indica*. **a**, **b** Sections stained with anti-H2B antibody or anti-H3 antibody, respectively, showing the positive staining of many of the nuclei of spermatogonia lying on the basement membrane of the seminiferous tubules and also in some of the spermatids near the lumen (*insets* in **a**, **b**). **c**, **d** Sections stained with antibodies against transition protein2 (TP2) or protamine, respectively, demonstrating positive staining in the nuclei of the late spermatids and spermatozoa (*insets* in **c**, **d**). *Bar* 5 μm (*insets*)

observations by determining the ultrastructural organization of the spermatids with special emphasis on chromatin organization.

The formation of the acrosomal granule, by the attachment of Golgi-body-derived vesicles to the outer nuclear envelope, was characteristic of the Golgi phase (steps 1–2) spermatids (Fig. 1a), similar to that in most mammalian species (Biggiogera et al. 1992; Courtens et al. 1991; Dooher and Bennett 1973; Loir and Courtens 1979). In the early cap phase (steps 3–4) of *B. indica* spermatids, the acrosomal granule became extremely large (Breed 1993) (see Fig. 1b), and the acrosomal matrix developed two regions of differing electron density (Fig. 2c-f) suggesting compartmentalization of the acrosomal contents in the granule. Thickening of the nuclear envelope occurred close to the acrosomal granule with an elongation of the acrosomal granule taking place during the late cap and acrosomal phases (steps 5–9), with the manchette forming around the nuclear periphery (Figs. 1c,d, 2a-d).

In the Golgi phase and early cap phase (steps 1–4) spermatids (Fig. 1a,b), the nuclear chromatin initially appeared as 10-nm and 20-nm scattered granules. In spermatids of the late cap phase (step 5), condensed 30-nm fibers of nucleochromatin began to appear in the central nuclear region (Fig. 1c). Whereas these chromatin fibers spread throughout the nucleus of the spermatids of early acrosome phase (steps 6–7), higher order condensation of chromatin fibers with a diameter of about 50 nm appeared close to the nuclear periphery at a distance from the acrosomal granule (Figs. 1d, 2a, insets). Vacuoles with electron-dense particles surrounded by an electron-lucent region often occurred near the center of the nuclei of these

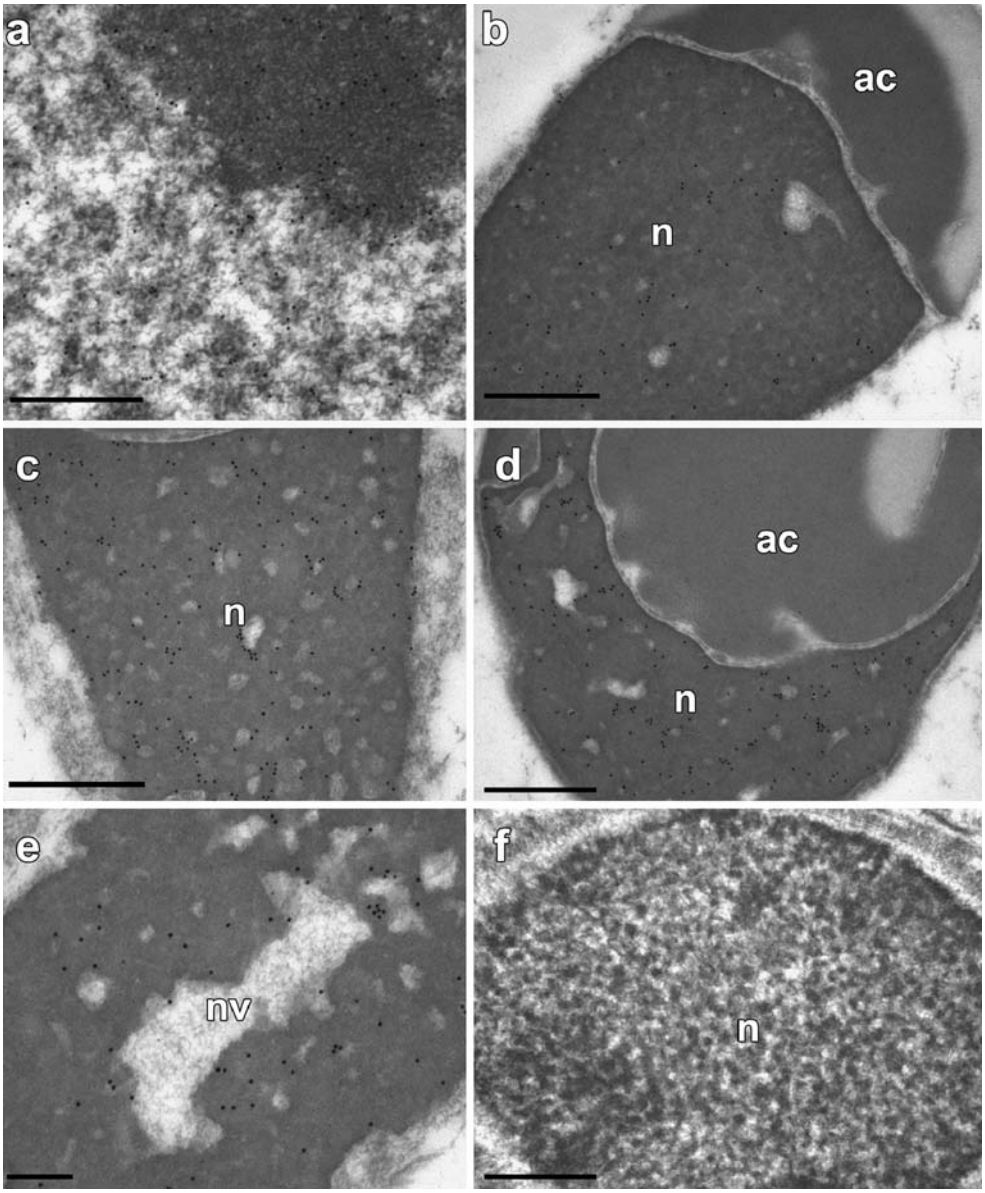


Fig. 4 Transmission electron micrographs of gold-immunolabeled nuclei of *B. indica* spermatocyte and spermatids after immunostaining with anti-histones antibodies (*n* nucleus). Immunostaining with the anti-H2B antibody demonstrated gold particles scattered throughout the condensing nuclear chromatin of a pachytene primary spermatocyte) serving as the positive control for histone (**a** and of a step 12 spermatid (**b**). Immunostaining with the anti-H3 antibody revealed numerous gold particles in the step 10 (**c**) and step 12 (**d**) late spermatids. The acrosome (*ac* in **b**, **d**) exhibited no labeling. No immunogold labeling occurred in the nuclear vacuole (*nv* in **e**) or in the control section (**f**). *Bars* 500 nm (**a-d**, **f**), 200 nm (**e**)

spermatids (Fig. 2b). In the mid-acrosome phase (step 8) spermatids, 50-nm diameter fibers were dispersed throughout much of the nucleus with larger 70-nm diameter fibers being present peripherally (Fig. 2b, inset). All chromatin fibers reached their maximal thickness of about 90 nm in spermatids of the late acrosome phase (step 9), leaving some spaces filled with unidentified material scattered randomly throughout the nucleus (Fig. 2c, inset). The thick chromatin cords in spermatids of the maturation phase (step 10–12) then associated with each other to become highly condensed chromatin patches, with the vacuoles containing the spherical electron-dense particles becoming reduced in size (Fig. 2d-f) as was the overall volume of the nucleus.

Distribution of BNPs in spermatids during spermiogenesis

Intense immunoreactivity to antibodies against histones H2B (Fig. 3a) and H3 (Fig. 3b) was detectable in some of the spermatogonia lining the base of seminiferous tubules. Similar immunostaining by both anti-H2B and anti-H3 was also observed in various spermatids in the adluminal compartment of the tubules (Fig. 3a,b, insets) indicating that these two histones were retained until late differentiation. At the TEM level, as in primary spermatocytes (Fig. 4a), deposition of gold particles was seen in spermatids from the late cap phase (step 9) to the late maturation phase after staining with histone antibodies (Fig. 4b-d). There was an absence of labeling against both anti-histones in the nuclear vacuoles of the late differentiating spermatid nuclei (Fig. 4e) and in the negative controls (Fig. 4f).

Immunoreactivity with anti-TP2 was initially found in step 7 spermatids and remained throughout nuclear maturation (Figs. 3c, 5a,b), whereas staining with the anti-protamine antibody was detected from the mid-acrosomal phase (step 8; Figs. 3d, 5c,d). At the TEM level, some deposition of gold particles initially appeared at step 7 after anti-TP2 staining (Fig. 5a) and in step 8 spermatids after anti-protamine staining (Fig. 5c,d). In step 11–12 spermatids, a slightly increased abundance of gold particles was evident, especially with the anti-protamine antibody, whereas no gold labeling was apparent in the negative controls.

Presence and expression level of TP and protamine of mature sperm

Profiles of BNPs extracted from *B. indica* spermatozoa were analyzed by AUT-PAGE (Fig. 6). Four major protein bands were found to occur, which had similar electrophoretic mobilities to those of the chicken erythrocyte histones H2A, H3, H2B, and H4 in sperm BNP extracts (Fig. 6a,

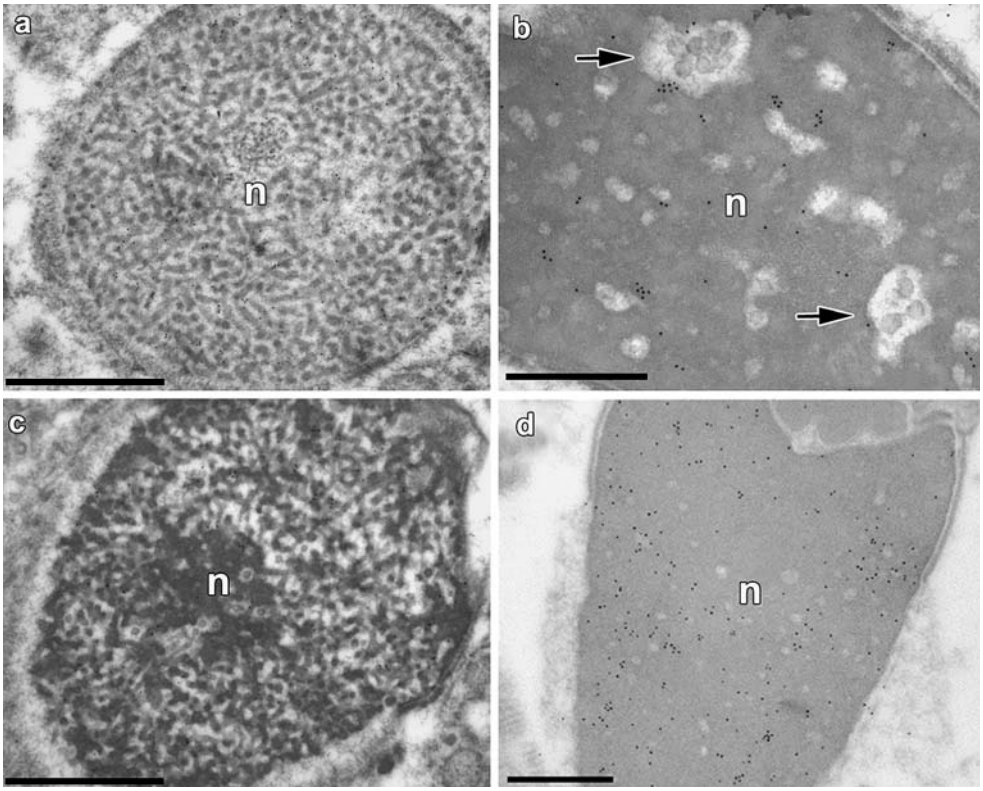


Fig. 5 Transmission electron micrographs of *B. indica* spermatids gold-labeled with the anti-TP2 or anti-protamine antibodies (*n* nucleus). Immunostaining with anti-TP2 antibody showed sparse gold labeling in the chromatin of spermatids at step 7 (**a**) and occurred throughout the chromatin at step 12 (**b**). No gold labelling was seen in the nuclear vacuoles (*arrows* in **b**). Immunostaining with anti-protamine antibody revealed the presence of gold particles in the chromatin of step 8 spermatids (**c**) and throughout the maturing spermatids (**d**). *Bars* 1 μm (**a**, **c**) 500 nm (**b**, **d**)

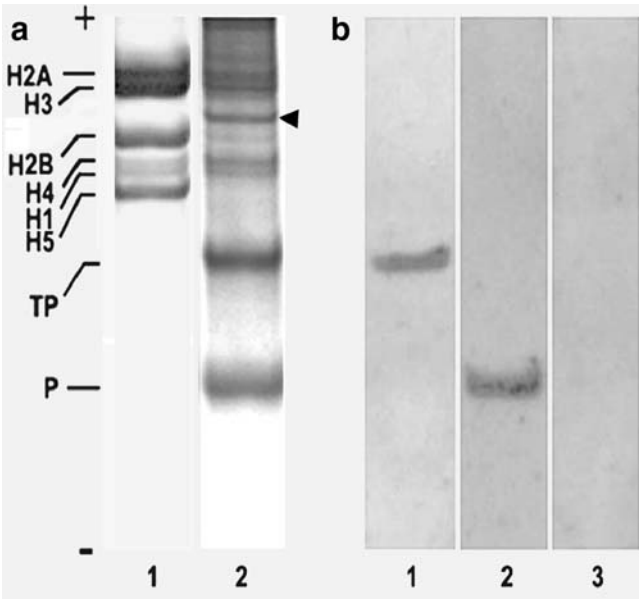


Fig. 6 **a** Comparison of BNPs from cauda epididymal spermatozoa of *B. indica* (*lane 2*) with BNPs from chick erythrocytes (*lane 1*) by 17% acid urea Triton X-100 polyacrylamide gel electrophoresis. Coomassie-blue-stained bands demonstrate core histones (*H2A*, *H3*, *H2B*, *H4*) together with TP and protamine (*P*) in *B. indica* sperm extracts. **b** Immunoblotting with anti-TP (*lane 1*) and anti-protamine (*lane 2*) of epididymal spermatozoa extracts (*lane 3* control–*arrowhead* presumed testis-specific H2B)

lanes 1, 2). Two other major basic proteins occurred, which were probably TP and protamine as judged by their positions on the gels. Results seen in gels of the cauda sperm extracts blotted with specific antibodies against TP and protamine supported the conclusion that TP and protamines occurred in the sperm extracts. The antibodies specifically recognized a single protein band whose mobility was similar to that of TP or protamine (Fig. 6b, lanes 1, 2, respectively). BNP extracts exposed to secondary antibody, as a negative control, revealed only background staining (Fig. 6b, lane 3).

Discussion

Unlike in most murine rodents that have a falciform-shaped sperm head (see Retzius 1909; Friend 1936; Bishop and Austin 1960), the sperm head in male greater bandicoot rats is globular and more like that in other, distantly related, eutherian mammals, with the shape of the nucleus generally reflecting that of the overall head shape (Breed 1993, 1998, 2004; Worawittayawong et al. 2005). Preliminary observations suggested that, during chromatin condensation, the chromatin organization differed from that of the laboratory rat (Breed 1993, 1998). Thus, the question arises as to whether the pattern of chromatin condensation could result, at least in part, in the different final form of the sperm nucleus. In the present study of spermiogenesis in the greater bandicoot rat, we have found that a filamentous organization of the chromatin is evident during early spermiogenesis, similar to that of the laboratory rat (Balhorn et al. 1999; Wanichanon et al. 2001), but that the chromatin fibers then appear to assemble to form thicker chromatin cords. In addition, we have observed that nuclear vacuoles, with electron-dense particles, also occur.

In maturing mammalian spermatids, histones are generally replaced by TPs, which are, in turn, then replaced by protamines (Grimes et al. 1977; Meistrich 1989; Oliva and Dixon 1991; Biggiogera et al. 1992; Oko et al. 1996;

Table 1 Occurrence (+) of histones, transition protein2 (*TP2*), and protamine and of the different sizes of chromatin fibers during spermiogenesis in *Bandicota indica* (*GP* Golgi phase, *ECP* early cap phase, *LCP* late cap phase, *EAP* early acrosome phase,*MAP* mid-acrosome phase, *LAP* late acrosome phase, *MP* maturation phase)

Presence of BNPs and sizes of chromatin fibers	Spermatid steps (1-12)											
	GP		ECP		LCP	EAP		MAP		LAP	MP	
	1	2	3	4	5	6	7	8	9	10	11	12
BNPs												
Histones	+	+	+	+	+	+	+	+	+	+	+	+
TP2							+	+	+	+	+	+
Protamine								+	+	+	+	+
Chromatin fibers (nm)												
10	+	+	+	+								
20	+	+	+	+	+	+						
30					+							
50						+	+	+				
70								+				
90									+			

Wouters-Tyrou et al. 1998). Nevertheless, in human spermatids, a small amount of histone is retained, perhaps localized to the telomere regions at the nuclear periphery (see, for example, Gatewood et al. 1990; Wykes and Krawetz 2003; Churikov et al. 2004), whereas in the laboratory mouse, sperm histones also occur around the peripheral nuclear region (Pittoggi et al. 1999). In the present study of the spermatids of the greater bandicoot rat, immunogold labeling suggests that, whereas only histones are present in the early spermatid nuclei, TPs and protamines are laid down at the time of the thickening of the chromatin fibers and the formation of cords. Information available from several species of mammals has revealed the toroidal chromatin structure of nucleoprotamine organization (Balhorn et al. 1999), but the structure of the DNA-TP complexes does not appear to have been determined. Our finding of chromatin fibers of ~50 nm in the mid-acrosomal phase spermatids suggests this may represent complexes of DNA and TPs (Akama et al. 1996; Singh and Rao 1988). These chromatin fibers then appear to associate with each other to form the thicker chromatin cords of ~90 to 100 nm, which are similar to nucleoprotamine complexes previously found in late spermatids of some other mammalian species (Sobhon et al. 1982; Balhorn et al. 1999) but quite unlike those in the spermatids of common laboratory rodents. The changes in the appearance of BNPs and the size of chromatin fibers in spermatids of the greater bandicoot rat during spermiogenesis is summarized in Table 1.

A further unusual characteristic suggested from the BNP profiles of the sperm extracts taken from the cauda epididymidis of the greater bandicoot rat is the apparent retention of TPs in the mature sperm nuclear extracts. TPs have been previously shown to play a role in chromatin condensation and perhaps in DNA repair during chromatin remodeling (Oko et al. 1996; Yu et al. 2000; Caron et al. 2001; Meistrich et al. 2003). These TPs are generally replaced by protamines (Zhao et al. 2001) and are thus eliminated prior to sperm maturation. However, the present study suggests that, in the sperm of the greater bandicoot rat, one of the TPs is retained even in the nuclei of the spermatozoa from the cauda epididymidis. Further work is now required to determine the distribution and relative abundance of the TPs in the mature sperm of this species. It also remains to be seen whether the remaining TPs and histones co-localize with protamines on the DNA strands to modulate DNA condensation or occur in the peripheral region of the nucleus leaving protamine as the major protein involved in DNA condensation.

Acknowledgements The authors thank Richard Oko for the transitional protein antibody, Sylviane Muller for the histone antibodies, and Rod Balhorn for the protamine antibody.

References

Akama K, Sato H, Furihata-Yamauchi M, Komatsu Y, Tobita T, Nakano M (1996) Interaction of nucleosome core DNA with transition proteins 1 and 3 from boar late spermatid nuclei. J Biochem (Tokyo) 119:448–455

Alfonso PJ, Kistler WS (1993) Immunohistochemical localisation of spermatid nuclear transition protein 2 in the testes of rats and mice. Biol Rep 48:522–539

Allen MJ, Dong XF, O'Neill TE, Yau P, Kowalczykowski SC, Gatewood J, Balhorn R, Bradbury EM (1993) Atomic force microscope measurement of nucleosome cores assembled along defined DNA sequences. Biochemistry 32:8390–8396

Balhorn R (1982) A model for the structure of chromatin in mammalian sperm. J Cell Biol 93:298–305

Balhorn R (1989) Mammalian protamines: structure and molecular interactions. In: Adolph, KW (eds) Molecular biology of chromosome function. Springer, New York, pp 366–395

Balhorn R, Weston S, Thomas C, Wyrobek AJ (1984) DNA packaging in mouse spermatids. Synthesis of protamine variants and four transition proteins. Exp Cell Res 150:298–308

Balhorn R, Cosman M, Thornton K, Krishnan VV, Corzett M, Bench G, Kramer C, Lee JD, Hud NV, Allen MJ, Prieto M, Meyer-Iese W, Brown JT, Kirz J, Zhang X, Bradbury EM, Maki G, Braun RE, Breed W (1999) Protamine mediated condensation of DNA in mammalian sperm. In: Gagnon, C (eds) The male gamete: from basic science to clinical applications. Cache River, Vienna, pp 55–70

Biggiogera M, Muller S, Courtens JL, Fakan S, Romanini MG (1992) Immunoelectron microscopical distribution of histones H2B and H3 and protamines in the course of mouse spermiogenesis. Microsc Res Tech 20:259–267

Bishop MWH, Austin CR (1960) Mammalian spermatozoa. Endeavour 16:137–150

Breed WG (1993) Novel organization of the spermatozoon in two species of murid rodents from southern Asia. J Reprod Fertil 99:149–158

Breed WG (1998) Interspecific variation in structural organisation of the spermatozoon in the Asian bandicoot rats, *Bandicota* species (family Muridae). Acta Zool 79:277–285

Breed WG (2004) The spermatozoon of Eurasian murine rodents: its morphological diversity and evolution. J Morphol 261:52–69

Brewer L, Corzett M, Balhorn R (2002) Condensation of DNA by spermatid basic nuclear proteins. J Biol Chem 277:38895–38900

Caron N, Veilleux S, Boissonneault G (2001) Stimulation of DNA repair by the spermatidal TP1 protein. Mol Reprod Dev 58:437–443

Churikov D, Zalenskaya IA, Zelensky AO (2004) Male germline-specific histones in mouse and man. Cytogenet Genome Res 105:203–214

Corzett M, Mazrimas J, Balhorn R (2002) Protamine 1:protamine 2 stoichiometry in the sperm of eutherian mammals. Mol Reprod Dev 61:519–527

Courtens JL, Loir M (1981) A cytochemical study of nuclear changes in boar, bull, goat, mouse, rat, and stallion spermatids. J Ultrastruct Res 74:327–340

Courtens JL, Biggiogera M, Fakan S (1991) A cytochemical and immunocytochemical study of DNA distribution in spermatid nuclei of mouse, rabbit, and bull. Cell Tissue Res 265:517–525

Dooher GB, Bennett D (1973) Fine structural observations on the development of the sperm head in the mouse. Am J Anat 136:339–361

Friend GF (1936) The sperms of British Muridae. Q J Microsc Sci 78:419–443

Gatewood JM, Cook GR, Balhorn R, Schmid CW, Bradbury EM (1990) Isolation of 4 core histones from human sperm chromatin

represents a minor set of somatic histones. J Biol Chem 265:20662–20666
Grimes SR, Meistrich ML, Platz RD, Hnilica LS (1977) Nuclear protein transitions in rat testis spermatids. Exp Cell Res 110:31–39
Kimmins S, Sassone-Corsi P (2005) Chromatin remodeling and epigenetic features of germ cells. Nature 434:583–589
Lalli M, Clermont Y (1981) Structural changes of the head components of the rat spermatid during spermiogenesis. Am J Anat 160:419–434
Loir M, Courtens JL (1979) Nuclear reorganization in ram spermatids. J Ultrastruct Res 67:309–324
Manochantr S, Sretarugsa P, Chavadej J, Sobhon P (2005) Chromatin organization and basic nuclear proteins in the male germ cells of *Rana tigerina*. Mol Reprod Dev 70:184–197
Meistrich ML (1989) Histone and basic nuclear protein transitions in mammalian spermatogenesis. In: Hnilica LS, Stein GS, Stein JL (eds) Histones and other basic nuclear proteins. CRC Press, Orlando, pp 165–182
Meistrich ML, Mohapatra B, Shirley CR, Zhao M (2003) Roles of transition nuclear proteins in spermiogenesis. Chromosoma 111:483–488
Oko RJ, Jando V, Wagner CL, Kistler WS, Hermo LS (1996) Chromatin reorganization in rat spermatids during the disappearance of testis-specific histone, H1t, and the appearance of transition proteins TP1 and TP2. Biol Reprod 54:1141–1157
Oliva R, Dixon GH (1991) Vertebrate protamine genes and the histone-to-protamine replacement reaction. Prog Nucleic Acid Res Mol Biol 40:25–94
Pittoggi C, Renzi L, Zaccagnini G, Cimini F, Degrassi F, Giordano R, Magnano AR, Lorenzini R, Lavia P, Spadafora C (1999) A fraction of mouse sperm chromatin is organized in nucleosomal hypersensitive domains enriched in retroposon DNA. J Cell Sci 112:3537–3548
Platz RD, Grimes SR, Meistrich ML, Hnilica LS (1975) Changes in nuclear proteins of rat testis cells separated by velocity sedimentation. J Biol Chem 250:5791–5800
Ploen L, Courtens J-L (1986) Comparative aspects of mammalian spermiogenesis. Scanning Electron Microsc 11:639–652
Pradeepa MM, Rao MRS (2007) Chromatin remodeling during mammalian spermatogenesis: role of testis specific histone variants and transition proteins. In: Gupta SK, Koyoma K, Murray JF (eds) Gamete biology: emerging frontiers on fertility and contraceptive development. Nottingham University Press, Nottingham
Queralt R, Adroer R, Oliva R, Winkfein RJ, Retief JD, Dixon GH (1995) Evolution of protamine P1 genes in mammals. J Mol Evol 40:601–607
Retzius G (1909) Spermien der Nagetiere. Biol Untersuch N F 14:133–162
Singh J, Rao MR (1988) Interaction of rat testis protein, TP, with nucleosome core particle. Biochem Int 17:701–710
Sobhon P, Chutatape C, Chalermisarachai P, Vongpayabal P, Tanphaichitr N (1982) Transmission and scanning electron microscopic studies of the human sperm chromatin decondensed by micrococcal nuclease and salt. J Exp Zool 221:61–79
Wanichanon C, Weerachatyanukul W, Suphamungmee W, Meepool A, Apisawetakan S, Linthong V, Sretarugsa P, Chavadej J, Sobhon P (2001) Chromatin condensation during spermiogenesis in rats. Sci Asia 27:211–220
Worawittayawong P, Leigh CM, Cozens G, Peirce EJ, Setchell BP, Sretarugsa P, Dharmarajan A, Breed WG (2005) Unusual germ cell organization in the seminiferous epithelium of a murid rodent from southern Asia, the greater bandicoot rat, *Bandicota indica*. Int J Androl 28:180–188
Wouters-Tyrou D, Martinage A, Chevaillier P, Sautiere P (1998) Nuclear basic proteins in spermiogenesis. Biochimie 80:117–128
Wykes SM, Krawetz SA (2003) The structural organization of sperm chromatin. J Biol Chem 278:29471–29477
Yu YE, Zhang Y, Unni E, Shirey CR, Deng JM, Russell LD, Weil MM, Behringer RR, Meistrich ML (2000) Abnormal spermatogenesis and reduced fertility in transition nuclear protein 1-deficient mice. Proc Natl Acad Sci USA 97:4683–4688
Zhao M, Shirley CR, Yu YE, Mohapatra B, Zhang Y, Unni E, Deng JM, Arango NA, Terry NHA, Weil MM, Russel LD, Behringer RR, Meistrich ML (2001) Targeted disruption of the transition protein 2 gene affects sperm chromatin structure and reduces fertility in mice. Mol Cell Biol 21:7243–7255
Zhao M, Shirley CR, Mounsey S, Meistrich ML (2004) Nucleoprotein transitions during spermiogenesis in mice with transition nuclear protein Tnp1 and TNP 2 mutations. Biol Rep 71:1016–1025
Zweidler A (1978) Resolution of histones by polyacrylamide gel electrophoresis in presence of nonionic detergents. Methods Cell Biol 17:223–233

Provided for non-commercial research and education use.
Not for reproduction, distribution or commercial use.



This article was published in an Elsevier journal. The attached copy is furnished to the author for non-commercial research and education use, including for instruction at the author's institution, sharing with colleagues and providing to institution administration.

Other uses, including reproduction and distribution, or selling or licensing copies, or posting to personal, institutional or third party websites are prohibited.

In most cases authors are permitted to post their version of the article (e.g. in Word or Tex form) to their personal website or institutional repository. Authors requiring further information regarding Elsevier's archiving and manuscript policies are encouraged to visit:

http://www.elsevier.com/copyright

Author's personal copy

Fish & Shellfish Immunology (2008) **24**, 426–435

available at www.sciencedirect.com

ScienceDirect

journal homepage: www.elsevier.com/locate/fsi

Histological and three dimensional organizations of lymphoid tubules in normal lymphoid organ of *Penaeus monodon*

Pornsawan Duangsuwan [a,b], Ittipon Phoungpetchara [a,c], Yotsawan Tinikul [a], Jaruwan Poljaroen [a], Chaitip Wanichanon [a], Prasert Sobhon [a,*]

[a] *Department of Anatomy, Faculty of Science, Mahidol University, Rama VI Road, Bangkok 10400, Thailand*
[b] *Department of Anatomy, Faculty of Science, Prince of Songkla University, Songkhla 90112, Thailand*
[c] *Department of Anatomy, Faculty of Medical Sciences, Naresuan University, Phitsanulok 65000, Thailand*

Received 14 October 2007; revised 17 December 2007; accepted 29 December 2007
Available online 9 January 2008

KEYWORDS
Penaeus monodon;
Lymphoid organ;
Histology;
Fibrous scaffold;
Three dimension;
Vimentin

Abstract The normal lymphoid organ of *Penaeus monodon* (which tested negative for WSSV and YHV) was composed of two parts: lymphoid tubules and interstitial spaces, which were permeated with haemal sinuses filled with large numbers of haemocytes. There were three permanent types of cells present in the wall of lymphoid tubules: endothelial, stromal and capsular cells. Haemocytes penetrated the endothelium of the lymphoid tubule's wall to reside among the fixed cells. The outermost layer of the lymphoid tubule was covered by a network of fibers embedded in a PAS-positive extracellular matrix, which corresponded to a basket-like network that covered all the lymphoid tubules as visualized by a scanning electron microscope (SEM). Argyrophilic reticular fibers surrounded haemal sinuses and lymphoid tubules. Together they formed the scaffold that supported the lymphoid tubule. Using vascular cast and SEM, the three dimensional structure of the subgastric artery that supplies each lobe of the lymphoid organ was reconstructed. This artery branched into highly convoluted and blind-ending terminal capillaries, each forming the lumen of a lymphoid tubule around which haemocytes and other cells aggregated to form a cuff-like wall. Stromal cells which form part of the tubular scaffold were immunostained for vimentin. Examination of the whole-mounted lymphoid organ, immunostained for vimentin, by confocal microscopy exhibited the highly branching and convoluted lymphoid tubules matching the pattern of the vascular cast observed in SEM.
© 2008 Elsevier Ltd. All rights reserved.

Introduction

The lymphoid or Oka organ was first described in *Penaeus orientalis* by Oka [1], and later in *Sicyonia ingentis* by

* Corresponding author. Tel.: +662 201 5406; fax: +662 354 7168.
E-mail address: scpso@mahidol.ac.th (P. Sobhon).

1050-4648/$ - see front matter © 2008 Elsevier Ltd. All rights reserved.
doi:10.1016/j.fsi.2007.12.011

Author's personal copy

Martin et al. [2] who incorrectly described it as haematopoietic nodules. The lymphoid organ of penaeid shrimp consists of two lobes situated ventro-anterior to the hepatopancreas [3]. Each lobe receives the haemolymph from the anterior aorta via the subgastric artery [3,4], which is further branched several times in each lobe of the lymphoid organ. At the light microscope level, the lymphoid organ is composed of two parts: lymphoid tubules and the spaces in between which are occupied by haemal sinuses. Lymphoid tubules consist of the central lumen lined by flattened endothelial cells. Next to the endothelial lining are two types of stromal cells. Cells in the inner layer have a clear, unstained cytoplasm, whereas those in the outer layer have a more darkly stained cytoplasm with H and E staining [4]. It is believed that haemocytes penetrate the endothelial cells into the space between stromal cells, where they settle and later migrate into the haemal sinuses which form part of the open circulatory system [3]. Apart from cellular constituents, there is a connective tissue scaffold that provides support for the lymphoid tubules. In penaeid shrimp, there is no detailed description of the fibrous scaffold of the lymphoid organ. Furthermore, the three dimensional structure of lymphoid tubules and their relationship with the branching subgastric artery have never been demonstrated. In this study the normal lymphoid organ of *Penaeus monodon*, which tested negative for white spot syndrome virus (WSSV) and yellow head virus (YHV), was studied by light microscopy using special staining and transmission electron microscopy in order to demonstrate the histological organization, cellular components, and the connective tissue scaffold, and by a vascular cast technique and SEM to visualize the three dimensional structure of the tubules.

Materials and methods

Shrimps

Wild caught fully mature *P. monodon* were obtained from the Gulf of Thailand. The shrimps were confirmed to be WSSV-negative by PCR and YHV-negative by RT-PCR using the IQ 2000 detection kit (Farming IntelliGene Technology Corporation, Taipei, Taiwan).

Tissue preparation for light microscopic observation

Dissected lymphoid organs were fixed in Davidson's fixative, dehydrated through ascending concentrations of ethanol, cleared with dioxane, and embedded in paraffin wax. Four to six micron thick sections were cut and stained with hematoxylin—eosin (H and E), Periodic acid-Schiff (PAS), and Gomori's stains. All images were captured in a Nikon microscope fitted with a digital camera DXM 1200.

Periodic acid-Schiff stain (PAS)

This staining method was used to identify carbohydrate components especially the extracellular matrix (ECM) in tissue sections. Briefly, the sections were deparaffinized and hydrated in distilled water. The sections were then oxidized by being immersed in 0.5% periodic acid solution for 5 min and washed thoroughly with three changes of distilled water. The sections were then placed in Schiff reagent for 15 min. The excess stain was removed by washing the sections thoroughly with two changes of 2% potassium metabisulfite before washing in running tap water for 10 min to develop full color. The sections were counterstained with hematoxylin, dehydrated with 95 and 100% ethanol, cleared with xylene, mounted with permount, and observed under a light microscope.

Gomori's stain

Gomori's stain was applied to detect reticular fibers in tissue sections because of their argyrophilic property. Briefly, the deparaffinized sections were treated with 0.5% potassium permanganate solution for 1 min and rinsed in tap water for 2 min. After that, the sections were differentiated in 2% potassium metabisulfite solution for 1 min and then washed in running tap water for 2 min. The sections were sensitized in 2% ferric ammonium sulfate for 1 min, washed thoroughly with tap water, and two changes of distilled water for 30 s each. The sections were then impregnated with 10% silver nitrate in distilled water for 1 min. Thereafter, the sections were rinsed in distilled water for 20 s, reduced for 3 min in the formalin solution and washed in tap water for 3 min. The sections were then toned in 0.2% gold chloride solution for 10 min and rinsed in distilled water. Subsequently, the sections were placed in 2% potassium metabisulfite for 1 min, in 2% sodium thiosulfate for 1 min, and washed in tap water for 2 min. Finally, the sections were dehydrated in 95 and 100% ethanol, cleared with xylene and mounted with permount before being observed under the light microscope.

Immunoperoxidase staining using antivimentin and anticytokeratin as cell markers

The deparaffinized sections of the lymphoid organ were prepared as mentioned above and haemolymph smears were prepared by taking haemolymph from the ventral sinus, fixing it with an equal volume of 4% paraformaldehyde for 1 h at 4 °C, and smearing onto glass slides, which were air-dried. Both the tissue sections and haemolymph smears were incubated in 0.3% hydrogen peroxide in methanol for 30 min to remove endogenous peroxidase activity. Thereafter, free aldehyde was quenched with 1% glycine in PBS for 5 min, followed by incubation in a blocking solution (4% BSA and 2% normal goat serum and 0.4% Triton X-100 in PBS) for 2 h. The sections were then incubated overnight at 4 °C in monoclonal antibodies against cytokeratin or vimentin (Sigma Chemical Co., St. Louis, MO, USA), as the primary antibodies, and goat anti-mouse IgG conjugated to HRP, as secondary antibody, for 1 h, respectively. Sections with the primary antibodies omitted or those treated with normal goat serum, served as controls. Subsequently, the sections were immersed in the substrate containing AEC-red (Zymed Laboratories, San Francisco, CA, USA) and counterstained with Mayer's hematoxylin. The sections were washed three times in PBS between each incubation step. All images were

Author's personal copy

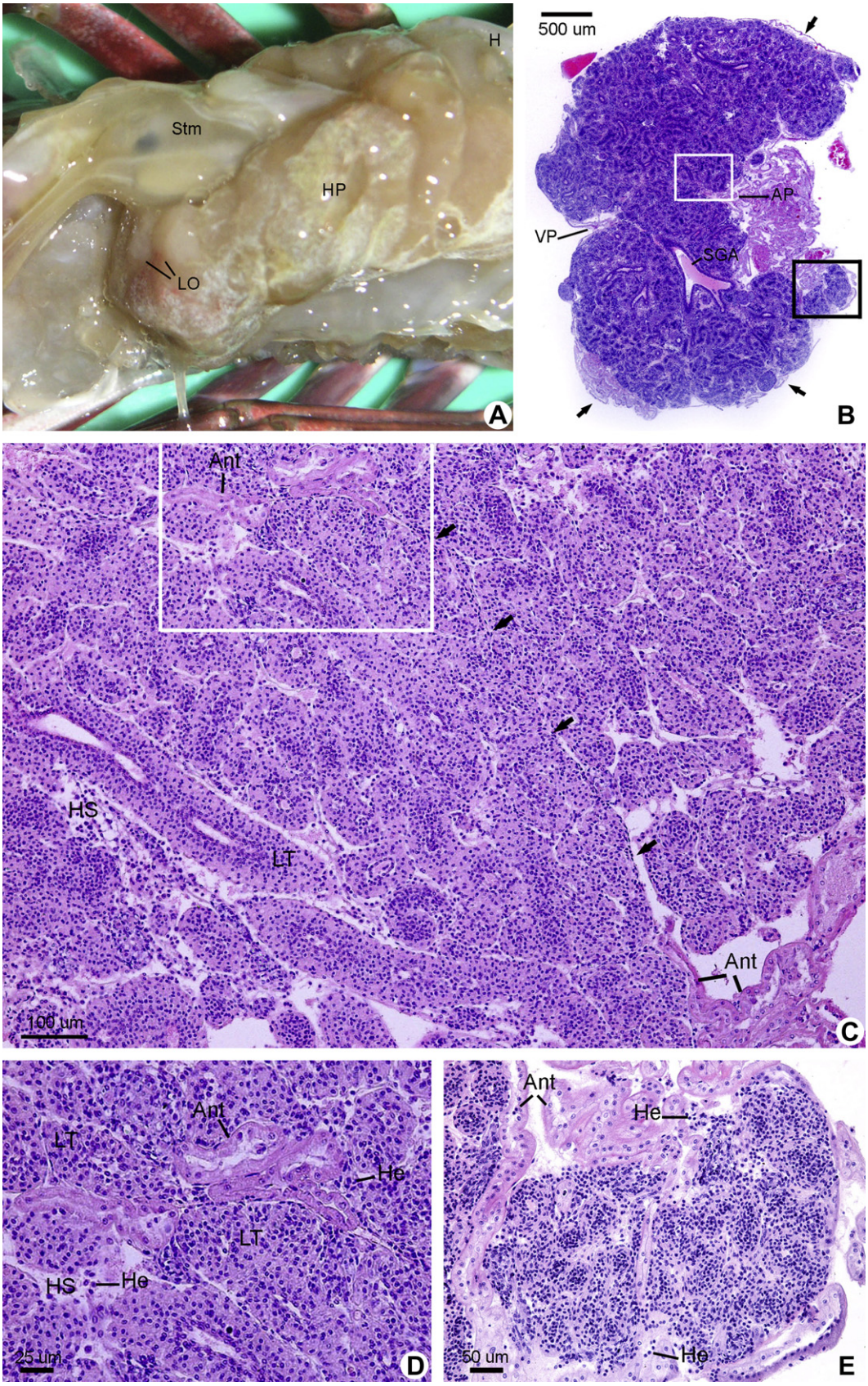


Figure 1 Position of lymphoid organ and light micrographs (LM) of paraffin sections stained with hematoxylin and eosin (H and E). (A) A photograph of the cephalothorax region of *Penaeus monodon* whose carapace was removed, showing the paired lymphoid organs (LO) lying ventral to the stomach (Stm) and dorso-anterior to the ventral hepatopancreas (HP). H: heart. (B) Low

Author's personal copy

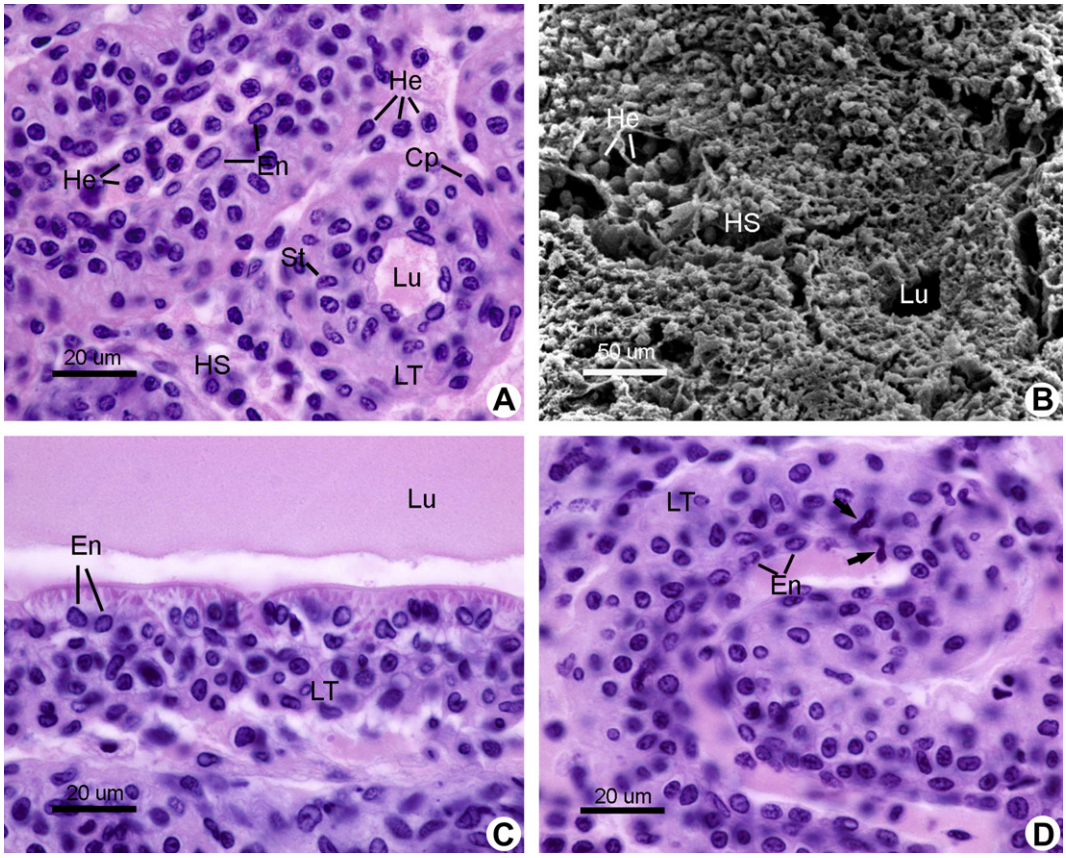


Figure 2 LM (H and E staining) and SEM micrographs of lymphoid tubules. (A, B) Comparable LM (A) and SEM (B) micrographs of lymphoid organs, showing lymphoid tubules (LT) and haemal sinuses (HS), which were packed with a large amount of haemocytes (He). The luminal surface of lymphoid tubule was lined by endothelial cells (En). Capsular cells (Cp) were located at the outermost layer of the lymphoid tubule. Stromal cells (St) were located between endothelial and capsular cells. (C) High magnification LM micrograph of a long section of the proximal part of the lymphoid tubule, showing high cuboidal endothelial cells (En) lining the lymphoid tubule (LT). Lu: lumen. (D) High magnification LM micrograph of a long section of the terminal blind ending of a lymphoid tubule (LT) where the endothelial cells (En) became simple squamous. Haemocytes (arrows) penetrating the endothelium into the wall of lymphoid tubules (LT) were observed.

captured in a Nikon microscope fitted with a digital camera DXM 1200.

Whole mount immunofluorescence observation

Dissected lymphoid organs were fixed with 4% paraformaldehyde, dehydrated in ascending concentrations of ethanol (70 to 100%), permeabilized with Dent's solution (80% ethanol and 20% DMSO) and rehydrated in descending concentrations of ethanol (100 to 50%). Whole lymphoid organs were then incubated in mouse monoclonal anti-vimentin antibody (Sigma Chemical Co., St. Louis, MO, USA) at 4 °C for 3 days and Alexa 594-conjugated goat anti-mouse IgG (Zymed Laboratories, San Francisco, CA, USA) overnight, respectively. The nuclei were stained with ToPro-3 (Zymed Laboratories, San Francisco, CA, USA). The specimens were then cleared in methyl salicylate before being observed under a confocal laser scanning microscope, Olympus FV1000.

Tissues preparation for electron microscopic observations

Dissected lymphoid organs were fixed in 4.2% glutaraldehyde and 1% paraformaldehyde in cacodylate buffer, post-fixed in 1% OsO_4, and dehydrated through ascending concentrations of ethanol. For scanning electron microscopic

magnification LM micrograph, showing the general feature of the lymphoid organ surrounded by a capsule (arrows). Subgastric artery (SGA) entered at the vascular pole (VP) and branched 4—5 times to form vascular plexuses in the lymphoid organ. An antennal tubule complex was situated at the antennal pole (AP). (C—E) Medium and high magnification LM micrographs from the white-boxed area in B (C), white-boxed area in C (D), and black-boxed area in B (E), showing antennal tubules (Ant) which were the invaginating parts from the antennal complex that projected inwards and partitioned the lymphoid organ into lymphoid lobules (arrows in C). Antennal tubules (Ant) and haemocytes (He) in haemal sinuses were also observed (D, E). LT: lymphoid tubule, HS: haemal sinus.

Author's personal copy

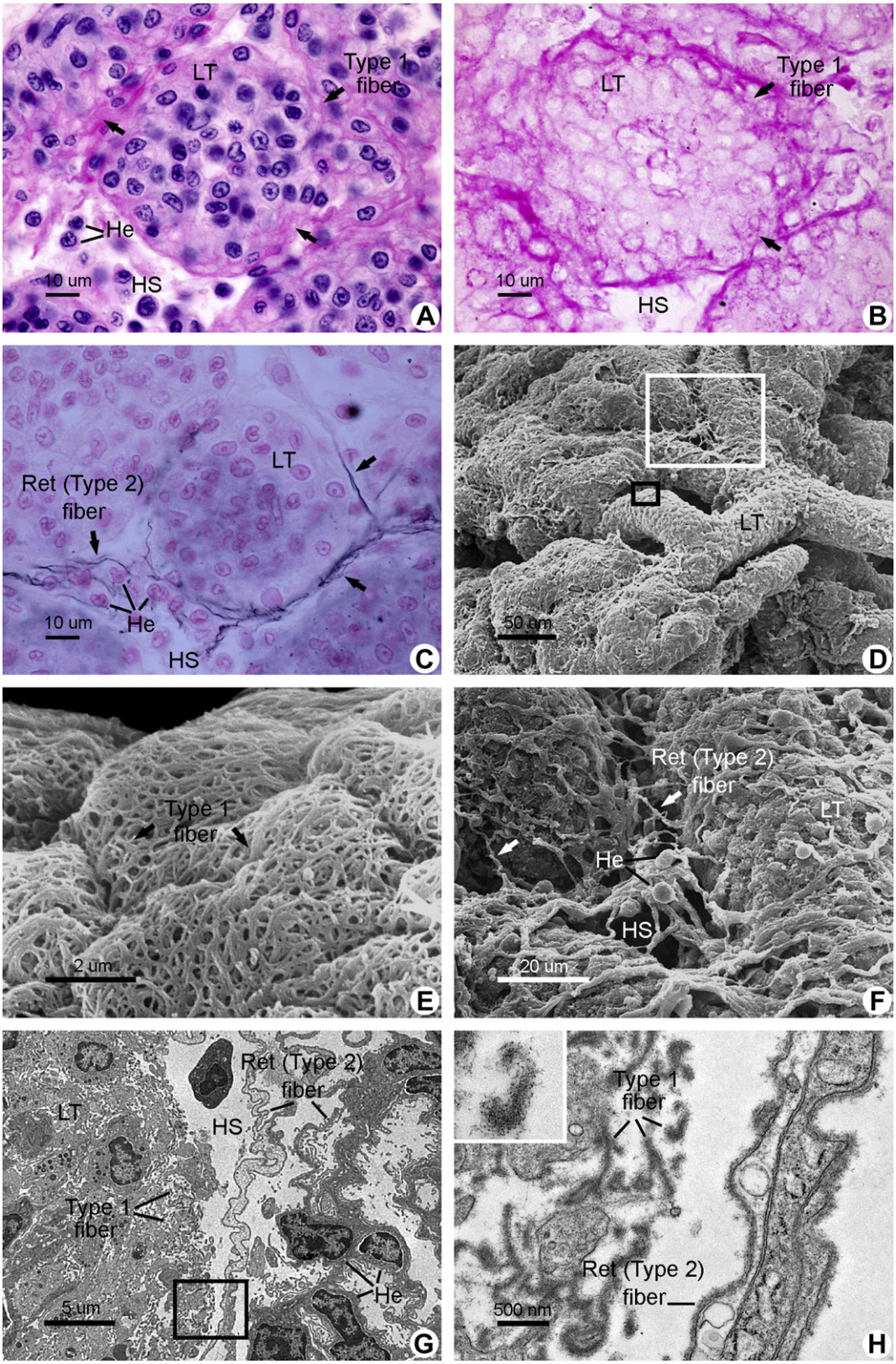


Figure 3 LM, SEM and TEM micrographs of normal lymphoid tubules. (A, B) High magnification LM micrographs of lymphoid tubule sections stained with PAS counterstained with Mayer's hematoxylin (in A) and uncounterstained (in B), showing intensely stained type 1 fibers and the extracellular matrix (ECM) in the capsular layer of lymphoid tubules (arrows), and there were also type 1 fibers running in the thinner ECM between stromal cells. There was no staining in haemal sinuses (HS). He: haemocyte. (C) High magnification LM micrograph of the lymphoid tubule section stained with Gomori's stain for reticular (type 2) fibers, showing thin black

Author's personal copy

observation, specimens were dried in a Hitachi HCP-2 critical point drying machine, mounted on aluminium planchettes and coated with platinum and palladium in an ion sputtering apparatus, Hitachi E-120, before being observed under a Hitachi scanning electron microscope S-2500, at an accelerating voltage of 15 kV. For transmission electron microscopic observation, specimens were embedded in Araldite-502 resin. Ultrathin sections were cut and stained with uranyl acetate and lead citrate before being observed under a Hitachi H600A and a Tecnai G^2 transmission electron microscope at 75 and 80 kV, respectively.

Vascular cast of lymphoid organ

A modified method of Chunhabundit and Somana [5] was used. Briefly, corrosion casts of the lymphoid organ vasculature were made by injecting the heart of the shrimps with Batson's No. 17 Anatomical Corrosion Kit (Polysciences Inc., Warrington, PA, USA). Soft tissues were removed by immersing the cast in 40% sodium hydroxide for 24—48 h, followed by slow rinsing in running tap water for 6—8 h, and washing in several changes of distilled water. Vascular casts were collected under a stereoscope, air-dried, mounted on aluminium planchettes, coated with platinum and palladium in an ion sputtering apparatus, Hitachi E-120, and then observed under a Hitachi scanning electron microscope S-2500 at an accelerating voltage of 15 kV.

Results

Gross anatomy of lymphoid organ

The lymphoid organs were paired and lay ventral to the stomach and dorso-anterior to the ventral hepatopancreas (Fig. 1A). Each lymphoid organ had an ovoid shape and was connected to the heart via the subgastric artery. In the fully mature shrimp (with the body length of 18—20 cm from head to telson, and body weight of 150—170 g), lymphoid organs were about 3—4 mm long, 2—3 mm wide, and 1—2 mm thick.

General histology of lymphoid organ

Each lymphoid organ was surrounded by a connective tissue capsule (Fig. 1B). The capsule invaginated inwards together with antennal tubules, and partitioned each lymphoid organ into lymphoid lobules (Fig. 1B, C). Antennal tubules were derived from the antennal tubule complex situated at the antennal pole of the lymphoid organ (Fig. 1B, C), and they were lined by simple cuboidal epithelium (Fig. 1C, D). The subgastric artery originated from the heart, entered the lymphoid organ at the side opposite to the antennal pole, and branched a further 4—5 times to form vascular plexuses in the lymphoid organ (Fig. 1B, C). Each terminal capillary formed a lumen of a lymphoid tubule, whose interstitial spaces were permeated with haemal sinuses that were packed with large numbers of haemocytes (Fig. 2A, B). Along their entire length, lymphoid tubules generally had the same histological appearance. At the vascular pole, each lymphoid tubule was lined with cuboidal epithelium (Fig. 2C), and had a diameter of approximately 200—250 μm. At the distal end, the endothelial cells decreased in height until they became squamous (Fig. 2A, D), and the diameter of the tubule reached 50—60 μm near the blind ending (Fig. 2C). Encircling the endothelium were 2—6 stromal cell layers (Fig. 2A) with intervening stromal matrix. Cells in the inner layer were tightly packed, whereas fewer cells were observed in the outer layer. The outermost layer was composed of ovoid-shaped capsular cells that ran circumferentially around the lymphoid tubule (Fig. 2A). Haemocytes appeared to penetrate the endothelium and move into the stromal cell layers in the wall of the lymphoid tubule (Fig. 2D).

Histology of the fibrous scaffold

Based on the histochemical staining and ultrastructural characteristics, the fibrous scaffold of the tubule was identified as fibers associated with the extracellular matrix (ECM) and reticular fibers. PAS stained the ECM and associated fibers (type 1) as pink structures, demonstrating the presence of carbohydrate components in both the fibers and ECM (Fig. 3A, B), while Gomori's stained reticular fibers which appeared as black lines representing the argyrophilic (type 2) fibers (Fig. 3C). In the normal lymphoid organ, the thick intensely PAS-positive ECM and associated type 1 fibers formed the capsular layer of each lymphoid tubule (Fig. 3A, B), and the lightly stained thinner ECM and associated type 1 fibers formed the scaffold between stromal cells (Fig. 3A, B). There was no staining of haemal sinuses. When observed by SEM, the type 1 fibers and ECM formed a basket-like network that covered all the lymphoid tubules (Fig. 3D, E). At the TEM level (Fig. 3G, H), the width of each type I fiber was about 100—150 nm. Unlike collagen fibers, no transverse striation was seen in these wavy type 1 fibers (inset in Fig. 3H). In contrast, black lines of argyrophilically stained reticular (type 2) fibers from Gomori's stain were observed around haemal sinuses and surrounding the outermost rim of lymphoid tubules (Fig. 3C). No Gomori's stain stained fibers were found within the wall of the lymphoid tubule (Fig. 3C). By SEM (Fig. 3D, F) and TEM (Fig. 3G, H),

lines around haemal sinuses and lymphoid tubules (arrows). (D) SEM micrograph of the outer surface of lymphoid tubules, showing the surface features of the lymphoid tubule (LT) and haemal sinus. (E) Higher magnification SEM micrograph of the black-boxed area in D, showing numerous basket-like networks of fine type 1 fibers (arrows) forming the capsular layer of lymphoid tubules. (F) Higher magnification SEM micrograph of the white-boxed area in D, showing reticular (type 2) fibers (arrows) surrounding the haemal sinus (HS) and lymphoid tubule (LT). (G) Low and (H) high TEM micrograph taken from the boxed area in G, showing wavy type 1 fibers embedded in the extracellular matrix (ECM) forming the capsular layer of lymphoid tubule. No cross-striation was observed in these fibers (inset in H) or reticular (type 2) fibers located around the lymphoid tubule and haemal sinuses (HS).

Author's personal copy

reticular fibers appeared as networks surrounding haemal sinuses and lymphoid tubules. The size of each reticular fiber was about 100—130 nm.

Immunolabelling with antibodies against cytoskeletal proteins

Cytokeratin and vimentin are cytoskeletal proteins which are specific for epithelial [6] and mesodermal [7] cells, respectively. Hence, the distributions of cytokeratin and vimentin were used as markers for the two types of cells that may come together to constitute the wall of the tubules. Cytokeratin was not observed in any cell type of the lymphoid organ (Fig. 4C). In contrast, vimentin was localized as a reddish reaction product due to AEC, in the cytoplasm of stromal cells which were located in the middle layer of lymphoid tubules (Fig. 4D—F), and in some interstitial cells around haemal sinuses (Fig. 4D, inset). There was no staining in the endothelial and capsular cells in the lymphoid tubule. The negative control experiment using normal goat serum in place of the primary antibodies did not show any immunostaining (Fig. 4B). Immunostaining for cytokeratin and vimentin was not detected in haemocytes within the tubular (Fig. 4B) wall or in haemolymph smears (Fig. 4A).

Visualization of the three dimensional structure of the vasculature in lymphoid organ

The three dimensional structure of the vascularization in the lymphoid organ was displayed by vascular corrosion cast and viewed by scanning electron microscopy (Fig. 5A—D). The two aorta arose anteriorly from the heart and each divided into subgastric and ophthalmic arteries (Fig. 5A). Each subgastric artery was further branched 4—5 times to form vascular plexuses in the lymphoid organ (Fig. 5B). Eventually, subgastric branches formed the highly convoluted and blind-ending terminal capillaries (Fig. 5C). Each capillary formed the lumen of a lymphoid tubule around which fixed and migratory cells form a cuff-like wall. This view was confirmed by the SEM micrograph of the cast whose soft tissues were not removed (Fig. 5D) and where lymphoid tubules exhibited a highly convoluted pattern matching the vascular network. However, the tubular wall was much thicker and not smooth as those appearing in the vascular cast (Fig. 5C). When the whole mounts of the lymphoid organ stained with anti-vimentin were viewed by confocal laser microscopy, the stromal cells that form part of the tubular wall showed an intense green fluorescent staining. This helped to trace the outline and branching pattern of the highly convoluted lymphoid tubules, and supports the notion that the lymphoid tubules were actually terminal branches of blood vessels (Fig. 5E, F).

Discussion

The structural organizations of lymphoid organs of penaeid shrimp have been studied by many authors, i.e., in *P. orientalis* by Oka [1], in *S. ingentis* by Martin et al. [2], and in *Penaeus stylirostris* by Bell and Lightner [4]. These authors described the lymphoid organ as being made up of lymphoid tubules which are the basic unit. It is believed that this organ plays a very important role against infection especially by viruses, as it is essentially a filtering organ that clears the haemolymph of viral particles [8—10]. However, it has not been made clear how lymphoid tubules are structurally related to each other, and how they appear in three dimension. This study is the first report that elucidates these points in the normal lymphoid organ of *P. monodon* that tested negative from WSSV and YHV which are the two major infections. The histology of these lymphoid organs was also judged to be normal. The detailed examination of the vascular cast of the lymphoid organ by SEM indicated clearly that this organ is actually the terminal part of subgastric arteries which branch off from the anterior aorta. The terminal branches of the subgastric artery are actually the blind-ending capillaries, each with a thick wall comprising endothelial cells, stromal cells and capsular cells which are the ''fixed'' cells. Together they formed the cellular scaffold that defined the structure of the lymphoid tubule, whereas haemocytes penetrated the endothelium to occupy the spaces between the stromal cells. In addition to these cellular components, elaborate connective tissue scaffolds were observed in and around lymphoid tubules. These scaffolds were formed by an extensive network of type 1 fibers which were embedded in an extracellular matrix (ECM). Both structures were PAS positive which implied that both were rich in carbohydrate content. This fiber-ECM network formed a thick layer at the capsular side of each tubule, where they appeared as ''basket-like'' in SEM. They, together with capsular cells, form a strong capsule around each tubule. From this capsular layer the fiber-ECM sheets permeated throughout the intercellular space in the tubular wall, and became less prominent only under the endothelial layer. The biochemical nature of this fiber-ECM structure needs to be studied further. However, by comparing with the vertebrate ECM, these combined structures appeared similar to the component of the basement membrane [11]. Moreover, the fibrous components appeared similar to protein fibers embedded in the basement membrane [11]. Interestingly, lymphoid tubules and haemal sinuses are circumscribed at their peripheries by argyrophilic filaments, whose affinity to silver staining and appearance are very much like ''reticular'' fibers in the vertebrate connective tissue [12]. In contrast, type 1 fiber-ECM components are not prevalent around the haemal sinuses and in the intertubular areas. Thus, we believe that this type 2 fiber (or reticular fibers) plays a major role in holding various structures of the lymphoid organ, particularly the lymphoid tubules, together.

Cytokeratin was not detected in any kind of cell, whereas vimentin was present in stromal cells but not in endothelial cells. Based on the vertebrate model of connective tissue, it is plausible that stromal cells, which are the ''fixed'' cells, could be derived from mesodermal origin like fibroblasts [13]. They may also act like fibroblasts in the sense that they provide the supporting scaffold for the lymphoid tubules, and they may even be responsible for the synthesis of type 1 fiber-ECM components, though this needs to be proven in further studies. Similarly, endothelial cells of lymphoid tubules, like endothelial cells of vertebrate capillaries and larger blood vessels, do not have cytokeratin [14,15].

Author's personal copy

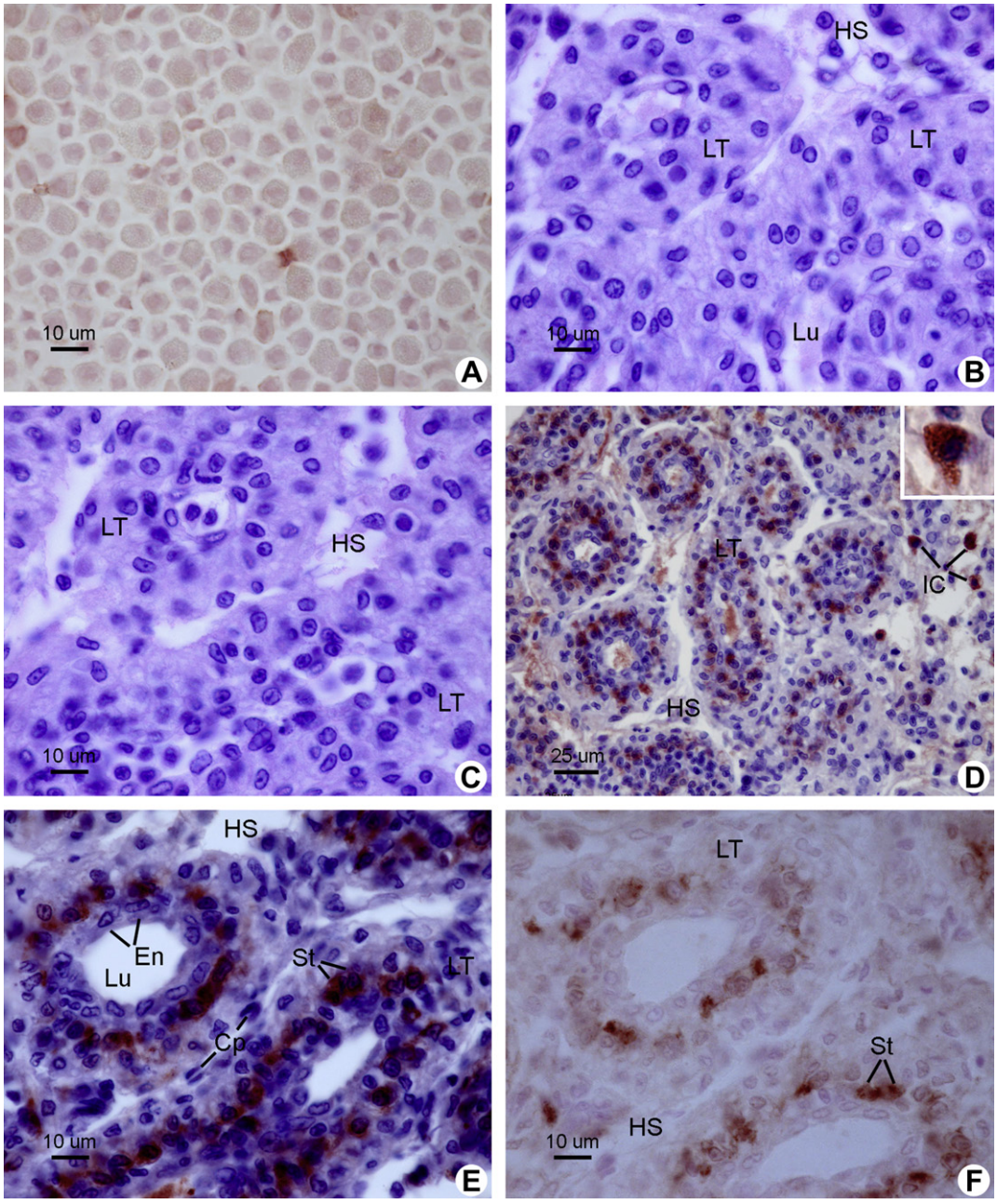


Figure 4 Light micrographs of haemolymph smear and the cross sections of normal lymphoid organ stained by immunoperoxidase technique using monoclonal antibodies (MoAb) against cytokeratin and vimentin as probes, and counterstained with Mayer's hematoxylin. (A) High magnification micrograph of haemolymph smear, showing no immunostaining in any type of haemocytes. (B) The control section of the normal lymphoid organ where the primary antibodies were omitted, showing no immunostaining while only Mayer's hematoxylin counterstaining was observed in the lymphoid tubules (LT) and haemal sinuses (HS). Lu: lumen. (C) High magnification micrograph of a normal lymphoid organ section stained by immunoperoxidase technique using MoAb against cytokeratin as a probe, showing no immunostaining while only Mayer's hematoxylin counterstaining was observed in the lymphoid tubules (LT) and haemal sinuses (HS). (D—F) Medium and high magnification micrographs of normal lymphoid organ sections stained by the immunoperoxidase technique using MoAb against vimentin as a probe and counterstained with Mayer's hematoxylin (in D and E) and uncounterstained (F), showing intense reddish immunostaining in the stromal cells (St) which were located in the middle layer of lymphoid tubules (LT), and some interstitial (IC) cells embedded around haemal sinuses (HS) (inset in D) were also stained. En: endothelial cell, Cp: capsular cell, Lu: lumen.

However, they have bundles of fine filamentous structure in their peripheral cytoplasm when viewed under TEM (data not shown), which could be actin-based microfilaments. Haemocytes, in both haemolymph smears and in sections of lymphoid tubules, do not exhibit either type of cytoskeletal filaments.

Haemal sinuses were described in penaeid shrimp's lymphoid organ by Oka [1], and Bell and Lightner [4], and

Author's personal copy

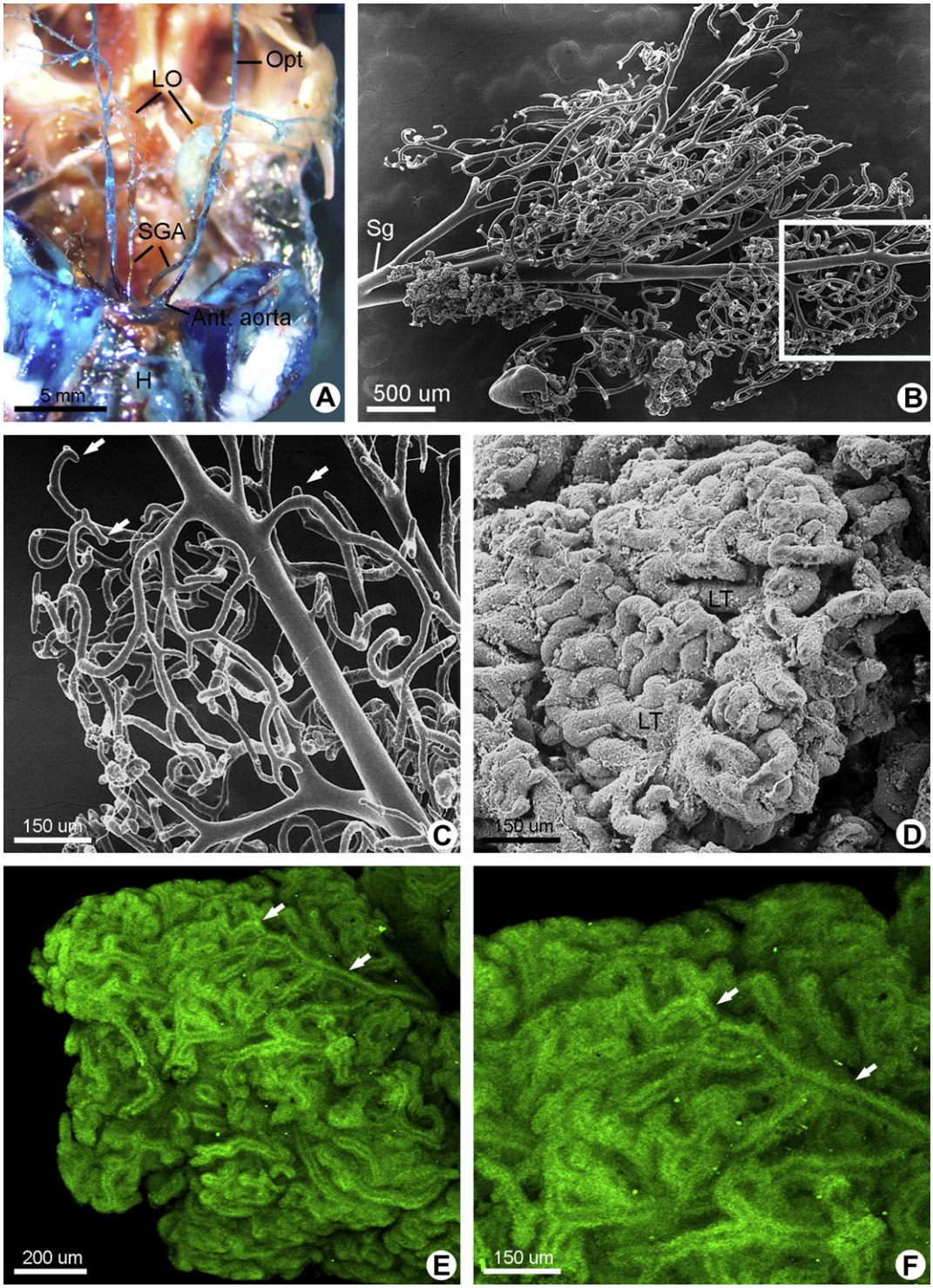


Figure 5 Light, SEM and confocal micrographs of subgastric artery which branched to form vascular plexus in the normal lymphoid organ of *Penaeus monodon*. (A) Overall view of a vascular cast of the cephalothorax region: anterior aorta (Ant. aorta) arose from the heart (H) and each divided into the ophthalmic (Opt) artery which gave off branches and terminated in eyestalk, and subgastric artery (SGA) which further branched to form vascular plexus in the lymphoid organ (LO). (B) Low and (C) medium magnification SEM micrograph taken from the boxed area in B of the normal lymphoid organ prepared by vascular cast technique, and viewed by SEM, showing the subgastric artery branched into highly convoluted and blind-ending terminal capillaries (arrows in C). Each capillary was the lumen of a lymphoid tubule which was surrounded by haemocytes and other cells aggregating to form a cuff-like wall. (D) Medium magnification SEM micrograph of the normal lymphoid organ, showing a large lymphoid tubule (LT) with thick wall branching into smaller highly convoluted tubules. (E, F) Low and medium magnification micrographs of the normal lymphoid organ prepared by staining the organ with anti-vimentin and observed by a confocal laser scanning microscope, showing intense fluorescence staining of stromal cells in the tubular wall (arrows), which could help to trace the outline and branching pattern of the highly convoluted lymphoid tubules comparable to the pattern in C.

Author's personal copy

these authors believed that they are the site where haemolymph is drained back to the circulation, and that they are actually the ''open'' part of the shrimp's open circulation. In addition to haemal sinuses we also observed the presence of an extensive branching system of ''antennal tubules''. This is a network of tubular structures that form part of the capsule of the lymphoid organs. They also branch extensively and permeate into the spaces between lymphoid tubules, sometimes, in close proximity to haemal sinuses. The antennal tubule is lined by cuboidal cells whose characteristics are quite similar to those found in the tubules of the antennal gland [4]. The aggregate of these tubules is observed at the antennal pole of the lymphoid organ (Fig. 1B). Since the lymphoid organ is physically quite close to the antennal gland, it is possible that this ''tuft'' of antennal tubules may be connected with the antennal gland. Since the latter is equivalent to the vertebrate kidney [16,17], it is plausible that these lymphoid associated-antennal tubules may function in controlling the electrolyte balance, osmotic regulation and disposal of wastes.

Taken together we agree with the ''filtering function'' of the lymphoid organ as proposed earlier by Oka [1], Bell and Lightner [4], and Kondo et al. [18]. However, we would like to propose more details to this concept as follows. The lymphoid tubules are essentially the blind-ending capillaries of the subgastric artery, where the haemolymph (blood) of the shrimp passes into, much like the blood circulating into the spleen of mammals. Once in the capillaries (lymphoid tubule lumens), the blood percolates through the endothelial cells and the tubular walls. Under normal situations, some haemocytes also routinely pass into the tubular wall and then traverse into the haemal sinuses with the filtrate. Judging from the extensive network of haemal sinuses, there must be a large volume of haemolymph flowing through the lymphoid organ at any one time. Because of this large amount of flow, part of this filtrate may pass into the antennal tubules which may exercise ''homeostatic control'' on the haemolymph filtered through the lymphoid organ. In other words, the lymphoid organ acts as a true filtering organ for the purposes of filtering and elimination of foreign materials and infectious agents from the haemolymph as well as for homeostatic improvement of the haemolymph filtrate.

Acknowledgements

This research was supported by the Commission on Higher Education (PhD. Scholarship to P. Duangsuwan and Research Group Grant to P. Sobhon) and TRF (Senior Research Scholar Fellowship to P. Sobhon).

References

[1] Oka M. Studies on *Penaeus orientalis* Kishinouye-VIII structure of the newly found lymphoid organ. Bull Jpn Soc Sci Fish 1969; 35:245—50.

[2] Martin GG, Hose JE, Kim JJ. Structure of hematopoietic nodules in the ridgeback prawn, *Sicyonia ingentis*: light and electron microscopic observations. J Morphol 1987; 192:193—204.

[3] Van de Braak CBT, Botterblom MHA, Taverne N, van Muiswinkel WB, Rombout JHWM, van der Knaap WPW. The roles of haemocytes and the lymphoid organ in the clearance of injected *Vibrio* bacteria in *Penaeus monodon* shrimp. Fish Shellfish Immunol 2002;13:293—309.

[4] Bell TA, Lightner DV. A handbook of normal penaeid shrimp histology. Baton Rouge: World Aquaculture Society; 1996. p. 14, 70—3.

[5] Chunhabundit P, Somana R. Scanning electron microscopic study on pineal vascularization of the common tree shrew (*Tupaia glis*). J Pineal Res 1991;10:59—64.

[6] Kummar S, Fogarasi M, Canova A, Mota A, Ciesielski T. Cytokeratin 7 and 20 staining for the diagnosis of lung and colorectal adenocarcinoma. Br J Cancer 2002;86:1884—7.

[7] Prelle K, Holtz W, Osborn M. Immunocytochemical analysis of vimentin expression patterns in porcine embryos suggests mesodermal differentiation from day 9 after conception. Anat Histol Embryol 2001;30:339—44.

[8] Anggraeni MS, Owens L. The haemocytic origin of lymphoid organ spheroid cells in the penaeid prawn *Penaeus monodon*. Dis Aquat Org 2000;40:85—92.

[9] Hasson KW, Lightner DV, Mohney LL, Redman RM, White BM. Role of lymphoid organ spheroids in chronic Taura syndrome virus (TSV) infections in *Penaeus vannamei*. Dis Aquat Org 1999;38:93—105.

[10] Kanobdee K, Soowannayan C, Flegel TW, Ubol S, Withyachumnarnkul B. Evidence for apoptosis correlated with mortality in the giant black tiger shrimp *Penaeus monodon* infected with yellow head virus. Dis Aquat Org 2002;48: 79—90.

[11] Brown B, Lindberg K, Reing J, Stolz DB, Badylak SF. The basement membrane components of biological scaffolds derived from extracellular matrix. Tissue Eng 2006;12:519—26.

[12] Montes GS, Kriszt RM, Shigihara KM, Tokoro R, Mourao PAS, Junqueira LCU. Histochemical and morphological characterization of reticular fibers. Histochemistry 1980;65:131—41.

[13] Salvatori G, Lattanzi L, Coletta M, Aguanno S, Vivarelli E, Kelly R, et al. Myogenic conversion of mammalian fibroblasts induced by differentiating muscle cells. J Cell Sci 1995;108: 2733—9.

[14] Mcdouall RM, Yacoub M, Rose ML. Isolation, culture, and characterisation of MHC class II-positive microvascular endothelial cells from the human heart. Microvasc Res 1996;51:137—52.

[15] Watanabe Y. Microfilaments and intermediate filaments in the fetal capillary endothelial cells of the human chorionic villi — ultrastructural and immunohistochemical study. Nippon Sanka Fujinka Gakkai Zasshi 1989;41:257—64.

[16] Lin S, Liou C, Chen J. The role of the antennal glands in ion and body volume regulation of cannulated *Penaeus monodon* reared in various salinity conditions. Comp Biochem Physiol A 2000;127:121—9.

[17] Johnson PT. A review of fixed phagocytic and pinocytotic cells of decapod crustaceans, with remarks on hemocytes. Dev Comp Immunol 1987;11:679—704.

[18] Kondo M, Itami T, Takahashi Y, Fujii R, Tomonaga S. Structure and function of the lymphoid organ in the kuruma prawn. Dev Comp Immunol 1994;18(Suppl. 1):S109.

Fish & Shellfish Immunology 25 (2008) 560–569

Contents lists available at ScienceDirect

Fish & Shellfish Immunology

journal homepage: www.elsevier.com/locate/fsi

Changes in the histological organization and spheroid formation in lymphoid organ of *Penaeus monodon* infected with yellow head virus

Pornsawan Duangsuwan [a,b], Yotsawan Tinikul [a], Charoonroj Chotwiwatthanakun [c,d], Rapeepun Vanichviriyakit [a,d], Prasert Sobhon [a,*]

[a] Department of Anatomy, Faculty of Science, Mahidol University, Rama VI Road, Bangkok 10400, Thailand
[b] Department of Anatomy, Faculty of Science, Prince of Songkla University, Songkhla 90112, Thailand
[c] Department of Biochemistry, Faculty of Science, Mahidol University, Rama VI Road, Bangkok 10400, Thailand
[d] Center of Excellence for Shrimp Biotechnology, Faculty of Science, Mahidol University, Rama VI Road, Bangkok 10400, Thailand

ARTICLE INFO

Article history:
Received 7 February 2008
Received in revised form 30 July 2008
Accepted 16 August 2008
Available online 29 August 2008

Keywords:
Penaeus monodon
Lymphoid organ
Yellow head virus
Histopathology
Lymphoid spheroid

ABSTRACT

The changes in the histological and three dimensional organizations of lymphoid organ and characteristics of lymphoid cells after chronic infection with yellow head virus (YHV) in *Penaeus monodon* were investigated. The vascular cast of infected lymphoid organ showed less branching and dramatically shortened terminal capillaries that formed the lymphoid tubules, and only large stumps of these lymphoid tubules remained. This might occur because the terminal ends of the tubules were damaged from YHV infection, as stromal cells and hemocytes in the LT wall were infected and formed foci that could give rise to lymphoid spheroids that broke away from the original lymphoid tubules. Histologically, there was a decrease of PAS-stained connective tissue materials in lymphoid spheroids as well as a decrease of stromal cells as marked by anti-vimentin antibody. This indicated that stromal cells together with type 1 fibers and associated extracellular matrix degenerated in lymphoid spheroids, while type 2 or reticular fibers proliferated and encapsulated the spheroids.

© 2008 Elsevier Ltd. All rights reserved.

1. Introduction

The lymphoid organ of penaeid shrimp functions as a hemolymph filter [1–3] and plays a central role in the immune response [4]. It is a major target organ of viral infection [5] and responsible for viral and bacterial clearance [4,6], and elimination of foreign substances from hemolymph [2,7]. Following infection by certain types of viruses, the lymphoid organ forms spheroids [8] which have been reported in infections by vacuolization virus (LOVV) [11], lymphoid parvo-like virus (LPV) [12], lymphoid organ virus (LOV) [13], rhabdovirus of penaeid shrimp (RPS) [14], yellow head virus (YHV) [15], and Taura syndrome virus (TSV) [8].

Hasson et al. [8] classified lymphoid spheroids of white shrimp, *Penaeus vannamei*, infected with Taura syndrome virus into three types. Type A, believed to be the earliest type to appear during the host-viral interaction, is characterized by the presence of lightly basophilic, homogeneous cell masses containing few or no necrotic cells or cell debris. Type B is believed to evolve from type A, but differs in being more basophilic, having higher number of necrotic cells and higher amount of cell debris, with few to moderate amounts of cytoplasmic vacuoles. Type C is believed to evolve from type B, and becomes the terminal lymphoid spheroid, which is characterized by intensely basophilic masses containing degenerating cells with numerous cytoplasmic vacuoles and highly basophilic nuclei [8]. Despite their common occurrence following infection, their origin, mode of formation and relationship to lymphoid tubules still remain unclear. In this study, we have addressed these questions by observing the three dimensional and histopathological changes that occurred in the lymphoid organ of *P. monodon* chronically infected with yellow head virus (YHV) by light microscopy with special stainings, confocal laser scanning (CLSM), scanning electron microscopy (SEM) using vascular cast technique, and transmission (TEM) electron microscopy.

2. Materials and methods

2.1. Shrimps

Thirty wild caught fully mature *Penaeus monodon* (~100–150 g) were obtained from the Gulf of Thailand. The shrimps were screened for white spot syndrome virus (WSSV), Taura syndrome virus (TSV), infectious hypodermal and hematopoietic necrosis virus (IHHNV), hepatopancreatic parvovirus (HPV), and yellow head virus (YHV) infections by RT-PCR using the IQ 2000 detection

* Corresponding author. Tel.: +66 2 201 5406; fax: +66 2 354 7168.
E-mail address: scpso@mahidol.ac.th (P. Sobhon).

1050-4648/$ – see front matter © 2008 Elsevier Ltd. All rights reserved.
doi:10.1016/j.fsi.2008.08.008

kit (Farming IntelliGene Technology Corporation, Taipei, Taiwan). Only shrimp that tested positive with YHV were selected and maintained in 300 L aquarium tanks filled with filtered sea water with continuous aeration at room temperature for at least 21 days. Eight surviving shrimps were considered as chronically infected with YHV and used in this study.

2.2. Nested-RT-PCR detection of YHV using IQ2000 kit

2.2.1. RNA extraction

Shrimp pleopods were excised and homogenized in 1 ml of TRI™ reagent (Pacific Science, USA). Chloroform (200 μl) was then added to the homogenate and the mixture was centrifuged to separate the insoluble materials at 12,000 × *g* for 10 min. The aqueous phase was collected and then 200 μl of chilled isopropanol was added to precipitate RNA. The RNA pellet was collected by centrifugation at 12,000 × *g* for 10 min, washed with cold 75% (v/v) ethanol, dried and re-suspended in 20 μl diethyl pyrocarbonate (DEPC)-treated water.

2.2.2. Nested-RT-PCR

Two microliters (50 ng) of extracted shrimp RNA were added to RT-PCR reaction consisting of 7 μl of RT-PCR premix, 0.50 μl of IQzyme DNA polymerase, and 0.5 μl RT Enzyme Mix. The RT-PCR reaction profile consisted of reverse transcription at 42 °C for 30 min, denaturation at 94 °C for 2 min, 15 cycles of denaturation at 94 °C for 20 s, annealing at 62 °C for 20 s, and extension at 72 °C for 30 s. The reaction was then extended at 72 °C for additional 30 s. The nested-PCR was carried out by adding 15 μl of nested-PCR mixture consisting of 14 μl Nested PCR premix and 1 μl IQzyme DNA Polymerase to the total RT-PCR reaction mixture, then the nested-PCR was performed by 30 cycles of denaturation at 94 °C for 20 s, annealing at 62 °C for 20 s and extension at 72 °C for 30 s. The reaction was then extended for completion at 72 °C for 30 s. A positive control was performed with standard YHV RNA 2000 copies. To the nested-RT-PCR reaction, 5 μl of 6× DNA loading dye was added and mixed. Ten μl of the mixture was fractionated by using 1.5% agarose gel electrophoresis. The bands at 277 and/or 777 base pairs indicated YHV infection (Fig. 1).

2.3. Localization of YHV Gp116 in YHV-infected lymphoid organ

To confirm that the shrimp were infected with YHV, their lymphoid organs were removed and fixed with Davison's fixative overnight. Subsequently, the samples were conventionally processed and embedded in paraffin blocks. The tissue sections (6-μm thick) were blocked with 4% BSA and 10% normal goat serum in Tris buffered saline containing 0.1% Tween 20 (TBST) and then incubated with the monoclonal antibody to YHV envelope glycoprotein 116 (gp116) (a kind gift from Dr. Paisarn Sithigorngul, Faculty of Science, Srinakharinwirot University, Bangkok, Thailand) at dilution of 1:500 for overnight at 4 °C.

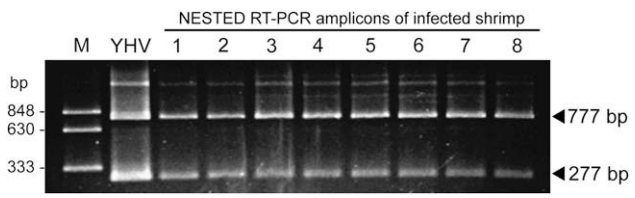


Fig. 1. Detection of YHV-infected shrimp used for the experiments: NESTED-RT-PCR detection of YHV from pleopods using IQ2000 detection kit. PCR amplicons at 277 and 777 bp indicated the specific YHV infection. Lane M: Standard DNA marker, Lane YHV: YHV positive control (2000 copies), lane 1–8; NESTED-RT-PCR product of the infected shrimp.

After washing, the sections were incubated with Alexa 594 conjugated goat anti-mouse IgG (Molecular Probe, Eugene, OR), at dilution 1:2000, for 1 h. The sections were then washed and observed under an Olympus FV1000 Laser Scanning Confocal Microscope (Fig. 2A–D). Exclusion of the primary antibody prior to incubation with secondary antibody was used as the negative control.

2.4. Reconstructing the three dimensional structure of the vascularization of lymphoid organ chronically infected with YHV

2.4.1. Vascular cast of infected lymphoid organ

The modified method of Chunhabundit and Somana (1991) was used [16]. Briefly, vascular-corrosion casts of the subgastric arteries, which supply lymphoid organs of the shrimp were made by injecting the hearts with Batson's #17 Anatomical Corrosion Kit (Polysciences Inc., Warrington, PA). Soft tissues were removed by immersing in 40% sodium hydroxide for 24–48 h, followed by slow rinsing in running tap water for 6–8 h and washed in several changes of distilled water. The vascular casts were collected under a stereoscope, air-dried, coated with platinum and palladium in an ion sputtering apparatus, Hitachi E-120, before being observed under a Hitachi scanning electron microscope S-2500 set at the accelerating voltage of 15 kV.

2.4.2. Whole mount immunofluorescence for visualizing lymphoid tubules

Dissected lymphoid organs were fixed with 4% paraformaldehyde, dehydrated in ascending concentrations of ethanol (70–100%), permeabilized with Dent's solution (80% ethanol and 20% DMSO) and redehydrated in descending concentrations of ethanol (100–50%). Whole lymphoid organs were then incubated in monoclonal anti-vimentin antibody (Sigma Chemical Co., St. Louise, MO) at 4 °C for three days and Alexa 594 conjugated goat anti-mouse IgG (Zymed Laboratories, San Francisco, CA) for overnight, respectively. The nuclei were stained with Topro-3 (Zymed Laboratories, San Francisco, CA). The specimens were then cleared in methyl salicylate before being observed under a confocal laser scanning microscope (CLSM) Olympus FV1000.

2.5. Tissue preparation for observing histopathological changes by light microscopy

Dissected lymphoid organs were fixed in Davidson's fixative, dehydrated through ascending concentrations of ethanol, cleared with dioxane, and embedded in paraffin wax. Four to six micron thick sections were cut and stained with hematoxylin and eosin, Periodic Acid-Schiff (PAS) for extracellular matrix (ECM) [17], Gomori's stain for reticular fibers [18], and immunoperoxidase staining with anti-vimentin and anti-cytokeratin. All images were acquired by a Nikon microscope fitted with digital camera DXM 1200.

2.5.1. Immunolabeling with anti-vimentin and anti-cytokeratin

Hemolymph drawn from the ventral sinus was fixed with an equal volume of 4% paraformaldehyde for 1 h at 4 °C, smeared on the glass slides, and air-dried. The deparaffinized sections, as prepared in Section 2.3, and hemolymph smears were devoided of endogenous peroxidase by being incubated in 0.3% hydrogen peroxide in methanol for 30 min. Thereafter, free aldehydes were quenched with 1% glycine in PBS for 5 min, followed by incubation in blocking solution (4% BSA and 2% normal goat serum and 0.4% Triton X-100 in PBS) for 2 h. The sections were then incubated overnight at 4 °C in the mouse monoclonal antibody (MoAb) against vimentin and cytokeratin (Sigma Chemical Co., St. Louis, MO), and then goat anti-mouse IgG

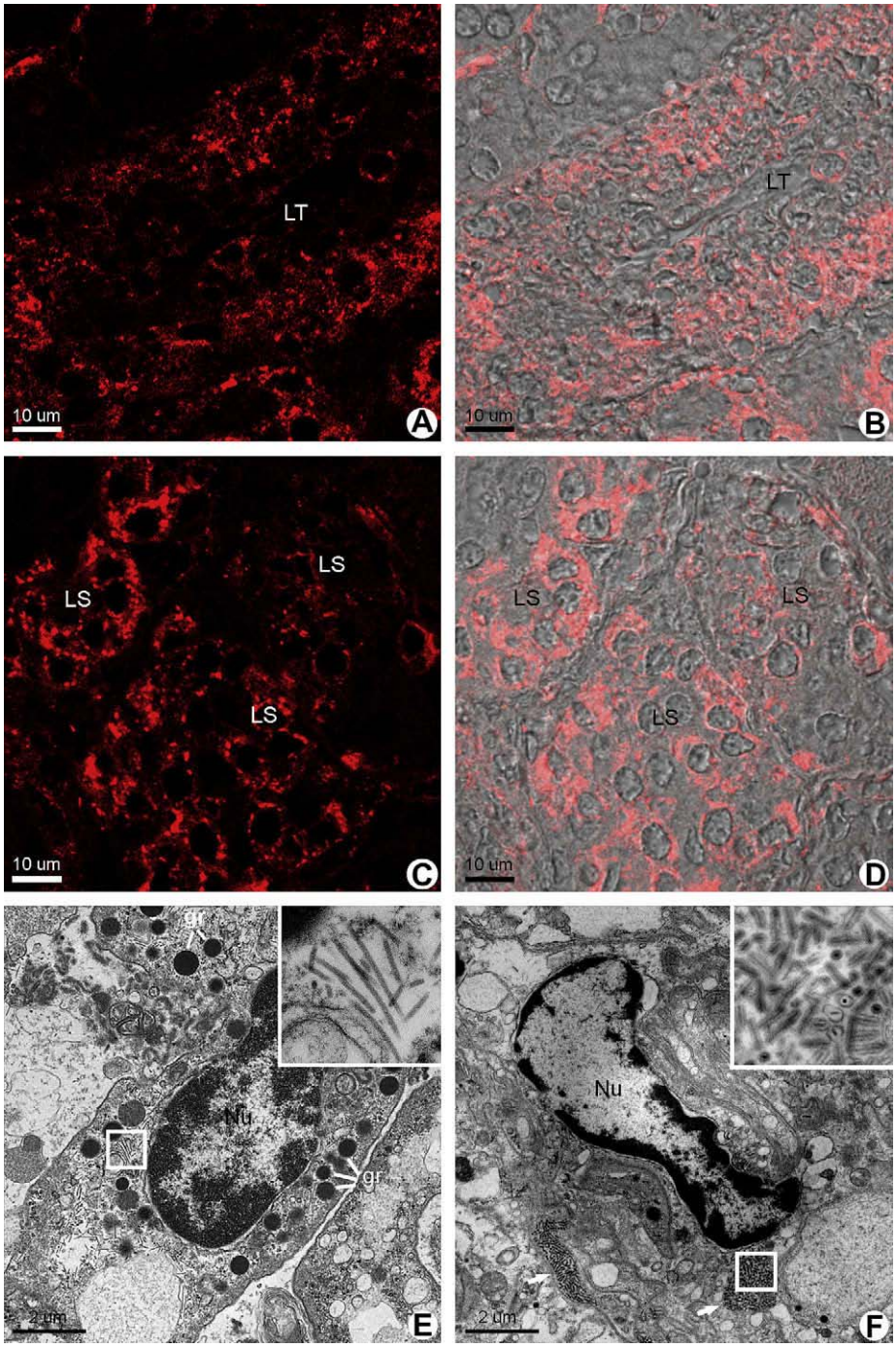


Fig. 2. Confocal laser scanning and TEM micrographs of YHV-infected lymphoid organ. **(A–D)** Confocal laser scanning micrographs of YHV-infected lymphoid organ sections immunostained with monoclonal antibody specific to YHV gp116 envelope glycoprotein. The immunoreactive fluorescence signal is present in cells of the lymphoid tubule with patent lumen (LT, in A), and cells of lymphoid spheroid (LS, in C). The superimposed fluorescence and phase-contrast images of immunostained sections, indicating the existence of YHV in the cytoplasm of cells in both LT (B) and LS (D). **(E)** Medium magnification micrograph of a granular hemocyte from the YHV-infected lymphoid tubule. Numerous unenveloped-YHV particles are observed in it's peripheral cytoplasm, an inset shows high magnification of YHV particles from the boxed area. Nu: Nucleus, gr: granule. **(F)** Medium magnification micrograph of a stromal cell from the infected lymphoid tubule. Numerous enveloped-YHV particles are observed in its cytoplasm (white arrows), and the inset shows high magnification of YHV particles from the boxed area. Nu: Nucleus, gr: granule.

conjugated to HRP, for 1 h. Sections with omitted primary antibodies or those treated with normal goat serum served as controls. Subsequently, the sections were immersed in the substrate containing AEC-red (Zymed Laboratories, San Francisco, CA) and counterstained with Mayer's hematoxylin. The sections were washed three times in PBS between each incubation step. All images were acquired by a Nikon microscope fitted with digital camera DXM 1200.

2.6. Tissue preparation for electron microscopy

Dissected lymphoid organs were fixed in 4.2% glutaraldehyde and 1% paraformaldehyde in 0.2 M cacodylate buffer, post-fixed in 1% OsO_4, dehydrated through ascending concentrations of ethanol. For scanning electron microscopy, specimens were dried in a Hitachi HCP-2 critical point drying machine under liquid CO_2, coated with platinum and palladium in an ion sputtering apparatus,

Hitachi E-120, before being observed under Hitachi scanning electron microscope S-2500 at the accelerating voltage of 15 kV. For transmission electron microscopy, specimens were embedded in Araldite-502 resin. Ultrathin sections were cut and stained with uranyl acetate and lead citrate before being observed under a FEI Tecnai G^2 transmission electron microscope at 80 kV.

3. Results

3.1. Nested-RT-PCR detection of YHV using IQ2000 kit

All the eight infected shrimps, used for vascular cast and histopathological studies were shown to be chronically infected with YHV by nested-RT-PCR as marked by PCR amplicons at 277 and 777 bp, which are specific for YHV infection (Fig. 1). Furthermore, the YHV infection was confirmed by detecting the presence of YHVgp116 envelope glycoprotein in the cells within the wall of intact lymphoid tubules with still patent lumen (Fig. 2A,B). Cells within a lymphoid spheroid without lumen also exhibited the presence of YHVgp116 (Fig. 2C,D). The intensity of fluorescence in the spheroid was more than in the tubule. Furthermore, YHV particles were detected in the hemocytes as well as stromal cells of the infected lymphoid tubule (Fig. 2E,F).

3.2. Changes of the three dimensional structure of lymphoid organ chronically infected with YHV

The vascular cast of a lymphoid organ chronically infected with YHV, viewed by SEM, showed subgastric artery branching into shorter, larger, less convoluted, blind-ending terminals (Fig. 3C,D) in comparison to those of the uninfected shrimp (Fig. 3A,B) (see ref. [23] for description of three dimensional organization of the normal lymphoid organ). It is possible that this occurred as the result of the breaking away of the terminal parts of the lymphoid tubules, some of which might become the lymphoid spheroids. As a result, only short stumps of the original tubules with blind endings remained (Fig. 3D).

When the chronically YHV-infected lymphoid organ was studied by confocal laser microscopy using MoAb against vimentin as a stromal cell marker [23], intense green fluorescence appeared in the lymphoid tubule wall (Fig. 3E) whereas this fluorescence was much less intense in the lymphoid organ spheroid (Fig. 3E,H). In contrast, nuclei stained by ToPro-3, showed intense red fluorescence in both lymphoid tubule and lymphoid spheroid (Fig. 3F,I). Merged pictures, showing orange color (Fig. 3G,J) in lymphoid tubule due to the combination of green and red colors from the presence of vimentin in stromal cells and nuclei of the same cells, whereas lymphoid spheroid exhibited more red staining (Fig. 3G,J) due to the lack of vimentin which implied a lower number of the stromal cells.

3.3. Histopathological changes in lymphoid organ chronically infected with YHV

Chronically YHV-infected lymphoid organ was still covered by a complete capsule bearing the antennal tubules (Fig. 4C). Within the lobules, lymphoid tubules were disorganized and had lost the normal appearance, and parts of the tubules were lymphoid spheroids that lacked a lumen (Fig. 4D–F) when compared to the normal lymphoid organ (Fig. 6A,B). The lymphoid spheroids could be classified into three types as described earlier by Hasson et al. in Taura syndrome virus infection in *P. vanamei* [8]. Spheroid type 1 (Fig. 4G) was a lightly basophilic, homogeneous mass. Cells in the spheroid contained hypertrophic nuclei with few or no cytoplasmic vacuoles. Spheroid type 2 (Fig. 4H), considered to develop from type 1, appeared more basophilic in staining, and was fully encapsulated with a fibrous connective sheet and a layer of cells with flat nuclei. There were increased numbers of apoptotic cells that contained intensely basophilic nuclei and a moderate number of cytoplasmic vacuoles. Spheroid type 3 (Fig. 4I) contained the most basophilic cells and was encapsulated by thick fibrous connective tissue. Most cells in this type of spheroid appeared highly vacuolated with apoptotic nuclei with dense and marginalized chromatin.

3.4. Ultrastructural changes of lymphoid organ chronically infected with YHV

Prior to the examination by TEM, the semithin plastic sections of the same tissue blocks were studied. In the methylene blue-stained semithin plastic sections, infected lymphoid tubules were still lined by endothelial cells (Fig. 5A). In a tubular wall, large numbers of small granular hemocytes surrounded a group of apoptotic cells (Fig. 5A), which were identified as stromal cells at TEM level (Fig. 5C,D). Lymphoid spheroids might form from these focal changes and sequentially transform into the 3 types as mentioned. Spheroid type 1, considered to be the first to develop from lymphoid tubule, appeared as a blue, homogeneous mass in methylene blue staining (Fig. 5B). At the ultrastructural level, spheroid type 1 contained degranulated small granular hemocytes surrounding stromal cells (Fig. 5E,F). No type 1 fiber and PAS-positive ECM were found in the spheroid (see ref. [23] for detailed description of type 1 fiber and ECM). Spheroid type 2 was paler blue when compared to spheroid type 1 (Fig. 5B). There were increasing numbers of hypertrophic and apoptotic cells in spheroid type 2 (Fig. 5B,G). Spheroid type 3 was a degenerating blue-staining mass with mostly vacuolated apoptotic cells (Fig. 5B). At TEM level, it became clear that most cells in this type of spheroid were highly vacuolated and contained apoptotic nuclei (Fig. 5H).

3.5. Change of fibrous scaffold in YHV-infected lymphoid organ

In general, both fibrous components exhibited similar patterns to those of normal lymphoid tubule where PAS-intensely stained extracellular matrix (ECM) were associated with type 1 fibers, and Gomori's stained type 2 (reticular) fibers (see ref. [23] for complete description). However, the staining of ECM and associated type 1 fibers within spheroids appeared much less intense, and less organized than in normal tubules (Fig. 6A,B). In contrast, intensely-stained argyrophilic fibers surrounding lymphoid spheroids became more prominent when compared to those around lymphoid tubules (Fig. 6C). When observed by SEM, spheroids showed a smooth surface (Fig. 6D–F) perhaps due to the loss or lower amount of ECM and type 1 fibers that formed the outer zone of the lymphoid tubules. In comparison, the surface of normal lymphoid tubules appeared rough and basket-like due to the presence of networks of numerous type 1 fibers and ECM (Fig. 6D–F).

3.6. Immunolabeling with anti-vimentin and anti-cytokeratin

No cytokeratin (Fig. 7B) and vimentin (Fig. 7C,D) immunostainings were detected in lymphoid spheroids. In contrast, intact lymphoid tubules in chronically YHV-infected lymphoid organ still showed positive immunostaining of vimentin in stromal cells. The negative control experiment using normal goat serum showed no staining (data not shown). Immunostaining for both cytokeratin and vimentin was not detected in hemocytes in tubular walls (Fig. 7B–D) or in the hemolymph smears (Fig. 7A) as in the case of uninfected shrimp.

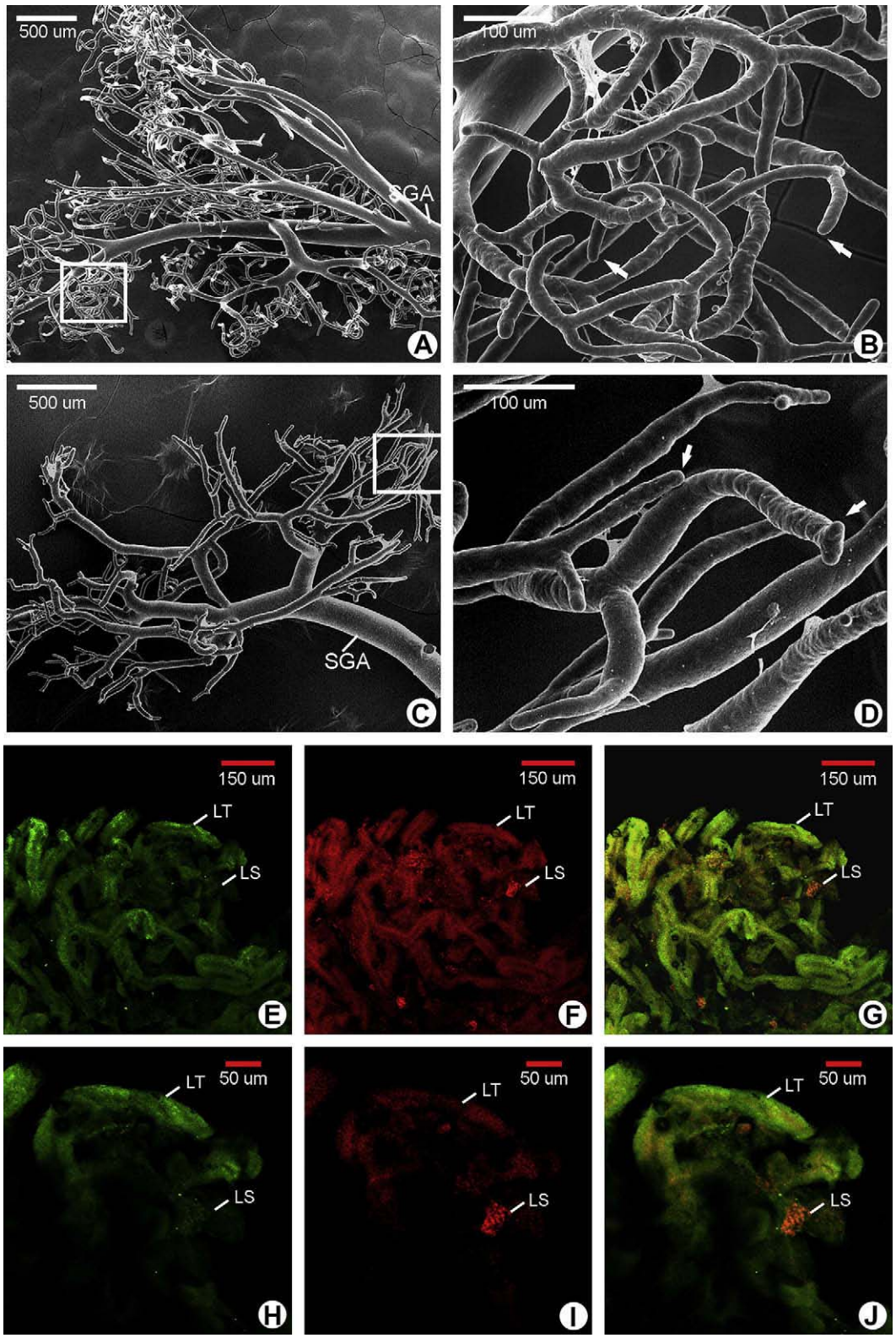


Fig. 3. Scanning electron (SEM) micrographs and confocal (CF) micrographs of normal and chronically YHV-infected lymphoid organs of *P. monodon*. **(A)** Low and **(B)** medium magnification SEM micrograph (taken from boxed area in A) of a normal lymphoid organ prepared by vascular cast technique and viewed by SEM, showing subgastric artery (SGA) branching into highly convoluted and blind-ending terminal capillaries (arrows in B). **(C)** Low and **(D)** medium magnification SEM micrograph (taken from boxed area in C) of chronically YHV-infected lymphoid organ prepared by vascular cast technique and viewed by SEM, showing the subgastric (SGA) artery branching into shorter, more limited number of branches that lead to the blind-ending stumps (arrows in D). It is believed that lymphoid spheroids lack a lumen, hence injected plastic would not fill them and consequently, most lymphoid organ spheroids might be disconnected from lymphoid tubules and washed out during the casting process. **(E–J)** Low and medium magnification CF micrographs of chronically YHV-infected lymphoid organ prepared by staining the whole-mounted lymphoid organ with MoAb against vimentin and viewed by confocal laser scanning microscopy, showing intense green fluorescence in lymphoid tubule (LT) but less intense fluorescence in lymphoid spheroid (LS) in E, H. Nuclei stained by ToPro 3 in F and I, show intense red fluorescence in both lymphoid tubule (LT) and lymphoid spheroid (LS). Merged pictures in G and J show orange color in lymphoid tubule (LT) due to the merged green fluorescence of vimentin and red fluorescence of nuclei in the same cells, whereas lymphoid spheroid (LS) was more red due to the lack of vimentin in stromal cells.

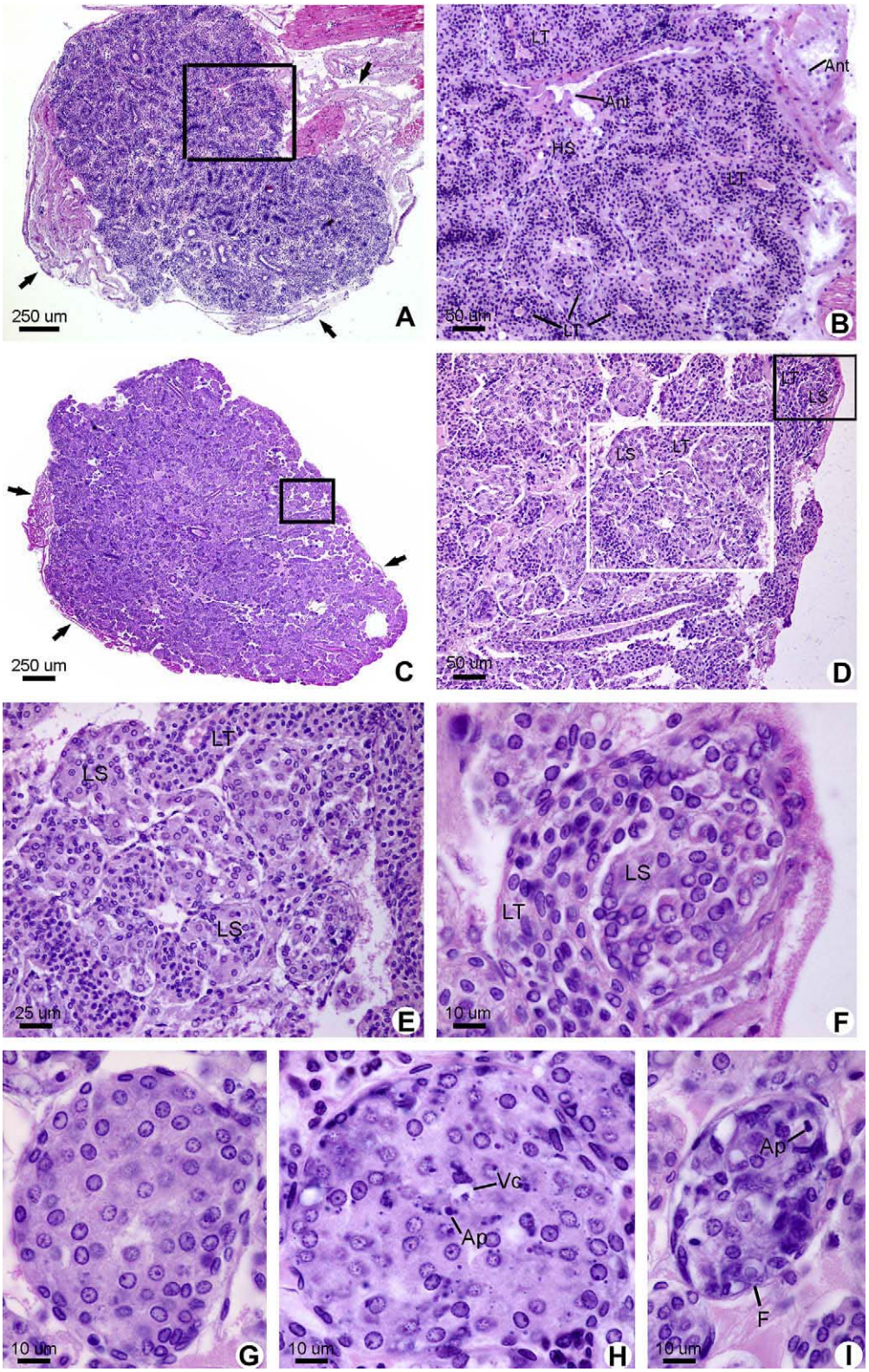


Fig. 4. Light micrographs (LM) of paraffin sections of normal and chronically YHV-infected lymphoid organs of *P. monodon* stained with hematoxylin and eosin. **(A, C)** Low magnification LM micrographs, showing the general features of normal (in A) and YHV-infected (in C) lymphoid organs surrounded by capsules containing antennal tubules embedded in the connective tissue (arrows in A and C). **(B)** A medium magnification LM micrograph taken from boxed area in A, showing antennal tubules (Ant) which are the invaginated parts from the antennal capsules that project inwards and partitioned the lymphoid organ into lymphoid tubules, each showing patent lumen. LT: lymphoid tubule, HS: hemal sinus. **(D)** A medium magnification LM micrograph taken from boxed area in C, showing lymphoid tubule (LT) transformed into lymphoid spheroid (LS) with occluded lumen. **(E, F)** High magnification micrographs, showing in E (taken from white-boxed area in D) the transitional zone from lymphoid tubule (LT) to the more disorganized lymphoid spheroid (LS), and in F (taken from black boxed area in D) long section of LS that lacked lumen. **(G)** A high magnification micrograph of a lymphoid spheroid type 1, showing light basophilic homogenous spheroid. The spheroid contained cells with hypertrophic nuclei with marginating heterochromatin along the nuclear periphery but no cytoplasmic vacuoles. **(H)** A high magnification micrograph of a lymphoid spheroid type 2, showing more intense basophilic spheroid. Prominent fibrous connective tissue capsule surrounded the spheroid. Increasing numbers of apoptotic (Ap) cells with fragmented nuclei with densely stained chromatin and cytoplasmic vacuoles (Vc) were observed. **(I)** A high magnification micrograph of a lymphoid spheroid type 3, showing the smallest and most basophilic spheroid clearly encapsulated by fibrous tissue (F). Vacuolized apoptotic (Ap) cells are present over the entire spheroid.

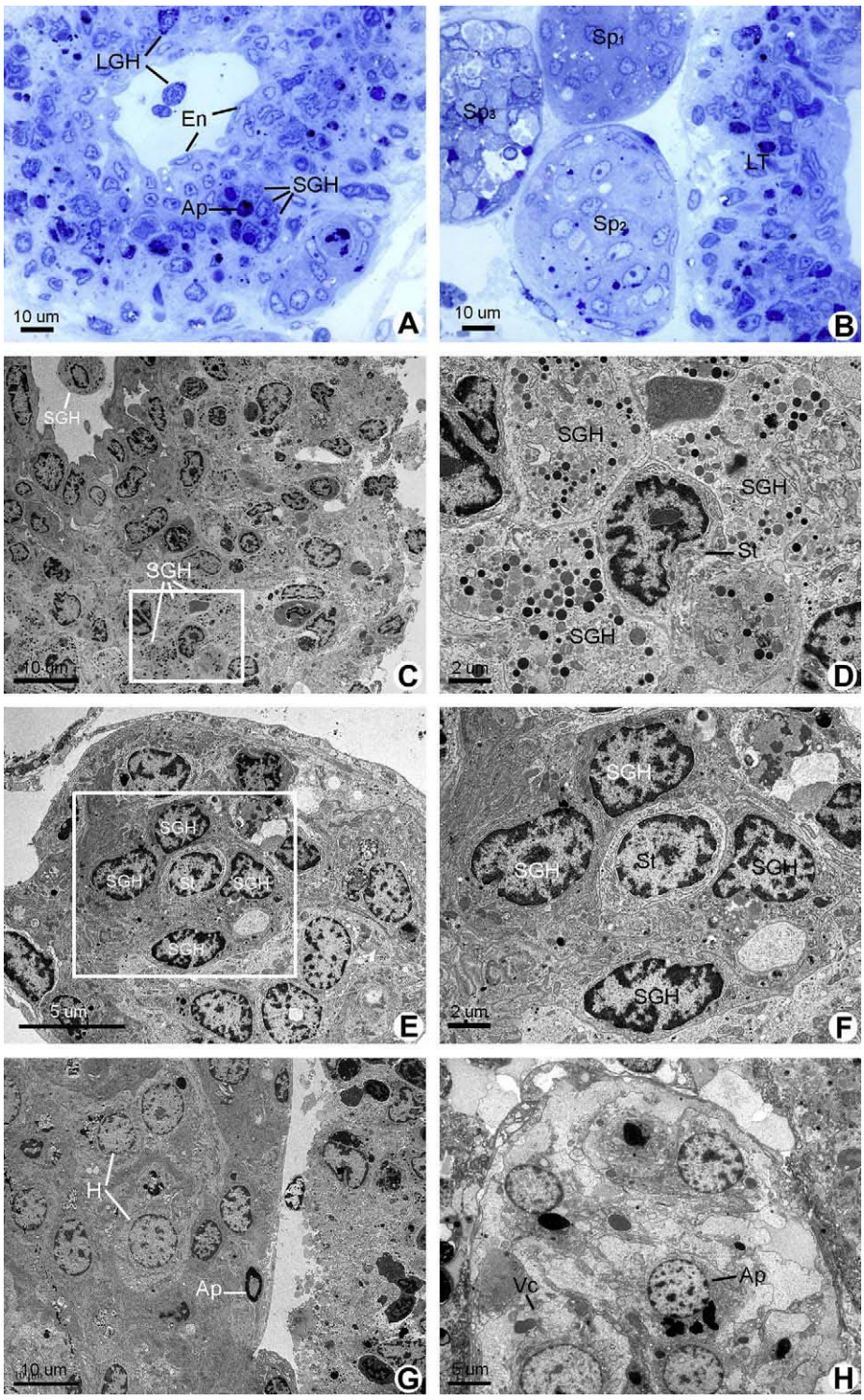


Fig. 5. Light (LM) and transmission electron (TEM) micrographs of chronically YHV-infected lymphoid organs of *P. monodon*. **(A, C, D)** High magnification LM micrographs of semi-thin sections of chronically YHV-infected lymphoid organ stained with methylene blue (in A) and TEM micrographs (in C and D), showing a large number of small granular hemocytes (SGH) surrounding apoptotic (Ap) cells (in A), which were identified as stromal cell (St). En: Endothelial cell. **(B)** A high magnification LM micrograph of semi-thin section of chronically YHV-infected lymphoid organ stained with methylene blue, showing infected lymphoid tubule (LT) and three types of spheroids: type 1 (Sp_1), type 2 (Sp_2) and type 3 (Sp_3). **(E)** Low and **(F)** medium magnification TEM micrograph (taken from boxed area in E) of lymphoid spheroid type 1, showing a group of degranulated small granular hemocytes (SGH) surrounding a stromal cell (St). **(G)** A low magnification TEM micrograph of lymphoid spheroid type 2, showing increasing number of hypertrophic (H) and apoptotic cells (Ap) in the spheroid. **(H)** A low magnification TEM micrograph of lymphoid spheroid type 3, showing vacuolized apoptotic (Ap) cells in the entire spheroid.

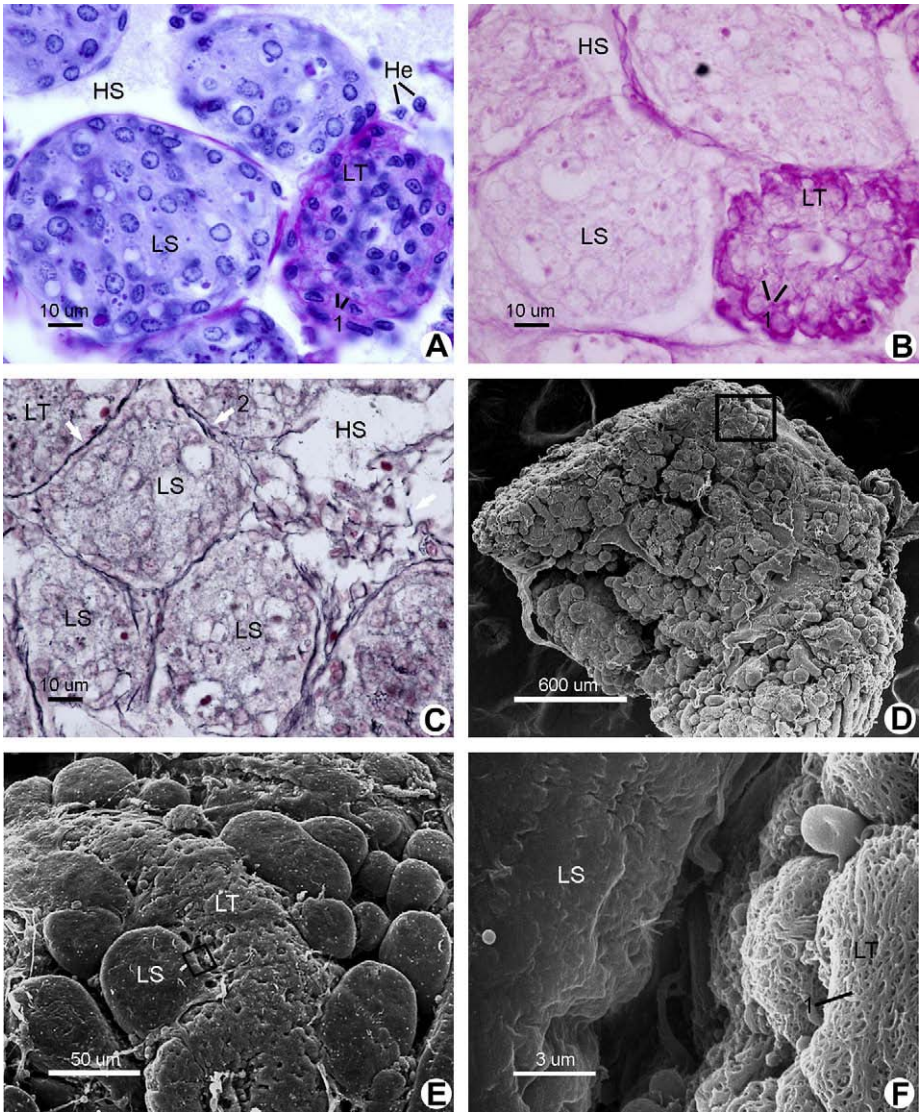


Fig. 6. Light and SEM micrographs of chronically YHV-infected lymphoid organs of *P. monodon*. **(A, B)** High magnification LM micrographs of lymphoid organ sections stained with PAS and counterstained with Mayer's hematoxylin (in A) and uncounterstained (in B), showing intense PAS staining of fibrous scaffold of type 1 fibers and extracellular matrix (ECM) at the capsular layer of lymphoid tubules (LT), and light staining of type 1 fibers running in ECM between stromal cells. However, the staining of ECM and associated type 1 fibers within the spheroid (LS) appeared much less intense and less organized. There was no staining in hemal sinuses (HS). He: Hemocyte, 1: type 1 fibers. **(C)** A high magnification LM micrograph of a lymphoid organ section stained with Gomori's stain for reticular fibers (type 2 fibers), showing black lines (arrows) around hemal sinuses (HS), and lymphoid spheroids (LS) and lymphoid tubules (LT). 2: type 2 fibers. **(D–F)** SEM micrographs, showing the surface of chronically YHV-infected lymphoid organ. Spheroids (LS) exhibited smooth surface due to the lack of type 1 fibers and ECM (in E-which was taken from the boxed area in D), whereas there were still numerous networks of type 1 fibers and ECM surrounding lymphoid tubule (LT), which make it's surface appearing rough and basket-like (in F which was taken from boxed area in E). 1: type 1 fibers.

4. Discussion

In this report, only the YHV-infected shrimp were selected for the histopathological study in order to make sure that any changes that occurred would be in response to a single species of virus. This was ascertained by the rigorous diagnosis of YHV infection with nested-RT-PCR. Furthermore, YHVgp116 envelope glycoprotein was detected specifically in cells within the wall of lymphoid tubules as well as lymphoid spheroids. The most obvious changes in the organization of lymphoid organ of the chronically YHV-infected shrimp were the presence of numerous lymphoid spheroids (LS) that were formed during the course of infection. Vascular casts of the infected lymphoid organ showed that the terminal lymphoid tubules (LT) were drastically shortened and the branching of LT was not as elaborate as normal LT. In many instances only the relatively large "stumps" of the terminal LT remained. Furthermore, observation by light microscopy of a large area and labeling of spheroid stromal cells by vimentin indicated that the lumen in the distal end of LT was obliterated and this end might breakdown thus shortening the original LT. The formation of LS in penaeid shrimp has been previously studied in *P. vannamei* [8] and in *P. monodon* [10]. These authors observed the presence of three types of spheroidal masses after infection with taura syndrome virus and proposed that they played roles in sequestering and finally eliminating viruses. The morphological transformation of lymphoid spheroid type 1–3 represented the viral sequestering stages largely by hemocytes, most of which became apoptotic in stage 3 spheroid. As a result, the viruses were prevented from spreading and were eliminated. However, in chronic infection a certain amount of viral particles remained, thus LT were re-infected and the cycle of LS formation was repeated and resulted in the abundance of LS in the lymphoid organ as observed in the present study. As for the

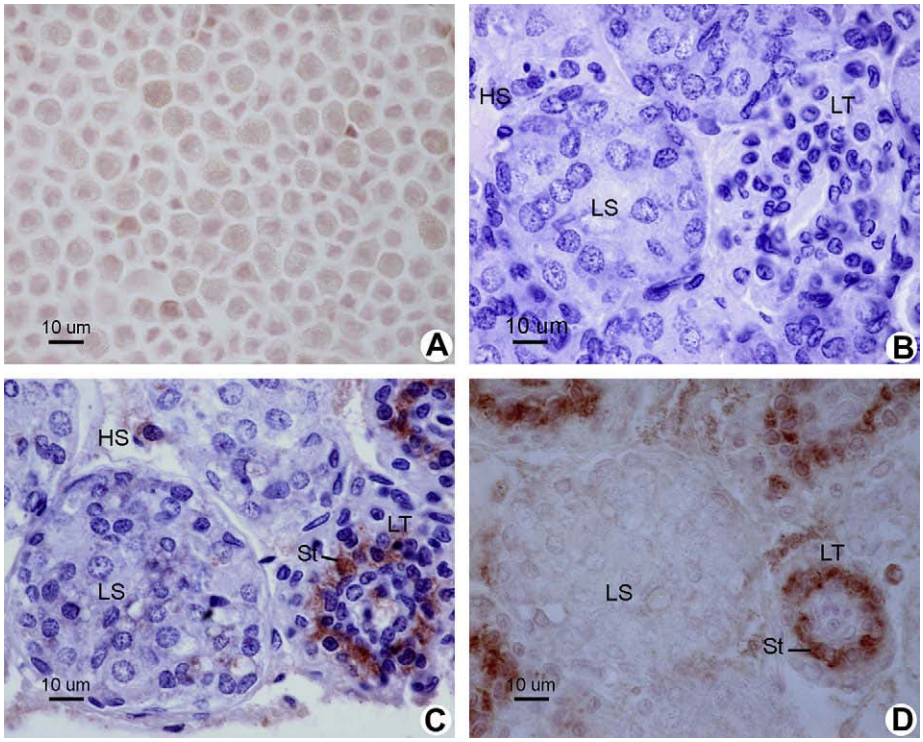


Fig. 7. Light micrographs of hemolymph smear and the cross sections of chronically YHV-infected lymphoid organ stained by immunoperoxidase technique using MoAb against cytokeratin and vimentin as probes. **(A)** A high magnification micrograph of hemolymph smear, showed no immunostaining in all types of hemocytes. **(B)** A high magnification micrograph of chronically YHV-infected lymphoid organ sections stained by immunoperoxidase technique using MoAb against cytokeratin as probe, showing no immunostaining while only Mayer's hematoxylin staining was observed in the lymphoid spheroid (LS), lymphoid tubules (LT) and hemal sinuses (HS). **(C, D)** High magnification micrographs of chronically YHV-infected lymphoid organ section stained by immunoperoxidase technique using MoAb against vimentin as probe (in D) and counterstained with Mayer's hematoxylin (in C), showing no immunostaining in lymphoid spheroid (LS), in contrast there was intense reddish immunostaining in the stromal cells (St) which was located in the middle layer of the wall of lymphoid tubules (LT).

relationship between LS and LT, Hasson et al. [8] reported that during acute infection with TSV, there is an increase of type 1 LS and a decrease of TSV-positive LT suggesting that LT might transform to LS. However, the authors were influenced by Anggraeni and Owen's suggestion [9,10] that LS were purely of hemocytic origin. According to this hypothesis LS may occur when resident LT phagocytes that sequestered TSV migrate into the intertubular hemal sinuses and hemocytes aggregate around them to form LS. In the present study, the decrease in number and shortening, possibly by breaking of the terminal parts of LT, were demonstrated by SEM and vascular cast, which could portray LT in three dimensions and covered a larger area than that which could be viewed in histological sections. This certainly demonstrated that LTs are structurally affected by YHV. Whether the broken-up terminal parts of LT became LS is still debatable. We believe that at least some parts of damaged LT became the seeding site for LS formation as in the present study we have also observed the dynamics of changes in LT cellular components and connective tissue scaffold in chronically YHV-infected lymphoid organ. There appeared to be more extravasation of hemocytes into the LT wall during YHV infection. So much that hemocytes were the major population of the LT wall. Viral particles were found in both stromal cells and hemocytes that aggregated together in the lymphoid tubule's wall (LTW). It is quite remarkable that the stromal cells and surrounding hemocyte's apoptosis occur before the degeneration of LTW. The role of stromal cells in processing antigens and in attracting hemocytes to LT needs to be verified in further studies. It is also interesting to note that most hemocytes in these foci were undergoing exocytosis of their granules, as in LS type 2 and 3 where granules were hardly visible in the hemocytes, which were similar to the spheroidal hemocytes reported by Anggraeni and Owen [10]. It is interesting to note that these authors also reported the presence of stromal cells like those in LTW in the LS even though they were not stained for phenol oxidase like hemocytes [10]. Since stromal cells are an intrinsic population of the LT wall, this suggested that part of LS cells were derived from LT cells. Therefore, even though it was suggested [10] that all LS may be formed *de novo* from hemocytes aggregating in the hemal sinuses, we believe that the LT origin of LS formation could not be ruled out. The compositions and possible functions of the released granular materials from hemocytes could partly be enzymes that break down viruses, while the rest could be proteins that were involved in the coagulation [19–22] and walling off (encapsulating) the spheroids, thus preventing viral particles and debris from the infected apoptotic cells from spreading. To ensure that this is the case, spheroids were surrounded by a thickened capsule which was made up of argyrophilic type 2 fibers (Fig. 6C). In contrast it was observed that type 1 fibers with associated ECM drastically decreased (Fig. 6A,B), as there was no more basket-like network (Fig. 6F) around LS as appearing around LT, resulting in the smooth appearance of LS when viewed under SEM. Labeling with vimentin also demonstrated there were much fewer stromal cells remaining in the LS (Fig. 7C,D), indicating their decreased number together with fiber type 1 and associated-EMC. Finally, LS were reduced in size after the apoptotic cells and their debris had been absorbed.

Acknowledgements

This research was supported by Commission on Higher Education (Ph.D. Scholarship to P. Duangsuwan and Research Group Development Grant to P. Sobhon) and TRF (Senior Research Scholar Fellowship to P. Sobhon). We would like to thank Dr. Paisarn

Sithigorngul, Department of Biology, Faculty of Science, Srinakharinwirot University, Bangkok, Thailand for generously providing the monoclonal antibody to YHV envelope glycoprotein 116 (gp116). We also thank Ms. Jaruwan Poljaroen for assistance with graphics.

References

[1] Oka M. Studies on *Penaeus orientalis* Kishinuoye-VIII structure of the newly found lymphoid organ. Bull Jpn Soc Sci Fish 1969;35:245–50.
[2] Kondo M, Itami T, Takahashi Y, Fujii R, Tomonaga S. Structure and function of the lymphoid organ in the Kuruma prawn. Dev Comp Immunol 1994;18. S109.
[3] Bell TA, Lightner DV. A Handbook of normal penaeid shrimp histology. Baton Rouge: World Aquaculture Society; 1996. p. 70-73.
[4] Van de Braak CBT, Botterblom MHA, Taverne N, van Muiswinkel WB, Rombout JHWM, van der Knaap WPW. The roles of the haemocytes and the lymphoid organ in the clearance of injected *Vibrio* bacteria in *Penaeus monodon* shrimp. Fish Shellfish Immunol 2002;13:293–309.
[5] Kanobdee K, Soowannayan C, Flegel TW, Ubol S, Withyachumnarnkul B. Evidence for apoptosis correlated with mortality in the giant black tiger shrimp *Penaeus monodon* infected with yellow head virus. Dis Aquat Org 2002;48:79–90.
[6] Martin GG, Hose JE, Minka G, Rosenberg S. Clearance of bacteria injected into hemolymph of Ridgeback prawn, *Sicyonia ingentis* (Crustacia: Decapoda): role of hematopoietic tissue. J Morphol 1996;227:227–33.
[7] Takahashi Y, Itami T, Kondo M. Immune system of crustacean. Fish Pathol 1995;30:141–50.
[8] Hasson KW, Lightner DV, Mohney LL, Redman RM, White BM. Role of lymphoid organ spheroids in chronic Taura syndrome virus (TSV) infections in *Penaeus vanamei*. Dis Aquat Org 1999;38:93–105.
[9] Anggraeni MS, Owen L. Evidence for the haemocytic origin of lymphoidal spheroids in *Penaeus monodon*. In: Flegel TW, editor. Advances in shrimp biotechnology. Bangkok: National Center for Genetic Engineering and Biotechnology; 1998. p. 137.
[10] Anggraeni MS, Owen L. The haemocytic origin of lymphoid organ spheroid cells in the penaeid prawn *Penaeus monodon*. Dis Aquat Org 2000;40:85–92.
[11] Bonami JR, Lightner DV, Redman RM, Poulos BT. Partial characterization of togavirus (LOVV) associated with histopathological changes of the lymphoid organ of penaeid shrimps. Dis Aquat Org 1992;14:145–52.
[12] Owens L, De Beer S, Smith J. Lymphoidal parvovirus-like particles in Australian penaeid prawns. Dis Aquat Org 1991;11:129–34.
[13] Spann KM, Vickers JE, Lester RJ. Lymphoid organ virus of *Penaeus monodon* from Australia. Dis Aquat Org 1995;23:127–34.
[14] Nadala ECB, Tapay LM, Loh PC. Yellow-head virus: a rhabdovirus-like pathogen of penaeid shrimp. Dis Aquat Org 1997;31:141–6.
[15] Flegel TW, Fegan DF, Kongsom S, Vuthikornudomkit S, Sriurairatana S, Boonyaratpalin S, et al. Occurrence, diagnosis and treatment of shrimp diseases in Thailand. In: Fulks W, Main KL, editors. Diseases of cultured penaeid shrimp in Asia and the United States. Honolulu: The Oceanic Institute; 1992. p. 57–112.
[16] Chunhabundit P, Somana R. Scanning electron microscopic study on pineal vascularization of the common tree shrew (*Tupaia glis*). J Pineal Res 1991;10:59–64.
[17] McManus JFA. Histological demonstration of mucin after periodic acid. Nature 1946;158:202.
[18] Jones Lamar. Connective tissues and stains. In: Bancroft JD, Gamble M, editors. Theory and practice of histological techniques. New York: Churchill Livingstone; 2002. p. 159–60.
[19] Huang CC, Sritunyalucksana K, Soderhall K, Song YL. Molecular cloning and characterization of tiger shrimp (*Penaeus monodon*) transglutaminase. Dev Comp Immunol 2004;28:279–94.
[20] Chen MY, Hu KY, Huang CC, Song YL. More than one type of transglutaminase in invertebrates? A second type of transglutaminase is involved in shrimp coagulation. Dev Comp Immunol 2005;29:1003–16.
[21] Yeh MS, Kao LR, Huang CJ, Tsai IH. Biochemical characterization and cloning of transglutaminases responsible for hemolymph clotting in *Penaeus monodon* and *Marsupenaeus japonicus*. Biochim Biophys Acta 2006;1764:1167–78.
[22] Yeh MS, Huang CJ, Cheng JH, Tsai IH. Tissue-specific expression and regulation of the haemolymph clottable protein of tiger shrimp (*Penaeus monodon*). Fish Shellfish Immunol 2007;23:272–9.
[23] Duangsuwan P, Phoungpetchara I, Tinikul Y, Poljaroen J, Wanichanon C, Sobhon P. Histological and three dimensional organizations of lymphoid tubules in normal lymphoid organ of *Penaeus monodon*. Fish Shellfish Immunol 2008;24:426–35.

EFFECTS OF SEROTONIN, DOPAMINE, OCTOPAMINE, AND SPIPERONE ON OVARIAN MATURATION AND EMBRYONIC DEVELOPMENT IN THE GIANT FRESHWATER PRAWN, MACROBRACHIUM ROSENBERGII (DE MAN, 1879)

BY

YOTSAWAN TINIKUL[1]), BOWORN SOONTHORNSUMRITH[1]), ITTIPON PHOUNGPETCHARA[1]), PRASERT MEERATANA[2]), JARUWAN POLJAROEN[1]), PORNSAWAN DUANGSUWAN[3]), NANTAWAN SOONKLANG[1]), A. JOFFRE MERCIER[4]), and PRASERT SOBHON [1,5])

[1])Department of Anatomy, Faculty of Science, Mahidol University, Rama VI Road, Ratchathewi, Bangkok 10400, Thailand

[2])Department of Medical Science, Faculty of Science, Burapha University, Chonburi 20131, Thailand

[3])Department of Anatomy, Faculty of Science, Prince of Songkla University, Songkhla 90112, Thailand

[4])Department of Biological Sciences, Brock University, St. Catharines, Ontario L2S 3A1, Canada

ABSTRACT

Mature female, Macrobrachium rosenbergii in stage I of their ovarian cycle were divided into 17 groups (14 experimental groups and 3 control groups) of 28 animals each. Animals in each experimental group were injected intramuscularly with 2-3 doses of serotonin (5-HT), dopamine (DA), octopamine (OA), spiperone (SP), or 5-HT plus SP, at four-day intervals from day 1 to 49. Five animals each in every group were sacrificed,

[5]) e-mail: Hscpso@mahidol.ac.thH or: Hanatch2002@yahoo.com

respectively, at day 14, 25, and 49 to evaluate the gonadosomatic index (GSI) and oocyte diameters. The experimental groups that received the doses of 2.5 x 10^{-5}, 2.5 x 10^{-6} mol of 5-HT/prawn, 2.5 x 10^{-5}, 2.5 x 10^{-6} , 2.5 x 10^{-7} mol of 5-HT/prawn plus 2.7 x 10^{-7} mol of SP/prawn, as well as SP alone at the dose of 5.4 x 10^{-7} mol of SP/prawn, exhibited significantly shorter periods of ovarian maturation and embryonic development, as well as increased GSI values and oocyte diameters, when compared with vehicle-injected and untreated control groups. In contrast, groups injected with DA and OA at similar doses showed decreased ovarian maturation, oocyte diameters, and embryonic periods, but no differences in GSI, when compared with control groups. For the number of eggs per spawn, the groups of animals that received 5-HT at doses of 2.5 x 10^{-5} and 2.5 x 10^{-6} mol/prawn, 5-HT at doses of 2.5 x 10^{-5} mol plus SP at 2.7 x 10^{-7} mol/prawn, 5-HT at 2.5 x 10^{-6} mol plus SP at 2.7 x 10^{-7} mol/prawn, and SP at a dose of 2.7 x 10^{-7} mol/prawn, yielded higher numbers than the control groups, and with a significant difference ($P<0.05$). All DA and OA injected groups showed lower numbers of eggs when compared to the control groups. Eggs from all these experimental groups exhibited equally good quality both among each other and in comparison with control groups, as judged from the percentage of fertilized eggs.

INTRODUCTION

The giant freshwater prawn, Macrobrachium rosenbergii (De Man, 1879), is an important food source that is cultured worldwide (Sandifer & Smith, 1985). Also, it is a highly valued aquatic animal in Thailand and other Asian countries. Hormonal regulation of the reproductive process of this decapod crustacean is not as well understood as in the crayfish, Procambarus clarkii (Girard, 1852), or the lobster, Homarus americanus (Milne-Edwards, 1837), in which a number of hormones from the eyestalk and other endocrine organs play roles in controlling the development of the gonads and of secondary sexual

characteristics (Fingerman, 1997; Herp & Soyez, 1997). Furthermore, in the crayfish, major neurotransmitters that could control ovarian maturation include serotonin (5-HT) and dopamine (DA): 5-HT has a stimulating effect on gonadal maturation, perhaps by inhibiting the release of gonad inhibiting hormone (GIH), and/or by stimulating the release of gonad stimulating hormone (GSH), whereas DA plays the opposite role (Sarojini et al., 1995b; Fingerman, 1997). Additionally, it was reported that female crayfish, given 5-HT, exhibit a significant increase in the ovarian index and in the size of the oocytes (Sarojini et al., 1995d). DA inhibits gonadal maturation in both sexes, apparently by inhibiting the release of GSH and possibly also by triggering the release of GIH. Interestingly, a DA antagonist, spiperone (SP), increases the gonadosomatic (GSI) index in P. clarkii when injected during early vitellogenesis (Rodríguez et al., 2002). SP also stimulates ovarian growth in the crab, Chasmagnathus granulatus (Dana, 1851) (cf. Zapata et al., 2003) and induces testicular maturation in the crayfish, P. clarkii (cf. Sarojini et al., 1995e). 5-HT induces ovarian maturation and spawning in Litopenaeus vannamei (Boone, 1931) (cf. Vaca & Alfaro, 2000). The aim of this study was to investigate whether these neurotransmitters and a DA antagonist have similar effects on ovarian maturation, embryonic development, and spawning in the giant freshwater prawn, Macrobrachium rosenbergii.

MATERIAL AND METHODS

Experimental animals

Mature female, Macrobrachium rosenbergii (giant freshwater prawns) (weighing on average 42.71 ± 5.8 g each) were obtained from commercial farms in Chonburi Province, Thailand. The animals were kept in outdoor concrete circular tanks, each with 1.50 m diameter and a water depth of 0.80 m; about 30% of the water was changed every 2 days. The prawns were fed commercial food pellets (Charoen Pokphand Group, Thailand) twice per

day. Aeration was given all day. To allow mating, blue-claw males and females were stocked at a ratio of 1 : 5, respectively, in the same tank. Thirty plastic cages were added into every tank for molting animals to hide in and avoid being killed as a result of the cannibalistic behaviour of this species. The prawns were acclimatized under a photoperiod of 12 : 12 h light : dark for two weeks before the beginning of the experiments. Female prawns were selected and used in the experiments to test the effects of 5-HT, DA, OA, and SP on the length of the ovarian cycle and embryonic development, as soon as they exhibited stage I of the ovarian cycle.

Effects of 5-HT, DA, OA, SP, and 5-HT plus SP on ovarian maturation, embryonic development, and spawning

Female prawns at ovarian stage I were divided into 17 groups, each with 28 animals. The prawns in the 14 treatment groups were injected with 5-HT at doses of 2.5×10^{-5}, 2.5×10^{-6}, and 2.5×10^{-7} mol of 5-HT/prawn, DA at doses of 2.5×10^{-5}, 2.5×10^{-6}, and 2.5×10^{-7} mol of DA/prawn, OA at doses of 2.5×10^{-5}, 2.5×10^{-6}, and 2.5×10^{-7} mol of OA/prawn, SP at doses of 2.7×10^{-7}, and 5.4×10^{-7}, mol of SP/prawn, and 5-HT plus SP at doses of 2.5×10^{-5} mol of 5-HT/prawn plus 2.7×10^{-7} mol of SP /prawn, 2.5×10^{-6} mol of 5-HT/prawn plus 2.7×10^{-7} mol of SP/prawn, and 2.5×10^{-7} mol of 5-HT/prawn plus 2.7×10^{-7} mol of SP/prawn. 5-HT, DA, and OA were dissolved in crustacean physiological saline (CPS, containing NaCl 29 g, KCl 0.71 g, $CaCl_2.2H_2O$ 2.38 g, $MgSO_4.7H_2O$ 3.16 g, $NaHCO_3$ 0.5 g, $MgCl_2.6H_2O$ 0.17 g, and HEPES 4.76 g in 1 liter of distilled water), whereas SP was dissolved in 95% ethanol. The injected volumes of 5-HT, DA, and OA were 0.10 ml, whereas SP was 0.05 ml. The females treated with 5-HT plus SP received 0.10 ml of 5-HT solution and 0.05 ml of SP solution, in separate injections. The doses of the chemicals used in this study were based on their positive effects as shown by Chen et al. (2003) for 5-HT and DA, and Alfaro et al.

(2004) for SP. All prawns could tolerate the injected doses of neurotransmitters without showing any abnormal behaviour. All injections were performed at 4-day intervals, covering a period of 49 days. The effects on the neurotransmitter-treated groups were compared with three control groups of 28 animals each: in the first group, each animal was injected with 0.1 ml of crustacean physiological saline (CPS), in the second each animal was injected with 0.1 ml CPS plus 0.05 ml 95% ethanol (CPSE), and the third group was an untreated negative control (NC) group. Animals in each group were identified by tying plastic loops of different colours around the eyestalk. The injections were performed via an intramuscular route at the lateral aspect of the second abdominal somite using a 1 ml syringe (NIPRO) fitted with 26 G x ½" (0.45 x 12 mm) thin-wall needles (NIPRO).

The weight and total length of the prawns were measured on every treatment day, before injection. Total length was taken from the base of the eyestalk to the telson (Eyestalk base-telson length, EBTL). Five animals in each group were randomly selected and sacrificed at days 14, 25, and 49 to evaluate the gonado-somatic index (GSI) and oocyte diameter. The GSI was calculated using the formula [ovarian weight (g) / body weight (g)] x 100. The rest of the prawns were allowed to proceed until they ovulated. The experiment was done in triplicate. All GSI values and oocytes diameters were then compared between the treated groups and the control groups. Pieces of ovary were subsequently fixed in Bouin's solution, and prepared by the paraffin technique for light microscopic observations to determine the ovarian stages and oocyte diameters.

Percentage of spawning prawn, and the quantity and quality of the spawned eggs

Percentage of spawning was determined from the number of spawning prawn in each group at the end of the experiment. The quality and quantity of spawned eggs were evaluated from the number of eggs per spawn and the percentage of fertilized eggs. The abdomen of

each spawning prawn was carefully scraped to obtain all the light yellow eggs from the brood chamber. All spawned eggs were mixed with 3% sodium hypochlorite (NaClO) in distilled water to thoroughly disperse the eggs. At least 300 eggs were observed under a compound or stereo-microscope for determining the morphology and percentage of developing embryos (successfully fertilized eggs). For evaluating the quantity of spawned eggs, the eggs were placed in 15 ml of 3% NaClO and mixed thoroughly. After that, 3 times aliquots of 10 µl of the egg suspension were randomly drawn from the 15 ml tube into a 0.6 ml tube to count the total number of eggs under a stereo-microscope. Counting was always triplicated, and the total number of eggs per spawn was calculated from the total volume of each egg suspension.

Determination of ovarian stages and embryonic stages

The ovarian cycle in female broodstocks was classified into five stages, based on ovarian size and colour as reported by Chang & Shih (1995). Fig. 1A shows stages 0 or I, which are spawned and spent phases, respectively. These ovarian stages appear white and when observed through the carapace, they do not seem to be different. However, after spawning, the ovary appears loose and empty, as it contains collapsed ovarian pouches with only strands of follicular cells and connective tissue remaining; thus this is called stage 0 (Meeratana and Sobhon, 2007). In stage II (Fig. 1B, C) (proliferative) a small yellow mass of ovary could be observed dorsally under the carapace. In stage III (Fig. 1D, E) (premature), the ovary became orange. In stage IV (Fig. 1F, G) (mature), the reddish-orange ovary extended from behind the eye posteriorly to the first abdominal somite. These ovarian stages were confirmed by histological study (Fig. 2) based on the criteria described by Meeratana & Sobhon (2007). Fig. 3 shows embryonic stages: the newly spawned eggs were characterized into 3 stages by their colour, i.e., the light yellow to orange stage, which gradually changed to the brown stage, and finally to the black stage just before hatching.

Determination of the mean oocyte diameters

Five stages of developing oocytes (Oc1, Oc2, Oc3, Oc4, and mOc) were classified according to Meeratana & Sobhon (2007). Fifty randomly selected oocytes at each stage in three widely separated ovarian sections from each animal were observed under the light microscope (LM). Diameters of the oocytes that contained full nuclear profiles were measured, and the data were expressed as the average diameters ± standard deviations.

Statistical analysis

Statistical significance was analysed with an SPSS program using one-way analysis of variance (ANOVA) and Duncan's multiple range test. A probability value less than 0.05 ($P<0.05$) indicated a significant difference. Data were presented as means ± standard deviations.

RESULTS

Effects of 5-HT, DA, and DA-antagonist on the ovary (Fig. 4A)

The ovarian maturation period (OMP) is defined as the time needed for the ovary to develop from stage I through stage II, III, and IV to spawning. The OMP of experimental subgroups that received 5-HT at doses of 2.5×10^{-5} , 2.5×10^{-6} mol/prawn (~34 and ~29 days, respectively), all groups of 5-HT plus SP (~24, ~25, and ~31 days, respectively), as well as the group treated with SP at a dose of 5.4×10^{-7} mol/prawn (~34 days), were all significantly shorter ($P<0.05$) than those of CPS (~41 days), CPSE (~41 days), and NC (~39 days). All DA treated groups (~70, ~64, ~67 days, respectively), and OA treated groups (~63, ~60, ~60 days, respectively) exhibited significantly longer OMP ($P<0.05$) than those of the control groups.

Effects on the embryonic development period (Fig. 4B)

The embryonic development period (EDP) is defined as the time needed from spawning to the appearance of the next black egg stage. The EDP of experimental groups that received 5-HT at doses of 2.5 x 10^{-5} and 2.5 x 10^{-6} mol/prawn (~20 and ~19 days, respectively), 5-HT plus SP at doses of 2.5 x 10^{-5} mol of 5-HT/prawn plus 2.7 x 10^{-7} mol of SP /prawn (~16 days), and SP alone at a dose of 2.7 x 10^{-7} mol/prawn (~20 days), were all significantly shorter ($P<0.05$) than the EDP of CPS (~28 days), CPSE (~26 days), and NC (~25 days). All DA-treated (~49, ~47, ~48 days, respectively), and OA-treated groups (~46, ~46, ~42 days, respectively), exhibited a significantly longer EDP ($P<0.05$) than those of the control groups.

Effects on GSI and oocyte diameters

Gonado-somatic index (GSI) (Fig. 5A)

When measured at days 14, 25, and 49, treatment with all doses of 5-HT, 5-HT plus SP, as well as SP alone, caused significantly higher GSI compared to those of the control groups. In contrast, treatment with all doses of DA and OA showed no significant difference in GSI compared to the control groups.

Mean oocyte diameter (Fig. 5B)

Mean oocyte diameter of vitellogenic oocytes (Oc3, Oc4) and mature oocytes (mOc) of all groups of prawns treated with those of 5-HT, 5-HT plus SP, and SP alone, exhibited significant increases when compared with the control groups. In contrast, all groups of prawns treated with DA and OA showed significantly decreased diameters of these last three steps of oocytes when compared with the control groups.

Effects on spawning

Number of spawned eggs (Fig. 6)

The number of eggs per spawn, after injection with 5-HT at doses of 2.5 x 10^{-5}, 2.5 x 10^{-6} mol/prawn (~92240 and 94,683 eggs, respectively), 5-HT plus SP at doses of 2.5 x 10^{-5} mol/prawn plus 2.7 x 10^{-7} mol/prawn, 2.5 x 10^{-6} mol/prawn plus 2.7 x 10^{-7} mol/prawn (~93,390 and ~93,270 eggs, respectively), and SP at a dose of 2.7 x 10^{-7} mol/prawn (~91,163 eggs) were significantly higher ($P<0.05$) than the control groups (~68,826, ~69,554, and 70,053, for NC, CPS, and CPSE, respectively). In contrast, DA injected groups at the doses of 2.5 x 10^{-5} and 2.5 x 10^{-6} mol/prawn (~46,112 and ~49,756, respectively), and OA injected group at the dose of 2.5 x 10^{-6} mol/prawn (~51,440 eggs) showed a lower number of eggs per spawn when compared to the control groups with significantly different ($P<0.05$). However, for other DA and OA injected groups, the data suggest that the number of eggs might be lower, but that the differences were not statistically significant ($P>0.05$).

Percentage of fertilized eggs (Fig. 7)

The number of fertilized eggs obtained after all of the treatments showed an equally good quality both among each other and in comparison with control groups as judged from the percentages of fertilized eggs, which were not statistically different.

DISCUSSION

Injection of 5-HT in mature Macrobrachium rosenbergii females shortened the ovarian maturation period by about 10 days compared to control groups (~29 days for 5-HT vs ~41 days for CPS, ~41 days for CPSE, ~39 days for NC). 5-HT injection also shortened the embryonic development period by about 6-9 days compared to the control groups (~19

days for 5-HT vs ~28 days for CPS, ~26 days for CPSE, ~25 days for NC). Both results were significantly different ($P<0.05$). 5-HT also caused significant increases in GSI index and mean oocyte diameter of vitellogenic and mature oocytes (from Oc3 to mOc), when compared with the control groups ($P<0.05$).

There have been several previous studies of the effect of 5-HT on gonadal maturation in other decapods. It was suggested that in the crayfish, Procambarus clarkii, and the lobster, Homarus americanus, 5-HT may act indirectly on the gonads by stimulating the release of a putative gonadotropic factor, gonad stimulating hormone (GSH), from the thoracic ganglia, and/or by inhibiting the release of gonad inhibiting hormone (GIH) from the optic lobe in the eyestalk (Kulkarni et al., 1992; Fingerman 1997). GSH activity in the thoracic ganglia was increased by 5-HT administration in the crab, Uca pugilator (Bosc, 1802) (cf. Richardson et al., 1991) and the freshwater crayfish, P. clarkii (cf. Kulkarni et al., 1991). The crayfish, P. clarkii, treated with 5-HT also showed significant increases in ovarian index and oocyte diameter (Kulkarni et al., 1992). In the white shrimp, Litopenaeus vannamei, 5-HT at doses of 15 and 50 μg g^{-1} BW induced ovarian maturation and spawning (Vaca & Alfaro, 2000). In the later report, it was demonstrated that 5-HT raised haemolymph vitellogenin 15-26 times over the normal level within 16 days in eyestalk-ablated M. rosenbergii female broodstock (Chen et al., 2003). Recently, it was also shown that the ovaries of Macrobrachium rosenbergii treated with the medium from 5-HT-primed thoracic ganglia exhibited higher numbers of oocytes that developed into the vitellogenic and the mature stage, despite pretreatment of the broodstocks with cyproheptadine (CYP), a 5-HT antagonist. This finding strongly suggested that 5-HT did not induce ovarian maturation directly, but through its action on the thoracic ganglia (Meeratana et al., 2006). As for the exact target and mechanism of action of 5-HT, Sáenz et al. (1997) reported that 5-HT could induce the bursting of action potentials and associated slow inward current in the intact X-organ axons as well as in the X-

organ neurons kept in culture. This bursting electrical activity by the X-organ neurons could mediate the release of CHH in the crayfish Orconectes limosus (Rafinesque, 1817) (Keller and Beyer, 1968). Similarly, 5-HT has been reported to elicit changes in the electrical activity of X-organ cells in the crabs Cardisoma carnifex (Herbst, 1794) and Podophthalmus vigil (Fabricius, 1798) (Nagano and Cooke, 1981). It was also reported that 5-HT could stimulate the release of molt-inhibit hormone (MIH) from the isolated eyestalks of crab, Cancer antennarius (Stimpson, 1856) by providing an excitatory input to MIH-containing neurosecretory cells (Mattson and Spaziani, 1985). Hence the primary target of 5-HT seems to be at the X-organ neurons. Whether it also affects the thoracic ganglion neurons directly remained to be studied.

SP, the DA antagonist, could also induce shorter ovarian maturation period (~34 days for SP vs ~41 days for CPS, ~41 days for CPSE, ~39 days for NC) and embryonic development periods (~ 20 days for SP vs ~28 days for CPS, ~26 days for CPSE, ~25 days for NC) than the control groups. Both results were statistically significant ($P<0.05$). The combined treatment, 5-HT plus SP, shortened the ovarian maturation period (~24 days) and embryonic development period (~16 days) even more than 5-HT-treated, SP-treated, and control groups. In vitro, SP has been shown to inhibit the secretion of a GIH-like factor from the eyestalks in Chasmagnathus granulata, which could explain its effect on the induction of ovarian growth (Zapata et al., 2003). In the penaeid shrimp, Litopenaeus stylirostris (Stimpson, 1874) and L. vannamei, combined treatment of 5-HT and SP not only induced ovarian maturation and spawning, but also stimulated the release of maturation promoting pheromones into the water (Alfaro et al., 2004). Our study is the first to report on the positive effects of 5-HT and SP alone, and in combination, on the development of ovaries and embryos of M. rosenbergii. The two chemicals appeared to be synergistic, and they might act

through the inhibition of GIH release and/or the stimulation of GSH release. This hypothesis needs, however, to be tested further.

Unlike 5-HT and SP, no dose of DA and OA shortened the ovarian maturation or embryonic development period. In the fiddler crab, Uca pugilator, it was shown that DA inhibits vitellogenin synthesis, either by inhibiting the release of GSH or by stimulating the release of GIH from the eyestalks, or through a combination of these two mechanisms (Sarojini et al., 1995e). Using HPLC, DA was detected in the brain and thoracic ganglia but not in the eyestalk of M. rosenbergii (cf. Chen et al., 2003). Taken together with the fact that DA was able to exert its effect in eyestalk-ablated prawns, it has been suggested that the action of DA on GIH release was unlikely in this species, and the most likely site of the action of DA could be at the thoracic ganglia through the inhibition of GSH release (Chen et al., 2003). It is presumed that DA exerts its inhibitory effect on vitellogenesis by acting indirectly via GSH, rather than directly on the target organ, the hepatopancreas (Chen et al., 1999). The action of OA on the gonads had not been studied previously. Our study is the first to show that this neurotransmitter exerts effects similar to those of DA, and that these effects may be mediated via the same mechanism as for DA.

Regarding the quantity and quality of the eggs, treatment with 5-HT, SP, and 5-HT plus SP resulted in significantly higher numbers of eggs per spawn than in the control groups ($P<0.05$). In contrast, DA and OA injected groups showed lower numbers of eggs per spawn than the control groups. The number of fertilized eggs obtained after all of the injections also showed equally good quality both among each other and in comparison with control groups. The number of eggs produced by each female was found to be directly proportional to the animal's size. A fully mature female might lay between 80,000 and 100,000 eggs per spawning, which is similar to that reported earlier (New, 2002). The fertilized eggs remained attached to the brood chamber between the pleopods for about 18–23 days after spawning.

The newly spawned eggs are characterized by a bright yellow to orange colour, which gradually changes to brown, and finally grey and black about 2–3 days before hatching. The quality of the spawned and fertilized eggs was equally good in all treatments, as the percentage of successfully developed zygotes was similar to those of the controls.

In summary, the present study shows that in Macrobrachium rosenbergii, 5-HT and SP exert a positive control, while DA and OA exert a negative control on ovarian maturation, oocyte development, and embryonic maturation, but these chemicals have no effect on spawning induction. In future, this knowledge could be adapted for improving prawn productivity.

ACKNOWLEDGEMENTS

This research was supported by the Thailand Research Fund (Royal Golden Jubilee Ph.D. Program (Grant No. PHD/0171/2547) to Yotsawan Tinikul and Prasert Sobhon, Senior Research Scholar Fellowship to Prasert Sobhon), and the Commission on Higher Education (Research Group Development Grant to Prasert Sobhon). For technical assistance, we thank Ms. Ratchanok Cheotacha and Mr. Anurak Prabyai.

REFERENCES

ALFARO, J., G. ZUNIGA & J. KOMEN, 2004. Induction of ovarian maturation and spawning by combined treatment of serotonin and a dopamine antagonist, spiperone in Litopenaeus stylirostris and Litopenaeus vannamei. Aquaculture, **236**: 511 –522.

BAUCHAU, A.G. & J. C. MANGEOT, 1966. Sérotonine et glycémie chez les crustacés. Experientia, **22**: 238–239.

CHANG, C.F. & T. W. Shih, 1995. Reproductive cycle of ovarian development and vitellogenin profiles in the freshwater prawn, Macrobrachium rosenbergii. Invertebr. Reprod. Dev., **27**: 11-20.

CHANG, E.S., 1985. Hormonal control of molting in decapod crustacea. American Zool., **25**: 179–185.

CHEN, Y.N., H.F. FAN, S.L. HAIEH & C. M. KUO, 2003. Physiological involvement of DA in ovarian development of the freshwater giant prawn, Macrobrachium rosenbergii. Aquaculture, **228**: 383–395.

CHEN, Y.N., D.Y. TSENG, P.Y. HO & C.M. KUO, 1999. Site of vitellogenin synthesis determined from a cDNA encoding a vitellogenin fragment in the freshwater giant prawn, Macrobrachium rosenbergii. Mol. Reprod. Dev., **54**: 215– 222.

FINGERMAN, M., 1997. Roles of neurotransmitters in regulating the reproductive hormone release and gonadal maturation in decapod crustaceans. Invertebr. Reprod. Dev., **31**: 47-54.

HERP, F. VAN. & D. SOYEZ, 1997. Arthropoda-Crustacea. In: R.G. Adiyodi, K.G. Adiyodi, T.S. Adams, (eds.), Reproductive biology of invertebrates, 3: 247-275. (John Wiley & Sons, New York).

KELLER, R. & J. BEYER, 1968. Zur hyperglykämischen Wirkung von Serotonin und Augenstielextrakt beim Flusskrebs Orconectes limosus. Z. vergl. Physiol. **59**: 78–85.

KULKARNI, G.K., L. GLADE & M. FINGERMAN, 1991. Oogenesis and effects of neuroendocrine tissues on in vitro synthesis of protein by the ovary of the red swamp crayfish Procambarus clarkii (Girard). Journ. Crust. Biol., **11**: 513–522.

KULKARNI, G.K., R. NAGABHUSHANAM, G. AMALDOSS, R.G. JAISWAL & M. FINGERMAN, 1992. In vitro stimulation of ovarian development in the red swamp crayfish, Procambarus clarkii (Girard), by 5-hydroxytryptamine. Invertebr. Reprod. Dev., **21**: 231–240.

MATTSON, M.P. & E. SPAZIANI, 1985. 5-hydroxytryptamine mediates release of molt inhibiting hormone activity from isolated crab eyestalk ganglia. Biol. Bull., **169**: 246–255.

MEERATANA, P. & P. SOBHON, 2007. Classification of differentiating oocytes during ovarian cycle in the giant freshwater prawn, Macrobrachium rosenbergii De Man. Aquaculture, **270**: 249-258.

MEERATANA, P., B. WITHYACHUMNARNKUL, P. DAMRONGPHOL, K. WONGPRASERT, A. SUSEANGTHAM & P. SOBHON, 2006. Serotonin induces ovarian maturation in giant freshwater prawn broodstock, Macrobrachium rosenbergii De Man. Aquaculture, **260**: 315–325.

NAGANO, M. & I. M. COOKE, 1981. Electrical activity in the crab X-organ sinus gland system: site of initiation, ionic bases and pharmacology. In: Neurosecretion, molecules, cells, systems (eds): 504–505. (Plenum Press, New York).

NEW, M.B., 2002. Farming freshwater prawns: a manual for the culture of the giant river prawn (Macrobrachium rosenbergii). FAO Fisheries Technical Paper, **428**: 1–10.

RICHARDSON, H.G.D., M. DECARAMAN & M. FINGERMAN, 1991. The effect of biogenic amines on ovarian development in fiddler crab, Uca pugilator. Comp. Biochem. Physiol., (C) **99:** 53–56.

RODRÍGUEZ, E.M., D.A. MEDESANI, L.S. LOPEZ GRECO & M. FINGERMAN, 2002. Effects of some steroids and other compounds on ovarian growth of the red swamp crayfish, Procambarus clarkii, during early vitellogenesis. Journ. exp. Zool., **292**: 82– 87.

SANDIFER, P.A. & T.J. SMITH, 1985. Freshwater prawn: crustacean and mollusk aquaculture in the United States: 1–15. (A Publishing Company Inc., West Port, Connecticut, USA).

SÁENZ, F., U. GARCÍA & H. ARÉCHIGA, 1997. Modulation of electrical activity by 5-hydroxytryptamine in crayfish neurosecretory cells. Journ. Exp. Biol. **200:** 3079–3090.

SAROJINI, R., R. NAGABHUSHANAM & M. FINGERMAN, 1995a. In vivo effects of DA and DArgic antagonists on testicular maturation in the red swamp crayfish, Procambarus clarkii. Biol. Bull., ……**189**: 340– 346.

----------,----------&----------, 1995b. Mode of action of the neurotransmitter 5-hydroxytryptamine in stimulating ovarian maturation in the red swamp crayfish, Procambarus clarkii: an in vivo and in vitro study. Journ. exp. Zool., **271:** 395–400.

SAROJINI, R., R. NAGABHUSHANAM, M. DEVI & M. FINGERMAN, 1995c. DArgic inhibition of 5-hydroxytryptamine-stimulated testicular maturation in the fiddler crab, Uca pugilator. Comp. Biochem. Physiol., (C) **111**: 287–292.

VACA, A.A. & J. ALFARO, 2000. Ovarian maturation and spawning in the white shrimp, Penaeus vannamei, by serotonin injection. Aquaculture, 182: 373-385.

ZAPATA, V., L.S. LOPEZ GRECO, D. MEDESENI & E.M. RODRIGEZ, 2003. Ovarian growth in the crab Chasmagnathus granulata induced by hormones and neuroregulators throughout the year. In vivo and in vitro studies. Aquaculture, **224**: 339-352.

CAPTIONS

Fig. 1. Top views of females of the giant freshwater prawn, Macrobrachium rosenbergii (De Man, 1979), whose bodies were in both unflexed and flexed positions to show various ovarian stages: A, stage 0 or I appears grossly as there is no yellow mass of ovary under the carapace; B and C, stage II shows small yellow mass; D and E, stage III shows enlarged yellow mass; F and G, stage IV shows full yellow mass.

Fig. 2. Light micrographs of H&E-stained ovarian sections showing various steps of oocyte development in Macrobrachium rosenbergii (De Man, 1979): A, ovarian stage I; B, stage II; C, stage III; and D, stage IV. Oog, oogonia; Oc1, early previtellogenic oocyte; Oc2, late previtellogenic oocytes; Oc3, early vitellogenic oocytes; Oc4, late vitellogenic oocytes; mOc, mature oocytes (classified according to Meeratana & Sobhon, 2007). Scale bars, 50 μm.

Fig. 3. Various stages of developing embryos of Macrobrachium rosenbergii (De Man, 1979): A, yellow egg stage; B, orange egg stage; C, brown egg stage; and D, black egg stage.

Fig. 4. A, Ovarian maturation period (defined as the time for ovarian development from ovarian stage I to spawning); and B, Embryonic developmental period (defined as the time for egg development from spawning to black egg stage), after injections with various doses of 5-HT, DA, OA, SP, and 5-HT plus SP, when compared with the control groups (NC, CPS, CPSE). The numbers indicate doses of chemicals in various groups in mol/prawn for 5-HT, DA, OA, 5-HT plus SP, and SP alone. Asterisks indicate significant differences ($P<0.05$) with respect to the control groups; one asterisk indicates significantly shorter/longer OMP and EMP periods than control groups.

Fig. 5. A, Mean gonadosomatic index (GSI) determined at days 14, 25, and 49 after the prawns were injected with various doses of 5-HT, DA, OA, 5-HT plus SP, and SP alone when compared with the control groups (NC, CPS, CPSE); B, Mean oocyte diameters of vitellogenic oocytes (Oc3, Oc4, and mOc), after the prawns were injected with various doses of 5-HT, DA, OA, 5-HT plus SP, and SP alone, when compared with the control groups. The numbers indicate doses of chemicals in various groups in mol/prawn for 5-HT, DA, OA, 5-HT plus SP, and SP alone. Asterisks indicate significant differences ($P<0.05$) with respect to the control groups; one asterisk indicated significant increase/decrease of GSI and oocyte diameters, when compared with control groups.

Fig. 6. Number of eggs per spawn, after injection with various doses of 5-HT, DA, OA, SP, and 5-HT plus SP, when compared to the control groups. Asterisks indicate significant differences ($P<0.05$) when compared to the control groups.

Fig. 7. Percentage of fertilized eggs of all experimental groups, after injection with various doses of 5-HT, DA, OA, SP, and 5-HT plus SP when compared to the control groups.

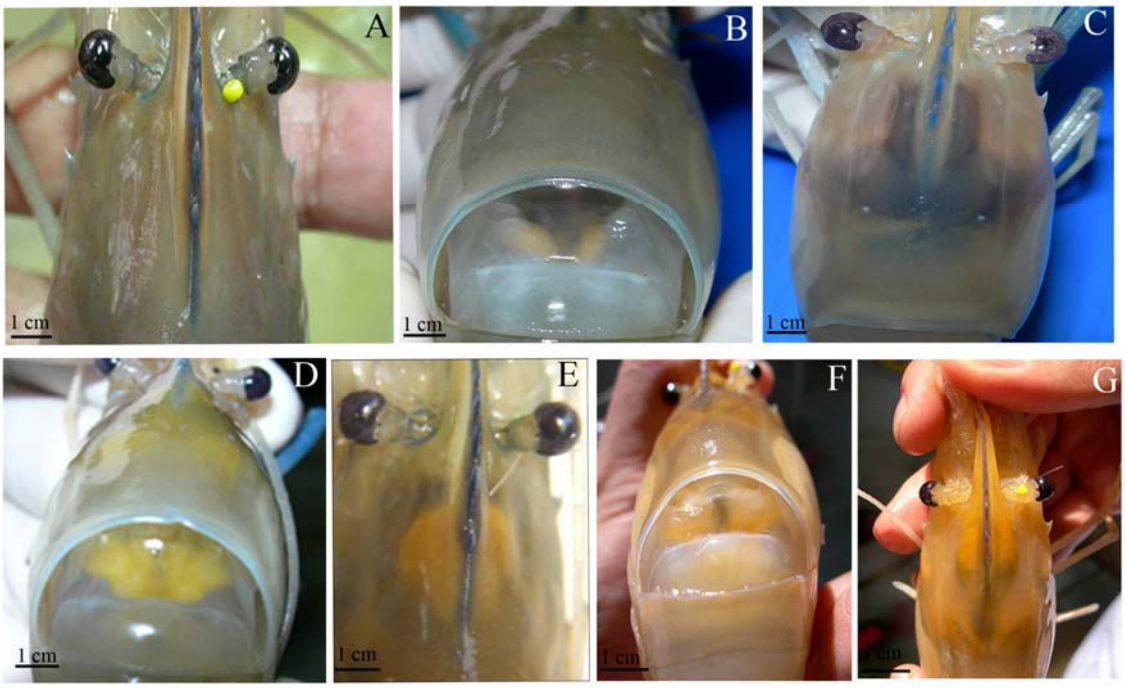


Figure 1

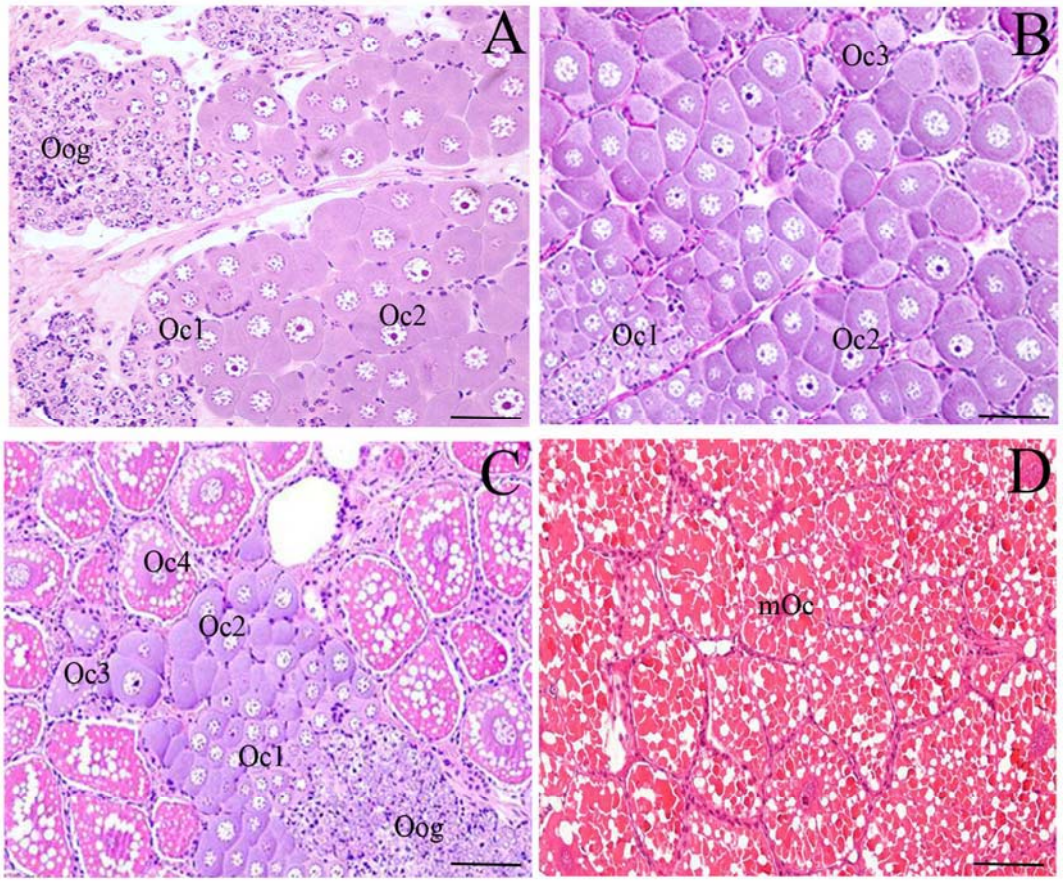


Figure 2

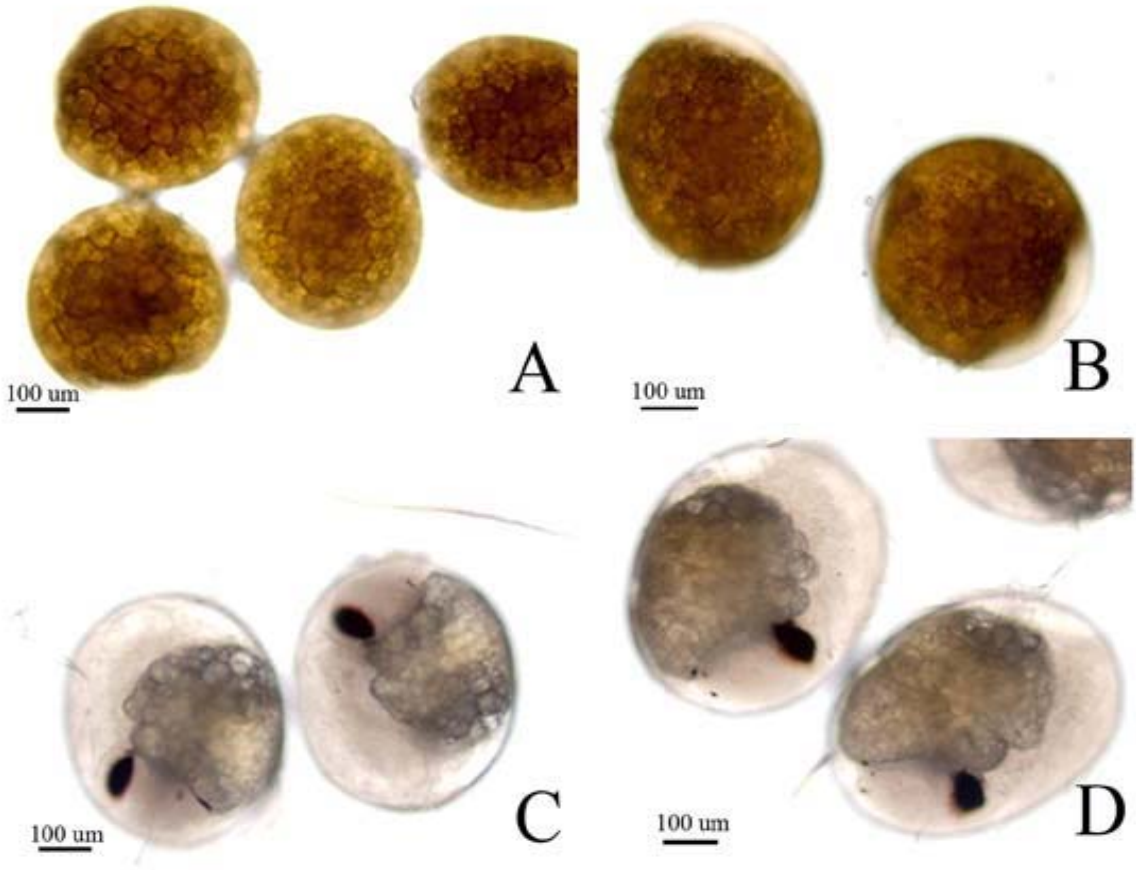
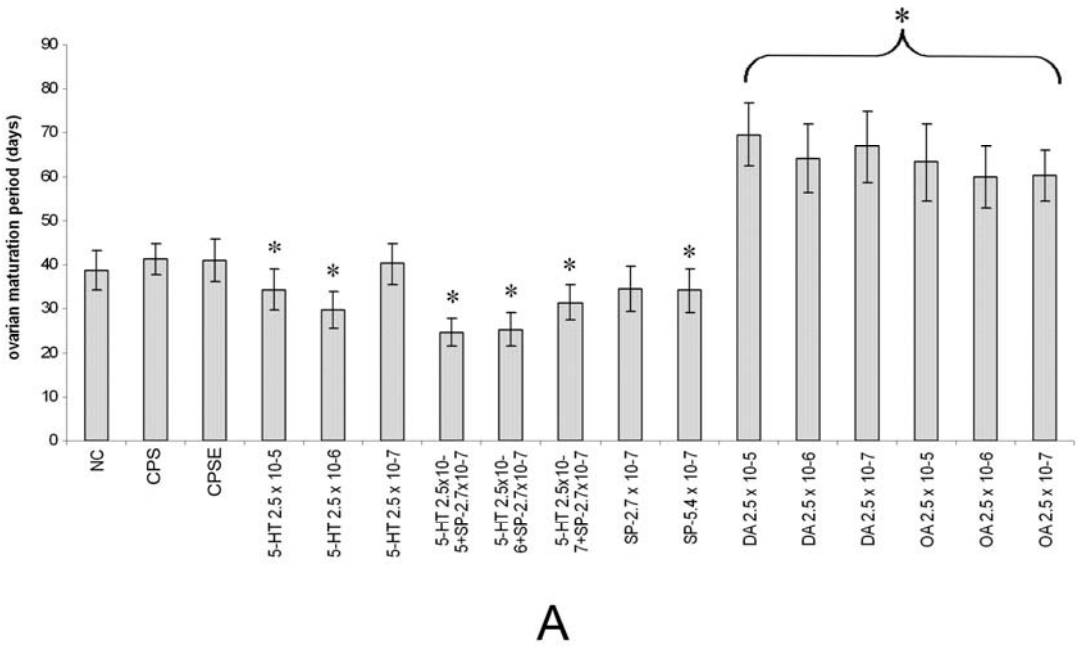
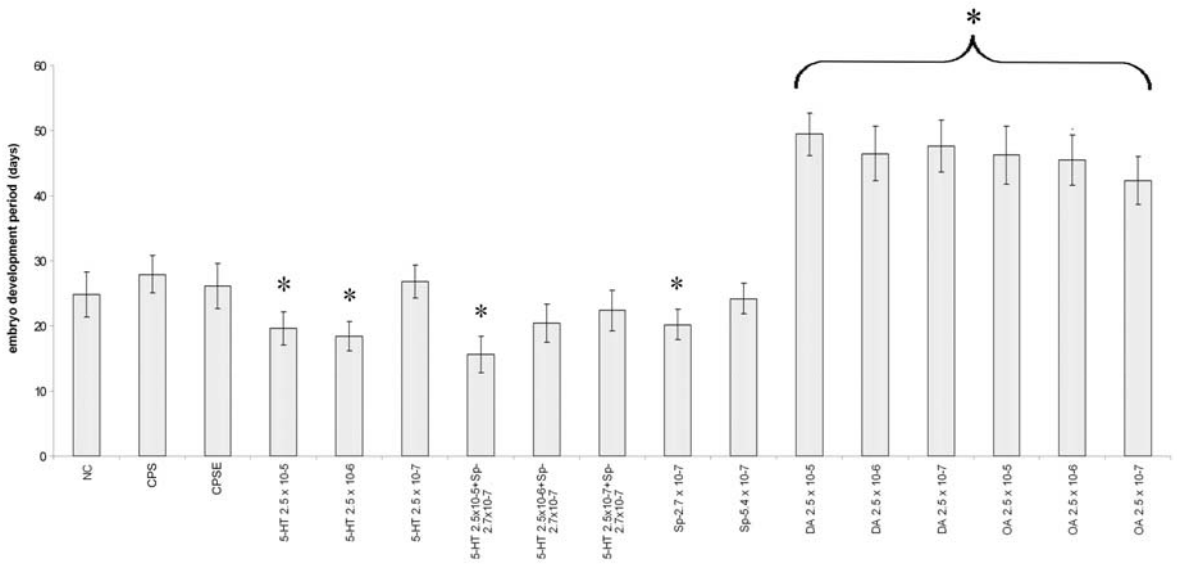


Figure 3.

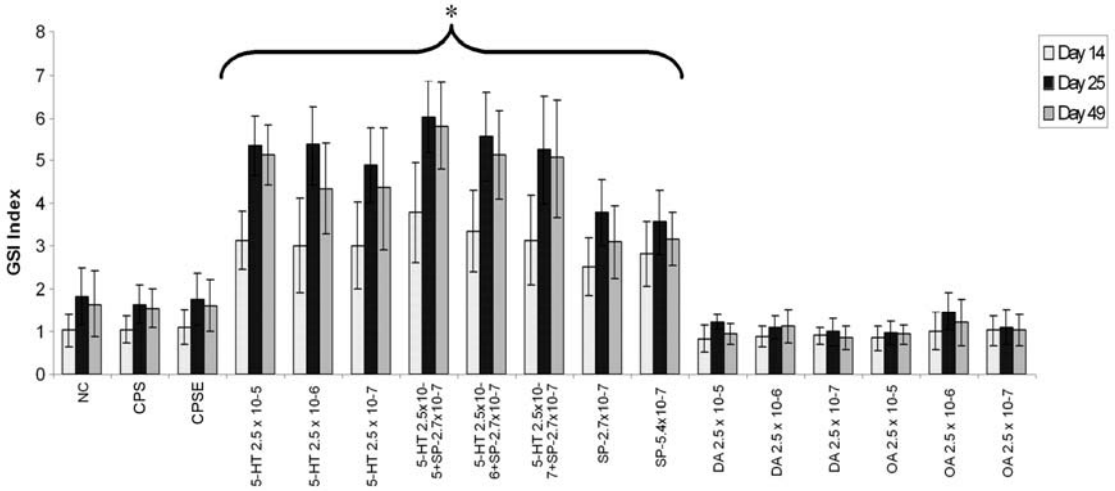

ovarian maturation period (days)
0
10
20
30
40
50
60
70
80
90
NC
CPS
CPSE
5-HT 2.5 x 10-5
5-HT 2.5 x 10-6
5-HT 2.5 x 10-7
5-HT 2.5x10-5+SP-2.7x10-7
5-HT 2.5x10-6+SP-2.7x10-7
5-HT 2.5x10-7+SP-2.7x10-7
SP-2.7 x 10-7
SP-5.4 x 10-7
DA 2.5 x 10-5
DA 2.5 x 10-6
DA 2.5 x 10-7
OA 2.5 x 10-5
OA 2.5 x 10-6
OA 2.5 x 10-7
*

A

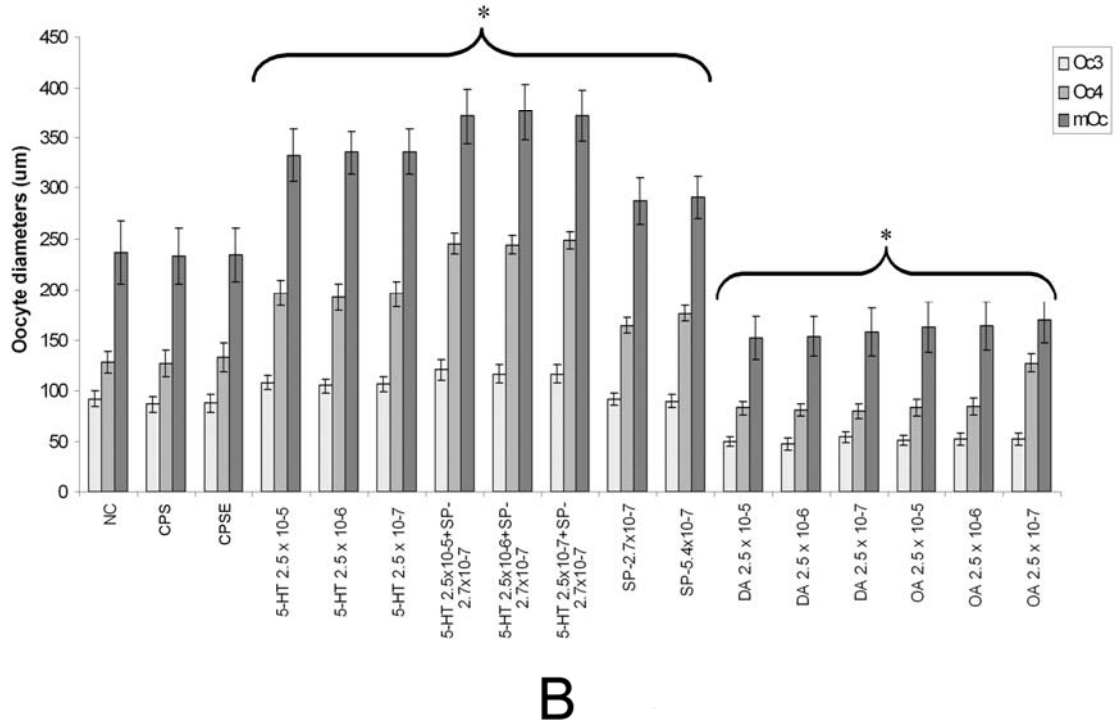

embryo development period (days)
0
10
20
30
40
50
60
NC
CPS
CPSE
5-HT 2.5 x 10-5
5-HT 2.5 x 10-6
5-HT 2.5 x 10-7
5-HT 2.5x10-5+Sp-2.7x10-7
5-HT 2.5x10-6+Sp-2.7x10-7
5-HT 2.5x10-7+Sp-2.7x10-7
Sp-2.7 x 10-7
Sp-5.4 x 10-7
DA 2.5 x 10-5
DA 2.5 x 10-6
DA 2.5 x 10-7
OA 2.5 x 10-5
OA 2.5 x 10-6
OA 2.5 x 10-7
*

B

Figure 4


GSI Index
Day 14
Day 25
Day 49
NC
CPS
CPSE
5-HT 2.5 x 10-5
5-HT 2.5 x 10-6
5-HT 2.5 x 10-7
5-HT 2.5x10-5+SP-2.7x10-7
5-HT 2.5x10-6+SP-2.7x10-7
5-HT 2.5x10-7+SP-2.7x10-7
SP-2.7x10-7
SP-5.4x10-7
DA 2.5 x 10-5
DA 2.5 x 10-6
DA 2.5 x 10-7
OA 2.5 x 10-5
OA 2.5 x 10-6
OA 2.5 x 10-7

A


Oocyte diameters (um)
Oc3
Oc4
mOc
NC
CPS
CPSE
5-HT 2.5 x 10-5
5-HT 2.5 x 10-6
5-HT 2.5 x 10-7
5-HT 2.5x10-5+SP-2.7x10-7
5-HT 2.5x10-6+SP-2.7x10-7
5-HT 2.5x10-7+SP-2.7x10-7
SP-2.7x10-7
SP-5.4x10-7
DA 2.5 x 10-5
DA 2.5 x 10-6
DA 2.5 x 10-7
OA 2.5 x 10-5
OA 2.5 x 10-6
OA 2.5 x 10-7

B

Figure 5

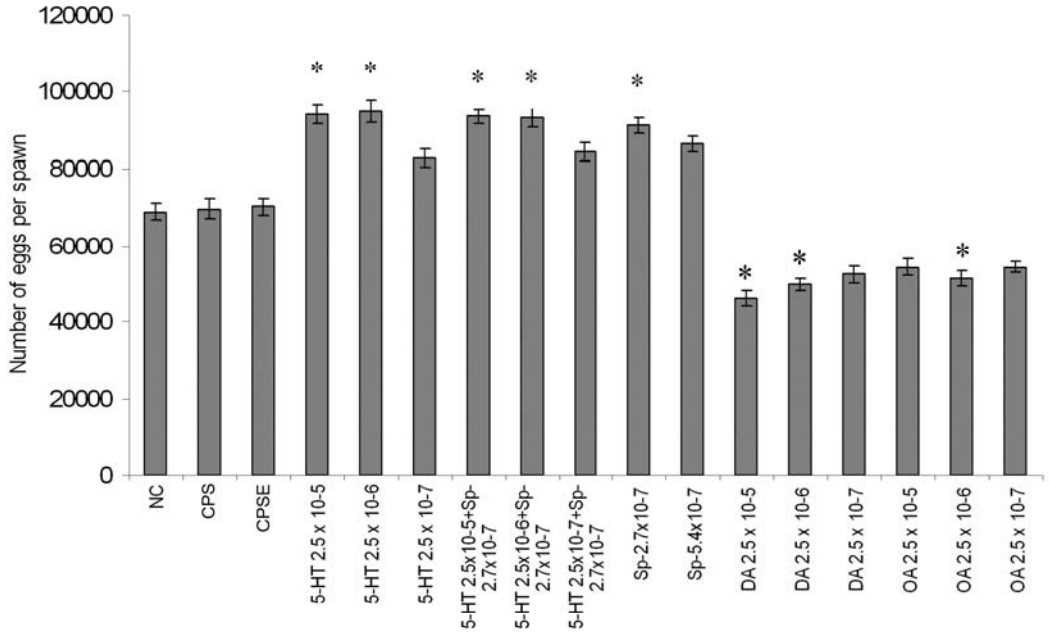

120000
100000
80000
60000
40000
20000
0
Number of eggs per spawn
*
NC
CPS
CPSE
5-HT 2.5 x 10-5
5-HT 2.5 x 10-6
5-HT 2.5 x 10-7
5-HT 2.5x10-5+Sp-2.7x10-7
5-HT 2.5x10-6+Sp-2.7x10-7
5-HT 2.5x10-7+Sp-2.7x10-7
Sp-2.7x10-7
Sp-5.4x10-7
DA 2.5 x 10-5
DA 2.5 x 10-6
DA 2.5 x 10-7
OA 2.5 x 10-5
OA 2.5 x 10-6
OA 2.5 x 10-7

Figure 6

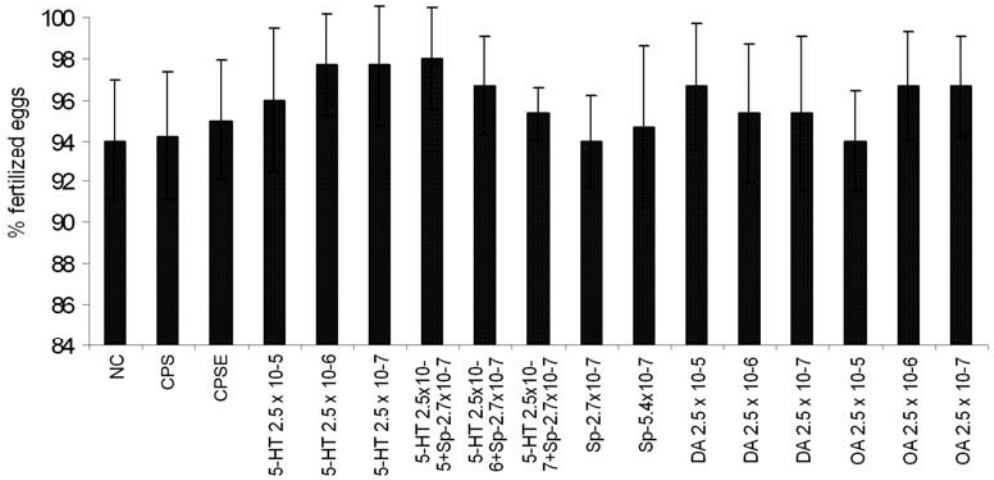

% fertilized eggs
100
98
96
94
92
90
88
86
84
NC
CPS
CPSE
5-HT 2.5 x 10-5
5-HT 2.5 x 10-6
5-HT 2.5 x 10-7
5-HT 2.5x10-5+Sp-2.7x10-7
5-HT 2.5x10-6+Sp-2.7x10-7
5-HT 2.5x10-7+Sp-2.7x10-7
Sp-2.7x10-7
Sp-5.4x10-7
DA 2.5 x 10-5
DA 2.5 x 10-6
DA 2.5 x 10-7
OA 2.5 x 10-5
OA 2.5 x 10-6
OA 2.5 x 10-7

Figure 7.

Comparative distribution of a putative egg-laying hormone in neural and reproductive tissues of four Decapoda crustaceans

Zhipeng Liu[1], John Donald[1], Peter Hanna[1,2], Parinyaphon Nuurai[2], Prasert Sobhon[2]

[1.] School of Life & Environmental Sciences, Deakin University, Geelong, VIC 3217 Australia

[2.] Department of Anatomy, Faculty of Science, Mahidol University, Bangkok 10400, Thailand

Corresponding author: **Prof. Prasert Sobhon**

Department of Anatomy

Faculty of Science

Mahidol University

Bangkok 10400

Thailand

Tel: +66 - 2 - 2015406

Email: scpso@mahidol.ac.th, anatch2002@yahoo.com

Abstract Evidence for the presence of a putative egg-laying (ELH) hormone has been previously described in the Black Tiger shrimp, *Penaeus monodon*, so a further investigation was carried out to detect its presence in a range of *Decapoda* crustaceans prior to a full molecular analysis. The crustaceans were represented by the Australian fresh water yabbie, *Cherax destructor*, the Australian southern rock lobster, *Jasus edwardsii*, the snow crab, *Chionoecetes opilio*, and the blue swimmer crab, *Portunus pelagicus*. Female cerebral ganglia, ventral nerve cords and gonads were investigated in a comparative study of the distribution of the immunoreactive hormone using immunoenzyme and immunofluorescence techniques. Immunoreactivity was detected in all tissues of interest, and the distribution patterns showed similarity within the four species, as well as that of *P.* monodon reported in the earlier study. There were minor variations. These data indicate that a putative ELH-like neuropeptide is widespread in crustaceans, and supports its previous identification in a range of molluscs and other invertebrates. Elucidation of the molecular structure of the peptide hormone and its encoding gene, as well as its involvement in spawning behaviour of crustaceans, is now fully under investigation.

Keywords Egg-laying like hormone – Decapoda crustaceans – Immunohistochemistry – Neurosecretory cells – Ovary – Oocytes

Introduction

There is limited success in the natural spawning of cultured crustaceans, such as the black tiger shrimp, *Penaeus monodon,* and therefore the artificial spawning of these crustacean species relies primarily on the collection of eggs from wild broodstock (Hoang et al., 2002). This has raised further problems which include the depletion of wild stocks, unknown disease status, and genetic unreliability (Liu et al., 2006). Spawning of wild and cultured broodstock is usually achieved by eyestalk ablation of females, such as with the white Pacific shrimp, *P. vannamei* (Palacios et al., 1999), the black tiger shrimp, *P. monodon* (Primavera, 1978), and the Kuruma prawn, *P. japonicus* (Tsutsui et al., 2005).

Eye ablation is generally practiced by most commercial hatcheries, and is known to function by decreasing the amount of gonad-inhibiting hormone (GIH), also known as vitellogenesis-inhibiting hormone (VIH). This loss of hormone is due to the removal of a neuroendocrine secretory tissue called the X-organ which is located in the terminal medulla, as well as the associated sinus gland, all within the eye stalk (Desai and Achuthankutty, 2000). The GIH inhibits female reproduction, i.e. ovarian development, and especially vitellogenesis (Keller, 1992). However, after eyestalk ablation, subsequent spawning and larval survival are markedly reduced, necessitating the replacement of broodstock a few weeks after eyestalk ablation (Palacios et al., 1999).

An approach to obviate eye ablation in crustacean farming could be the use of techniques that increase reproductive hormone(s), such as the egg-laying hormone (ELH) identified in the sea hare, *Aplysia californica* (Scheller et al., 1982; Nambu and Scheller, 1986). This may be achieved by supplying excitatory hormone(s) in sufficient quantities to override the inhibitory hormones, such as GIH in crustaceans (Lacombe et al., 1999). It has been reported that spawning

of female molluscs can be achieved by injection of neural tissue homogenates from sexually mature females; examples include the sea hare, *Aplysia californica* (Kupferman, 1967), and the disk abalone, *Haliotis discus* (Yahata, 1973). As well, injection of a recombinant abalone ELH from *H. discus hannai* has been used to spawn ripe females of the California red abalone, *H. rufescens*, and the blacklip abalone, *H. rubra* (unpublished data). Therefore, a means to activate crustacean spawning could be through the characterisation and application of spawning inducing hormone(s). This method could lead to a convenient crustacean farming practice, compared with the current high cost of using wild spawners and relative lack of control in all species (Primavera, 1978).

Immunocytochemical studies have identified an ELH type of immunoreactivity in a range of invertebrates. These include gastropod molluscs, such as the sea hare, *A. californica* (Shyamala et al., 1986), the great pond snail, *Lymnaea stagnalis* (Vreugdenhil et al., 1988), the brown garden snail, *Helix aspersa* (Van Minnen et al., 1992), the Australian blacklip abalone, *H. rubra* (Cummins et al., 2001), the tropical abalone, *H. asinina* (Saitongdee et al., 2005), the giant garden slug, *Limax maximus* (Van Minnen et al., 1992), a few basommatophoran snails, including *Bulinus truncates, B. glabrata, Listera ovata, Planorbarius corneus, P. planoribis* and *P. vortex* (Roubos and van de Ven, 1987); the bloodfluke planorb, *Biomphalaria glabrata*; annelids, including the rhyonobdellid leech, *Theromyzon tessulatum* (Salzet et al., 1997); and arthropods, including the Colorado potato beetle, *Leptinotarsa decemlineata*, the flesh fly, *Sarcophaga bullata*, the migratory locust *Locusta migratoria*, the American cockroach *Periplaneta Americana* (Theunis et al., 1990), the fruit fly, *Drosophila melanogaster* (Herndon and Wolfner, 1995), and the black tiger shrimp, *P. monodon* (Liu et al., 2006). A sequence alignment of *T. tessulatum* LELH, *A. californica* ELH, *A. parvula ELH* and *L. stagnalis* CDCH, has shown conserved regions within the 36 amino acid peptides which could act as cross-reactive

epitopes (Salzet et al., 1997). The *H. rubra* aELH peptide [LSITNDLRAIADSYLYDQHKLRERQEENLRRRFLRL], which is identical with CDCH except for Arg rather than Glu in residue 35 (Wang and Hanna, 1998), was used as the peptide to make antisera.

Although a putative ELH was recently identified in *P. monodon* (Liu et al., 2006), there has been no evidence for the putative neuropeptide being present in other crustaceans. Therefore, we carried out a comparative immunocytochemical study to investigate the presence of a putative ELH in four crustacean species, namely the Australian fresh water yabbie, *Cherax destructor*, the Australian southern rock lobster, *Jasus edwardsii*, the snow crab, *Chionoecetes opilio*, and the blue swimmer crab, *Portunus pelagicus*.

Materials and methods

Animals and tissue preparations

C. destructor (n=5) were captured in a local reservoir at Deakin University, Waurn Ponds, Victoria, Australia; live *J. edwardsii* (n=3) and *C. opilio* (n=3) were obtained from a commercial seafood supplier in Melbourne, Australia. Paraffin embedded blocks of tissues of *P. pelagicus* (n=3) were produced at the Anatomy Department, Faculty of Science, Mahidol University, Bangkok, Thailand, from live animals obtained at a local seafood supplier. Only females were investigated in this research. Target tissues, i.e. cerebral ganglia, ventral nerve cords and ovaries, were dissected and fixed immediately in 20 volumes of 4% paraformaldehyde in phosphate-buffered saline (PBS), pH 7.4. The fixation was carried out at 4^{o}C for 24 h, after which tissue samples were dehydrated in an ascending ethanol series (70%, 80% and 90%) and three final changes of 100% ethanol for 30 min each at room temperature. The ethanol in the tissue samples

was cleared using three changes of dioxane for 30 min each at room temperature, and the tissues were then embedded in melted Paraplastic Plus (Kendall) at 65^{o}C with three changes of 30 min each. Serial sections of prepared blocks were cut with a Reichert-Jung microtome and mounted onto silane-coated slides. Before immunostaining, the tissue sections were dewaxed in three change of xylene for 2 min each, rehydrated in a descending ethanol series (100%, 90%, 80% and 70% for 2 min each), then running tap water for 5 min. The tissue sections were then stored in a moist chamber prior to immunostaining. Twenty sections of each tissue were used to confirm immunostaining.

Immunostaining

The primary polyclonal antibody was produced in mouse against expressed recombinant abalone (*H. rubra*) egg-laying hormone (aELH; Sequence is given in the Introduction section), at Mahidol University. Immunoenzyme studies utilised horse radish peroxidase (HRP) with an avidin-biotin amplification step. Rehydrated tissue sections were treated with 10% v/v H_2O_2 in 80% v/v methanol to quench potential endogenous HRP activity. They were rinsed in PBS, and underwent a microwave treatment to nearly boiling in PBS for 15 min. The sections were blocked with 1% w/v gelatin in PBS for 30 min, and then 4% bovine serum albumin (BSA) and 2% goat serum w/v in PBS for another 30 min. Following this, the blocking solution was removed and primary antibody was applied. Sections were incubated at 4^{o}C overnight, and then washed three times in PBS. Secondary antibody (i.e. biotinylated polyclonal goat anti-mouse IgG (Sigma), was applied and the sections were then incubated at room temperature for 45 min. Following another series of washes in PBS, as above, the sections were incubated with HRP-avidin conjugate (Sigma) for a further 45 min. This was followed by another series of washes in PBS, and a freshly prepared NovaRED^{TM} (Vector Laboratory) substrate was then applied to

develop a colour reaction, which was stopped by rinsing in dH_2O. The sections were then counterstained in 0.1% haematoxylin (Mayer), rinsed in dH_2O, soaked in formulated tap water (i.e. 0.35% w/v $NaHCO_3$, 2% w/v $MgSO_4$) for 30 s and rinsed again in dH_2O. Sections were finally mounted in aqueous mounting medium (DAKO) and examined under a Zeiss Axioskop MC 80 microscope. Images were captured with a Spot cooled CCD camera.

In immunofluorescence studies, and prior to the application of secondary antibody, sections were treated the same as for immunoenzyme preparations, except that the enzyme quenching step was omitted. After the washes in PBS, the sections were incubated in secondary antibody, a polyclonal sheep anti-mouse IgG-FITC conjugate (Sigma), in the dark for 45 min. Following further washes in PBS, in the dark, the sections were mounted in FITC-mounting medium (50% glycerol in PBS), and images were captured under a fluorescence microscope (Leica).

Positive controls for the two methods were performed using the primary antibody on sections of known immunoreactive abalone tissues, i.e. cerebral ganglia, pleuropedal ganglia, and gonads, of reproductively mature *H. asinina* and *H. rubra* female as used by Saitongdee et al. (2005) and Cummins et al. (2001). Negative controls were made by substituting the primary antibody incubation step with pre-immune mouse serum. As well, preabsorption controls were used to show specificity of the antiserum to ELH epitopes.

Results

ELH-immunoreactivity (ELH-ir) was observed in neural and ovarian tissues of the Decapods, *Cherax destructor*, *Jasus edwardsii*, *Chionoecetes opilio*, and *Portunus pelagicus*, and with similar distribution patterns to that previously observed in *Penaeus monodon*. All tissues

studied showed ELH-ir, viz the cerebral ganglia, ventral nerve cords connecting thoracic and abdominal ganglia, and gonads. However, there were some minor variations. Positive controls using *Haliotis rubra* and *H. asinina* sections all showed ELH-ir in the expected tissues and cells. In all negative controls using both immunoperoxidase and immunofluorescence, there was no detection of any positive ELH-ir (data not shown).

Australian fresh water yabbie, *Cherax destructor*

ELH-ir was identified in the cerebral ganglion and the ventral nerve cord. In the cerebral ganglion region (Fig. 1A), dense ELH-ir was observed in the dorsal giant neurons (DGN), the olfactory lobe (OL), and in the neurons of the ventral paired lateral cluster (VPLC) or cluster 9 (LI-C9). It was also found in the interneuron cell cluster 11 (DCI-C11) of the central body (CB), in which the ELH-like peptide was located around the nuclei. In the ventral nerve cord (Fig. 1B, Fig. 5A), the ELH-ir was localised around the nuclei of small neural cells that were densely distributed along the nerve fibers of the cord (Fig. 1B).

In the ovary (Fig. 1C), ELH-ir was detected in the cells of ovarian capsule (OC) and the follicular cells which surround mature oocytes (Ocy). The ELH-ir were identified in most, but not all, follicular cells. Early previtellogenic oocyte stages were not detected in these ovarian sections and these lacked the sheath of follicular cells.

Australian southern rock lobster, *Jasus edwardsii*

ELH-ir was found to have an almost identical distribution to that observed in *C. destructor*. In the cerebral ganglion (Fig. 2A), ELH-ir was detected in the CB with highest staining density observed near the nuclei of the DCI-C9, and within the DCI-C11. However, there was low staining density in the OL and VPLC (data not shown). ELH-ir was also found in

the olfactory globular tract neuropil (OGTN), in which the staining was located around the nuclei of DGN. In the ventral nerve cord (Fig. 2B, Fig. 5B), ELH-ir was observed around nuclei in some small neurons within the nerve bundle, and these neurons also had positive granules in their axons.

In the ovary (Fig. 2C), ELH-ir was strong near the nuclei of most, but not all, follicular cells which surrounded mature oocytes (Ocy). Unlike the mature Ocy, the previtellogenic (POcy) stages exhibited some cytoplasmic ELH-ir.

Snow crab, *Chionoecetes opilio*

ELH-ir was detected in the OL, the VPLC and the ventral nerve cord. In the cerebral ganglion region (Fig. 3A), dense ELH-ir was observed in both the OL and the VPLC. In the OL, the ELH-ir was densely distributed around the nuclei of DGN. However, in the VPLC, ELH-ir was observed in the cytoplasm of neurons in LI-C9. There was a lower level of ELH-ir in the CB (data not shown). In the ventral nerve cord (Fig. 3B, Fig. 5C), dense ELH-ir was found in the axons and perinuclear region of neurons distributed among nerve bundles.

In the ovary (Fig. 3C), ELH-ir was detected in most, but not all, follicular cells which surrounded mature oocytes (Ocy). These oocytes did not show ELH-ir, whereas the early stage oocytes at the previtellogenic stages exhibited some cytoplasmic ELH-ir (Fig. 3C).

Blue swimmer crab, *Portunus pelagicus*

ELH-immunoreactivity was observed in both neural and reproductive tissues of *P. pelagisus*. In the cerebral ganglion region (Fig. 4A), dense ELH-ir was observed in both the OL and CB, but low density immunoreactivity was found in the VPLC (data not shown). In the OL, ELH-ir was distributed mainly in the cytoplasm of DGN and neurons of the CB. In the ventral

nerve cord (Fig. 4B, Fig. 5D), dense ELH-ir was found within cells in the nerve capsule, but relatively little ELH-ir was found in the cells residing in the nerve bundles.

In the ovary (Fig. 4C), strong ELH-ir was observed around the nuclei of most of the follicular cells surrounding mature oocytes (Ocy). Early stage previtellogenic oocytes were not detected in these ovarian sections.

Discussion

This research shows evidence for the existence for an ELH-like regulatory peptide in four Decapoda species: the Australian fresh water yabbie, *Cherax destructor*, the Australian southern rock lobster, *Jasus edwardsii*, the snow crab, *Chionoecetes opilio,* and the blue swimmer crab, *Portunus pelagicus*. It also reveals similar distribution patterns of ELH-ir in the selected female tissues, i.e. cerebral ganglia, ventral nerve cords and ovaries (Table 1).

Although ELH-ir was observed in the similar tissues and cell clusters within all four species, some differences of signal strength and specific locations were observed and are summarised in Table 1. For example, a strong ELH-ir signal was found in the olfactory lobe (OL) of *C. destructor*, *C. opilio* and *P. pelagicus*, but there was considerably less in *J. edwardsii*. Strong ELH-ir was observed around the nuclei of neural cells and within axons of *C. opilio* ventral nerve cord, but this was not present in the other species. A low level of ELH-ir was observed in *P. pelagicus* ventral nerve cord fibers, compared with a high level in the same structures of the other species. These differences could be due to the fact that animals used in this study were at different stages of gonad maturity (e.g. some previtellogenic oocytes were observed in *J. edwardsii* and *C. opilio* ovaries, but not in *C. destructor* and *P. pelagicus*).

In the ovary, most but not all follicular cells surrounding mature oocytes consistently showed strong immunoreactivity, a feature also characteristic of pre-spawned *P. monodon* which is lost following spawning (Lui et al., 2006). The loss of a putative ELH hormone during spawning could be linked to an active role in the release of oocytes. Previtellogenic oocytes, but not mature oocytes, also exhibited some immunoreactivity, which may indicate the role for the putative ELH hormone in stimulating the development of the early previtellogenic oocytes.

In the black tiger shrimp, *P. monodon*, ELH-ir was identified in the subesophageal-thoracic ganglia region and the supraesophageal ganglion which is known as the brain (Liu et al., 2006). In particular, the ELH-ir in the *P. monodon* brain was within the cytoplasm of the neurosecretory cells and neurons, and a similar pattern was observed in all four species investigated in this study. In eumalacostracan crustaceans, such as crayfish, lobster and crabs, the olfactory neuropil has a principal role in control of mating, feeding and territorial behaviours (Sullivan and Beltz, 2004). In these organisms, outputs from the OL which is the primary olfactory centre, are conveyed to the medulla terminalis and hemiellipsoid body in the lateral protocerebrum, a higher order centre, and this transmission is carried out by a large population of associated neurons (Sullivan and Beltz, 2004). These neurons showed ELH reactivity in the present study.

However, in the present study there were some ELH-ir variations and these are reported in Table 1. For example, some ELH-ir variations were within the OL, DGN, VPLC, LI-C9, DCI-C9, and DCI-C11. These may reflect a status of reproductive maturation as *J. edwardsii* and *C. opilio* appeared to be more sexually mature (see ovary results in Table 1).

In the ventral nerve cords of the four species, the ELH-ir was high, and tended to be denser along the nerve fibers. This may indicate that ELH might be transmitted to the more

caudal region of the CNS and possibly the gonads, thus a cascading mechanism might be involved for spawning control.

ELH was firstly identified in bag cells of the abdominal ganglia of the sea hare, *Aplysia californica*, (Kupfermann, 1967). Expression of ELH genes were later shown to occur, not only in the bag cells, but in an extensive system of neurons distributed in four of the five ganglia of the central nervous system (Scheller et al., 1982; McAllister et al. 1983). These locations are similar to the ELH immunoreactivity in the abdominal ganglia and associated ventral nerve cord of eumalacostracan crustaceans. ELH in *A. californica*, has been characterised as a 36 amino acid peptide (Chiu et al., 1979) acting as a neuromodulator from the abdominal ganglia (Branton et al., 1978), and alerting defined neurons (Mayeri et al., 1985). It is also distributed via the hemolymph throughout the individual, arriving at the target organ which is the female gonad, causing smooth muscle contraction and discharge of the eggs (Rothman et al., 1983). However, in terms of behaviour, ELH and associated peptides, cleaved from a preprohormone, generate a stereotypic repertoire during spawning (Garden et al., 1998), inducing cessation of walking, feeding inhibition, head weaving, and finally, egg expulsion (Scheller et al., 1982).

A seminal fluid protein, Acp26aa, identified in male *Drosophila melanogaster* was found to contain a conserved ELH region to *A. californica* ELH, and features to stimulate female spawning when transferred during mating (Herndon and Wolfner, 1995). This raises interest as to whether a similar process is also involved in crustacean reproduction, utilising a crustacean ELH-like hormone. A crustacean ELH might also be produced in males but requires further testing.

As indicated by the molluscs and insect ELH data, a crustacean ELH might play a multifunctional role in a spawning process. Signaled by either internal or external or both environmental factors for spawning. A crustacean ELH preprohormone might firstly be

expressed in neurosecretory cells located in cerebral ganglia (e.g. OL cells and VPLC cells) and certain neurons in the ventral nerve cord; this immature product was then distributed to the circulation and cleaved into different mature hormones before arriving at individual responsive targets, e.g. smooth muscles in trabaculae and capsule of the female ovaries; and therefore triggered defined activities, one of which is egg-laying. It is also possible that such a preprohormone or certain final product, i.e. ELH, could be produced by male individuals, transferred to and stored by females, which leads to spawning activities as above. Futhermore, the presence of strong ELH immunoreactivity in the follicular cells surrounding mature oocytes and in the cytoplasm of previtellogenic oocytes implies that this hormone may be involved in some way with the process of oocyte maturation.

In summary, a putative ELH in *Decapoda* crustacean has been identified, and as a consequence of its similar distribution in various crustaceans and molluscs, it is likely that the putative crustacean ELH serves as an endocrine factor in the spawning behaviour. Male crustaceans are now being investigated to determine whether they express a putative ELH. We are also investigating the molecular basis of the putative endocrine hormone for better understanding of its function in crustacean reproductive biology. The ability to reliably spawn female crustaceans using an egg-laying hormone, rather than the using eye ablation, would be very important to aquaculture production by having a regulated reproductive cycle. This would then provide for the selection of females with genetically desirable traits, including growth, colour and disease resistance.

Acknowledgements

We thank Deakin University for a PhD scholarship to Z. Liu, the Thailand Research Fund (TRF) for a PhD scholarship to P. Nuurai and a Senior Research Fellowship to Professor P. Sobhon, and

the Commision on Higher Education (CHE) for a Research Group Development grant to P. Sobhon.

References

Branton WD, Arch S, Smock T, Mayeri E (1978) Evidence for mediation of a neuronal interaction by a behaviorally active peptide. Proc Nat Acad Sci USA 75:5732-5736

Chiu AY, Hunkapiller MW, Heller E, Stuart DK, Hood LE, Strumwasser F (1979) Purification and primary structure of the neuropeptide egg-laying hormone of *Aplysia californica*. Proc Natl Acad Sci USA 76:6656-6660

Cummins S, Thongkukiatkul A, Hanna PJ (2001) Location of egg-laying hormone in reproductive structures and neurons of *Haliotis rubra* (Leach) using antibodies raised against recombinant fusion proteins. J Shell Res 20:705-710

Desai UM, Achuthankutty CT (2000) Complete regeneration of ablated eyestalk in penaeid shrimp, *Penaeus monodon*. Curr Sci 79:1602-1603

Garden RW, Shippy SA, Li L, Moroz TP, Sweedler JV (1998) Proteolytic processing of the *Aplysia* egg-laying hormone prohormone. Proc Nat Acad Sci USA 95:3972-3977

Herndon L, Wolfner M. (1995) A *Drosophila* seminal fluid protein, Acp26Aa, stimulates egg laying in females for 1 day after mating. Proc Natl Acad Sci USA 92:10114-10118

Hoang T, Lee ST, Keenan CP, Marsden GE (2002) Observations on growth, sexual maturity and spawning performance of pond-reared *Penaeus merguiensis*. Aquac Res 33:863-873

Keller R (1992) Crustacean neuropeptides: structures, functions and comparative aspects. Experientia 48:439-449

Kupferman I (1967) Stimulation of egg laying: possible neuroendocrine function of bag cells of abdominal ganglion of *Aplysia californica*. Nature 216:814-815

Lacombe C, Greve P, Martin G (1999) Overview on the sub-grouping of the crustacean hyperglycemic hormone family. Neuropeptides 33:71-80

Liu Z, Sobhon, P, Withyachumnarnkul B, Hanna P (2006) Identification of a putative egg-laying hormone in neural and ovarian tissues of the black tiger shrimp, *Penaeus monodon*, using immunocytochemistry. Invert Neurosci 6:41-46

McAllister LB, Scheller RH, Kandel ER, Axel R (1983) In situ hybridization to study the origin and fate of identified neurons. Science 222:800-808

Mayeri E, Rothman BS, Brownell PH, Branton WD, Padgett L (1985) Nonsynaptic characteristics of neurotransmission mediated by egg-laying hormone in the abdominal ganglion of *Aplysia*. J Neurosci 5**:**2060-2077

Nambu JR, Scheller RH (1986) Egg-laying hormone genes of *Aplysia*: evolution of the ELH gene family. J Neurosci 6:2026-2036

Palacios E, Carreño D, Rodríguez-Jaramillo MC, Racotta IS (1999) Effect of eyestalk ablation on maturation, larval performance and biochemistry of white pacific shrimp *Penaeus vannamei*, broodstock. J Appl Aquac 9:1-23

Primavera JH (1978) Induced mauration and spawning in five-month-old *Penaeus monodon* Fabricius by eyestalk ablation. Aquaculture 13:355-359

Rothman BS, Weir G, Dudek FE (1983) Egg-laying hormone: Direct action on ovotestis of *Aplysia*. Gen Comp Endocrinol 52**:**134-141

Roubos EWR, van de Ven AMH (1987) Morphology of neurosecretory cells in basommatophoran snails homologous with egg-laying and growth hormone producing cells of *Lymnaea stagnalis*. Gen Comp Endocrinol 67:7-23

Saitongdee P, Apisawetakan S, Anunruang N, Poomthong T, Hanna PJ, Sobhon P (2005) Egg-laying-hormone immunoreactivity in the neural ganglia and ovary of *Haliotis asinina* Linnaeus. Invert Neurosci 5:165-172

Salzet M, Verger-Gocquet M, Vandenbulcke F.Minnen JV (1997) Leech egg-laying-like hormone: structure, neuronal distribution and phylogeny. Mol Brain Res 49:211-221

Scheller RH, Jackson JF, McAllister LB, Schwartz JH, Kandel ER, Axel R (1982) A family of genes that codes for ELH, a neuropeptide eliciting a stereotyped pattern of behavior in *Aplysia*. Cell 28:707-719

Shyamala M, Nambu JR, Scheller RH (1986) Expression of the egg-laying hormone gene family in the head ganglia of *Aplysia*. Brain Res 371:49-57

Sullivan JM, Beltz BS (2004) Evolutionary changes in the olfactory projection neuron pathways of Eumalacostracan crustaceans. J Comp Neurol 470:25-38

Theunis W, Van Minnen J, De Loof A (1990) Immunocytochemical localization in the central nervous system of four different insect species of molecules immunoreactive against peptides present in the causodorsal cells of *Lymnaea stagnalis*. Gen Comp Endocrinol 79:415-422

Tsutsui N, Kim YK, Jasmani S, Ohira T, Wilder MN, Aida K (2005) The dynamics of vitellogenin gene expression differs between intact and eyestalk ablated kuruma prawn *Penaeus (Marsupenaeus) japonicus*. Fish Sci 71:249-256

Van Minnen J, Schallin HDFH, Ramkema MD (1992) Identification of putative egg-laying hormone containing neuronal systems in *gastropod molluscs*. Gen Comp Endocrinol 86:96-102

Vreugdenhil E, Jackson JF, Bouwmeester T, Smit AB, Van Minnen J, Van Heerikhuizen H, Klootwijk J, Joosse H (1988) Isolation, characterization, and evolutionary aspects of a cDNA clone encoding multiple neuropeptides involved in the stereotyped egg-laying behavior of the fresh water snail *Lymnaea stagnalis*. J Neurosci 8:4184-4191

Wang L, Hanna PJ (1998). Isolation, cloning, and expression of a DNA sequence encoding an egg-laying hormone of the blacklip abalone (*Haliotis rubra* Leach). J Shellfish Res 17:789-793

Yahata T (1973) Induced spawning of abalone (*Nordotis discus* REEVE) injected with ganglional suspensions. Bull Jap Soc Sci Fish 39:1117-1122

Figure legends

Fig. 1 Immunocytochemical detection of ELH in *C. destructor* tissues. Mouse anti *H. rubra* ELH polyclonal antibody as primary antibody, biotinylated goat anti mouse IgG monoclonal antibody as secondary antibody, avidin linked horse radish peroxidase (HRP) as tertiary binding, and a NovaRED substrate, were used for visualization of ELH. Reactions at the black arrows indicate ELH immunoreactive cells and the white arrow indicates no ELH detection. High magnification insets are shown. **A**. Section of the cerebral ganglion showing the olfactory lobe (OL), with ELH immunoreactive dorsal giant neurons (DGN), the ventral paired lateral cluster (VPLC), with ELH immunoreactive local interneurons cluster 9 (LI-C9), and the central body (CB) containing an ELH positive deutocerebral commissure interneurons cell cluster 11 (DCI-C11) and DGN. A high density of ELH is observed within the cytoplasm of LI-C9 in the VPLC (inset 1), and around the DGN nuclear region in OL (inset 2). **B**. A section of the ventral nerve cord showing the ventral nerve capsule (VNC) and the ventral nerve neurofibres (VNF). ELH is mainly distributed in the axon of neurons within the neurofibres, as indicated in the inset. **C**. An ovarian section showing the ovarian capsule (OC), oocyte (Ocy) and the surrounding connective tissue. High power inset showing ELH immunoreactivity around the nuclei of the positive follicular cells and some connective tissue in the OC. Scale bars are 100 μm in A-C, and 10 μm in insets.

Fig. 2 Immunocytochemical detection of ELH in *J. edwardsii* tissues, using the same technique as in Fig. 1. Black arrows indicate ELH positive cells and the white arrow indicates an ELH negative cell. High magnifications are shown in insets. **A**. A section of the cerebral ganglion showing the CB and OGTN containing DCI-C9, DCI-C11 and DGN, all of which are

immunoreactive for ELH. Inset shows a high density of ELH around the nucleus in a DCI-C11 cell of the CB. **B.** A section of the ventral nerve cord showing the VNC and VNF. The majority of ELH is located in the axons of neurons within the VNF, and shown by the inset. **C.** An ovarian section showing the trabaculae (Tr) and Ocy. High power inset shows intense ELH immunoreactivity around the nuclei of many follicular cells. Scale bars are 100 μm in A-C, and 10 μm in insets.

Fig. 3 Detection of ELH in *C. opilio* tissues, using the same immunocytochemistry technique as in Fig. 1. Black arrows indicate ELH positive cells and the white arrow indicates an ELH negative cell. High magnification insets are shown. **A.** A cerebral ganglion section showing the OL and VPLC, containing ELH immunoreactive DGN and LI-C9 cells, respectively. High density of ELH signal is observed around the nuclei of the DGN in the OL (inset 1), and in the cytoplasm of cells in LI-C9 within the VPLC (inset 2). **B.** A section of the ventral nerve cord showing VNC and VNF. Insets show ELH distribution occurs around the nucleus and along the axon of a neuron. **C.** An ovarian section showing the Tr and Ocy. ELH immunoreactivity is identified around the nuclei of many follicular cells which surround each Ocy. Scale bars are 100 μm in A-C, and 10 μm in insets.

Fig. 4 ELH detection in *P. pelagicus* tissues, using the same immunocytochemistry technique as in Fig. 1. Black arrows indicate ELH positive cells and the white arrow indicates an ELH negative cell. High magnification insets are shown. **A.** A cerebral ganglion section showing the OL and CB, which contain DGN and LI-C9 respectively. Inset shows a high density of ELH signal around the nuclei of DGN in the OL. **B.** A section through the ventral nerve cord showing the VNC and VNF. ELH appears to be located more around the nuclei of the VNC cells than in

neurons of the VNF (see inset). **C.** An ovarian section showing oocytes (OC) and eggs (E). The inset shows ELH immunoreactivity around the nuclei of the follicular cells surrounding an egg. Scale bars are 100 μm in A-C, and 10 μm in insets.

Fig. 5 ELH immunofluorescence confirming the ELH immunoenzyme results represented by nerve cells within the VNC of the four species investigated. Mouse anti *H. rubra* ELH polyclonal antibody was used as the primary antibody and fluorescein isothiocyanate-labelled sheep anti mouse IgG monoclonal antibody used as the secondary antibody, and green fluorescence represents a positive ELH immunoreactive signal. **A.** *C. destructor*. **B.** *J. edwardsii*. **C.** *C. opilio*. **D.** *P. pelagicusis*. Scale 10 μm.

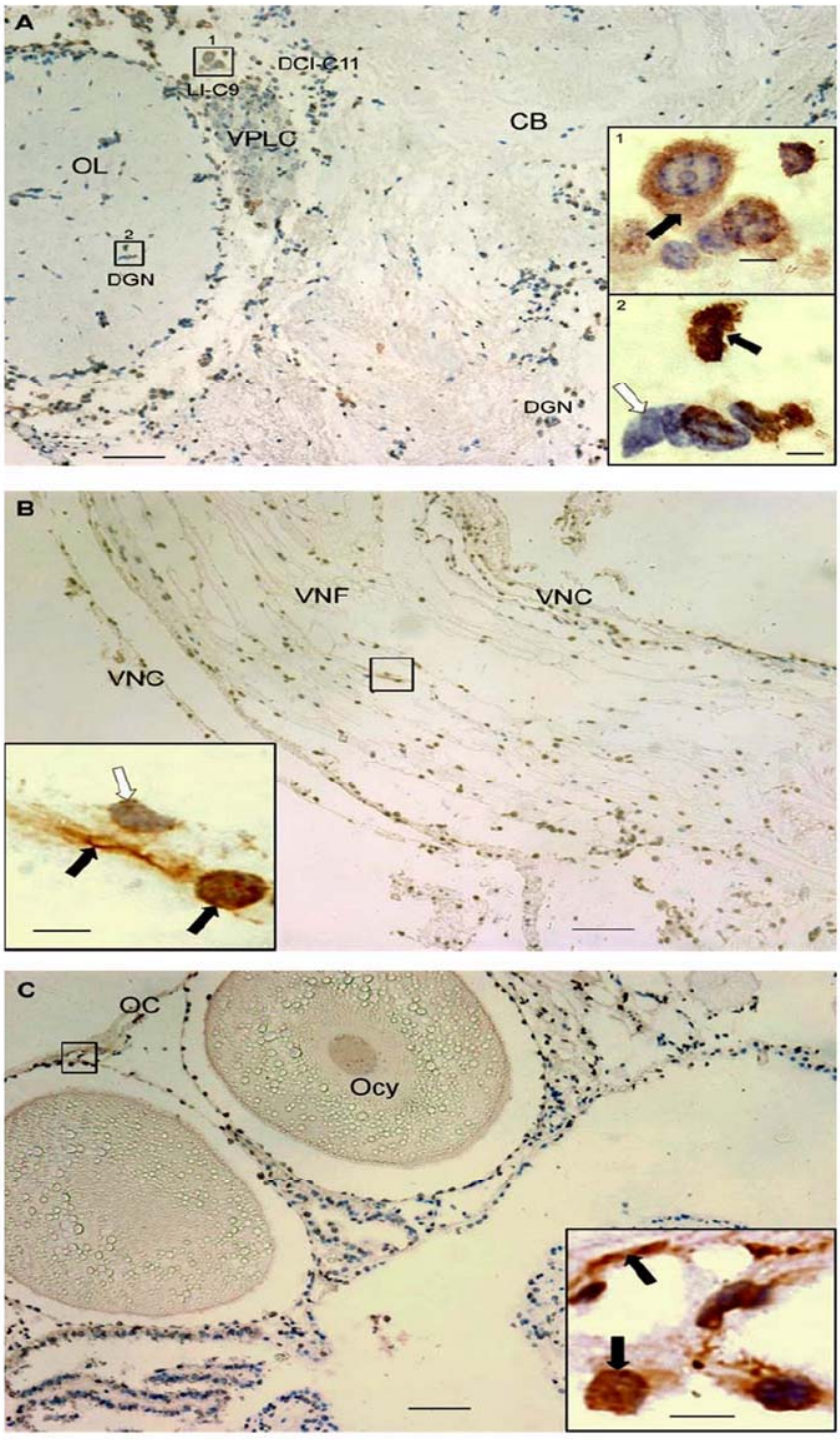


Figure 1

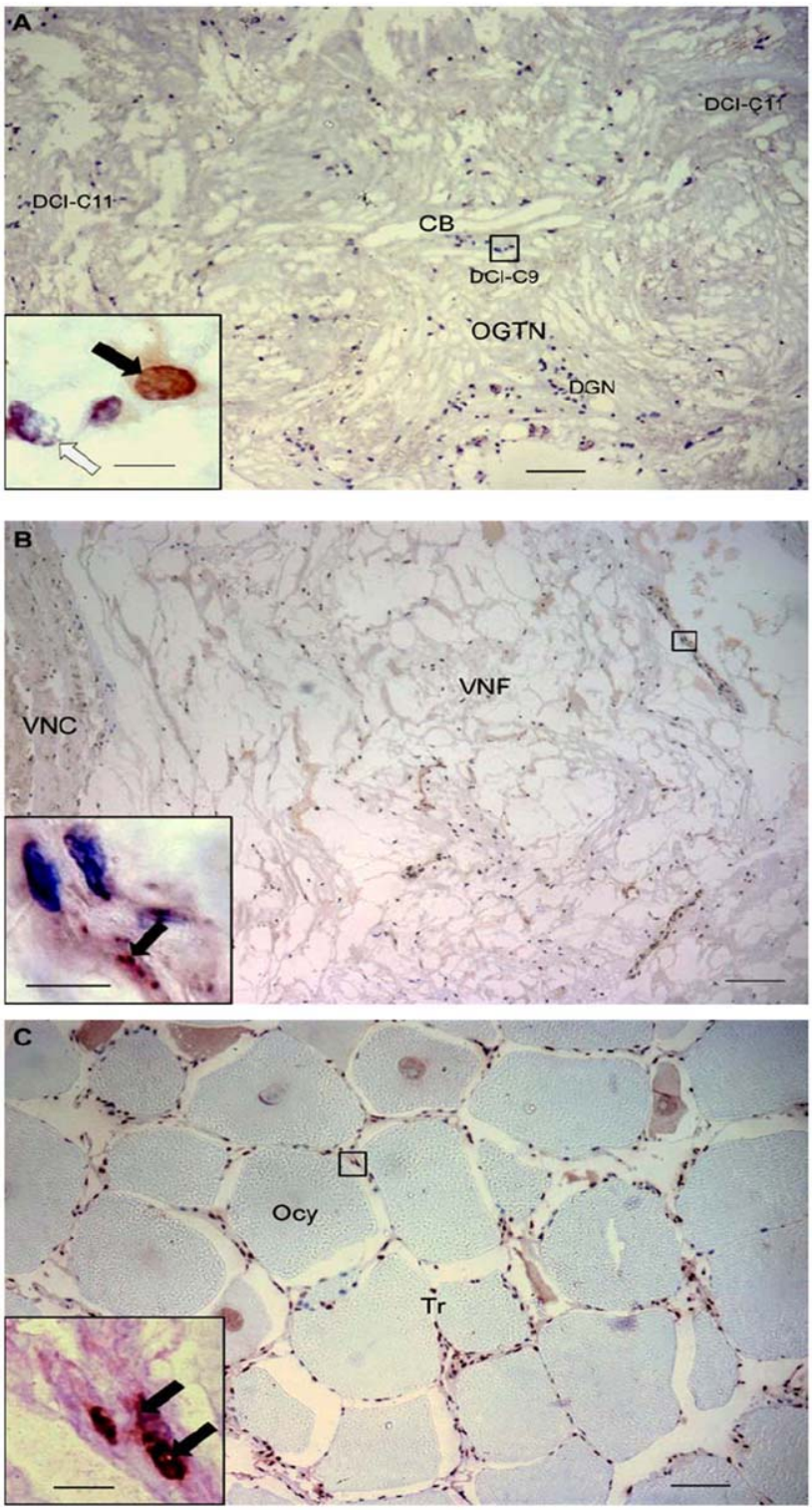


Figure 2

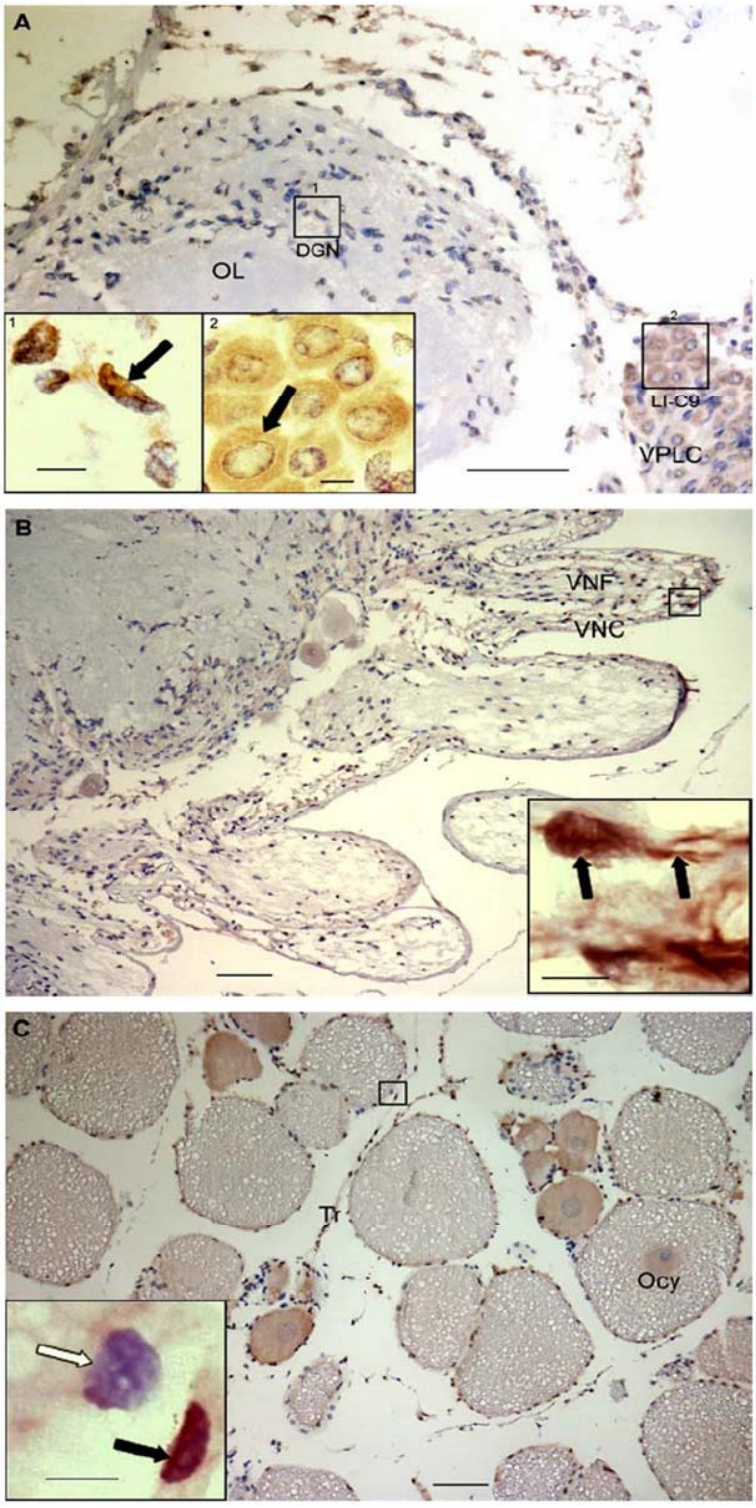


Figure 3

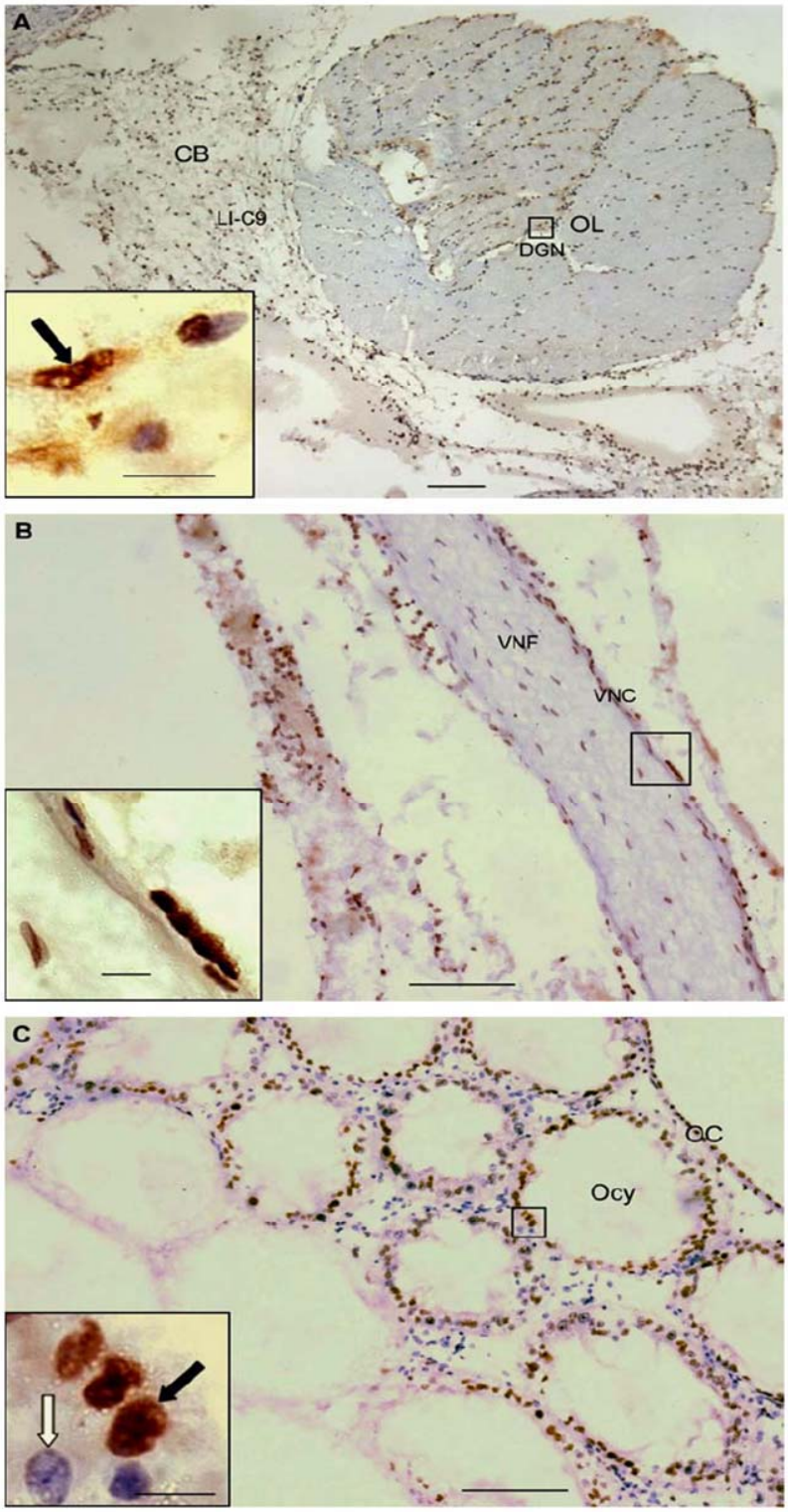


Figure 4

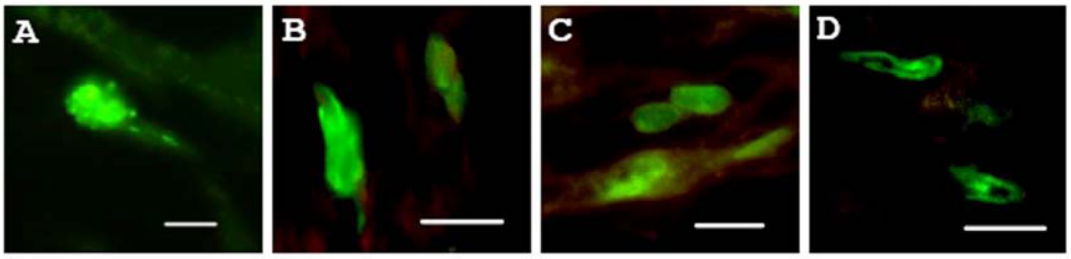


Figure 5

Table 1. Relative density of ELH-immunoreactivity in neural and ovarian tissues.

Species	Cerebral ganglia						Cephalothorax ventral nerve cord			Ovary	
	OL	**DGN**	**VPLC**	**LI-C9**	**DCI-C9**	**DCI-C11**	**Neurons**	**Axons**	**FC**	**Tr**	**Pre-Ocy**
Cherax destructor	high	high	high	high	medium	medium	medium	high	medium	medium	NO
Jasus edwardsii	low	medium	low	medium	high	high	medium	high	medium	medium	high
Chionoecetes opilio	high	high	high	medium	high	medium	medium	high	high	high	high
Portunus pelagicus	high	high	low	medium	medium	medium	medium	medium	medium	medium	NO

Ol, Olfactory Lobe; DGN, Dorsal Giant Neuron; VPLC, Ventral Paired Lateral Cluster; LI-C9, Local Interneurone Cluster 9; DCI-C9, Deutocerebral Commissure Interneurone Cluster 9; DCI-C11, Deutocerebral Commissure Interneurone Cluster 11; FC, Folicular Cells; Tr, Trabaculae; Pre-Ocy, Pre-vitellogenic Oocyte (Note: mature Ocy negative), NO, Not Observed.

Molecular Characterization and Analysis of a Truncated Serotonin Receptor Gene Expressed in Neural and Reproductive Tissues of Abalone.

Sasiporn Panasophonkul[1], Somjai Apisawettakan[1], Scott F. Cummins[3], Patrick S. York[3], Bernard M. Degnan[3], Peter J. Hanna[1,2], Porncharn Saitongdee[1], Prasert Sobhon[1], Prapee Sretarugsa[1*]

1 Department of Anatomy, Faculty of Science, Mahidol University, Bangkok, 10400, Thailand
2 School of Life & Environmental Sciences, Deakin University, Geelong, VIC 3217, Australia
3 School of Integrative Biology, University of Queensland, Brisbane, QLD 4072, Australia

Deleted: *St. Lucia*

Abbreviated Title (40 characters or less): Truncated 5-HT Receptor in Abalone

*Correspondence author and requests for reprints: Dr. Prapee Sretarugsa, Department of Anatomy, Faculty of Science, Mahidol University, Bangkok, 10400, Thailand. Email: scpsr@mahidol.ac.th

Three Key Words: Serotonin receptor, Abalone, Reproduction

Supporting Grants: This work was supported by the Thailand Research Fund (Royal Golden Jubilee Ph.D. Program, Grant No. PHD/0150/2543 to S. Pansophonkul and P. Sretarugsa), the Commission on Higher Education with a grant to P. Sobhon, a University of Queensland Fellowship to S. Cummins and ARC grants to BMD.

Deleted: s

Deleted: and

In molluscs, the neurotransmitter serotonin (5-HT) has been linked to a variety of biological roles including gamete maturation and spawning. Physiological functions associated with 5-HT, are mediated through binding to 5-HT receptors. A cDNA encoding a putative 5-HT receptor consisting of 359 amino acids was isolated from the tropical abalone *Haliotis asinina*, termed 5-HT_{1Hal}. The 5-HT_{1Hal} [seems like an odd naming convention – how about Has-5HT1] shares G-protein-coupled receptor motifs with metazoan 5-HT receptors, including predicted transmembrane domains, active sites for protein kinase action, and N-linked glycosylation sites. However, the third intracellular loop of 5-HT_{1Hal} is relatively short, and only six transmembrane domains are predicted, implying a truncated receptor. Phylogenetic analysis with known 5-HT receptor genes suggests that 5-HT_{1Hal} belongs to the type 1 5-HT receptor family. Expression analysis by RT-PCR showed that 5-HT_{1Hal} mRNA was present in all tissues examined, including the neural ganglia and gonad tissues. Immunocytochemistry revealed the presence of 5-HT_{1Hal} specifically within the soma of neuronal cells located in the outer cortex of both cerebral and pleuropedal ganglia. In ovarian and testicular tissues, 5-HT_{1Hal} immunoreactivity was observed in epithelial cells of the outer capsule and connective tissue of the trabeculae to which the gamete follicles adhere. The possible involvement of 5-HT in oocyte and sperm release was demonstrated by a dose-dependent increase in *Haliotis rubra* gonad contractile bioactivity following 5-HT stimulation.

Deleted: invertebrate and vertebrate

Deleted: homolog

Abbreviations: AEBSF, 4-(2-Aminoethyl) benzenesulfonyl fluoride; cg, cerebral ganglia; ppg, pleuropedal ganglia; fgo, female gonad; mgo, male gonad; GAFS, Gomori's aldehyde-fuchsin staining; 5-HT, 5-hydroxytryptamine, serotonin; 5-HT_{1Hal}, abalone serotonin receptor; 5-HT_{1Hal}-ir, 5-HT_{1Hal} immunoreacitivity; TM domains, transmembrane domains; RT-PCR, reverse transcription-polymerase chain reaction.

SEROTONIN (5-HT, 5-hydroxytryptamine) has been established as a major neurotransmitter in vertebrates and invertebrates. In molluscs, bioassays, as well as electrophysiological, immunocytochemical and genetic studies, have implicated it in behaviours and physiological processes such as sensitisation, feeding, development, and locomotion (Rathouz and Kirk, 1988, Croll, 1988; Barlow and Truman, 1991, Kuhl *et al*., 1992, Satterlie *et al*., 1995). Serotonin also plays an important role in reproduction through the biosynthesis and release of active egg-laying peptides precursor proteins, gamete maturation, and the control and initiation of gamete release in several molluscan species (Ram *et al*., 1992, Krantic *et al*., 1993; Fong *et al*., 1994; Vaca and Alfaro, 2000, Ouimet and Castellucci, 1997, Zatylny *et al*., 2000). Administration of 5-HT has been shown to induce spawning in bivalves (Matsutani and Nomura, 1982; Gibbons and Castagna, 1984; Hirai *et al*., 1988; Ram *et al*., 1992). However, the interaction of 5-HT with its receptors, particularly in the reproductive process, is not yet fully understood.

Deleted: or

In vertebrates, the effects of 5-HT are mediated by a large family of receptors, either ionotropic or coupled to second messenger cascades. Thus, 5-HT receptors are known to display diverse functions and play a critical role in modulating cognitive and behavioural functions. Numerous invertebrate 5-HT receptor genes have also been characterised and are known to mediate a variety of functions (reviewed by Tierney, 2001). In molluscs, most is known from the gastropods *Aplysia californica* and *Lymnaea stagnalis*. In *L. stagnalis,* a cDNA sequence encoding a mature 509 amino acid 5-HT receptor (5-HT_{1lym}) was cloned from the nervous system (Sugamori *et al*., 1993). It had highest sequence homology with *Drosophila* 5-$HTdro_{2B}$ (61%) and mammalian 5-HT_{1A}-type (53%) receptors. The 5-HT_{1lym} receptor contained seven regions of hydrophobic amino acids representing seven transmembrane (TM) domains. Another *L. stagnalis* 5-HT receptor, designated 5-HT_{2Lym}, was identified that resembled members of the mammalian 5-HT_2-type receptor subfamily (Gerhardt *et al*., 1996).

In *Aplysia*, sensory neurons are known to contain at least three 5-HT receptor subtypes. They include: (1) 5-HT_{1ap} which is coupled to a cAMP/protein kinase A pathway (Li *et al*., 1995); (2) Ap5-HT_{B1} and Ap5-HT_{B2} that are coupled to an inositol triphosphate/protein kinase C pathway and thereby induce a dose-dependent increase in phospholipase C in response to 5-HT (Angers *et al*., 1998); and (3) 5-HT_{1ap} which is localised in a variety of tissues, including the ganglia of the nervous system and is negatively coupled to adenylate cyclase. The 5-HT_{1ap} receptor has significant amino acid sequence identity with 5-HT_{1lym} (62%) (Angers *et al*., 1998) and, therefore, also closely resembles the mammalian 5-HT_1 receptor subfamily.

In the present study, we aimed to identify and analyse an abalone 5-HT receptor (5-HT_{1Hal}). We discovered that the tropical abalone *Haliotis asinina* contains a truncated 5-HT receptor that is most homologous to *Aplysia* 5-HT_{1ap}. Reverse transcription-polymerase chain reactions (RT-PCR) revealed mRNA expression in numerous tissues, including the ganglia and gonad tissues. An antibody generated to the predicted third intracellular loop of 5-HT_{1Hal} was used to localize receptor expression to cells of the neural and gonad tissues. The functional significance of 5-HT in abalone reproduction is shown by *in vitro* organ bath gonad contraction assays in the related abalone species, *Haliotis rubra*.

Materials and Methods

Animals

H. asinina used for gene identification were collected from Heron Island reef, Australia. *H. asinina* used for immunocytochemical localization were provided by the Coastal Aquaculture Development Center, Prachup Khiri Khan, Thailand. Tissues were dissected and immediately prepared for nucleic acid extractions, protein extractions and serial sectioning. *H. rubra* (Leach) were collected from Pt. Cook, Port Phillip Bay, under a Fisheries Victoria research permit (97/R/049A).

Oligonucleotide Primers

The sequences of oligonucleotide (OL) primers used to clone 5-HT_{1Hal} (OL1-OL11), to perform RT-PCR expression studies (OL4, OL7), and for recombinant expression (OL12-OL13) are listed as follows:
OL1, AAGCAGTGGTATCAACGCAGAGTGAATTCT$_{17}$
OL2, GC(C/T)AT(A/C/T)GC(A/C)ATGGA(C/T)AG(A/G/T)TACTGG
OL3, (A/G/C)AT(A/G/T)A(A/T/G/C)GAAAGC(C/T)CCAGTGATGAT
OL4, GGCGTGTGCGTTATTAGCCAAGACCAT
OL5, CGGAAAGCAGCCAGAACTCTCG
OL6, GTCGTCGTCGTTGCGTCCTCTTTAACC
OL7, GCACCCATTGCAGTTGGACACAACACT
OL8, ATCCGTTTAGCACTGCGGTTACG
OL9, GCTCTAATACGACTCACTATAGG
OL10, AAGCAGTGGTATCAACGCAGAGT
OL11, CACATGAGCGATGTTCGTCTTAACGTG
OL12, GTCAATGGATCCTGTTCCCCAGAAAA
OL13, TTGACGAATTCCTTCCGAGACATGG

cDNA cloning of an abalone 5-HT receptor gene - 5-HT_{1Hal}

Total RNA was extracted from juvenile (40 day old) *H. asinina* using a Tripure® Isolation Reagent (Roche). Any contaminating genomic DNA was removed by treatment with DNase I (Sigma). First strand cDNA synthesis was performed using 1 μg of total RNA in a 20 μl reverse transcription mixture containing OL1 and 200 U SUPERSCRIPT™ III RNase H^- reverse transcriptase (Invitrogen), following the manufacturer's instructions.

H. asinina juvenile cDNA (1 µl) was used as template in PCRs. Each PCR was performed in a final concentration of 1x PCR Buffer, 2.0 mM $MgCl_2$, 200 µM dNTPs, 1.0 µM of sense (OL2) and antisense primer (OL3), 0.25 units of *Taq* Ti polymerase (Fisher Biotec, Australia) and ddH_2O, to a final volume of 25 µl. Sterile water was substituted for DNA in negative control reactions. The PCR consisted of 35 cycles, with 2 min denaturation at 94°C, 1 min annealing at 50°C, and a 1 min extension at 74°C. PCR products were detected using 2% agarose gel electrophoresis, and appropriate size bands were extracted and TA cloned using a TA Cloning Kit (Promega), following the manufacturer's instructions. Recombinant plasmid DNA was purified from positive clones, as determined by colony PCR, and inserts then sequenced in both directions and analysed using ClustalW.

The 3' and 5'-end gene sequences were identified by rapid amplification of cDNA ends (RACE). In both cases, PCR was performed using gene-specific primers, and confirmed by DNA sequence analysis. For 5'-RACE, antisense primers OL6-8 were used in combination with the 5'-RACE sense primer OL9. For 3'-RACE, sense primers OL2 and OL5, respectively, were used in combination with the 3'-RACE antisense primer OL10. Due to the apparent truncation of the 3'-RACE transcript, a further RT-PCR was performed using an antisense primer (OL11) with OL5, to ensure transcript entirety. A Kyte-Doolittle hydropathy profile of the deduced amino acid sequence was performed using TMbase (Hofmann and Stoffel, 1993).

Sequence alignment and phylogenetic analysis

Sequences were aligned using Clustal X, 8.1 (Thompson et al., 1997). Phylogenetic trees were constructed from respective multiple alignments using MEGA3 software (Kumar et al., 2004). The unrooted tree was generated with 1000 bootstrap trials using the neighbor-joining method (Saitou and Nei 1987) and presented with a cut-off bootstrapping value of 50.

Identification of 5-HT_{1Hal} mRNA expression in tissues using RT-PCR

Tissue-specific expressions of 5-HT_{1Hal} mRNA were examined by RT-PCR, and expected to have product sizes of 246-bp. Total RNA was extracted from cerebral ganglia (cg), pleuro-pedal ganglia (ppg), female gonad (fgo), male gonad (mgo), 40 day juvenile, mantle, cephalic tentacle, eye stalk, gill, and foot muscle tissues of *H. asinina* using a Tripure® Isolation Reagent (Roche). Any contaminating genomic DNA was removed by treatment with DNase I. First strand cDNA synthesis was performed using 1 µg of total RNA in a 20 µl reverse transcription mixture containing oligo $d(T)_{12-18}$ (Invitrogen) and 200 U SUPERSCRIPT™ III RNase H^- reverse transcriptase, following the manufacturer's instructions. PCR was performed using 1 µl of cDNA and the following sequence-specific primers were designed from existing 5-HT_{1Hal} cDNA sequence (see Results section): OL4 and OL7. Each reaction was performed in a final concentration of 1 x PCR Buffer, 2.0 mM $MgCl_2$, 200 µM of each dNTP, 1 µM of sense and antisense primer, 0.25 units of *Taq* Ti polymerase and ddH_2O to a final volume of 25 µl. Recombinant plasmid containing the 5-HT receptor gene sequence was used as positive controls, and negative controls are substituting cDNA with water or RT absent samples. PCR consisted of 36 cycles, including a 2 min denaturation at 94°C, a 30 sec annealing at 58°C, and a 1 min extension at 74°C. Following PCR, 15 µl of reaction mix was fractionated on 2% agarose gel containing ethidium bromide (0.5 µg/ml).

Production of a recombinant 5-HT_{1Hal} fusion protein

A 5-HT_{1Hal} cDNA sequence encoding 51 amino acids of the predicted third intracellular loop corresponding to Cys^{265}-Glu^{315} (see RESULTS, **Fig. 1A**), was PCR amplified using the following primers which incorporated terminal restriction sites for *Bam* HI and *Eco* RI sequences, OL12 and OL13. PCR consisted of 36 cycles, including a 2 min denaturation at 94°C, a 1 min annealing at 40°C, and a 2 min extension at 72°C. A PCR product of expected 173-bp size was gel extracted, double digested,

directionally ligated into pGEX-2T (Pharmacia), and then transformed into *E. coli* strain DH5α (Stratagene). Positive recombinant clones were subjected to plasmid purification and sequencing of inserts, prior to sub-culture in LB medium, expression of a glutathione S-transferase (GST)-5-HT_{1Hal} fusion protein using 0.1 mM IPTG inducer, and protein purification, according to the manufacturer's instructions. The integrity of the expressed protein was verified by 12% SDS-PAGE and Coomassie blue staining.

Antisera production against recombinant 5-HT_{1Hal} fusion protein

Two 6-weeks old female BALB/c mice were injected intraperitoneally with 100 μg fusion protein as an emulsion in Freund's complete adjuvant (Sigma). Booster injections were done with the same immunogen in Freund's incomplete adjuvant (Sigma) three times at intervals of 2 weeks. Retro-orbital plexus blood was collected and then centrifuged to collect antiserum, which was then preabsorbed with GST overnight at 4°C, and subsequently stored at -20ºC.

Immunocytochemistry

*H. asinin*a cerebral and pleuropedal ganglia, ovaries, and testes were fixed in Bouin's solution and processed routinely for paraffin embedding. The sections were deparaffinized, rehydrated, immersed in 70% ethanol containing 1% saturated $LiCO_3$ and 1% H_2O_2, and subsequently immersed in 0.1 M glycine and 0.4% Triton X-100 in order to remove picric acid, endogenous peroxidase, free aldehyde groups, and for tissue permeabilization, respectively. Sections were rinsed three times in PBS, and then incubated for 1 h at room temperature in antisera diluted 1:1,000 in PBS. After three washes in PBS, and incubation with HRP-conjugated goat anti-mouse IgG for 1 h, detection was performed with Nova Red substrate solution. The sections were then dehydrated, cleared, mounted with mounting medium, observed under a Nikon ECLIPESE E600 light microscope, and images captured by a Nikon ECIPESE 2000 CCD camera. The experiments were repeated at least three times for each tissue.

Gomori's aldehyde-fuchsin staining (GAFS)

GAFS was used to identify neurosecretory cells in the neural ganglia (Cameron and Steele, 1959), but modified to study both immunoperoxidase staining and GAFS within the same section. After taking images of immunoreactivities within sections following immunoperoxidase staining, the sections were rehydrated in a graded series of ethyl alcohol. They were then oxidized in potassium permanganate solution (0.3% potassium permanganate and 0.3% concentrated sulfuric acid) for 1 min and rinsed in distilled water. The sections were bleached in 2.5% sodium bisulfite solution until permanganate colour was removed and then washed in running tap water for 5 min before transferring into 70% ethanol for 2 min. For neurosecretory cell detection, the sections were stained in aldehyde-fuchsin solution (0.5% basic fuchsin, 1% concentrated hydrochloric acid, 1% paraldehyde solution) for 10 min, then rinsed in 95% ethyl alcohol and further differentiated in fresh 95% ethanol until no more aldehyde-fuchsin was removed. The sections were transferred to 70% ethyl alcohol for 2 min, rinsed in distilled water for 1 min, and then stained in Halmi solution (0.2% light green SF, yellowish, 1% orange G and 0.5% chromotrope 2R). They were then differentiated in 95% ethyl alcohol containing 0.2% acetic acid for 3 min, rinsed in fresh 95% ethanol, dehydrated in absolute alcohol, cleared in xylene, and mounted with permount.

Immunofluorescence localisation of 5-HT and 5-HT$_{1Hal}$ in neural tissues

H. asinina ganglia were fixed in 4% paraformaldehyde containing 5% sucrose for 12-16 h. After three washes, the tissues were immersed in 30% sucrose-PBS overnight. The specimens were embedded in Tissue Tek (Sakulra Finetek, U.S.A.) and directly frozen in liquid nitrogen. Cryosections of approximately 15 µm were cut and mounted on poly-L-lysine (Sigma) coated slides. After rinsing in PBS, the sections were incubated in glycine for 5 min and pre-incubated in blocking buffer (4% BSA and 2% normal goat serum in PBS containing 0.1% Tween 20) for 30 min before incubation overnight with a mixture of rabbit anti-5-HT and mouse anti-5-HT$_{1Hal}$ diluted 1: 200 and 1: 50, respectively, in blocking buffer. Sections were washed three times in PBS and incubated with goat anti mouse antiserum conjugated to the Alexa 568 fluorochrome and anti-rabbit antiserum conjugated to Alexa 488 fluorochrome diluted 1: 200 in blocking buffer for 1 h. After three washes in PBS, the sections were nuclear stained with TO-PRO-3 (MolecularProbes, U.S.A.), diluted 1: 1000 in PBS, for 5 min. They were then rinsed in PBS and mounted with Vectashield (Vector Lab). Negative controls included the omission of primary antibody, replaced with blocking buffer. Immunolabeled sections were examined by an Olympus FV1000 confocal laser scanning microscope (Tokyo, Japan). Serial optical sections were taken at interval of 0.5 µm, and confocal stacks (3-6 images) were reconstructed using Olympus Fluoview software. All specimens were examined within 24 h of immunolabeling.

In vitro *organ bath gonad contraction bioassays*

A previous molecular study has demonstrated the existence of 5-HT-like receptor in *H. rubra* (unpublished) that is highly homologous (96%) to *H. asinina* 5-HT$_{1Hal}$. Physiological experiments were performed on gonad tissue of mature *H. rubra*. After the animal was anesthetized by injection of isotonic $MgCl_2$ (25-50% body weight), freshly dissected gonad rings were prepared for analysis. Transverse cuts were made 1 cm from the tip of the gonad to release a ring of tissue. Hooks were inserted between the hepatopancreas capsule and the capsule of the gonad, which consists of dense collagenous fibres mixed with muscle cells that surround both the testis and ovaries (Apisawetakan *et al*., 1997).

Preparations were placed into organ baths containing 15 ml of molluscan Ringer's solution (Tucker, 1970) at 23°C, and suspended between a force transducer (Grass-FT03) and a fixed steel hook using cotton thread. Prior to assay, tissues were given a 15 min relaxation and acclimation period, and were allowed 10 min to recover initial tonus after washing. In males, bioactivities were tested using 10^{-4} to 10^{-6} M 5-HT solutions, diluted in 50 µl of molluscan Ringer's solution, and contractions monitored with a force-displacement transducer which was linked to a PowerLab™ data collection system. Mean rate of contractility was calculated over a 2 min period and statistical differences between the values were determined using Student's t-test for paired comparisons with significance assumed at a $P \leq 0.05$. In females, bioactivity was measured using a 10^{-6} M 5-HT solution.

Results

Cloning and characterization of an abalone 5-HT receptor gene

PCR amplification of juvenile *H. asinina* cDNA using degenerate primers generated an amplification product of 633-bp. The amplification product was successfully cloned and sequenced. Subsequently, the full-length gene was identified by 5' and 3' RACE, containing 1633-bp and encoding a protein of 359 amino acids **(Fig. 1A)**. The sequence data has been submitted to the GenBank database under the accession number EU342382. Partial 5-HT receptor sequences of approximately 785 bp, covering predicted TM domains 3 to 7, were obtained previously from *H. rubra* (GenBank accession number AY237917) and *Haliotis laevigata* (GenBank accession number AY237918). These were 96% identical at the nucleotide level???, but the data may reflect sequencing of genomic DNA as DNase I treatments

Deleted: homologous

Formatted: Not Highlight

were not implemented in the earlier mRNA extractions prior to cDNA synthesis (data not shown). Not sure of relevance of this statement

Protein sequence analysis using the Protein Families database of alignments and hidden Markov models, revealed that the deduced amino acid sequence has characteristics common to mammalian and invertebrate G-protein-coupled 5-HT receptors. It possesses a G-protein coupled motif, represented by a conserved triplet in the region A^{121}SILHLVAIAMDRYWAV^{137}, and spanning the TM3 and carboxyl end of the second intracellular loop. Four potential phosphorylation sites for protein kinase C (S^{147}AK, S^{251}PK, S^{270}MK and S^{312}RK) and a single cAMP phosphorylation site (K^{149}RIS) were identified. The sequence has four potential sites for N-linked glycosylation (N^{3}QT, N^{18}VT, N^{145}RS and N^{277}SS) within the predicted N-terminal region and intracellular loop domains.

Kyte-Doolittle hydropathy profiles of the deduced 5-HT_{1Hal} amino acid sequence (**Fig. 1B**) showed that it contained 6 hydrophobic TM segments that were composed of between 20 to 25 residues. A phylogenetic tree of molluscan and selected vertebrate 5-HT receptors, based on amino acid identity, is shown in **Fig. 1C**. The abalone (*Haliotis*) 5-HT receptor is most closely related to molluscan homologs and to human 5-HT Type 1 receptors, and is therefore named 5-HT_{1Hal}.

Sequence alignment of *H. asinina* 5-HT_{1Hal} with *Aplysia* and *Panulirus* (Lobster) homologs show 40% and 41% identity, respectively, with most similarity observed within the TM regions (**Fig. 2**). Most divergence is found within the N-terminus, the third intracellular loop, prior to the first TM domain, and the C-terminus. Within the predicted third intracellular loop of 5-HT_{1Hal}, there are only 111 amino acids, compared to 154 amino acids for 5-HT_{1ap}. However, the relatively short domain is consistent with the size of the equivalent domain of the *Panulirus* 5-HT receptor. The deduced 5-HT_{1Hal} obtained did not appear to contain the predicted seventh TM domain and intracellular C-termini which is common to other known 5-HT receptors.

Production of a recombinant 5-HT_{1Hal} fusion protein and antisera

A 153-bp PCR product, encoding the 51 amino acid sequence of the third intracellular loop (see underlined amino acids in **Fig. 1A**) was directional cloning into a pGEX-2T expression vector following double digestion of the *Bam* HI and *Eco* RI terminal restriction sites. A GST-5-HT_{1Hal} fusion protein of 34.5 kDa was then expressed in *E. coli* cells and used to produce murine 5-HT_{1Hal} antisera.

Tissue specific expression of 5-HT_{1Hal} mRNA

In RT-PCR using template cDNAs produced from *H. asinina* cg, ppg, fgo, mgo, 40 day juvenile, mantle, cephalic tentacle, eye stalk, gill, and foot muscle tissues, predicted 246-bp amplicons were obtained in all tissues (**Fig. 3 upper panel**). Control PCRs using recombinant plasmid 5-HT_{1Hal} sequence as template gave a positive result (PCR +), and those using no cDNA template gave a negative result (PCR -), indicating no contaminating genomic DNA. Controls where PCR was performed upon respective samples without the RT reactions were also negative (**Fig. 3 lower panel**).

Immunoperoxidase and Gomori's aldehyde fuschin (GAF) staining

The 5-HT_{1Hal}-immunoreactivity (5-HT_{1Hal}-ir) was detected in the soma of neuronal cells located in the outer cortex of both cerebral and pleuropedal ganglia **(Fig. 4**). Based on histological characteristics, the immunoreactive cells could be classified as type I (NS1) and type II neurosecretory cells (NS2) according to Upatham et al. (1998) and Kruatrachue et al. (1999). The NS1 was the largest in size, containing cytoplasmic granules and a euchromatic nucleus, whereas the NS2 was smaller with a round nucleus having patches of heterochromatin. NS1 and NS2 in the cerebral and pleuropedal ganglia were positively stained with GAF, especially their secretory granules which exhibited a dark-violet color (**Fig. 4A1, A2, B1, C1**). In addition, 5-HT_{1Hal}-ir was also detected in the fibers distributed within the medullar of cerebral and pleuropedal ganglia (**Fig. 4A1**).

In the ovarian tissue, 5-HT_{1Hal}-ir was observed in epithelial cells of the outer capsule and connective tissue of the trabeculae to which the ovarian follicles adhered (**Fig. 5A, A1**). Additionally, 5-HT_{1Hal}-ir was also expressed in the cytoplasm of late stage oocytes (Oc4, Oc5) (**Fig. 5A2, B**). In the testis, 5-HT_{1Hal}-ir was also present in the outer capsule and connective tissue of the trabeculae (**Fig. 5C, C1**).

Colocalization of 5-HT-ir and 5-HT_{1Hal}-ir in neural tissues by immunofluorescence

Fluorescence staining showed that 5-HT_{1Hal}-ir and 5-HT-ir were present in separate cells of both cerebral and pleuropedal ganglia, i.e. they were not co-localized (**Fig. 6**). Strikingly, numerous 5-HT-ir fibers were present in the medulla region of both ganglia whereas 5-HT_{1Hal}-ir fibers were fewer than that of 5-HT-ir fibers (**Fig. 6B, D**). Furthermore, some 5-HT-ir fibers appeared to innervate the 5-HT_{1Hal}-ir neuronal cells, both in cerebral and pleuropedal ganglia (**Fig. 6B, D**).

The 5-HT_{1Hal} receptor was also found to be expressed in several other tissues (data not shown). In particular, it was observed in the vascularized connective tissues of the eye, epipodial and cephalic tentacles (i.e. connective tissue beneath the surface epithelium and muscle fibers within the central region), and pedal muscle (i.e. around the epithelial cells of foot epithelium, but not in the muscle fibers).

In vitro *gonad contraction bioassays*

Abalone gonad muscle tissue was monitored for contraction bioactivity following stimulation with 5-HT (10^{-4} to 10^{-6} M; **(Fig. 7**). Application of 5-HT typically led to the increase of irregular phasic contractions and relaxations in male *H. rubra* gonad preparations compared to control (**Fig. 7A)**. The use of 0.018 % v/v H_2O_2, commonly used to induce spawning in abalone, had no effect on contractility (data not shown). Also, control experiments where molluscan Ringer's solution was substituted for test solution, did not affect basal contractility (negative control).

A dose-response of gonad contraction induced by 5-HT was determined at concentrations of 10^{-4} M to 10^{-6} M (**Fig. 7A**). At each concentration, 5-HT induced a dose-dependent increase in irregular rhythmic contraction, compared with control preparations. The most dramatic effect was observed at 10^{-6} M ($P<0.05$, $n = 6$), in which the rate of phasic contraction and relaxation increased more than 200% and continued for at least 10 min, after which the rate decreased. A significant increase in the rate of gonad contraction and relaxation ($P<0.05$, $n = 6$) was also demonstrated upon application of 10^{-4} M and 10^{-5} M 5-HT. Application of 10^{-6} M 5-HT also led to the increase of irregular phasic contractions and relaxations in female *H. rubra* gonad preparations compared to control (**Fig. 7B)**.

Discussion

A putative abalone truncated 5-HT receptor

This study has identified a putative abalone 5-HT receptor, termed 5-HT_{1Hal}. Using RT-PCR with degenerate primers, followed by 5' and 3' -RACE, we initially cloned the full-length gene from 40-day *H. asinina* juveniles. Comparative analysis of known nucleotide and predicted amino acid 5-HT receptor sequences, as well as the identification of associated protein motifs, suggests that 5-HT_{1Hal} is a homologue to the molluscan *Aplysia* CNS 5-HT_{1ap} (Angers *et al*., 1998) and the crustacean *Panulirus* CNS 5-HT_{1Pan} (Sosa *et al*., 2004). Furthermore, phylogenetic analysis established that the 5-HT_{1Hal} belongs to the 5-HT type 1 receptor cluster and represents the first 5-HT receptor transcript identified in 'prosobranchs'.

Pharmacological, ligand-binding and site-directed mutagenesis studies have defined structural and functional properties required for G-protein coupled receptors (GPCRs). Many of these are present in 5-HT_{1Hal}. First, serine residues present within cytoplasmic domains can be phosphorylated by protein kinases (Strosberg, 1996). It was notable that the 5-HT_{1Hal} had one less potential phosphorylation site for protein kinase C in the third intracellular loop, possibly relating to function. The serine residue within

TM5 domain, may be part of a binding site, already defined for 5-HT (Li *et al*., 1995). Second, the highly conserved ''DRY'' motif is present and is located at the C-terminal end of the TM3. The aspartic acid (D) residue is important for the maintenance of the three-dimensional structure of GPCRs. Finally, studies involving site-directed mutation and receptor antibodies have shown that the second intracellular loop is important in receptor G-protein interaction (Ostrowski *et al*., 1992; Hedin *et al*., 1993). Specifically, a conserved threonine residue in this loop is involved in G-protein coupling for calcium mobilisation, and to inhibition of calcium channel activation (Lembo *et al*., 1997). It is also thought to play a minor role in the inhibition of cAMP accumulation (Lembo *et al*., 1997). In addition, regions of the third intracellular loop are known to dictate the specificity of interaction with different G proteins (Kobilka *et al*., 1987). A large third intracellular loop is typical of GPCRs coupled to G-inhibitory subunits (Sugamori *et al*., 1993) as has been demonstrated in the 5-HT_{1ap} (Angers *et al*., 1998). Comparative sequence analyses show that 5-HT_{1Hal} demonstrates significant divergence in the third intracellular loop compared with other known molluscan 5-HT receptors. We have found that this loop is considerably shorter by 40 amino acids in the internal portion, which may have important secondary signalling implications. However, it has been established that the primary regions of receptor G-protein interaction are the amino and carboxyl terminal portions of the loop (Ostrowski, *et al*., 1992), thus the removal of this internal region may not be of significant functional importance. In fact, the amino and carboxyl regions of this loop are largely conserved when compared with 5-HT_{1ap}. So although we do not yet know the effector mechanisms associated with the putative 5-HT_{1Hal} receptor, we do know that the 5-HT receptor type 1 family signals through pertussis toxin-sensitive Gi/Go proteins to mediate a range of actions that include the ubiquitous inhibition of cAMP formation via Gi, as well as cell-specific G-mediated effects. Future pharmacological analysis is necessary to verify these assumptions.

Interestingly, analysis of the 5-HT_{1Hal} transcript showed that the deduced protein appears to be truncated following the TM6 domain. Repeated 3'-RACE did not reveal a larger transcript that may encode a predicted seventh TM and C-terminal intracellular domain. DNase I treatment of isolated RNA ensured that contaminating genomic DNA, which could potentially contain introns leading to mispriming, was not an issue. The published sizes of 5-HT1 homologs vary with the species, typically ranging from around 50–92 kDa. Variation is largely the result of differences in the third intracellular loop as well as differences in the lengths of the N-termini, but rarely the C-termini. However, Sosa et al (2004) have demonstrated in *Panulirus* the expression of a 40 kDa 5-HT_{1Pan}, and this may contain a similar truncation to that observed with the abalone 5-HT_{1Hal} (predicted to encode a protein of 40 kDa). Western blots have suggested that crustacean 5-HT receptors are alternately spliced and/or differentially modified posttranslationally.

Truncated GPCRs appear to modulate the function of the full-length version of the receptor as shown for the α1A-adrenergic receptor (Cogé *et al*., 1999), the dopamine D3 receptor (Karpa *et al*., 2000), the gonadotropin receptor (Grosse *et al*., 1997), the prostaglandin E2 EP1 receptor subtype (Okuda-Ashitaka et al., 1996), the secretin receptor (Ding et al., 2002), the V2 vasopressin receptor (Zhu and Wess, 1998), and the ghrelin receptor (Gnanapavan *et al*., 2002). The human wild-type ghrelin receptor consists of 366 amino acids with seven TM domains and has a truncated splice variant consisting of 289 amino acids with only five predicted TM domains which fails to bind ghrelins. It has been demonstrated that the truncated form mRNA exceeds that of wild type in normal human tissues (Gnanapavan *et al*., 2002). In fact, a 13-fold excess of the truncated ghrelin receptor mRNA compared with its wild-type attenuates trafficking to the cell surface and decreases constitutive activity. The full-length receptor physically interacts with its truncated splice variant and thereby can exist as heterodimers. We hypothesize that the truncated 5-HT_{1Hal} may play a similar role in modulation of a full-length serotonin receptor in abalone.

Expression of 5-HT_{1Hal} in abalone tissues and its potential role in reproductive processes

Due to the high degree of 5-HT_{1Hal} sequence identity with 5-HT_{1ap}, we expected a similar expression pattern with 5-HT_{1Hal}. In *Aplysia*, 5-HT_{1ap} mRNA has been localised to all ganglia tested, and antibody probes have been used to identify widespread receptor protein expression in the gill, heart,

Formatted: Font: 11 pt

Formatted: Left, Right: 1.1 pt, Space After: 4 pt, Adjust space between Latin and Asian text, Adjust space between Asian text and numbers

hermaphroditic duct, kidney and ovotestis (Angers *et al*., 1998). Indeed, *H. asinina* 5-HT_{1Hal} mRNA transcripts and protein appeared in all tissues examined. The existence of this receptor in neural and reproductive tissues is of particular significance given existing evidence showing that 5-HT has reproduction-related bioactivity in other molluscs. Like most marine invertebrates, abalone have a well defined annual reproductive cycle culminating in the initiation of spawning (Counihan, R.T., McNamara, D.C., Souter, D.C., Jebreen, E.J., Preston, N.P., Johnson, C.R. and Degnan, B.M. 2001. Pattern, synchrony and predictability of spawning of the tropical abalone *Haliotis asinina* from Heron Reef, Australia. *Mar. Ecol. Prog. Ser.* 213, 193-202.). Upon initiation, detached oocytes undergo germinal vesicle breakdown and start the first meiotic division (Jebreen, E.J., Counihan, R.T., Fielder, D.T. and Degnan , B.M. 2000. Synchronous oogenesis during the semilunar spawning cycle of the tropical abalone *Haliotis asinina*. *J. Shellfish Res.* 19, 845-852). Mature gametes are conveyed to the cavity of the right renal organ, where they escape into the seawater through the respiratory pores of the shell by continual lifting of the shell and rotation of the foot. Our findings suggest that the 5-HT_{1Hal} may play an important role in this, such as modulating the release of active reproductive peptides precursor proteins, gamete maturation, and/or the control and initiation of gamete release.

Formatted: Font: Times New Roman

Formatted: Font: Times New Roman

Formatted: Font: 11 pt

Formatted: Font: Times New Roman, 11 pt

Formatted: Font: 11 pt

This is supported by our *in vitro* organ bath experiments. Application of 5-HT solution was shown to induce an increase in the rate of phasic contraction and relaxation of muscle within male and female abalone gonad capsules. We hypothesize that this neurotransmitter could be required to induce contraction of the gonad in the process of gamete expulsion. Serotonin released from neurones in gonads may bind directly to receptors on muscle cells to induce contractions. In our study, we found examples of colocalization of receptor cells with 5-HT in axons, consistent with the short-term modulatory role of 5-HT in neural and possibly reproductive tissues. Likewise, it has been shown that ovarian muscle contraction is an important process in the movement of gametes prior to egg-laying or spawning (Howard and Talbot, 1992; Henry *et al*., 1999; Zatylny *et al*., 2000). For example, in the lobster, 5-HT can induce significant ovarian muscle contraction (Howard and Talbot, 1992). The exact mechanism by which transmitters elicit smooth muscle contraction is unknown, but it may involve a cAMP or Ca^{2+} secondary messenger system (Howard and Talbot, 1992).

It is also possible that 5-HT released may function in a similar way to that in the zebra mussel. In zebra mussel, prior to spawning, 5-HT from the gonadal nerve endings acts via a 5-HT receptor to initiate oocyte maturation, including germinal vesicle breakdown (Fong *et al*., 1994). These events could also be artificially induced by administration of 5-HT to surf clams, ultimately leading to spawning (Hirai *et al*., 1988). Other research groups have implicated 5-HT in the induction of molluscan oocyte maturation via a single class of 5-HT receptor (Matsutani and Nomura, 1982; Krantic *et al*., 1993). Based on ligand-binding and pharmacological studies, this receptor appears to be most similar to the 5-HT_{1A} type receptor, although it has certain properties that makes it novel (Krantic *et al*., 1993).

Summary

Advances in biotechnology have meant that molecules such as hormones and neurotransmitters may be used for aquaculture purposes to enhance market potential. The results from the current study contribute to our understanding of abalone reproduction and suggest 5-HT and 5-HT receptors may interact in a complex way to control reproduction. Multiple genes encoding 5-HT receptors in vertebrates and invertebrates have been described, and therefore it would be of interest to identify whether this type of complexity also exists in abalone.

Acknowledgments

We are grateful to Mr. Tanes Poomtong and staff at the Coastal Development Center, Klongwan, Prachaubkirikhun, and Mr. Tony Smith at the Bay City Seafarm, Geelong, Australia, for provision of animals.

References

1. **Rathouz MM, Kirk MD** 1988 Localization of catecholamines in the buccal ganglia of *Aplysia californica*. Brain Res 458:170-175
2. **Croll RP** 1988 Distribution of monoamines within the central nervous system of the juvenile pulmonate snail, *Achatina fulica*. Brain Res 460:29-49
3. **Barlow LA, Truman JW** 1991 Patterns of serotonin and SCP immunoreactivity during metamorphosis of the nervous system of the red abalone, *Haliotis rufescens*. J. Neurobiology 23:829-844
4. **Kuhl D, Kennedy TE, Barzilai A, Kandel ER** 1992 Long-term sensitization training in *Aplysia* leads to an increase in the expression of BiP, the major protein chaperone in the ER. J Cell Biol 119:1069-1076
5. **Satterlie RA, Norekian TP, Jordan S, Kazilek CJ** 1995 Serotonergic modulation of swimming speed in the pteropod mollusc *clione limacina*. J Exp Zool 198:895-904
6. **Bruehl C, Berry R** 1985 Regulation of synthesis of the neurosecretory egg-laying hormone of *Aplysia*: Antagonistic roles of calcium and cylic adenosine 3':5'-monophosphate. Soc Neuroscience 5:1233-1238
7. **Ram JL, Fong PP, Croll RP, Nichols SJ, Wall D** 1992 The zebra mussel (*Dreissena polymorpha*), a new pest in North America: reproductive mechanisms as possible targets of control strategies. Inv Reprod Dev 22:77-86
8. **Krantic S, Dube F, Guerrier P** 1993 Evidence for a new subtype of serotonin receptor in oocytes of the Surf Clam *Spisula solidissima*. Gen Comp Endocrinol 90:125-131
9. **Fong PP, Kyozuka K, Abdelghani H, Hardege JD, Ram JL** 1994 *In vivo* and *in vitro* induction of germinal vesicle breakdown in a freshwater bivalve, the zebra mussel *Dreissena polymorpha* (Pallas). J Exp Zool 269:467-474
10. **Vaca AA, Alfaro J** 2000 Ovarian maturation and spawning in the white shrimp, *Penaeus vannamei*, by serotonin injection. Aquaculture 182:373-385
11. **Ouimet T, Castellucci VF** 1997 Gene expression and regulation of *Aplysia californica* prohromone convertases aPC1B and aPC2. J Neurochem 68:1031-1039
12. **Zatylny C, Durantou F, Boucaud-Camou E, Henry J** 2000 Evidence of 5-hydroxytryptamine synthesis in the follicles of *Sepia officinalis* and direct involvement in the control of egg-laying. Mol Reprod Dev 55:182-188
13. **Matsutani T, Nomura T** 1982 Induction of spawning by serotonin in the scallop, *Patinopecten yessoensis* (Jay). Mar Biol Lett 3: 353-358
14. **Gibbons M, Castagna M** 1984 Serotonin as an inducer of spawning in six bivalve species. *Aquaculture* 40:189-191
15. **Hirai S, Kishimoto T, Kadam AL, Kanatani H, Koide SS** 1988 Induction of spawning and oocyte maturation by 5-hydroxytryptamine in the Surf Clam. J Exp Zool 245:318-321.
16. **Tierney AJ** 2001 Structure and function of invertebrate 5-HT receptors: a review. Comp Biochem Physiol A 128:791-804
17. **Sugamori KS, Sunahara RK, Guan H, Bulloch AGM, Tensen CP, Seeman P, Niznik HB, Van Tol HM** 1993 Serotonin receptor cDNA cloned from *Lymnaea stagnalis*. Proc Natl Acad Sci USA 90: 11-15.
18. **Gerhardt CC, Leysen JE, Planta RJ, Vreugdenhil E, and Van Heerikhuizen H** 1996 Functional characterisation of a 5-HT_2 receptor cDNA cloned from *Lymnaea stagnalis*. Eur J Pharmacol 311:249-258
19. **Li X, Giot J, Kuhl D, Hen R, Kandel ER** 1995 Cloning and characterization of two related serotonergic receptors from the brain and the reproductive system of *Aplysia* that activate phospholipase C. J Neurosci 15(11):7585-7591.

20. **Angers A, Storozhuk MV, Duchaine T, Castellucci VF, DesGroseillers L.** 1998 Cloning and functional expression of an *Aplysia* 5-HT receptor negatively coupled to adenylate cyclase. J Neurosci 18(15):5586-5589.
21. **Hofmann K, Stoffel W** 1993 TMbase - A database of membrane spanning proteins segments. Biol Chem Hoppe-Seyler 374,166.
22. **Thompson JD, Gibson TJ, Plewniak F, Jeanmougin F, Higgins** DG 1997 The CLUSTAL_X windows interface: flexible strategies for multiple sequence alignment aided by quality analysis tools. Nucl Acids Res 25:4876-4882.
23. **Kumar S, Tamura K, Nei M** 2004 MEGA3: Integrated software for molecular evolutionary genetics analysis and sequence alignment, Briefings in Bioinformatics 5:150-163.
24. **Saitou N, Nei M** 1987 The neighbor-joining method: a new method for reconstructing phylogenetic trees, Mol Biol Evol 4:406-425.
25. **Cameron ML, Steel JE** 2001 Simplified aldehyde-fuchsin staining of neurosecretory cells. Stain Technology 34:265-266.
26. **Apisawetakan S, Thongkukiatkul A, Wanichanon C, Linthong V, Kruatrachue M, Upatham ES, Poomthong T, Sobhon P** 1997 The gametogenic processes in a tropical abalone, *Haliotis asinina* Linnaeus. J Sci Soc Thailand 23:225-240.
27. **Tucker LE** 1970 Effects of external salinity on *Scutus breviculus* (Gastropoda, Prosobranchia) - II. Nerve conduction. Comp Biochem Physiol 37:467-480.
28. **Upatham ES, Thongkukiatkul A, Kruatrachue M, Wanichanon. C, Chitramwong YP, Sahavacharin S, Sobhon P** 1998 Classification of neurosecretory cells, neurons and neuroglia in the cerebral ganglia of *Haliotis asinina* Linnaeus **by light microscopy**. J Shellfish Res 17:737-742.
29. **Kruatrachue M, Thongkukiatkul A, Sobhon P, Upatham ES, Wanichanon. C, Sretarugsa P** 1999 The ultrastructure of neuron and neuroglia in the cerebral and pleuro-pedal ganglia of *Haliotis asinine* Linnaeus. Science Asia 25:134-142.
30. **Sosa MA, Spitzer N, Edwards DH, Baro DJ**A crustacean serotonin receptor: cloning and distribution in the thoracic ganglia of crayfish and freshwater prawn. J Comp Neurol 2004 Jun 7:473(4):526-37.
31. **Strosberg AD** 1996 G protein coupled R_7G receptors. Cell Signalling. Cold Spring Harbor Laboratory Press. 27:65-83.
32. **Ostrowski J, Kjelsberg MA, Caron MG, Lefkowitz RJ** 1992 Mutagenesis of the β_2-adrenergic receptor: how structure elucidates function. Annu Rev Pharmacol Toxicol 32:167-183.
33. **Hedin KE, Duerson K, Clapham DE** 1993 Specificity of receptor G-protein interaction: searching for the structure behind the signal. Cell Signal 5:505-518.
34. **Lembo PMC, Ghahremani MH, Morris SJ, Albert PR** 1997 A conserved threonine residue in the second intracellular loop of the 5-hydroxytryptamine 1A receptor directs signaling specificity. Molecular Pharmacology 52:164-171.
35. **Kobilka BK, Frielle T, Collins S, Yang-Feng TL, Kobilka TS, Francke U, Lefkowitz, RJ, Caron MG** 1987 An intronless gene encoding a potential member of the family of receptors coupled to guanine nucleotide regulatory proteins. Nature 329:75-79.
36. **Cogé F, Guenin SP, Renouard-Try A, Rique H, Ouvry C, Fabry N, Beauverger P, Nicolas JP, Galizzi JP, Boutin JA, Canet E** 1999 Truncated isoforms inhibit [^{3}H]prazosin binding and cellular trafficking of native human α_{1A}-adrenoceptors. J. Biochemistry, 343:231-239
37. **Karpa KD, Lin R, Kabbani N, Levenson R** 2000 The dopamine D3 receptor interacts with itself and the truncated D3 splice variant d3nf: D3-D3nf interaction causes mislocalization of D3 receptors. Mol Pharmacol 58:677-683
38. **Grosse R, Schultz G, Gudermann T** 1997 Inhibition of gonadotropin-releasing hormone receptor signaling by expression of a splice variant of the human receptor. Mol Endocrinol 11:1305-1318
39. **Okuda-Ashitaka E, Sakamoto K, Ezashi T, Miwa K, Ito S, Hayaishi O** 1996 Suppression of prostaglandin E receptor signalling by the variant form of EP1 subtype. J. Biol. Chem. 271:31255-31261.

Formatted: English (Australia)

40. **Ding WQ, Cheng ZJ, McElhiney J, Kuntz SM, Miller LJ** 2002 Silencing of secretin receptor function by dimerization with a misspliced variant secretin receptor in ductal pancreatic adenocarcinoma. Cancer Res 62:5223-5229
41. **Zhu X, and Wess J** 1998 Truncated V2 vasopressin receptors as negative regulators of wild-type V2 receptor function. Biochemistry 37:15773-15784.
42. **Gnanapavan S, Kola B, Bustin SA, Morris DG, McGee P, Fairclough P, Bhattacharya S, Carpenter R, Grossman AB, Korbonits M** 2002 The tissue distribution of the mRNA of ghrelin and subtypes of its receptor, GHS-R, in humans. J Clin Endocrinol Metab 87(6):2988.
43. **Howard DR, and Talbot P** 1992 *In vitro* contraction of lobster (*Homarus*) ovarian muscle: Methods for assaying contraction and effects of biogenic amines. J Exp Zool 263:356-366.
44. **Henry J, Zatylny C, Boucaud-Camou E** 1999 Peptidergic control of egg-laying in the cephalopod *Sepia officinalis*: involvement of FMRFamide and FMRFamide-related peptides. Peptides 20:1061-1070.

FIG. 1. Molecular identification of a 5-HT receptor in the abalone, *H. asinina*. **A**, Nucleotide sequence (1633-bp) and deduced amino acid sequence (359 aa) of a *H. asinina* 5-HT_{1Hal} receptor. Boxed grey areas indicate predicted TM domains (TM1-6; http://www.enzim.hu/hmmtop/html/submit.html). The 50 amino acids (underlined) of *H. asinina* are those which were expressed as a recombinant peptide to make an antibody probe. Inset: RT-PCR using primers (double underlined) spanning the coding and untranslated regions, followed by agarose gel electrophoresis visualization. PCR – represents a negative control with RT absent. **B**, Kyte-Doolittle hydropathy profile of the deduced *H. asinina* 5-HT receptor sequence. **C**, Phylogenetic tree of molluscan 5-HT receptors compared with selected non-molluscan 5-HT receptors. A tree was constructed from deduced amino acid sequences by using the neighbor-joining method. The number at each branch point represents the bootstrap probability that two lineages join together to form a cluster. Genbank accession numbers: *Lymnaea* (Q25414), *Heliothis* (AY395746), *Aplysia* 1a (AAM46088), *Haliotis* (EU342382), *Mizuhopecten* (AB209935), *Aplysia* 1b (AAC28786), *Panulirus* (AY528822), *Takifugu* 1a (CAA65175), *Oreochromis* (AAP83427), *Takifugu* 1b (CAA65176), *Mus* (NP_032334), *Homo* 1A (NM_000524), *Oreochromis* (AAP83428), *Homo* 1D (NM_000864), *Homo* 1B (NM_000863), *Homo* 2C (NM_000868), *Homo* 2A (NM_000621), *Xenopus* 2B (NP_001082744), *Homo* 2B (NM_000867), *Homo* 7 (NM_000872), and *Homo* 5A (NM_024012).

FIG. 2. Comparative analysis of deduced 5-HT receptor sequences. Comparison of deduced amino acid sequences from *H. asinina* 5-HT_{1Hal} receptor, with *Aplysia* CNS (5-HT_{1ap}; AF041039) and *Panulirus interruptus* (5-HT_{1Pan}; AY528822). The identical residues are shaded in black, similar residues are shaded in grey, - represents gaps in the alignment. A schematic diagram shows the relative length of deduced 5-HT receptor proteins and dark boxes represent transmembrane domains.

FIG. 3. Tissue-specific expression of the 5-HT_{1Hal} mRNA using gene specific primers OL5 and OL7 in PCRs with cDNAs prepared from different tissues. Amplification products were separated on 2% agarose gels and stained with ethidium bromide. Amplification products were 246-bp. All tissues tested were positive for 5-HT_{1Hal} mRNA: cerebral ganglia (CG), pleuro-pedal ganglia (PPG), female gonad (FGO), male gonad (MGO), 40 day juvenile (40 day), mantle, cephalic tentacle (Ctent), eye stalk (Eye), gill, and foot muscle tissues. PCR + represent the positive control using recombinant plasmid containing the 5-HT receptor gene sequence, PCR - represents the negative control using water instead of cDNA, and Control includes respective samples without RT reaction.

FIG. 4. Immunoperoxidase staining of the 5-HT_{1Hal} in cerebral ganglion (**A**) and pleuropedal ganglion (**B and C**), together with Gomori's aldehyde-fuschin staining (GAFS) (**A2, B1,** lower). **A,** Cross-section of cerebral ganglion showing the distribution of 5-HT_{1Hal} immunoreactivity (5-HT-ir) in cells within the cortical region (arrows). **A1**. High power micrograph of boxed 1 area in **A** showing 5-HT_{1Hal}-ir in type1 neurosecretory cells (NS1) and fibers (arrow heads). **A2**. High power micrograph of boxed 2 area in A showing NS1 stained with immunoperoxidase method (upper), and GAFS (lower), repectively. **B and C**, Low power micrographs of a section of the pleuropedal ganglion showing the distribution of 5-HT_{1Hal}-ir in the cells (arrows). **B1**, High power micrograph of boxed 1 area in **B** showing NS1 stained with immunoperoxidase (upper), and GAFS (lower), respectively. **C,** Cross-section of lower pleuropedal horn showing 5-HTR-ir in cells located at the peripheral region. **C1**, High power of boxed area 1 in **C** showing both NS1 and NS2 contain 5-HT_{1Hal}-ir in the cytoplasm. Scale bars: 100 μm (**A, B, C**); 10 μm (**A1, A2, B1, C1**)

FIG. 5. Immunoperoxidase staining of 5-HT_{1Hal}-ir in the gonads. **A**, Low power of ovary showing the distribution of 5-HT_{1Hal}-ir in the outer capsule (arrows), trabeculae (arrow heads) and late stage oocytes (asterisks). **A1 and A2**. High power inset of boxes 1 and 2 in A, showing 5-HT_{1Hal}-ir in the trabeculae (arrow heads) and the cytoplasm of stage 4 oocyte (Oc4), respectively. No immunostaining of 5-HT_{1Hal} occurs in previttellogenic oocytes (Oc2, Oc3). **B,** High power of Oc5 showing immunostaining of 5-HT_{1Hal} in the cytoplasm. **C**. Medium power of testis showing the distribution of 5-HT_{1Hal} in the outer

capsule (arrows) and the trabeculae (arrow heads). **C1**, high power from box 1 in **C** showing 5-HT_{1Hal}-ir in trabeculae (arrow heads). Scale bars: 50 μm (**A, C**); 10 μm (**A1, A2, B, C1**)

FIG. 6. Immunofluorescent staining of cerebral (**A and B**) and pleuropedal ganglia (**C and D**) illustrating the distribution of 5-HT_{1Hal} immunoreactivity (red) and 5-HT immunoreactivity (green), and nuclear staining (blue). **A and C**, Medium power micrographs of cerebral (**A**) and pleuropedal ganglia (**C**) showing 5-HT neurons (S) and neurosecretory cells (NSs) containing 5-HT_{1Hal} (R) localized in the cortex. Abundant 5-HT positive fibers are present in the medulla of both ganglia. **B and D**, High power micrograph of cerebral and pleuropedal ganglia demonstrating the 5-HT fibers innervating the NSs (red) (**B**, inset; **D**, inset) respectively. Some fibers of NSs are observed (**B, D** arrows). Scale bars: 40 μm (**A**); 10 μm (**B**, **B** inset, **D**); 20 μm (**C, D** inset)

FIG. 7. Contractility of male and female gonad rings following 5-HT stimulation. **A,** Representative trace of the effect of 5-HT (10^{-6} M) on male gonad muscle. Time of application of 5-HT is shown by the arrow. Dose-response for the effect of 5-HT on change in rate of gonad contraction (n = 6, mean $\pm$ S.D.). Asterisks indicate significant different compared to the control ($p<0.05$). **B,** Representative trace of the effect of 5-HT (10^{-6} M) on female gonad muscle.

Title: Ultrastructure, Compositions and Possible Roles of the Egg Coats in *Haliotis asinina*

Authors: Worawit Suphamungmee[a], Wattana Weerachatyanukul[a], Tanes Poomtong[b], Rapeepun Vanichviriyakit[a] and Prasert Sobhon[a]*

Affiliations:

[a]Department of Anatomy, Faculty of Science, Mahidol University, Rama VI Road, Bangkok 10400, Thailand

[b]The Coastal Aquaculture Research and Development Center, Department of Fisheries, Klong-wan, Prachuabkirikhun 77000, Thailand

***Address for manuscipt correspondence:**

Professor Prasert Sobhon

Department of Anatomy, Faculty of Science,

Mahidol University, Rama VI Road,

Bangkok 10400, Thailand

Email: scpso@mahidol.ac.th

Tel. (+66) 2-201-5406

Fax. (+66) 2-354-7168

Short title: Study of abalone egg coats

SUMMARY

Spawned egg of a tropical abalone *H. asinina* has two protective barriers, i.e., the egg jelly coat (EJ) and the vitelline envelope (VE). At electron microscopic level, EJ is shown to be composed of a network of large fibers (40-50 nm thick) cross-linked by smaller fibers (15-20 nm thick) while VE is a thin tough sheet containing pores that might be channels for sperm contact and entry. Electrophoretically, EJ contains two major glycoproteins at 107 and 178 kDa, while VE contains a broad spectrum of protein bands ranging from 15-200 kDa which also includes the corresponding EJ protein bands. Glycoproteins of EJ and VE exhibit strong cross reactivities and they appear around late oocytes (Oc_4, Oc_5). Glucose is the major sugar composition of both EJ and VE glycoproteins, while a minor proportion of arabinose, fructose, galactose and fucose is detected in both EJ and VE. Our findings suggest that sperm acrosome reaction could be induced by isolated VE glycoproteins, whereas acceleration of the sperm motility could be stimulated by EJ glycoproteins.

Keywords: *Haliotis asinina*, egg jelly, vitelline envelope, acrosome reaction, motility

INTRODUCTION

Molecules on sperm and egg surfaces that mediate gamete recognition and fertilization in broadcast-spawning marine invertebrates have been extensively studied, especially in sea urchins (Darszon et al., 2001; Hirohashi and Vacquier, 2003; Moy et al., 1996; SeGall and Lennarz, 1979; Vilela-Silva et al., 2002), and in two abalone species, *Haliotis rufescens* and *Haliotis corrugata*. It was demonstrated in the latter that the sperm acrosomal lysin binds to the vitelline envelop (VE) receptor and creates a hole through which sperm could pass and fuse with the egg cell membrane, and this is non-enzymatic species-specific mechanism (Kresge et al., 2001; Lewis et al., 1982; Vacquier et al., 1999). Mechanistically, sperm lysin binds to a 1,000-kDa glycoprotein molecule, named vitelline envelope receptor for lysin (VERL) that is a major constituent of the egg VE. This receptor molecule is composed of at least 50% carbohydrate (Swanson and Vacquier, 1997), containing predominantly glucose and mannose residues. Lysin dimers make the tight, species-specific binding to VERL. Upon binding to lysin, the fibrous VERL molecules lose cohesion and are splayed apart, creating hole for sperm passage (Vacquier et al., 1999). However, it was not demonstrated that this VE molecules could induce acrosome reaction (AR).

Structurally, the eggs of red abalone, *Haliotis rufescens*, and Japanese abalone, *Haliotis discus*, are covered by a coat of fibrous jelly layer (EJ) (Mozingo et al., 1995; Shiroya and Sakai, 1995). The role of EJ has not yet been fully demonstrated, whilst in sea urchins, EJ is thought to be involved in sperm acrosome reaction (AR) induction. Sperm AR is believed to be induced on the sea urchins' egg surface by sulfated fucose polymer (FSP) in the jelly layer (SeGall and Lennarz, 1979). Similarly, AR-inducing

substance (ARIS) and its cofactor molecule (CoARIS) are reported to reside in starfish egg's jelly coat (Gunaratne et al., 2003). In abalone, the agents for AR induction have not exactly been identified.

In this study, we have investigated the ultrastructure of egg surface coatings, namely, the jelly coat (EJ) and vitelline envelope (VE) of a tropical abalone *Haliotis asinina*, using electron microscopies. The glycoprotein compositions of the egg coatings were analyzed for their proteins and carbohydrate compositions. And lastly the roles of EJ and VE in sperm AR induction and enhancing motility were demonstrated.

MATERIALS AND METHODS

Ultrastructure of the egg coats

Eggs spawned into seawater were settled down for 5 min and pipetted into fixative solution containing 2.5% glutaraldehyde in 0.1 M cacodylate buffer, pH 7.8 at 4°C, and left for overnight. After washing with 50 mM cacodylate buffer, pH 7.8, the samples were postfixed in 1% osmium tetroxide in the same buffer, at 4°C, for 1 hr. Subsequently, the fixed eggs were washed twice with the same buffer, dehydrated in increasing concentrations of ethanol (from 50% to 100%), and embedded in Araldite 502 resin (Electron Microscopy Sciences, Fort Washington, PA, USA). Semithin and thin sections were cut with ultramicrotome. Semithin sections were stained with 1% methylene blue, and then observed under a light microscope (LM) (Nikon Eclipse E600). Thin sections were placed on 300-mesh copper grids, stained sequentially with uranyl acetate and lead citrate, and then observed under a transmission electron microscope (TEM) (Hitachi H-300), operating at 75 kV. In order to observe the surface features of

the egg's coats, spawned eggs were similarly prepared and fixed as described. Samples were dehydrated in a critical point-drying apparatus (Hitachi HCP-2), sputter-coated with palladium. Finally, they were observed under a scanning electron microscope (SEM) (Hitachi S-2500) operating at 20 kV.

Molecular composition of the egg coats

About 1,000 spawned eggs were washed and settled in 3 ml filtered seawater. The jelly coat was extracted by dropping 1 N HCl to the egg suspension to lower the pH to 5.0 (Lewis et al., 1982). After thorough mixing, the suspension was incubated for 30 min at 4°C by continuous shaking. Then, drops of 1 M Tris-HCl (pH 8.0) were added to readjust the final pH of the egg suspension to 7.0. Seawater above the settled eggs was pipetted into a tube, leaving the dejellied eggs which were then kept at 4°C for further studies. Egg jelly in seawater was separated from cellular debris by centrifugation at 10,000 *xg*, 4°C, for 30 min. Supernatant containing the egg jelly (EJ) proteins was collected and dialyzed (with molecular weight cut off at 10 kDa) against 10 mM Tris-HCl, pH 7.4, containing 150 mM NaCl (TBS) at 4°C for overnight. Later, EJ proteins were concentrated, using microCON (Millipore Corperation, Billerica, MA, USA) with a 10-kDa cut off and kept at 4°C for further experiment.

To isolate proteins from the egg vitelline envelope (VE), the dejellied eggs were washed several times in 3 ml filtered seawater, and then 5 volumes of salt medium (454 mM NaCl, 9.7 mM KCl, 24.9 mM $MgCl_2$, 27.1 mM $MgSO_4$, 4.4 mM $NaHCO_3$, 10 mM Tris base, and 10 mM EGTA, pH 7.0) was added to 1 volume of the dejellied eggs in seawater. This suspension was homogenized by 10 strokes at 4°C and filtered through 3 layers of gauze. The homogenate was spun at 190 *xg*, 4°C, for 5 minutes. Then, the pellet

was washed twice by resuspension in the salt medium and subjected to centrifugation (50 *×g*, 4°C, 5 min). The solution appeared as 2 layers: the lower layer containing pigment granules, and the fainter upper layer containing VE. The upper layer was removed and then transferred to a new tube. After the third wash with the salt medium and centrifugation, VE pellet appeared colorless and free from cytoplasmic contaminants, as observed by light microscopy. To further purify VE, the isolate was overlaid on Percoll gradient (40%-80%) (Sigma-Aldrich Chemical Co., Saint Louis, MO, USA) and subjected to 1,000 *×g* centrifugation, for 20 min. The intact VE appeared at the interface of 40% and 60% Percoll, and was separated from the debris of nucleus and cytoplasmic granules at the bottom of the tube. Solution containing only intact VE was collected by a Pasture pipette and washed with the salt medium until pure envelopes were obtained. The sample was stored in the salt medium at 4°C until use. To solubilize the vitelline envelope, acetic acid was added to the purified VE for 2 min to adjust pH to 2.8. The reaction was stopped by a dropwise addition of 1 M Tris-HCl, pH 8.0 into the solution for the readjustment of pH to 7.8. Then, the solution was centrifuged at 5,000 ×*g*, at 4°C, for 3 min, the supernatant containing soluble VE was dialyzed against TBS. VE proteins were concentrated using microCON with 10 kDa cut off, and kept for protein analysis and for inducing the sperm acrosome reaction. The protein quantification was done by Lowry's method using bovine serum albumin (BSA) as the standard (Lowry et al., 1951).

Analysis of protein and glycoprotein components

SDS-PAGE was carried out using a stacking gel of 5% acrylamide and separating gel of 10%. Proteins (~10 μg) from both EJ and VE were denatured in sample buffer containing 0.125 mM Tris base, pH 6.8, 4% SDS, 10% β-mercaptoethanol, 20% glycerol,

0.2% bromophenol blue. The broad range molecular weight standard was used as the molecular weight markers (Biorad Laboratories, Ltd., Hercules, CA, USA). Gels were run at constant current (40 mA) for 50 min, and visualized by staining with 0.125% Coomassie brilliant blue R-250. For identification of glycoproteins, the gels were visualized by staining with Periodic acid-Schiff (PAS). A parallel histological experiment was performed by staining semithin sections of ovaries and spawned eggs with PAS to demonstrate whether they were invested with carbohydrate-containing coats.

Analysis of sugar moieties by HPLC

Isolated EJ and VE proteins were analyzed for the sugar compositions by HPLC. The HPLC system was set at room temperature on a Prevail Carbohydrate Column (15 × 0.46 cm in size) (Alltech Associates, Inc., Deerfield, IL, USA). EJ and VE proteins were prepared at 1 mg/ml in seawater, and were carefully pushed through 0.22-μm nylon filter to exclude the particulate contaminants. The samples were chromatographed using a mixture of acetronitrile:deionized distilled water in the ratio of 80:20 as a mobile phase. The refractive index (RI) detector was set at a flow rate of 1 ml/min, for 2.5-30 min. A solution containing a mixture of fucose, fructose, galactose, glucose, sucrose, mannose, arabinose and maltose (50 μg for each sugar) was run as the standards. Chromatograms indicated various kinds of sugar and their amount present in the injected samples.

Production of antibodies against EJ and VE proteins

Polyclonal antibodies against EJ and VE proteins were produced by immunizing isolated EJ or VE proteins into six-week old female ICR mice. Each animal was first subcutaneously injected with the EJ or VE proteins (~300 μg) that were emulsified with an equal volume of Freund's complete adjuvant. Two boosting injections, each

containing the same amount of proteins with Freund's incomplete adjuvant, were given twice at two-week intervals. Immune sera were collected by the tail bleeding and the presence of antibodies was tested by Western blotting, using preimmune sera as the control. The animals, whose antisera were found to be reacting exclusively with the targeted antigens, were sacrificed at the seventh day after the second boosting, and blood was collected from the heart. After centrifugation, the antisera were kept at -20°C until use.

Cross-reactivities and immunolocalization of EJ and VE proteins

The separated EJ or VE proteins were transferred onto nitrocellulose membrane in an electrophoretic transfer chamber (LKB Bromma, Hoefer Scientific Instruments, San Francisco, CA, USA) using the constant voltage set at 100 V, for 1 hr, in a transfer buffer (0.028 mM Tris base, 0.039 mM glycine, 20% methanol). Following the blocking step with 5% skim milk in TBST (Tris buffer saline containing 0.05% Tween 20), the membrane strips were incubated with mouse antiserum to EJ or VE proteins (at the dilution of 1:100), for 1 hr at room temperature. For the negative control, the membranes were incubated with preimmune serum instead of primary antibody. Then, the membranes were incubated in rabbit anti-mouse IgG conjugated to horseradish peroxidase (Zymed Laboratories, Inc., San Francisco, CA, USA) in TBST at 1:3,000 dilution, for 30 min at room temperature. The specific reaction was visualized by using ECL substrate kit (Amersham Pharmacia, Buckinghamshire, UK).

To investigate the expression of EJ and VE proteins in oocytes and spawned eggs, pieces of ovarian tissue and freshly spawned eggs were immersed in a fixative solution of 0.5% glutaraldehyde, 4% paraformaldehyde in 0.1 M phosphate buffer, pH 7.8 at 4^{o}C, for

2 hr. After washing, the samples were sequentially dehydrated in increasing concentrations of ethanol (from 50% to 100%), and embedded in LR White resin (London Resin Co., Thule, UK). Semithin sections were cut and mounted on the gelatin-coated glass slides. The sections were then incubated in 0.15 M glycine in order to block free aldehyde groups, and then in 4% BSA for blocking non-specific bindings. The sections were incubated in mouse anti-EJ or anti-VE antisera (at dilution 1:80) or preimmune sera (control) in TBST, for 1 hr at 37°C, and then washed by TBST. The sections were further exposed to biotinylated rabbit anti-mouse IgG (Zymed Laboratories, Inc.) in TBST at 1:100 dilution, and then with FITC-conjugated streptavidin (Sigma-Aldrich Chemical Co.) in TBST at 1:100 dilution, 37°C, for 30 min. After washing, samples were mounted with cover glasses, using Vectashield mounting medium (Vector Laboratories, Inc., Burlingame, CA, USA), observed and photographed under a Nikon Eclipse 600 fluorescence microscope equipped with a Nikon DXM 2000 CCD camera.

Induction of sperm acrosome reaction and assessment of sperm motility

EJ and VE proteins were prepared at various concentrations, i.e., 10 μg/ml, 100 μg/ml, 500 μg/ml and 1 mg/ml of proteins in filtered seawater. Sperm were incubated in each concentration of EJ and VE proteins, and AR induction was stopped at 2 min by fixing with 1% paraformaldehyde, and the occurrence of AR was observed by a light microscope. Acrosome intact (AI) sperm possess a round-shaped head with smooth anterior while the acrosome reacted (AR) sperm contain a long-extended filament projection at the anterior region. Sperm incubated in filtered seawater were used as the control. Approximately 200 sperm were counted for each data point from four separated experiments.

Sperm motility was assessed by observing under an inverted light microscope. A droplet of 50 µl sperm suspension taken from non-treated, EJ or VE treated sperm were plated onto a slide and a 40× objective was used for analyzing the sperm that were motile in the total sperm population.

RESULTS

Ultrastructure of spawned eggs' coatings

When observed at LM level, a normal live egg exhibited round shape with green color due to the presence of its yolk (Fig. 1A, B). There were two covering layers over the egg, i.e., jelly layer (EJ) and vitelline envelope (VE) (Fig. 1B). The space between VE and the egg cell membrane, so called perivitelline space, was filled with fluid. The size of a live egg was approximately 160-200 µm in diameter. The thickness of EJ was about 100 µm, whereas the thickness of VE was about 1 µm. EJ was easily torn off the egg when the eggs were left in seawater for a prolonged period (>1 hr). It could also be separated by mechanical force, such as continuous shaking in seawater for 20-40 min. In this study, EJ was isolated by mild acid (~0.1 N HCl) at pH 5.0 in the seawater, which resulted in the eggs being devoided off EJ (Fig. 1C). After homogenization and several washes, VE could be detached from the eggs (Fig. 1D).

At TEM level, EJ appeared as a network of fibrous structures, while VE was a thin, condensed sheet, comprising two dense lines separated by a light zone about 0.25 µm in width (Fig. 2A-C). The subjacent egg cytoplasm contained numerous mitochondria, yolk granules and lipid droplets (Fig. 2E, F). At the egg cell membrane, there were microvilli projecting outwards into the perivitelline space (Fig. 2B, D). Higher

magnification demonstrated a network of fine fibers linking between neighboring microvilli (Fig. 2D). The spawned egg' s EJ (Fig. 2C) exhibited two-sized fibers tightly attached to VE as well as loosely distributed around the egg (Fig. 2B, C). Large fibers were approximate 40-50 nm in thickness, and they were interconnected by smaller fibers, each approximately 15-20 nm in thickness.

When observed by SEM, the spawned egg's EJ exhibited spongy appearance (Fig. 3A, B). After the removal of EJ, VE exhibited smooth surface with small pores distributed throughout its entire surface (Fig. 3C, D). Each pore was measured about 190-200 nm.

Molecular compositions of EJ and VE

When separated by 10% SDS-PAGE, EJ consisted of the only two major bands of proteins at molecular mass of 107 and 178 kDa, while there were also some proteins larger than 200 kDa left in the stacking gel (Fig. 4A). VE consisted of several proteins ranging from 15 kDa to 200 kDa with the major bands appeared at 29-32, 45, 48 and 82 kDa, while the 107 kDa and 178 kDa and some larger proteins were also found in lesser amount than in EJ. The separated protein bands from EJ and VE were also stained with PAS that identified the carbohydrate-conjugated proteins. In EJ, the intensely PAS-positive bands were at 107 kDa, 178 kDa, and some other bands larger than 200 kDa remaining in the stacking gel. VE showed weak PAS stained bands at the lower molecular weights, whereas larger proteins at 107 kDa, 178 kDa, and over 200 kDa were also strongly PAS-positive (Fig. 4A).

In the ovarian oocytes (Fig. 4B), a thick PAS-positive layer of jelly coat appeared in premature stage 4 oocyte (Oc_4) and mature stage 5 oocyte (Oc_5), while the surfaces of

253 early stage oocytes (Oc_1 to Oc_3) were not stained (oocyte classification based on
254 Apisawatakan et al., 2001). Very weak PAS staining was also detected in the ovarian
255 trabeculae and inside oocyte cytoplasm. In spawned eggs (Fig. 4C), a weak PAS staining
256 could also be observed at VE and throughout EJ. The histochemical stain and SDS-PAGE
257 results suggested that both EJ and VE were composed of glycoproteins, which were laid
258 down in the late stage oocytes (Oc_4 and Oc_5).

259 The carbohydrate compositions of the EJ and VE proteins was quantitatively
260 analyzed by HPLC (Fig. 5). The result revealed that EJ contained a large amount of
261 glucose (~81% per total content), whereas fructose (~6%) and galactose (~1.5%) were
262 barely present. In comparison, VE also contained the highest amount of glucose (~73%)
263 and smaller amount of fucose (2.7%).

264 **Cross reactions and expression of EJ and VE components**

265 Cross-reactivity of the antibodies raised against EJ and VE proteins was tested by
266 Western blotting (Fig. 6). It was shown that anti-EJ strongly reacted with EJ proteins,
267 specifically at 107 kDa, 178 kDa, and to a small extent with the bands over 200 kDa
268 (remaining in the stacking gel). Anti-EJ showed a slight cross-reactivity with VE proteins
269 at the 107 kDa protein band. In comparison, anti-VE reacted strongly with the 30 kDa VE
270 protein and to a lesser extent with the 48 and 82 kDa proteins. A trace staining could also
271 be observed at a 107 kDa band. When this antibody was applied to EJ protein isolate,
272 some cross reactivity with the 30 and 48 kDa proteins were notable. These results
273 indicated that some isolated proteins from EJ and VE may share common epitopes,
274 though the degree of their cross reactivities varied. It may also be possible that some
275 contamination from the EJ components may be left during VE extraction, dispite a

careful cleaning process was done to wash away EJ proteins. This could be because some EJ fibers were seen tightly adhered to VE under TEM.

Immunofluorescent staining of ovarian sections with anti-EJ showed that the fluorescence was firstly detected in the jelly layer of the mature oocytes at Oc_4-Oc_5 stages, whereas no fluorescence was observed in immature oocytes at Oc_1-Oc_3 (Fig. 7A, B). Similarly, anti-VE showed an intense fluorescence in Oc_4-Oc_5 (Fig. 7C, D). This strong fluorescence was particularly prominent over the entire region of the two layers and seemed to occupy larger area than those detected by anti-EJ. For the spawned eggs, both anti-EJ and anti-VE showed strong fluorescence at the jelly coat and vitelline envelope as in mature ovarian oocytes (Fig.7E, F). In controls, there was no fluorescence signal detected either on VE or EJ. However, some autofluorescence (exhibited a yellow color) was observed in the oocyte cytoplasm in both ovarian sections and the spawned eggs (Fig. 7G, H).

Induction of sperm acrosome reaction and motility

Sperm acrosome reaction (AR) and its associated morphological changes were observed by SEM, which revealed that the acrosome of most sperm disappeared from the head after contact with VE region following the incubation of spawned eggs with sperm. These AR-sperm possessed filamentous structure projecting from the anterior region of the head (Fig 8A-C). In contrast, some sperm remaining on EJ had an intact acrosomal integrity showing still smooth anterior end (Fig. 8D).

To confirm the above SEM observations of intact and AR-sperm and study the role of EJ and VE proteins in inducing sperm AR, freshly spawned sperm were treated with proteins isolated from both layers at various concentrations in seawater. At 10 μg/ml

299 of EJ proteins (Fig. 9, black bars), most sperm still exhibited normal head bearing
300 acrosomal vesicle with no anterior projection. The pattern of their swimming, as observed
301 by LM, did not differ from the normal spawned sperm. Similar characteristics were
302 observed when sperm were treated with EJ proteins at higher concentrations at 100 μg/ml
303 (5.4%), 500 μg/ml (5.6%) and 1 mg/ml (4.5%). However, at 1 mg/ml EJ, the proportion
304 of sperm showing motility was increased from ~60% to >90%, whereas other
305 characteristics of sperm still remained normal. When sperm were treated with VE
306 proteins at concentrations 10 μg/ml and 100 μg/ml (Fig. 9, hatched bars), most sperm still
307 exhibited normal morphological features while the percentage of AR sperm detected at
308 concentrations of 10 μg/ml (5.1%) and 100 μg/ml (5.4%) were comparable to those of the
309 control group (4.7%). At higher concentrations of 500 μg/ml and 1 mg/ml VE, the
310 number of AR sperm was significantly increased to 19.8% and 25.9%, respectively. All
311 VE-treated AR sperm exhibited heads with anterior projections which were subacrosomal
312 filaments, while other characteristics were still normal, and their motility was unaltered.
313
314 **DISCUSSION**
315 **Ultrastructure of the egg coats**
316 We have recently described oogenesis in *H. asinina* and the formation of EJ in
317 ovarian oocytes (Apisawetakan et al., 2001). EJ surrounding the mature ovarian oocytes
318 at Oc_4 and Oc_5 stages appears to be a thick homogeneous structure. In contrast, EJ of the
319 spawned egg shown in this study appeared as a fibrous meshwork of glycoprotein fibers.
320 High magnification TEM micrographs of the spawned eggs could define the fibrous
321 nature of EJ, which was clearly separated from VE. This EJ fibrous network was formed

by interconnection between the large fibers (40-50 nm) and smaller fibers (~20 nm). Similar filamentous network has been observed around the egg of sea urchin, *Strongylocentrotus purpuratus* (Chandler and Heuser, 1980; Chandler and Kazilek, 1986), red abalone (Mozingo et al., 1995) and Japanese abalone (Shiroya and Sakai, 1995). However, the sizes of both types of fibers are variable according to species. It has also been reported in *H. discus* that the jelly-freed eggs are found to be 90% fertilizable, suggesting that EJ has no direct role in the process of fertilization and gamete fusion (Shiroya and Sakai, 1995). In contrast to EJ, VE was not as clearly defined in the mature ovarian oocyte (Oc_5) as in the spawned egg, where it appeared as a thin tough sheet. In addition, the surface of VE exhibited pores which could not be easily visualized in TEM micrographs of VE cross sections, partly due to the fact that they were small in size and widely separated. The function of these pores is, at present, not known, but they could be channels for sperm penetration.

The compositions of EJ and VE

We found that EJ could be easily isolated and dissolved in buffer, whereas VE was harder to be solubilized, supporting the compact nature of VE composition as a thin tough sheet. These VE proteins could be extracted by acetic acid, which yielded higher amount of proteins than other chemical treatments, such as mercaptoethanol or SDS. Electrophoretic analyzes showed that *H. asinina* EJ contained major glycoproteins with molecular weights at 107 and 178 kDa. VE also contained both proteins and other smaller glycoproteins at the range of 15-82 kDa. Staining with PAS in sections of mature ovary and spawned egg indicated that these glycoproteins started to be deposited around the late vitellogenic oocytes (Oc_4), in consistent with the previous morphological study showing

345 that EJ coating started to be visible in Oc_4 (Apisawetakan et al., 2001). The detailed
346 carbohydrate compositions analyzed by HPLC revealed a high amount of glucose in EJ
347 and VE proteins, whereas other sugars were present in much smaller quantities. Highly
348 variable corbohydrate compositions of the egg outer coats have been reported in a broad
349 spectrum of species from invertebrates to vertebrates which are known to serve the
350 functions in gamete recognition and/or AR induction. In the well studied model of
351 invertebrate, sea urchin, the egg's jelly layer is composed mainly of sulfated
352 polysaccharides, i.e., fucose sulfate polymer (FSP) with the various bands of
353 glycoproteins at molecular mass ranging between 120 kDa to 260 kDa and over 10^4 kDa
354 depending on species (Shimizu et al., 1990). It is well estabished that these egg FSP
355 glycoproteins initiate AR in the species-specific manner in sea urchin (Hirohashi and
356 Vacquier, 2002; SeGall and Lennarz, 1979; Vilela-Silva et al., 2002). In oocytes of
357 amphibians, *Bufo arenarum*, mannose is the most abundant carbohydrate residue which is
358 involved in recognition of sperm (Omata and Katagiri, 1996), whereas sulfated
359 glycoproteins riched in hexosamines, fucose, and galactose are found in *Xenopus laevis*
360 EJ and act in a similar manner (Yurewicz et al., 1975). In comparison, mammalian eggs'
361 coating (zona pellucida) has large oligomers of carbohydrate-conjugated proteins, such as
362 β-N-acetylglucosamine (GlcNAc), which is involved in sperm-egg binding (Miller et al.,
363 1993; Wassarman, 1999; Wassarman, 2005). Whether the carbohydrate moieties of EJ
364 and VE of *H. asinina* involved in sperm binding and AR modulation are still unknown
365 and remain to be investigated.
366

Induction of sperm acrosome reaction (AR) and motility

AR in abalone sperm involves the exocytosis of the acrosomal vesicle and the polymerization of subacrosomal materials, composed mainly of actin, to form the anterior spike called acrosomal process (Neill and Vacquier, 2004). Abalone sperm can undergo AR after exposing to high concentration of calcium ions and then lysin, which could bind to VE (Lewis et al., 1980). Few studies have shown that egg VE might be responsible for the induction of sperm AR in abalone (Sakai et al., 1982). By contrast, in sea urchin, EJ glycoconjugates rich in fucose sulfate (FSP) has reported to be the AR inducer (Hirohashi and Vacquier, 2002; SeGall and Lennarz, 1979; Vilela-Silva et al., 2002). Interestingly, constituents of FSP that regulates AR in sea urchins were pure polysaccharides, with no associated protein (Mengerink and Vacquier, 2001; Vacquier and Moy, 1997). In fact, the significance of carbohydrate moieties on regulating fertilization has not only been shown in invertebrates but also in mammals including human (Shalgi and Raz, 1997; Wassarman, 2005; Zara and Naz, 1998). Surprisingly, although we showed herein that EJ of *H. asinina* were enriched in carbohydrate compositions (Fig. 4), they were not involved in initiating sperm AR, but rather in regulating sperm motility. In sea urchins, motility was activated when sperm were spawned into seawater. It is believed that some factors associated with the EJ may function as “chemoattractants” to stimulate sperm motility (Neill and Vacquier, 2004). In red abalone *H. rufescens*, L-tryptophan has been shown to be released from the eggs into seawater, which serves dual functions in triggering both sperm activation and chemotaxis (Riffell et al., 2002; Riffell et al., 2004). Experimental evidence in the present study also showed acceleration of sperm motility in

388 the presence of high concentration of isolated EJ proteins, though the exact protein
389 inducer(s) have yet to be identified.
390
391

ACKNOWLEDGEMENTS

This research was supported by the Thailand Research Funds (Senior Research Scholar Fellowship to PS, Research scholar to WW and RGJ-Ph.D. scholarship to WS) and Mahidol University.

REFERENCES

Apisawetakan, S., Linthong V., Wanichanon, C., Panasophonkul, S., Meepool, A., Kruatrachue, M., Upatham, E. S., Pumthong, T. and Sobhon, P. (2001). Ultrastructure of female germ cells in Haliotis asinina Linnaeus. *Inv Reprod Dev* **39**, 67-79.

Chandler, D. E. and Heuser, J. (1980). The vitelline layer of the sea urchin egg and its modification during fertilization. A freeze-fracture study using quick-freezing and deep-etching. *J Cell Biol* **84**, 618-32.

Chandler, D. E. and Kazilek, C. J. (1986). Extracellular coats on the surface of Strongylocentrotus purpuratus eggs: stereo electron microscopy of quick-frozen and deep-etched specimens. *Cell Tissue Res* **246**, 153-61.

Darszon, A., Beltran, C., Felix, R., Nishigaki, T. and Trevino, C. L. (2001). Ion transport in sperm signaling. *Dev Biol* **240**, 1-14.

Gunaratne, H. M., Yamagaki, T., Matsumoto, M. and Hoshi, M. (2003). Biochemical characterization of inner sugar chains of acrosome reaction-inducing substance in jelly coat of starfish eggs. *Glycobiology* **13**, 567-80.

Hirohashi, N. and Vacquier, V. D. (2002). High molecular mass egg fucose sulfate polymer is required for opening both Ca2+ channels involved in triggering the sea urchin sperm acrosome reaction. *J Biol Chem* **277**, 1182-9.

Hirohashi, N. and Vacquier, V. D. (2003). Store-operated calcium channels trigger exocytosis of the sea urchin sperm acrosomal vesicle. *Biochem Biophys Res Commun* **304**, 285-92.

418 **Kresge, N., Vacquier, V. D. and Stout, C. D.** (2001). Abalone lysin: the dissolving and
419 evolving sperm protein. *Bioessays* **23**, 95-103.
420 **Lewis, C. A., Leighton, D. L. and Vacquier, V. D.** (1980). Morphology of abalone
421 spermatozoa before and after the acrosome reaction. *J Ultrastruct Res* **72**, 39-46.
422 **Lewis, C. A., Talbot, C. F. and Vacquier, V. D.** (1982). A protein from abalone sperm
423 dissolves the egg vitelline layer by a nonenzymatic mechanism. *Dev Biol* **92**, 227-
424 39.
425 **Lowry, O. H., Rosebrough, N. J., Farr, A. L. and Randall, R. J.** (1951). Protein
426 measurement with the Folin phenol reagent. *J Biol Chem* **193**, 265-75.
427 **Mengerink, K. J. and Vacquier, V. D.** (2001). Glycobiology of sperm-egg interactions
428 in deuterostomes. *Glycobiology* **11**, 37R-43R.
429 **Miller, D. J., Gong, X. and Shur, B. D.** (1993). Sperm require beta-N-
430 acetylglucosaminidase to penetrate through the egg zona pellucida. *Development*
431 **118**, 1279-89.
432 **Moy, G. W., Mendoza, L. M., Schulz, J. R., Swanson, W. J., Glabe, C. G. and**
433 **Vacquier, V. D.** (1996). The sea urchin sperm receptor for egg jelly is a modular
434 protein with extensive homology to the human polycystic kidney disease protein,
435 PKD1. *J Cell Biol* **133**, 809-17.
436 **Mozingo, N. M., Vacquier, V. D. and Chandler, D. E.** (1995). Structural features of the
437 abalone egg extracellular matrix and its role in gamete interaction during
438 fertilization. *Mol Reprod Dev* **41**, 493-502.
439 **Neill, A. T. and Vacquier, V. D.** (2004). Ligands and receptors mediating signal
440 transduction in sea urchin spermatozoa. *Reproduction* **127**, 141-9.

441 **Omata, S. and Katagiri, C.** (1996). Involvement of carbohydrate moieties of the toad
442 egg vitelline coat in binding with fertilizing sperm. *Dev Growth Differ* **38**, 663-672.
443 **Riffell, J. A., Krug, P. J. and Zimmer, R. K.** (2002). Fertilization in the sea: the
444 chemical identity of an abalone sperm attractant. *J Exp Biol* **205**, 1439-50.
445 **Riffell, J. A., Krug, P. J. and Zimmer, R. K.** (2004). The ecological and evolutionary
446 consequences of sperm chemoattraction. *Proc Natl Acad Sci U S A* **101**, 4501-6.
447 **Sakai, Y. T., Shiroya, Y. and Haino-Fugushima, K.** (1982). Fine structural changes in
448 the acrosome reaction of the Janpanese abalone, Hailotis discus. *Dev Growth Differ*
449 **24**, 531-542.
450 **SeGall, G. K. and Lennarz, W. J.** (1979). Chemical characterization of the component
451 of the jelly coat from sea urchin eggs responsible for induction of the acrosome
452 reaction. *Dev Biol* **71**, 33-48.
453 **Shalgi, R. and Raz, T.** (1997). The role of carbohydrate residues in mammalian
454 fertilization. *Histol Histopathol* **12**, 813-22.
455 **Shimizu, T., Kinoh, H., Yamaguchi, M. and Suzuki, N.** (1990). Purification and
456 characterization of the egg jelly macromolecules, sialoglycoprotein and fucose
457 sulfate glycoconjugate, of the sea urchin Hemicentrotus pulcherrimus. *Dev Growth*
458 *Differ* **32**, 473-487.
459 **Shiroya, T. and Sakai, Y. T.** (1995). Filamentous structure of the external surface of
460 abalone eggs revealed by quick-freeze deep-etch technique. *Dev Growth Differ* **37**,
461 85-91.

462 **Swanson, W. J. and Vacquier, V. D.** (1997). The abalone egg vitelline envelope
463 receptor for sperm lysin is a giant multivalent molecule. *Proc Natl Acad Sci U S A*
464 **94**, 6724-9.
465 **Vacquier, V. D. and Moy, G. W.** (1997). The fucose sulfate polymer of egg jelly binds
466 to sperm REJ and is the inducer of the sea urchin sperm acrosome reaction. *Dev*
467 *Biol* **192**, 125-35.
468 **Vacquier, V. D., Swanson, W. J., Metz, E. C. and Stout, C. D.** (1999). Acrosomal
469 proteins of abalone spermatozoa. *Adv Dev Biochem* **5**, 49-81.
470 **Vilela-Silva, A. C., Castro, M. O., Valente, A. P., Biermann, C. H. and Mourao, P. A.**
471 (2002). Sulfated fucans from the egg jellies of the closely related sea urchins
472 Strongylocentrotus droebachiensis and Strongylocentrotus pallidus ensure species-
473 specific fertilization. *J Biol Chem* **277**, 379-87.
474 **Wassarman, P. M.** (1999). Mammalian fertilization: molecular aspects of gamete
475 adhesion, exocytosis, and fusion. *Cell* **96**, 175-83.
476 **Wassarman, P. M.** (2005). Contribution of mouse egg zona pellucida glycoproteins to
477 gamete recognition during fertilization. *J Cell Physiol* **204**, 388-91.
478 **Yurewicz, E. C., Oliphant, G. and Hedrick, J. L.** (1975). The macromolecular
479 composition of Xenopus laevis egg jelly coat. *Biochemistry* **14**, 3101-3107.
480 **Zara, J. and Naz, R. K.** (1998). The role of carbohydrates in mammalian sperm-egg
481 interactions: how important are carbohydrate epitopes? *Front Biosci* **3**, D1028-38.
482
483
484
485

485 **FIGURE LEGENDS**

486 **Figure 1 (A, B)** Light micrographs of live *H. asinina* spawned egg showing two coating
487 layers, jelly coat (EJ) and vitelline envelope (arrow head). After acid treatment, jelly coat
488 is detached from the egg **(C)**, and then its vitelline envelope is isolated using
489 homogenization **(D)**.

490

491 **Figure 2 (A, B)** Ultrastructure of the coatings of the spawned egg displaying a fibrous
492 network in the jelly coat (EJ) and thin dense double lines of vitelline envelope (VE). **(C)**
493 In EJ, large, 40-50 nm thick (1) and small, 15-20 nm thick (2) fibers are interconnected.
494 **(D)** At the egg cell membrane, microvilli (arrows) are present over the entire surface, and
495 they are linked by small fibers (arrow heads). **(E, F)** Egg's peripheral cytoplasm contains
496 abundant lipid droplets (L), yolk granules (G) and small mitochondria (Mi). P –
497 perivitelline space

498

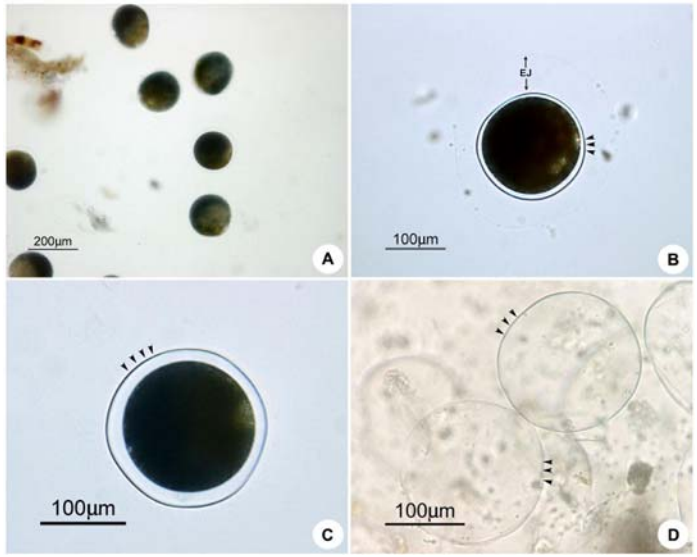
499 **Figure 3 (A, B)** The jelly coat (EJ) exhibits a network of thick and thin fibers that give
500 spongy appearance. **(C, D)** The vitelline envelope (VE) exhibits smooth surface with
501 numerous pores (arrow heads).

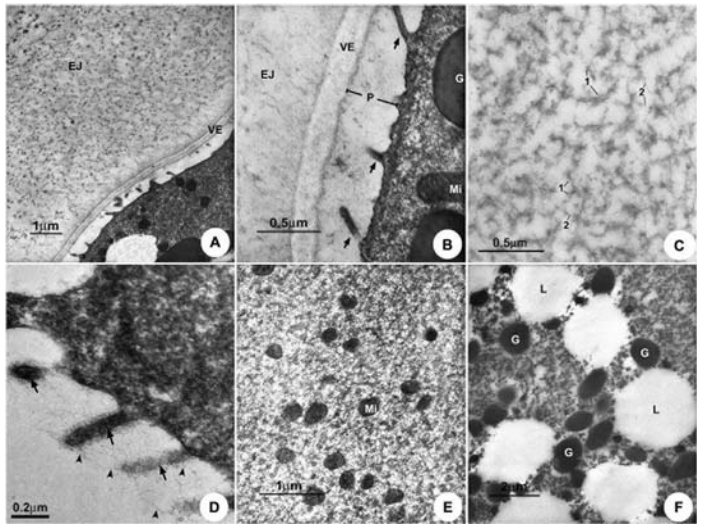
502

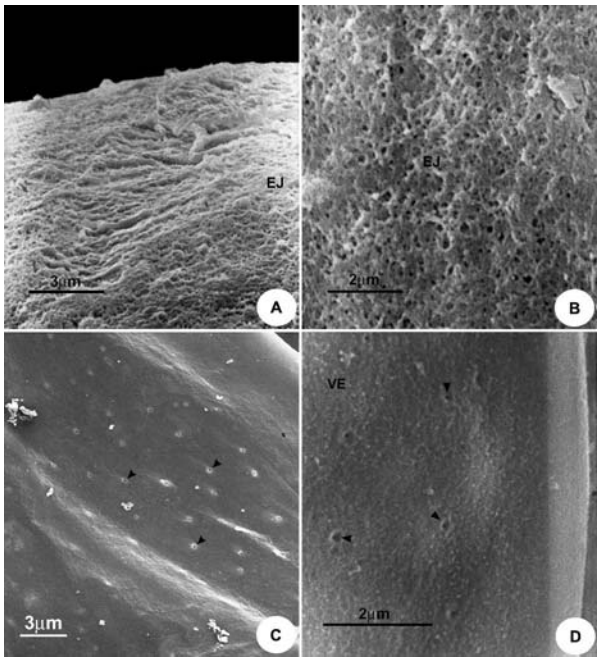
503 **Figure 4 (A)** Electrophoretograms of egg jelly (EJ) and vitelline envelope (VE) proteins
504 separated on 10% SDS-PAGE, stained by Coomassie blue (CB) and Periodic acid-Schiff
505 (PAS). PAS-stained mature ovarian oocytes (Oc_4, Oc_5) **(B)** and spawned egg **(C)** showing
506 strong-PAS positive jelly coat (EJ) and vitelline envelope (VE). Oc - developing oocyte
507 stage, Tr - connective tissue trabeculae

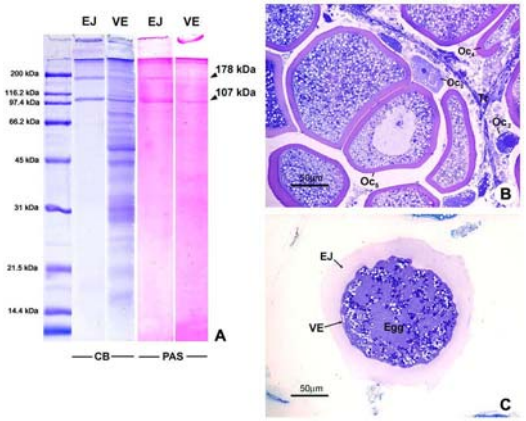
508 **Figure 5** HPLC chromatograms exhibiting percentages of the constituent sugars in the
509 extracted EJ and VE glycoproteins. The numbers on arrows indicate types of sugar that
510 are used as standards for HPLC: 1) = fucose, 2) = fructose, 3) = mannose, 4) = glucose, 5)
511 = galactose, 6) = sucrose, 7) = maltose
512
513 **Figure 6** Western blottings of extracted EJ and VE proteins, probed with anti-EJ and
514 anti-VE, showing the cross-immunoreactivities among both groups of separated proteins.
515
516 **Figure 7** Indirect immunofluorescent staining of ovarian sections **(A-D)** and spawned
517 eggs **(E, F)** using mouse anti-EJ and anti-VE anti-sera, demonstrating strong
518 immunoreactivities in both jelly coat and vitelline envelope. Control slides were
519 incubated with mouse preimmune sera instead of primary antibodies **(G, H)**. Cp - ovarian
520 capsule, Oc5 - stage 5 oocyte, EJ - jelly coat, VE - vitelline envelope
521
522 **Figure 8 (A-C)** SEM micrographs of sperm undergoing acrosome reaction (AR) on VE
523 (arrows) after 2-min incubation with the spawned eggs, compared to acrosme intact (AI)
524 sperm on EJ **(D)**. Extension of acrosomal filament (**C)** is clearly observed in AR sperm in
525 contact with VE surface, while the heads of AI sperm on EJ appear smooth (D).
526
527 **Figure 9** Histogram displaying percents of acrosome-reacted (AR) sperm after incubating
528 sperm in various concentrations of EJ (black bars) and VE (hatched bars) proteins in
529 seawater. Numbers of AR sperm with acrosomal filament (inset, arrowheads) are counted

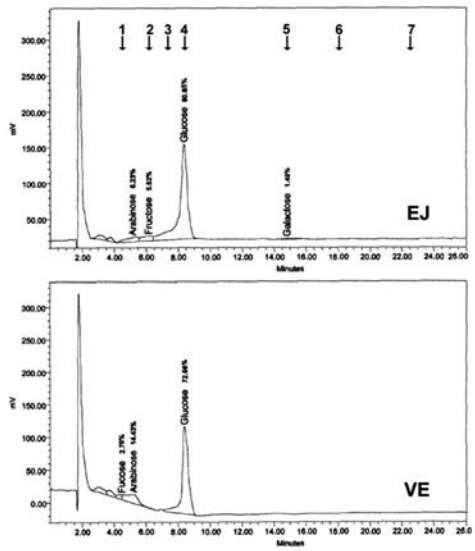
530 from at least 200 sperm. Control represents sperm incubated in filtered seawater. The
531 experiments are repeated four times, and bars indicate standard errors.
532
533


200µm
A
EJ
100µm
B
100µm
C
100µm
D


EJ
VE
1µm
A
VE
EJ
G
P
Mi
0.5µm
B
1
2
1'
2'
0.5µm
C
0.2µm
D
Mi
1µm
E
L
G
G
L
G
F

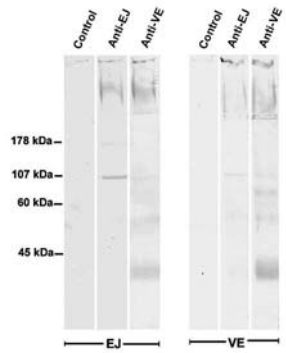

EJ
3µm
A
EJ
2µm
B
3µm
C
VE
2µm
D

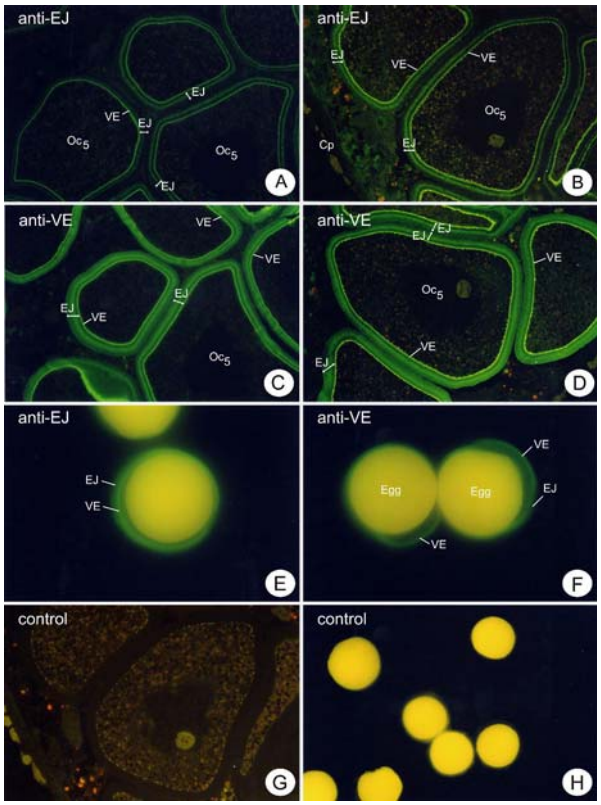

EJ
VE
EJ
VE
200 kDa
116.2 kDa
97.4 kDa
66.2 kDa
45 kDa
31 kDa
21.5 kDa
14.4 kDa
178 kDa
107 kDa
A
CB
PAS
Oc4
Oc3
Y
Oc2
Oc1
B
EJ
VE
Egg
50μm
C

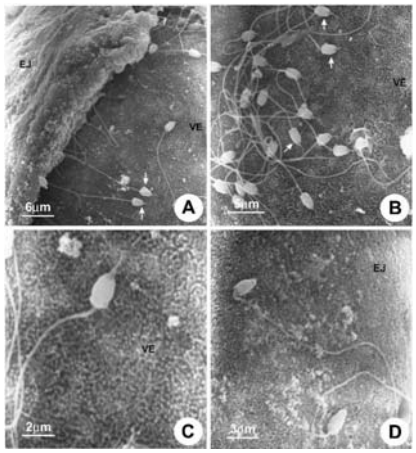


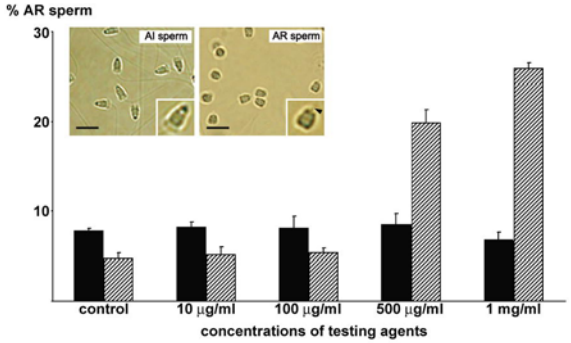
	Percent sugar compositions	
	EJ elute	VE elute
Glucose	80.85	72.66
Arabinose	6.23	14.43
Fructose	5.62	ND*
Galactose	1.49	ND*
Fucose	ND*	2.70

*ND = non detectable


Control
Anti-EJ
Anti-VE
Control
Anti-EJ
Anti-VE
178 kDa
107 kDa
60 kDa
45 kDa
EJ
VE


anti-EJ
EJ
VE
EJ
Oc5
Oc5
EJ
A
anti-EJ
EJ
VE
VE
Oc5
Cp
EJ
B
anti-VE
VE
VE
EJ
EJ
VE
Oc5
C
anti-VE
EJ
EJ
VE
Oc5
VE
EJ
D
anti-EJ
EJ
VE
E
anti-VE
VE
Egg
Egg
EJ
VE
F
control
G
control
H


EJ
VE
6µm
A
VE
5µm
B
VE
2µm
C
EJ
3µm
D


% AR sperm
30
20
10
AI sperm
AR sperm
control
10 μg/ml
100 μg/ml
500 μg/ml
1 mg/ml
concentrations of testing agents